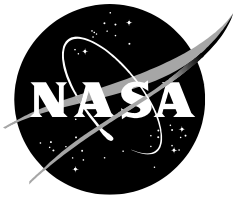
NASA/ TM-20250008197



GISS Research Publications 2024

De Leon, Priscilla (Editor)
Autonomic Integra, LLC., New York
NASA Goddard Institute for Space Studies, New York

Schmunk, Robert (Editor)
Autonomic Integra, LLC., New York
NASA Goddard Institute for Space Studies, New York

Mora, Josefina (Editor)
Autonomic Integra, LLC., New York
NASA Goddard Institute for Space Studies, New York

August 2025

NASA STI Program Report Series

The NASA STI Program collects, organizes, provides for archiving, and disseminates NASA's STI. The NASA STI program provides access to the NTRS Registered and its public interface, the NASA Technical Reports Server, thus providing one of the largest collections of aeronautical and space science STI in the world. Results are published in both non-NASA channels and by NASA in the NASA STI Report Series, which includes the following report types:

- TECHNICAL PUBLICATION. Reports of completed research or a major significant phase of research that present the results of NASA Programs and include extensive data or theoretical analysis. Includes compilations of significant scientific and technical data and information deemed to be of continuing reference value. NASA counterpart of peer-reviewed formal professional papers but has less stringent limitations on manuscript length and extent of graphic presentations.

- TECHNICAL MEMORANDUM. Scientific and technical findings that are preliminary or of specialized interest, e.g., quick release reports, working papers, and bibliographies that contain minimal annotation. Does not contain extensive analysis.

- CONTRACTOR REPORT. Scientific and technical findings by NASA-sponsored contractors and grantees.

- CONFERENCE PUBLICATION. Collected papers from scientific and technical conferences, symposia, seminars, or other meetings sponsored or co-sponsored by NASA.

- SPECIAL PUBLICATION. Scientific, technical, or historical information from NASA programs, projects, and missions, often concerned with subjects having substantial public interest.

- TECHNICAL TRANSLATION. English-language translations of foreign scientific and technical material pertinent to NASA's mission.

Specialized services also include organizing and publishing research results, distributing specialized research announcements and feeds, providing information desk and personal search support, and enabling data exchange services.

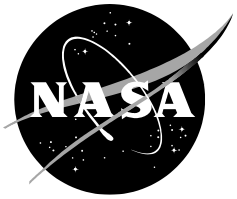
For more information about the NASA STI program, see the following:

- Access the NASA STI program home page at http://www.sti.nasa.gov

- Help desk contact information:

https://www.sti.nasa.gov/sti-contact-form/ and select the "General" help request type.

NASA/ TM-20250008197



GISS Research Publications 2024

De Leon, Priscilla
Autonomic Integra, LLC., New York
NASA Goddard Institute for Space Studies, New York

Schmunk, Robert
Autonomic Integra, LLC., New York
NASA Goddard Institute for Space Studies, New York

Mora, Josefina
Autonomic Integra, LLC., New York
NASA Goddard Institute for Space Studies, New York

National Aeronautics and
Space Administration

NASA Goddard Institute for Space Studies
New York

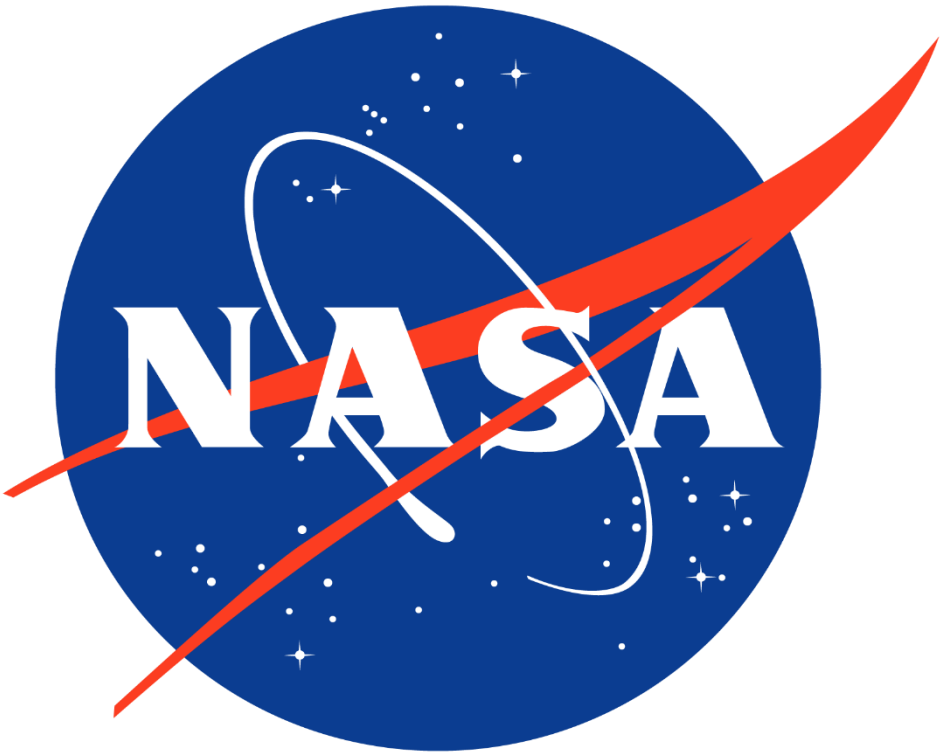
August 2025

The use of trademarks or names of manufacturers in this report is for accurate reporting and does not constitute an official endorsement, either expressed or implied, of such products or manufacturers by the National Aeronautics and Space Administration.

Available from:

NASA STI Program / Mail Stop 050
NASA Langley Research Center
Hampton, VA 23681-2199

GODDARD INSTITUTE FOR SPACE STUDIES



Research Publications 2024

National Aeronautics and Space Administration
Goddard Space Flight Center

2880 Broadway
New York, NY 10025
(212) 678-5500

GISS Research Publications 2024

The GISS Research Publications document was initiated in 1992 as an annual summary of our research based on quick inexpensive reproduction of excerpts of published papers. Its aim is twofold: to communicate in and outside the GISS community what we do and how we got about it, as well as to record annual accomplishments, providing a continual basis for measuring progress.

Background

Pictured below, GISS is a laboratory of NASA's Goddard Space Flight Center (GSFC) in Goddard's Earth Sciences Division and is located at Columbia University's Armstrong Hall in New York City. GISS was established in 1961 by Dr. Robert Jastrow. Our mission is to conduct basic research in support of NASA programs. Led by Dr. James E. Hansen from 1981 to 2013, the prime objective has been improved understanding of global change. Research areas include global climate, biogeochemical cycles, planetary atmospheres, earth observations and related interdisciplinary studies. In 2014, Dr. Gavin A. Schmidt was named Chief of GISS.

Research is carried out in cooperation with the academic community, especially Columbia University, near whose campus GISS is housed, City University of New York (CUNY) and the Massachusetts Institute of Technology (MIT). Typically, about six graduate students carry out their Ph.D. thesis research under the supervision of GISS staff members at any given time. GISS is made up of approximately 150 employees including high school, undergraduate, graduate students, post-doctoral scientists, university research associates and visiting faculty, all of whom contribute to collaborative research projects.



Table of Contents

1. OUTREACH

A. World Wide Web: GISS Home Page 4

B. Global Data and Model Simulations 8

C. Research News, Features, and Science Nuggets.....11

D. Science Education at GISS 41

2. PUBLICATIONS

A. GISS Best Publication Award 43

B. Journal Papers ….....45

C. Chapters, Conferences, Workshops, and Other Publications……226

3. AUTHOR INDEX 236

1. OUTREACH

A. WORLD WIDE WEB: GISS HOME PAGE

The GISS homepage on the Word Wide Web is located at the URL:

https://www.giss.nasa.gov/

All of the GISS website can be reached via the GISS homepage. These sites host a growing body of datasets, journal papers, preprints, software, and educational material. Sample GISS websites are depicted on the following pages including the GISS Publications main page.

The extensive GISS publications database is located at the URL:

https://pubs.giss.nasa.gov/

The publications website presently includes abstracts for more than 6000 GISS papers published since the institution's creation in 1961, with near complete coverage of papers published since 1990. Additionally, the publications site includes downloadable copies of about a third of these papers, almost all of them in the widely used Acrobat/PDF format.

Information about GISS Research Projects and Groups can be found at:

https://www.giss.nasa.gov/projects/

The research combines analysis of comprehensive global datasets with global models of atmospheric, land surface, and oceanic processes and includes study of past events on Earth such as paleoclimate change and the study of other planets as an aid to prediction of future evolution of Earth on a planetary scale.

Individual GISS projects can be accessed from the "Projects & Groups" tab on the GISS homepage. Some of these websites include:

Astrobiology — ROCKE-3D,

https://www.giss.nasa.gov/projects/astrobio/

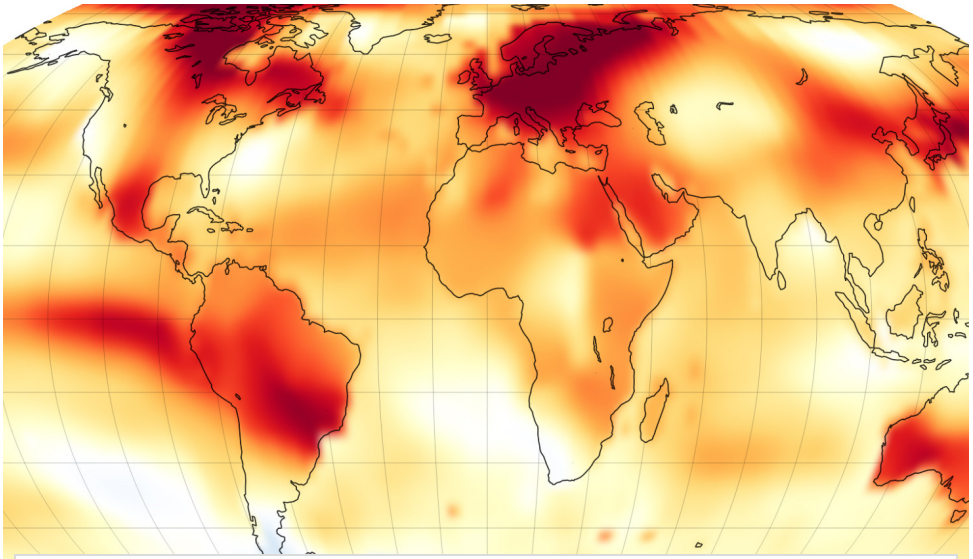
Climate Impacts,

https://www.giss.nasa.gov/projects/impacts/

Goddard Institute Surface Temperature Analysis (GISTEMP),

https://data.giss.nasa.gov/gistemp/

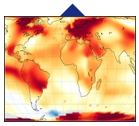
Charting the Exceptional, Unexpected Heat of 2023 and 2024

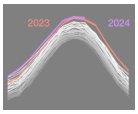


Global temperatures have soared in recent years and climate scientists are trying to understand why. (2024-11-20)


Columbia Univ.

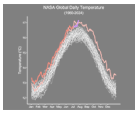

Cooling Cities


Charting Heat



Summer Temps

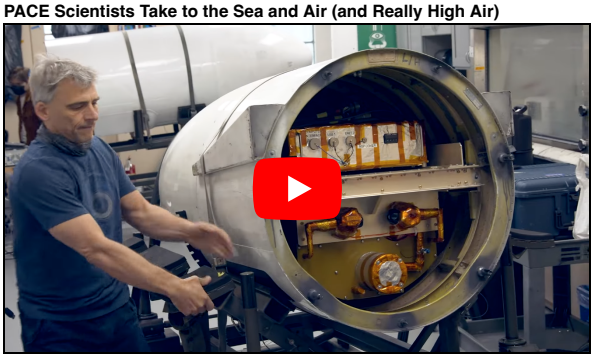

Verifying PACE


July 22 Temps

More News & Features

Featured Video

PACE Scientists Take to the Sea and Air (and Really High Air)



About GISS

Research at NASA's Goddard Institute for Space Studies (GISS) emphasizes a broad study of global change, which is an interdisciplinary initiative addressing natural and man-made changes in our environment that occur on various time scales — from one-time forcings such as volcanic explosions, to seasonal and annual effects such as El Niño, and on up to the millennia of ice ages — and that affect the habitability of our planet.

GISS is located at Columbia University in New York City. The institute is a laboratory in the Earth Sciences Division of NASA's Goddard Space Flight Center and is affiliated with the Columbia Climate School and School of Engineering and Applied Science.

+ More About GISS

Recent Publications

Lin, Y.-J., G.V. Cesana, C. Proistosescu, M.D. Zelinka, and K.C. Armour, 2025: The relative importance of forced and unforced temperature patterns in driving the time variation of low-cloud feedback. *J. Climate*, **38**, no. 2, 513-529, doi:10.1175/JCLI-D-24-0014.1.

Bruning, E.C., K.N. Brunner, M. van Lier-Walqui, T. Logan, and T. Matsui, 2024: Lightning and radar measures of mixed phase updraft variability in tracked storms during the TRACER field campaign in Houston, Texas. *Mon. Weather Rev.*, **152**, no. 12, 2753-2769, doi:10.1175/MWR-D-24-0060.1.

Peteet, D.M., R. Ibe, E. Stone, C. Zajac, and C. Chang, 2024: Paleoecological history of Maplecrest Fen, Catskill Mountains (NY, USA) from deglaciation to the Industrial Age. *J. Biogeogr.*, early on-line, doi:10.1111/jbi.15052.

Zhang, X., D.W. Waugh, I. Mitevski, C. Orbe, and L.M. Polvani, 2024: Decreased Northern Hemisphere precipitation from consecutive CO_2 doublings is associated with significant AMOC weakening. *Environ. Res. Clim.*, **3**, no. 4, 041005, doi:10.1088/2752-5295/ad929c.

+ More Publications



These database pages index about 6000 publications authored or co-authored by NASA Goddard Institute for Space Studies scientists and colleagues since the institute was founded in 1961. Most entries are refereed journal articles, but the database also includes tech reports and tech notes, report chapters, book chapters, conference proceedings papers, doctoral dissertations, and other research publications as well as some popular science articles. The database is not complete but is nearly so for the years after 1990.

Copies of some listed publications are also available here in PDF form. Otherwise, entries are citation and abstract only. Most listings also include a link to the appropriate journal website. Some include links to related news releases, features, or non-technical science briefs describing the research.

Some complete papers provided here differ from the published form, most likely because they are post-publication versions that include typographical or other corrections. Unless otherwise indicated, the published version is the version intended by the author(s).

Recent Publications

Lin, Y.-J., G.V. Cesana, C. Proistosescu, M.D. Zelinka, and K.C. Armour, 2025: The relative importance of forced and unforced temperature patterns in driving the time variation of low-cloud feedback. *J. Climate*, **38**, no. 2, 513-529, doi:10.1175/JCLI-D-24-0014.1.

Bruning, E.C., K.N. Brunner, M. van Lier-Walqui, T. Logan, and T. Matsui, 2024: Lightning and radar measures of mixed phase updraft variability in tracked storms during the TRACER field campaign in Houston, Texas. *Mon. Weather Rev.*, **152**, no. 12, 2753-2769, doi:10.1175/MWR-D-24-0060.1.

Peteet, D.M., R. Ibe, E. Stone, C. Zajac, and C. Chang, 2024: Paleoecological history of Maplecrest Fen, Catskill Mountains (NY, USA) from deglaciation to the Industrial Age. *J. Biogeogr.*, early on-line, doi:10.1111/jbi.15052.

Ehsan, M.A., M.L. L'Heureux, M.K. Tippett, A.W. Robertson, and J. Turmelle, 2024: Real-time ENSO forecast skill evaluated over the last two decades, with focus on onset of ENSO events. *NPJ Clim. Atmos. Sci.*, **7**, 301, doi:10.1038/s41612-024-00845-5.

Mülmenstädt, J., A.S. Ackerman, A.M. Fridlind, M. Huang, P.-L. Ma, N. Mahfouz, S.E. Bauer, S.M. Burrows, M.W. Christensen, S. Dipu, A. Gettelman, L.R. Leung, F. Tornow, J. Quaas, A.C. Varble, H. Wang, K. Zhang, and Y. Zheng, 2024: Can general circulation models (GCMs) represent cloud liquid water path adjustments to aerosol-cloud interactions? *Atmos. Chem. Phys.*, **24**, no. 23, 13633-13652, doi:10.5194/acp-24-13633-2024.

Zhang, X., D.W. Waugh, I. Mitevski, C. Orbe, and L.M. Polvani, 2024: Decreased Northern Hemisphere precipitation from consecutive CO_2 doublings is associated with significant AMOC weakening. *Environ. Res. Clim.*, **3**, no. 4, 041005, doi:10.1088/2752-5295/ad929c.

Romanou, A., G. Hegerl, S. Seneviratne, B. Abis, A. Bastos, A. Conversi, A. Landolfi, H. Kim, P. Lerner, J. Mekus, B. Otto-Bliesner, F. Pausata, I. Pinto, and L. Suarez-Guiterrez, 2024: Extreme events contributing to tipping elements and tipping points. *Surv. Geophys.*, early on-line, doi:10.1007/s10712-024-09863-7.

Schmidt, G.A., J. Arblaster, K.D. Mankoff, A. Pauling, and Q. Li, 2024: Lessons learned from running a virtual global workshop. *Eos*, **105**, on-line, doi:10.1029/2024EO240514.

Annual Lists

Publications in
2025, 2024, 2023, 2022, 2021,
2020, 2019, 2018, 2017, 2016,
2015, 2014, 2013, 2012, 2011,
2010, 2009, 2008, 2007, 2006,
2005, 2004, 2003, 2002, 2001,
2000, 1999, 1998, 1997, 1996,
1995, 1994, 1993, 1992, 1991,
1990, 1989, 1988, 1987, 1986,
1985, 1984, 1983, 1982, 1981,
1980, 1979, 1978, 1977, 1976,
1975, 1974, 1973, 1972, 1971,
1970, 1969, 1968, 1967, 1966,
1965, 1964, 1963, 1962, 1961.

Papers in press or accepted for publication.

Other Lists

+ Author Bibliographies
+ Best Paper of the Year
+ Most Cited Papers
+ Doctoral Dissertations

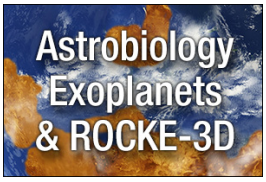
Publication Links

+ GSFC Earth Sciences Publications
+ SAO/NASA Astrophysics Data System
+ NASA Technical Reports Server
+ DOI Resolver
+ IPCC Assessment Reports



Following are links to some homepages for projects and groups in which researchers at NASA's Goddard Institute for Space Studies are involved.

Astrobiology, Exoplanets and ROCKE-3D



The GISS Astrobiology and Exoplanets group is an interdisciplinary team of scientists interested in understanding our solar system through time — from the early configuration of the planets nearly 4 billion years ago to their modern state. Our focus, using the ROCKE-3D model, is on characterizing the habitability of rocky planets, extending that understanding to the climates of extrasolar planets, but also includes understanding environments as diverse as Venus, Titan and Archean Earth.
+ Read More

Climate Adaptation Science Investigators



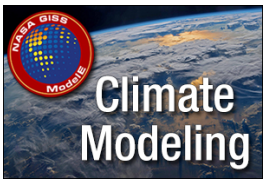
The goal of the CASI workgroup is to provide the latest scientific research on climate change that will help NASA facilities managers adapt to increasing climate risks in timely and effective ways. The CASI initiative is a partnership between NASA's Earth Science Division and Office of Strategic Infrastructure geared towards enhancing climate resilience at agency facilities.
+ Read More

Climate Impacts



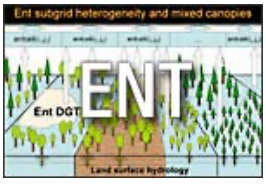
The Climate Impacts group at NASA GISS seeks to improve understanding of how climate affects human society through assessment of the effect of current climate variability and of potential climate change impacts caused by anthropogenic emissions of greenhouse gases and aerosols. Impacts research includes development of a framework to analyze complex interactions among biophysical and socio-economic processes.
+ Read More

Climate Modeling



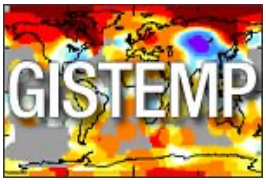
The climate modeling program at GISS is primarily aimed at the development of 3D general circulation models (GCMs) and coupled atmosphere-ocean models for simulating Earth's climate system, although some research may include the use of regional climate models, 2D energy balance models, and 1D radiative-convective models. Primary emphasis is placed on investigation of climate sensitivity, including the climate system's response to forcings such as solar variability, anthropogenic and natural emissions of greenhouse gases and aerosols, etc.
+ Read More

Ent Terrestrial Biosphere Model (Ent TBM)



The Ent model is a demographic dynamic global vegetation model developed specifically for coupling with Earth system models. Ent provides the GISS model with satellite-observed vegetation canopy structure, land surface albedo, and surface fluxes of water and carbon dioxide to the atmosphere, with canopy structure also used as boundary conditions for dust dynamics and vegetation emissions for atmospheric chemistry. Ent is also slated to serve as a lidar observation simulator of vertical canopy structure and to provide prognostic vegetation growth and decadal to century-scale alterations in vegetation cover and soil carbon and nitrogen.
+ Read More

Goddard Institute Surface Temperature Analysis (GISTEMP)



Surface air temperature change is a primary measure of global climate change. The GISTEMP project started in the late 1970s to provide an estimate of the changing global surface air temperature which could be compared with the estimates obtained from climate models simulating the effect of changes in atmospheric carbon dioxide, volcanic aerosols, and solar irradiance. The continuing analysis updates global temperature change from the late 1800s to the present.
+ Read More

For more, see https://www.giss.nasa.gov/projects/

B. Global Data and Model Simulations

GISS datasets are accessible from our main datasets index at:

https://data.giss.nasa.gov/

This page links to introductory pages for each available dataset, which in turn link to the actual data and to sample code snippets and images. In many cases, such as model simulation datasets and the GISS global temperature analysis, the user can interactively create graphics from the data.

Ready access to our global data sets and the results of our model simulations facilitates interactions with the outside community. It is with this in mind that we are giving priority to putting these data in convenient forms.

This section also includes the GISS "Software Tools" homepage, which can be found at:

https://www.giss.nasa.gov/tools/

This page provides an index of downloadable GISS-created software applications, including versions of the GISS climate model and other research tools. Among these are the FORTRAN source code for the GISS ModelE coupled atmosphere-ocean model, the ROCKE-3D exoplanet modeling code, and the cross-platform Panoply netCDF data viewer.



Datasets and derived material are available from the NASA GISS websites for the following research projects:

Climate Simulations

GISS ModelE

- Earth's Energy Imbalance
- Efficacy of Climate Forcings
- Climate Simulations for 1880-2003
- Dangerous Human-Made Interference
- Transient Simulations with Beryllium-10
- Simulated Greenland Surface Mass Balance
- Desert Dust, Industrialization and Agricultural Fires

SWING2 Stable Water Isotope Intercomparisons

Climate Forcings

- Forcings in GISS Climate Model
- Dust Mineral Fractions at Emission
- Globally Uniform Mineral Dust Aerosols
- Global Land Cover Datasets
- Surface Exchange of Carbon Dioxide
- Surface Exchange of Methane

Climate Impacts

- AgMIP Climate Forcing Datasets for Agricultural Modeling
- Evolving Fragility of the Global Food System
- Global Fire Weather Database (GFWED)

Planets, Exoplanets and Astrobiology

- Simulations of Planetary Climates with ROCKE-3D
- Saturn Mean Zonal Winds and Eddy Momentum Fluxes
- Objective Classification of Saturn Cloud Features

Astrophysics

- Molecular Collision Rates Relevant to Microwave and IR Astronomy

Earth Observations

Temperature

- GISS Surface Temperature Analysis (GISTEMP)
- GISTEMP Uncertainty Quantification
- Common Sense Climate Index (CSCI)

Aerosols

- Research Scanning Polarimeter (RSP)
- Global Aerosol Climatology Project (GACP)
- Stratospheric Aerosol and Gas Experiment II (SAGE II) V6.20

Clouds

- International Satellite Cloud Climatology Project (ISCCP)
- GEWEX Cloud System Study Data Integration for Model Evaluation (GCSS-DIME)
- Cumulus And Stratocumulus Cloudsat-CAlipso Dataset (CASCCAD)

Oceans

- Global Seawater Oxygen-18 Database
- Ocean Carbon States — Database and Toolbox

Precipitation

- Observed Land Surface Precipitation Data: 1850-1995

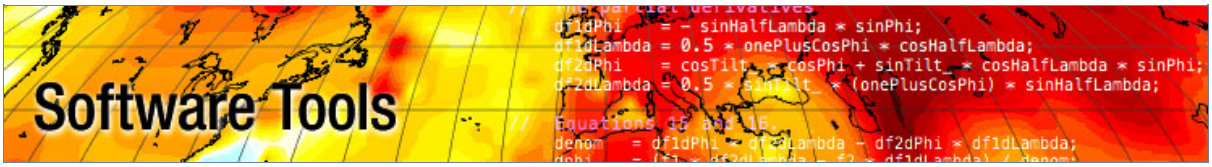
Radiative Flux

- ISCCP-FH Global Surface and Atmospheric Radiative Fluxes
- ISCCP-FH Radiative Kernels
- Surface Solar Irradiance: Datasets Produced for SeaWiFS

Storms

- Atlas of Extratropical Storm Tracks
- Observations of Extratropical Cyclones — Databases

National Aeronautics and Space Administration
Goddard Institute for Space Studies



This page provides links to several self-contained, downloadable software products that have been developed by GISS personnel, either for specific research purposes or for more general analytic use.

Climate Modeling

GISS GCM - Model E

Fortran 90 source and documentation for the GISS ModelE series of coupled atmosphere-ocean models. These models have been used for our contribution to the CMIP3 and CMIP5 archives of model simulation results.
+ Read More

Exoplanets & Planetary Science

GISS GCM - ROCKE-3D

Fortran 90 source and documentation for a version of GISS modelE GCM specially adapted for planetary (non-modern-Earth) simulations.
+ Read More

Mars24

Desktop application that calculates the solar and mean time for any location on the planet Mars, presenting the data as digital readouts and in "sunclock" format. (Requires Java)
+ Read More

Radiation

T-Matrix Codes

Fortran source code for computing electromagnetic scattering by nonspherical and aggregated particles.
+ Read More

Bidirectional Reflection Codes

Fortran source code for computing bidirectional reflection function for a semi-infinite homogeneous slab composed of arbitrarily shaped, randomly oriented particles.
+ Read More

Data Visualization

Panoply

Desktop application that interactively plots georeferenced and other data encoded in netCDF, HDF and GRIB file formats. (Requires Java)
+ Read More

G.Projector

Desktop application that explores over 200 map projections, including transformation of input equirectangular map images. (Requires Java)
+ Read More

Numerical Tools

JIGSAW(GEO)

C++ package that generates variable resolution unstructured mesh grids in complex domains. It is useful for multi-resolution GCMs and climate process modeling.
+ Read More

Astrophysics

MOLSCAT

Fortran source for quantum mechanical solution of nonreactive molecular scattering, useful in astrophysical studies.
+ Read More

C. Research News, Features, and Science Nuggets

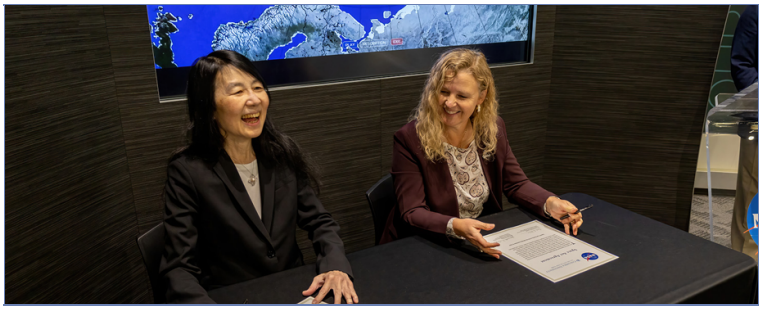
The communication of research goals and results with the public is one important aspect of our research program. GISS researchers are encouraged to prepare one-page summaries of their principal publications, in language meaningful to the educated laity.

To further our communication of GISS research, this publications document also includes "News & Features," NASA media releases about notable GISS research accomplishments. Following are copies of this year's "NASA News and Feature Releases" and "Science Nuggets." All belong to a larger collection of articles which are available at the GISS homepage.



Following are news releases, features and updates about research at NASA's Goddard Institute for Space Studies written by NASA news services, GISS personnel, and affiliated offices.

NASA, Columbia U. Enact Collaborative Space Act Agreement



NASA's Goddard Space Flight Center in Greenbelt, Maryland, and Columbia University in New York, enacted a collaborative Space Act Agreement to advance research and education opportunities during a signing ceremony on December 16. (2024-12-18)

+ Go to NASA Release

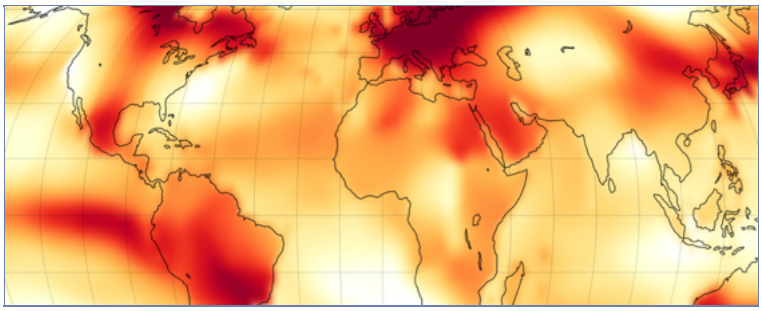
NASA Data Reveals Role of Green Spaces in Cooling Cities



A recent study used NASA satellite data to identify a major gap in global resilience to climate change: cities in the Global South have far less green space — and therefore less cooling capacity — than cities in the Global North. (2024-11-24)

+ Go to NASA Release

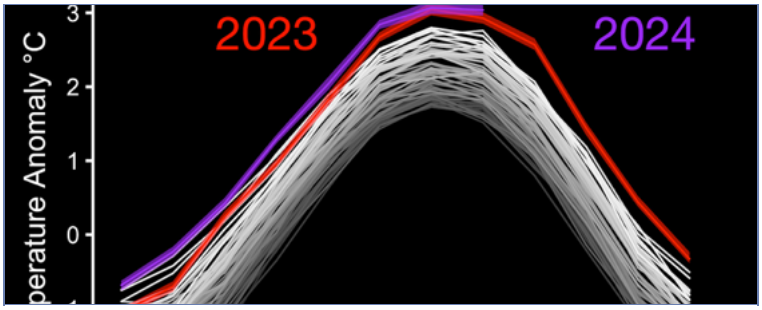
Charting the Exceptional, Unexpected Heat of 2023 and 2024



Global temperatures have soared in recent years and climate scientists are trying to understand why. (2024-11-20)

+ Go to NASA EO Feature

NASA Finds Summer 2024 Hottest to Date



August 2024 set a new monthly temperature record, capping Earth's hottest summer since global records began in 1880, according to scientists at NASA's Goddard Institute for Space Studies. (2024-09-11)

+ Go to NASA Release

For more 2024 GISS Research News & Features, see https://www.giss.nasa.gov/research/

NASA News & Feature Releases

NASA Analysis Confirms 2023 as Warmest Year on Record

By Roxana Barden — Release 24-008 — Jan. 12, 2024

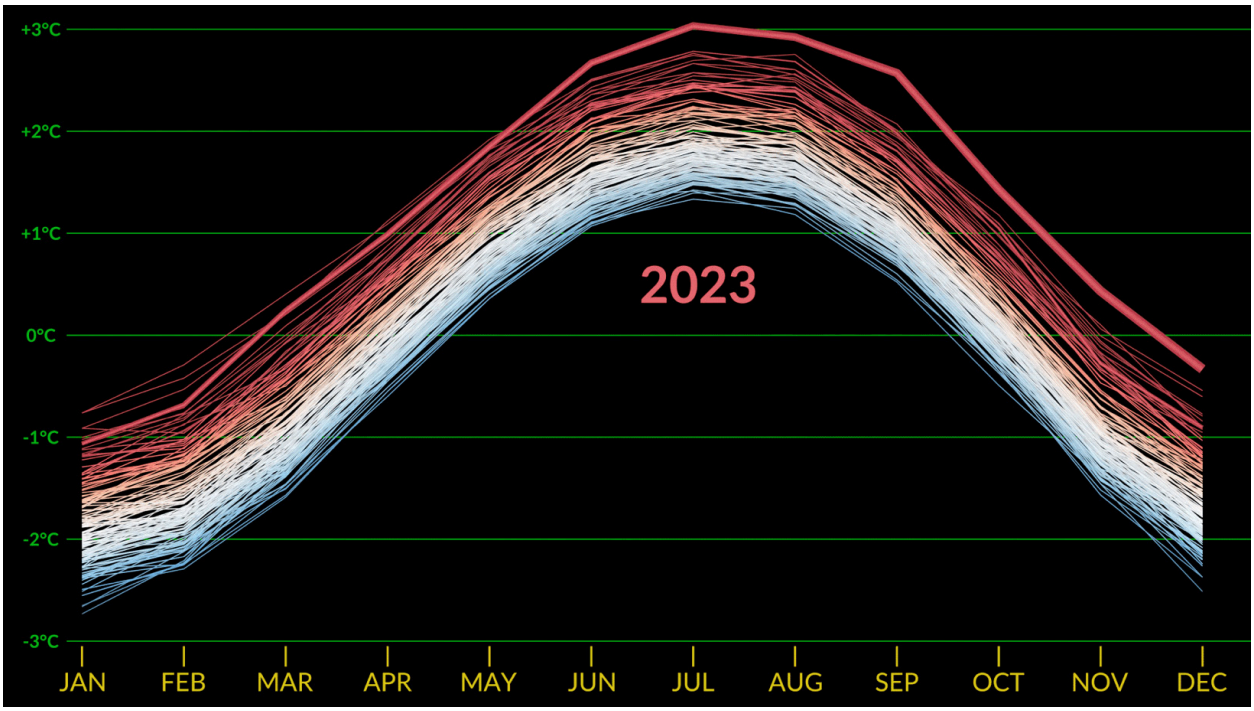
Earth's average surface temperature in 2023 was the warmest on record, according to an analysis by NASA. Global temperatures last year were around 2.1 degrees Fahrenheit (1.2 degrees Celsius) above the average for NASA's baseline period (1951-1980), scientists from NASA's Goddard Institute for Space Studies (GISS) in New York reported.

"NASA and NOAA's global temperature report confirms what billions of people around the world experienced last year; we are facing a climate crisis," said NASA Administrator Bill Nelson. "From extreme heat, to wildfires, to rising sea levels, we can see our Earth is changing. There's still more work to be done, but President Biden and communities across America are taking more action than ever to reduce climate risks and help communities become more resilient – and NASA will continue to use our vantage point of space to bring critical climate data back down to Earth that is understandable and accessible for all people. NASA and the Biden-Harris Administration are working to protect our home planet and its people, for this generation – and the next."

In 2023, hundreds of millions of people around the world experienced extreme heat, and each month from June through December set a global record for the respective month. July was the hottest month ever recorded. Overall, Earth was about 2.5 degrees Fahrenheit (or about 1.4 degrees Celsius) warmer in 2023 than the late 19th-century average, when modern record-keeping began.

"The exceptional warming that we're experiencing is not something we've seen before in human history," said Gavin Schmidt, director of GISS. "It's driven primarily by our fossil fuel emissions, and we're seeing the impacts in heat waves, intense rainfall, and coastal flooding."

Though scientists have conclusive evidence that the planet's long-term warming trend is driven by human activity, they still examine other phenomena that can affect yearly or multi-year changes in climate such as El Niño, aerosols and pollution, and volcanic eruptions.



This data visualization, which is updated monthly, shows the seasonal cycle of temperature variation on the Earth's surface, and how those temperatures deviate from the average from 1951 to 1980. The data come from the GISS Surface Temperature Analysis and are publicly accessible here. The seasonal temperature offsets are based on the MERRA-2 reanalysis data here. **NASA's Scientific Visualization Studio**

Typically, the largest source of year-to-year variability is the El Niño – Southern Oscillation ocean climate pattern in the Pacific Ocean. The pattern has two phases – El Niño and La Niña – when sea surface temperatures along the equator switch between warmer, average, and cooler temperatures. From 2020-2022, the Pacific Ocean saw three consecutive La Niña events, which tend to cool global temperatures. In May 2023, the ocean transitioned from La Niña to El Niño, which often coincides with the hottest years on record.

However, the record temperatures in the second half of 2023 occurred before the peak of the current El Niño event. Scientists expect to see the biggest impacts of El Niño in February, March, and April.

Scientists have also investigated possible impacts from the January 2022 eruption of the Hunga Tonga-Hunga Ha'apai undersea volcano, which blasted water vapor and fine particles, or aerosols, into the stratosphere. A recent study found that the volcanic aerosols – by reflecting sunlight away from Earth's surface – led to an overall slight cooling of less than 0.2 degrees Fahrenheit (or about 0.1 degrees Celsius) in the Southern Hemisphere following the eruption.

"Even with occasional cooling factors like volcanoes or aerosols, we will continue to break records as long as greenhouse gas emissions keep going up," Schmidt said. "And, unfortunately, we just set a new record for greenhouse gas emissions again this past year."

"The record-setting year of 2023 underscores the significance of urgent and continued actions to address climate change," said NASA Deputy Administrator Pam Melroy. "Recent legislation has delivered the U.S. government's largest-ever climate investment, including billions to strengthen America's resilience to the increasing impacts of the climate crisis. As an agency focused on studying our changing climate, NASA's fleet of Earth observing satellites will continue to provide critical data of our home planet at scale to help all people make informed decisions."

Open Science in Action

NASA assembles its temperature record using surface air temperature data collected from tens of thousands of meteorological stations, as well as sea surface temperature data acquired by ship- and buoy-based instruments. This data is analyzed using methods that account for the varied spacing of temperature stations around the globe and for urban heating effects that could skew the calculations.

Independent analyses by NOAA and the Hadley Centre (part of the United Kingdom Met Office) concluded the global surface temperatures for 2023 were the highest since modern record-keeping began. These scientists use much of the same temperature data in their analyses but use different methodologies. Although rankings can differ slightly between the records, they are in broad agreement and show the same ongoing long-term warming in recent decades.

Building on a half century of research, observations, and models, the Biden-Harris Administration including NASA and several federal partners recently launched the U.S. Greenhouse Gas Center to make critical climate data readily available to decisionmakers and citizens. The center supports collaboration across U.S. government agencies and the non-profit and private sectors to make air-, ground-, and space-borne data and resources available online.

NASA's full dataset of global surface temperatures through 2023, as well as details with code of how NASA scientists conducted the analysis, are publicly available from GISS. GISS is a NASA laboratory managed by the Earth Sciences Division of the agency's Goddard Space Flight Center in Greenbelt, Maryland. The laboratory is affiliated with Columbia University's Earth Institute and School of Engineering and Applied Science in New York

For more information on NASA, visit: https://www.nasa.gov.

-end-

Karen Fox / Katherine Rohloff, Headquarters, Washington
202-358-1600, karen.fox@nasa.gov / Katherine.a.rohloff@nasa.gov

Peter Jacobs, NASA Goddard Space Flight Center, Greenbelt, Md
301-286-0535, peter.jacobs@nasa.gov

From https://www.nasa.gov/news-release/nasa-analysis-confirms-2023-as-warmest-year-on-record/

NASA Earth Observatory: Image of the Day

Five Factors to Explain the Record Heat in 2023

By Angela Colbert (NASA JPL), with Sally Younger (NASA JPL) — Jan. 13, 2024

NASA announced that 2023 was the hottest year on record, according to an analysis of annual global average temperatures by the Goddard Institute for Space Studies. Scientists who maintain the temperature record, which begins in 1880, calculate a global temperature anomaly each year to determine how much temperatures have changed compared to temperatures from 1951–1980.

Every month from June through December 2023 came in as the hottest month on record. July ranked as the hottest month ever recorded.

But what caused 2023, especially the second half of it, to be so hot? Scientists asked themselves this same question. Here is a breakdown of primary factors that scientists considered to explain the record-breaking heat.

The long-term rise in greenhouse gases is the primary driver.

For more than 100 years, humans have been burning fossil fuels such as coal, gas, and oil to power everything from lightbulbs and cars to factories and cities. These actions, along with changes in land use, have led to a rise in greenhouse gases in the atmosphere. Greenhouse gases act like a blanket trapping heat around the planet. The more of them you add, the thicker that blanket becomes, further heating Earth.

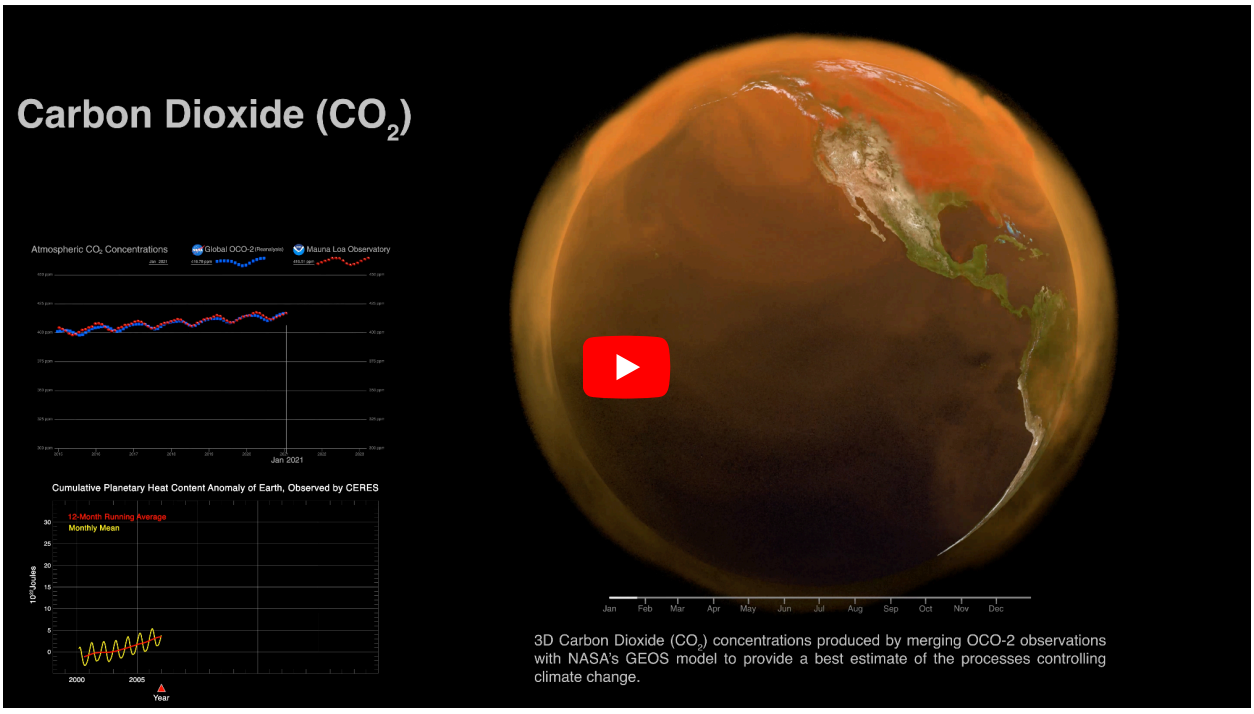
In May 2023, carbon dioxide concentrations in the atmosphere peaked at 424 parts per million at NOAA's Mauna Loa Observatory, Hawaii. The annual peak has been steadily rising since measurements began in 1958. (Other global carbon measurement projects showed similarly high numbers.) Extending the record back even further with ice cores, carbon dioxide concentrations are the highest they have been in at least 800,000 years.

"We're going to continue to have records be broken because the baseline temperature is moving up all the time," said Gavin Schmidt, director of NASA's Goddard Institute for Space Studies in New York City. "The cause of that warming trend over the last 50 to 60 years is dominated by our changes to greenhouse gases, particularly carbon dioxide and methane."

The return of El Niño added to the heat.

On top of the long-term global warming trend are natural variations in the climate. One of the largest sources of such year-to-year variability is the El Niño Southern Oscillation (ENSO), which occurs in the tropical Pacific.

ENSO transitions between three phases: El Niño, La Niña, and neutral, or average. During El Niño, trade winds weaken; that is, winds that normally blow from east to west in the tropical Pacific weaken. The sea surface around the equator in the central and eastern Pacific near South America also becomes warmer (and higher) than normal. El Niño often coincides



January 1 - December 31, 2021

MPEG

with the warmest years in the global average.

During La Niña, the opposite happens: the trade winds strengthen and the sea surface temperatures in the eastern Pacific are cooler than normal. This can help offset some of the rising temperatures from long-term global warming.

From 2020–2022, the Pacific saw three years of La Niña conditions. Then El Niño returned beginning in May 2023. This El Niño has not yet been as strong as those in 2015–2016 or 1997–1998, both of which caused large global average temperature spikes. However, when you add this ocean warming to the long-term warming trend from greenhouse gases, the start of El Niño helped temperatures jump enough to create a new record for heat.

"For the most part, it's us and El Niño," said Josh Willis, a climate scientist at NASA's Jet Propulsion Laboratory. "At the end of the day, humans are heating the planet, and El Niño is dancing on our heads."

Globally, long-term ocean warming and hotter-than-normal sea surface temperatures played a part.

Looking more broadly, the tropical Pacific wasn't the only part of the ocean that was hotter than normal this year. The global sea surface temperature set new records in 2023, with the North Atlantic and other parts of the ocean experiencing several marine heat waves.

"Just like global temperatures, ocean temperatures are on the rise," said Willis. "They have been rising for the last century or more, and they are not slowing down. If anything, they are speeding up."

What's behind the rise in ocean temperatures? Greenhouse gases warming the planet. Around 90 percent of the heat trapped by rising greenhouse gases is absorbed by the ocean. That means that as greenhouse gases continue to increase, so will ocean temperatures, which raises temperatures across the globe.

Aerosols are decreasing, so they are no longer slowing the rise in temperatures.

Another global trend that scientists are monitoring is a change in aerosols in the atmosphere. Aerosols are small particles in the air—such as smoke, dust, volcanic gases, sea spray, air pollution or soot—that can impact the climate. Airborne particles can either reflect sunlight, causing a slight cooling of the air, or absorb sunlight, causing a slight warming of it.

As governments have passed regulations to reduce air pollution and improve air quality, the abundance of aerosols has been decreasing in most areas. Many of these human-produced particles are the type that cool the climate slightly, so with less of them in the air, the result is a slight warming effect. But this contribution is quite small in comparison to the much greater warming from rising greenhouse gases.

Scientists at NASA and around the world are investigating how a reduction in aerosols from new shipping regulations potentially change how much solar energy is reflected back into space. While these changes can be notable on regional scales, the global impact is likely small, Schmidt said.

Scientists found that the Hunga Tonga-Hunga Ha'apai volcanic eruption did not substantially add to the record heat.

In January 2022, the eruption of the Hunga Tonga-Hunga Ha'apai undersea volcano blasted an unprecedented amount of water vapor and fine particles, or aerosols, into the stratosphere. Water vapor, a greenhouse gas, can produce a warming effect on the atmosphere, so scientists investigated the impact of the eruption on the global temperature. Sulfate aerosols from eruptions, on the other hand, have sometimes led to some global cooling events.

A recent study found that the volcanic sulfate aerosols reflected some sunlight away from Earth's surface, leading to a slight cooling of less than 0.1 degrees in the southern hemisphere following the eruption. Essentially, the warming that occurred from the increase in water vapor in the stratosphere was offset by the cooling caused by volcanic sulfate aerosols leading to a slight cooling lower in the atmosphere. This means the eruption likely did not add to the record heat in 2023.

"We are very interested in the weather and extremes of any particular year because those are the things that impact us," said Schmidt. "But the key difference between this decade and the ones before is that the temperatures keep rising because of our activities, principally the burning of fossil fuels."

Carbon dioxide animation by Helen-Nicole Kostis, NASA's Scientific Visualization Studio.

NASA Earth Observatory map (top) by Lauren Dauphin, based on data from the NASA Goddard Institute for Space Studies. Carbon dioxide animation by Helen-Nicole Kostis, NASA's Scientific Visualization Studio. Sea surface height anomaly map by Lauren Dauphin, using modified Copernicus Sentinel data (2023) processed by the European Space Agency and further processed by Josh Willis, Severin Fournier, and Kevin Marlis/NASA/JPL-Caltech. Sea surface temperature anomaly map by Lauren Dauphin, using data from the Multiscale Ultrahigh Resolution (MUR) project. Wildland fire smoke image by Lauren Dauphin, using Terra MODIS data from NASA EOSDIS LANCE and GIBS/Worldview. Eruption image courtesy of NOAA and the National Environmental Satellite, Data, and Information Service (NESDIS). Story by Angela Colbert (NASA JPL), with Sally Younger (NASA JPL).

From https://earthobservatory.nasa.gov/images/152313/five-factors-to-explain-the-record-heat-in-2023

NASA Launches New Climate Mission to Study Ocean, Atmosphere

By Jennifer M. Dooren — Release 24-021 — Feb. 8, 2024

NASA's satellite mission to study ocean health, air quality, and the effects of a changing climate for the benefit of humanity launched successfully into orbit at 1:33 a.m. EST Thursday.

Known as PACE, the Plankton, Aerosol, Cloud, ocean Ecosystem satellite, launched aboard a SpaceX Falcon 9 rocket from Space Launch Complex 40 at Cape Canaveral Space Force Station in Florida. NASA confirmed signal acquisition from the satellite about five minutes after launch, and the spacecraft is performing as expected.



NASA's Plankton, Aerosol, Cloud, ocean Ecosystem (PACE) satellite launched aboard a SpaceX Falcon 9 rocket at 1:33 a.m. EST, Feb. 8, 2024, from Space Launch Complex 40 at Cape Canaveral Space Force Station in Florida. From its orbit hundreds of miles above Earth, PACE will study microscopic life in the oceans and microscopic particles in the atmosphere to investigate key mysteries of our planet's interconnected systems. **NASA**

"Congratulations to the PACE team on a successful launch. With this new addition to NASA's fleet of Earth-observing satellites, PACE will help us learn, like never before, how particles in our atmosphere and our oceans can identify key factors impacting global warming," said NASA Administrator Bill Nelson. "Missions like this are supporting the Biden-Harris Administration's climate agenda and helping us answer urgent questions about our changing climate."

From hundreds of miles above Earth, the PACE mission will study the impact of tiny, often invisible things: microscopic life in water and microscopic particles in the air.

The satellite's hyperspectral ocean color instrument will allow researchers to measure oceans and other waterbodies across a spectrum of ultraviolet, visible, and near-infrared light. This will enable scientists to track the distribution of phytoplankton and – for the first time from space – identify which communities of these organisms are present on daily, global scales. Scientists and coastal resource managers can use the data to help forecast the health of fisheries, track harmful algal blooms, and identify changes in the marine environment.

The spacecraft also carries two polarimeter instruments, Hyper-Angular Rainbow Polarimeter #2 and Spectro-polarimeter for Planetary Exploration. These will detect how sunlight interacts with particles in the atmosphere, giving researchers new information on atmospheric aerosols and cloud properties, as well as air quality at local, regional, and global scales.

With the combination of the instrument and the polarimeters, PACE will provide insights into the interactions of the ocean and atmosphere, and how a changing climate affects these interactions.

“Observations and scientific research from PACE will profoundly advance our knowledge of the ocean’s role in the climate cycle,” said Karen St. Germain, director, Earth Science Division, Science Mission Directorate, at NASA Headquarters in Washington. “The value of PACE data skyrockets when we combine it with data and science from our Surface Water and Ocean Topography mission – ushering in a new era of ocean science. As an open-source science mission with early adopters ready to use its research and data, PACE will accelerate our understanding of the Earth system and help NASA deliver actionable science, data, and practical applications to help our coastal communities and industries address rapidly evolving challenges.”

“It’s been an honor to work with the PACE team and witness firsthand their dedication and tenacity in overcoming challenges, including the global pandemic, to make this observatory a reality,” said Marjorie Haskell, PACE program executive at NASA Headquarters. “The passion and teamwork are matched only by the excitement of the science community for the data this new satellite will provide.”

Earth’s oceans are responding in many ways to climate change – from sea level rise to marine heat waves to a loss of biodiversity. With PACE, researchers will be able to study climate change’s effects on phytoplankton, which play a key role in the global carbon cycle by absorbing carbon dioxide from the atmosphere and converting it into their cellular material. These tiny organisms drive larger aquatic and global ecosystems that provide critical resources for food security, recreation, and the economy.

“After 20 years of thinking about this mission, it’s exhilarating to watch it finally realized and to witness its launch. I couldn’t be prouder or more appreciative of our PACE team,” said Jeremy Werdell, PACE project scientist at NASA’s Goddard Space Flight Center in Greenbelt, Maryland. “The opportunities PACE will offer are so exciting, and we’re going to be able to use these incredible technologies in ways we haven’t yet anticipated. It’s truly a mission of discovery.”

NASA’s Launch Services Program, based at the agency’s Kennedy Space Center in Florida, managed the launch services for the mission. The PACE mission is managed by NASA Goddard, which also built and tested the spacecraft and the ocean color instrument. The Hyper-Angular Rainbow Polarimeter #2 was designed and built by the University of Maryland, Baltimore County, and the Spectro-polarimeter for Planetary Exploration was developed and built by a Dutch consortium led by Netherlands Institute for Space Research, Airbus Defence, and Space Netherlands.

For more information on PACE, visit: https://www.nasa.gov/pace

-end-

Faith McKie / Karen Fox
Headquarters, Washington
202-358-1600 / 240-285-5155
faith.d.mckie@nasa.gov / karen.c.fox@nasa.gov

Jake Richmond
Goddard Space Flight Center, Greenbelt, Md.
240-713-1618
jacob.a.richmond@nasa.gov

From https://www.nasa.gov/news-release/nasa-launches-new-climate-mission-to-study-ocean-atmosphere/

Can Volcanic Super Eruptions Lead to Major Cooling? Study Suggests No

By Sally Younger— Feb. 8, 2024

New research suggests that sunlight-blocking particles from an extreme eruption would not cool surface temperatures on Earth as severely as previously estimated.

Some 74,000 years ago, the Toba volcano in Indonesia exploded with a force 1,000 times more powerful than the 1980 eruption of Mount St. Helens. The mystery is what happened after that – namely, to what degree that extreme explosion might have cooled global temperatures.

When it comes to the most powerful volcanoes, researchers have long speculated how post-eruption global cooling – sometimes called volcanic winter – could potentially pose a threat to humanity. Previous studies agreed that some planet-wide cooling would occur but diverged on how much. Estimates have ranged from 3.6 to 14 degrees Fahrenheit (2 to 8 degrees Celsius).

In a new study in the Journal of Climate, a team from NASA's Goddard Institute for Space Studies (GISS) and Columbia University in New York used advanced computer modeling to simulate super-eruptions like the Toba event. They found that post-eruption cooling would probably not exceed 2.7 degrees Fahrenheit (1.5 degrees Celsius) for even the most powerful blasts.

"The relatively modest temperature changes we found most compatible with the evidence could explain why no single super-eruption has produced firm evidence of global-scale catastrophe for humans or ecosystems," said lead author Zachary McGraw, a researcher at NASA GISS and Columbia University.

To qualify as a super eruption, a volcano must release more than 240 cubic miles (1,000 cubic kilometers) of magma. These eruptions are extremely powerful – and rare. The most recent super-eruption occurred more



Crew aboard the International Space Station photographed the eruption of Mount Etna in Sicily in October 2002. Ashfall was reported more than 350 miles away. When it comes to explosive power, however, no eruption in modern times can compare with a super eruption – which hasn't occurred for tens of thousands of years. **NASA**

than 22,000 years ago in New Zealand. The best-known example may be the eruption that blasted Yellowstone Crater in Wyoming about 2 million years ago.

Small Particles, Big Questions

McGraw and colleagues set out to understand what was driving the divergence in model temperature estimates because "models are the main tool for understanding climate shifts that happened too long ago to leave clear records of their severity." They settled on a variable that can be difficult to pin down: the size of microscopic sulfur particles injected miles high into the atmosphere.

In the stratosphere (about 6 to 30 miles in altitude), sulfur dioxide gas from volcanoes undergoes chemical reactions to condense into liquid sulfate particles. These particles can influence surface temperature on Earth in two counteracting ways: by reflecting incoming sunlight (causing cooling) or by trapping outgoing heat energy (a kind of greenhouse warming effect).

Over the years, this cooling phenomenon has also spurred questions about how humans might turn back global warming – a concept called geoengineering – by intentionally injecting aerosol particles into the stratosphere to promote a cooling effect.

The researchers showed to what extent the diameter of the volcanic aerosol particles influenced post-eruption temperatures. The smaller and denser the particles, the greater their ability to block sunlight. But estimating the size of particles is challenging because previous super eruptions have not left reliable physical evidence. In the atmosphere, the size of the particles changes as they coagulate and condense. Even when particles fall back to Earth and are preserved in ice cores, they don't leave a clear-cut physical record because of mixing and compaction.

By simulating super-eruptions over a range of particle sizes, the researchers found that super-eruptions may be incapable of altering global temperatures dramatically more than the largest eruptions of modern times. For instance, the 1991 eruption of Mount Pinatubo in the Philippines caused about a half-degree drop in global temperatures for two years.

Luis Millán, an atmospheric scientist at NASA's Jet Propulsion Laboratory in Southern California who was not involved in the study, said that the mysteries of super-eruption cooling invite more research. He said the way forward is to conduct a comprehensive comparison of models, as well as more laboratory and model studies on the factors determining volcanic aerosol particle sizes.

Given the ongoing uncertainties, Millán added, "To me, this is another example of why geoengineering via stratospheric aerosol injection is a long, long way from being a viable option."

The study, titled "Severe Global Cooling After Volcanic Super-Eruptions? The Answer Hinges on Unknown Aerosol Size," was published in the *Journal of Climate*.

From https://www.nasa.gov/earth/can-volcanic-super-eruptions-lead-to-major-cooling-study-suggests-no/

Jennifer Krottinger: Designing Ways to Serve

By Elizabeth M. Jarrell — Mar. 5, 2024

At NASA's Goddard Institute for Space Studies in New York City, Jennifer Krottinger pairs her artistic vision with a passion for public service.

Name: Jennifer Krottinger

Title: Business Manager

Formal Job Classification: Business Management Specialist

Organization: Goddard Institute for Space Studies, Science and Exploration Directorate (Code 611)



Jennifer Krottinger is a business management specialist at NASA's Goddard Institute for Space Studies in New York City. Courtesy of Jennifer Krottinger

What do you do and what is most interesting about your role here at Goddard?

I play a key role in decision making on institutional support, and provide authoritative, technical advice, and consultation on the laboratory's grants, cooperative agreements, personnel management, and procurement actions. Because no two days are alike, and I have the honor of working alongside brilliant, awesome, and equally humble people, my role is very interesting.

What is your educational background?

In 2002, I received my undergraduate degree, a bachelor's in business administration, from Midwestern State University in Wichita Falls, Texas. In 2008, I received my graduate degree, a master's in public administration, specializing in analysis and research, from Portland State University in Portland, Oregon. In 2019, I received another undergraduate degree, an associate of applied science in fashion design, from Parsons School of Design, School of Fashion, in New York, New York.

Please tell us about your service in Volunteers in Service to America (VISTA).

I worked for a small business during my undergrad and continued to after graduation. I was born into a family of entrepreneurs, maternally and paternally, and small business is in my DNA. I was ready for something different, yearning to "give back." I applied to VISTA, the domestic version of the Peace Corps. I was ultimately offered a few different positions, opting for the West Coast, leaving Texas in 2003 to begin VISTA service. I worked on economic development initiatives, in California and Oregon at the county, city, and state levels of government. I served for three-and-a-half years and fell in love with public service. Thinking I would pursue an MBA post-service, I decided to study for a master's in public administration instead, studying full-time while working part-time as a graduate research assistant for a department chair.

After graduating with my MPA, I returned to the private sector for a few years, and decided to take another leap of faith, answering the call of international service with the Peace Corps.

Please tell us about your experience in the Peace Corps.

From 2011 to 2015, I served in the Peace Corps, and my post was Sarteneja, Belize, Central America. My primary project was Sarteneja Alliance for Conservation and Development (SACD), a non-governmental organization working on communications ranging from basic skills, such as teaching Belizeans how to use Google, to more advanced, working with the SACD Board of Directors on the development and implementation of the communications plan.

My secondary project was helping 10 women found a women-owned, -operated, and -led sewing and handicraft cooperative, Las Sartenejeñas Cooperative. They make and sell indigenous artisan work and school uniforms for the local schools. The project won the 2013 Charlotte Daniels Champions of Change award, selected from world-wide projects, from World Connect, and the cooperative is still flourishing. These women inspire me to this day.

After completing Peace Corps service, I stayed in-country working on projects, with the cooperative, as the technical business development manager, working for almost a year, post-service.

And, in the summer of 2022, while working at GISS, I participated voluntarily in the Peace Corps Virtual Service Pilot Program (VSPP), in Namibia, to capitate Ngato Vocational Training Centre staff in developing a financially, viable business plan for the center, enabling greater sustainability, an increase in student enrollment capacity, and expansion of scholarship

program for youth who come from traditionally marginalized and disadvantaged communities.

What inspired you to attend Parsons School of Design?
The women at the cooperative were a great catalyst for me. Since I was five years old, I wanted to be a fashion designer, and it was time. The opportunity was presenting itself and working with the women fueled the motivation. It was the education I always wanted and deserved, and decided to go for it.

I returned to Texas in June of 2015 from Belize, and moved to New York City in July 2015. In August 2015, I started my position with the Small Business Administration Region II, New Jersey District Office, later transferring to the New York Metro District Office, and Parsons.

It was a tall order to work full time, while adapting back to the United States, let alone coming from a rural, remote village of about 3,500, to a city of about 8.7 million, and attend Parsons part time which was rigorous and grueling, with little to no fashion design experience. I loved my time at Parsons, learning a lot about myself, the grit and the gumption, including how strong I really was and how to successfully manage priorities, attaining almost straight A's, graduating with top honors.

What did you do for the Small Business Administration (SBA)?
From 2015 to 2020, I worked at SBA, in Region II District Offices located in Newark, New Jersey, and New York City in government contracting and business development. The position as a business opportunity specialist allowed me to continue working cross-culturally with socioeconomic groups through managing portfolios of socially and economically disadvantaged small businesses, participating in federal government contract certification programs such as 8(a), Women Owned Small Business (WOSB), HUBZone, Veteran Owned Small Business (VOSB) and other certifications offered, providing technical assistance on the development of comprehensive business plans including robust financial planning. I also served as a district office technical representative for the Women's Business Centers funded by SBA.

Why did you come to GISS?
In May 2020, I landed at GISS. NASA has always been an aspiration for me. One of my heroes is Katherine Goble Johnson, a NASA mathematician and "Hidden Figure." One of my favorite quotes of hers is, "I'm always interested in learning something new." I hold this quote near and dear to my heart; growth and learning are two of my values. I included this quote and explained its importance on my NASA application. If you are always learning something new, you are continuously improving and growing.

What do you do at GISS?
Every day is different, and as mentioned earlier, no two days are alike. My major duties are program management and coordination of GISS strategic planning activities, oversight of GISS partnership agreements and procurement duties as the contracting officer representative (COR). This tends to involve problem-solving, working through and undoing complexities, establishing and refining policies and procedures, providing guidance and technical assistance, implementing innovative and creative approaches, and a lot of listening. I'm also one of the founding members of the newly established GISS DEIA Committee and serve as a vice co-chair for the Women's Employee Resource Group and Network (WEN) at NASA's Goddard Space Flight Center.

What is the coolest part about working at GISS?
Working at GISS is truly the coolest part, because again, NASA was an aspiration and achieving this, well sometimes I feel like pinching myself, ensuring its real. Also working directly and alongside Gavin Schmidt, the GISS director, and Ron Miller, the GISS deputy director, two incredibly brilliant and people-first leaders, who demonstrate everyday humility and humanity in leadership. For example, during the pandemic, when there was civil unrest across the country, Gavin told everyone at the weekly staff meeting that it was OK not to be OK, normalizing the taboo.

[…]

What are you currently doing for the United Nations?
The third goal of Peace Corps is to "help promote a better understanding of other peoples on the part of Americans," bringing back the country of service, to the United States. In March 2023, I became a representative for the Economic and Social Council (ECOSOC) of the United Nations. Five Returned Peace Corps Volunteers, are voluntarily consulting on addressing worldwide poverty and the 17 Sustainable Development Goals (SDG). My focus is SDG 5 Gender Equality, SDG 8 Decent Work and Economic Growth, and SDG 10 Reduced Inequalities. The consultancy involves attending UN meetings, summits, side events, briefings, and official ECOSOC written and oral statements.

What do you do for fun?
In January 2023, I launched my own fashion brand of prêt-à-couture garments and accessories with a focus on creative

Interview continues at
https://www.nasa.gov/people-of-nasa/goddard-people/jennifer-krottinger-designing-ways-to-serve/

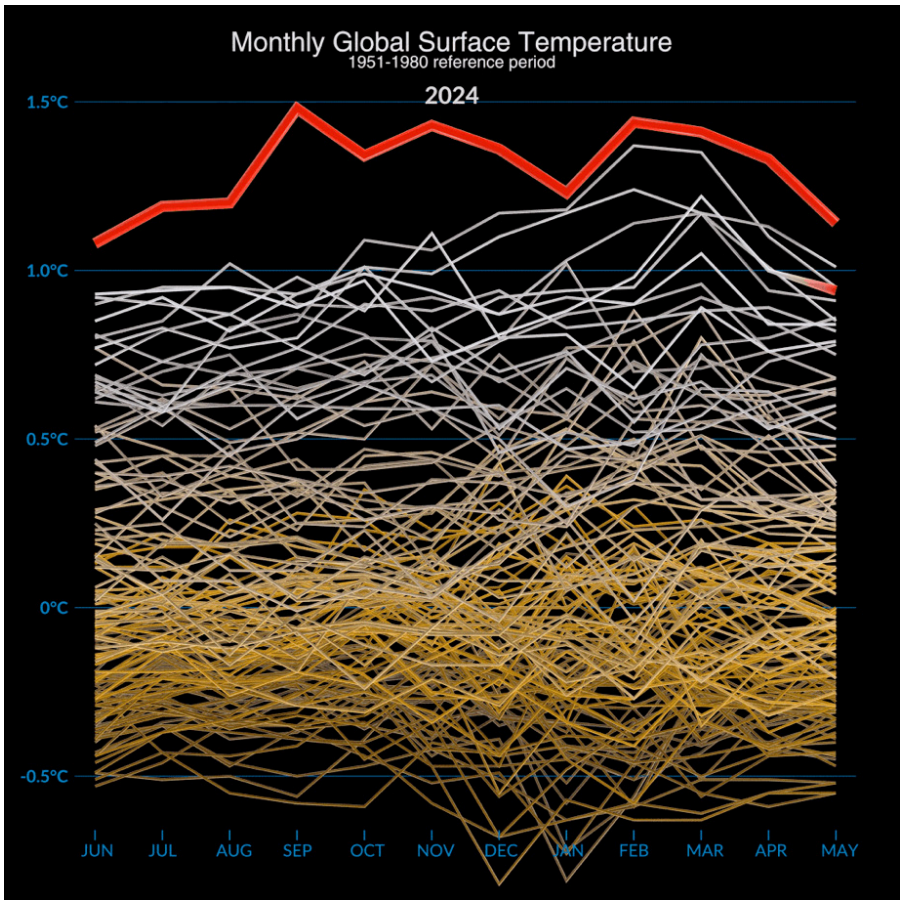
NASA Analysis Confirms a Year of Monthly Temperature Records

By Sally Younger — June 11, 2024

May 2024 was the warmest May on the books, marking a full year of record-high monthly temperatures, NASA scientists found. Average global temperatures for the past 12 months hit record highs for each respective month – an unprecedented streak – according to scientists from NASA's Goddard Institute for Space Studies (GISS) in New York.

"It's clear we are facing a climate crisis," said NASA Administrator Bill Nelson. "Communities across America—like Arizona, California, Nevada—and communities across the globe are feeling first-hand extreme heat in unprecedented numbers. NASA and the Biden-Harris Administration recognize the urgency of protecting our home planet. We are providing critical climate data to better lives and livelihoods, and benefit all humanity."

The run of record temperatures fits within a long-term warming trend driven by human activity — primarily greenhouse gas emissions. The trend has become evident over the past four decades, with the last 10 consecutive years being the warmest 10 since record-keeping began in the late 19th century. Before this streak of 12 straight months of record temperatures, the second longest streak lasted for seven months between 2015 and 2016.



This visualization shows monthly global surface temperatures from 1880 to May 2024. The last 12 months (June 2023 through May 2024) hit record highs for each respective month. Download this visualization from NASA Goddard's Scientific Visualization Studio: https://svs.gsfc.nasa.gov/5311 — **NASA's Scientific Visualization Studio**

"We're experiencing more hot days, more hot months, more hot years," said Kate Calvin, NASA's chief scientist and senior climate advisor. "We know that these increases in temperature are driven by our greenhouse gas emissions and are impacting people and ecosystems around the world."

In NASA's analysis, a temperature baseline is defined by several decades or more – typically 30 years. The average global temperature over the past 12 months was 2.34 degrees Fahrenheit (1.30 degrees Celsius) above the 20th century baseline (1951 to 1980). This is slightly over the 2.69 degree Fahrenheit (1.5 degree Celsius) level with respect to the late 19th century average.

To calculate Earth's global temperature, NASA scientists gather data from tens of thousands of meteorological stations on land, plus thousands of instruments on ships and buoys on the ocean surface. This raw data is analyzed using methods that account for the varied spacing of temperature stations around the globe and for urban heating effects that could skew the calculations.

El Niño Subsiding, La Niña Arriving?

Phenomena such as El Niño and La Niña, which alternately warm and cool the tropical Pacific Ocean, can contribute a small amount of variability in global temperatures from year to year. The strong El Niño that began in spring 2023 helped stoke last year's extreme summer and fall heat.

As of May 2024, scientists at the NOAA (National Oceanic and Atmospheric Administration) Climate Prediction Center projected a 49% chance of La Niña developing between June and August, and a 69% chance of it developing between July and September. By cooling a large swath of the tropical Pacific, a La Niña event could partially suppress average global temperatures this year.

It's hard to know whether 2024 will set another global heat record. Factors like volcanic eruptions and sun-blocking aerosol emissions can affect our climate in any given year. NASA missions are actively studying these influences, said Gavin Schmidt, director of GISS.

"There are open questions that can impact our predictions over the next few years and decades, and we're in evidence-gathering mode," Schmidt said. "This year may well end up setting another global temperature record. Right now, it's in line to be close to 2023."



Dr. Kate Calvin, NASA's Chief Scientist and Senior Climate Advisor, answers some of the top questions pertaining to these temperature records and our changing climate. **NASA's Goddard Space Flight Center/ Katie Jepson**

Ocean Temperatures and Hurricanes

Scientists are watching to see how ocean temperatures may influence this year's hurricane season. Temperatures remained high as the 2024 hurricane and typhoon seasons got underway. Across the Northern Hemisphere, ocean temperatures for the January-April period were 2.12 degrees Fahrenheit (1.18 degrees Celsius) above average, according to NOAA. Despite the waning El Niño, temperatures at the sea surface and at deeper depths are still above average in many places, said Josh Willis, an oceanographer at NASA's Jet Propulsion Laboratory in Southern California.

Willis cited rising carbon dioxide emissions as the main driver of ocean warming. As much as 90% of the excess atmospheric heat in recent decades has been absorbed by the ocean, with much of that heat stored near the water surface.

"The ocean is the flywheel of our climate," Willis said. "Since the ocean covers more than two-thirds of Earth, whatever sea surface temperatures are, the rest of the planet follows."

La Niña years also can contribute to more active Atlantic hurricane seasons. That's because La Niña conditions weaken westerly winds high in the atmosphere near the Americas, over the Caribbean Sea and tropical Atlantic Ocean. Wind shear – abrupt changes in wind speed and direction – can cut hurricanes down before they grow. La Niña effectively lifts this brake, allowing tropical storms to form and intensify unimpeded.

NASA's full dataset of global surface temperatures, as well as details of how NASA scientists conducted the analysis, are publicly available from GISS, a NASA laboratory managed by the agency's Goddard Space Flight Center in Greenbelt, Maryland.

From https://www.nasa.gov/earth/nasa-analysis-confirms-a-year-of-monthly-temperature-records/

NASA Earth Observatory: Image of the Day

In the Grip of Global Heat

By Adam Voiland — June 28, 2024

It's only the beginning of the summer season in the Northern Hemisphere, but Earth is already roasting.

Scientists from NASA's Goddard Institute for Space Studies recently reported that May 2024, the hottest May in NASA's global surface temperature analysis, marked a full year of record-high monthly temperatures. Likewise, NOAA recently reported that January through May 2024 ranked warmest on its 175-year temperature record. On June 19, 2024, the Northern Hemisphere was running 1.1 degrees Celsius (1.9 degrees Fahrenheit) above normal, according to an analysis of meteorological data from Climate Reanalyzer.

In this context, early summer heatwaves in the Northern Hemisphere have been fierce. Just as Central America and the southwestern and eastern United States saw blasts of heat in May and June, temperatures also soared in the Middle East, South Asia, and Africa. The series of heat waves has contributed to large numbers of deaths, strained power grids, and challenged meteorological records.

The animation above shows the daily maximum surface air temperature across Northern Africa, the Middle East, and South Asia from June 15 to June 25, 2024. It was produced by combining satellite observations with temperatures predicted by a version of the Goddard Earth Observing System (GEOS) global model, which uses mathematical equations to represent physical processes in the atmosphere. The darkest red areas indicate temperatures of more than 40°C (104°F).

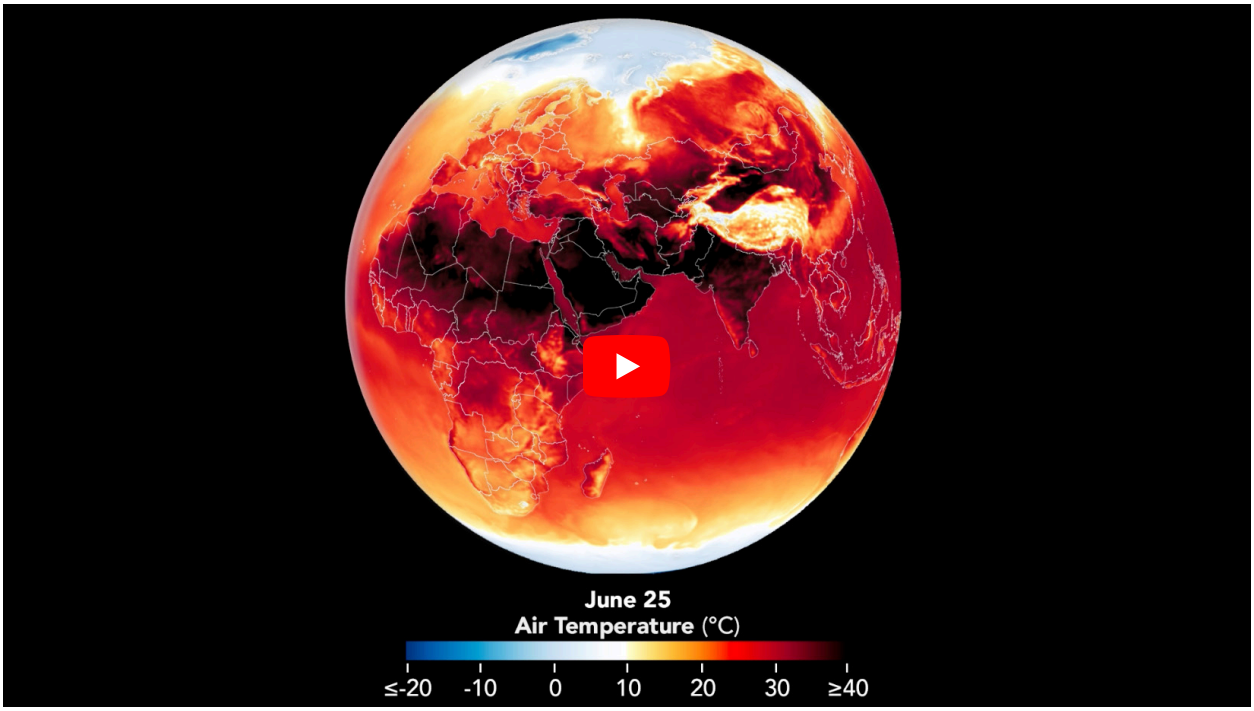
According to news reports, nighttime temperatures were as high as 35.2°C (95.4°F) in Delhi on June 18, one of the hottest nights the city has seen in decades. In Greece, temperatures soared to 44.5°C (112.1°F) amid the closure of schools and historical sites. The Saudi National Center for Meteorology reported temperatures up to 49°C (120°F) in and around Mecca during Hajj.

In many cities, extreme temperatures collided with limited access to air conditioning, large outdoor events, high nighttime temperatures, a lack of green space, urban heat islands, and other factors to leave millions of people in hot and often humid conditions. The circumstances triggered not just discomfort but heat exhaustion and heatstroke in some places. The annual Hajj pilgrimage to Mecca in Saudi Arabia proved particularly deadly in mid-June, but news reports indicate that the heat was associated with hospitalizations and deaths in India, Pakistan, Egypt, and Greece as well.

According to the World Health Organization, heat stress is the world's leading cause of weather-related deaths and can exacerbate underlying illnesses including cardiovascular disease, diabetes, mental health conditions, and asthma. Researchers have calculated that roughly 489,000 heat-related deaths occur each year, with 45 percent of the deaths in Asia and 36 percent in Europe.

"For older adults with physical health problems, temperatures as low as 26.7°C (80°F) can pose significant danger. And when humidity is as high as 90 percent, even 25.6°C (78°F) can be hazardous," said Deborah Carr, a Boston University sociologist who specializes in the study of aging. "Nighttime heat is especially harmful for older adults whose homes lack air conditioning or who can't afford to run their air conditioners for long periods."

Carr is part of a research team that used temperature and climate data archived by NASA and demographic data to identify which parts of the world are at the greatest risk of current and future heat exposure. They published their results in *Nature Communications* in May 2024. They found that, in 2020, about 14 percent of the world's population 69 years of age or older resided in areas where the average maximum temperature exceeded 37.5°C (99.5°F)—the level at which even brief exposure can be dangerous for older adults. The researchers projected that by 2050, more than 23 percent of that age group will face maximum temperatures that exceed 37.5°C—an increase of around 200 million older adults.



June 15 - 25, 2024

MPEG

To prepare, Giacomo Falchetta, one of the authors of the study and a researcher at the Euro-Mediterranean Center on Climate Change, recommended a number of tailored public approaches. Well-resourced cities might increase investments in early warning systems and ride services to cooling centers and hospitals. By using remote sensing and geographic information systems, public officials could identify neighborhoods with high levels of heat exposure, and expand power grids to manage the increasing demand for air conditioning, he said. In contrast, improving access to high-quality housing, air conditioning, and clean water could have the greatest impact in cities with fewer resources, he added.

There are steps individuals can take to minimize risks as well. “The number one thing that older adults need to recognize is that they’re not the same person they were 50 years ago,” said Carr. “Biological changes mean that we can’t tolerate heat as well in our older years. Stay indoors during heat waves. If you have to go outside, get your activities done in the early morning or evening, when temperatures cool down. Drink plenty of water. Don’t use the oven, especially in small homes. Be sensitive to symptoms like dizziness and call for medical attention.”

NASA Earth Observatory video by Lauren Dauphin, using GEOS data from the Global Modeling and Assimilation Office at NASA GSFC.

From https://earthobservatory.nasa.gov/images/152995/in-the-grip-of-global-heat

NASA Earth Observatory: Image of the Day

El Niño Exits

By Emily Cassidy — July 15, 2024

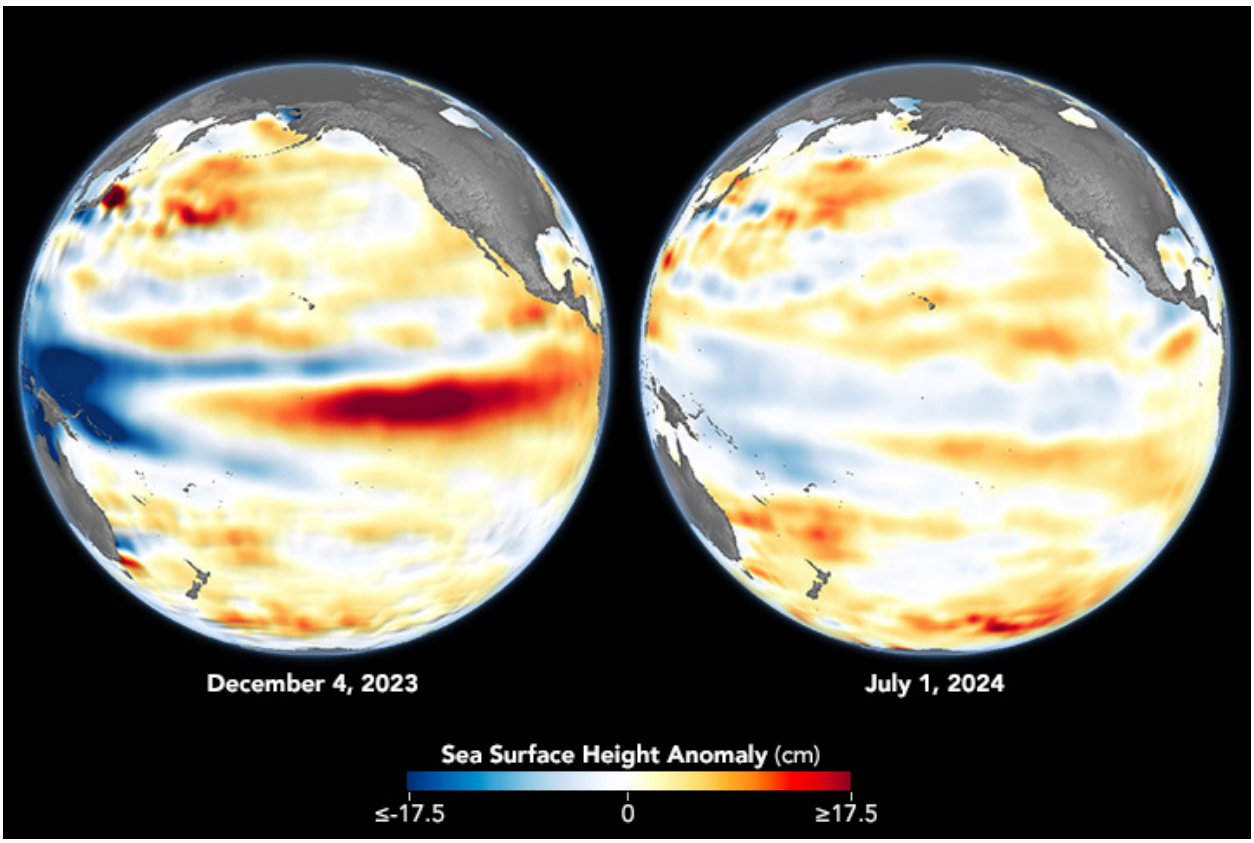
After heating up the eastern Pacific Ocean for about a year, El Niño finally died out in May 2024. The natural climate phenomenom contributed to many months of record-high ocean temperatures, precipitation extremes in Africa, low ice cover on the Great Lakes, and severe drought in the Amazon and Central America. As of July 2024, the eastern Pacific was in a neutral phase, but the reprieve may be short-lived.

In tropical latitudes of the eastern Pacific, the ocean's surface cools and warms cyclically in response to the strength of the trade winds—a phenomenon known as the El Niño Southern Oscillation (ENSO). In turn, the changing ocean disrupts atmospheric circulation in ways that intensify rainfall in some regions and bring drought to others.

In May 2023, easterly trade winds weakened and warm water from the western Pacific moved toward the western coast of the Americas, signs that an El Niño had begun, after three consecutive years of La Niña conditions. El Niño continued to strengthen into December 2023 and then faded by mid-May 2024.

"This was a sizable El Niño, but not the biggest we've seen in the last 30 years," said Josh Willis, an oceanographer at NASA's Jet Propulsion Laboratory (JPL). Willis tracks the signature of sea level change across the globe by using satellite measurements of sea surface height. Warmer water expands, raising sea levels, while cooler water contracts, lowering them.

The maps above depict sea surface height anomalies across the central and eastern Pacific Ocean as observed on July 1, 2024 (right), during the neutral phase, compared to December 4, 2023 (left), near the peak of the El Niño. Shades of red indicate areas where the ocean stood higher than normal; blues indicate sea levels



December 4, 2023 - July 1, 2024

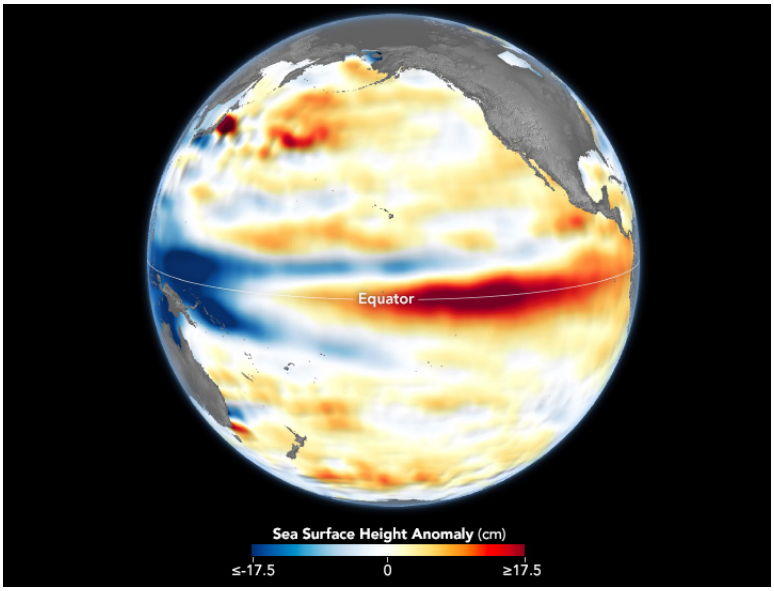
JPEG

that were lower than average; and normal sea level conditions appear white. In a report from NOAA's Climate Prediction Center, the sea surface temperatures in December for the key tropical Pacific monitoring region (from 170° to 120° West longitude) measured 2° Celsius above the 1991–2020 average.

Data for the maps were acquired by the Sentinel-6 Michael Freilich satellite and processed by Willis and colleagues at JPL. Note that signals related to seasonal cycles and long-term trends have been removed to highlight sea level anomalies associated with El Niño and other short-term natural phenomena.

Even at its peak in November and December, the intensity of the 2023 El Niño did not match that of the largest events in recent decades. During the previous record-setting events of 1997–1998 and 2015–2016, sea levels were much higher (warmer), and the high sea levels were spread over a much larger area of the central and eastern Pacific.

Even so, this moderately intense El Niño contributed to climate disturbances around the world. Precipitation patterns were disrupted in Africa: southern parts of the country suffered a dry spell that parched almost half the corn grown in Zambia, while the Horn of Africa saw devastating flooding. Severe drought in the Amazon led to huge understory fires in the northern state of Roraima. El Niño also contributed to heat stress in coral reefs, intense precipitation on the U.S. West Coast, low ice on the Great Lakes, and fires in Indonesia.



December 4, 2023 - July 1, 2024 JPEG

El Niño often coincides with the warmest years in the global temperature record. Warm sea surface temperatures, on top of the long-term warming trend from greenhouse gases, helped global temperatures jump enough to create a new record for heat in 2023. An analysis by scientists at NASA's Goddard Institute for Space Studies (GISS) found that May 2023 to May 2024 marked a full year of record-high monthly temperatures—an unprecedented streak. Before the consecutive 12 straight months of record temperatures, the second longest streak lasted for seven months, during the El Niño between 2015 and 2016.

In May 2024, easterly trade winds picked back up, bringing sea surface temperatures (and sea surface heights) back to normal in the eastern Pacific. NOAA's Climate Prediction Center estimates these neutral conditions will stick around until August. They forecast that La Niña is 70 percent likely to emerge sometime between August and October and persist into the Northern Hemisphere winter.

NASA Earth Observatory image by Lauren Dauphin, using modified Copernicus Sentinel data (2023) processed by the European Space Agency and further processed by Josh Willis, Severin Fournier, and Kevin Marlis/NASA/JPL-Caltech.

From https://earthobservatory.nasa.gov/images/153058/el-nino-exits

NASA Data Shows July 22 Was Earth's Hottest Day on Record

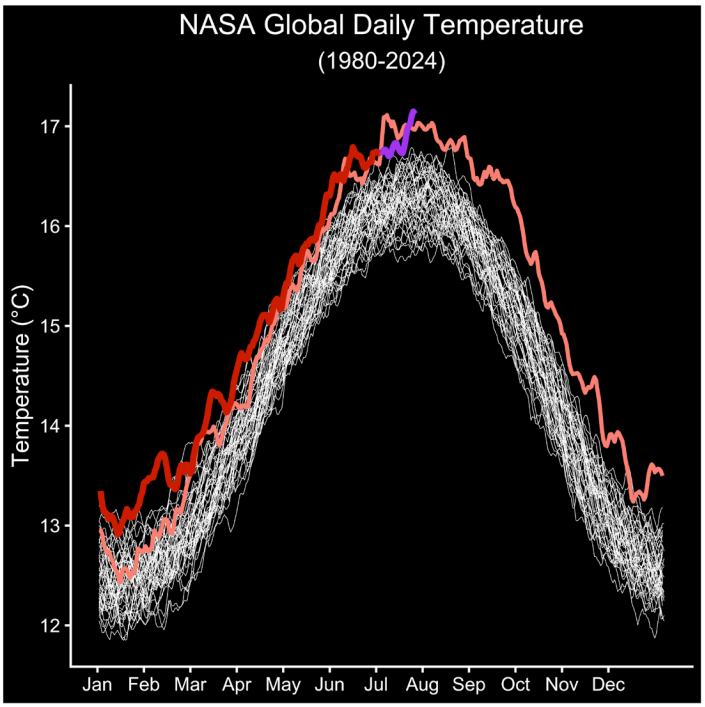
July 29, 2024

July 22, 2024, was the hottest day on record, according to a NASA analysis of global daily temperature data. July 21 and 23 of this year also exceeded the previous daily record, set in July 2023. These record-breaking temperatures are part of a long-term warming trend driven by human activities, primarily the emission of greenhouse gases. As part of its mission to expand our understanding of Earth, NASA collects critical long-term observations of our changing planet.

"In a year that has been the hottest on record to date, these past two weeks have been particularly brutal," said NASA Administrator Bill Nelson. "Through our over two dozen Earth-observing satellites and over 60 years of data, NASA is providing critical analyses of how our planet is changing and how local communities can prepare, adapt, and stay safe. We are proud to be part of the Biden-Harris Administration efforts to protect communities from extreme heat."

This preliminary finding comes from data analyses from Modern-Era Retrospective analysis for Research and Applications, Version 2 (MERRA-2) and Goddard Earth Observing System Forward Processing (GEOS-FP) systems, which combine millions of global observations from instruments on land, sea, air, and satellites using atmospheric models. GEOS-FP provides rapid, near-real time weather data, while the MERRA-2 climate reanalysis takes longer but ensures the use of best quality observations. These models are run by the Global Modeling and Assimilation Office (GMAO) at NASA's Goddard Space Flight Center in Greenbelt, Maryland.

Daily global average temperature values from MERRA-2 for the years 1980-2022 are shown in white, values for the year 2023 are shown in pink, and values from 2024 through June are shown in red. Daily global temperature values from July 1 to 23, 2024, from GEOS-FP are shown in purple. The results agree with an independent analysis from the European Union's Copernicus Earth Observation Programme. While the analyses have small differences, they show broad agreement in the change in temperature over time and hottest days.



Daily global average temperature values from MERRA-2 for the years 1980-2022 are shown in white, values for the year 2023 are shown in pink, and values from 2024 through June are shown in red. Daily global temperature values from July 1-July 23, 2024, from GEOS-FP are shown in purple. **NASA/ Global Modeling and Assimilation Office/Peter Jacobs**

The latest daily temperature records follow 13 months of consecutive monthly temperature records, according to scientists from NASA's Goddard Institute for Space Studies in New York. Their analysis was based on the GISTEMP record, which uses surface instrumental data alone and provides a longer-term view of changes in global temperatures at monthly and annual resolutions going back to the late 19th century.

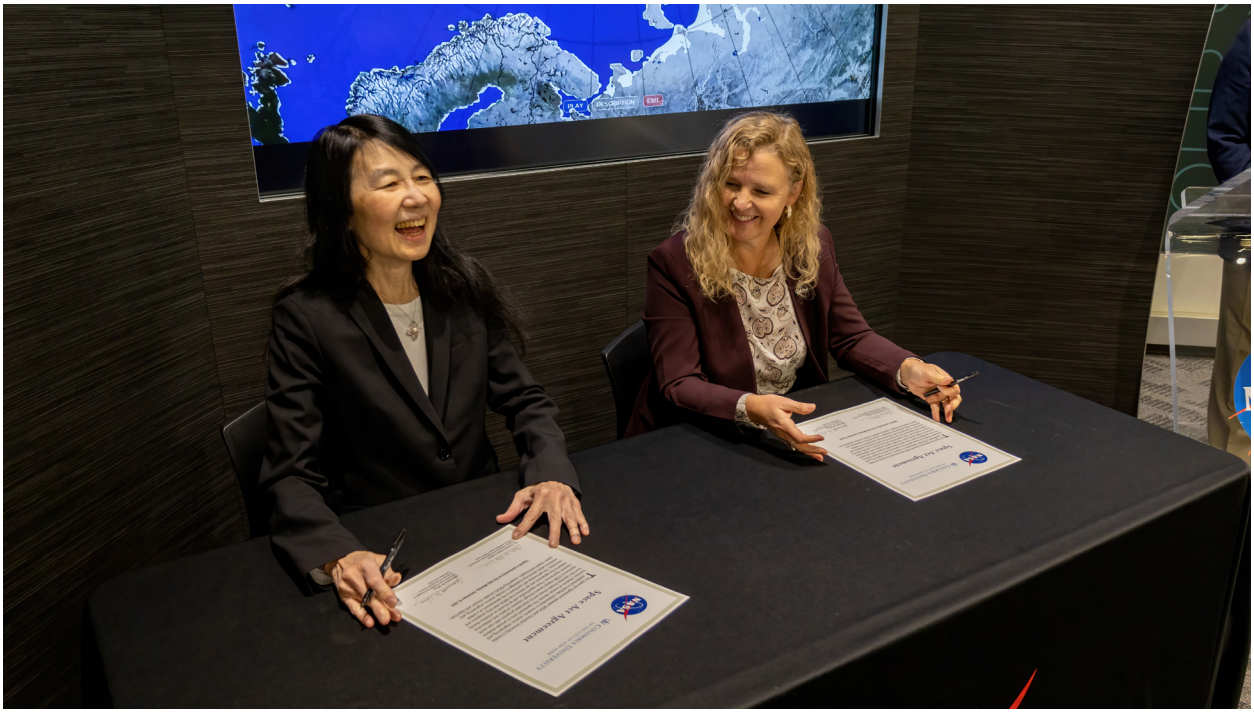
Media Contact:
Liz Vlock, NASA Headquarters, Washington
202-358-1600, elizabeth.a.vlock@nasa.gov

From https://www.nasa.gov/earth/nasa-data-shows-july-22-was-earths-hottest-day-on-record/

NASA, Columbia U. Enact Collaborative Space Act Agreement

By Jeremy Eggers — Dec. 18, 2024

NASA's Goddard Space Flight Center in Greenbelt, Maryland, and Columbia University in New York, New York, enacted a collaborative Space Act Agreement to advance research and education opportunities during a signing ceremony Monday, Dec. 16, at Goddard.



Dr. Jeannette Wing and Dr. Christa Peters-Lidard sign a collaborative Space Act Agreement at NASA's Goddard Space Flight Center on Monday, Dec. 16, 2024. **— NASA/Travis Wohlrab**

Presiding over the ceremony were Dr. Christa Peters-Lidard, director of Goddard's Sciences and Exploration directorate, and Dr Jeannette Wing, executive vice president for research and professor of computer science at Columbia University.

Columbia University has been a trusted partner for many years and has a long history of interactions with Goddard Space Flight Center. Notably, the Goddard Institute for Space Studies (GISS) is located at Columbia University serving as a laboratory in Goddard's Earth Sciences Division and is affiliated with the Columbia Climate School and School of Engineering and Applied Science.

The agreement expands NASA's CU partnership to Goddard's Greenbelt campus and will be centered around collaborative research, education, technology development, workforce development, science and engineering exchanges, applied science, commercial as well as nonprofit research along with technology infusion.

Areas of mutual interest include but are not limited to: artificial intelligence, foundation models, machine learning, and data science; climate sustainability, justice, adaptation, and resilience; materials and sensors; quantum sensing and computing; Earth science, planetary science, heliophysics, physics and astrophysics.

From https://www.nasa.gov/image-article/nasa-cu-enact-collaborative-space-act-agreement/

NASA Earth Scientists Take Flight, Set Sail to Verify PACE Satellite Data

By Erica McNamee — Sep. 4, 2024

- More than 100 scientists will participate in a field campaign involving a research vessel and two aircraft this month to verify the accuracy of data collected by NASA's new PACE satellite: the Plankton, Aerosol, Cloud, ocean Ecosystem mission.
- The process of data validation includes researchers comparing PACE data with data collected by similar, Earth-based instruments to ensure the measurements match up.
- Since the mission's Feb. 8, 2024 launch, scientists around the world have successfully completed several data validation campaigns; the September deployment — PACE-PAX — is its largest.

From sea to sky to orbit, a range of vantage points allow NASA Earth scientists to collect different types of data to better understand our changing planet. Collecting them together, at the same place and the same time, is an important step used to verify the accuracy of satellite data.

NASA's Plankton, Aerosol, Cloud, ocean Ecosystem (PACE) satellite launched in February 2024 and is collecting observations of the ocean and measuring atmospheric particle and cloud properties. This data will help inform scientists and decision makers about the health of Earth's ocean, land surfaces, and atmosphere and the interactions between them.

To make sure the data from PACE's instruments accurately represent the ocean and the atmosphere, scientists compare (or "validate") the data collected from orbit with measurements they collect at or near Earth's surface. The mission's biggest validation campaign, called PACE Postlaunch Airborne eXperiment (PACE-PAX), began on Sept. 3, 2024, and will last the entire month.

"If we want to have confidence in the observations from PACE, we need to validate those observations," said Kirk Knobelspiesse, mission scientist for PACE-PAX and an atmospheric scientist at NASA's Goddard Space Flight Center in Greenbelt, Maryland. "This field campaign is focused on doing just that."



Technicians work to process the NASA's Plankton, Aerosol, Cloud, ocean Ecosystem (PACE) observatory on a spacecraft dolly in a high bay at the Astrotech Space Operations Facility near the agency's Kennedy Space Center in Florida on Monday, Dec. 4, 2023. **— Credit: NASA/Kim Shiflett**

Scientists will make measurements both from aircraft and ships. Based out of three locations across California — Marina, Santa Barbara, and NASA's Armstrong Flight Research Center in Edwards — the campaign includes more than 100 people working in the field and several dozen instruments.

"This campaign allows us to validate data for both the atmosphere and the ocean, all in one campaign," said Brian Cairns, deputy mission scientist for PACE-PAX and an atmospheric scientist at NASA's Goddard Institute for Space Studies in New York City.

On the ocean, ships, including the National Oceanic and Atmospheric Administration (NOAA) research vessel

Shearwater, will gather data on ocean biology and the optical properties of the water. Scientists onboard will gather water samples to help define the types of phytoplankton at different locations and their relative abundance, something that PACE's hyperspectral Ocean Color Instrument measures from orbit.

Overhead, a Twin Otter research aircraft operated by the Naval Postgraduate School in Monterey, California, will collect data on the atmosphere. At altitudes of up to 10,000 feet, the aircraft will sample and measure cloud droplet sizes, aerosol sizes, and the amount of light that those particles scatter and absorb. These are the atmospheric properties that PACE observes with its two polarimeters, SPEXOne and HARP2.

At a higher altitude — approximately 70,000 feet up — NASA's ER-2 aircraft will provide a complementary view from above clouds, looking down on the atmosphere and ocean in finer detail than the satellite, but with a narrower view.

The plane will carry several instruments that are similar to those on PACE, including two prototypes of PACE's polarimeters, called SPEXAirborne and AirHARP. In addition, two instruments called the Portable Remote Imaging SpectroMeter and Pushbroom Imager for Cloud and Aerosol Research and Development — from NASA's Jet Propulsion Laboratory in Pasedena, California, and NASA's Ames Research Center in California's Silicon Valley, respectively — will measure essentially all the wavelengths of visible light (color). The remote sensing measurements are key for scientists who want to test the methods they use to analyze PACE satellite data.

Together, the instruments on the ER-2 approximate the data that PACE gathers and complement the in situ measurements from the ocean research vessel and the Twin Otter.



The NASA ER-2 high-altitude aircraft preparing for flight on Jan. 29, 2023. The aircraft is based at NASA's Armstrong Flight Research Center Building 703 in Palmdale, California. **— Credit: NASA/Carla Thoma**

As the field campaign team gathers data, PACE will be observing the same areas of the ocean surface and atmosphere. Once the campaign is over, scientists will look at the data PACE returned and compare them to the measurements they took from the other three vantage points.

"Once you launch the satellite, there's no more tinkering you can do," said Ivona Cetinic, deputy mission scientist for PACE-PAX and an ocean scientist at NASA Goddard.

Though the scientists cannot alter the satellite anymore, the algorithms designed to interpret PACE data can be adjusted to make the measurements more accurate. Validation checks from campaigns like PACE-PAX help scientists ensure that PACE will be able to return accurate data about our oceans and atmosphere — critical to better understand our changing planet and its interconnected systems — for years to come.

"The ocean and atmosphere are such changing environments that it's really important to validate what we see," Cetinic said. "Understanding the accuracy of the view from the satellite is important, so we can use the data to answer important questions about climate change."

From https://www.nasa.gov/earth/nasa-earth-scientists-take-flight-set-sail-to-verify-pace-satellite-data/

NASA Earth Observatory: Image of the Day

Charting the Exceptional, Unexpected Heat of 2023 and 2024

By Emily Cassidy — Nov. 20, 2024

In 2024, global temperatures for June through August were the hottest on record, narrowly topping the same period in 2023. The exceptional heat extended throughout other seasons, too, with global temperatures breaking records for 15 straight months from June 2023 until August 2024, according to scientists from NASA's Goddard Institute for Space Studies (GISS).

Although this spell of record heat fits within a long-term warming trend driven by human activity—primarily greenhouse gas emissions—the intensity of the heat, which reached a crescendo in the last half of 2023, surprised leading climate scientists. In a commentary in *Nature*, Gavin Schmidt, the director of GISS, used words like "humbling" and "confounding" to explain just how far temperatures overshot expectations during that period.

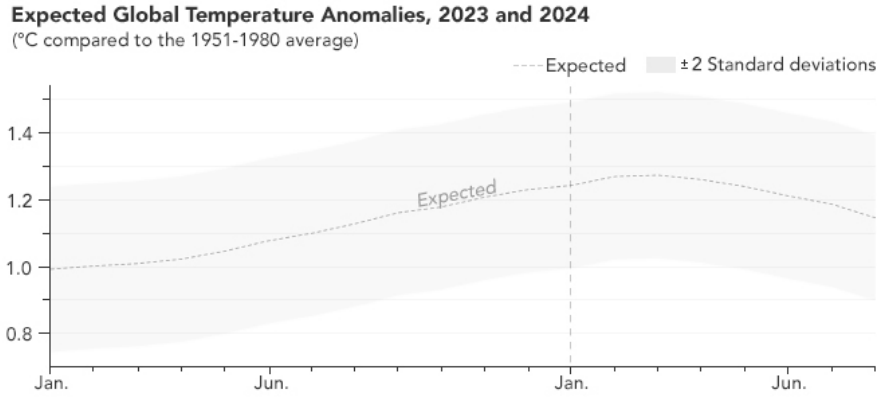
The charts on this page show how much global temperatures in 2023 and 2024 diverged from expectations based on NASA's temperature record. Roughly a year later, Schmidt and other climatologists are still trying to understand why.

"Warming in 2023 was head-and-shoulders above any other year, and 2024 will be as well," Schmidt said. "I wish I knew why, but I don't. We're still in the process of assessing what happened and if we are seeing a shift in how the climate system operates."

Setting Expectations

Earth's air and ocean temperatures during a given year typically reflect a combination of long-term trends, such as those associated with climate change, and shorter-term influences, such as volcanic activity, solar activity, and the state of the ocean.

In late 2022, as he has done each year since 2016, Schmidt used a statistical model to project global temperatures for the coming year. La Niña—which cools sea surface temperatures in the tropical Pacific—was present for the first part of 2023 and should have taken the edge off global temperatures. Schmidt calculated that average 2023 global temperatures would reach about 1.22 degrees Celsius above the baseline, putting it in the top three or four warmest years, but that it would not be a record-breaking year. Scientists at the UK Met Office, Berkeley Earth, and Carbon Brief made similar assessments using a variety of methods.



This chart shows Schmidt's expectation for how much monthly temperatures from January 2023 to August 2024 would differ from NASA's 1951-1980 baseline (also known as an anomaly). The expectation (represented as the dashed line in the chart) was based on an equation that calculates global average temperature based on the most recent 20-year rate of warming (about 0.25°C per decade) and NOAA's sea surface temperature measurements from the tropical Pacific, accounting for a three-month delay for these temperatures to affect the global average. The shaded area shows the range of variability (plus or minus two standard deviations).

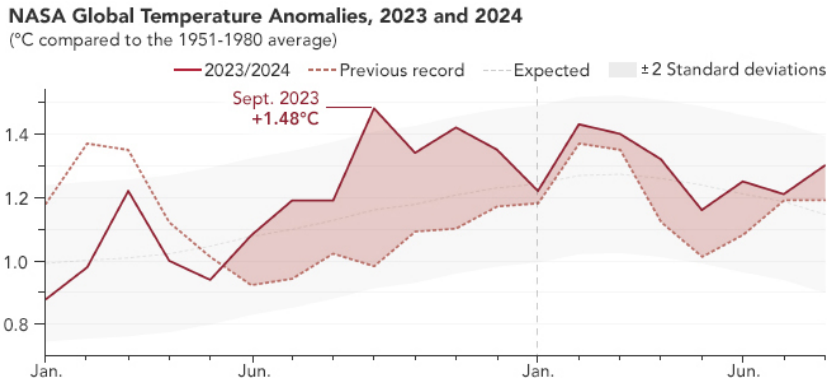
"More complex global climate models are helpful to predict long-term warming, but statistical models like these help us project year-to-year variability, which is often dominated by El Niño and La Niña events," said Zeke Hausfather, a climate scientist at the University of California, Berkeley. Hausfather helps produce the Berkeley Earth global temperature record and also generates annual predictions of global temperature changes based on those data.

Schmidt's statistical model—which successfully predicted the global average temperature every year since 2016—underestimated the exceptional heat in 2023, as did the methods used by Hausfather and other climatologists. Schmidt expected global temperature anomalies to peak in February or March 2024 as a lagged response to the additional warming from El Niño. Instead, the anomalous heat emerged well before El Niño had peaked. And the heat came with unexpected intensity—first in the North Atlantic Ocean and then virtually everywhere.

"In September, the record was broken by an absolutely astonishing 0.5 degrees Celsius," Schmidt said. "That has not happened before in the GISS record."

The second chart shows how global temperatures calculated from January 2023 to August 2024 differed from NASA's baseline (1951–1980). The previous record temperature anomalies for each month—set in 2016 and 2020—are indicated

by the red dashed line. Starting in June 2023, temperatures exceeded previous records by 0.3 to 0.5°C every month. Although temperature anomalies in 2024 were closer to past anomalies, they continued to break records through August 2024. The global average temperature in September 2024 was 1.26°C above NASA's baseline—lower than September 2023 but still 0.3°C above any September in the record prior to 2023.



To calculate Earth's global average temperature changes, NASA scientists analyze data from tens of thousands of meteorological stations on land, plus thousands of instruments on ships and buoys on the ocean surface. The GISS team analyzes this information using methods that account for the varied spacing of temperature stations around the globe and for urban heating effects that could skew the calculations.

Investigating Possible Contributors

Since May 2024, Schmidt has been compiling research about possible contributors to the unexpected warmth, including changes in greenhouse gas emissions, incoming radiation from the Sun, airborne particles called aerosols, and cloud cover, as well as the impact of the 2022 Hunga Tonga-Hunga Ha'apai volcanic eruption. However, none of these factors provide what Schmidt and other scientists consider a convincing explanation for the unusual heat in 2023.

Atmospheric greenhouse gas levels have continued to rise, but Schmidt estimates that the extra load since 2022 only accounted for additional warming of about 0.02°C. The Sun was nearing peak activity in 2023, but its roughly 11-year cycle is well measured and not enough to explain the temperature surge either.

Major volcanic eruptions, such as El Chichón in 1982 and Pinatubo in 1991, have caused brief periods of global cooling in the past by lofting aerosols into the stratosphere. And research published in 2024 indicates the eruption in Tonga had a net cooling effect in 2022 and 2023. "If that's the case, there's even more warming in the system that needs to be explained," Schmidt said.

Another possible contributor is reduced air pollution. A research team led by Tianle Yuan, an atmospheric research scientist at NASA's Goddard Space Flight Center, has found a significant drop in aerosol pollution from shipping since 2020. The drop coincides with new international regulations on sulfur content in shipping fuels and with sporadic drops in shipping due to the coronavirus pandemic.

Sulfur aerosol emissions promote the formation of bright clouds that reflect incoming sunlight back to space and have a net cooling effect. Reducing this pollution has the opposite effect: clouds are less likely to form, which could warm the climate. Although scientists, including Yuan, generally agree that the drop in sulfur emissions likely caused a net warming in 2023, the scientific community continues to debate the precise size of the effect.

"All of these factors explain, perhaps, a tenth of a degree in warming," Schmidt said. "Even after taking all plausible explanations into account, the divergence between expected and observed annual mean temperatures in 2023 remains near 0.2°C—roughly the gap between the previous and current annual record."

Grappling With Uncertainty

Both Hausfather and Schmidt expressed concern that these unexpected temperature changes could signal a shift in how the climate system functions. It could also be some combination of climate variability and a change in the system, Schmidt said. "It doesn't have to be an either-or."

One of the biggest uncertainties in the climate system is how aerosols affect cloud formation, which in turn affects the amount of radiation reflected back to space. However, one challenge for scientists trying to piece together what happened in 2023 is the lack of updated global aerosol emissions data. "Reliable assessments of aerosol emissions depend on networks of mostly volunteer-driven efforts, and it could be a year or more before the full data from 2023 are available," Schmidt said.

NASA's PACE (Plankton, Aerosol, Cloud, ocean Ecosystem) satellite, which launched in February 2024, could help shed light on these uncertainties. The satellite will help scientists make a global assessment of the composition of various aerosol particles in the atmosphere. PACE data may also help scientists understand cloud properties and how aerosols influence cloud formation, which is essential to creating accurate climate models.

Schmidt and Hausfather invite scientists to discuss research related to the contributors of the 2023 heat at a session they are convening at the fall meeting of the American Geophysical Union in Washington, D.C., on December 9–13, 2024.

From https://earthobservatory.nasa.gov/images/153588/charting-the-exceptional-unexpected-heat-of-2023-and-2024

NASA Data Reveals Role of Green Spaces in Cooling Cities

By Madeleine Gregory —Nov. 26, 2024

As any urban dweller who has lived through a heat wave knows, a shady tree can make all the difference. But what happens when there's no shade available?

A recent study in *Nature Communications* used NASA satellite data to identify a major gap in global resilience to climate change: cities in the Global South have far less green space — and therefore less cooling capacity — than cities in the Global North. The terms Global North and Global South were used in the study to distinguish developed countries (mostly in the Northern Hemisphere) from developing nations (mostly in the Southern Hemisphere).

Cities tend to be hotter than nearby rural areas because of the urban heat island effect. Heat-trapping dark surfaces such as sidewalks, buildings, and roads absorb heat from the Sun's rays, which raises the temperature of the city. Extreme heat poses serious health threats for urban residents, including dehydration, heat stroke, and even death. Though not a cure-all, greenery provides shade and releases moisture into the air, cooling the surroundings.

"Cities can strategically prioritize developing new green spaces in areas that have less green space," said Christian Braneon, a climate scientist at NASA's Goddard Institute for Space Studies in New York who was not affiliated with this study. "Satellite data can be really helpful for this."



The Operational Land Imager (OLI) on the NASA and U.S. Geological Survey's Landsat 8 satellite captured this natural color image of Sanaa, Yemen, on June 8, 2024. Sanaa, which has a hot, dry climate and little green space, had the second-lowest cooling capacity of 500 cities studied in a paper recently published in the journal Nature Communications. **— Wanmei Liang, NASA Earth Observatory**

An international team of researchers led by Yuxiang Li, a doctoral student at Nanjing University, analyzed the 500 largest cities in the world to compare their cooling capacities. They used data from the Landsat 8 satellite, jointly managed by NASA and the U.S. Geological Survey, to determine how effective green space was at cooling each city.

First, they calculated the average land surface temperature for the hottest month of 2018 for each city, as well as the average of the hottest months from 2017 to 2019. Next, the researchers used a metric called the Normalized Difference Vegetation Index (NDVI) to map how much green space each city had. The NDVI relies on the fact that healthy vegetation absorbs red light and reflects infrared light: the ratio of these wavelengths can show the density of healthy vegetation in a given satellite image.

Researchers found that cities in the Global South have just 70% of the greenery-related cooling capacity of cities in the Global North. The green spaces in an average Global South city cool the temperature by about 4.5 F (2.5 C). In an average Global North city, that cooling capacity is 6.5 F (3.6 C). This compounds an existing problem: cities in the South tend to be at lower latitudes (that is, nearer to the Equator), which are predicted to see more heat extremes in the coming years.

“It’s already clear that Global South countries will be impacted by heat waves, rising temperatures, and climatic extremes more than their Global North counterparts,” said Chi Xu, a professor of ecology at Nanjing University and a co-author of the study. The Global South has less capacity to adapt to heat because air conditioning is less common and power outages are more frequent.

Why do cities in the Global South struggle to stay cool? Cities in the Global South tend to have less green space than cities in the Global North. This mirrors studies of the disparities within cities, sometimes referred to as the “luxury effect”: wealthier neighborhoods tend to have more green space than poorer neighborhoods. “Wealthier cities also have more urban green spaces than the poorest cities,” Chi said.

It’s unlikely that urban planners can close the gap between the study’s worst-performing city (Mogadishu, Somalia) and the best-performing one (Charlotte, North Carolina).

Mogadishu is a dense city with a dry climate that limits vegetation growth. Still, there’s a lot that each city can learn from its neighbors. Within a given region, the researchers identified the city with the greatest cooling capacity and used that as a goal. They calculated the difference between the best-performing city in the region and every city nearby to get the potential additional cooling capacity. They found that cities’ average cooling capacity could be increased substantially — to as much as 18°F (10°C) — by systematically increasing green space quantity and quality.

“How you utilize green space is really going to vary depending on the climate and the urban environment you’re focused on,” said Braneon, whose research at NASA focuses on climate change and urban planning.

Greener cities in the U.S. and Canada have lower population densities. However, fewer people per square mile isn’t necessarily good for the environment: residents in low-density cities rely more on cars, and their houses tend to be bigger and less efficient. Braneon noted that there’s a suite of solutions beyond just planting trees or designating parks: Cities can increase cooling capacity by creating water bodies, seeding green roofs, and painting roofs or pavement lighter colors to reflect more light.

With a global study like this, urban planners can compare strategies for cities within the same region or with similar densities. “For newly urbanized areas that aren’t completely built out, there’s a lot of room to still change the design,” Braneon said.

From https://science.nasa.gov/earth/climate-change/nasa-data-reveals-role-of-green-spaces-in-cooling-cities/

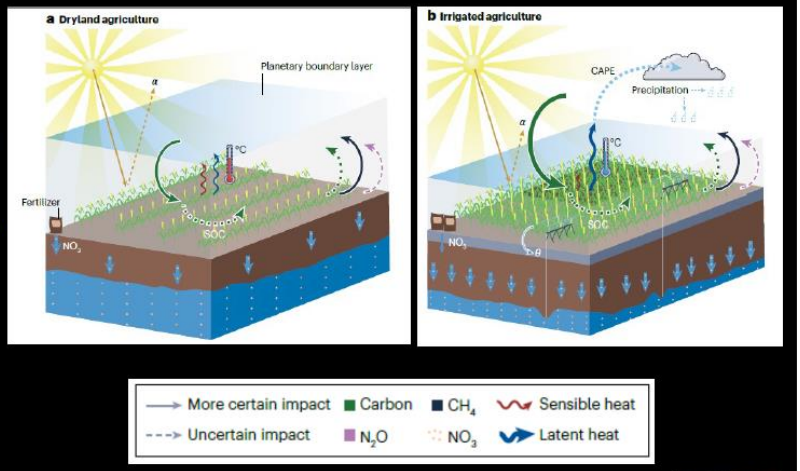
Irrigation Impacts in the Earth System: Much More Understanding Needed

Irrigation accounts for ~70% of global freshwater withdrawals and ~90% of consumptive water use, driving myriad Earth system impacts. Estimates suggest there are more than 3.6 million square kilometers of currently irrigated land, with hot spots in the intensively cultivated U.S. High Plains, California Central Valley, and elsewhere in the world.

Major uncertainties and gaps remain in irrigation research and modeling. Irrigation could enhance cropland carbon uptake; however, it can also contribute to elevated methane fluxes in rice systems and mobilize nitrogen loading to groundwater.

Irrigation impacts weather and climate processes by altering surface energy and moisture balances, exchanges with the atmosphere and biogeochemical cycling. These irrigation–Earth system interactions have implications for a range of ecosystem services, such as crop production, carbon sequestration on agricultural lands, water availability and even human health.

Paper: Irrigation in the Earth system | Nature Reviews Earth & Environment





Dr. Patricia M. Parker

Studying decarbonization effects on premature deaths in U.S., China, & South Asia

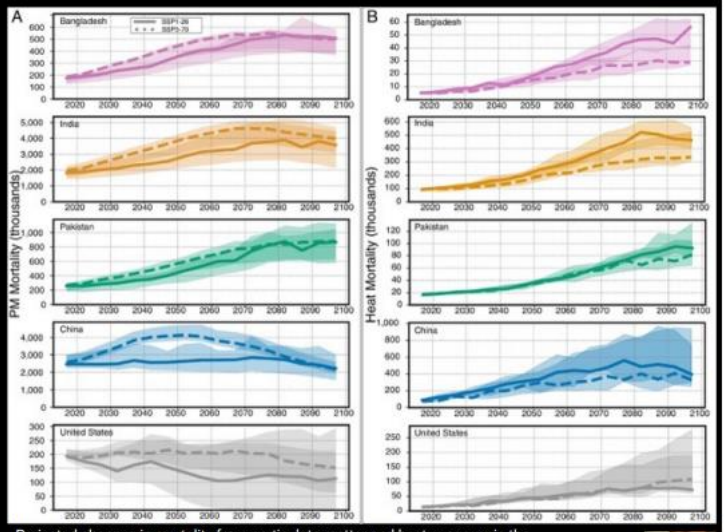
The perception that emissions reductions will require near-term sacrifices but only provide distant future benefits may be unfortunately slowing movement toward decarbonization.

However, certain policies can offer rapid, local health benefits via improved air quality, as well as longer term avoided heat exposure.

We quantify these benefits, showing that they avert millions of premature deaths annually, with valuations in developing Asia that outweigh the costs of mitigation.

The results demonstrate that a global transition from a high-emission scenario to a sustainability scenario including clean energy access, strong air quality policies, and rapid decarbonization consistent with keeping warming below 2 °C provides far greater public health benefits in the near term via improved air pollution than it does via reduced heat exposure.

As populations age and become increasingly sensitive to environmental exposures, mitigating both climate change and air pollution will become an increasingly important component of ensuring public health.



Projected changes in mortality from particulate matter and heat exposure in the indicated countries under the two scenarios. SSP1-2.6 is a sustainable development scenario and SSP3-7.0 is a high-emissions reference case.



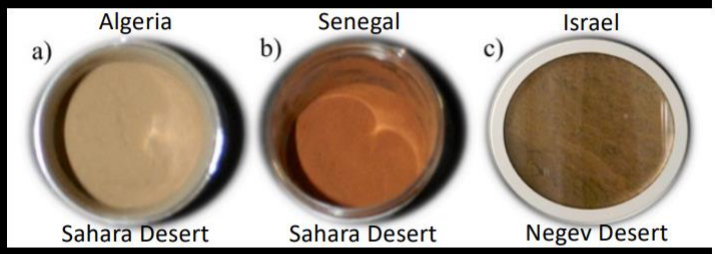
Author spotlight: ***Greg Faluvegi,*** *GSFC Code 611 (GISS)*

Paper: Reductions in premature deaths from heat and particulate matter air pollution under decarbonization

Dust on Earth and Mars: Optical Properties for Remote Sensing and Modeling

Dust plays a key role in many Earth system processes and is ubiquitous in the Martian atmosphere. Researchers are intensively trying to characterize dust optical properties with field campaigns, laboratory analyses, space-based remote sensing missions, and global modeling efforts.

This is a bountiful time for dust scientists, but the uncertainty between measurements and models is complicated by conflicting assumptions. For example, the conversion of satellite radiance measurements into products like aerosol optical depth for model evaluation depends upon aerosol properties like particle size and shape that are often prescribed and not part of the retrieval.



Soil samples from desert regions taken for the Fennec field campaign and the Statistical Evaluation of Aerosol Retrievals (STEAR) experiment. The different hues illustrate the high variability of mineral composition of dust sources.

Current measurements of optical properties of bulk dust and fundamental dust minerology components vary widely, which creates problems for scientists trying to interpret satellite observations of dust and estimate its climate impacts. Field observations indicate the persistence of coarse and giant dust particles at higher altitudes and farther downwind from their source than previously expected with consequences for climate. The lack of comprehensive and realistic shape models for dust is an outstanding issue in the research community.

Paper: Mineral dust optical properties for remote sensing and global modeling: A review - ScienceDirect

Atmospheric CO2 emissions and ocean acidification from bottom-trawling

Marine sediments are thought to be the ultimate long-term carbon store. Buried below the active layer, organic carbon can remain unmineralized for millennia to eons.

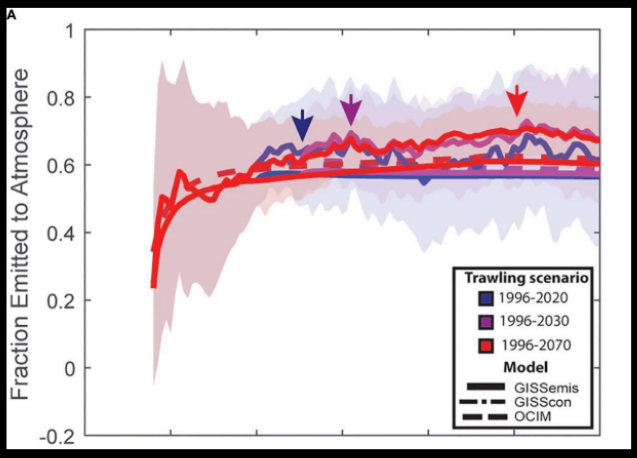
In the case of bottom-trawling, heavy fishing gear is dragged across the seafloor, re-exposing significant amounts of buried organic carbon.

This study shows that 55-60% of CO2 produced from bottom-trawling is released into the atmosphere within nine years.

The study also found that 40-45% of the cumulative trawling-induced CO2 emissions remained dissolved in seawater, augmenting the ocean acidification already occurring from the burning of fossil fuels.

Ocean-based climate solutions offer promise in closing the emissions gap to limit global temperature increases to 1.5°C, while also supporting co-benefits like biodiversity preservation and food security.

However, current climate policies and carbon markets require estimates of avoided atmospheric emissions. Such frameworks overlook the total impact of ocean-use change activities on the carbon cycle because they ignore factors such as the pool of dissolved inorganic carbon that remains sequestered by the ocean.



The fraction of trawled CO2 emitted to the atmosphere from historical trawling (1996-2020) and future projections. Colors represent different trawling scenarios, with blue denoting historical trawling from 1996-2020 and zero trawling thereafter, magenta denoting a future scenario where trawling stops in 2030, and red denoting a future scenario where global trawling ceases in 2070.

Journal Article: Atwood TB, Romanou A, DeVries T, Lerner PE, Mayorga JS, Bradley D, Cabral RB, Schmidt GA and Sala E (2024) Atmospheric CO2 emissions and ocean acidification from bottom-trawling. *Front. Mar. Sci.* 10:1125137.

URL or DOI: https://doi.org/10.3389/fmars.2023.1125137

D. Science Education at GISS

Information about the GISS educational programs are available at:
https://www.giss.nasa.gov/edu/

GISS personnel include students and educations who participate as partners with the Institute's scientists in their research. Typically, six graduate students carry out their Ph.D. thesis research under the supervision of GISS staff members at any given time. Other participants include students and teachers from junior and senior high schools and senior colleges.

The Climate Change Research Initiative (CCRI) is a year-long STEM engagement program for educators and graduate students to work directly with NASA scientists and lead research teams in a NASA research project. Participating educators become associate researchers at NASA GISS and integrate NASA education resources and content into their classrooms while improving STEM education within their communities. During the summer session, CCRI teams add undergraduate and high school interns.

Further information about CCRI and other GISS student internship programs is available at: https://www.giss.nasa.gov/edu/intern/

Education @ GISS

Intern and Educator Opportunities



Internships
All about high school and undergraduate student internships at NASA/GISS and its NYC-area research partners.
+ Read More



Climate Change Research Initiative
Year-round STEM engagement program allowing educators and graduate students to work directly with NASA scientists, with a summer internship program.
+ Read More

Past Programs



New York City Research Initiative
Intern and educator program in which teams

affiliated university researchers. NYCRI concluded in 2014.
+ Read More

GISS Institute on Climate and Planets
A collaborative program between GISS, Columbia University, and the City University of New York. ICP concluded in 2004
+ Go to Website

More About NASA Education

+ NASA STEM Engagement
+ NASA ESD Early Career Research Program

Advanced Study Programs



Columbia University Graduate Study
Study toward an advanced degree in the atmospheric sciences may be conducted at GISS through enrollment at Columbia University.
+ Read More



Postdoctoral Research Programs
Advanced programs in which early career scientists may participate in GISS research include NASA and Columbia University postdoctoral appointments.
+ Read More

Resource Materials

CCRI STEM Curriculum Modules
Instructional modules developed during the GISS Climate Change Research Initiative and NASA/SMD approved.
+ Read More

ICP Educational Materials Archive
Curriculum modules and learning tools developed during the Institute for Climate and Planets program (1994-2004) for use in classroom learning about climate and environmental research.
+ Read More

GISS Best Publication Award

Each spring/summer, scientists at NASA's Goddard Institute for Space Studies vote on the "best" paper published during the previous calendar year by a member or members of the institute. We consider this peer award to be the highest scientific honor that we bestow. The winners of this award since 1993 are listed below.
Beginning in 2023, scientists have also voted on the best paper whose first author was an early career researcher (i.e., a postdoctoral scientist or graduate student). Such papers are also included below and are prefixed by an "(ECR)" notation.

2024

⋆ & ECR– DeLessio, M.A., K. Tsigaridis, S.E. Bauer, J. Chowdhary, and G.L. Schuster, 2024: Modeling atmospheric brown carbon in the GISS ModelE Earth system model. *Atmos. Chem. Phys.*, **24**, no. 10, 6275-6304, doi:10.5194/acp-24-6275-2024.

2023

⋆ – Orbe, C., D. Rind, R.L. Miller, L. Nazarenko, A. Romanou, J. Jonas, G. Russell, M. Kelley, and G. Schmidt, 2023: Atmospheric response to a collapse of the North Atlantic circulation under a mid-range future climate scenario: A regime shift in Northern Hemisphere dynamics. *J. Climate*, **36**, no. 19, 6669-6693, doi:10.1175/JCLI-D-22-0841.1.
(ECR) – Singh, R., K. Tsigaridis, A.N. LeGrande, F. Ludlow, and J.G. Manning, 2023: Investigating hydroclimatic impacts of the 168-158 BCE volcanic quartet and their relevance to the Nile River basin and Egyptian history. *Clim. Past*, **19**, no. 1, 249-275, doi:10.5194/cp-19-249-2023.

2022

⋆ – Bauer, S.E., K. Tsigaridis, G. Faluvegi, L. Nazarenko, R.L. Miller, M. Kelley, and G. Schmidt, 2022: The turning point of the aerosol era. *J. Adv. Model. Earth Syst.*, **14**, no. 12, e2022MS003070, doi:10.1029/2022MS003070.

2021

⋆ – Miller, R.L., G.A. Schmidt, L. Nazarenko, S.E. Bauer, M. Kelley, R. Ruedy, G.L. Russell, A. Ackerman, I. Aleinov, M. Bauer, R. Bleck, V. Canuto, G. Cesana, Y. Cheng, T.L. Clune, B. Cook, C.A. Cruz, A.D. Del Genio, G.S. Elsaesser, G. Faluvegi, N.Y. Kiang, D. Kim, A.A. Lacis, A. Leboissetier, A.N. LeGrande, K.K. Lo, J. Marshall, E.E. Matthews, S. McDermid, K. Mezuman, L.T. Murray, V. Oinas, C. Orbe, C. Pérez García-Pando, J.P. Perlwitz, M.J. Puma, D. Rind, A. Romanou, D.T. Shindell, S. Sun, N. Tausnev, K. Tsigaridis, G. Tselioudis, E. Weng, J. Wu, and M.-S. Yao, 2021: CMIP6 historical simulations (1850-2014) with GISS-E2.1. *J. Adv. Model. Earth Syst.*, **13**, no. 1, e2019MS002034, doi:10.1029/2019MS002034.

2020

⋆ – Kelley, M., G.A. Schmidt, L. Nazarenko, S.E. Bauer, R. Ruedy, G.L. Russell, A.S. Ackerman, I. Aleinov, M. Bauer, R. Bleck, V. Canuto, G. Cesana, Y. Cheng, T.L. Clune, B.I. Cook, C.A. Cruz, A.D. Del Genio, G.S. Elsaesser, G. Faluvegi, N.Y. Kiang, D. Kim, A.A. Lacis, A. Leboissetier, A.N. LeGrande, K.K. Lo, J. Marshall, E.E. Matthews, S. McDermid, K. Mezuman, R.L. Miller, L.T. Murray, V. Oinas, C. Orbe, C. Pérez García-Pando, J.P. Perlwitz, M.J. Puma, D. Rind, A. Romanou, D.T. Shindell, S. Sun, N. Tausnev, K. Tsigaridis, G. Tselioudis, E. Weng, J. Wu, and M.-S. Yao, 2020: GISS-E2.1: Configurations and climatology. *J. Adv. Model. Earth Syst.*, **12**, no. 8, e2019MS002025, doi:10.1029/2019MS002025.

2019

⋆ – Carlson, B., A. Lacis, C. Colose, A. Marshak, W. Su, and S. Lorentz, 2019: Spectral signature of the biosphere: NISTAR finds it in our solar system from the Lagrangian L-1 point. *Geophys. Res. Lett.*, **46**, no. 17-18, 10679-10686, doi:10.1029/2019GL083736.

2018

⋆ – Marvel, K.D., R. Pincus, G.A. Schmidt, and R.L. Miller, 2018: Internal variability and disequilibrium confound estimates of climate sensitivity from observations. *Geophys. Res. Lett.*, **45**, no. 3, 1595-1601, doi:10.1002/2017GL076468.

2017

⋆ – Elsaesser, G.S., A.D. Del Genio, J. Jiang, and M. van Lier-Walqui, 2017: An improved convective ice parameterization for the NASA GISS Global Climate Model and impacts on cloud ice simulation. *J. Climate*, **30**, no. 1, 317-336, doi:10.1175/JCLI-D-16-0346.1.

2016

⋆ – Way, M.J., A.D. Del Genio, N.Y. Kiang, L.E. Sohl, D.H. Grinspoon, I. Aleinov, M. Kelley, and T. Clune, 2016: Was Venus the first habitable world of our solar system? *Geophys. Res. Lett.*, **43**, no. 16, 8376-8383, doi:10.1002/2016GL069790.

2015

⋆ – Hall, T.M., and K. Hereid, 2015: The frequency and duration of U.S. hurricane droughts. *Geophys. Res. Lett.*, **42**, no. 9, 3482-3485, doi:10.1002/2015GL063652.

2014

⋆ – Miller, R.L., G.A. Schmidt, L.S. Nazarenko, N. Tausnev, S.E. Bauer, A.D. Del Genio, M. Kelley, K.K. Lo, R. Ruedy, D.T. Shindell, I. Aleinov, M. Bauer, R. Bleck, V. Canuto, Y. Chen, Y. Cheng, T.L. Clune, G. Faluvegi, J.E. Hansen, R.J. Healy, N.Y. Kiang, D. Koch, A.A. Lacis, A.N. LeGrande, J. Lerner, S. Menon, V. Oinas, C. Pérez García-Pando, J.P. Perlwitz, M.J. Puma, D. Rind, A. Romanou, G.L. Russell, M. Sato, S. Sun, K. Tsigaridis, N. Unger, A. Voulgarakis, M.-S. Yao, and J. Zhang, 2014: CMIP5 historical simulations (1850-2012) with GISS ModelE2. *J. Adv. Model. Earth Syst.*, **6**, no. 2, 441-477, doi:10.1002/2013MS000266.

2013

⋆ – Lacis, A.A., J.E. Hansen, G.L. Russell, V. Oinas, and J. Jonas, 2013: The role of long-lived greenhouse gases as principal LW control knob that governs the global surface temperature for past and future climate change. *Tellus B*, **65**, 19734, doi:10.3402/tellusb.v65i0.19734.

2012

⋆ – Shindell, D., J.C.I. Kuylenstierna, E. Vignati, R. van Dingenen, M. Amann, Z. Klimont, S.C. Anenberg, N. Muller, G. Janssens-Maenhout, F. Raes, J. Schwartz, G. Faluvegi, L. Pozzoli, K. Kupiainen, L. Höglund-Isaksson, L. Emberson, D. Streets, V. Ramanathan, K. Hicks, N.T.K. Oanh, G. Milly, M. Williams, V. Demkine, and D. Fowler, 2012: Simultaneously mitigating near-term

climate change and improving human health and food security. *Science*, **335**, 183-189, doi:10.1126/science.1210026.

2011

⋆ – Hansen, J., M. Sato, P. Kharecha, and K. von Schuckmann, 2011: Earth's energy imbalance and implications. *Atmos. Chem. Phys.*, **11**, 13421-13449, doi:10.5194/acp-11-13421-2011.

2010

⋆ – Lacis, A.A, G.A. Schmidt, D. Rind, and R.A. Ruedy, 2010: Atmospheric CO2: Principal control knob governing Earth's temperature. *Science*, **330**, 356-359, doi:10.1126/science.1190653.

2009

⋆ – Del Genio, A.D., R.K. Achterberg, K.H. Baines, F.M. Flasar, P.L. Read, A. Sánchez-Lavega, and A.P. Showman, 2009: Saturn atmospheric structure and dynamics. In *Saturn from Cassini-Huygens*. M.K. Dougherty, L.W. Esposito, and S.M. Krimigis, Eds., Springer-Verlag, pp. 113-159, doi:10.1007/978-1-4020-9217-6_6.

2008

⋆ – Rosenzweig, C., D. Karoly, M. Vicarelli, P. Neofotis, Q. Wu, G. Casassa, A. Menzel, T.L. Root, N. Estrella, B. Seguin, P. Tryjanowski, C. Liu, S. Rawlins, and A. Imeson, 2008: Attributing physical and biological impacts to anthropogenic climate change. *Nature*, **453**, 353-357, doi:10.1038/nature06937.

2007

⋆ – Del Genio, A.D., M.-S. Yao, and J. Jonas, 2007: Will moist convection be stronger in a warmer climate? *Geophys. Res. Lett.*, **34**, L16703, doi:10.1029/2007GL030525.

2006

⋆ – Hansen, J., M. Sato, R. Ruedy, K. Lo, D.W. Lea, and M. Medina-Elizade, 2006: Global temperature change. *Proc. Natl. Acad. Sci.*, **103**, 14288-14293, doi:10.1073/pnas.0606291103.

2005

⋆ – Hansen, J., L. Nazarenko, R. Ruedy, M. Sato, J. Willis, A. Del Genio, D. Koch, A. Lacis, K. Lo, S. Menon, T. Novakov, J. Perlwitz, G. Russell, G.A. Schmidt, and N. Tausnev, 2005: Earth's energy imbalance: Confirmation and implications. *Science*, **308**, 1431-1435, doi:10.1126/science.1110252.

2004

⋆ – Hansen, J., and L. Nazarenko, 2004: Soot climate forcing via snow and ice albedos. *Proc. Natl. Acad. Sci.*, **101**, 423-428, doi:10.1073/pnas.2237157100.

2003

⋆ – Koch, D., J. Park, and A. Del Genio, 2003: Clouds and sulfate are anticorrelated: A new diagnostic for global sulfur models. *J. Geophys. Res.*, **108**, no. D24, 4781, doi:10.1029/2003JD003621.

2002

⋆ – Chen, J., B.E. Carlson, and A.D. Del Genio, 2002: Evidence for strengthening of the tropical general circulation in the 1990s. *Science*, **295**, 838-841, doi:10.1126/science.1065835.

2001

⋆ – Allison, M., and D.H. Atkinson, 2001: Galileo Probe Doppler residuals as the wave-dynamical signature of weakly stable, downward-increasing stratification in Jupiter's deep wind layer. *Geophys. Res. Lett.*, **28**, 2747-2750, doi:10.1029/2001GL012927.

2000

⋆ – Del Genio, A.D., and A.B. Wolf, 2000: The temperature dependence of the liquid water path of low clouds in the southern Great Plains. *J. Climate*, **13**, 3465-3486, doi:10.1175/1520-0442(2000)013<3465:TTDOTL>2.0.CO;2.

⋆ – Hansen, J., M. Sato, R. Ruedy, A. Lacis, and V. Oinas, 2000: Global warming in the twenty-first century: An alternative scenario. *Proc. Natl. Acad. Sci.*, **97**, 9875-9880, doi:10.1073/pnas.170278997.

1999

⋆ – Shindell, D.T., R.L. Miller, G.A. Schmidt, and L. Pandolfo, 1999: Simulation of recent northern winter climate trends by greenhouse-gas forcing. *Nature*, **399**, 452-455, doi:10.1038/20905.

1998

⋆ – Shindell, D.T., D. Rind, and P. Lonergan, 1998: Increased polar stratospheric ozone losses and delayed eventual recovery owing to increasing greenhouse-gas concentrations. *Nature*, **392**, 589-592, doi:10.1038/33385.

1997

⋆ – Miller, R.L., 1997: Tropical thermostats and low cloud cover. *J. Climate*, **10**, 409-440, doi:10.1175/1520-0442(1997)010<0409:TTALCC>2.0.CO;2.

1996

⋆ – Tegen, I., A.A. Lacis, and I. Fung, 1996: The influence of mineral aerosols from disturbed soils on the global radiation budget. *Nature*, **380**, 419-422, doi:10.1038/380419a0.

1995

⋆ – Russell, G.L., J.R. Miller, and D. Rind, 1995: A coupled atmosphere-ocean model for transient climate change studies. *Atmos.-Ocean*, **33**, 683-730, doi:10.1080/07055900.1995.9649550.

1994

⋆ – Del Genio, A.D., W. Kovari, Jr., and M.-S. Yao, 1994: Climatic implications of the seasonal variation of upper troposphere water vapor. *Geophys. Res. Lett.*, **21**, 2701-2704, doi:10.1029/94GL02658.

1993

⋆ – Tselioudis, G., A.A. Lacis, D. Rind, and W.B. Rossow, 1993: Potential effects of cloud optical thickness on climate warming. Nature, **366**, 670-672, doi:10.1038/366670a0.

B. Journal Papers

1. **Alexandrov, M.D.**, **B. Cairns**, C. Emde, and B. van Diedenhoven, 2024: Correction of cloud optical thickness retrievals from nadir reflectances in the presence of 3D radiative effects. Part I: Concept and tests on 3D RT simulations. *Front. Remote Sens.*, **5**, 1397631, doi:10.3389/frsen.2024.1397631…….....66

2. Anchukaitis, K., R. Touchan, D. Meko, D. Kherchouche, S. Slimani, F. Sivrikaya, R. Ilmen, I. Mitsopoulos, J. Stephan, J. Attieh, F. Hasnaoui, J.J. Camarero, R. Sánchez-Salguero, F. Guibal, A. Piermattei, A. Christou, J. Krcmaric, and **B. Cook**, 2024: Enhancing spatiotemporal reconstructions of hydroclimate variability across the Mediterranean during the last millennium. *Clim. Dyn.*, **62**, no. 6, 5351-5371, doi:10.1007/s00382-024-07166-6……..... 67

3. Anderson, W., S. Shukla, J. Verdin, A. Hoell, C. Justice, B. Barker, K. Slinski, N. Lenssen, J. Lou, **B.I. Cook**, and A. McNally, 2024: Preseason maize and wheat yield forecasts for early warning of crop failure. *Nat. Commun.*, **15**, no. 1, 7262, doi:10.1038/s41467-024-51555-8…….....68

4. **Arouf, A.**, H. Chepfer, J.E. Kay, T. L'Ecuyer, and J. Lac, 2024: Surface cloud warming increases as Fall Arctic sea ice cover decreases. *Geophys. Res. Lett.*, **51**, no. 3, e2023GL105805, doi:10.1029/2023GL105805……...……69

5. Asadi Shamsabadi, E., **S.M.H. Erfani**, C. Xu, and D. Dias-da-Costa, 2024: Efficient semi-supervised surface crack segmentation with small datasets based on consistency regularisation and pseudo-labelling. *Autom. Constr.*, **158**, 105181, doi:10.1016/j.autcon.2023.105181…….....70

6. Atwood, T.B., **A. Romanou**, T. DeVries, **P.E. Lerner**, J.S. Mayorga, D. Bradley, R.B. Cabral, **G.A. Schmidt**, and E. Sala, 2024: Atmospheric CO_2 emissions and ocean acidification from bottom-trawling. *Front. Mar. Sci.*, **10**, 1125137, doi:10.3389/fmars.2023.1125137…….....71

7. Balk, D., **C. Braneon**, R. Leichenko, R. Moss, and J. Towers, 2024: NPCC4: Climate risk and equity — Advancing knowledge toward a sustainable future — Introduction. *Ann. New York Acad. Sci.*, **1539**, no. 1, 3-12, doi:10.1111/nyas.15149…….....72

8. **Barbara, J.M.**, R.A. West, **A.D. Del Genio**, and J.A. Sinclair, 2024: A study of Jupiter's UV Great Dark Spot and tropopause to stratosphere winds in the high northern latitudes as seen by Cassini imaging. *Icarus*, **410**, 115913, doi:10.1016/j.icarus.2023.115913…...73

9. Bierman, P., H. Mastro, L. Corbett, E. Steig, C. Halsted, M. Caffee, A. Hidy, G. Balco, **D. Peteet**, O. Bennike, and B. Rock, 2024: Plants, insects and fungi fossils under the center of Greenland's ice sheet are evidence of ice-free times. *Proc. Natl. Acad. Sci.*, **121**, no. 33, e2407465121, doi:10.1073/pnas.2407465121……..74

10. Bo, Y., X. Wang, K.J. van Groenigen, B.A. Linquist, C. Müller, T. Li, J. Yang, **J. Jägermeyr**, Y. Qin, and F. Zhou, 2024: Improved alternate wetting and drying irrigation increases global water productivity. *Nat. Food*, **5**, no. 12, 1005-1013, doi:10.1038/s43016-024-01081-z……75

11. **Bong, H.**, A. Cauquoin, A. Okazaki, E.-C. Chang, M. Werner, Z. Wei, N. Yeo, and K. Yoshimura, 2024: Process-based intercomparison of water isotope-enabled models and reanalysis nudging effects. *J. Geophys. Res. Atmos.*, **129**, no. 1, e2023JD038719, doi:10.1029/2023JD038719……76

12. **Braneon, C.**, L. Ortiz, **D. Bader**, N. Devineni, P. Orton, B. Rosenzweig, T. McPhearson, L. Smalls-Mantey, **V. Gornitz**, T. Mayo, S. Kadam, H. Sheerazi, E. Glenn, L. Yoon, A. Derras-Chouk, J. Towers, R. Leichenko, D. Balk, P. Marcotullio, and R. Horton, 2024: NPCC4: New York City climate risk information 2022 — Observations and projections. *Ann. New York Acad. Sci.*, **1539**, no. 1, 13-48, doi:10.1111/nyas.15116……..…77

13. Bruning, E.C., K.N. Brunner, **M. van Lier-Walqui**, T. Logan, and T. Matsui, 2024: Lightning and radar measures of mixed phase updraft variability in tracked storms during the TRACER field campaign in Houston, Texas. *Mon. Weather Rev.*, **152**, no. 12, 2753-2769, doi:10.1175/MWR-D-24-0060.1……...…78

14. Bushuk, M., S. Ali, D.A. Bailey, Q. Bao, L. Batté, U.S. Bhatt, E. Blanchard-Wrigglesworth, E. Blockley, G. Cawley, J. Chi, F. Counillon, P.G. Coulombe, R.I. Cullather, F.X. Diebold, A. Dirkson, E. Exarchou, M. Göbel, W. Gregory, V. Guemas, L. Hamilton, B. He, S. Horvath, M. Ionita, J.E. Kay, E. Kim, N. Kimura, D. Kondrashov, Z.M. Labe, W. Lee, Y.J. Lee, C. Li, X. Li, Y. Lin, Y. Liu, W. Maslowski, F. Massonnet, W.N. Meier, W.J. Merryfield, H. Myint, J.C.A. Navarro, A. Petty, F. Qiao, D. Schröder, A. Schweiger, Q. Shu, M. Sigmond, M. Steele, J. Stroeve, N. Sun, S. Tietsche, M. Tsamados, K. Wang, J. Wang, W. Wang, Y. Wang, Y. Wang, **J. Williams**, Q. Yang, X. Yuan, J. Zhang, and Y. Zhang, 2024: Predicting September Arctic sea ice: A multimodel seasonal skill comparison. *Bull. Amer. Meteorol. Soc.*, **105**, no. 7, E1170-E1203, doi:10.1175/BAMS-D-23-0163.1……79

15. Carter, J.L., R.D. Perera, and **M.J. Way**, 2024: Hyper illumination of exoplanets: Analytical and numerical approaches. *Astron. J.*, **167**, no. 5, 222, doi:10.3847/1538-3881/ad33c1…….....80

16. Castellanos, P., P. Colarco, W.R. Espinosa, S.D. Guzewich, R.C. Levy, **R.L. Miller**, M. Chin, R.A. Kahn, O. Kemppinen, H. Moosmüller, E.P. Nowottnick, A. Rocha-Lima, M.D. Smith, J.E. Yorks, and H. Yu, 2024: Mineral dust optical properties for remote sensing and global modeling: A review. *Remote Sens. Environ.*, **303**, 113982, doi:10.1016/j.rse.2023.113982…….....81

17. **Cesana, G.**, **A.S. Ackerman**, **A.M. Fridlind**, I. Silber, **A. Del Genio**, M. Zelinka, H. Chepfer, T. Khadir, and R. Roehrig, 2024: Observational constraint on a feedback from supercooled clouds reduces projected warming uncertainty. *Commun. Earth Environ.*, **5**, 181, doi:10.1038/s43247-024-01339-1…….82

18. **Cesana, G.V.**, **O. Pierpaoli**, **M. Ottaviani**, **L. Vu**, and **Z. Jin**, 2024: The correlation between Arctic sea ice, cloud phase and radiation using A-train satellites. *Atmos. Chem. Phys.*, **24**, no. 13, 7899-7909, doi:10.5194/acp-24-7899-2024……83

19. Chellappan, S., P. Zuidema, S. Kirschler, C. Voigt, **B. Cairns**, E.C. Crosbie, R. Ferrare, J. Hair, D. Painemal, T. Shingler, M. Shook, K.L. Thornhill, **F. Tornow**, and A. Sorooshian, 2024: Microphysical evolution in mixed-phase midlatitude marine cold-air outbreaks. *J. Atmos. Sci.*, **81**, no. 10, 1725-1747, doi:10.1175/JAS-D-23-0203.1…….84

20. Chemyakin, E., S. Stamnes, J. Allen, S.P. Burton, J. Hair, C. Hostetler, **J. Chowdhary**, B. van Diedenhoven, and **B. Cairns**, 2024: Efficient single-scattering lookup table for lidar and polarimeter phytoplankton studies. *Opt. Lett.*, **49**, no. 9, 2453-2456, doi:10.1364/OL.513735……85

21. Cheng, L., K. von Schuckmann, A. Minière, M.Z. Hakuba, S. Purkey, **G.A. Schmidt**, and Y. Pan, 2024: Ocean heat content in 2023. *Nat. Rev. Earth Environ.*, **5**, no. 4, 232-234, doi:10.1038/s43017-024-00539-9……86

22. **Clifton, O.E.**, **S.E. Bauer**, **K. Tsigaridis**, **I. Aleinov**, **T.G. Cowan**, **G. Faluvegi**, and **M. Kelley**, 2024: Influence of more mechanistic representation of particle dry deposition on historical changes in global aerosol burdens and radiative forcing. *J. Adv. Model. Earth Syst.*, **16**, no. 3, e2023MS003952, doi:10.1029/2023MS003952…….....87

23. **Cook, B.I.**, E.R. Cook, K.J. Anchukaitis, and D. Singh, 2024: Characterizing the 2010 Russian heatwave-Pakistan flood concurrent extreme over the last millennium using the Great Eurasian Drought Atlas. *J. Climate*, **37**, no. 17, 4389-4401, doi:10.1175/JCLI-D-23-0773.1…….....88

24. **Cook, B.I.**, W. Anderson, K. Slinski, S. Shukla, and A. McNally, 2024: Investigating the strength and variability of El Niño-Southern Oscillation teleconnections to hydroclimate and maize yields in Southern and East Africa. *J. Hydrometeorol.*, **25**, no. 1, 257-275, doi:10.1175/JHM-D-23-0098.1…….....89

25. Couëdel, A., G.N. Falconnier, M. Adam, R. Cardinael, K. Boote, E. Justes, W.N. Smith, A.M. Whitbread, F. Affholder, J. Balkovic, B. Basso, A. Bhatia, B. Chakrabarti, R. Chikowo, M. Christina, B. Faye, F. Ferchaud, C. Folberth, F.M. Akinseye, T. Gaiser, M.V. Galdos, S. Gayler, A. Gorooei, B. Grant, H. Guibert, G. Hoogenboom, B. Kamali, M. Laub, F. Maureira, F. Mequanint, C. Nendel, C.H. Porter, D. Ripoche, **A.C. Ruane**, L. Rusinamhodzi, S. Sharma, U. Singh, J. Six, A. Srivastava, B. Vanlauwe, A. Versini, M. Vianna, H. Webber, T. Weber, C. Zhang, and M. Corbeels, 2024: Long-term soil organic carbon and crop yield feedbacks differ between 16 soil-crop models in sub-Saharan Africa. *Eur. J. Agron.*, **155**, 127109, doi:10.1016/j.eja.2024.127109…….....90

26. Crosbie, E., L. Ziemba, M. Shook, T. Shingler, J. Hair, A. Sorooshian, R. Ferrare, **B. Cairns**, Y. Choi, J. DiGangi, G. Diskin, C. Hostetler, S. Kirschler, R.H. Moore, D. Painemal, C. Robinson, S. Seaman, K. Thornhill, C. Voigt, and E. Winstead, 2024: Measurement report: Cloud and environmental properties associated with aggregated shallow marine cumulus and cumulus congestus. *Atmos. Chem. Phys.*, **24**, no. 10, 6123-6152, doi:10.5194/acp-24-6123-2024……...91

27. De Wit, J., R. Doyon, B.V. Rackham, O. Lim, E. Ducrot, L. Kreidberg, B. Benneke, I. Ribas, D. Berardo, P. Niraula, A. Iyer, A. Shapiro, N. Kostogryz, V. Witzke, M. Gillon, E. Agol, V. Meadows, A.J. Burgasser, J.E. Owen, J.J. Fortney, F. Selsis, A. Bello-Arufe, Z. de Beurs, E. Bolmont, N. Cowan, C. Dong, J.J. Drake, L. Garcia, T. Greene, T. Haworth, R. Hu, S.R. Kane, P. Kervella, D. Koll, J. Krissansen-Totton, P.-O. Lagage, T. Lichtenberg, J. Lustig-Yaeger, M. Lingam, M. Turbet, S. Seager, K. Barkaoui, T.J. Bell, A. Burdanov, C. Cadieux, B. Charnay, R. Cloutier, N.J. Cook, A.C.M. Correia, L. Dang, T. Daylan, L. Delrez, B. Edwards, T.J. Fauchez, L. Flagg, F. Fraschetti, J. Haqq-Misra, Z. Huang, N. Iro, R. Jayawardhana, E. Jehin, M. Jin, E. Kite, D. Kitzmann, Q. Kral, D. Lafrenière, A.-S. Libert, B. Liu, S. Mohanty, B.M. Morris, C.A. Murray, C. Piaulet, F.J. Pozuelos, M. Radica, S. Ranjan, A. Rathcke, P.-A. Roy, E.W. Schwieterman, J.D. Turner, A. Triaud, and **M.J. Way**, 2024: A roadmap for the atmospheric characterization of terrestrial exoplanets with JWST. *Nat. Astron.*, **8**, no. 7, 810-818, doi:10.1038/s41550-024-02298-5…….92

28. **DeLessio, M.A.**, **K. Tsigaridis**, **S.E. Bauer**, **J. Chowdhary**, and G.L. Schuster, 2024: Modeling atmospheric brown carbon in the GISS ModelE Earth system model. *Atmos. Chem. Phys.*, **24**, no. 10, 6275-6304, doi:10.5194/acp-24-6275-2024……....93

29. **Derras-Chouk, A.**, and Z.J. Luo, 2024: A geostationary satellite-based approach to estimate convective mass flux and revisit the hot tower hypothesis. *Surv. Geophys.*, **45**, no. 6, 1959-1977, doi:10.1007/s10712-024-09856-6……94

30. **Ehsan, M.A.**, M.L. L'Heureux, M.K. Tippett, **A.W. Robertson**, and J. Turmelle, 2024: Real-time ENSO forecast skill evaluated over the last two decades, with focus on onset of ENSO events. *NPJ Clim. Atmos. Sci.*, **7**, 301, doi:10.1038/s41612-024-00845-5……..95

31. Eidhammer, T., A. Gettelman, K. Thayer-Calder, D. Watson-Parris, **G. Elsaesser**, H. Morrison, **M. van Lier-Walqui**, C. Song, and D. McCoy, 2024: An extensible perturbed parameter ensemble (PPE) for the Community Atmosphere Model Version 6. *Geosci. Model Dev.*, **17**, no. 21, 7835-7853, doi:10.5194/gmd-17-7835-2024……..96

32. **Erfani, S.M.H.**, M. Erfani, S. Cohen, A.R.J. Downey, and E. Goharian, 2024: A large dataset of fluvial hydraulic and geometry attributes derived from USGS field measurement records. *Environ. Model. Softw.*, **180**, 106136, doi:10.1016/j.envsoft.2024.106136……...97

33. Eriksen, S.H., N.P. Simpson, B. Glavovic, D. Ley, E.R. Carr, L. Fernández-Carril, B. Hayward, M.D. Morecroft, M. Pathak, J.J. Pereira, H.-O. Pörtner, D.C. Roberts, **A.C. Ruane**, R. Sánchez-Rodríguez, E.L.F. Schipper, W. Solecki, L.C. Stringer, E. Totin, A. Birt, and F. Degvold, 2024: Pathways for urgent action towards climate resilient development. *Nat. Clim. Change*, **14**, no. 12, 1212-1215, doi:10.1038/s41558-024-02190-0……..98

34. Ficklin, D.L., D. Touma, **B.I. Cook**, S.M. Robeson, T. Hwang, J. Scheff, A.P. Williams, H. Watson, B. Livneh, M.R. Tye, and L. Wang, 2024: Vegetation greening mitigates the impacts of increasing extreme rainfall on runoff events. *Earth's Future*, **12**, no. 12, e2024EF004661, doi:10.1029/2024EF004661……99

35. Fiedler, S., V. Naik, F.M. O'Connor, C.J. Smith, R. Pincus, P. Griffiths, R. Kramer, T. Takemura, R.J. Allen, U. Im, M. Kasoar, A. Modak, S. Turnock, A. Voulgarakis, D. Watson-Parris, **D.M. Westervelt**, L.J. Wilcox, A. Zhao, W.J. Collins, M. Schulz, G. Myhre, and P.M. Forster, 2024: Interactions between atmospheric composition and climate change — Progress in understanding and future opportunities from AerChemMIP, PDRMIP, and RFMIP. *Geosci. Model Dev.*, **17**, no. 5, 2387-2417, doi:10.5194/gmd-17-2387-2024……100

36. **Field, R.D.**, M. Luo, **S.E. Bauer**, **J.E. Hickman**, **G.S. Elsaesser**, **K. Mezuman, M. van Lier-Walqui**, **K. Tsigaridis**, and **J. Wu**, 2024: Estimating the impact of a 2017 smoke plume on surface climate over northern Canada with a climate model, satellite retrievals, and weather forecasts. *J. Geophys. Res. Atmos.*, **129**, no. 15, e2023JD039396, doi:10.1029/2023JD039396……....101

37. Flammini, A., H. Adzmir, R. Pattison, **K. Karl**, Y. Allouche, and F.N. Tubiello, 2024: Greenhouse gas emissions from cold chains in agrifood systems. *MDPI Sustainability*, **16**, no. 21, 9184, doi:10.3390/su16219184…….....102

38. Frieler, K., J. Volkholz, S. Lange, J. Schewe, M. Mengel, M.R. Rivas López, C. Otto, C.P.O. Reyer, D.N. Karger, J.T. Malle, S. Treu, C. Menz, J.L. Blanchard, C.S. Harrison, C.M. Petrik, T.D. Eddy, K. Ortega-Cisneros, C. Novaglio, Y. Rousseau, R.A. Watson, C. Stock, X. Liu, R. Heneghan, D. Tittensor, O. Maury, M. Büchner, T. Vogt, T. Wang, F. Sun, I.J. Sauer, J. Koch, I. Vanderkelen, **J. Jägermeyr**, C. Müller, J. Klar, I.D. Vega del Valle, G. Lasslop, S. Chadburn, E. Burke, A. Gallego-Sala, N. Smith, J. Chang, S. Hantson, C. Burton, A. Gädeke, F. Li, S.N. Gosling, H. Müller Schmied, F. Hattermann, J. Wang, F. Yao, T. Hickler, R. Marcé, D. Pierson, W. Thiery, D. Mercado-Bettín, R. Ladwig, A.I. Ayala-Zamora, M. Forrest, and M. Bechtold, 2024: Scenario set-up and forcing data for impact model evaluation and impact attribution within the third round of the Inter-Sectoral Model Intercomparison Project (ISIMIP3a). *Geosci. Model Dev.*, **17**, no. 1, 1-51, doi:10.5194/gmd-17-1-2024…….....103

39. Fronzek, S., H. Webber, R. Rötter, **A.C. Ruane**, and F. Evert, 2024: A daily time-step observed and scenario climate dataset on a European grid for crop modelling applications. *Open Data J. Agric. Res.*, **10**, 28-34, doi:10.18174/odjar.v10i0.16398.....104

40. **Gao, C.Y.**, **S.E. Bauer**, **K. Tsigaridis**, and U. Im, 2024: Global influence of organic aerosol volatility on aerosol microphysical processes: Composition and number. *J. Adv. Model. Earth Syst.*, **16**, no. 10, e2023MS004185, doi:10.1029/2023MS004185……....105

41. Gonçalves, I.Z., I.M. Fattori, C.M.U. Neale, C.A.C. Santos, **A.C. Ruane**, **M.M. Phillips**, and F.R. Marin, 2024: How can future climate change affect the corn production system in Nebraska, USA? *Int. J. Plant Prod.*, **18**, no. 4, 563-577, doi:10.1007/s42106-024-00310-6……106

42. Gonzalez, A.O., I. Ganguly, M. Osterloh, **G.V. Cesana**, and C.A. DeMott, 2024: Dynamical importance of the trade wind inversion in suppressing the southeast Pacific ITCZ. *J. Geophys. Res. Atmos.*, **129**, no. 24, e2023JD039571, doi:10.1029/2023JD039571…….....107

43. Govindjee, G., O. Canaani, R.A. Cellarius, B. Diner, E. Greenbaum, H. Hou, **N.Y. Kiang**, J.S. Lindsey, D.L. Mauzerall, M.E. Mauzerall, M. Seibert, and A. Stirbet, 2024: Contributions of David Mauzerall to photosynthesis research — Celebrating his 95th birthday. *Photosynthetica*, **62**, no. 3, 271-288, doi:10.32615/ps.2024.029……108

44. Grise, K.M., and **G. Tselioudis**, 2024: Understanding the relationship between cloud controlling factors and the ISCCP weather states. *J. Climate*, **37**, no. 20, 5387-5403, doi:10.1175/JCLI-D-24-0011.1…….....109

45. **Guarin, J.R.**, **J. Jägermeyr**, E.A. Ainsworth, F.A.A. Oliveira, S. Asseng, K. Boote, J. Elliott, L. Emberson, I. Foster, G. Hoogenboom, D. Kelly, **A.C. Ruane**, and K. Sharps, 2024: Modeling the effects of tropospheric ozone on the growth and yield of global staple crops with DSSAT v4.8.0. *Geosci. Model Dev.*, **17**, no. 7, 2547-2567, doi:10.5194/gmd-17-2547-2024……....110

46. Gurazada, M., **S. McDermid**, R. DeFries, K.F Davis, J. Singh, and D. Singh, 2024: El Niño and positive Indian Ocean Dipole conditions simultaneously reduce the production of multiple cereals across India. *Environ. Res. Lett.*, **19**, no. 10, 104059, doi:10.1088/1748-9326/ad6a6f……..….....111

47. **Haas, H.**, L. Kalin, and E. Baltaci, 2024: How wide is the problem? Leveraging alternative data sources to enhance channel width representation in watershed modeling. *Environ. Model. Softw.*, **172**, 105935, doi:10.1016/j.envsoft.2023.105935.....112

48. **Haas, H.**, L. Kalin, and H. Yen, 2024: Improved forest canopy evaporation leads to better predictions of ecohydrological processes. *Ecol. Model.*, **489**, 110620, doi:10.1016/j.ecolmodel.2024.110620……...113

49. Han, J., Z. Zhang, J. Xu, Y. Chen, **J. Jägermeyr**, J. Cao, Y. Luo, F. Cheng, H. Zhuang, H. Wu, Q. Mei, J. Song, and F. Tao, 2024: Threat of low-frequency high-intensity floods to global cropland and crop yields. *Nat. Sustain.*, **7**, no. 8, 994-1006, doi:10.1038/s41893-024-01375-x……...114

50. Hartig, E.K., C. Haight, M. Hsu, N. Auyeung, R. Swadek, J. Ong, **V. Gornitz**, and R. Boger, 2024: A decade of salt marsh elevation change in New York City's coastal urban parks. *Estuar. Coasts*, **47**, no. 7, 1941-1954, doi:10.1007/s12237-024-01374-3…….....115

51. Hofer, S., L.C. Hahn, J.K. Shaw, **Z.S. McGraw**, O. Bruno, F. Hellmuth, M. Pietschnig, I.A. Mostue, R.O. David, T. Carlsen, and T. Storelvmo, 2024: Realistic representation of mixed-phase clouds increases future climate warming. *Commun. Earth Environ.*, **5**, 390, doi:10.1038/s43247-024-01524-2……116

52. Hsiao, W.-T., E.D. Maloney, **N.M. Leitmann-Niimi**, and C.D. Kummerow, 2024: Observed relationships between sea surface temperature, vertical wind shear, tropical organized deep convection, and radiative effects. *J. Climate*, **37**, no. 4, 1277-1293, doi:10.1175/JCLI-D-23-0262.1……....117

53. Ing, R.N., P.W. Nienow, A.J. Sole, A.J. Tedstone, and **K.D. Mankoff**, 2024: Minimal impact of late-season melt events on Greenland ice sheet annual motion. *Geophys. Res. Lett.*, **51**, no. 4, e2023GL106520, doi:10.1029/2023GL106520…….118

54. **Ivanovich, C.C.**, **R.M. Horton**, A.H. Sobel, and D. Singh, 2024: Subseasonal variability of humid heat during the South Asian summer monsoon. *Geophys. Res. Lett.*, **51**, no. 6, e2023GL107382, doi:10.1029/2023GL107382…….119

55. **Ivanovich, C.C.**, A.H. Sobel, **R.M. Horton**, and C. Raymond, 2024: Stickiness: A new variable to characterize the temperature and humidity contributions toward humid heat. *J. Atmos. Sci.*, **81**, no. 5, 819-837, doi:10.1175/JAS-D-23-0072.1……120

56. Johnson, S., **C. Ivanovich**, **R.M Horton**, M. Ting, K. Kornhuber, and **C. Lesk**, 2024: Temporal connections between extreme precipitation and humid heat. *Environ. Res. Lett.*, **19**, 114076, doi:10.1088/1748-9326/ad7edc…….....121

57. Jun, T., and **D. Rind**, 2024: Increasing contribution of the atmospheric vertical motion to precipitation in a warming climate. *Commun. Earth Environ.*, **5**, 541, doi:10.1038/s43247-024-01676-1……..122

58. **Karl, K.**, R. DeFries, W. Baethgen, M. Furtado, J. Potent, E.M. Leal, **E. Mencos Contreras**, and **C. Rosenzweig**, 2024: Toward a holistic and data-driven framework to evaluate livestock-derived protein systems. *One Earth*, **7**, no. 4, 572-588, doi:10.1016/j.oneear.2024.02.003…….....…123

59. Kim, D., M. Chin, G. Schuster, H. Yu, T. Takemura, P. Tuccella, P. Ginoux, X. Liu, Y. Shi, H. Matsui, **K. Tsigaridis**, **S.E. Bauer**, J.F. Kok, and M. Schulz, 2024: Where dust comes from: Global assessment of dust source attributions with AeroCom models. *J. Geophys. Res. Atmos.*, **129**, no. 16, e2024JD041377, doi:10.1029/2024JD041377….124

60. Korolev, A., Z. Qu, J. Milbrandt, I. Heckman, M. Cholette, M. Wolde, C. Nguyen, G. McFarquhar, P. Lawson, and **A.M. Fridlind**, 2024: High ice water content in tropical mesoscale convective systems (a conceptual model). *Atmos. Chem. Phys.*, **24**, no. 20, 11849-11881, doi:10.5194/acp-24-11849-2024……125

61. Kothari, K., R. Battisti, K.J. Boote, S.V. Archontoulis, A. Confalone, J. Constantin, S.V. Cuadra, P. Debaeke, B. Faye, B. Grant, G. Hoogenboom, Q. Jing, M. van der Laan, F.A.M. da Silva, F.R. Marin, A. Nehbandani, C. Nendel, L.C. Purcell, B. Qian, **A.C. Ruane**, C. Schoving, E.H.F.M. Silva, W. Smith, A. Soltani, A. Srivastava, N.A. Vieira, and M. Salmerón, 2024: Evaluating differences among crop models in simulating soybean in-season growth. *Field Crops Res.*, **309**, 109306, doi:10.1016/j.fcr.2024.109306……. 126

62. Kuhla, K., **M.J. Puma**, and C. Otto, 2024: International cooperation was key to stabilize wheat prices after the Russian invasion of Ukraine. *Commun. Earth Environ.*, **5**, no. 1, 481, doi:10.1038/s43247-024-01638-7……127

63. Lac, J., H. Chepfer, **A. Arouf**, M.D. Shupe, and M.R. Gallagher, 2024: Polar low circulation enhances Greenland's west coast cloud surface warming. *J. Geophys. Res. Atmos.*, **129**, no. 11, e2023JD040450, doi:10.1029/2023JD040450……....128

64. Lamb, K., **M. van Lier-Walqui**, S. Santos, and H. Morrison, 2024: Reduced order modeling for linearized representations of microphysical process rates. *J. Adv. Model. Earth Syst.*, **16**, no. 7, e2023MS003918, doi:10.1029/2023MS003918……...129

65. Larose, J., É. Boucher, A. de Vernal, I. Hermoso de Mendoza, F. Gennaretti, A. Lavergne, L. Andreu-Hayles, and **R.D. Field**, 2024: Labrador Sea's influence on black spruce forests: Insights from tree-ring stable oxygen isotopes. *Commun. Earth Environ.*, **5**, 108, doi:10.1038/s43247-024-01271-4……..…..130

66. **LeGrande, A.N.**, J.F. Booth, **C.M. Naud**, C. Ordaz, and J. Crespo, 2024: Just how river-like are atmospheric rivers? *Geophys. Res. Lett.*, **51**, no. 10, e2023GL105828, doi:10.1029/2023GL105828……131

67. **Lenssen, N.**, **G.A. Schmidt**, **M. Hendrickson**, P. Jacobs, M. Menne, and **R. Ruedy**, 2024: A GISTEMPv4 observational uncertainty ensemble. *J. Geophys. Res. Atmos.*, **129**, no. 17, e2023JD040179, doi:10.1029/2023JD040179……132

68. **Lerner, P.**, **A. Romanou**, D. Nicholson, **M. Kelley**, **R. Ruedy**, and **G. Russell**, 2024: The sensitivity of the Equatorial Pacific ODZ to particulate organic matter remineralization in a climate model under pre-industrial conditions. *Ocean Model.*, **188**, 102303, doi:10.1016/j.ocemod.2023.102303……..133

69. Li, J.-L.F., K.-M. Xu, J.H. Jiang, W.-L. Lee, J.-Y. Yu, J.-D. Chern, **G.V. Cesana**, L. Wu, and G. Stephens, 2024: Investigating the "too bright" issue pertaining to non-PBL clouds over the South Pacific trade-wind region in CMIP6 global climate models. *Geophys. Res. Lett.*, **51**, no. 22, e2024GL112006, doi:10.1029/2024GL112006……...134

70. Li, L., N.M. Mahowald, M. Gonçalves Ageitos, **V. Obiso**, **R.L. Miller**, C. Pérez García-Pando, C. Di Biagio, P. Formenti, P.G. Brodrick, R.N. Clark, R.O. Green, R. Kokaly, G. Swayze, and D.R. Thompson, 2024: Improved constraints on hematite refractive index for estimating climatic effects of dust aerosols. *Commun. Earth Environ.*, **5**, no. 1, 295, doi:10.1038/s43247-024-01441-4……..135

71. Li, T., **S.S. McDermid**, R.O. Valdivia, and P. Sundaram, 2024: Climate change mitigation and adaptation for rice-based farming systems in the Red River Delta, Vietnam. *CABI Agric. Biosci.*, **5**, no. 1, 109, doi:10.1186/s43170-024-00308-0……136

72. Li, X.-Y., H. Wang, M.W. Christensen, J. Chen, S. Tang, S. Kirschler, E. Crosbie, L.D. Ziemba, D. Painemal, A.F. Corral, K.A. McCauley, S. Dmitrovic, A. Sorooshian, M. Fenn, J.S. Schlosser, S. Stamnes, J.W. Hair, **B. Cairns**, R. Moore, R.A. Ferrare, M.A. Shook, Y. Choi, J. DiGangi, J.B. Nowak, C. Robinson, T.J. Shingler, K.L. Thornhill, and C. Voigt, 2024: Process modeling of aerosol-cloud interaction in summertime precipitating shallow cumulus over the Western North Atlantic. *J. Geophys. Res. Atmos.*, **129**, no. 7, e2023JD039489, doi:10.1029/2023JD039489……137

73. Lichstein, J.W., T. Zhang, **E. Weng**, C.E. Farrior, R. Dybzinski, S. Malyshev, E. Shevliakova, R.A. Birdsey, and S.W. Pacala, 2024: Effects of water limitation and competition on tree carbon allocation in an Earth system modeling framework. *J. Ecol.*, **112**, no. 11, 2522-2539, doi:10.1111/1365-2745.14416……..…138

74. Lumsden, C.L., **J. Jägermeyr**, L. Ziska, and J. Fanzo, 2024: Critical overview of the implications of a global protein transition in the face of climate change: Key unknowns and research imperatives. *One Earth*, **7**, no. 7, 1187-1201, doi:10.1016/j.oneear.2024.06.013……..139

75. Luo, M., H.M. Worden, **R.D. Field**, **K. Tsigaridis**, and **G.S. Elsaesser**, 2024: TROPESS-CrIS CO single-pixel vertical profiles: Intercomparisons with MOPITT and model comparisons for 2020 western US wildfires. *Atmos. Meas. Tech.*, **17**, no. 9, 2611-2024, doi:10.5194/amt-17-2611-2024……140

76. **Ma, Q.**, and C. Boulet, 2024: Branch dependence of halfwidths: Theoretical analysis of N2-broadened halfwidths of CH3Br in the ν6 band. *J. Quant. Spectrosc. Radiat. Transfer*, **320**, 108972, doi:10.1016/j.jqsrt.2024.108972……....141

77. Mahowald, N., P. Ginoux, G.S. Okin, J. Kok, S. Albani, Y. Balkanski, M. Chin, G. Bergametti, T.F. Eck, C. Pérez García-Pando, A. Gkikas, M. Gonçalves Ageitos, D. Kim, M. Klose, S. LeGrand, L. Li, B. Marticorena, **R.L. Miller**, C. Ryder, C. Zender, and Y. Yu, 2024: Letter to the Editor regarding Chappell et al., 2023, "Satellites reveal Earth's seasonally shifting dust emission sources". *Sci. Total Environ.*, **949**, 174792, doi:10.1016/j.scitotenv.2024.174792……...…142

78. Mariotti, A., **D.C. Bader**, **S.E. Bauer**, G. Danabasoglu, J.P.P. Dunne, B. Gross, L.R. Leung, S. Pawson, W.M Putman, V. Ramaswamy, **G.A. Schmidt**, and V. Tallapragada, 2024: Envisioning U.S. climate predictions and projections to meet new challenges. *Earth's Future*, **12**, no. 6, e2023EF004187, doi:10.1029/2023EF004187….143

79. Martre, P., S. Dueri, H. Brown, S. Asseng, F. Ewert, H. Webber, M. George, R. Craigie, **J. Guarin**, D. Pequeno, T. Stella, M. Ahmed, P. Alderman, B. Basso, A. Berger, G. Bracho Mujica, D. Cammarano, Y. Chen, B. Dumont, E. Rezaei, E. Fereres, R. Ferrise, T. Gaiser, Y. Gao, M. Garcia-Vila, S. Gayler, Z. Hochman, G. Hoogenboom, K. Kersebaum, C. Nendel, J. Olesen, G. Padovan, T. Palosuo, E. Priesack, J. Pullens, A. Rodríguez, R. Rötter, M. Ruiz Ramos, M. Semenov, N. Senapati, S. Siebert, A. Srivastava, C. Stöckle, I. Supit, F. Tao, P. Thorburn, E. Wang, T. Weber, L. Xiao, C. Zhao, J. Zhao, Z. Zhao, and Y. Zhu, 2024: Winter wheat experiments to optimize sowing dates and densities in a high-yielding environment in New Zealand: field experiments and AgMIP-Wheat multi-model simulations. *Open Data J. Agric. Res.*, **10**, 14-21, doi:10.18174/odjar.v10i0.18442…….144

80. Martre, P., S. Dueri, **J.R. Guarin**, F. Ewert, H. Webber, D. Calderini, G. Molero, M. Reynolds, D. Miralles, G. Garcia, H. Brown, M. George, R. Craigie, J.-P. Cohan, J.-C. Deswarte, G. Slafer, F. Giunta, D. Cammarano, R. Ferrise, T. Gaiser, Y. Gao, Z. Hochman, G. Hoogenboom, L.A. Hunt, K.C. Kersebaum, C. Nendel, G. Padovan, **A.C. Ruane**, A.K. Srivastava, T. Stella, I. Supit, P. Thorburn, E. Wang, J. Wolf, C. Zhao, Z. Zhao, and S. Asseng, 2024: Global nitrogen needs to improve wheat yield under climate change. *Nat. Plants*, **10**, 1081-1090, doi:10.1038/s41477-024-01739-3…….....145

81. **Marvel, K.D.**, and M. Webb, 2024: Towards robust community assessments of the Earth's climate sensitivity. *Earth Syst. Dyn.*, **16**, no. 1, 317, doi:10.5194/esd-16-317-2025…….....146

82. Matsui, T., D. Hernandez-Deckers, S. Giangrande, T. Biscaro, **A.M. Fridlind**, and S. Braun, 2024: A thermal-driven graupel generation process to explain dry-season convective vigor over the Amazon. *Atmos. Chem. Phys.*, **24**, no. 18, 10793-10814, doi:10.5194/acp-24-10793-2024…….....147

83. McBride, B.A., J.V. Martins, J.D. Cieslak, R. Fernandez-Borda, A. Puthukuddy, X. Xu, N. Sienkiewicz, **B. Cairns**, and H.M.J. Barbosa, 2024: Pre-launch calibration and validation of the Airborne Hyper-Angular Rainbow Polarimeter (AirHARP) instrument. *Atmos. Meas. Tech.*, **17**, no. 19, 5709-5729, doi:10.5194/amt-17-5709-2024…….148

84. McConnell, K., and **C.V. Braneon**, 2024: Post-wildfire neighborhood change: Evidence from the 2018 Camp Fire. *Landsc. Urban Plan.*, **247**, 104997, doi:10.1016/j.landurbplan.2023.104997…….....149

85. **McGraw, Z.**, L.M. Polvani, B. Gasparini, E.K. Van De Koot, and A. Voigt, 2024: The cloud radiative response to surface warming weakens hydrological sensitivity. *Geophys. Res. Lett.*, **52**, no. 2, e2024GL112368, doi:10.1029/2024GL112368……..150

86. **McGraw, Z.**, **K. DallaSanta**, L. Polvani, **K. Tsigaridis**, **C. Orbe**, and **S.E. Bauer**, 2024: Severe global cooling after volcanic super-eruptions? The answer hinges on unknown aerosol size. *J. Climate*, **37**, no. 4, 1449-1464, doi:10.1175/JCLI-D-23-0116.1…….....151

87. **McGraw, Z.**, and L.M. Polvani, 2024: How volcanic aerosols globally inhibit precipitation. *Geophys. Res. Lett.*, **51**, no. 13, e2023GL107930, doi:10.1029/2023GL107930…….....152

88. **Menzel, M.E.**, D. Waugh, Z. Wu, and T. Reichler, 2024: Replicating the Hadley Cell and subtropical jet disconnect in idealized atmospheric models. *Weather Clim. Dynam.*, **5**, no. 1, 251-261, doi:10.5194/wcd-5-251-2024…….....153

89. Metz, C.O., **N.Y. Kiang**, G.L. Villanueva, M.N. Parenteau, and V. Kofman, 2024: Detectability simulations of a NIR surface biosignature on Proxima Centauri b with future space observatories. *Planet. Sci. J.*, **5**, 228, doi:10.3847/PSJ/ad769d…….....154

90. Mitevski, I., R. Chemke, **C. Orbe**, and L.M. Polvani, 2024: Southern Hemisphere winter storm tracks respond differently to low and high CO_2 forcings. *J. Climate*, **37**, no. 20, 5355-5372, doi:10.1175/JCLI-D-23-0758.1…….....155

91. Monaco, H., C. Ortiz, L. Caetano, C. Müller, and **J. Jägermeyr**, 2024: The economics of farming expansion in the Brazilian Cerrado under possible effects of climate change. *Int. Food Agribus. Manag. Rev.*, **27**, no. 3, 441-462, doi:10.22434/ifamr1028……156

92. Mortelmans, J., A. Felsberg, G.J.M. De Lannoy, S. Veraverbeke, **R.D. Field**, N. Andela, and M. Bechtold, 2024: Improving the fire weather index system for peatlands using peat-specific hydrological input data. *Nat. Hazards Earth Syst. Sci.*, **24**, no. 2, 445-464, doi:10.5194/nhess-24-445-2024……157

93. Mroz, K., A. Battaglia, and **A.M. Fridlind**, 2024: Enhancing consistency of microphysical properties of precipitation across the melting layer in the Dual-frequency Precipitation Radar data. *Atmos. Meas. Tech.*, **17**, no. 5, 1577-1597, doi:10.5194/amt-17-1577-2024……....158

94. Müller, C., **J. Jägermeyr**, J.A. Franke, **A.C. Ruane**, J. Balkovic, P. Ciais, M. Dury, P. Falloon, C. Folberth, T. Hank, M. Hoffmannn, C. Izaurralde, I. Jacquemin, N. Khabarov, W. Liu, S. Olin, T.A.M. Pugh, X. Wang, K. Williams, F. Zabel, and J.W. Elliott, 2024: Substantial differences in crop yield sensitivities between models call for functionality-based model evaluation. *Earth's Future*, **12**, no. 3, e2023EF003773, doi:10.1029/2023EF003773……...….159

95. Mülmenstädt, J., **A.S. Ackerman**, **A.M. Fridlind**, M. Huang, P.-L. Ma, N. Mahfouz, **S.E. Bauer**, S.M. Burrows, M.W. Christensen, S. Dipu, A. Gettelman, L.R. Leung, **F. Tornow**, J. Quaas, A.C. Varble, H. Wang, K. Zhang, and Y. Zheng, 2024: Can general circulation models (GCMs) represent cloud liquid water path adjustments to aerosol-cloud interactions? *Atmos. Chem. Phys.*, **24**, no. 23, 13633-13652, doi:10.5194/acp-24-13633-2024……...…160

96. Mülmenstädt, J., E. Gryspeerdt, S. Dipu, J. Quaas, **A.S. Ackerman**, **A.M. Fridlind**, **F. Tornow**, **S.E. Bauer**, A. Gettelman, Y. Ming, Y. Zheng, P.-L. Ma, H. Wang, K. Zhang, M.W. Christensen, A.C. Varble, L.R. Leung, X. Liu, D. Neubauer, D.G. Partridge, P. Stier, and T. Takemura, 2024: General circulation models simulate negative liquid water path-droplet number correlations, but anthropogenic aerosols still increase simulated liquid water path. *Atmos. Chem. Phys.*, **24**, no. 12, 7331-7345, doi:10.5194/acp-24-7331-2024……...…161

97. Muneepeerakul, R., J. Johnson, **M. Puma**, and M. Zurek, 2024: Triadic signatures of global refugee and migrant flow networks. *PLOS ONE*, **19**, no. 2, e0298876, doi:10.1371/journal.pone.0298876…….....…162

98. **Nakad, M.**, 2024: Discounting water for optimal carbon gain as a basis of stomatal closure. *AGU Adv.*, **5**, no. 3, e2024AV001287, doi:10.1029/2024AV001287…….....163

99. Nakamura, J., R. Seager, H. Liu, F. Cottier, **M.J. Puma**, D.J. Wrathall, B. Katz, A. de Sherbinin, and S.B. Adamo, 2024: Recent trends in agriculturally relevant climate in Central America. *Int. J. Climatol.*, **44**, no. 8, 2701-2724, doi:10.1002/joc.8476……164

100. **Naud, C.M.**, P. Ghosh, J.E. Martin, **G.S. Elsaesser**, and D.J. Posselt, 2024: A CloudSat-CALIPSO view of cloud and precipitation in the occluded quadrants of extratropical cyclones. *Q. J. Roy. Meteorol. Soc.*, **150**, 1336-1356, doi:10.1002/qj.4648……...…165

101. **Nielsen, M.**, **B.I. Cook**, **K.D Marvel**, M. Ting, and J.E. Smerdon, 2024: The changing influence of precipitation on soil moisture drought with warming in the Mediterranean and Western North America. *Earth's Future*, **12**, no. 5, e2023EF003987, doi:10.1029/2023EF003987……...166

102. **Obiso, V.**, M. Gonçalves Ageitos, C. Pérez García-Pando, G.L. Schuster, **S.E. Bauer**, C. Di Biagio, P. Formenti, **J.P. Perlwitz**, **K. Tsigaridis**, and **R.L. Miller**, 2024: Observationally constrained regional variations of shortwave absorption by iron oxides emphasize the cooling effect of dust. *Atmos. Chem. Phys.*, **24**, no. 9, 5337-5367, doi:10.5194/acp-24-5337-2024……167

103. **Orbe, C.**, **D. Rind**, D. Waugh, **J. Jonas**, X. Zhang, G. Chiodo, **L. Nazarenko**, and **G.A. Schmidt**, 2024: Coupled stratospheric ozone and Atlantic Meridional Overturning Circulation feedbacks on the Northern Hemisphere midlatitude jet response to 4×CO_2. *J. Climate*, **37**, no. 10, 2897-2917, doi:10.1175/JCLI-D-23-0119.1……..…168

104. **Ordaz Osorio, C.**, J.F. Booth, **A.N. LeGrande**, and **C.M. Naud**, 2024: Assessing the impact of climate change on atmospheric rivers: A modeling perspective. *J. Geophys. Res. Atmos.*, **129**, no. 12, e2023JD040074, doi:10.1029/2023JD040074……..169

105. Orlov, A., **J. Jägermeyr**, C. Müller, A.S. Daloz, F. Zabel, S. Minoli, W. Liu, T.-S. Lin, A.K. Jain, C. Folberth, M. Okada, B. Poschlod, A. Smerald, J.M. Schneider, and J. Sillmann, 2024: Human heat stress could offset potential economic benefits of CO2 fertilization in crop production under a high-emissions scenario. *One Earth*, **7**, no. 7, 1250-1265, doi:10.1016/j.oneear.2024.06.012…….170

106. Ortiz, L., **C. Braneon**, R. Horton, **D. Bader**, P. Orton, **V. Gornitz**, B. Rosenzweig, T. McPhearson, L. Smalls-Mantey, H. Sheerazi, F. Montalto, M.R. Golkhandan, C. Evans, A. Degaetano, E. Mallen, L. Carter, K. McConnell, T. Mayo, and M. Buchanan, 2024: NPCC4: Tail risk, climate drivers of extreme heat, and new methods for extreme event projections. *Ann. New York Acad. Sci.*, **1539**, no. 1, 49-76, doi:10.1111/nyas.15180……...171

107. **Ottaviani, M.**, G.H. Myers, and N. Chen, 2024: Global Sensitivity Analysis of simulated polarimetric remote sensing observations over snow. *Atmos. Meas. Tech.*, **17**, no. 15, 4737-4756, doi:10.5194/amt-17-4737-2024……..172

108. Paerl, H.W., J.D. Chaffin, J.H. Cheshire, **H.E. Plaas,** M.A. Barnard, L.B. Goerlitz, J.S. Braddy, A. Sabo, L.M. Nelson, and L. Yue, 2024: Dual phosphorus and nitrogen nutrient reduction will be more effective than a phosphorus-only reduction in mitigating diatom and cyanobacterial blooms in Lake Erie, USA-Canada. *Limnol. Oceanogr.*, **69**, no. 12, 2913-2928, doi:10.1002/lno.12719……...……173

109. Paerl, H.W., **H.E. Plaas**, L.M. Nelson, A.S. Korbobo, J.H. Cheshire, L. Yue, and E.P. Preece, 2024: Dual nitrogen and phosphorus reductions are needed for long-term mitigation of eutrophication and harmful cyanobacterial blooms in the hydrologically-variable San Francisco Bay Delta, CA. *Sci. Total Environ.*, **957**, 177499, doi:10.1016/j.scitotenv.2024.177499…….174

110. Palmer, J.G., D. Verdon-Kidd, K.J. Allen, P. Higgins, **B.I. Cook**, E.R. Cook, C.S.M. Turney, and P.J. Baker, 2024: Drought and deluge: the recurrence of hydroclimate extremes during the past 600 years in eastern Australia's Natural Resource Management (NRM) clusters. *Nat. Hazards*, **120**, no. 4, 3565-3587, doi:10.1007/s11069-023-06288-0……....……....175

111. **Pilewskie, J.**, G. Stephens, H. Takahashi, and T. L'Ecuyer, 2024: A multi-satellite perspective on "hot tower" characteristics in the equatorial trough zone. *Surv. Geophys.*, **45**, no. 6, 1933-1958, doi:10.1007/s10712-024-09868-2…….176

112. Preece, E.P., J. Cooke, **H. Plaas**, A. Sabo, L. Nelson, and H.W. Paerl, 2024: Managing a cyanobacteria harmful algae bloom "hotspot" in the Sacramento — San Joaquin Delta, California. *J. Environ. Manag.*, **351**, 119606, doi:10.1016/j.jenvman.2023.119606…….177

113. Ren, F., J. Lin, C. Xu, J.A. Adeniran, J. Wang, R.V. Martin, A. van Donkelaar, M. Hammer, L. Horowitz, S.T. Turnock, N. Oshima, J. Zhang, **S.E. Bauer**, **K. Tsigaridis**, Ø. Seland, P. Nabat, D. Neubauer, G. Strand, T. van Noije, P. Le Sager, and T. Takemura, 2024: Evaluation of CMIP6 model simulations of $PM_{2.5}$ and its components over China. *Geosci. Model Dev.*, **17**, no. 12, 4821-4836, doi:10.5194/gmd-17-4821-2024……..……178

114. Rigatti, E., **S.S. McDermid**, **B.I. Cook**, and M.G. De Kauwe, 2024: The impact of drought on terrestrial carbon in the West African Sahel: Implications for natural climate solutions. *J. Geophys. Res. Biogeosci.*, **129**, no. 10, e2024JG008143, doi:10.1029/2024JG008143…….....179

115. Riihimaki, L.D., M.F. Cronin, R. Acharya, N. Anderson, J. Augustine, K.A. Balmes, P. Berk, R. Bozzano, A. Bucholtz, K.J. Connell, C. Cox, A.G. Di Sarra, J.B. Edson, C. Fairall, J.T. Farrar, K. Grissom, M.T. Guerra, V. Hormann, K.J. Joseph, C. Lanconelli, F. Melin, D. Meloni, **M. Ottaviani**, S. Pensieri, K Ramesh, D. Rutan, N. Samarinas, S.R. Smith, S. Swart, A. Tandon, R. Venkatesan, E. Thompson, R.K. Verma, V. Vitale, K.S. Watkins-Brandt, R.A. Weller, C.J. Zappa, and D. Zhang, 2024: Ocean surface radiation measurement best practices. *Front. Mar. Sci.*, **11**, 1359149, doi:10.3389/fmars.2024.1359149……..180

116. Rivera, A., **K. Tsigaridis**, **G. Faluvegi**, and D. Shindell, 2024: Assessing acetone for the GISS ModelE2.1 Earth system model. *Geosci. Model Dev.*, **17**, no. 8, 3487-3505, doi:10.5194/gmd-17-3487-2024……181

117. **Roach, L.A.**, 2024: Accelerating Antarctic research amid rapid changes. *Nat. Water*, **2**, 604-605, doi:10.1038/s44221-024-00266-x……182

118. **Roach, L.A.**, and W.N. Meier, 2024: Sea ice in 2023. *Nat. Rev. Earth Environ.*, **5**, no. 4, 235-237, doi:10.1038/s43017-024-00542-0……183

119. **Ruane, A.C.**, **M. Phillips**, **J. Jägermeyr**, and C. Müller, 2024: Non-linear climate change impacts on crop yields may mislead stakeholders. *Earth's Future*, **12**, no. 4, e2023EF003842, doi:10.1029/2023EF003842……184

120. Salesin, K., K.D. Knobelspiesse, **J. Chowdhary**, P.-W. Zhai, and W. Jarosz, 2024: Unifying radiative transfer models in computer graphics and remote sensing, Part II: A differentiable, polarimetric forward model and validation. *J. Quant. Spectrosc. Radiat. Transfer*, **315**, 108849, doi:10.1016/j.jqsrt.2023.108849……185

121. Salesin, K., K.D. Knobelspiesse, **J. Chowdhary**, P.-W. Zhai, and W. Jarosz, 2024: Unifying radiative transfer models in computer graphics and remote sensing, Part I: A survey. *J. Quant. Spectrosc. Radiat. Transfer*, **314**, 108847, doi:10.1016/j.jqsrt.2023.108847……..…..186

122. Schlosser, J.S., R. Bennett, **B. Cairns**, G. Chen, B.L. Collister, J.W. Hair, M. Jones, M.A. Shook, A. Sorooshian, K.L. Thornhill, L.D. Ziemba, and S. Stamnes, 2024: Maximizing the volume of collocated data from two coordinated suborbital platforms. *J. Atmos. Ocean. Technol.*, **41**, no. 2, 189-201, doi:10.1175/JTECH-D-23-0001.1……187

123. **Schmidt, G.A.**, J. Arblaster, **K.D. Mankoff**, A. Pauling, and Q. Li, 2024: Lessons learned from running a virtual global workshop. *Eos*, **105**, on-line, doi:10.1029/2024EO240514……188

124. **Schmidt, G.A.**, 2024: Climate models can't explain 2023's huge heat anomaly — We could be in uncharted territory. *Nature*, **627**, 467, doi:10.1038/d41586-024-00816-z……..……189

125. Shindell, D., R. Hunter, **G. Faluvegi**, and L. Parsons, 2024: Premature deaths due to heat exposure: The potential effects of neighborhood-level versus city-level acclimatization within US cities. *GeoHealth*, **8**, no. 1, e2023GH000970, doi:10.1029/2023GH000970……190

126. Shindell, D., **G. Faluvegi**, E. Nagamoto, L. Parsons, and Y. Zhang, 2024: Reductions in premature deaths from heat and particulate matter air pollution in South Asia, China, and the US under decarbonization. *Proc. Natl. Acad. Sci.*, **121**, no. 5, e2312832120, doi:10.1073/pnas.2312832120……..……191

127. Shindell, D., I. Petropoulos, **G. Faluvegi**, L. Parsons, and M. Bergin, 2024: The impact of decarbonization on particulate soiling of solar panels. *ACS EST Air*, **1**, no. 12, 1531-1540, doi:10.1021/acsestair.4c00105……..192

128. Shindell, D., P. Sadavarte, I. Aben, T. de Oliveira Bredariol, G. Dreyfus, L. Höglund-Isaksson, B. Poulter, M. Saunois, **G.A. Schmidt**, S. Szopa, K. Rentz, L. Parsons, Z. Qu, **G. Faluvegi**, and J.D. Maasakkers, 2024: The methane imperative. *Front. Sci.*, **2**, 1349770, doi:10.3389/fsci.2024.1349770……...193

129. Sillmann, J., T.H. Raupach, K.L. Findell, M. Donat, L.M. Alves, L. Alexander, L. Borchert, P.B. de Amorim, C. Buontempo, E.M. Fischer, C.L. Franzke, B. Guan, M. Haasnoot, E. Hawkins, D. Jacob, R. Mahon, D. Maraun, M.A. Morrison, B. Poschlod, **A.C. Ruane**, Shampa, T. Stephenson, N. van der Wel, Z. Wang, X. Zhang, and J. Županić, 2024: Climate extremes and risks: links between climate science and decision-making. *Front. Clim.*, **6**, 1499765, doi:10.3389/fclim.2024.1499765……194

130. Silvy, Y., T.L. Frölicher, J. Terhaar, F. Joos, F.A. Burger, F. Lacroix, M. Allen, R. Bernadello, L. Bopp, V. Brovkin, J.R. Buzan, P. Cadule, M. Dix, J. Dunne, P. Friedlingstein, G. Georgievski, T. Hajima, S. Jenkins, M. Kawamiya, **N.Y. Kiang**, V. Lapin, D. Lee, **P. Lerner**, N. Mengis, E.A. Monteiro, D. Paynter, G.P. Peters, **A. Romanou**, J. Schwinger, S. Sparrow, E. Stofferahn, J. Tjiputra, E. Tourigny, and T. Ziehn, 2024: AERA-MIP: Emission pathways, remaining budgets and carbon cycle dynamics compatible with 1.5°C and 2°C global warming stabilization. *Earth Syst. Dyn.*, **15**, no. 6, 1591-1608, doi:10.5194/esd-15-1591-2024…….195

131. Siu, L.W., J.S. Schlosser, D. Painemal, **B. Cairns**, M.A. Fenn, R.A. Ferrare, J.W. Hair, C.A. Hostetler, L. Li, M.M. Kleb, A.J. Scarino, T.J. Shingler, A. Sorooshian, S.A. Stamnes, and X. Zeng, 2024: Retrievals of aerosol optical depth over the western North Atlantic Ocean during ACTIVATE. *Atmos. Meas. Tech.*, **17**, no. 9, 2739-2759, doi:10.5194/amt-17-2739-2024…….....196

132. Siu, L.W., X. Zeng, A. Sorooshian, **B. Cairns**, R.A. Ferrare, J.W. Hair, C.A. Hostetler, D. Painemal, and J.S. Schlosser, 2024: Summarizing multiple aspects of triple collocation analysis in a single diagram. *Front. Remote Sens.*, **5**, 1395442, doi:10.3389/frsen.2024.1395442……197

133. **Sohl, L.E.**, T.J. Fauchez, S. Domagal-Goldman, D.A. Christie, R. Deitrick, J. Haqq-Misra, C.E. Harman, N. Iro, N.J. Mayne, **K. Tsigaridis**, G.L. Villanueva, A.V. Young, and G. Chaverot, 2024: The CUISINES framework for conducting exoplanet model intercomparison projects, version 1.0. *Planet. Sci. J.*, **5**, 175, doi:10.3847/PSJ/ad5830……....198

134. Song, C., D.T. McCoy, T. Eidhammer, A. Gettelman, I.L. McCoy, D. Watson-Parris, C.J. Wall, **G. Elsaesser**, and R. Wood, 2024: Buffering of aerosol-cloud adjustments by coupling between radiative susceptibility and precipitation efficiency. *Geophys. Res. Lett.*, **51**, no. 11, e2024GL108663, doi:10.1029/2024GL108663……199

135. Song, Q., P. Ginoux, M. Gonçalves Ageitos, **R.L. Miller**, **V. Obiso**, and C. Pérez García-Pando, 2024: Modeling impacts of dust mineralogy on Earth's radiation and climate. *Atmos. Chem. Phys.*, **24**, no. 12, 7421-7446, doi:10.5194/acp-24-7421-2024……200

136. Sparrman, V., S. Bladh, and **M.J. Way**, 2024: Multiple habitable phases on outer exosolar worlds. *Astrophys. J.*, **962**, no. 1, 83, doi:10.3847/1538-4357/ad1685……..…201

137. **Stanford, M.**, A.C. Varble, and H. Morrison, 2024: Evaluation of a stochastic mixing scheme in the deep convective gray zone using a tropical oceanic deep convection case study. *J. Adv. Model. Earth Syst.*, **16**, no. 1, e2023MS003748, doi:10.1029/2023MS003748……202

138. Steinbuks, J., Y. Cai, **J. Jaegermeyr**, and T.W. Hertel, 2024: Assessing effects of climate and technology uncertainties in large natural resource allocation problems. *Geosci. Model Dev.*, **17**, no. 12, 4791-4819, doi:10.5194/gmd-17-4791-202……..…203

139. Stephens, G.L., K.A. Shiro, M.Z. Hakuba, H. Takahashi, **J.A. Pilewskie**, T. Andrews, C.J. Stubenrauch, and L. Wu, 2024: Tropical deep convection, cloud feedbacks and climate sensitivity. *Surv. Geophys.*, **45**, no. 6, 1903-1931, doi:10.1007/s10712-024-09831-1…….....…204

140. Stuart, L., M. Hobbins, E. Neibuhr, **A. Ruane**, R. Pulwarty, A. Hoell, W. Thiaw, **C. Rosenzweig**, F. Muñoz-Arriola, M. Jahn, and M. Farrar, 2024: Enhancing global food security: Opportunities for the American Meteorological Society. *Bull. Amer. Meteorol. Soc.*, **125**, no. 4, E760-E777, doi:10.1175/BAMS-D-22-0106.1……205

141. Takahashi, H., **C.M. Naud**, D.J. Posselt, and G.A. Duffy, 2024: Systematic differences between the Northern and Southern Hemispheres: Warm frontal ice water path linked to the origin of extratropical cyclones. *J. Climate*, **37**, no. 8, 2491-2504, doi:10.1175/JCLI-D-23-0391.1……...……206

142. Tan, C., D.T. McCoy, and **G. Elsaesser**, 2024: Constraints on Southern Ocean shortwave cloud feedback from the hydrological cycle. *J. Geophys. Res. Atmos.*, **129**, no. 6, e2023JD040489, doi:10.1029/2023JD040489……..…207

143. Tan, I., M.D. Zelinka, Q. Coopman, B.H. Kahn, L. Oreopoulos, **G. Tselioudis**, D.T. McCoy, and N. Li, 2024: Contributions from cloud morphological changes to the interannual shortwave cloud feedback based on MODIS and ISCCP satellite observations. *J. Geophys. Res. Atmos.*, **129**, no. 8, e2023JD040540, doi:10.1029/2023JD040540…….....208

144. Thompson, D.R., R.O. Green, C. Bradley, P.G. Brodrick, N. Mahowald, E.B. Dor, M. Bennett, M. Bernas, N. Carmon, K.D. Chadwick, R.N. Clark, R.W. Coleman, E. Cox, E. Diaz, M.L. Eastwood, R. Eckert, B.L. Ehlmann, P. Ginoux, M.G. Ageitos, K. Grant, L. Guanter, D.H. Pearlshtien, M. Helmlinger, H. Herzog, T. Hoefen, **Y. Huang**, A. Keebler, O. Kalashnikova, D. Keymeulen, R. Kokaly, M. Klose, L. Li, S.R. Lundeen, J. Meyer, E. Middleton, **R.L. Miller**, P. Mouroulis, B. Oaida, **V. Obiso**, F. Ochoa, W. Olson-Duvall, G.S. Okin, T.H. Painter, C. Pérez García-Pando, R. Pollock, V. Realmuto, L. Shaw, P. Sullivan, G. Swayze, E. Thingvold, A.K. Thorpe, S. Vannan, C. Villarreal, C. Ung, D.W. Wilson, and S. Zandbergen, 2024: On-orbit calibration and performance of the EMIT imaging spectrometer. *Remote Sens. Environ.*, **303**, 113986, doi:10.1016/j.rse.2023.113986……..209

145. Towers, J., R. Leichenko, **C. Braneon**, D. Balk, L. Yoon, G. Wagner, J. Ventrella, J.K.W. Tchen, B. Rosenzweig, P. Orton, L. Ortiz, R. Moss, F. Montalto, T. McPhearson, K. McComas, P. Marcotullio, T. Matte, N. Maher, K. Knowlton, **R. Horton**, S. Foster, D. Bader, and A. Baptista, 2024: NPCC4: Climate risk and equity — Advancing knowledge toward a sustainable future — Conclusions. *Ann. New York Acad. Sci.*, **1539**, no. 1, 323-334, doi:10.1111/nyas.15150……210

146. Trotechaud, S., B. Tremblay, **J. Williams**, **J. Romanski**, **A. Romanou**, M. Bushuk, W. Merryfield, and R. Msadek, 2024: Predictability of the minimum sea ice extent from winter Fram Strait Ice Area Export: Model versus observations. *J. Climate*, **37**, no. 7, 2361-2377, doi:10.1175/JCLI-D-22-0931.1……..211

147. **Tselioudis, G.**, W.B. Rossow, F. Bender, L. Oreopoulos, and **J. Rémillard**, 2024: Oceanic cloud trends during the satellite era and their radiative signatures. *Clim. Dyn.*, **62**, no. 9, 9319-9332, doi:10.1007/s00382-024-07396-8……..212

148. Varnam, M., C.W. Hamilton, **I. Aleinov**, and J.J. Barnes, 2024: Composition and speciation of volcanic volatiles on the Moon. *Icarus*, **413**, 116009, doi:10.1016/j.icarus.2024.116009……213

149. Wang, S., Y. Qian, K. Yoshimura, **H. Bong**, C. Risi, Z. Wei, H. Pang, W. Xiao, S. Lei, M. Xing, P. Zhao, H. Wu, Y. Shi, D. Wang, and M. Zhang, 2024: Skill of isotope-enabled climate models for daily surface water vapour in East Asia. *Glob. Planet. Change*, **239**, 104502, doi:10.1016/j.gloplacha.2024.104502……....214

150. Watson, A., C. Birkel, S. Arciniega-Esparza, J. de Waal, J. Miller, Y. Vystavna, J. van Rooyen, A. Welham, **H. Bong**, K. Yoshimura, J. Helmschrot, A. Künne, and S. Kralisch, 2024: Evaluating input data sources for isotope-enabled rainfall-runoff models. *Hydrol. Process.*, **38**, no. 9, e15276, doi:10.1002/hyp.15276……215

151. Weiskopf, S., F. Isbell, M.I. Arce-Plata, M. Di Marco, M. Harfoot, J. Johnson, S.B. Lerman, B.W. Miller, T. Morelli, A. Mori, **E. Weng**, and S. Ferrier, 2024: Biodiversity loss reduces global terrestrial carbon storage. *Nat. Commun.*, **15**, no. 4354, doi:10.1038/s41467-024-47872-7……....216

152. Werapitiya, G., D. McCoy, **G. Elsaesser**, P. Field, and S. Rahimi, 2024: Meteorology modulates the impact of GCM horizontal resolution on underestimation of midlatitude ocean wind speeds. *Geophys. Res. Lett.*, **51**, no. 13, e2024GL108512, doi:10.1029/2024GL108512……217

153. Williams, A.S., J.L. Dedrick, L.M. Russell, **F. Tornow**, I. Silber, **A.M. Fridlind**, B. Swanson, P.J. DeMott, P. Zieger, and R. Krejci, 2024: Aerosol size distribution properties associated with cold-air outbreaks in the Norwegian Arctic. *Atmos. Chem. Phys.*, **24**, no. 20, 11791-11805, doi:10.5194/acp-24-11791-2024……...…218

154. Wilson, A.J., R.D. Bressler, **C. Ivanovich**, C. Tuholske, C. Raymond, **R.M. Horton**, A. Sobel, P. Kinney, T. Cavazos, and J.G. Shrader, 2024: Heat disproportionately kills young people: Evidence from wet-bulb temperature in Mexico. *Sci. Adv.*, **10**, no. 49, eadq3367, doi:10.1126/sciadv.adq3367……219

155. Winstrup, M., H. Ranndal, S.H. Larsen, S.B. Simonsen, **K.D. Mankoff**, R.S. Fausto, and L. Sandberg Sørensen, 2024: PRODEM: An annual series of summer DEMs (2019 through 2022) of the marginal areas of the Greenland Ice Sheet. *Earth Syst. Sci. Data*, **16**, no. 11, 5405-5428, doi:10.5194/essd-16-5405-2024……..…220

156. Wood, M., A. Khazendar, I. Fenty, **K.D. Mankoff**, A.T. Nguyen, K. Schulz, J.K. Willis, and H. Zhang, 2024: Decadal evolution of ice-ocean interactions at a large East Greenland glacier resolved at fjord scale with downscaled ocean models and observations. *Geophys. Res. Lett.*, **51**, no. 7, e2023GL107983, doi:10.1029/2023GL107983……221

157. Young, A., T. Robinson, J. Krissansen-Totton, E.W. Schwieterman, N. Wogan, **M. Way**, **L. Sohl**, G. Arney, C. Reinhard, M. Line, D. Catling, and J. Windsor, 2024: Inferring chemical disequilibrium biosignatures for proterozoic Earth-like exoplanets. *Nat. Astron.*, **8**, no. 1, 101-110, doi:10.1038/s41550-023-02145-z……222

158. Zhang, X., D.W. Waugh, I. Mitevski, **C. Orbe**, and L.M. Polvani, 2024: Decreased Northern Hemisphere precipitation from consecutive CO_2 doublings is associated with significant AMOC weakening. *Environ. Res. Clim.*, **3**, no. 4, 041005, doi:10.1088/2752-5295/ad929c……223

159. Zhang, Y., S. He, B. Wee, **A.N. LeGrande**, J. Wang, N. Goodkin, and X. Wang, 2024: Precipitation ^{17}O-excess altered during tropical convection: Evidence from monsoon cold surges in Singapore. *J. Geophys. Res. Atmos.*, **129**, no. 9, e2023JD040437, doi:10.1029/2023JD040437……...…224

160. Zheng, C., Y. Wu, M. Ting, and **C. Orbe**, 2024: Influence of atmospheric circulation on the interannual variability of transport from global and regional emissions into the Arctic. *Atmos. Chem. Phys.*, **24**, no. 12, 6965-6985, doi:10.5194/acp-24-6965-2024……225

161. **Zhou, T.**, **K.J. DallaSanta**, **C. Orbe**, **D.H. Rind**, **J.A. Jonas**, **L. Nazarenko**, **G.A. Schmidt**, and **G. Russell**, 2024: Exploring the ENSO modulation of the QBO periods with GISS E2.2 models. *Atmos. Chem. Phys.*, **24**, no. 1, 509-532, doi:10.5194/acp-24-509-2024……226

Frontiers Remote Sensing, vol. 5, 1397631, doi:10.3389/frsen.2024.1397631

Correction of cloud optical thickness retrievals from nadir reflectances in the presence of 3D radiative effects. Part I: Concept and tests on 3D RT simulations.

Alexandrov, M.D.[1,2], **B. Cairns**[1], C. Emde, and B. van Diedenhoven, 2024

NASA Goddard Institute for Space Studies, New York, NY, USA[1]
Department of Applied Physics and Applied Mathematics, Columbia University, New York, NY, USA[2]

Abstract. 3D effects cause substantial underestimation of cloud optical thickness (COT) in airborne and satellite retrievals based on 1D radiative transfer computations (such as in the case of widely used bi-spectral technique). For a single-layer isolated cloud we propose a simple linear correction of the retrieved COT with the renormalization factor dependent on the cloud's aspect ratio (the ratio between vertical and horizontal dimensions of the cloud). This is an empirical assumption which we successfully test using synthetic 3D RT data. We introduce a heuristic "block model" of 3D radiative effects and show that the functional form of the renormalization factor is consistent with the process of radiation escape from cloud sides in an essentially 3D geometry. We also extend the block model to the case of single-layer broken cloud field with radiative interaction between the neighboring clouds. In this case the

Introduction. Currently operational algorithms for satellite retrievals of cloud optical thickness (COT) and droplet size are based on bi-spectral measurements in absorbing and non-absorbing bands (Nakajima and King, 1990). Such algorithms are used, e.g., to generate data products based on the Moderate Resolution Imaging Spectroradiometer (MODIS) measurements (Platnick et al., 2003). Similar algorithm (along with its modified version relying on cloud droplet size derived from polarized reflectances) is also applied to measurements made by the airborne Research Scanning Polarimeter (RSP). These retrieval techniques have certain limitations owing to the influence of 3D structure of clouds (especially broken) on the reflected solar radiation, which is not accounted for in the look-up tables (LUTs) based on 1D radiative transfer models (Marshak et al., 2006; Zinner et al., 2010). The satellite data survey by Di Girolamo et al. (2010) found that the retrieved cloud reflectance is consistent with plane-parallel RT model only in 24% of cases, mostly limited to regions dominated by stratiform clouds at solar zenith angles less than 60° (for other regions or solar angles this frequency drops sharply to as low as a few percent). 3D radiative effects, such as escape of light through cloud sides and shadowing, can cause substantial underestimation of COT by 1D-RT-based retrieval techniques. Zhang and Platnick (2011) also reported significant overestimation of droplet size by the MODIS bispectral algorithm.

Correct COT is also important because of its role in calibration of the extinction coefficient fields computed using the tomographic technique designed by Alexandrov et al. (2021). The subjects of tomographic retrievals are isolated clouds such as Cu or CuCg (Tcu), which radiative properties are significantly impacted by 3D effects.

In this study (Part I of the series) we introduce the concept of linear correction of COTs of single-layer clouds retrieved using LUT based on 1D RT computations. This correction is simply multiplication of COT value by a renormalization factor depending on the cloud aspect ratio. We also present validation of this correction method based on 3D RT simulations. And finally, we provide theoretical justification of our technique based on a simple geometrical model, which allows for estimation of the effect of radiation escape through cloud sides on the cloud-top reflectance and subsequently on COT retrievals. We also extend this model designed for isolated cloud case to that for broken cloud field. In the upcoming Part II of the series we will present a comprehensive COT renormalization theory accounting for the relationship between reflectance and COT. We will also derive correction factors for essentially 3D (close to isotropic) scattering.

Climate Dynamics, vol. 62, issue no. 6, pp. 5351-5371, doi:10.1007/s00382-024-07166-6

Enhancing spatiotemporal reconstructions of hydroclimate variability across the Mediterranean during the last millennium.

Anchukaitis, K., R. Touchan, D. Meko, D. Kherchouche, S. Slimani, F. Sivrikaya, R. Ilmen, I. Mitsopoulos, J. Stephan, J. Attieh, F. Hasnaoui, J.J. Camarero, R. Sánchez-Salguero, F. Guibal, A. Piermattei, A. Christou, J. Krcmaric, and **B. Cook**[1], 2024

NASA Goddard Institute for Space Studies, New York, NY, USA[1]

Abstract. The Mediterranean region is projected to experience severe drying trends and more extreme hydroclimate events as a consequence of anthropogenic climate change over the next century. In some places this signal may have already emerged from natural variability, but uncertainty in long-term paleoclimate reconstructions can be a significant challenge to the detection of the influence of rising CO2 on droughts. Here we provide expanded context for recent and future hydroclimate changes with a new high-resolution (0.5o) spatial reconstruction of the Palmer Drought Severity Index (PDSI) using a tree-ring network that spans much of the last millennium. This network provides new perspective on the existing Old World Drought Atlas (OWDA) and allows us to characterize differences between OWDA and our reconstruction. In light of the uncertainties we identify, we also reexamine previous conclusions about the severity of recent droughts in the context of earlier centuries. We find that, in both the western Mediterranean and the Levant, recent dry periods remain the worst in at least the last 500 years, but our assessment of the significance and confidence in this finding is affected by differences in the tree-ring networks used for the reconstructions. Long millennium-length hydroclimate reconstructions in the Mediterranean do provide the opportunity to understand variability and trends in the hydroclimate of the region, but extant uncertainties arising from the existing tree-ring chronology network and methodological choices call attention to locations that require further proxy collection, chronology updates, and statistical scrutiny.

Introduction. Ongoing and future climate change is a global phenomenon, but it is projected to have a disproportionate impact on certain regions of the world, in particular the Mediterranean (Allen and Ingram 2002; Giorgi 2006; Christensen et al. 2007; García-Ruiz et al. 2011; Kelley et al. 2012a; Tuel and Eltahir 2020; Tramblay et al. 2020; Cook et al. 2020a; Douville et al. 2021; Cos et al. 2022). The region is projected to experience reductions in rainfall in all seasons that will be further exacerbated by the effects of higher temperatures on drought severity (García-Ruiz et al. 2011; Cook et al. 2014; Vicente-Serrano et al. 2014; Tramblay et al. 2020; Vicente-Serrano et al. 2020; Cook et al. 2020a). The risk of a severe megadrought event also increases in the future (Cook et al. 2020a; Stevenson et al. 2022). In some parts of the region the signal of anthropogenic influence on precipitation and drought may already be emerging from natural variability (Touchan et al. 2011; Kelley et al. 2012a, 2015; Cook et al. 2016; Seager et al. 2019).

However, the importance of internal variability at interannual to decadal scales, climate model limitations in simulating the complete range of precipitation processes, and the influence of various large-scale ocean–atmosphere dynamics all affect the robust detection and attribution of trends in Mediterranean drought (Altava-Ortiz et al. 2011; Kelley et al. 2012b; Barkhordarian et al. 2013; Mariotti et al. 2015; Anchukaitis et al. 2019; Seager et al. 2020; Suárez-Moreno et al. 2022). For instance, Kelley et al. (2012a) identified important differences between climate model simulations and the observed patterns of drying in the Mediterranean over the late 20th century, particularly in winter, a discrepancy that Kelley et al. (2012b) subsequently linked to the importance of internal climate variability. Observed drought patterns reflect a combination of the unforced internal variability and the forced response of the hydroclimate system (Cook et al. 2011; Suárez-Moreno et al. 2022). Mariotti et al. (2015) concluded that the signal of forced changes in precipitation in the region would emerge later in the century due to the influence of large internal climate system variability.

Nature Communications, vol. 15, issue no. 1, 7262, doi:10.1038/s41467-024-51555-8

Preseason maize and wheat yield forecasts for early warning of crop failure.

Anderson, W.[1], S. Shukla, J. Verdin, A. Hoell, C. Justice, B. Barker, K. Slinski[1], N. Lenssen, J. Lou, **B.I. Cook**[2,3], and A. McNally[1], 2024

NASA Goddard Space Flight Center, Greenbelt, MD, USA[1]
NASA Goddard Institute for Space Studies, New York, NY, USA[2]
Lamont-Doherty Earth Observatory, Palisades, NY, USA[3]

Abstract. Provided the considerable logistical challenges of anticipatory action and disaster response programs, there is a need for early warning of crop failures at lead times of six to twelve months. But crop yield forecasts at these lead times are virtually nonexistent. By leveraging recent advances in climate forecasting, we demonstrate that global preseason crop yield forecasts are not only possible but are skillful over considerable portions of cropland. Globally, maize and wheat forecasts are skillful at lead times of up to a year ahead of harvest for 15% and 30% of harvested areas, respectively. Forecasts are most skillful in Southeast Africa and Southeast Asia for maize and parts of South and Central Asia, Australia, and Southeast South America for wheat. Wheat forecasts, furthermore, remain skillful at lead times of over 18 months ahead of harvest in some locations. Our results demonstrate that the potential for preseason crop yield forecasts is greater than previously appreciated.

Introduction. Early warning systems that produce accurate and timely information provide vital decision support for effective humanitarian responses to food crises[1,2]. Many of the programs implemented by government and non-governmental organizations (NGOs) to anticipate and respond to food crises require months to plan and execute. Examples include the distribution of farming inputs and drought-tolerant seed ahead of the growing season, securing the funds needed for disaster response, procurement and distribution of food aid, and scaling up of nutrition assistance programs[3,4,5,6]. Anticipatory actions, such as the distribution of drought-tolerant seed varieties or switching to planting small grains on marginal lands instead of water-intensive crops can only be taken in advance of planting[3]. Even many disaster response policies, such as the shipment of in-kind food aid coming from the United States, to take one example, typically take around six months to reach target populations[4]. Likewise, the logistics of scaling up nutrition assistance programs can take months due to the time required to obtain the funds needed to finance such an operation, plan and conduct nutrition surveys to identify vulnerable populations, and set up food distribution sites in targeted regions[7]. Even in the absence of exceptional funding needs, routine funding mechanisms for disaster response programs require months of advanced planning[6].

Provided the considerable logistical challenges of anticipating and responding to disasters, there is a clear need for early warning information at lead times of six to twelve months. Crop yield forecasts made at these lead times could provide information on expected crop failures affecting the income of or food availability for vulnerable populations. But routine crop yield forecasts at lead times of a year do not currently exist. Research on crop yield forecast systems has been overwhelmingly focused on within-season forecasts, which are issued a few months prior to crop harvest, rather than preseason forecasts, which are issued prior to the start of the cropping season[8,9]. The primary utility of preseason forecast systems is that they issue forecasts several months earlier than within-season forecast systems[10].

Geophysical Research Letters, vol. 51, issue no. 3, e2023GL105805, doi:10.1029/2023GL105805.

Surface cloud warming increases as Fall Arctic sea ice cover decreases.

Arouf, A.[1], H. Chepfer, J.E. Kay, T. L'Ecuyer, and J. Lac, 2024

NASA Goddard Institute for Space Studies, New York, NY, USA[1]

Abstract. During the Arctic night, clouds regulate surface energy budgets through longwave warming alone. During fall, any increase in low-level clouds will increase surface cloud warming and could potentially delay sea ice formation. While an increase in clouds due to fall sea ice loss has been observed, quantifying the surface warming is observationally challenging. Here, we use a new observational data set of surface cloud warming at instantaneous 330 m × 90 m spatial resolution. By instantaneously co-locating surface cloud warming and sea ice observations in regions where sea ice varies, we find October large surface cloud warming values (>80 W m^{-2}) are much more frequent (∼+50%) over open water than over sea ice. Notably, in November large surface cloud warming values (>80 W m^{-2}) occur more frequently (∼+200%) over open water than over sea ice. These results suggest more surface warming caused by low-level opaque clouds in the future as open water persists later into the fall.

Introduction. Over the past 40 years, the Arctic has warmed nearly four times faster than the global average (Rantanen et al., 2022) and also lost sea ice, especially in late summer and early fall since the satellite record began (Stroeve et al., 2012). More summer melt and a longer melt season has long been known to lead to more shortwave absorption in the Arctic ocean and greater ocean warming (Manabe & Stouffer, 1980). Warming large areas of open water can influence the adjacent ice cover, contributing to further thinning and delaying sea ice freeze-up (Stroeve et al., 2012, 2014).

Enhanced surface longwave radiation due to increased water vapor and cloudiness may accelerate sea ice melt in early spring (Huang et al., 2019) and would delay sea ice freeze-up in fall (Morrison et al., 2018), resulting in a longer melt season. Cloud-sea ice interactions is exciting to study due to their complexity but still poorly understood. Therefore, it has been the focus of several recent studies (e.g., Kay & Gettelman, 2009; Li et al., 2023; Maillard et al., 2021; Morrison et al., 2018; Monroe et al., 2021; Taylor & Monroe, 2023; Taylor et al., 2015; Yu et al., 2019). Air-sea coupling during non-summer season promotes the formation of low-level liquid clouds above open water in response to sea ice loss (Kay & Gettelman, 2009). These low-level clouds affect surface radiative fluxes and may affect sea ice formation (e.g., Taylor & Monroe, 2023). Indeed, clouds radiatively warm the surface in the longwave by trapping upward longwave earth surface radiation that would otherwise escape the earth system. Conversely, clouds radiatively cool the surface in the shortwave by reflecting solar radiation back to space. Low-level clouds play a stronger influence on the surface energy budget both in the longwave and the shortwave because they are usually more opaque (supercooled clouds) (Kay & Gettelman, 2009; Shupe & Intrieri, 2004; Taylor et al., 2015). During Arctic summer over the ocean, the shortwave effect dominates over the longwave effect and clouds cool the surface. In all other seasons, clouds warm the surface and may enhance sea ice loss. On average overall, Arctic clouds warm the ocean surface (e.g., Boeke & Taylor, 2016; Intrieri et al., 2002; Kay & L'Ecuyer, 2013; Schweiger & Key, 1994).

In fall, previous studies (e.g., Monroe et al., 2021; Morrison et al., 2018; Taylor & Monroe, 2023; Yu et al., 2019) found more low-level liquid clouds over open water than over sea ice. However, quantifying the surface radiative impact of these low-level clouds formed over newly open water over the entire Arctic for more than a decade is challenging.

Automation in Construction, vol. 158, 105181, doi:10.1016/j.autcon.2023.105181

Efficient semi-supervised surface crack segmentation with small datasets based on consistency regularisation and pseudo-labelling.

Asadi Shamsabadi, E., **S.M.H. Erfani**[1], C. Xu, and D. Dias-da-Costa, 2024

NASA Goddard Institute for Space Studies, New York, NY, USA[1]

Abstract. Despite promising results in vision-based surface crack detection, data-driven approaches still suffer from the scarcity of rich labelled datasets. Such a limitation has hindered a wider practical application of detection models. To address this issue, a semi-supervised framework is proposed, capable of learning from a substantial amount of unlabelled data and achieving high accuracy, even when the available labelled datasets are of limited size. The framework is designed by tailoring supervised training, semi-supervised consistency regularisation, and self-training with certainty-based pseudo-labelling, resulting in a simple yet effective approach. Despite using only 2% of the total labelled Concrete and Asphalt datasets, the resulting mIoU was only 2.6% and 4.7%, respectively, lower than the best performance of the model trained on 100% of the labelled data. Remarkably, the designed framework assisted the model in approaching and even exceeding saturation levels with as little as 20% and 25% of the Concrete and Asphalt datasets.

Introduction. As one of the most common defects in infrastructures, cracks can considerably decrease the designed performance of structural components [1]. Cracks cause material discontinuities and reduce the load-bearing capacity of structures with risks to infrastructure assets. The ingress of chemicals through cracked sections may also impact the durability and further reduce service life [2,3]. Although preventing the initiation of cracks is often unfeasible, structures can be incrementally repaired to divert major failures and offset costs if damages are detected in the early stages [4]. In this regard, the advancements in drone technology could enable more regular and closely spaced inspections while undergoing automation, as novel frameworks have the potential to reach accuracy higher than humans in controlled settings [5].

The seemingly effortless generalisation of the human recognition system provides increased certainty in detecting structural defects [6]. Nonetheless, manual inspection is time-consuming, arduous, sometimes dangerous, and inefficient, particularly after disasters [7], [8], [9]. It is also commonly argued that human recognition may be influenced by particular skills and have inconsistencies [6]. The automation of defect detection with computer vision coupled with machine learning (ML) seems an effective way forward [10,11]. With deep learning in image processing, the low generalisation of traditional image processing methods in the presence of noise can be improved [12,13]; as a result, different ML-based frameworks have been deployed for crack detection [14], [15], [16], [17].

Initial works on vision-based detection adopted patch-based image classification approaches [18] that have limited capability in localising objects in large images; patch-based methods cannot provide pixel-level detection accuracy. Considering the importance of the geometry of the defects in ranking the condition of structural elements, semantic segmentation has gradually replaced patch-based approaches [19,20]. Research has assessed the ability of Convolutional Neural Network (CNN)-based models to detect cracks in asphalt, concrete, and masonry surfaces and confirmed their high accuracy in controlled environments [21], [22], [23], [24], [25]. CNN architectures, like fully convolutional networks (FCNs) [26], [27], [28], [29], U-Net [30], and DeepLabv3+ [22], have been examined for vision-based defect detection.

Frontiers in Marine Science, vol. 10, 1125137, doi:10.3389/fmars.2023.1125137

Atmospheric CO_2 emissions and ocean acidification from bottom-trawling.

Atwood, T.B., **A. Romanou**[1], T. DeVries, **P.E. Lerner**[1,2], J.S. Mayorga, D. Bradley, R.B. Cabral, **G.A. Schmidt**[1,2], and E. Sala, 2024

NASA Goddard Institute for Space Studies, New York, NY, USA[1]
Department of Applied Physics and Applied Mathematics, Columbia University, New York, NY, USA[2]

Abstract. Trawling the seafloor can disturb carbon that took millennia to accumulate, but the fate of that carbon and its impact on climate and ecosystems remains unknown. Using satellite-inferred fishing events and carbon cycle models, we find that 55-60% of trawling-induced aqueous CO_2 is released to the atmosphere over 7-9 years. Using recent estimates of bottom trawling's impact on sedimentary carbon, we found that between 1996-2020 trawling could have released, at the global scale, up to 0.34-0.37 Pg CO_2 yr^{-1} to the atmosphere, and locally altered water pH in some semi-enclosed and heavy trawled seas. Our results suggest that the management of bottom-trawling efforts could be an important climate solution.

Introduction. Marine sediments are thought to be the ultimate long-term carbon store; once buried below the active layer, organic carbon can remain unmineralized for millennia to eons (Burdige, 2007; LaRowe et al., 2020). However, disturbances to the seabed by human activities threaten the permanency of this marine carbon (Levin et al., 2020; Paradis et al., 2021). In the case of bottom trawling, heavy fishing gear that is dragged across the seafloor mixes and resuspends sediments, exposing 0.16-0.40 Pg C yr^{-1} of previously buried organic carbon to potential microbial degradation (Sala et al., 2021). However, the ultimate fate of this disturbed organic carbon stock is as yet unquantified, hampering our understanding of the effects that bottom trawling has on the global carbon cycle and the potential implications for climate policies.

The protection of organic carbon stored in marine sediments, plants, and animals has been identified as a powerful tool for tackling climate change (Hoegh-Guldberg et al., 2019). However, the uptake of ocean-based climate solutions has been slow due to prevailing climate policies and carbon markets that only recognize mitigation activities with measurable impacts on atmospheric emissions. The challenge with identifying ocean-based solutions under those current paradigms lies in the complexity of quantifying atmospheric emissions generated by anthropogenic activities that occur below the ocean's surface (Luisetti et al., 2020). Therefore, research addressing this challenge is crucial for discovering new opportunities that can harness the full potential of the ocean in contributing to mitigating climate change.

Here, we examined the fate of trawling-induced carbon released into the global ocean between 1996-2020 and under future scenarios, as well as estimated the fraction of CO_2 emitted to the atmosphere. To estimate trawling-induced CO_2 emissions, we used assumptions and data from Sala et al. (2021), the only study to date to estimate the global impact of trawling on CO_2 fluxes from marine sediments, and two classes of ocean circulation models: (I) the Ocean Circulation Inverse Model (OCIM; 2° resolution; Holzer et al., 2021) and (II) the NASA Goddard Institute for Space Studies (GISS) ModelE2.1 (1° x 1.25° ocean model resolution; Lerner et al., 2021). The latter was used in coupled climate simulations under two realizations: prescribed atmospheric CO_2 concentrations (GISScon) and prognostic atmospheric CO_2 based on anthropogenic emissions, the land and ocean sink, and benthic trawling (GISSemis; Ito et al., 2020).

Annals New York Academy Sciences, vol. 1539, issue no. 1, pp. 3-12, doi:10.1111/nyas.15149

NPCC4: Climate risk and equity — Advancing knowledge toward a sustainable future — Introduction.

Balk, D., **C. Braneon**[1], R. Leichenko, R. Moss, and J. Towers, 2024

NASA Goddard Institute for Space Studies, New York, NY, USA[1]

Abstract. This Introduction to NPCC4 provides an overview of the first three NPCC Reports and contextualizes NPCC4's deliberate decision to address justice, equity, diversity, and inclusion in its collective work and in its own practices, procedures, and methods of assessment. Next, it summarizes the assessment process, including greater emphasis on sustained assessment. Finally, it introduces the NPCC4 chapters and their scope.

Introduction. On December 19, 2019, the Mayor of New York appointed a group of five academics, researchers, and practitioners as co-chairs to lead the fourth New York City Panel on Climate Change. Providing expertise in climate science, engineering, social science, policy, design, and planning, the NPCC4 leadership team was convened with the ambition to support catalytic change during this next, and perhaps most crucial, decade of climate response in NYC. The co-chairs began meeting regularly with the Deputy Director for Climate Science and Risk Communication in the Mayor's Office of Resiliency,1 now the Mayor's Office of Climate and Environmental Justice (MOCEJ). Together, they established a set of goals for the assessment, including identifying near, intermediate, and long-term quantitative and qualitative climate trends; assessing potential impacts of climate change on the city's communities, vulnerable populations, public health, natural systems, critical infrastructure, and buildings; and expanding ways to use climate research to inform decision-making. From the outset, NPCC4 committed to strengthening participation by agencies and the public in the assessment process (see Section 4). The co-chairs and the Deputy Director then turned to identifying candidates to recommend to the mayor to complete the full panel, ensuring NPCC would meet its mandate to provide authoritative, actionable information on future climate change and its potential impacts in support of science-based decision-making by the City. However, between late December 2019 and June 2020, when the full panel was charged by the mayor, the novel SARS-CoV-2/COVID-19 pandemic emerged in full and, in a trauma that would lay bare the modern brutality of structural racism in the United States, George Floyd's murder in police custody was filmed in a live-streamed video that quickly spread worldwide. Other systemic shocks would follow, including an extreme rainfall and flooding event associated with the remnants of Hurricane Ida and the 13 deaths in NYC (and more than 45 deaths in the New York metropolitan region) that followed in its wake. As events continued to confirm that the context of the fourth assessment was shifting in real-time, the full panel went to work assuring NPCC4 would produce a report in support of the City's initiatives to build resilience and equity into climate adaptation.

The profound system-level shock of COVID-19 revealed additional challenges to the city's resilience that will likely be exacerbated by current and future climate change. Climate change, like COVID-19, demands the full attention and commitment of the city government and the cooperation of local, state, federal, and global government, NGO, and private entities alike. Layering the impacts of significant, and likely, climate-related system-level perturbations such as a hurricane or a sustained heat wave that threatens electrical grid capacity on top of a public health crisis, multiplies the complexity of the management challenge in the acute moment of impact, and complicates the long-term economic and ecological recovery. Advanced planning, dynamic and sustained adaptation, environmental and climate justice, as well as a commitment to ongoing assessment that reflects the state of emerging science are the hallmarks of a resilient city and the bedrock commitment of the NPCC.

Icarus, vol. 410, 115913, doi:10.1016/j.icarus.2023.115913

A study of Jupiter's UV Great Dark Spot and tropopause to stratosphere winds in the high northern latitudes as seen by Cassini imaging.

Barbara, J.M.[1,2], R.A. West[3], **A.D. Del Genio**[1], and J.A. Sinclair[3], 2024

NASA Goddard Institute for Space Studies, New York, NY, USA[1]
Autonomic Integra, LLC, Institute for Space Studies, New York, NY, USA[2]
NASA Jet Propulsion Laboratory, California Institute of Technology, Pasadena, USA[3]

Abstract. Images of Jupiter taken during the year 2000 Cassini flyby revealed the early stages and evolution of a high northern-latitude UV Great Dark Spot over a three-month period. They also provided a window on the circulation of Jupiter's polar stratosphere. Jupiter's rarely-detected UV Great Dark Spot (UVGDS) is unusual in several respects. It is an ephemeral feature, twice appearing as an oval with size and shape similar to Jupiter's Great Red Spot (GRS). Like the GRS, it is an anticyclonic feature. It is unlike the GRS in that: (1) A gas, and/or very small particles (radius < < 1 micro meter, of unknown composition but likely hydrocarbon) is responsible for its contrast with its surroundings; (2) It appears to be a shallow feature, confined to the stratosphere; (3) It evolves (moves in System III longitude, elongates and tilts) over a period of months; and (4) It may be produced by an auroral event as inferred by its proximity to the southern extent of Jupiter's main auroral oval. However, we did not identify a specific auroral trigger event. We measure the rotation rate for the UVGDS to have been ~20° per Earth day. To investigate the dynamical regime of this feature, we applied an automated cloud feature tracking algorithm to Cassini Imaging Science Subsystem images of Jupiter's northern hemisphere (30°N – 80°N) in the near-IR continuum, methane band, and ultraviolet filters. From these images we were able to derive zonal wind profiles from the middle troposphere cloud tops to the lower stratosphere and track the evolution of the UV Great Dark Spot. Differences in mean zonal wind speed between the continuum and methane band filters indicate a weakening of jets with altitude as far north as 75°N latitude at the altitudes sampled by these filters. We also observe notable differences between the ultraviolet and the other two filters: (1) Winds are significantly weaker and mostly westward in the ultraviolet relative to lower altitudes at all latitudes equatorward of 60°N latitude; (2) Poleward of 60°N latitude, winds observed in the ultraviolet may be faster than those observed in the continuum and methane bands, though we are less confident in this result as Jupiter's haze morphology and the lack of small, discrete, unambiguous trackable features present unique challenges to obtaining reliable mean zonal winds in the ultraviolet at high latitudes.

Introduction. Jupiter's Great Red Spot (GRS) is perhaps its most well-known feature because of its large size, observability to even small telescopes, and its longevity. It has attracted the attention of numerous investigators and is the subject of many publications. For the entirety of telescopic observations of Jupiter, it has been the largest cloud feature (Beebe et al., 1989). It is therefore remarkable that a dark oval with nearly the same size and shape as the GRS appeared in Hubble Space Telescope (HST) Wide Field and Planetary Camera 2 (WFPC2) images in 1997, as shown in Fig. 1 (West, 1999) and shown as a polar-projection mosaic shown in Fig. 5.13 of West et al. (2004). In West et al. (2004), the text pointing to Fig. 5.13 listed October, but the correct month is September.

Proceedings of the National Academy of Sciences of the USA, vol. 121, issue no. 33, e2407465121,
doi:10.1073/pnas.2407465121

Plants, insects and fungi fossils under the center of Greenland's ice sheet are evidence of ice-free times.

Bierman, P., H. Mastro, L. Corbett, E. Steig, C. Halsted, M. Caffee, A. Hidy, G. Balco, **D. Peteet**[1,2], O. Bennike, and B. Rock, 2024

NASA Goddard Institute for Space Studies, New York, NY, USA[1]
Lamont-Doherty Earth Observatory, Palisades, NY, USA[2]

Abstract. The persistence and size of the Greenland Ice Sheet (GrIS) through the Pleistocene is uncertain. This is important because reconstructing changes in the GrIS determines its contribution to sea level rise during prior warm climate periods and informs future projections. To understand better the history of Greenland's ice, we analyzed glacial till collected in 1993 from below 3 km of ice at Summit, Greenland. The till contains plant fragments, wood, insect parts, fungi, and cosmogenic nuclides showing that the bed of the GrIS at Summit is a long-lived, stable land surface preserving a record of deposition, exposure, and interglacial ecosystems. Knowing that central Greenland was tundra-covered during the Pleistocene informs the understanding of Arctic biosphere response to deglaciation.

Introduction. Although marine sediment provides information about long-term Greenland Ice Sheet (GrIS) history (1), terrestrial materials older than about 21 ka are scarce (2). Thus, the information needed to reconstruct the size of the GrIS over time is lacking. Analysis of marine sediment reveals the distribution of terrestrial ecosystems during interglacials, but it cannot provide high spatial resolution (3). In contrast, materials collected from below the GrIS record location-specific ice extent and climate, providing direct evidence for past ice sheet absence and biosphere response. For example, data from the 1966 Camp Century (CC) core in northwest Greenland elucidate retreat timing, glacial processes, and former tundra ecosystems within 150 km of the ice margin (4, 5). Because there is a wide range of ice-extent scenarios under which CC could be ice-free, that core provides little information about central Greenland, the thickest and largest part of the ice sheet, which dominates GrIS contributions to global sea level (Fig. 1*A*).

In 1993, the Greenland Ice Sheet Project 2 (GISP2) recovered the only basal material from central Greenland: 40 cm of erratic boulders, 8 cm of till, and 105 cm of rock (Fig. 1*B*) [6–8]. Analysis of sediment in the lowest basal ice revealed substantial organic carbon and nitrogen and meteoric ^{10}Be—consistent with limited erosion, long subaerial exposure, and the presence of soil [(9)]. A depth profile of cosmogenic nuclides from the GISP2 subglacial rock core indicated that central Greenland deglaciated at least once in the last 1.1 My (6). Summit.

Results. Purified quartz, isolated from sand in the till, had 32,820 ± 2,780 atoms g^{-1} ^{10}Be, 91,150 ± 18,290 g^{-1} ^{26}Al, and ^{26}Al/^{10}Be of 2.8 ± 0.6, indicative of no more than 2.0 ± 0.4 million years of burial after the last substantive near-surface exposure (Fig. 1*D*). When sieving the sediment (Fig. 2*A*), we found vegetation fragments (Fig. 2*B*) including a bud scale of *Salix* sp. (willow) and 129 megaspores of *Selaginella rupestris* (rock spike-moss) with interwoven reticulation. Some megaspores had a visible trilete scar (y-shaped suture) on the surface and others did not, a phenomenon common in *S. rupestris* (10). We also found a *Papaver* sect. *Scapiflora* (poppy) seed, 155 sclerotia of the soil fungus *Cenococcum geophilum*, and the remains of an insect leg and compound eye. We isolated seven pieces of angiosperm wood. In three wood samples, scanning electron microscopy showed vessel elements with simple perforation plates and large simple lateral wall pitting indicative of *Salix*. Helical wall thickenings suggest that this wood was from immature plants.

Nature Food, vol. 5, issue no. 12, pp. 1005-1013, doi:10.1038/s43016-024-01081-z

Improved alternate wetting and drying irrigation increases global water productivity.

Bo, Y., X. Wang, K.J. van Groenigen, B.A. Linquist, C. Müller, T. Li, J. Yang, **J. Jägermeyr**[1,2], Y. Qin, and F. Zhou, 2024

NASA Goddard Institute for Space Studies, New York, NY, USA[1]
Center for Climate Systems Research, Columbia University, New York, NY, USA[2]

Abstract. Rice is the staple food for half of the world's population but also has the largest water footprint among cereal crops. Alternate wetting and drying (AWD) is a promising irrigation strategy to improve paddy rice's water productivity—defined as the ratio of rice yield to irrigation water use. However, its global adoption has been limited due to concerns about potential yield losses and uncertainties regarding water productivity improvements. Here, using 1,187 paired field observations of rice yield under AWD and continuous flooding to quantify AWD effects (ΔY), we found that variation in ΔY is predominantly explained by the lowest soil water potential during the drying period. We estimate that implementing a soil water potential-based AWD scheme could increase water productivity across 37% of the global irrigated rice area, particularly in India, Bangladesh and central China. These findings highlight the potential of AWD to promote more sustainable rice production systems and provide a pathway toward the sustainable intensification of rice cultivation worldwide.

Introduction. Rice is the most irrigation-intensive cereal crop, accounting for 30% of global irrigation water use[1]. By 2050, a 50% to 60% increase in global rice production while a 15% increase in irrigation water use are required to feed the growing population[2], which will intensify water competition between agriculture and other sectors, threatening global rice supply[3]. Thus, saving water in rice cultivation is critical to ensure food security of nearly half the world's population with rice as its main staple food.

Alternate wetting and drying (AWD) is a promising and widely recommended water-saving irrigation strategy for paddy rice[4]. With AWD, irrigation water is applied to reflood the field a certain number of days after the subsidence of ponded water. The timing of re-flooding is a key management decision that could be determined by metrics of soil moisture status, such as volumetric or gravimetric water content, soil water potential or field water depth falling below a predetermined threshold[5,6]. Previous studies showed that AWD could reduce irrigation water use by approximately a quarter compared to continuous flooding[7] and might reduce rice yields in some circumstances (such as alkaline soils)[5,7]. Trade-offs between water saving and yield losses remain a fundamental obstacle for large-scale application of AWD. To avoid yield losses, several thresholds have been proposed. For example, the International Rice Research Institute (IRRI) recommends 15 cm below the ground surface (that is, −15 cm) as a safe threshold for the field water depth-based AWD scheme to avoid yield loss[5]. Also, two global meta-analyses indicated −15 to −20 kPa as safe thresholds for the soil water potential-based AWD scheme[6,7]. However, various case studies also reported varying safe threshold of soil water potential from −70 to −10 kPa across a wide range of global rice cultivation area[8,9]. This large variation in thresholds underlines that despite increasing research on AWD practices, a spatially explicit application guideline is still lacking. Resolving this challenge requires increased understanding of the factors driving variations in rice yield responses to AWD management practices.

In this Article, we synthesized 1,187 field observations of AWD-induced changes in rice yield (Δ*Y*) from 123 studies covering all major global rice baskets to identify the predominant driver of Δ*Y* (Supplementary Fig. 1). The observations in our dataset are up to 7 times larger as those in previous analyses[6,7,10,11] and include the field sites representing >80% of the climatic and edaphic covariate space across global irrigated rice area (Supplementary Table 1 and Supplementary Fig. 2).

Journal of Geophysical Research: Atmospheres, vol. 129, issue no. 1, e2023JD038719, doi:10.1029/2023JD038719

Process-based intercomparison of water isotope-enabled models and reanalysis nudging effects.

Bong, H.[1], A. Cauquoin, A. Okazaki, E.-C. Chang, M. Werner, Z. Wei, N. Yeo, and K. Yoshimura, 2024

NASA Goddard Institute for Space Studies, New York, NY, USA[1]

Abstract. The products from the Stable Water Isotope Intercomparison Group, Phase 2, are currently used for numerous studies, allowing water isotope model-data comparisons with various isotope-enabled atmospheric general circulation model (AGCMs) outputs. However, the simulations under this framework were performed using different parameterizations and forcings. Therefore, a uniform experimental design with state-of-the-art AGCMs is required to interpret isotope observations rigorously. Here, we evaluate the outputs from three isotope-enabled numerical models nudged by three different reanalysis products and investigate the ability of the isotope-enabled AGCMs to reproduce the spatial and temporal patterns of water isotopic composition observed at the surface and in the atmospheric airborne water. Through correlation analyses at various spatial and temporal scales, we found that the model's performance depends on the model or reanalysis we use, the observations we compare, and the vertical levels we select. Moreover, we employed the stable isotope mass balance method to conduct decomposition analyses on the ratio of isotopic changes in the atmosphere. Our goal was to elucidate the spread in simulated atmospheric column δ18O, which is influenced by factors such as evaporation, precipitation, and horizontal moisture flux. Satisfying the law of conservation of water isotopes, this budget method is expected to explain various fractionation phenomena in atmospheric meteorological and climatic events. It also aims to highlight the spreads in modeled isotope results among different experiments using multiple models and reanalyses, which are primarily dominated by uncertainties in moisture flux and precipitation, respectively.

Introduction. As humanity's greenhouse gas emissions have increased, atmospheric temperatures have risen, affecting the Earth's hydrological cycle. The escalation in emissions has changed the amount of water vapor the atmosphere can hold, thereby amplifying uncertainties in climate model simulations due to changes in linear or non-linear feedback processes in different regions. Understanding these uncertainties, which contribute to the spread of modeled variables, is crucial for improving the accuracy and reliability of climate projections. In the wake of climate change, the atmospheric circulation is undergoing significant shifts, making some regions wetter and others drier, leading to unprecedented weather and climatic phenomena. Such changes necessitate increasingly accurate tools for understanding and prediction.

To shed light on these complexities, stable oxygen and hydrogen isotopes in water ($H_2{}^{16}O$: 99.75%, $HD^{16}O$: 0.02%, $H_2{}^{18}O$: 0.20%, hereafter referred to as water isotopes) serve as a powerful tool for delving into these challenges. They are widely used in hydrological studies to document Earth's climate variability (Craig & Gordon, 1965; Dansgaard, 1964). The water isotopes possess nearly identical chemical properties to their counterparts but differ in mass. This unique feature makes them invaluable for inferring phase changes in environmental conditions, such as evaporation and condensation (Wright et al., 2009). This distinctive characteristic enables researchers to trace the trajectory of atmospheric moisture from its source to its various destinations (Aemisegger et al., 2014; Diekmann et al., 2021; Dütsch et al., 2018; Fiorella et al., 2018; Lewis et al., 2010; Nusbaumer & Noone, 2018; Sodemann et al., 2008).

Annals of the New York Academy of Sciences, vol. 1539, issue no. 1, pp. 13-48, doi:10.1111/nyas.15116

NPCC4: New York City climate risk information 2022 — Observations and projections.

Braneon, C.[1,2], L. Ortiz, **D. Bader**[1,2], N. Devineni, P. Orton, B. Rosenzweig, T. McPhearson, L. Smalls-Mantey, **V. Gornitz**[1,3], T. Mayo, **S. Kadam**[1,2], H. Sheerazi, E. Glenn, L. Yoon, **A. Derras-Chouk**[1], J. Towers, R. Leichenko, D. Balk, P. Marcotullio, and **R. Horton**[1,2,4], 2024

NASA Goddard Institute for Space Studies, New York, NY, USA[1]
Center for Climate Systems Research, Columbia University, New York, NY, USA[2]
Autonomic Integra, LLC, New York, NY, USA[3]

Abstract. New York City (NYC) faces many challenges in the coming decades due to climate change and its interactions with social vulnerabilities and uneven urban development patterns and processes. This New York City Panel on Climate Change (NPCC) report contributes to the Panel's mandate to advise the city on climate change and provide timely climate risk information that can inform flexible and equitable adaptation pathways that enhance resilience to climate change. This report presents up-to-date scientific information as well as updated sea level rise projections of record. We also present a new methodology related to climate extremes and describe new methods for developing the next generation of climate projections for the New York metropolitan region. Future work by the Panel should compare the temperature and precipitation projections presented in this report with a subset of models to determine the potential impact and relevance of the “hot model” problem. NPCC4 expects to establish new projections-of-record for precipitation and temperature in 2024 based on this comparison and additional analysis. Nevertheless, the temperature and precipitation projections presented in this report may be useful for NYC stakeholders in the interim as they rely on the newest generation of global climate models.

Introduction. New York City (NYC) faces many challenges in the coming decades due to climate change and its interactions with social vulnerabilities and uneven urban development patterns and processes. This New York City Panel on Climate Change (NPCC) report contributes to the Panel's mandate to advise the city on climate change and provide timely climate risk information that can inform flexible and equitable adaptation pathways that enhance resilience to climate change. This report presents up-to-date scientific information as well as updated sea level rise projections of record. We also present a new methodology related to climate extremes and describe new methods for developing the next generation of climate projections for the New York metropolitan region. Future work by the Panel should compare the temperature and precipitation projections presented in this report with a subset of models to determine the potential impact and relevance of the “hot model” problem. NPCC4 expects to establish new projections-of-record for precipitation and temperature in 2024 based on this comparison and additional analysis. Nevertheless, the temperature and precipitation projections presented in this report may be useful for NYC stakeholders in the interim as they rely on the newest generation of global climate models.

Key Message 1: Sea level is projected to rise for centuries and remain elevated for thousands of years. Glaciers and ice sheets combined are now the dominant contributors to global mean sea level rise (GMSLR). In the future, the cryosphere contributions will dominate, especially in higher GMSLR scenarios. Changes in ocean circulation, such as the Atlantic Meridional Overturning Circulation (AMOC), may also play an increasing role in the future. Coastal locations in the NYC metropolitan region continue to experience higher rates of relative sea level rise (SLR) as compared to the global mean, a trend that is generally expected to continue into the future. Projected SLR for NYC will exacerbate the destructive hazards posed by storm surges and cause more frequent high-tide flooding. Although many improvements have been made to protect neighborhoods and secure critical infrastructure in future floods, many neighborhoods remain vulnerable to coastal flooding. More research is needed on both the baseline storm surge hazard as well as its potential future changes.

Monthly Weather Review, vol.152, issue no. 12, pp. 2753-2769, doi:10.1175/MWR-D-24-0060.1

Lightning and radar measures of mixed phase updraft variability in tracked storms during the TRACER field campaign in Houston, Texas.

Bruning, E.C., K.N. Brunner, **M. van Lier-Walqui**[1,2], T. Logan, and T. Matsui, 2024

NASA Goddard Institute for Space Studies, New York, NY, USA[1]
Center for Climate Systems Research, Columbia University, New York, NY, USA[2]

Abstract. Properties of 7488 thunderstorms are summarized for June–September 2022 during the Tracking Aerosol Convection Interactions Experiment (TRACER) field campaign Houston, Texas, using polarimetric weather radar and VHF 3D Lightning Mapping Array data. Automated tracking of storms linked each instrument's measurements to a data-defined, time-evolving storm footprint. Within each storm, the depth and magnitude of episodic columns of radar differential reflectivity and specific differential phase quantified the prevalence of updrafts that activated mixed-phase precipitation pathways. Lightning measurements further distinguished the degree of rimed precipitation formation: the fraction of tracks with lightning varied from day to day and cells with lightning had stronger polarimetric columns. Track-level correlation of the lightning flash rate with radar polarimetric measures had substantial spread, showing that lightning provides an additional signal of mixed-phase precipitation processes that can complement future studies of thermodynamic and aerosol controls on cloud microphysics in the Houston region.

Introduction. Clouds, including precipitating deep cumulus convection and thunderstorms, are among the most uncertain processes in models of the climate system (Morrison et al. 2020b; Stephens et al. 2010) and among the most challenging and relevant phenomena to predict on weather forecast time scales (Stensrud et al. 2009). Thunderstorms are influenced by the thermodynamics of the atmosphere, large-scale dynamical forcing from weather systems, mesoscale boundaries such as sea breezes, and atmospheric composition. Each of these factors can also be influenced by urban areas (Shepherd 2013). Recognizing that the Houston, Texas, metropolitan area was influenced by all of these processes, the Tracking Aerosol Convection Interactions Experiment (TRACER) and Experiment of Sea Breeze Convection, Aerosols, Precipitation and Environment (ESCAPE) field campaigns (Jensen et al. 2019, 2022; Kollias et al. 2024) were conducted in 2021–22 to observe thunderstorms as they developed within and moved across this unique natural laboratory.

Background. The life cycle of isolated precipitating deep convection in the atmosphere has long been understood as a thunderstorm cell that typically lasts 20–30 min and begins with an updraft, followed by a downdraft and the cell's dissipation (Byers and Braham 1949). Any longer-lived complexes of storms result from a multicellular sequence of updrafts, often forced along rain-cooled outflow (a cold pool) that provides a low-level convergence to force new updrafts and sustain their life cycle. In environments without substantial wind shear, the up-scale mesoscale organization is rare (Weisman and Klemp 1982).

One possible model of atmospheric deep convection analogizes a thunderstorm updraft to a dry thermal plume, which is produced by a continuous point source of buoyancy and expands due to lateral entrainment (Squires and Turner 1962). These idealized plumes allow for the properties of turbulent deep convection to be treated in terms of their averages, making such plumes especially suitable for parameterization of deep convection.

In contrast to the steady-state plume model, observational studies have observed impulsive behavior in thunderstorm updrafts (Anderson 1960) that are more in line with the discrete, bubble-like idealization of convection as a spherical vortex (Levine 1959).

Bulletin of the American Meteorological Society, vol. 105, issue no. 7, pp. E1170-E1203, doi:10.1175/BAMS-D-23-0163.1

Predicting September Arctic sea ice: A multimodel seasonal skill comparison.

Bushuk, M., S. Ali, D.A. Bailey, Q. Bao, L. Batté, U.S. Bhatt, E. Blanchard-Wrigglesworth, E. Blockley, G. Cawley, J. Chi, F. Counillon, P.G. Coulombe, R.I. Cullather[1], F.X. Diebold, A. Dirkson, E. Exarchou, M. Göbel, W. Gregory, V. Guemas, L. Hamilton, B. He, S. Horvath, M. Ionita, J.E. Kay, E. Kim[1], N. Kimura, D. Kondrashov, Z.M. Labe, W. Lee, Y.J. Lee, C. Li, X. Li, Y. Lin, Y. Liu, W. Maslowski, F. Massonnet, W.N. Meier, W.J. Merryfield, H. Myint, J.C.A. Navarro, A. Petty, F. Qiao, D. Schröder, A. Schweiger, Q. Shu, M. Sigmond, M. Steele, J. Stroeve, N. Sun, S. Tietsche, M. Tsamados, K. Wang, J. Wang, W. Wang, Y. Wang, Y. Wang, **J. Williams[2]**, Q. Yang, X. Yuan, J. Zhang, and Y. Zhang, 2024

NASA Goddard Space Flight Center, Greenbelt, MD, USA[1]
NASA Goddard Institute for Space Studies, New York, NY, USA[2]

Abstract. This study quantifies the state of the art in the rapidly growing field of seasonal Arctic Sea ice prediction. A novel multi-model dataset of retrospective seasonal predictions of September Arctic Sea ice is created and analyzed, consisting of community contributions from 17 statistical models and 17 dynamical models. Prediction skill is compared over the period 2001–20 for predictions of pan-Arctic Sea ice extent (SIE), regional SIE, and local sea ice concentration (SIC) initialized on 1 June, 1 July, 1 August, and 1 September. This diverse set of statistical and dynamical models can individually predict linearly detrended pan-Arctic SIE anomalies with skill, and a multimodel median prediction has correlation coefficients of 0.79, 0.86, 0.92, and 0.99 at these respective initialization times. Regional SIE predictions have similar skill to pan-Arctic predictions in the Alaskan and Siberian regions, whereas regional skill is lower in the Canadian, Atlantic, and central Arctic sectors. The skill of dynamical and statistical models is generally comparable for pan-Arctic SIE, whereas dynamical models outperform their statistical counterparts for regional and local predictions. The prediction systems are found to provide the most value added relative to basic reference forecasts in the extreme SIE years of 1996, 2007, and 2012. SIE prediction errors do not show clear trends over time, suggesting that there has been minimal change in inherent sea ice predictability over the satellite era. Overall, this study demonstrates that there are bright prospects for skillful operational predictions of September Sea ice at least 3 months in advance.

Introduction. The rapid decline of summer Arctic Sea ice over the satellite era (Fig. 1) has led to increased socioeconomic activity in the region and an emerging need for skillful predictions of sea ice conditions (Jung et al. 2016; Wagner et al. 2020). Following the then-record-setting 2007 September Arctic Sea ice extent (SIE) minimum, a new research subfield emerged focused on scientific understanding of sea ice predictability and prediction. At the core of this research community has been the Sea Ice Outlook (SIO), which collects, analyzes, and synthesizes real-time seasonal predictions of September pan-Arctic SIE [Stroeve et al. (2014); see arcus.org/sipn/sea-ice-outlook]. From 2008 to the present, the SIO has collected predictions of September SIE initialized on 1 June, 1 July, and 1 August, months that span the summer Arctic melt season. The SIO began additionally collecting 1 September initialized predictions in 2021. The number of annual SIO submissions has grown steadily over time, with approximately 40 groups submitting predictions in recent years. These submissions are provided by an international community of polar scientists and employ a diverse mix of dynamical modeling, statistical, and heuristic approaches.

The Astronomical Journal, vol. 167, issue no. 5, 222, doi:10.3847/1538-3881/ad33c1

Hyper illumination of exoplanets: Analytical and numerical approaches.

Carter, J.L., R.D. Perera, and **M.J. Way**[1], 2024

NASA Goddard Institute for Space Studies, New York, NY, USA[1]

Abstract. This work describes the illumination of exoplanets whose orbits are close enough to their host star that the finite angular size of their host star causes hyper illumination, in which more than 50% of the planet receives light. Such exoplanets include the hot Jupiters KELT-9 b (64.5% illuminated) and Kepler-91 b (69.6% illuminated). We describe the geometry of three primary illumination zones: the fully illuminated zone, penumbral zone, and unilluminated zone. The integrals required to determine the incident radiation as a function of position from the substellar point on the exoplanet are explained and derived, and the analytical solution is presented within the fully illuminated zone. We find that the illumination predicted by our model is greater at the substellar point than the typical plane-parallel ray model used would suggest. In addition, it is greater within the region of the penumbral zone extending into the antistellar side of the exoplanet. Finally, we compare our model to that used in starry, an open-source software package used to create albedo maps. It appears that starry may be overestimating the illumination of closely orbiting exoplanets because the foreshortening of the area element of the host star is not included in its calculation.

Introduction. Over 5000 exoplanets have been discovered and characterized using a variety of methods, including precise photometric data from instruments such as Kepler, which allow researchers to estimate planetary parameters such as albedo and temperature. 5 To do so, scientists must first create mathematical models of the system in question. In this work, we concern ourselves with the modeling of the illumination of an exoplanet. The illumination of an exoplanet by its host star determines its atmospheric characteristics by contributing to the energy balance of the atmosphere, and the light reflected and absorbed by the planet.

For most exoplanetary systems, it is sufficient to assume that the planet is far enough away from its host star that its rays arrive as plane-parallel rays, as shown in Figure 1. In which case, the illumination of the exoplanet is greatest at the substellar point and decreases with the cosine of the zenith angle (Cowan et al. 2013, Equation (38)). Many methods of modeling the phase curve of exoplanets for the purposes of parameter estimation and albedo mapping make use of this assumption (Madhusudhan & Burrows 2012; Farr et al. 2018; Haggard & Cowan 2018; Berdyugina & Kuhn 2019; Kawahara 2020; Heng et al. 2021; Teinturier et al. 2022). The assumption has also been used in ocean glint studies by comparing a planet's apparent albedo at different orbital phases (Lustig-Yaeger et al. 2018). It is also implemented as part of 1D climate modeling code, such as PICASO (Batalha et al. 2019), and 3D climate modeling code such as ROCKE-3D (Way et al. 2017) and the Community Atmosphere Model (Neale et al. 2010; Wolf 2017).

Yet, for exoplanets that orbit very close to their host star the plane-parallel ray illumination assumption breaks down due to the finite angular size of the star and its area elements, and the presence of penumbral effects. Here, we define such exoplanets as being hyper illuminated. In Lillo-Box et al. (2014), the authors note that the hot Jupiter Kepler-91 b was approximately 70% illuminated due to its proximity to its host star. In addition, Guillot (2010) note that the use of the plane-parallel ray approximation would result in an overestimation of the dayside/nightside temperature difference for exoplanets experiencing more than 50% illumination. In Léger et al. (2011), the authors compare the modeled temperature distribution of CoRot-7 b using the plane-parallel ray approximation to a model that accounts for the finite angular size of its host star in their Figure 4, noting that the temperature effects within the penumbral region are significant. To correctly characterize such exoplanets, the spherical and finite angular size of an exoplanet's host star must be taken into account, as demonstrated in Knuth et al. (2017) and Carter (2018).

Remote Sensing Environment, vol. 303, 113982, doi:10.1016/j.rse.2023.113982

Mineral dust optical properties for remote sensing and global modeling: A review.

Castellanos, P.[1], P. Colarco[1], W.R. Espinosa[1], S.D. Guzewich[1], R.C. Levy[1], **R.L. Miller[2]**, M. Chin[1], R.A. Kahn[1], O. Kemppinen[1], H. Moosmüller, E.P. Nowottnick[1], A. Rocha-Lima, M.D. Smith[1], J.E. Yorks[1], and H. Yu[1], 2024

NASA Goddard Space Flight Center, Greenbelt, MD, USA[1]
NASA Goddard Institute for Space Studies, New York, NY, USA[2]

Abstract. Dust plays a key role in many Earth system processes and is ubiquitous in the Martian atmosphere. Various intensive field campaigns, laboratory analyses, space-based remote sensing missions, and global modeling efforts aim to characterize dust optical properties. This is a bountiful time for dust scientists, and yet the interpretation of retrievals and comparison to models remains complicated by various conflicting assumptions that are part of each algorithm. For example, the conversion of satellite radiance measurements into products like aerosol optical depth for model evaluation depends upon aerosol properties like particle size and shape that are often prescribed and not part of the retrieval. Conversely, the model calculation of aerosol optical depth often uses different assumptions. The goal of this review is to first document algorithmic assumptions by various satellite retrieval products and models and identify where there is consistency and where there are differences. In general, the differences documented in this paper reflect uncertainties resulting from incomplete observational characterization of dust aerosols and limitations in our understanding.

Second, we note what observations might reduce uncertainties in our knowledge and bring greater consistency to retrievals and models, allowing for a more rigorous and harmonious comparison. The lack of comprehensive and realistic shape models for dust is an outstanding issue, such that closure between forward modeling from particle refractive index, shape, and size and observed optical properties cannot be achieved. Limitations in the computational methods that must be applied to model scattering from complex shapes also makes accurate optical modeling for dust challenging. Field observations indicate the persistence of coarse and giant dust particles at higher altitudes and farther downwind from their source than previously expected. Remote sensing retrieval algorithms based on observations at visible wavelengths have limited sensitivity to these particles and generally do not consider them, although a recent product based on longwave radiances is encouraging.

Current measurements of the refractive index of bulk dust and fundamental dust minerology components such as hematite vary widely, inhibiting attempts to represent the variability in dust optical properties and forcing, as expected from different major dust source regions on Earth that have varying mineralogical composition. Some remote sensing retrieval algorithms allow for limited refractive index variability in their inversion solutions through mixing with other fine mode aerosol models, or optimizing the single scattering albedo, but Earth system models surveyed for this paper assume a globally uniform, size-invariant refractive index. Although no Martian dust samples have yet been returned to Earth, remote sensing observations indicate that Martian dust is globally homogenous in composition, and a single spectral refractive index assumption has been widely adopted to represent Martian dust.

The lack of comprehensive, statistically representative measurements of dust particle microphysical properties (size distribution, morphology, complex index of refraction spectra, internal structure heterogeneity), and the resulting optical properties, limits our ability to verify the fidelity of these assumptions. A chain of measurements is needed, ranging from characterizing individual dust mineralogy components (e.g., pure hematite and goethite) to in situ sampling of complex atmospheric aerosol mixtures. Such results could be applied to both remote sensing retrievals that characterize the optical properties of the total aerosol burden in the atmosphere from total radiance measurements, and to global models that represent the total aerosol burden in the atmosphere by building it up from the balance of individual aerosol sources and sinks.

Communications Earth & Environment, vol. 5, issue no.181, doi:10.1038/s43247-024-01339-1



Observational constraint on a feedback from supercooled clouds reduces projected warming uncertainty.

Cesana, G.[1,2], **A. Ackerman**[1], **A. Fridlind**[1], I. Silber, **A. Del Genio**[1,3], M. Zelinka, H. Chepfer, T. Khadir, and R. Roehrig, 2024

NASA Goddard Institute for Space Studies, New York, NY, USA[1]
Center for Climate Systems Research, Columbia University, New York, NY, USA[2]
Department of Applied Physics and Applied Mathematics, Columbia University, New York, NY, USA[3]

Abstract. The increase of carbon-dioxide-doubling-induced warming (climate sensitivity) in the latest climate models is primarily attributed to a larger extratropical cloud feedback. This is thought to be partly driven by a greater ratio of supercooled liquid-phase clouds to all clouds, termed liquid phase ratio. We use an instrument simulator approach to show that this ratio has increased in the latest climate models and is overestimated rather than underestimated as previously thought. In our analysis of multiple models, a greater ratio corresponds to stronger negative cloud feedback, in contradiction with single-model-based studies. We trace this unexpected result to a cloud feedback involving a shift from supercooled to warm clouds as climate warms, which corresponds to greater cloud amount and optical depth and weakens the extratropical cloud feedback. Better constraining this ratio in climate models – and thus this supercooled cloud feedback – impacts their climate sensitivities by up to 1 ˚C and reduces inter-model spread.

Introduction. In response to climate warming, statistically more liquid phase clouds and fewer ice clouds are likely. For the same mass of condensate, liquid phase clouds are more reflective than ice clouds, and they tend to precipitate less efficiently. Since a warmer climate favors more liquid phase clouds, this implies that warming will lead to clouds with greater optical depth[1,2,3] and spatial coverage[1,2,3]. As a result, the solar radiation reflected back to space would be greater, weakening the initial warming, a negative cloud feedback commonly referred to as the "cloud phase feedback"[3,4,5]. Although this feedback has not been explicitly characterized in climate models to date, it is hypothesized to substantially affect the strength of the negative cloud optical depth feedback and that of the negative cloud amount feedback to a lesser degree[4,5] – two feedbacks that are well documented in Earth System Models (ESM). The magnitude of these two modeled feedbacks, while largely unconstrained by observations, is maximum in the extratropics, particularly over the Southern Ocean[6,7,8,9]. This is because mixed-phase temperatures, i.e., temperatures at which both liquid and ice can exist ($0\ ^{\circ}\mathrm{C} > T \gtrsim -40\ ^{\circ}\mathrm{C}$), are omnipresent in the troposphere at these latitudes. In addition to its connection to precipitation processes[1,10], the optical depth feedback seems to depend on the presence of supercooled liquid relative to total cloud water at mixed-phase temperatures. The overall weakening of this negative feedback in the extratropics in present generation Coupled Model Intercomparison Project phase 6 (CMIP6) models relative to the previous CMIP5 models has contributed to increased CMIP6 equilibrium climate sensitivity[9] (ECS) estimates (including their upper range)[9], making them substantially larger than values derived from independent lines of evidence[11,12].

Given the crucial role of supercooled clouds in projected warming, recent efforts have been devoted to evaluating cloud phase in ESMs and studying the relationship between Liquid Phase Ratio (LPR) and cloud feedback. Some studies have reported a link between increased liquid water mass relative to all condensed water ($\mathrm{LPR_{mass}}$) in the current climate and reduced negative optical depth feedback in individual ESMs[13,14,15].

Atmospheric Chemistry and Physics, vol. 24, issue no. 13, pp. 7899-7909, doi:10.5194/acp-24-7899-2024

The correlation between Arctic sea ice, cloud phase and radiation using A-train satellites.

Cesana, G.V.[1,2], **O. Pierpaoli**[1], **M. Ottaviani**[1,3], **L. Vu**[1], and **Z. Jin**[1], 2024

NASA Goddard Institute for Space Studies, New York, NY, USA[1]
Center for Climate Systems Research, Columbia University, New York, NY, USA[2]
Terra Research Inc., Hoboken, NJ, USA[3]

Abstract. Climate warming has a stronger impact on Arctic climate and sea ice cover (SIC) decline than previously thought. Better understanding and characterization of the relationship between sea ice and clouds and the implications for surface radiation is key to improving our confidence in Arctic climate projections. Here we analyze the relationship between sea ice, cloud phase and surface radiation over the Arctic, defined as north of 60° N, using active- and passive-sensor satellite observations from three different datasets. We find that all datasets agree on the climatology of and seasonal variability in total and liquid-bearing (liquid and mixed-phase) cloud covers. Similarly, our results show a robust relationship between decreased SIC and increased liquid-bearing clouds in the lowest levels (below 3 km) for all seasons (strongest in winter) but summer, while increased SIC and ice clouds are positively correlated in two of the three datasets. A refined map correlation analysis indicates that the relationship between SIC and liquid-bearing clouds can change sign over the Bering, Barents and Laptev seas, likely because of intrusions of warm air from low latitudes during winter and spring. Finally, the increase in liquid clouds resulting from decreasing SIC is associated with enhanced radiative cooling at the surface. Our findings indicate that the newly formed liquid clouds reflect more shortwave (SW) radiation back to space compared to the surface, generating a cooling effect of the surface, while their downward longwave (LW) radiation is similar to the upward LW surface emission, which has a negligible radiative impact on the surface. This overall cooling effect should contribute to dampening future Arctic surface warming as SIC continues to decline.

Introduction. Clouds can have different radiative effects over the Arctic (Curry et al., 1996; Shupe and Intrieri, 2004), defined as north of 60° N: cooling in summer generated by sunlight reflection and warming in winter through longwave (LW) radiative heating of the surface. In a region where the warming can be up to 4 times larger than in the rest of the world (Boeke and Taylor, 2018), it is crucial to determine how clouds respond to climate change and whether their feedback will enhance or dampen the warming. While cloud feedback was shown to play a minor role in polar amplification in CMIP5 (Pithan and Mauritsen, 2014; Middlemas et al., 2020), studies using the most recent climate model generation (CMIP6) unveil a strong impact of extratropical mixed-phase clouds on global climate (Zelinka et al., 2020). Part of the uncertainty in determining cloud variability in polar regions stems from the extent to which Arctic clouds respond to sea ice loss (e.g., Kay and Gettelman, 2009; Morrison et al., 2018; Taylor and Monroe, 2023), which is still debated. Within the context of substantial decrease in sea ice extent over the past few decades (Kim et al., 2023), determining how clouds may be affected by this tremendous change is necessary to simulate realistic projections of polar climate.

The analysis of various observational datasets has led to consensus on the sensitivity of cloud fraction to sea ice extent variability in the fall but not in the summer (Kay and Gettelman, 2009; Morrison et al., 2018). As the sea ice cover (SIC) decreases in the fall, the cloud fraction increases, mostly attributable to low-level liquid clouds (Morrison et al., 2018). A more recent study also found a larger cloud fraction over open ocean than over sea ice in winter and spring (Taylor and Monroe, 2023). In general, these studies try to better understand the relationship between sea ice and clouds at the process level and show that clouds are most likely controlled by air–surface coupling.

Journal of the Atmospheric Sciences, vol. 81, issue no. 10, pp. 1725-1747, doi:10.1175/JAS-D-23-0203.1

Microphysical evolution in mixed-phase midlatitude marine cold-air outbreaks.

Chellappan, S., P. Zuidema, S. Kirschler, C. Voigt, **B. Cairns**[1], E.C. Crosbie, R. Ferrare[2], J. Hair[2], D. Painemal, T. Shingler[2], M. Shook[2], K.L. Thornhill[2], **F. Tornow**[1], and A. Sorooshian, 2024

NASA Goddard Institute for Space Studies, New York, NY, USA[1]
NASA Langley Research Center, Hampton, VA, USA[2]

Abstract. Five cold-air outbreaks are investigated with aircraft offshore of continental northeast America. Flight paths aligned with the cloud-layer flow from January through March span cloud-top temperatures from −5° to −12°C, in situ liquid water paths of up to 500 g m^{-2}, while in situ cloud droplet number concentrations exceeding 500 cm^{-3} maintain effective radii below 10 μm. Rimed ice is detected in the four colder cases within the first cloud pass. After further fetch, ice particle number concentrations reaching 2.5 L^{-1} support an interpretation that secondary ice production is occurring. Rime splintering is clearly evident, with dendritic growth increasing ice water contents within deeper clouds with colder cloud-top temperatures. Buoyancy fluxes reach 400–600 W m^{-2} near the Gulf Stream's western edge, with 1-s updrafts reaching 5 m s^{-1} supporting closely spaced convective cells. Near-surface rainfall rates of the three more intense cold-air outbreaks are a maximum near the Gulf Stream's eastern edge, just before the clouds transition to more open-celled structures. The milder two cold-air outbreaks transition to lower-albedo cumulus with little or no precipitation. The clouds thin through cloud-top entrainment.

Introduction. Cold-air outbreaks (CAOs) off of the eastern U.S. seaboard provide dramatic visual examples of cloud morphology, with cloud streets and closed-cell circulations transitioning to more open-celled or thinner cloud structures with fetch. The CAOs typically occur behind cold fronts, suppressed by upper-level subsidence within the trough and trough-to-ridge portions of eastward-moving midlatitude cyclones (Painemal et al. 2023). Coastal northerly winds turning eastward support strong moisture and heat fluxes off of the warm Gulf Stream (GS). The sea surface temperature (SST) gradient to the cold nearshore Labrador Current further encourages secondary mesoscale circulations that aid cloud deepening (Liu et al. 2014; Naud et al. 2020).

Outflow of urban anthropogenic pollution elevates the cloud condensation nucleus (CCN) concentrations and cloud droplet number concentrations N_d (Corral et al. 2021; Dadashazar et al. 2021; Kirschler et al. 2022; Gryspeerdt et al. 2022). Space-based characterizations indicate supercooled liquid, wherein produced ice can become melting snow (Field and Heymsfield 2015; Mülmenstadt et al. 2015; Matus and L'Ecuyer 2017). The precipitation in turn can alter the cloud morphology (Abel et al. 2017; Field et al. 2017). Mixed-phase CAOs represent a modeling challenge in that the small-scale microphysical and turbulence processes must be accurately represented as well as the larger-scale synoptics. Interest in improving the understanding, modeling, and prediction of mixed-phase CAOs for both weather and climate has motivated multiple recent observational campaigns (Wendisch et al. 2019; McFarquhar et al. 2021; Geerts et al. 2022).

We contribute to this growing literature with detailed fetch-following characterizations of five winter days with CAOs over the northwest Atlantic (Table 1), using aircraft measurements from the NASA Earth Venture Suborbital-3 Aerosol Cloud Meteorology Interactions over the Western Atlantic Experiment (ACTIVATE; Sorooshian et al. 2019), held from 2020 through 2022. A major observational strategy was to fly a high and low plane, both at speeds of ~120 m s^{-1}, within 5 min and 6 km of each other (Sorooshian et al. 2023). The low-flying Langley Falcon HU-25 plane followed a set flight pattern (Fig. 1) to collect in situ cloud and aerosol microphysical measurements.

Nature Review & Earth Environment, vol. 5, issue no. 4, pp. 232-234, doi:10.1038/s43017-024-00539-9

Ocean heat content in 2023.

Cheng, L.[1], K. von Schuckmann, A. Minière, M.Z. Hakuba[1], S. Purkey, **G.A. Schmidt[1]**, and Y. Pan, 2024

NASA Jet Propulsion Laboratory, California Institute of Technology, Pasadena, CA, USA[1]
NASA Goddard Institute for Space Studies, New York, NY, USA[2]

Abstract. In 2023, global full-depth ocean heat content (OHC) reached a record increase of 464 ± 55 ZJ since 1960, with strong heat gain observed in the Southern and Atlantic Oceans. OHC was 16 ± 10 ZJ higher than in 2022, continuing the long-term increasing trend that started in 1960.

Introduction. Rice is the most irrigation-intensive cereal crop, accounting for 30% of global irrigation water use[1]. By 2050, a 50% to 60% increase in global rice production while a 15% increase in irrigation water use are required to feed the growing population[2], which will intensify water competition between agriculture and other sectors, threatening global rice supply[3]. Thus, saving water in rice cultivation is critical to ensure food security of nearly half the world's population with rice as its main staple food.

Alternate wetting and drying (AWD) is a promising and widely recommended water-saving irrigation strategy for paddy rice[4]. With AWD, irrigation water is applied to reflood the field a certain number of days after the subsidence of ponded water. The timing of re-flooding is a key management decision that could be determined by metrics of soil moisture status, such as volumetric or gravimetric water content, soil water potential or field water depth falling below a predetermined threshold[5,6]. Previous studies showed that AWD could reduce irrigation water use by approximately a quarter compared to continuous flooding[7] and might reduce rice yields in some circumstances (such as alkaline soils)[5,7]. Trade-offs between water saving and yield losses remain a fundamental obstacle for large-scale application of AWD. To avoid yield losses, several thresholds have been proposed. For example, the International Rice Research Institute (IRRI) recommends 15 cm below the ground surface (that is, −15 cm) as a safe threshold for the field water depth-based AWD scheme to avoid yield loss[5]. Also, two global meta-analyses indicated −15 to −20 kPa as safe thresholds for the soil water potential-based AWD scheme[6,7]. However, various case studies also reported varying safe threshold of soil water potential from −70 to −10 kPa across a wide range of global rice cultivation area[8,9]. This large variation in thresholds underlines that despite increasing research on AWD practices, a spatially explicit application guideline is still lacking. Resolving this challenge requires increased understanding of the factors driving variations in rice yield responses to AWD management practices.

In this Article, we synthesized 1,187 field observations of AWD-induced changes in rice yield (ΔY) from 123 studies covering all major global rice baskets to identify the predominant driver of ΔY (Supplementary Fig. 1). The observations in our dataset are up to 7 times larger as those in previous analyses[6,7,10,11] and include the field sites representing >80% of the climatic and edaphic covariate space across global irrigated rice area (Supplementary Table 1 and Supplementary Fig. 2). Our overall objectives were to (1) identify the predominant driver of variation in ΔY, (2) develop a spatially explicit AWD scheme to avoid yield loss and improve water productivity (that is, the ratio of rice yield to irrigation water use) and (3) determine the priority areas for implementing the spatially explicit AWD scheme.

Journal of Advances in Modeling Earth Systems, vol. 16, issue no. 3, e2023MS003952, doi:10.1029/2023MS003952

Influence of more mechanistic representation of particle dry deposition on historical changes in global aerosol burdens and radiative forcing.

Clifton, O.E.[1,2], **S.E. Bauer**[1], **K. Tsigaridis**[1,2], **I. Aleinov**[1,2], **T.G. Cowan**[1,3], **G. Faluvegi**[1,2], and **M. Kelley**[1], 2024

NASA Goddard Institute for Space Studies, New York, NY, USA[1]
Center for Climate Systems Research, Columbia University, New York, NY, USA[2]
Autonomic Integra, LLC., New York, NY, USA[3]

Abstract. Robust estimates of historical changes in aerosols are key for accurate constraints on climate sensitivity. Dry deposition is a primary sink of aerosols from the atmosphere. However, most global climate models do not accurately represent observed strong dependencies of dry deposition following turbulent transport on aerosol size. It is unclear whether there is a substantial impact of mischaracterized aerosol deposition velocities on historical aerosol changes. Here we describe improved mechanistic representation of aerosol dry deposition in the NASA Goddard Institute for Space Studies (GISS) global climate model, ModelE, and illustrate the impact on 1850–2000 changes in global aerosol burdens as well as aerosol direct and cloud albedo effects using a set of 1850 and 2000 time slice simulations. We employ two aerosol configurations of ModelE (a "bulk" mass-based configuration and a configuration that more explicitly represents aerosol size distributions, internal mixing, and microphysics) to explore how model structural differences in aerosol representation alter the response to representation of dry deposition. Both configurations show larger historical increases in the global burdens of non-dust aerosols with the new dry deposition scheme, by 11% in the simpler mass-based configuration and 23% in the more complex microphysical configuration. Historical radiative forcing responses, which vary in magnitude from 5% to 12% as well as sign, depend on the aerosol configuration.

Introduction. Aerosols (or particles) influence climate by scattering or absorbing solar radiation and influencing cloud formation and lifetimes. Preindustrial-to-present increases in aerosol abundances have had a net cooling effect on climate, which has offset warming from increases in greenhouse gases. However, the magnitude of the net cooling effect from aerosols is highly uncertain (Bellouin et al., 2020; Myhre et al., 2013; Szopa et al., 2021), challenging accurate constraints on the global climate sensitivity from observations. Better constraints on processes governing the distributions and fate of aerosols are needed to advance predictive ability of aerosol impacts on climate (Kinne et al., 2003; Szopa et al., 2021).

Dry deposition occurs when particles are transported to the Earth's surface via turbulence (hereinafter, "turbulent" dry deposition) or gravitational settling and then stick to surfaces. Regional and global chemical transport and climate models largely employ crude approaches for estimating aerosol dry deposition (Fanourgakis et al., 2019; Textor et al., 2006). Most previous work tends to focus on wet deposition of aerosols, which is the larger sink globally, and has considered dry deposition less important, especially in considering decadal changes (e.g., Fuzzi et al., 2015). However, there has always been the question of how well do we need to understand particle dry deposition (Penner et al., 1994). Further, model intercomparison studies highlight the need to perform analyses investigating different dry deposition schemes (Galmarini et al., 2021), especially how particle size distributions play a role in differences (Textor et al., 2006).

Journal of Climate, vol 37, issue no. 17, pp. 4389-4401, doi:10.1175/JCLI-D-23-0773.1

Characterizing the 2010 Russian heatwave-Pakistan flood concurrent extreme over the last millennium using the Great Eurasian Drought Atlas.

Cook, B.I.[1,2], E.R. Cook[2], K.J. Anchukaitis[2], and D. Singh, 2024

NASA Goddard Institute for Space Studies, New York, NY, USA[1]
Lamont-Doherty Earth Observatory, Palisades, NY, USA[2]

Abstract. During summer 2010, exceptional heat and drought in western Russia (WRU) occurred simultaneously with heavy rainfall and flooding in northern Pakistan (NPK). Here, we use the Great Eurasian Drought Atlas (GEDA), a new 1021-yr tree-ring reconstruction of summer soil moisture, to investigate the variability and dynamics of this exceptional spatially concurrent climate extreme over the last millennium. Summer 2010 in the GEDA was the second driest year over WRU and the largest wet–dry contrast between NPK and WRU; it was also the second warmest year over WRU in an independent 1015-yr temperature reconstruction. Soil moisture variability is only weakly correlated between the two regions, and 2010 event analogs are rare, occurring in 31 (3.0%) or 52 (5.1%) years in the GEDA, depending on the definition used. Post-1900 is significantly drier in WRU and wetter in NPK compared to previous centuries, increasing the likelihood of concurrent wet NPK–dry WRU extremes, with over 20% of the events in the record occurring in this interval. The dynamics of wet NPK–dry WRU events like 2010 are well captured by two principal components in the GEDA, modes correlated with ridging over northern Europe and western Russia and a pan-hemispheric extratropical wave train pattern similar to that observed in 2010. Our results highlight how high-resolution paleoclimate reconstructions can be used to capture some of the most extreme events in the climate system, investigate their physical drivers, and allow us to assess their behavior across longer time scales than available from shorter instrumental records.

Introduction. In the summer of 2010, Eurasia experienced a spatially concurrent extreme climate event, characterized by severe drought and heat over western Russia and heavy precipitation and flooding over northern Pakistan (Dole et al. 2011; Lau and Kim 2012; Webster et al. 2011). Europe and western Russia experienced one of the hottest summers of the last 500 years (Barriopedro et al. 2011), with pervasive impacts across the region including over 11 000 excess deaths from heat and wildfire smoke (Shaposhnikov et al. 2014) and a 34% reduction in wheat production compared to the previous 2 years (Hunt et al. 2021). The Pakistan floods affected over 20 million people, resulting in over 1000 human deaths, the loss of 20 000 cattle, and estimated damages of $40 billion (U.S. dollars) (Houze et al. 2011; Lau and Kim 2012; Webster et al. 2011).

The main driver of this spatially concurrent extreme was a circumglobal Rossby wave train in the atmosphere. This gave rise to a persistent ridge over western Russia, amplifying heat and drought through anomalous subsidence and suppression of precipitation, and a trough over northern Pakistan that caused a series of extreme rainfall events (Di Capua et al. 2021; Lau and Kim 2012). These waves, and the related dynamics, are one of the main drivers of summer season climate extremes over extratropical Eurasia (Schubert et al. 2014). For 2010, the occurrence of this wave train was favored by both the state of the tropical oceans, including a La Niña in the tropical Pacific and a negative Indian Ocean dipole (IOD), and high-latitude warming (Di Capua et al. 2021). Dry soil moisture conditions in western Russia likely further amplified extreme heat in this region (Christian et al. 2020; Hauser et al. 2016; Lau and Kim 2012; Miralles et al. 2014) and may have enhanced heavy rainfall in northern Pakistan by reinforcing the wave response (Di Capua et al. 2021). Indian Ocean sea surface temperatures also likely increased advection of moisture that fed into the heavy rainfall in northern Pakistan (Priya et al. 2015).

Journal of Hydrometeorology, vol. 25, issue no. 1, pp. 257-275, doi:10.1175/JHM-D-23-0098.1

Investigating the strength and variability of El Niño-Southern Oscillation teleconnections to hydroclimate and maize yields in Southern and East Africa.

Cook, B.I.[1,2], W. Anderson[3], K. Slinski[3], S. Shukla, and A. McNally[3], 2024

NASA Goddard Institute for Space Studies, New York, NY, USA[1]
Division of Ocean and Climate Physics, Lamont-Doherty Earth Observatory, Palisades, NY, USA[2]
NASA Goddard Space Flight Center, Greenbelt, MD[3]

Abstract. The state of the El Niño–Southern Oscillation (ENSO) is critical for seasonal climate forecasts, but recent events diverged substantially from expectations in many regions, including sub-Saharan Africa where seasonal forecasts are critical tools for addressing food security. Here, we evaluate 39 years (1982–2020) of data on hydroclimate, leaf area index, and maize yields to investigate the strength of ENSO teleconnections in southern and East Africa. Teleconnections to precipitation, soil moisture, and leaf area index are generally stronger during ENSO phases that cause drought conditions (El Niño in southern Africa and La Niña in East Africa), with seasonality that aligns well with the maize growing seasons. Within maize growing areas, however, ENSO teleconnections to hydroclimate and vegetation are generally weaker compared to the broader geographic regions, especially in East Africa. There is also little evidence that the magnitude of the ENSO event affects the hydroclimate or vegetation response in these maize regions. Maize yields in Kenya, Malawi, South Africa, and Zimbabwe all correlate significantly with hydroclimate and leaf area index, with South Africa and Zimbabwe showing the strongest and most consistent yield responses to ENSO events. Our results highlight the chain of causality from El Niño and La Niña forcing of regional anomalies in hydroclimate to vegetation health and maize yields in southern and East Africa. The large spread across individual ENSO events, however, underscores the limitations of this climate mode for seasonal climate prediction in the region, and the importance of finding additional sources of skill for improving climate and yield forecasts.

Introduction. The state of the El Niño–Southern Oscillation (ENSO) system is one the most important sources of skill in seasonal climate forecasts (Goddard et al. 2001). This is because cold (La Niña) and warm (El Niño) ENSO states, and their regional climate impacts, can be skillfully predicted at least several months in advance (Barnston et al. 2019; Goddard et al. 2001; Lenssen et al. 2020). As such, ENSO events often have major implications for crop yields and malnutrition (Anttila-Hughes et al. 2021; Guimarães Nobre et al. 2019; Sazib et al. 2020; Ubilava and Abdolrahimi 2019), highlighting the value of using ENSO-informed forecasts to monitor and predict changes in food security (Guimarães Nobre et al. 2019; Goddard and Dilley 2005). The Famine Early Warning Systems Network (FEWS NET), for example, uses seasonal climate and ENSO forecasts, with other information, to monitor and forecast levels of food insecurity in many developing regions around the world (Backer and Billing 2021; Funk et al. 2019; Ross et al. 2009). This includes countries in central Asia, sub-Saharan Africa, and Central America, developing regions often dependent on international aid when food insecurity arises.

Despite their value for seasonal climate predictions, however, there have been several recent incidents where seasonal climate forecasts diverged significantly from what was expected given the ENSO state at the time. One of the more notable occurrences in the last decade was the 2015/16 El Niño, at the time the strongest El Niño event in 36 years (Kogan and Guo 2017). Despite the magnitude of this El Niño event, however, regional hydroclimate and food security conditions deviated substantially from forecasts in regions like East Africa (Choularton and Krishnamurthy 2019; Krishnamurthy et al. 2020), the western United States (Jong et al. 2018; Paek et al. 2017), and Peru and Ecuador (Cai et al. 2020).

European Journal of Agronomy, vol. 155, 127109, doi:10.1016/j.eja.2024.127109

Long-term soil organic carbon and crop yield feedbacks differ between 16 soil-crop models in sub-Saharan Africa.

Couëdel, A., G.N. Falconnier, M. Adam, R. Cardinael, K. Boote, E. Justes, W.N. Smith, A.M. Whitbread, F. Affholder, J. Balkovic, B. Basso, A. Bhatia, B. Chakrabarti, R. Chikowo, M. Christina, B. Faye, F. Ferchaud, C. Folberth, F.M. Akinseye, T. Gaiser, M.V. Galdos, S. Gayler, A. Gorooei, B. Grant, H. Guibert, G. Hoogenboom, B. Kamali, M. Laub, F. Maureira, F. Mequanint, C. Nendel, C.H. Porter, D. Ripoche, **A.C. Ruane**[1], L. Rusinamhodzi, S. Sharma, U. Singh, J. Six, A. Srivastava, B. Vanlauwe, A. Versini, M. Vianna, H. Webber, T. Weber, C. Zhang, and M. Corbeels, 2024

NASA Goddard Institute for Space Studies, New York, NY, USA[1]

Abstract. Food insecurity in sub-Saharan Africa is partly due to low staple crop yields, resulting from poor soil fertility and low nutrient inputs. Integrated soil fertility management (ISFM), which includes the combined use of mineral and organic fertilizers, can contribute to increasing yields and sustaining soil organic carbon (SOC) in the long term. Soil-crop simulation models can help assess the performance and trade-offs of a range of crop management practices including ISFM, under current and future climate. Yet, uncertainty in model simulations can be high, resulting from poor model calibration and/or inadequate model structure. Multi-model simulations have been shown to be more robust than those with single models and help understand and reduce modelling uncertainty. In this study, we aim to perform the first multi-model comparison for long-term simulations of crop yield and SOC and their feedbacks in SSA. We evaluated the performance of 16 soil-crop models using data from four long-term maize experiments at sites in SSA with contrasting climates and soils. Each experiment had four treatments: i) no exogenous inputs, ii) addition of mineral nitrogen (N) fertilizer, iii) use of organic amendments, and iv) combined use of mineral and organic inputs. We assessed model performance in two steps: through blind calibration involving a minimum level of experimental data provided to the modeling teams, and subsequently through full calibration, which included a more extensive set of observational data. Model ensemble accuracy was greater with full calibration than blind calibration. Improvement in model accuracy was larger for maize yields (nRMSE 48 vs 18%) than for topsoil SOC (nRMSE 22 vs 14%). Model ensemble uncertainty (defined as the coefficient of variation across the 16 models) increased over the duration of the long-term experiments. Uncertainty of SOC simulations increased when organic amendments were used, whilst uncertainty of yield predictions was largest when no inputs were applied. Our study revealed large discrepancies among the models in simulating i) crop-to-soil feedbacks due to uncertainties in simulated carbon coming from roots, and ii) soil-to-crop feedbacks due to large uncertainties in simulated crop N supply from soil organic matter decomposition. These discrepancies were largest when organic amendments were applied. The results highlight the need for long-term experiments in which root and soil N dynamics are monitored. This will provide the corresponding data to improve and calibrate soil-crop models, which will lead to more robust and reliable simulations of SOC and crop productivity, and their interactions.

Introduction. Food insecurity in sub-Saharan Africa (SSA) can be largely attributed to low cereal crop yields often caused by low soil fertility and low external input use (Sanchez, 2002). In fact, the large yield gaps of cereal crops in SSA can mostly be explained by soil nutrient limitations rather than climate factors (Van Ittersum et al., 2016). Soil fertility has declined in many regions of SSA as a result of the low use of mineral and organic fertilizers, the shortening of fallow periods and soil erosion (Falconnier et al., 2023, Vanlauwe et al., 2015b, Vanlauwe and Giller, 2006). Sustainable intensification schemes, such as Integrated soil fertility management (ISFM), aiming at maximizing the agronomic use efficiency of nutrients through the combined use of mineral and organic fertilizers, are promising entry points to increase both crop yield and soil organic carbon (SOC), with potential positive impacts on food security and adaptation to climate change (Gram et al., 2020, Vanlauwe et al., 2010)

.

Atmospheric Chemistry and Physics, vol. 24, issue no. 10, pp. 6123-6152, doi:10.5194/acp-24-6123-2024

Measurement report: Cloud and environmental properties associated with aggregated shallow marine cumulus and cumulus congestus.

Crosbie, E.[1], L. Ziemba[1], M. Shook[1], T. Shingler[1], J. Hair[1], A. Sorooshian, R. Ferrare[1], **B. Cairns[2]**, Y. Choi[1], J. DiGangi[1], G. Diskin[1], C. Hostetler[1], S. Kirschler, R.H. Moore[1], D. Painemal[1], C. Robinson[1], S. Seaman[1], K. Thornhill[1], C. Voigt, and E. Winstead[1], 2024

NASA Langley Research Center, Hampton, Va, USA[1]
NASA Goddard Institute for Space Studies, New York, NY, USA[2]

Abstract. Mesoscale organization of marine convective clouds into linear or clustered states is prevalent across the tropical and subtropical oceans, and its investigation served as a guiding focus for a series of process study flights conducted as part of the Aerosol Cloud meTeorology Interactions oVer the western ATlantic Experiment (ACTIVATE) during summer 2020, 2021, and 2022. These select ACTIVATE flights involved a novel strategy for coordinating two aircraft, with respective remote sensing and in situ sampling payloads, to probe regions of organized shallow convection for several hours. The main purpose of this measurement report is to summarize the aircraft sampling approach, describe the characteristics and evolution of the cases, and provide an overview of the datasets that can serve as a starting point for more detailed modeling and analysis studies.

Six flights are described, involving a total of 80 dropsonde profiles that capture the environment surrounding clustered shallow convection. The flights include detailed observations of the vertical structure of cloud systems, comprising up to 20 in situ sampling levels. Four cases involved deepening convection rooted in the marine boundary layer that developed vertically to 2–5 km with varying precipitation amounts, while two cases captured more complex and developed cumulus congestus systems extending above 5 km. In addition to the thermodynamic and dynamic characterization afforded by dropsonde and in situ measurements, the datasets include cloud and aerosol microphysics, trace gas concentrations, aerosol and droplet composition, and cloud and aerosol remote sensing from high-spectral-resolution lidar and polarimetry.

Introduction. Cumulus convection is a pervasive component of the marine atmosphere above the global tropical and subtropical oceans (Warren et al., 1988; Johnson and Lin, 1997; Bony et al., 2004) where vertical transport and overturning circulations are tightly coupled to diabatic processes associated with radiative and latent heating (Riehl and Malkus, 1958; Johnson et al., 1999; Sobel and Bretherton, 2000). In addition to their role in the heat, moisture, and momentum budgets, convective clouds across all scales affect the production, loss, and vertical distribution of atmospheric trace gases (e.g., Dickerson et al., 1987; Fried et al., 2016; Li et al., 2018) and aerosol particles (e.g., Koch et al., 2003; Berg et al., 2015; Corr et al., 2016; Wonaschuetz et al., 2012; Reid et al., 2019; Leung and van den Heever, 2022). Tropical cloudiness has been associated with three major modes (Johnson et al., 1999; Haynes and Stephens, 2007): (i) a shallow cumulus mode often capped by a trade wind inversion; (ii) a middle mode associated with cumulus congestus and altocumulus, often associated with enhanced stability near the melting level (Posselt et al., 2008); and (iii) a deep mode (not considered here) associated with cumulonimbus and anvil cirrus, capped by the tropopause.

Oceanic regions that frequently accommodate deep convection are also subject to suppressed periods with shallow convection (Johnson and Lin, 1997; Malkus and Riehl, 1964). The vertical distribution and extent of clouds capable of supporting deep convection in unstable environments are also strongly dependent on the moisture profile (Redelsperger et al., 2002; Jensen and Del Genio, 2006; Takayabu et al., 2006) because of the inhibiting influences of entrainment and mixing on updraft buoyancy (Derbyshire et al., 2004).

Naure Astronomy, vol. 8, issue no. 7, pp. 810-818, doi:10.1038/s41550-024-02298-5

A roadmap for the atmospheric characterization of terrestrial exoplanets with JWST.

De Wit, J., R. Doyon, B.V. Rackham, O. Lim, E. Ducrot, L. Kreidberg, B. Benneke, I. Ribas, D. Berardo, P. Niraula, A. Iyer, A. Shapiro, N. Kostogryz, V. Witzke, M. Gillon, E. Agol, V. Meadows, A.J. Burgasser, J.E. Owen, J.J. Fortney, F. Selsis, A. Bello-Arufe, Z. de Beurs, E. Bolmont, N. Cowan, C. Dong, J.J. Drake, L. Garcia, T. Greene, T. Haworth, R. Hu, S.R. Kane, P. Kervella, D. Koll, J. Krissansen-Totton, P.-O. Lagage, T. Lichtenberg, J. Lustig-Yaeger, M. Lingam, M. Turbet, S. Seager, K. Barkaoui, T.J. Bell, A. Burdanov, C. Cadieux, B. Charnay, R. Cloutier, N.J. Cook, A.C.M. Correia, L. Dang, T. Daylan, L. Delrez, B. Edwards, T.J. Fauchez, L. Flagg, F. Fraschetti, J. Haqq-Misra, Z. Huang, N. Iro, R. Jayawardhana, E. Jehin, M. Jin, E. Kite, D. Kitzmann, Q. Kral, D. Lafrenière, A.-S. Libert, B. Liu, S. Mohanty, B.M. Morris, C.A. Murray, C. Piaulet, F.J. Pozuelos, M. Radica, S. Ranjan, A. Rathcke, P.-A. Roy, E.W. Schwieterman, J.D. Turner, A. Triaud, and **M.J. Way**[1], 2024

NASA Goddard Institute for Space Studies, New York, NY, USA[1]

Abstract. Ultracool dwarf stars are abundant, long-lived and uniquely suited to enable the atmospheric study of transiting terrestrial companions with the JWST. Among them, the most prominent is the M8.5V star TRAPPIST-1 and its seven planets. While JWST Cycle 1 observations have started to yield preliminary insights into the planets, they have also revealed that their atmospheric exploration requires a better understanding of their host star. Here we propose a roadmap to characterize the TRAPPIST-1 system — and others like it — in an efficient and robust manner with JWST. We notably recommend that — although more challenging to schedule — multi-transit windows be prioritized to mitigate the effects of stellar activity and gather up to twice more transits per JWST hour spent. We conclude that, for such systems, planets cannot be studied in isolation by small programmes but rather need large-scale, joint space- and ground-based initiatives to fully exploit the capabilities of JWST for the exploration of terrestrial planets.

Introduction. Terrestrial planets surrounding M dwarfs are abundant[1,2,3]. As these stars dominate the galactic population[4], planetary systems around M dwarfs can be viewed as windows on the galactic terrestrial planet population (Fig. 1a). Unfortunately, terrestrial exoplanets are only amenable for atmospheric studies with the James Webb Space Telescope (JWST) when found around mid- to late-M dwarfs (Fig. 1b), specifically around ultracool dwarf stars (UCDs, with effective temperature less than 3,000 K) for those within the temperate zone—defined as receiving a flux between 4× and 0.25× that of Earth5. Figure 1b highlights the handful of systems with transiting terrestrial exoplanets amenable for atmospheric characterization with JWST known so far (including L 98-59 (ref. 6), LHS 1140 (ref. 7), LHS 3844 (ref. 8), LP 791-18 (refs. 9·10), LP 890-9 (ref. 11), TOI-540 (ref. 12) and TRAPPIST-1 (refs. [13,14])). The small sizes of UCDs yield favourable planet-to-star radius ratios that enable the detectability of terrestrial planet atmospheres via transmission spectroscopy.

If temperate planets around UCDs are able to acquire a moderate amount of atmospheric volatiles during planet formation[15] and preserve it during their star's extended pre-main-sequence phase[16,17], our Galaxy may be host to billions of habitable oases. Alternative scenarios, depending on volatile inventories and age, may include scorched desert, runaway greenhouse or frigid ice-locked ocean worlds[18,19,20,21,22,23,24]. Other factors such as large extreme ultraviolet fluxes, stellar winds, flares and coronal mass ejections can evaporate and erode planetary atmospheres and remain at high levels on billion-year timescales, thus supporting the desert fate[25,26,27,28]. In addition, after the protoplanetary disk phase collisions with planetesimals may deliver volatiles to the outermost planets but erode the atmospheres of the innermost ones[29].

Atmospheric Chemistry and Physics, vol. 24, issue no. 10, pp. 6275-6304, doi:10.5194/acp-24-6275-2024

Modeling atmospheric brown carbon in the GISS ModelE Earth system model.

DeLessio, M.A.[1,2], **K. Tsigaridis**[1,3], **S.E. Bauer**[1,3], **J. Chowdhary**[1,4], and G.L. Schuster[5], 2024

NASA Goddard Institute for Space Studies, New York, NY, USA[1]
Department of Earth and Environmental Sciences, Columbia University, New York, NY, USA[2]
Center for Climate Systems Research, Columbia University, New York, NY, USA[3]
Department of Applied Physics and Applied Mathematics, Columbia University, New York, NY, USA[4]
NASA Langley Research Center, Hampton, VA, USA[5]

Early Career Winner

Abstract. Brown carbon (BrC) is an absorbing organic aerosol (OA), primarily emitted through biomass burning (BB), which exhibits light absorption unique to both black carbon (BC) and other organic aerosols. Despite many field and laboratory studies seeking to constrain BrC properties, the radiative forcing (RF) of BrC is still highly uncertain. To better understand its climate impact, we introduced BrC to the One-Moment Aerosol (OMA) module of the GISS ModelE Earth system model (ESM). We assessed ModelE sensitivity to primary BrC processed through a novel chemical aging scheme and to secondary BrC formed from biogenic volatile organic compounds (BVOCs). Initial results show that BrC typically contributes a top-of-the-atmosphere (TOA) radiative effect of 0.04 W m^{-2}. Sensitivity tests indicate that explicitly simulating BrC (separating it from other OAs), including secondary BrC, and simulating chemical bleaching of BrC contribute distinguishable radiative effects and should be accounted for in BrC schemes. This addition of prognostic BrC to ModelE allows greater physical and chemical complexity in OA representation with no apparent trade-off in model performance, as the evaluation of ModelE aerosol optical depth against Aerosol Robotic Network (AERONET) and Moderate Resolution Imaging Spectroradiometer (MODIS) retrieval data, with and without the BrC scheme, reveals similar skill in both cases. Thus, BrC should be explicitly simulated to allow more physically based chemical composition, which is crucial for more detailed OA studies like comparisons to in situ measurement campaigns. We include a summary of best practices for BrC representation within ModelE at the end of this paper.

Introduction. Carbonaceous aerosols are important, short-lived climate forcers. Black carbon (BC), a strongly absorbing carbonaceous aerosol produced from fuel and biomass burning (BB), contributes a significant positive radiative forcing (RF) to the atmosphere (Hansen et al., 1997; Jacobson, 2001; Ramanathan and Carmichael, 2008; Bond et al., 2013). The Sixth Assessment Report (AR6) of the Intergovernmental Panel on Climate Change (IPCC, 2023) estimates a BC effective RF of 0.11 W m^{-2} (Szopa et al., 2021). BB also emits organic aerosols (OAs) (Ito and Penner, 2005), another type of carbonaceous aerosol, which cool the atmosphere at an estimated RF of −0.21 W m^{-2} (Szopa et al., 2021). Beyond BB, secondary production is a key source of OAs: isoprene and other biogenic or anthropogenic volatile organic compounds (VOCs) partition and react in the atmosphere to form secondary organic aerosols (SOAs; Shrivastava et al., 2017; Mahilang et al., 2021).

As warming temperatures and changes in precipitation drive increases in wildfire frequency and intensity (Flannigan et al., 2009; Keywood et al., 2013), and emission controls and cleaner technologies lead to a further reduction in other aerosol sources (Bauer et al., 2022), carbonaceous aerosols, including OAs, could possibly become more prominent. Observations at Whiteface Mountain, downwind of the US West Coast BB region, have already shown an increase in OAs found in cloud water over the last 10 years, suggesting a growing influence of wildfire smoke (Lawrence et al., 2023). SOAs from biogenic VOCs (BVOCs) are also expected to grow in importance; the SOA burden could possibly be greater than that of sulfate aerosols by 2100 (Tsigaridis and Kanakidou, 2007). Despite their growing importance, OAs still pose a large gap in aerosol modeling: the IPCC Sixth Assessment Report estimated an OA RF uncertainty of 0.23 W m^{-2}, about the same magnitude as the cooling effect itself (Szopa et al., 2021).

Surveys in Geophysics, vol. 45, issue no. 6, pp. 1959-1977, doi:10.1007/s10712-024-09856-6

A geostationary satellite-based approach to estimate convective mass flux and revisit the hot tower hypothesis.

Derras-Chouk, A.[1,2], and Z.J. Luo[2], 2024

NASA Goddard Institute for Space Studies, New York, NY, USA[1]
Department of Earth and Atmospheric Sciences, The City College of the New York of City University of New York (CUNY), New York, NY, USA[2]

Abstract. This study aims to revisit the classic "hot tower" hypothesis proposed by Riehl and Simpson (Malkus) in 1958 and revisited in 1979. Our investigation centers on the convective mass flux of hot towers within the tropical trough zone, using geostationary (GEO) satellite data and an innovative analysis technique, known as ML16, which integrates various data sources, including hot tower heights, ambient profiles, and a plume model, to determine convective mass flux. The GEO-based ML16 approach is evaluated against collocated ground-based radar wind profiler observations, showing broad agreement. Our GEO-based estimate of hot tower convective mass flux, 2.8×10^{11}–3.4×10^{11} kg s^{-1}, is similar to the revisited estimate in Riehl and Simpson (1979), 2.6–3.0×10^{11} kg s^{-1}. Additionally, our analysis gives a median count of around 550 hot towers with a median size of about 11 km, in contrast to the previous estimates of 1600–2400 hot towers, each characterized by a fixed size of 5 km. We discuss the causes of these discrepancies, emphasizing the fundamental differences between the two approaches in characterizing tropical hot towers. While both approaches have various uncertainties, the evidence suggests that greater credibility should be placed on results derived from direct satellite observations. Finally, we identify future opportunities in Earth Observations that will provide more accurate measurements, enabling further evaluation of the role played by tropical hot towers in mass transport.

Introduction. The "hot tower" hypothesis was originally introduced by Riehl and Malkus (1958) to clarify the process of heat transport from the surface to the upper troposphere within the tropical trough zone, providing an explanation for the vertical movement of air against energy gradient to reach high altitudes. At that time, the term "hot tower" had not yet been coined; the authors used the terms "undilute cloud towers" and "cumulonimbus chimneys."

Subsequent studies revised the undilute requirement for cloud towers defined as deep convective clouds originating in the planetary boundary layer and extending near the upper tropospheric outflow layer, allowing for some entrainment of ambient air (Zipser 2003; Fierro et al. 2009), although the requirement remains in Riehl (1979) revision.

Nevertheless, the core idea of the hypothesis remains: Vertical heat transport, required for energy balance of the tropical trough zone, is achieved through hot towers and not through gradual, large-scale ascent of air masses, which fails to overcome the mid-tropospheric energy minimum. Furthermore, through energy balance and continuity considerations, Riehl and Malkus (1958) estimated the mass flux in undilute hot towers, and, with assumptions about the sizes and vertical velocities within cloud towers, they postulated that a total of 1500–5000 active hot towers embedded within the tropical trough zone maintain the tropical energy balance. A later study by Riehl (1979) revised the hot tower count to 1600–2400.

The "hot tower" concept and subsequent inferences about the properties of tropical deep convective cloud were ground-breaking achievements at a time when global observations were scarce. Nevertheless, any quantitative conclusion about mass and energy transport by hot towers in those early studies should be considered tentative. Indeed, Riehl and Malkus (1958) acknowledged that "lack of [global] data prevents a definitive treatment" and their attempt should be treated as "an initial study proceeding a much more extensive analysis."

NPJ Climate and Atmospheric Science, vol. 7, 301, doi:10.1038/s41612-024-00845-5

Real-time ENSO forecast skill evaluated over the last two decades, with focus on onset of ENSO events.

Ehsan, M.A.[1,2,3], M.L. L'Heureux, M.K. Tippett, **A.W. Robertson**[1,2,3], and J. Turmelle[3], 2024

NASA Goddard Institute for Space Studies, New York, NY, USA[1]
Center for Climate Systems Research, Columbia University, New York, NY, USA[2]
International Research Institute for Climate and Society, Columbia Climate School, Columbia University, New York, NY[3]

Abstract. This paper provides an updated assessment of the "International Research Institute for Climate and Society's (IRI) El Niño Southern Oscillation (ENSO) Predictions Plume". We evaluate 253 real-time forecasts of the Niño 3.4 index issued from February 2002 to February 2023 and examine multimodal means of dynamical (DYN) and statistical (STAT) models separately. Forecast skill diminishes as lead time increases in both DYN and STAT forecasts, with peak accuracy occurring post-northern hemisphere spring predictability barrier and preceding seasons. The DYN forecasts outperform STAT forecasts with a pronounced advantage in forecasts initiated from late boreal winter through spring. The analysis uncovers an asymmetry in predicting the onset of cold and warm ENSO episodes, with warm episode onsets being better forecasted than cold onsets in both DYN and STAT models. The DYN forecasts are found to be valuable for predicting warm and cold ENSO episode onsets at least several months in advance, while STAT forecasts are less informative about ENSO phase transitions. The results indicate that predicting ENSO onset is challenging and that the ability to do so is both model- and event-dependent.

Introduction. Since February 2002, the International Research Institute for Climate and Society (IRI) has routinely disseminated forecasts of the El Niño Southern Oscillation (ENSO) every month, in both deterministic and probabilistic formats. These forecasts, generated by forecast producers around the world, employ a range of dynamical and statistical models. Referred to as the IRI ENSO predictions plume, this resource provides valuable insights into the expected ENSO conditions over the next nine overlapping 3-month periods, corresponding to a maximum lead time of 9 months. The identification of the ENSO state relies on the Niño3.4 index, which tracks the progression of sea surface temperature (SST) anomalies in the central-eastern equatorial Pacific region spanning from 5°S to 5°N and 170°W to 120°W. The objective of this paper is to conduct a reassessment of the IRI ENSO predictions over the extended period of February 2002—February 2023, encompassing a total of 253 real-time forecasts. This paper reevaluates the performance of the multimodel mean of dynamical and statistical real-time forecasts issued during last two decades, updating earlier analyses that were limited to the 2002–2011 period[1,2], with a focus on the ability of dynamical and statistical models to predict the onset of ENSO.

Supplementary Figure S1 illustrates the IRI ENSO predictions plume (henceforth the plume) released in mid-February 2023 (the last issued forecast considered in this study). This example encompasses the forecast period from Feb–Apr 2023 through Oct–Dec 2023, showcasing predictions from various dynamical and statistical models. Additionally, it includes the multimodel mean (thick solid lines), which combines the predictions from both types of models. The plume stands out for its distinctiveness in two key aspects. It provides real-time ENSO forecasts issued monthly from various dynamical and statistical models, while keeping a track record of the models used and forecasts issued, and includes a forecast discussion released on the 19th of each month. The IRI website (https://iri.columbia.edu/our-expertise/climate/forecasts/enso/current/) hosts archived forecasts data and discussions, enabling users to retrospectively review past forecasts. This extensive compilation of real-time forecasts from diverse models, accompanied by pertinent discussions, stands as a vital asset, strengthening the efficacy of utilizing the plume for real-time ENSO predictions.

Geoscientific Model Development, vol. 17, issue no. 21, pp.7835-7853, doi:10.5194/gmd-17-7835-2024

An extensible perturbed parameter ensemble (PPE) for the Community Atmosphere Model Version 6.

Eidhammer, T., A. Gettelman, K. Thayer-Calder, D. Watson-Parris, **G. Elsaesser**[1,2], H. Morrison, **M. van Lier-Walqui**[1,3], C. Song, and D. McCoy, 2024

NASA Goddard Institute for Space Studies, New York, NY, USA[1]
Department of Applied Physics and Applied Mathematics, Columbia University, New York, NY, USA[2]
Center for Climate Systems Research, Columbia University, New York, NY, USA[3]

Abstract. This paper documents the methodology and preliminary results from a perturbed parameter ensemble (PPE) technique, where multiple parameters are varied simultaneously and the parameter values are determined with Latin hypercube sampling. This is done with the Community Atmosphere Model version 6 (CAM6), the atmospheric component of the Community Earth System Model version 2 (CESM2). We apply the PPE method to CESM2–CAM6 to understand climate sensitivity to atmospheric physics parameters. The initial simulations vary 45 parameters in the microphysics, convection, turbulence and aerosol schemes with 263 ensemble members. These atmospheric parameters are typically the most uncertain in many climate models. Control simulations and targeted simulations to understand climate forcing due to aerosols and fast climate feedbacks are analyzed. The use of various emulators is explored in the multi-dimensional space mapping input parameters to output metrics. Parameter impacts on various model outputs, such as radiation, cloud and aerosol properties, are evaluated. Machine learning is also used to probe optimal parameter values against observations. Our findings show that PPE is a valuable tool for climate uncertainty analysis. Furthermore, by varying many parameters simultaneously, we find that many different combinations of parameter values can produce results consistent with observations, and thus careful analysis of tuning is important. The CESM2–CAM6 PPE is publicly available and extensible to other configurations to address questions of other model processes in the atmosphere and other model components (e.g., coupling to the land surface).

Introduction. General circulation models (GCMs) have numerous and long-standing biases due in part to uncertain representations of the physical processes (e.g., Trenberth and Fasullo, 2010). This is especially true for processes that occur at subgrid scales, such as microphysics, turbulence, convection and aerosol processes. Because these processes are not resolved, their effects on the grid-scale model state variables are represented via parameterizations rather than the process equations being explicitly solved at the natural scale of the phenomena being represented. For example, the evolution of a single cloud drop in a turbulent flow over a small domain can be simulated explicitly, but the evolution of a cloud drop population cannot be directly simulated directly due to the sheer number of drops within each grid volume of typical atmospheric models (with grid spacing of tens of meters to tens of kilometers). Moreover, for many processes, including cloud and aerosol microphysics, even at the natural scale of the phenomenon (e.g., scale of an individual drop) there are uncertainties in the underlying physical processes. That is to say that for many processes there are no governing equations at any scale. For example, for cloud microphysics there are fundamental uncertainties in how drops collide and either bounce, coalesce or breakup. Most ice microphysical processes, including nucleation, diffusional growth, riming and aggregation, remain highly uncertain even at the scale of individual particles (e.g., Morrison et al., 2020).

Parameterizations typically include parameters whose values are constrained by theory, high-resolution process models and observations. To varying degrees, these parameter values are uncertain because of both uncertainty in how to best represent the impact of subgrid-scale processes at the grid scale and fundamental uncertainty at the process scale. In climate models, parameter values are adjusted within the bounds of uncertainty to produce realistic output relative to observations. However, this process, usually referred to as “tuning”, faces several challenges (Hourdin et al., 2016).

Environmental Modelling & Software, vol. 180, 106136, doi:10.1016/j.envsoft.2024.106136

A large dataset of fluvial hydraulic and geometry attributes derived from USGS field measurement records.

Erfani, S.M.H.[1,2], M. Erfani, S. Cohen, A.R.J. Downey, and E. Goharian, 2024

NASA Goddard Institute for Space Studies, New York, NY, USA[1]
Center for Climate Systems Research, Columbia University, New York, NY, USA[2]

Abstract. Accurate representation of river channel geometry is important for hydrologic and hydraulic modeling of fluvial systems. Often, channel geometry is estimated using simple rating curves that can be applied across various spatial scales. However, such methods are limited to power law relations that do not employ many potentially relevant catchment and river attributes. This paper introduce a new dataset, IFMHA (Inventory of Field Measurement of Hydraulic Attributes), to enable research studies on channel geometry and streamflow characteristics. IFMHA is derived from the National Water Information System (NWIS) site inventory for surface water field measurements and stream attributes from the National Hydrography Dataset (NHD). IFMHA includes 2,802,532 records from 10,050 sites (NWIS streamgaging stations). The dataset utility is demonstrated here by presenting a series of conceptual models for estimating channel geometry parameters (i.e., channel mean depth, channel maximum depth, wetted perimeter, and roughness) based on the available field attributes within IFMHA. Such a dataset and attributed channel geometry parameters can enhance the performance of operational flood forecasting frameworks (e.g. National Water Model) by providing more accurate initial conditions used in hydrologic and hydraulic routing models.

Introduction. Hydrological models are prominent tools for flood forecasting, water resources management, and the study of climate change impacts (Bárdossy and Singh, 2008, Mendoza et al., 2016, Krysanova et al., 2018). Hydrological models often require a routing method to estimate discharge hydrograph through a river channel (Yoo et al., 2017, Zhao et al., 2017, Nguyen-Quang et al., 2018). The accuracy of the representation of channel geometry can significantly impact routing simulations within hydrological models (Orlandini and Rosso, 1998, Hutton et al., 2012, Brackins et al., 2021). Since obtaining accurate channel geometry using surveying methods is costly, simplifying assumptions are often used (Brackins et al., 2021). An example of this approach is the representation of channel geometry in the National Water Model (NWM) developed by the National Oceanic and Atmospheric Administration (NOAA), National Weather Service. At present, the NWM is using a compound channel formulation that incorporates trapezoidal bankfull and rectangular floodplain cross sections as a means of simplifying the behavior of the flow (Gochis et al., 2020).

The importance of proper representation of channel geometry and the lack of surveyed data in most rivers has motivated research in the field of hydraulic geometry, mostly focusing on power-law equations that relate channel width, depth, and velocity with drainage area or discharge (Leopold and Maddock, 1953, Parker et al., 2007, Ferguson, 1986, Dingman, 2007, Stewardson, 2005). In locations where no or limited discharge data is available, drainage area is often used (Dunne and Leopold, 1978, Ames et al., 2009). It has been shown that regional calibration of hydraulic geometry equations provides a more robust estimation of channel parameters (Bieger et al., 2015, Bieger et al., 2016). This, however, requires much larger and spatially diverse datasets. Attempting to overcome this challenge, a combined dataset from 50 studies was used to develop regional calibrations for estimation of bankfull hydraulic geometry (Blackburn-Lynch et al., 2017), which are currently being used in NWM to estimate reach-averaged geometry (Gochis et al., 2020). Moreover, taking advantage of satellite measurements, the Surface Water and Ocean Topography (SWOT) mission by NASA and CNES, focuses on providing several river data products such as river width and water surface elevation (Lettenmaier et al., 2015, Altenau et al., 2021). However, remote sensing products such as those offered by SWOT, are not without limitations as they cannot observe below the water surface and the small rivers are unobserved (Mersel et al., 2013, Nickles et al., 2020).

Nature Climate Change, vol. 14, issue no. 12, pp. 1212-1215, doi:10.1038/s41558-024-02190-0

Pathways for urgent action towards climate resilient development.

Eriksen, S.H., N.P. Simpson, B. Glavovic, D. Ley, E.R. Carr, L. Fernández-Carril, B. Hayward, M.D. Morecroft, M. Pathak, J.J. Pereira, H.-O. Pörtner, D.C. Roberts, **A.C. Ruane**[1], R. Sánchez-Rodríguez, E.L.F. Schipper, W. Solecki, L.C. Stringer, E. Totin, A. Birt, and F. Degvold, 2024

NASA Goddard Institute for Space Studies, New York, NY, USA[1]

Abstract. There is a closing window of opportunity to ensure a sustainable future for all, with deep and rapid action needed this decade. Inclusive and just climate resilient development advances sustainable development and keeps open pathways to a livable planet but requires urgent and fundamental shifts in prevailing development politics and practice.

Introduction. Development pathways have failed to deliver the rapid, deep and just climate action necessary for enduring human well-being and planetary health[1]. The interconnected nature of climate impacts and geopolitical instability, pervasive injustices, biodiversity loss and other socioenvironmental challenges underlines the urgent need to shift to new development pathways.

Climate action is currently woefully inadequate to meet scientifically informed and politically agreed targets to halt global warming, reduce vulnerability and adapt. Slow progress is attributed to systemic failures in the structure of the political economy, development framings, technological and institutional challenges, lack of political will, and insufficient access to and levels of finance, among many other constraints[1,2]. Political commitment has stalled and competes with multiple crises from COVID-19 to conflicts in Ukraine, Sudan and the Middle East. These crises compound climate-related, humanitarian and sustainability challenges. Pressing development needs, such as education, health and peace building, make it difficult to prioritize climate action and priority is given to gross domestic product growth at the expense of human well-being and the environment.

A major advance in the IPCC sixth assessment cycle that charts pathways to overcome these challenges was the articulation of climate resilient development (CRD) as closely intertwined with ecosystem stewardship, social justice and sustainable development. This Comment explains how CRD — the integration of adaptation and mitigation action to advance sustainable development for all — frames the kind of development actions urgently needed this decade to limit global warming for a liveable planet, support adaptation, address inequities and make progress towards the Sustainable Development Goals (SDGs)[1,3].

Closing window of opportunity. The costs for not acting urgently on effective climate policies and actions are substantial. Climate change has negatively affected socioenvironmental systems around the world, including freshwater, health, food, land and oceans ecosystems, cities, infrastructure and energy systems, making it difficult to realize sustainable development outcomes[3]. The annual economic damages from climate change are rising. Global income is expected to be US$38 trillion less by 2049 than in a world without climate change[4]. These costs outweigh the mitigation costs required to limit global warming to 2 °C by sixfold[4]. Climate change is a risk multiplier, precluding sustainable development and increasing costs of future climate impacts and adaptation with each increment of global warming[1,3].

Current development trajectories and delaying climate action close down opportunities for sustainable development1 (Fig. 1). Increased warming, adaptation limits and inequitable and unsustainable development cause path dependencies that constrain future adaptation, mitigation and development options, and hence future prospects for human and ecosystem well-being1. Adaptation cannot therefore be delinked from mitigation and the development choices driving climate change.

Earth's Future, vol. 12, issue no. 12, e2024EF004661, doi:10.1029/2024EF004661

Vegetation greening mitigates the impacts of increasing extreme rainfall on runoff events.

Ficklin, D.L., D. Touma, **B.I. Cook**, S.M. Robeson, T. Hwang, J. Scheff, A.P. Williams, H. Watson, B. Livneh, M.R. Tye, and L. Wang, 2024

NASA Goddard Institute for Space Studies, New York, NY, USA[1]
Lamont-Doherty Earth Observatory, Palisades, NY, USA[2]

Abstract. Future flood risk assessment has primarily focused on heavy rainfall as the main driver, with the assumption that projected increases in extreme rain events will lead to subsequent flooding. However, the presence of and changes in vegetation have long been known to influence the relationship between rainfall and runoff. Here, we extract historical (1850–1880) and projected (2070–2100) daily extreme rainfall events, the corresponding runoff, and antecedent conditions simulated in a prominent large Earth system model ensemble to examine the shifting extreme rainfall and runoff relationship. Even with widespread projected increases in the magnitude (78% of the land surface) and number (72%) of extreme rainfall events, we find projected declines in event-based runoff ratio (runoff/rainfall) for a majority (57%) of the Earth surface. Runoff ratio declines are linked with decreases in antecedent soil water driven by greater transpiration and canopy evaporation (both linked to vegetation greening) compared to areas with runoff ratio increases. Using a machine learning regression tree approach, we find that changes in canopy evaporation is the most important variable related to changes in antecedent soil water content in areas of decreased runoff ratios (with minimal changes in antecedent rainfall) while antecedent ground evaporation is the most important variable in areas of increased runoff ratios. Our results suggest that simulated interactions between vegetation greening, increasing evaporative demand, and antecedent soil drying are projected to diminish runoff associated with extreme rainfall events, with important implications for society.

Introduction. Hydrologic extremes have severe consequences for human, environmental, and economic sectors. One of the well-established outcomes of ongoing climate change is an increase in the number and magnitude of extreme precipitation events even with minimal changes in annual or seasonal precipitation (Kirchmeier-Young & Zhang, 2020; Pendergrass & Knutti, 2018; Polson et al., 2013). Even for areas that are projected to experience a decline in annual precipitation, the number and intensity of short duration heavy precipitation events are likely to increase (Allan et al., 2021). This increase in precipitation extremes has already been observed throughout the world (Barbero et al., 2017; Westra et al., 2013), with sub-daily extreme precipitation changes generally aligning at or above the Clausius-Clapeyron relationship (~7%°C^{-1}; Visser et al., 2021) and a lower precipitation sensitivity (2%–3%°C^{-1}) for longer time intervals due to energetic constraints (Allen & Ingram, 2002; Visser et al., 2021). Climate model projections agree with these observations and suggest that precipitation extremes will continue to increase into the future with increases in air temperature (Ficklin et al., 2022; Visser et al., 2021) with high confidence (Allan et al., 2021).

It is often assumed that extreme precipitation increases also will lead to increases in extreme runoff. However, previous work has suggested that this is not always the case (Ivancic & Shaw, 2015; Sharma et al., 2018; Wasko et al., 2021; Zhang et al., 2022), resulting in uncertain regional runoff and subsequent flooding trends under increasing extreme precipitation (Blöschl et al., 2019; Mallakpour & Villarini, 2015; Wasko & Nathan, 2019; Wasko et al., 2021; Zhang et al., 2022). Prior work suggests that these discrepancies might stem from changes in the extreme runoff generation mechanisms, where increases in rain-induced extreme runoff events are offset by decreases in snowmelt-induced extreme runoff events (Burn & Whitfield, 2023; Zhang et al., 2022). However, there remains a lack of consensus of runoff trends from extreme precipitation events (Mallakpour & Villarini, 2015; Wasko et al., 2021), suggesting that (a) we lack a thorough understanding of how the interaction between climate and biotic factors affect precipitation partitioning into runoff and soil-water infiltration, and (b) mechanistic drivers of the changes in antecedent conditions need to be examined in more detail.

Geoscientific Model Development, vol. 17, issue no. 5, pp. 2387-2417, doi:10.5194/gmd-17-2387-2024

Interactions between atmospheric composition and climate change — Progress in understanding and future opportunities from AerChemMIP, PDRMIP, and RFMIP.

Fiedler, S., V. Naik, F.M. O'Connor, C.J. Smith, R. Pincus, P. Griffiths, R. Kramer[1], T. Takemura, R.J. Allen, U. Im, M. Kasoar, A. Modak, S. Turnock, A. Voulgarakis, D. Watson-Parris, **D.M. Westervelt[2,3]**, L.J. Wilcox, A. Zhao, W.J. Collins, M. Schulz, G. Myhre, and P.M. Forster, 2024

NASA Goddard Space Flight Center, Greenbelt, MD, USA[1]
NASA Goddard Institute for Space Studies, New York, NY, USA[2]
Lamont-Doherty Earth Observatory, Palisades, NY, USA[3]

Abstract. The climate science community aims to improve our understanding of climate change due to anthropogenic influences on atmospheric composition and the Earth's surface. Yet not all climate interactions are fully understood, and uncertainty in climate model results persists, as assessed in the latest Intergovernmental Panel on Climate Change (IPCC) assessment report. We synthesize current challenges and emphasize opportunities for advancing our understanding of the interactions between atmospheric composition, air quality, and climate change, as well as for quantifying model diversity. Our perspective is based on expert views from three multi-model intercomparison projects (MIPs) – the Precipitation Driver Response MIP (PDRMIP), the Aerosol Chemistry MIP (AerChemMIP), and the Radiative Forcing MIP (RFMIP). While there are many shared interests and specializations across the MIPs, they have their own scientific foci and specific approaches. The partial overlap between the MIPs proved useful for advancing the understanding of the perturbation–response paradigm through multi-model ensembles of Earth system models of varying complexity. We discuss the challenges of gaining insights from Earth system models that face computational and process representation limits and provide guidance from our lessons learned. Promising ideas to overcome some long-standing challenges in the near future are kilometer-scale experiments to better simulate circulation-dependent processes where it is possible and machine learning approaches where they are needed, e.g., for faster and better subgrid-scale parameterizations and pattern recognition in big data. New model constraints can arise from augmented observational products that leverage multiple datasets with machine learning approaches. Future MIPs can develop smart experiment protocols that strive towards an optimal trade-off between the resolution, complexity, and number of simulations and their length and, thereby, help to advance the understanding of climate change and its impacts.

Introduction. A central aim of climate science is to advance our understanding of how the Earth system responds to human activities. This endeavor involves the assessment of numerous spatiotemporally changing variables in the Earth system, which can be determined by multiple interacting physical, chemical, and biological processes. For example, changes in irradiance, land use, and atmospheric composition, including, for instance, aerosols and their precursors (greenhouse gases such as carbon dioxide and methane), perturb the radiation fluxes in and at the top of the atmosphere and hence the Earth's radiation balance. On a timescale of several decades, the Earth's temperature is controlled by a balance between the net amount of absorbed sunlight (solar radiation) and the radiation emitted by the planet and its atmosphere (terrestrial radiation). A perturbation of this balance is called “radiative forcing” – a concept embedded in the study of the physical basis of climate (Ramaswamy et al., 2019) – and is measured as energy flux (in W m^{-2}).

Changes to atmospheric composition have distinct effects on the Earth's energy budget and climate, which are classified into radiative forcing, climate response, and feedbacks. Instantaneous radiative forcing (IRF) is the initial change in radiation fluxes that arises from a perturbation in a climate forcer, which could be, for instance, associated with increased greenhouse gas concentrations in the atmosphere due to anthropogenic emissions in the absence of other changes.

Journal of Geophysical Research Atmospheres, vol. 129, issue no. 15, e2023JD039396, doi:10.1029/2023JD039396



Estimating the impact of a 2017 smoke plume on surface climate over northern Canada with a climate model, satellite retrievals, and weather forecasts.

Field, R.D.[1,2], M. Luo[3], **S.E. Bauer**[1], **J.E. Hickman**[1,4], **G.S. Elsaesser**[1,2], **K. Mezuman**[1,4], **M. van Lier-Walqui**[1,4], **K. Tsigaridis**[1,4], and **J. Wu**[1,2], 2024

NASA Goddard Institute for Space Studies, New York, NY, USA[1]
Department of Applied Physics and Applied Mathematics, Columbia University, New York, NY, USA [2]
NASA Jet Propulsion Laboratory, California Institute of Technology, Pasadena, CA, USA[3]
Center for Climate Systems Research, Columbia University, New York, NY, USA[4]

Abstract. In August 2017, a smoke plume from wildfires in British Columbia and the Northwest Territories recirculated and persisted over northern Canada for over two weeks. We compared a full-factorial set of NASA Goddard Institute for Space Studies ModelE simulations of the plume to satellite retrievals of aerosol optical depth and carbon monoxide, finding that ModelE performance was dependent on the model configuration, and more so on the choice of injection height approach, aerosol scheme and biomass burning emissions estimates than to the choice of horizontal winds for nudging. In particular, ModelE simulations with free-tropospheric smoke injection, a mass-based aerosol scheme and comparatively high fire NO_x emissions led to unrealistically high aerosol optical depth. Using paired simulations with and without fire emissions, we estimated that for 16 days over an 850,000 km^2 region, the smoke decreased planetary boundary layer heights by between 253 and 547 m, decreased downward shortwave radiation by between 52 and 172 Wm^{-2}, and decreased surface temperature by between 1.5°C and 4.9°C, the latter spanning an independent estimate from operational weather forecasts of a 3.7°C cooling. The strongest surface climate effects were for ModelE configurations with more detailed aerosol microphysics that led to a stronger first indirect effect.

Introduction. The stratospheric smoke plume from Pacific Northwest Event (PNE) wildfires on August 12 and 13, 2017 has been studied observationally for its source strength, injection altitude, lifetime, and dynamical effects (Fromm et al., **2021**; Lestrelin et al., **2021**; Peterson et al., **2018**; Torres et al., **2020**) and with models to determine the role of "self-lofting" in its ascent (Yu et al., **2019**) and its radiative impacts (Das et al., **2021**). At about the same time there was also high fire danger and extensive fire southeast of Great Slave Lake in Northwest Territories (NWT) of Canada (Figure **1**) which contributed to the persistent smoke plume (Figure **2**) in an otherwise fairly clean environment. Wizenberg et al. (**2023**) considered both the PNE and NWT emissions at different altitudes in their comparison of chemical transport model simulations to satellite and ground-based trace gas retrievals.

This is a useful natural experiment to evaluate a model against satellite data and to estimate the regional effects of smoke on surface climate. Our study follows basic model-observation comparisons for, for example, smoke events in Russia (Huijnen et al., **2012**; Palacios-Peña et al., **2018**; Toll et al., **2015**) and North America (Carter et al., **2020**; Lu & Sokolik, **2013**; Mallet et al., **2017**). The effects of smoke on surface climate have been examined using discrepancies between operational weather forecasts and observations (Jones et al., **2022**; Mitchell et al., **2006**; Robock, **1988**, **1991**; Wexler, **1950**) or with models comparing experiments with and without smoke or its radiative effects (Kochanski et al., **2019**; Toll et al., **2015**; Walter et al., **2016**; Westphal & Toon, **1991**). By absorbing and scattering incoming shortwave radiation, wildfire smoke can directly and indirectly reduce the amount of radiation reaching the surface, leading to warming of the smoke layer, cooling at the surface, reductions in planetary boundary layer (PBL) height, and reductions in horizontal wind speeds.

MDPI Sustainability, vol. 16, issue no. 21, 9184, doi:10.3390/su16219184

Greenhouse gas emissions from cold chains in agrifood systems.

Flammini, A., H. Adzmir, R. Pattison, **K. Karl**[1,2], Y. Allouche, and F.N. Tubiello, 2024

NASA Goddard Institute for Space Studies, New York, NY, USA[1]
Centre on Global Energy Policy, Columbia University, New York, NY, USA[2]

Abstract. Cold chains are essential components of agrifood system activities, from storage and food processing to transport, retail, and household consumption. We devise a comprehensive methodology, validated against established data, to estimate both direct (due to refrigerant use) and indirect (from energy use) greenhouse gas emissions from agrifood system cold chains, expanding previous approaches, which had focused on direct emissions only. We found that in 2022, world-total indirect emissions from energy use in cold chains were more than twice the direct component from refrigerants. This resulted in a new estimate of world-total GHG emissions from agrifood system cold chains of 1.32 Gt CO_2eq in 2022, with significant growth over the past two decades (0.52 Gt CO_2eq in 2000). Household consumption and food processing represented the most significant contributors to agrifood system emissions from cold chains, together representing in 2022 three-fourths of the total. These results align well with known global patterns of energy use in the refrigeration sector and highlight the importance of targeting cold chains within agrifood system with GHG emission mitigation actions.

Introduction. Agrifood systems encompass the farm gate, land use change and pre- and post-agricultural production activities, with significant contributions to anthropogenic greenhouse gas (GHG) emissions, representing approximately one-third of the total [1]. Several recent studies have sought to quantify emissions from post-farm activities with the aim of identifying the highest emitting components, propose energy-efficient technologies, and provide roadmaps and mitigation strategies to support and shape policy decisions for the agrifood sector. According to FAO [1], pre-and post-agricultural production activities encompass a range of operations, including manufacturing of fertilizers and pesticides, food processing, packaging, retailing, transport, household consumption, and waste disposal.

Cold chains are a critical infrastructure of agrifood systems, playing a vital role in preserving perishable food and enabling its distribution from local to global scales. The interconnected processes of precooling, refrigerated transport, storage, and distribution are crucial for maintaining food quality and safety from production to consumption. While it is well understood that a lack of refrigeration capacity is a major driver of food loss globally [2,3], targeted research on the synergies and trade-offs of future cold chains development in agrifood systems with respect to climate and sustainable development goals and targets remains limited [4,5].

As efforts to combat hunger and food insecurity intensify, the demand for refrigeration processes will continue to rise. Therefore, developing sustainable food cold chains with minimal GHG emissions impact is crucial [6]. Moreover, development of cold chains has important positive spill-over effects across agrifood systems [7].

The direct component of GHG emissions from agrifood system cold chains, i.e., those related to the use of refrigerant F-gases, is available with country detail from FAO [8], showing a world total of 0.52 Gt CO_2eq in the year 2021, with a nearly five-fold increase since the year 2000. Conversely, similarly detailed data on the indirect emissions from agrifood system cold chains, i.e., from energy consumption, do not yet exist. This indirect component may in fact be significant, considering that published global estimates suggest that up to 5% of the worlds' electricity is currently used to operate agrifood system cold chains [9,10].

Geoscientific Model Development, vol. 17, issue no. 1, pp. 1-51, doi:10.5194/gmd-17-1-2024

Scenario set-up and forcing data for impact model evaluation and impact attribution within the third round of the Inter-Sectoral Model Intercomparison Project (ISIMIP3a).

Frieler, K., J. Volkholz, S. Lange, J. Schewe, M. Mengel, M.R. Rivas López, C. Otto, C.P.O. Reyer, D.N. Karger, J.T. Malle, S. Treu, C. Menz, J.L. Blanchard, C.S. Harrison, C.M. Petrik, T.D. Eddy, K. Ortega-Cisneros, C. Novaglio, Y. Rousseau, R.A. Watson, C. Stock, X. Liu, R. Heneghan, D. Tittensor, O. Maury, M. Büchner, T. Vogt, T. Wang, F. Sun, I.J. Sauer, J. Koch, I. Vanderkelen, **J. Jägermeyr**[1,2,3], C. Müller, J. Klar, I.D. Vega del Valle, G. Lasslop, S. Chadburn, E. Burke, A. Gallego-Sala, N. Smith, J. Chang, S. Hantson, C. Burton, A. Gädeke, F. Li, S.N. Gosling, H. Müller Schmied, F. Hattermann, J. Wang, F. Yao, T. Hickler, R. Marcé, D. Pierson, W. Thiery, D. Mercado-Bettín, R. Ladwig, A.I. Ayala-Zamora, M. Forrest, and M. Bechtold, 2024

NASA Goddard Institute for Space Studies, New York, NY, USA[1]
Center for Climate Systems Research, Columbia University, New York, NY, USA[2]
Potsdam Institute for Climate Impact Research, Potsdam, Germany[3]

Abstract. This paper describes the rationale and the protocol of the first component of the third simulation round of the Inter-Sectoral Impact Model Intercomparison Project (ISIMIP3a, http://www.isimip.org, last access: 2 November 2023) and the associated set of climate-related and direct human forcing data (CRF and DHF, respectively). The observation-based climate-related forcings for the first time include high-resolution observational climate forcings derived by orographic downscaling, monthly to hourly coastal water levels, and wind fields associated with historical tropical cyclones. The DHFs include land use patterns, population densities, information about water and agricultural management, and fishing intensities. The ISIMIP3a impact model simulations driven by these observation-based climate-related and direct human forcings are designed to test to what degree the impact models can explain observed changes in natural and human systems. In a second set of ISIMIP3a experiments the participating impact models are forced by the same DHFs but a counterfactual set of atmospheric forcings and coastal water levels where observed trends have been removed. These experiments are designed to allow for the attribution of observed changes in natural, human, and managed systems to climate change, rising CH_4 and CO_2 concentrations, and sea level rise according to the definition of the Working Group II contribution to the IPCC AR6.

Introduction. The Inter-Sectoral Impact Model Intercomparison Project ISIMIP (http://www.isimip.org, last access: 2 November 2023) provides a common scenario framework for cross-sectorally consistent climate impact simulations currently covering the following sectors: agriculture (global, in cooperation with AgMIP's Global Gridded Crop Model Intercomparison Project – GGCMI, water – global and regional, lakes – global and regional, biomes – global, forest – regional, fisheries and marine ecosystems – global and regional, terrestrial biodiversity – global, fire – global, permafrost – global, peat – global, coastal systems – global, energy – global, health: temperature-related mortality, waterborne diseases, vector-borne diseases, and food security and nutrition – global and local, labor productivity – global and local). The impact model simulations are made freely available, allowing for all types of follow-up analysis. The consistent design of the simulations does allow for the comparison of climate impact simulations within each sector. However, it also enables the bottom-up integration of impacts across sectors. Thus, it provides a unique basis for the estimation of the effects of climate change on, e.g., the economy, displacement and migration, health, or water quality, resolving the mechanisms along different impact channels and fully exploiting the process understanding represented in the biophysical impact models.

Open Data Journal for Agricultural Research, vol. 10, pp. 28-34, doi:10.18174/odjar.v10i0.16398

A daily time-step observed and scenario climate dataset on a European grid for crop modelling applications.

Fronzek, S., H. Webber, R. Rötter, **A.C. Ruane**[1], and F. Evert, 2024

NASA Goddard Institute for Space Studies, New York, NY, USA[1]

Abstract. This paper describes a daily time-step observed and scenario climate dataset on a European grid with 25 km x 25 km spatial resolution. The dataset was developed for crop modelling applications in the MACSUR project. The dataset covers the period 1980-2010 for observations; this is, for a baseline period of 1981-2010 and the year 1980 for crop model simulations with sowing dates in the autumn. It also covers the periods 2040-2069 and 2070-2099 for 5 Global Climate Models (GCMs) x 2 forcing scenarios (RCP4.5 and RCP8.5) and 2 GCMs with RCP2.6. The Joint Research Centre's (JRC) Agri4Cast gridded dataset was used for the baseline. The scenarios have been calculated using an enhanced delta change method that applies changes in aspects of temperature and precipitation variability in addition to changes in mean climate.

Introduction. A consistent daily weather dataset with historic data for 1981-2010 and a set of scenarios for the periods 2040-2069 and 2070-2099 has been constructed for agricultural applications on a regular grid for Europe covering the EU-27 countries plus Norway, Liechtenstein, Switzerland, the Balkan region and Kaliningrad. The primary purpose for this dataset was to serve as input data for gridded crop model simulation experiments, in which the effect of processes on drought and heat stress were evaluated (Webber et al. 2018), and future prospects for soybean cultivation were assessed (Nendel et al. 2023). The dataset is suitable for crop modelling and other applications requiring agroclimatic data under different climate change scenarios.

Three versions of the dataset have been prepared: version 1 consisting of 8709 grid cells) that was used by Webber et al. (2018), an updated version 2 consisting of 8748 grid cells) that corrects an error that occurred when a correction for differences in altitude was applied to agricultural cultivation areas, and version 3 consisting of 9220 grid cells that corrects an error in the scenario values for vapour pressure and dew point temperature and expands the study region to include Switzerland, Lichtenstein, the Balkan region and Kaliningrad. It is recommended to use the latest version, unless the data are intended to be used for direct comparison with the crop model results of Webber et al. (2018, 2020).

2. Data and Methods. 2 .1 Baseline climate data Weather data source. Daily weather data was downloaded from the JRC Agri4Cast database (version 1.0) for grid cells covering the EU-27 countries (Austria, Belgium, Bulgaria, Cyprus, Denmark, Finland, France, Germany, Greece, Ireland, Italy, Luxembourg, Malta, Netherlands, Portugal, Romania, Spain, Sweden, United Kingdom, Czech Republic, Estonia, Hungary, Latvia, Lithuania, Poland, Slovenia, Slovak Republic) and Norway, Liechtenstein, Switzerland, the Balkan region and Kaliningrad. The data were interpolated from approximately 4000 weather stations in Europe to a regular grid of25 km x 25 km resolution with the Lambert Azimuthal Equal Area projection (Toreti et al. 2019; Van der Goot et al. 2004). In version 1.0of the AgriCast dataset used here, interpolated temperature variables are corrected by altitude by using the median of all arable land points within a grid cellif arable land covers more than 5%, and the lower quartile of all points (arable and not arable) within grid cell is if arable land covers less than 5% (A. Toreti, pers. comm.).

Journal of Advances in Modeling Earth Systems, vol. 16, issue no. 10, e2023MS004185, doi:10.1029/2023MS004185

Global influence of organic aerosol volatility on aerosol microphysical processes: Composition and number.

Gao, C.Y.[1], **S.E. Bauer**[1], **K. Tsigaridis**[1,2], and U. Im, 2024

NASA Goddard Institute for Space Studies, New York, NY, USA[1]
Center for Climate Systems Research, Columbia University, New York, NY, USA[2]

Abstract. We present MATRIX-VBS, a new aerosol scheme that simulates organic partitioning in an aerosol microphysics model, as part of the NASA GISS ModelE Earth System Model. MATRIX-VBS builds on its predecessor aerosol microphysics model MATRIX (Bauer et al., 2008, **https://doi.org/10.5194/acp-8-6003-2008**) and was developed in the box model framework (Gao et al., 2017, **https://doi.org/10.5194/gmd-10-751-2017**). The scheme features the inclusion of organic partitioning between the gas and particle phases and the photochemical aging process using the volatility-basis set (Donahue et al., 2006, **https://doi.org/10.1021/es052297c**). To assess the performance of the new model, we compared its mass concentration, number concentration, and activated number concentration to the original scheme MATRIX, and evaluated its mass concentrations in four seasons against data from the NASA Atmospheric Tomography Mission (ATom) aircraft campaign. Results from MATRIX-VBS show that organics are transported further away from their source, and their mass concentration increases aloft and decreases at the surface compared to those in MATRIX. The mass concentration of organics at the surface agrees well with measurements, and there are discrepancies for vertical profiles aloft. In the new scheme, the global mass load of organic aerosols increased by 50%, there is also an increased number of particles at the surface and fewer activated ones in most regions. The new scheme presents advanced and more comprehensive capability in simulating aerosol processes.

Introduction. The chemical composition of aerosols is key to understanding their impact on climate (Seinfeld & Pandis, **2016**). Thanks to advancements in aerosol measurement techniques and an increased number of field campaigns, our knowledge of the chemical composition and evolution of aerosols in the real world has rapidly improved. At the same time, in the simulated Earth system, the modeling community has also made significant strides by including more comprehensive aerosol physical processes in models, narrowing the gap between simulated aerosols and those observed, and reducing uncertainties in climate impact predictions.

Despite continuing efforts, the bias between measurements and simulated organic aerosols remains. Inter-model comparisons against measurements show that most models underestimate organic aerosol concentrations (e.g., Tsigaridis et al., **2014**) due to missing sources of secondary organic aerosols. In addition, aerosol formation rates, especially those for organic aerosols, should be at least an order of magnitude higher in models (Heald et al., **2005**; Hodzic et al., **2010**; Spracklen et al., **2011**; Volkamer et al., **2006**).

Subsequent modeling efforts aimed to improve organic aerosol representation in models and fill the gap between measurements and models by including semi-volatile primary organic aerosol (POA) and intermediate volatility organic compound (IVOCs) as secondary organic aerosol SOA precursors in regional (Ahmadov et al., **2012**; Athanasopoulou et al., **2013**; Ciarelli et al., **2017**; Fountoukis et al., **2014**; Koo et al., **2014**; Lane et al., **2008**; Murphy & Pandis, **2009**; Shrivastava et al., **2008**; Tsimpidi et al., **2010**, **2011**) and global (Chen et al., **2021**; Hodzic et al., **2010**, **2016**; Jathar et al., **2011**; Jo et al., **2013**; Pye & Seinfeld, **2010**; Tsimpidi et al., **2014**, **2018**) models using the volatility-basis set (VBS), an organic aerosol parameterization by Donahue et al. (**2006**) that resolves the volatility space of organic aerosols.

However, to our knowledge, no global climate model with aerosol microphysics that tracks aerosol mixing state has considered semi-volatile organics, and our understanding of the impact of semi-volatile organics on aerosol microphysics and climate at the global scale remains limited (Mann et al., **2014**).

International Journal of Plant Production, vol. 18, issue no. 4, pp. 563-577, doi:10.1007/s42106-024-00310-6

How can future climate change affect the corn production system in Nebraska, USA?

Gonçalves, I.Z., I.M. Fattori, C.M.U. Neale, C.A.C. Santos, **A.C. Ruane**[1], **M.M. Phillips**[1], and F.R. Marin, 2024

NASA Goddard Institute for Space Studies, New York, NY, USA[1]

Abstract. The increasing temperatures and changing precipitation patterns have affected both crop yields and water requirements challenging agricultural systems in sustaining high crop yields and ensuring water and food security. In the present study, we evaluated the impact of climate change on the corn production under irrigated and rainfed cropping systems in Nebraska considering four climate zones until 2100 as a case study for the US Corn Belt. Additionally, suggests ways to reduce the impact of climate change on corn yield and water resources. Five global circulation model datasets from the sixth phase of the Coupled Model Intercomparison Project (CMIP6) interconnected to Shared Socioeconomic Pathways (SSPs), were selected. Three future periods: near (2020–2039), mid (2040–2069), and far future (2070–2100) under SSP226, SSP370, and SSP585 scenarios were used to predict the climate changes, crop cycle length, crop yield, and crop water requirement. Additionally, we input annual CO_2 concentration scenarios for each SSP scenario to model changes from 2015 to 2100 using the CERES-Maize model. Temperatures are forecasted to rise, precipitation to decline, and crop cycle length to decrease, particularly for SSP370 (up to 49% yield decrease) and SSP585 (up to 67% yield decrease) by 2070–2100. Yields are expected to decline across all scenarios and periods for irrigated and rainfed fields due to the reduction in crop cycle length. Crop water demand is projected to increase, with rainfed systems facing heightened impact due to reduced precipitation. Addressing climate change in Nebraska requires actions like developing new corn varieties to longer the crop season, transitioning to efficient irrigation systems, improving irrigation management for water and food security, and reducing the risk of conflicts over its use. These results open possibilities for discussion about the actions that can be taken to cope with climate change and guarantee water and food security in the US Corn Belt.

Introduction. Increasing temperature is projected to increase even more in the next few decades (Intergovernmental Panel on Climate Change, 2022), which has raised questions about its impacts on long-term agricultural production and how we can adapt to these changes and ensure water security and food supply for future generations. Projections for U.S. agriculture indi-cate that its impact can transform through changes in yield (Wang et al., 2019; Schauberger et al., 2017; Schlenker & Roberts, 2009; Zhao et al., 2017; Liang et al., 2017; Ortiz-Bobea et al., 2021) and shifts in the cultivation geographies of many crops (Burchfield, 2022).

The United States is the world's largest corn exporter and exports between 10% and 20% of its total production volume (USDA-ERS, 2023a), and Nebraska, located in the midwestern United States, in the U.S. "Corn Belt," is well known for its agricultural and livestock production. In 2023, Nebraska generated around $31.1 billion in agricultural cash receipts, with the highest-valued commodities being cattle and calves, corn, and soybeans (USDA, 2023b). The state ranks third in the nation in corn production (over 4 mil-lion hectares), with important uses such as feed for livestock and ethanol production and is the second-largest ethanol-producing state in the U.S. and one of the most important beef producers (USDA, 2023b).

Unprecedented climate changes have become a major challenge for sustainable crop production globally and put food supplies at risk (Marin et al., 2022). Thus, crop simula-tion models have been widely used to understand the impact of climate change projections on the agricultural system across large temporal and spatial scales (Jägermeyr et al. 2021). However, important aspects of supporting decision-making for current weather and future climates need to be developed on a small scale, considering the specific traits of the production area.

Journal of Geophysical Research Atmospheres, vol. 129, issue no. 24, e2023JD039571, doi:10.1029/2023JD039571

Dynamical importance of the trade wind inversion in suppressing the southeast Pacific ITCZ.

Gonzalez, A.O., I. Ganguly, M. Osterloh, **G.V. Cesana**[1,2], and C.A. DeMott, 2024

NASA Goddard Institute for Space Studies, New York, NY, USA[1]
Center for Climate Systems Research, Columbia University, New York, NY, USA[2]

Abstract. Sea surface temperature (SST) gradients are a primary driver of low-level wind convergence in the east Pacific Inter-Tropical Convergence Zone (ITCZ) through their hydrostatic relationship to the surface pressure gradient force (PGF). However, the surface PGF may not always align with SST gradients due to variations in boundary layer temperature gradients with height, that is, the boundary layer contribution to the surface PGF. In this study, we investigate the observed northern hemisphere position of the east Pacific ITCZ using a slab boundary layer model (SBLM) driven by different approximations of the boundary layer virtual temperature field. SBLM simulations using the entire boundary layer virtual temperature profile produce a realistic northern hemisphere ITCZ. However, SST-only simulations produce excessive equatorial divergence and southern hemisphere convergence, resulting in a latitudinally confined double ITCZ-like structure. Observed virtual temperature gradients highlight the importance of northward temperature gradients strengthening with height from the equator to 15°S below the trade wind inversion (TWI). Our interpretation is that the equatorial cold tongue induces relatively weak high surface pressure and double ITCZ-like convergence because the resulting layer of cold air is shallow. Concurrently, relatively strong high surface pressure spreads out in the southern hemisphere due to interactions between stratocumulus clouds and the ocean surface. Together, the equatorial cold tongue and the TWI/stratocumulus clouds enable a more northern hemisphere dominant ITCZ. Thus, we provide evidence of a dynamical link between the equatorial cold tongue, low clouds, and double ITCZs, which continue to be problematic in Earth system models.

Introduction. The east Pacific Ocean intertropical convergence zone (ITCZ) is highly modulated by variations in the tropical boundary layer winds, which often produce horizontal convergence that is co-located with ITCZ precipitation (Gonzalez et al., 2022; Lindzen & Nigam, 1987; Liu & Xie, 2002). The cause of these boundary layer wind variations is commonly diagnosed through the zonal and meridional momentum budgets (Back & Bretherton, 2009a; Gonzalez & Schubert, 2019; Gonzalez et al., 2022; Holton, 1975; Holton et al., 1971; Lindzen & Nigam, 1987; Mahrt, 1972a, 1972b; McGauley et al., 2004; Raymond et al., 2006; Sobel & Neelin, 2006; Tomas et al., 1999). A leading term in boundary layer momentum budgets is the pressure gradient force (PGF), especially in regions where there are strong sea surface temperature (SST) gradients (Back & Bretherton, 2009b; Duffy et al., 2020; Lindzen & Nigam, 1987). The link between SST and boundary layer pressure gradients comes from hydrostatic balance when integrated vertically. In a hydrostatic atmosphere, the surface pressure is determined by the density of the overlying atmospheric column. Therefore, regions with cool SSTs tend to have a higher surface pressure due to a heavier column above, and regions with warm SSTs tend to have a lower surface pressure due to a lighter column above.

Lindzen and Nigam (1987); Stevens et al. (2002); Back and Bretherton (2009a); Duffy et al. (2020), and Zhou et al. (2020) used hydrostatic balance and different forms of a linear boundary layer model to quantify how well SST gradients explain large-scale surface winds and convergence in the tropics. When integrating vertically to solve for the surface pressure gradient, most of these studies assume temperature gradients decrease with height in the boundary layer at a constant rate determined solely from the SST distribution (i.e., larger lapse rates for warm than cool SSTs). However, this assumption does not always hold true because of variations in boundary layer lapse rates that are inconsistent with SST over wide swaths of tropical latitudes. For example, near the equatorial cold tongue, SST gradients are large.

Photosynthetica, vol. 62, issue no. 3, pp. 271-288, doi:10.32615/ps.2024.029

Contributions of David Mauzerall to photosynthesis research — Celebrating his 95th birthday.

Govindjee, G., O. Canaani, R.A. Cellarius, B. Diner, E. Greenbaum, H. Hou, **N.Y. Kiang**[1], J.S. Lindsey, D.L. Mauzerall, M.E. Mauzerall, M. Seibert, and A. Stirbet, 2024

NASA Goddard Institute for Space Studies, New York, NY, USA[1]

Abstract. We honor here Professor David Mauzerall, a pioneer in the fields of photochemistry and photobiology of porphyrins and chlorophylls *in vitro* and *in vivo*, on the occasion of his 95th birthday. Throughout his career at The Rockefeller University, he refined our understanding of how chlorophyll converts light energy into chemical energy. He exploited top-of-the-line laser technology in developing photoacoustics and a variety of other innovative experimental approaches. His experimental work and conceptual insights contributed greatly to our understanding of photosynthesis and the possible role of photosynthesis in the origin of life. His contributions include many landmark single-authored and collaborative papers, and his legacy includes the training of others who have become authorities themselves. After providing a brief description of his research accomplishments, we include tributes from several of his coworkers and his daughters highlighting their valuable experiences with David Mauzerall on this milestone birthday.

Introduction. David Charles Mauzerall (born 22 July 1929) grew up under humble circumstances in the French-speaking section of a small, textile town (Sanford) in Maine, USA. His early life, high school and college education, and extracurricular activities are recounted in depth in a recent article (Lindsey 2024). He attended graduate school at the University of Chicago where he did novel research on the physical organic chemistry of NADPH (Mauzerall and Westheimer 1955) in the laboratory of Professor Frank Henry Westheimer (1912–2007; see: https://en.m.wikipedia.org/wiki/Frank_Westheimer). After completing his PhD in 1954, he joined the lab of Professor Sam Granick (1909–1977; see: https://en.m.wikipedia. org/wiki/Sam_Granick) at The Rockefeller Institute for Medical Research. In the Granick lab, he began research on the fundamental reactivity of molecules in the tetrapyrrole biosynthetic pathway. He rose through the ranks there, becoming a full professor at The Rockefeller University in 1969. Fig. 1 shows a photo of David (Dave) Mauzerall.

Given his physical organic background and research in enzyme-mimetic chemistry, the question arises when did Mauzerall's interest in photosynthesis begin? His first paper on photochemistry, concerning the photoreduction of porphyrins with amines, was in 1960 (Mauzerall 1960). In the 1950s, the Granick lab was routinely generating mutants of photosynthetic bacteria for studies of tetrapyrrole biosynthesis. A further spark appears to have come from Mauzerall's first graduate student, Richard Cellarius, who arrived with a physics background, having done studies on photosynthesis as a solid-state phenomenon; Cellarius and Mauzerall (1966) published together on a model light-harvesting system. From the 1960s on, David's studies were centered on questions about the mechanisms of photosynthesis, and the role of photosynthesis in the origin of life. For a broad overview of Mauzerall's life and far-reaching scientific contributions, see Lindsey (2024). In his personal life, Dave was married to Dr. Miriam Jacob (1924–2023; a summary of her life is included in Appendix 1), a cell physiologist and scientific writer, for 64 years. They have two daughters, Denise and Michele. Below, we present some selected contributions of Professor David C. Mauzerall to the field of photosynthesis and related processes. Appendix 2 provides URLs for websites about Dave Mauzerall.

Journal of Climate, vol. 37, issue no. 20, pp. 5387-5403, doi:10.1175/JCLI-D-24-0011.1

Understanding the relationship between cloud controlling factors and the ISCCP weather states.

Grise, K.M., and **G. Tselioudis**[1,2], 2024

NASA Goddard Institute for Space Studies, New York, NY, USA[1]
Department of Applied Physics and Applied Mathematics, Columbia University, New York, NY, USA[2]

Abstract. Two common methods used to develop a process-level understanding of global cloud cover are 1) analyzing large-scale meteorological variables (cloud controlling factors) associated with cloud variability and 2) classifying cloud types using clustering algorithms applied to satellite data, such as the International Satellite Cloud Climatology Project (ISCCP) weather states. The cloud controlling factor method is advantageous to apply to climate models, as it does not rely on cloud parameterizations or the availability of satellite simulator output. The purpose of this study is to document the relationship between cloud controlling factors and the ISCCP weather states in the observational record, providing a benchmark for the application of cloud controlling factors to study individual cloud types in future studies. Most ISCCP weather states are linked to distinct dynamical regimes characterized by unique combinations of six cloud controlling factors. These relationships are present in both the long-term mean climatology and daily-to-monthly climate variability. For example, deep convective and midlatitude storm clouds dominate ascending regions. In descending regions, shallow cumulus is more frequent in regimes characterized by weak boundary layer temperature inversions [estimated inversion strength (EIS)] and strong subsidence, and stratocumulus is more frequent in regimes with larger values of EIS, weaker subsidence, and relatively weak near-surface cold advection. Midlevel clouds are prominent in descending regions with strong cold advection. Overall, the results of this study suggest promise in using cloud controlling factors to identify dynamical regimes where individual cloud types are more or less likely and to understand the physical processes responsible for the transitions among them.

Introduction. Clouds remain one of the largest sources of uncertainty in global climate projections (e.g., Bony and Dufresne 2005; Webb et al. 2013; Zelinka et al. 2020). Cloud processes are challenging to simulate directly in present-generation global climate models because they occur on spatial and temporal scales too small to be resolved in models and must therefore be parameterized. Efforts to improve the representation of clouds in models rely on a process-level understanding of the factors that govern various cloud types.

One common method to understand the processes responsible for global cloud cover and its variability is the cloud controlling factor framework (e.g., Stevens and Brenguier 2009; Klein et al. 2017). Cloud controlling factors are large-scale meteorological variables that have been linked to variability in global cloud cover and its radiative properties in the observed climate system, serving as proxies for the turbulent fluxes of heat, moisture, and momentum relevant for cloud formation (Scott et al. 2020). The advantage of the cloud controlling factor approach is that large-scale meteorological fields are more well represented in models than the smaller-scale cloud properties that depend upon them. Therefore, by understanding how observed cloud properties respond to perturbations in the cloud controlling factors, the response of model clouds to climate change can be inferred solely from the models' projected future changes in large-scale meteorological factors, circumventing the need to rely on the models' cloud parameterizations. This method has been used by a number of recent studies to provide observational constraints on global cloud feedbacks (Qu et al. 2015; Myers et al. 2021; Cesana and Del Genio 2021).

The cloud controlling factor framework is most commonly applied to understand marine low cloud variability, not only in the tropics and subtropics (e.g., Norris and Iacobellis 2005; Myers and Norris 2013, 2015; Qu et al. 2014; Seethala et al. 2015) but also in the extratropics (e.g., Wall et al. 2017; Zelinka et al. 2018; Kelleher and Grise 2019; Grise and Kelleher 2021; Blanco et al. 2023).

Geoscientific Model Development, vol. 17, issue no. 7, pp. 2547-2567, doi:10.5194/gmd-17-2547-2024

Modeling the effects of tropospheric ozone on the growth and yield of global staple crops with DSSAT v4.8.0.

Guarin, J.R.[1,2], **J. Jägermeyr**[1,2], E.A. Ainsworth, F.A.A. Oliveira, S. Asseng, K. Boote, J. Elliott, L. Emberson, I. Foster, G. Hoogenboom, D. Kelly, **A.C. Ruane**[1], and K. Sharps, 2024

NASA Goddard Institute for Space Studies, New York, NY, USA[1]
Center for Climate Systems Research, Columbia University, New York, NY, USA[2]

Abstract. Elevated surface ozone (O_3) concentrations can negatively impact growth and development of crop production by reducing photosynthesis and accelerating leaf senescence. Under unabated climate change, future global O_3 concentrations are expected to increase in many regions, adding additional challenges to global agricultural production. Presently, few global process-based crop models consider the effects of O_3 stress on crop growth. Here, we incorporated the effects of O_3 stress on photosynthesis and leaf senescence into the Decision Support System for Agrotechnology Transfer (DSSAT) crop models for maize, rice, soybean, and wheat. The advanced models reproduced the reported yield declines from observed O_3-dose field experiments and O_3 exposure responses reported in the literature (O_3 relative yield loss RMSE <10 % across all calibrated models). Simulated crop yields decreased as daily O_3 concentrations increased above 25 ppb, with average yield losses of 0.16 % to 0.82 % (maize), 0.05 % to 0.63 % (rice), 0.36 % to 0.96 % (soybean), and 0.26 % to 1.23 % (wheat) per ppb O_3 increase, depending on the cultivar O_3 sensitivity. Increased water deficit stress and elevated CO_2 lessen the negative impact of elevated O_3 on crop yield, but potential yield gains from CO_2 concentration increases may be counteracted by higher O_3 concentrations in the future, a potentially important constraint to global change projections for the latest process-based crop models. The improved DSSAT models with O_3 representation simulate the effects of O_3 stress on crop growth and yield in interaction with other growth factors and can be run in the parallel DSSAT global gridded modeling framework for future studies on O_3 impacts under climate change and air pollution scenarios across agroecosystems globally.

Introduction. Surface or ground-level, ozone (O_3) is a major air pollutant that causes adverse impacts on agricultural productivity worldwide (Mills et al., 2018a; Emberson et al., 2018; Tai et al., 2021). O_3 is formed through photochemical reactions between incoming solar radiation and primary pollutants such as nitrogen oxides (NO_x= NO + NO_2), volatile organic compounds (VOCs), carbon monoxide (CO), or methane (CH_4) across all areas of the globe (Cooper et al., 2014; Simpson et al., 2014). Global O_3 concentrations have increased 2 %–7 % per decade in northern mid-latitude regions and 2 %–12 % per decade in tropical regions since the mid-1990s (IPCC, 2021; Arias et al., 2021). Future O_3 concentrations are projected to continue increasing if O_3 precursor emissions are not mitigated, i.e., following the shared socio-economic pathways where regional rivalry leads to doubling of CO_2 emissions by 2100 (SSP3-7.0) or where fossil-fuel-enabled growth leads to doubling of CO_2 emissions by 2050 (SSP5-8.5) (IPCC, 2021; Arias et al., 2021; Szopa et al., 2021; Griffiths et al., 2021).

Crops exposed to elevated levels of O_3 concentrations can experience reduced photosynthesis, accelerated senescence, foliar chlorosis, and even necrosis from increased cumulative oxidative stress (Ainsworth, 2017). These negative effects lead to decreased productivity resulting in global yield losses between 2 %–16 % for the four main staple crops, maize, rice, soybean, and wheat (Ainsworth, 2017; Schiferl and Heald, 2018; Emberson, 2020), with global annual economic damages of approximately USD 34 billion (Sampedro et al., 2020; Feng et al., 2022). Climate change may exacerbate the negative effects from elevated O_3 concentrations because O_3 concentrations are highest in summer months, and the projected higher temperatures with more frequent heat waves may lead to a longer period of more active photochemical reactions (Zhang and Wang, 2016; Hou and Wu, 2016; Szopa et al., 2021).

Environmental Research Letters, vol. 19, issue no. 10, 104059, doi:10.1088/1748-9326/ad6a6f

El Niño and positive Indian Ocean Dipole conditions simultaneously reduce the production of multiple cereals across India.

Gurazada, M., **S. McDermid**[1,2], R. DeFries, K.F Davis, J. Singh, and D. Singh, 2024

NASA Goddard Institute for Space Studies, New York, NY, USA[1]
Department of Environmental Studies, New York University, New York, NY, USA[2]

Abstract. Natural climate phenomena like El Niño Southern Oscillation (ENSO) and the Indian Ocean Dipole (IOD) influence the Indian monsoon and thereby the region's agricultural systems. Understanding their influence can provide seasonal predictability of agricultural production metrics to inform decision-making and mitigate potential food security challenges. Here, we analyze the effects of ENSO and IOD on four agricultural production metrics (production, harvested area, irrigated area, and yields) for rice, maize, sorghum, pearl millet, and finger millet across India from 1968 to 2015. El Niños and positive-IODs are associated with simultaneous reductions in the production and yields of multiple crops. Impacts vary considerably by crop and geography. Maize and pearl millet experience large declines in both production and yields when compared to other grains in districts located in the northwest and southern peninsular regions. Associated with warmer and drier conditions during El Niño, >70% of all crop districts experience lower production and yields. Impacts of positive-IODs exhibit relatively more spatial variability. La Niña and negative-IODs are associated with simultaneous increases in all production metrics across the crops, particularly benefiting traditional grains. Variations in impacts of ENSO and IOD on different cereals depend on where they are grown and differences in their sensitivity to climate conditions. We compare production metrics for each crop relative to rice in overlapping rainfed districts to isolate the influence of climate conditions. Maize production and yields experience larger reductions relative to rice, while pearl millet production and yields also experience reductions relative to rice during El Niños and positive-IODs. However, sorghum experiences enhanced production and harvested areas, and finger millet experiences enhanced production and yields. These findings suggest that transitioning from maize and rice to these traditional cereals could lower interannual production variability associated with natural climate variations.

Introduction. Oscillations in tropical sea-surface temperatures drive variations in global rainfall and temperature patterns that affect food production and livelihoods worldwide [1, 2]. India is particularly vulnerable to such natural climate variations, as the country's agricultural activities and water availability closely depend on the Indian summer monsoon rainfall (ISMR). Agriculture is crucial to the Indian economy, contributing substantially to employment, food security, and economic growth. According to the Indian Economic Association [3], agriculture employed about 46.5% of the workforce in 2020–21 and constituted one-fifth of India's economy (Gross Value Added). Fluctuations in temperature and monsoonal rainfall can impact food production, food prices, agricultural activities, and socioeconomic stability of the agricultural workforce [4], thereby affecting food security within India and beyond [5–8].

El Niño Southern Oscillation (ENSO) is a primary mode of natural variability in Earth's climate system and a major driver of ISMR variability [9]. The Indian Ocean Dipole (IOD) also influences the ISMR and modulates monsoon-ENSO teleconnections [10–13]. Typically, the Indian monsoon experiences below average rainfall during El Niño [9] and excess rainfall during La Niña [14]. Positive IOD events typically enhance the monsoon but are associated with delayed monsoon onset over southwestern India [15]. Strong El Niño events often co-occur with positive IOD (IOD^{+}) events, and recent research suggests these co-occurrences have become more frequent in recent decades [16]. However, the impacts of their co-occurrences are not well understood due to the relatively short instrumental record.

Environmental Modelling & Software, vol. 172, 105935, doi:10.1016/j.envsoft.2023.105935

How wide is the problem? Leveraging alternative data sources to enhance channel width representation in watershed modeling.

Haas, H.[1], L. Kalin, and E. Baltaci, 2024

NASA Goddard Institute for Space Studies, New York, NY, USA[1]

Abstract. Watershed models have been increasingly applied to investigate the impacts of environmental changes on water quantity and quality and to support decision-making. Thus, accurately capturing physical processes and the characteristics of the watershed system is vital to achieving reliable results. Channel geometry features such as cross-sectional shape, bankfull channel width, and depth affect hydraulic parameters like hydraulic radius, wetted perimeter, and cross-sectional area. These, in turn, play important roles in streamflow dynamics, flow velocity, erosion, nutrient transport, and stream ecology. However, the representation of bankfull channel width is often oversimplified in watershed models. Power-law regression equations relating geometric parameters and upstream drainage area are commonly used to calculate bankfull channel width in watershed models. This approach has limitations and may resonate in the misrepresentation of channel geometry with implications for water quantity and quality estimations. This study evaluates how bankfull channel width is represented in a popular watershed model and presents alternative data sources derived from aerial measurements, empirical models, LiDAR, and a global database to mitigate potential misrepresentations. To assess the impacts of bankfull channel width on water quantity and quality, we designed a series of modeling experiments through the Soil and Water Assessment Tool (SWAT) model. We test our methodology in the Alabama-Coosa-Tallapoosa river basin, a large watershed system draining to the Gulf of Mexico coast. Our findings indicate that, overall, the regression equation used in the ArcSWAT program (SWAT's GIS interface) can overestimate bankfull channel width by as much as three times in our study domain. In testing the effects of bankfull width on model simulations we found negligeable implication for water yield predictions. On the other hand, 1-day maximum flows were greatly increased (20%) by using channel width values from the alternative data sources. Simulated water quality was also affected, with stream water temperature showing better agreement with observations under the proposed scenarios. Sediment loadings increased by as much as 118% under the alternative data sources of channel width. Nitrate and phosphate loadings had opposite responses and showed decreases as high as 8.3 and 18.8%, respectively, relative to the default model. Our findings demonstrate that bankfull channel width is misrepresented in watershed models with underlying impacts on simulated water quantity, quality, and ecological flows. Our analysis found bankfull channel width as an important parameter affecting high flows and water quality, and the freely available data sources tested in this study showed good matches with field measurements, making our findings readily available and broadly useful to the modeling community.

Introduction. Channel geometry features such as cross-sectional shape, bankfull channel width and depth affect hydraulic parameters like hydraulic radius, wetted perimeter, and cross-sectional area. These variables, in turn, play a crucial role in determining water velocity, volume, sediment, and pollutant transport within the channel, thereby affecting both streamflow and water quality (Choi et al., 2018; Stewardson, 2005). In terms of streamflow, wider channels can mitigate flood risk by accommodating larger water volumes during high-flow events (Kale and Hire, 2004), while narrower channels can increase water flow velocity, leading to increased erosive potential, channel instability, and bank erosion (Fisher et al., 2013; Michalková et al., 2011). In terms of water quality, bankfull width and depth influence the residence time of water and the exchange of water between the channel and surrounding riparian areas, with underlying implications for nutrient cycling and pollutant transport (Baradei, 2020; Sharpley et al., 2013).

Ecological Modelling, vol. 489, 110620, doi:10.1016/j.ecolmodel.2024.110620

Improved forest canopy evaporation leads to better predictions of ecohydrological processes.

Haas, H.[1], L. Kalin, and H. Yen, 2024

NASA Goddard Institute for Space Studies, New York, NY, USA[1]

Abstract. Canopy evaporation (E_i) is a vital process in forest ecosystems impacting hydrology and biogeochemistry through the redistribution of gross rainfall and gradual infiltration of water into the soil profile. Inaccurate representation of E_i in models may lead to flawed predictions of ecohydrological processes such as water availability, soil erosion, nutrient transport, and ecosystem productivity, thus compromising the reliability of model outputs. The Soil and Water Assessment Tool (SWAT) ecohydrological model has been widely used for various purposes worldwide. However, SWAT has shown limitations in forest ecosystems. SWAT employs a single equation to calculate canopy evaporation for crops and trees, which may not accurately account for the differences in ecophysiology and aerodynamic resistance between short and tall vegetation. In SWAT, canopy interception is calculated as a function of canopy storage and is normalized by the maximum plant leaf area index (LAI). Here we present an alternative approach to simulate forest canopy interception and evaporation with SWAT. Under our proposed approach, the LAI normalization is eliminated, and canopy storage is computed as a linear function of daily LAI and a user-defined parameter. We used remote-sensing (R-S) estimates of E_i to accurately parameterize forest canopy evaporation in the modified and default models. The Alabama-Coosa-Tallapoosa, a large (55,000 km^2) and forested watershed system in the Southeast United States, is utilized as testbed. Results showed that the default SWAT largely underestimated (> 70%) forest E_i across our study domain. The modified model better matched R-S estimates of E_i, showing a mere 2% overestimation. Additionally, the modified model yielded better agreement with R-S transpiration and total evapotranspiration compared to the default model. Our alternative approach positively affected the model simulation of daily streamflow and ecologically relevant flow metrics, reducing model overestimations and leading to better agreement with observations. Also, the modified model led to reduced sediment, nitrate, and organic nitrogen loadings, with sediment and organic nitrogen being particularly affected, witnessing reductions of 13 and 11%, respectively, compared to the default model. Finally, our proposed approach resonated in better agreement between simulated net primary productivity (NPP) and R-S estimates. Although our study is in the context of SWAT, our findings can be useful to the broader modeling community since other popular process-based models are based on similar modeling assumptions. Our findings demonstrate the benefits of improved forest evapotranspiration partitioning for simulating ecological processes with SWAT.

Introduction. Canopy rainfall interception is the process by which vegetation captures and temporarily stores gross rainfall (P) before it reaches the ground (Lawrence et al., 2007; Nicholls and Carey, 2021; Paul-Limoges et al., 2020; Stoy et al., 2019) - being the first of several land surface hydrological processes affecting the redistribution of rainwater (Brantley et al., 2019; Miralles et al., 2010). Canopy evaporation (E_i) represents a major fraction of the global terrestrial evapotranspiration (ET), making it a key, yet understudied, component of the terrestrial water and energy budgets (Hadiwijaya et al., 2021; Muzylo et al., 2009). This process is particularly relevant in forest ecosystems, where E_i usually represents 10 to 40% of the total ET (Brantley et al., 2019; Kofroňová et al., 2021; Miralles et al., 2010). Canopy interception and evaporation may also influence soil erosion and nutrient exports by facilitating the gradual infiltration of water into the soil profile and thereby minimizing the erosive power of rapid surface runoff (Zore et al., 2022). In forest ecosystems, the nexus between the soil-plant-atmosphere is stronger because of higher aerodynamic conductance associated with taller vegetation (Miralles et al., 2010; Muzylo et al., 2009). Thus, forest canopy interception is an important link between land surface and atmosphere influencing terrestrial biogeochemistry and water balance.

Nature Sustainability, vol. 7, issue no. 8, pp. 994-1006, doi:10.1038/s41893-024-01375-x

Threat of low-frequency high-intensity floods to global cropland and crop yields.

Han, J., Z. Zhang, J. Xu, Y. Chen, **J. Jägermeyr**[1,2,3], J. Cao, Y. Luo, F. Cheng, H. Zhuang, H. Wu, Q. Mei, J. Song, and F. Tao, 2024

NASA Goddard Institute for Space Studies, New York, NY, USA[1]
Center for Climate Systems Research, Columbia University, New York, NY, USA[2]
Potsdam Institute for Climate Impacts Research, Leibniz Association, Potsdam, Germany[3]

Abstract. Flood hazards pose a significant threat to agricultural production. Agricultural adaptations tend to be prevalent and systematic in high-frequency flood (HFF) areas but neglected in low-frequency flood (LFF) areas. Here, using satellite imagery, we map global spatial distributions of LFF and HFF at 250 m resolution for 3,427 flood events between 2000 and 2021. We show that LFF affected a larger proportion of cropland area (4.7%) than HFF (1.2%), and HFF occurred in smaller regions with less intensity. Cropland expansion between 2000 and 2019 increased the area affected by LFF (3.1×10^4 km^2) more than that affected by HFF (1.3×10^4 km^2). Moreover, the mean yield losses of wheat and rice from LFF were greater than those from HFF, owing to the higher precipitation anomalies, soil moisture anomalies and greater crop flooding during their growing seasons. Our findings highlight the urgency of this issue and identify priority areas to prevent these neglected low-frequency but high-impact floods, providing valuable information for developing flood-adapted policy.

Introduction. Floods affect agricultural production widely across the world[1,2]. Although numerous studies have reported the impacts of drought and heat stress on global crop yields, the impacts of floods have been less studied because most current crop models are not well developed in representing the impact processes of flooding and excess moisture[3,4,5,6,7]. Flooding poses a significant threat to global agricultural production, and this threat may increase as floods are projected to become more frequent and severe in many breadbasket regions under future climate change[8,9,10]. A comprehensive impact assessment of future floods on global agricultural production is therefore critical to identifying adaptation priorities.

Recently, some studies applied process-based crop models or satellite-based damage indices to investigate yield losses from floods regionally[11,12,13]. Process-based crop models are generally used to attribute the spatiotemporal change in flood-induced crop yield losses[14]. These models are improved to simulate the impacts of flooding or waterlogging on crop phenology, photosynthesis, nitrogen uptake, grain formation and yield penalties, but they are still at an infant stage[6,12,14]. Some studies use extreme precipitation as an indicator, but without accounting for land surface characteristics, which can lead to misrepresented impacts as flooded areas often occur downstream from the precipitation areas[14,15,16]. A study based on crop yield statistics showed that drought and heat stresses lead to severe yield losses at the national level, whereas the impacts of floods are insignificant because they generally occur more regionally[4]. Flooding areas can be precisely captured by medium- to high-resolution inundation maps from satellite observations. However, climate and yield data with a coarser spatial resolution make it difficult to quantify the exposure of crop production to floods, especially at a national or global scale[15,17]. Previous empirical studies are thus often limited by the lack of crop yield statistics at a subnational scale[4], which render it difficult to accurately assess crop yield changes associated with flooding globally. A spatially explicit global archive of historical flooding events will help strengthen the flood–yield relationship and develop adaptation strategies, but it has been available rarely so far.

Flooding frequency varies by region[2,18,19]. We categorized these events into low-frequency floods (LFF) and high-frequency floods (HFF) according to annual flooding frequency. We defined an area as an LFF (HFF) area if the frequency of flood-event occurrence was <0.5 (≥0.5) within a six-year window (Supplementary Figs. 1, 7 and 8).

Estuaries and Coasts, vol. 47, issue no. 7, pp. 1941-1954, doi:10.1007/s12237-024-01374-3

A decade of salt marsh elevation change in New York City's coastal urban parks.

Hartig, E.K., C. Haight, M. Hsu, N. Auyeung, R. Swadek, J. Ong, **V. Gornitz**[1,2], and R. Boger, 2024

NASA Goddard Institute for Space Studies, New York, NY, USA[1]
Autonomic Integra, LLC., New York, NY, USA[2]

Abstract. Coastal salt marshes of the eastern United States are particularly vulnerable to accelerated sea level rise, and urban marshes are at greater risk of erosion, inundation, and conversion to mudflat if left unmanaged. To guide New York City (NYC) salt marsh restoration strategies, NYC Parks collected up to 10 years of salt marsh elevation change data through 2020 at six salt marsh sites using the Surface Elevation Table-Marker Horizon (SET-MH) method, conducted a salt marsh trends analysis to determine shoreline change from 1974 to 2012, and conducted a salt marsh conditions assessment. We found that the citywide average surface elevation trend of 3.31 mm yr^{-1} was not significantly different from the 30-year (1990–2020) Relative Sea Level Rise of 4.23 mm yr^{-1} at The Battery, NY, tide station, probably due to high variability across and within sites. We also found that accretion rates differed across sites and watersheds, and sites situated lower in the tidal zone had higher accretion rates. Notably, Jamaica Bay's Idlewild salt marsh, long suspected of being sediment-starved and ranking lowest in our conditions assessment, had the highest accretion rate at 9.5 mm yr^{-1}. Our salt marsh trends analysis also showed marsh loss at the shoreline edge, bare ground cover, and other indicators of marsh degradation. In mitigating marsh loss, the design grades for our recent wetland restoration projects enlarge the upper elevation ranges of the low- and high-marsh zones and incorporate wider and more gradual slopes in upland transition zones to enable inland marsh migration.

Introduction. Coastal wetlands worldwide are vulnerable to climate change, and this risk is particularly high in the mid-Atlantic region of the United States (U.S.), where sea level rise risks are exacerbated by glacial isostatic adjustment (peripheral bulge collapse) following the last ice age (Sallenger et al. 2012). Centuries of alterations have filled and dammed tributaries for development, dredged and armored shorelines for shipping and industry, and crisscrossed marshes with ditches for agriculture and mosquito control (Black 1981; Adamowicz and Roman 2005; Adamowicz et al. 2020). In New York City (NYC), numerous present-day stressors further increase the vulnerability of existing salt marshes to deterioration. Stressors include increases in nutrient loading in coastal waterways, especially nitrogen effluent inputs from wastewater treatment plants (WWTPs) (Anisfeld and Hill 2011; Peteet et al. 2018; Rosenzweig et al. 2018; Watson et al. 2018). By the late 1990s, the rapid decline of NYC salt marshes was discernible from aerial imagery (Hartig et al. 2002; Mushacke and Picard 2002). Between 1974 and 1999, the marsh islands of the Jamaica Bay Wildlife Refuge lost 304 hectares (1.5% per year) (Hartig et al. 2002). Swanson and Wilson (2008) tracked how a century of dredge and fill practices altered the bathymetry by deepening the bay. The resulting wider and deeper channels increased the tidal range and effectively increased inundation at the marsh surface. Once the marsh surface can no longer drain sufficiently, hydrogen sulfide (H_2S) toxicity can trigger plant dieback and subsequent conversion to mudflat (Kolker 2005; Wigand et al. 2014; Alldred et al. 2020; Krause et al. 2020). Despite existing regulations intended to protect wetlands and clean water, NYC continues to lose salt marshes to erosion and drowning (Basso et al. 2015; Campbell et al. 2017; Haight et al. 2019). This trend is expected to worsen with sea level rise.

In the highly urbanized NYC setting, the loss of salt marsh is extremely concerning. Salt marshes filter contaminants and thus reduce pollutant loads in receiving waters, sequester carbon through mineral and organic sediment accretion (Pace et al. 2021), protect urban infrastructure from wave damage due to coastal storms (Gornitz et al. 2001), offer recreational opportunities for visitors and coastal communities, and support nursery habitat for fish and wildlife (Mitsch and Gosselink 2000; Gedan et al. 2009).

Communications Earth & Environment, vol. 5, 390, doi:10.1038/s43247-024-01524-2

Realistic representation of mixed-phase clouds increases future climate warming.

Hofer, S., L.C. Hahn, J.K. Shaw, **Z.S. McGraw**[1,2], O. Bruno, F. Hellmuth, M. Pietschnig, I.A. Mostue, R.O. David, T. Carlsen, and T. Storelvmo, 2024

NASA Goddard Institute for Space Studies, New York, NY, USA[1]
Department of Applied Physics and Applied Mathematics, Columbia University, New York, NY, USA[2]

Abstract. Clouds are the main source of uncertainties when projecting climate change. Mixed-phase clouds that contain ice and supercooled-liquid particles are especially hard to constrain, and climate models neither agree on their phase nor their spatial extent. This is problematic, as models that underestimate contemporary supercooled-liquid in mixed-phase clouds will underestimate future warming. Furthermore, it has recently been shown that supercooled-liquid water in mixed-phase clouds is not homogeneously-mixed, neither vertically nor horizontally. However, while there have been attempts at observationally constraining mixed-phase clouds to constrain uncertainties in future warming, all studies only use the phase of the interior of mixed-phase clouds. Here we show, using novel satellite observations that distinguish between cloud-top and interior phase in mixed-phase clouds, that mixed-phase clouds are more liquid at the cloud top globally. We use these observations to constrain the cloud top phase in addition to the interior in a global climate model, leading to +1 °C more 21st century warming in NorESM2 SSP5-8.5 climate projections. We anticipate that the difference between cloud top and interior phase in mixed-phase clouds is an important new target metric for future climate model development, because similar mixed-phase clouds related biases in future warming are likely present in many climate models.

Introduction. Clouds can consist of liquid, ice or a mixture of both, with distinctly different impacts on the Earth's radiation budget[1,2,3,4,5]. A greater fraction of liquid particles within a cloud generally leads to a higher cloud albedo and less shortwave radiation reaching the surface. Concurrently, a higher liquid water content will also increase the cloud's longwave emissivity and therefore, increase the amount of trapped longwave radiation[5,6]. Between −38 and 0 °C, liquid and ice particles can coexist, forming a mixed-phase cloud (MPC)[7,8]. Most of these MPCs are found over the Southern Ocean and the Northern Hemisphere extratropical storm track[9], but they can also exist in more extreme environments such as the Arctic and over high-latitude polar ice sheets[7,10,11,12]. Active satellite observations between 2006 and 2011 suggest that MPCs have a global mean cloud radiative effect of $-3.4\ \mathrm{W\ m^{-2}}$, driven by a strong cooling in the shortwave part of the spectrum[4]. While passive satellite sensors struggle to accurately detect cloud phase[13,14], active satellite sensors such as onboard Cloudsat and the Cloud-Aerosol Lidar and Infrared Pathfinder Satellite Observation (CALIPSO) satellites provide a more accurate picture of the global distribution and climate impacts of MPCs.

MPCs are still one of the leading causes of uncertainties in projecting global climate change[15,16,17,18], despite the fact that Cloudsat and CALIPSO have been in orbit for 16 years[19], advances in ground-based observations of MPCs and more sophisticated cloud parameterizations in state-of-the-art climate models. A notable part of the uncertainty from MPCs results from the fact that even within one mixed-phase cloud system, the water and ice phases are not homogenously mixed, neither horizontally nor vertically[20,21]. Because cloud parameterizations assume homogeneously mixed ice and liquid particles, cloud parameterizations often grow too much ice at the expense of supercooled liquid droplets via a too-efficient Wegener–Bergeron–Findeisen (WBF) process[22,23]. This leads to an underestimation of liquid water at mixed-phase temperatures across most climate models[24,25,26,27]. Climate models that have too much ice in the current climate will also underestimate the temperature sensitivity to anthropogenic greenhouse gas forcing, as with warming the transition from ice to liquid produces an unrealistic increase in cloud albedo[15].

Journal of Climate, vol. 37, issue no. 4, pp. 1277-1293, doi:10.1175/JCLI-D-23-0262.1

Observed relationships between sea surface temperature, vertical wind shear, tropical organized deep convection, and radiative effects.

Hsiao, W.-T., E.D. Maloney, **N.M. Leitmann-Niimi**[1,2], and C.D. Kummerow, 2024

NASA Goddard Institute for Space Studies, New York, NY, USA[1]
Department of Atmospheric Science, Colorado State University, Fort Collins, CO, USA[2]

Abstract. Organized deep convective activity has been routinely monitored by satellite precipitation radar from the Tropical Rainfall Measuring Mission (TRMM) and Global Precipitation Mission (GPM). Organized deep convective activity is found to increase not only with sea surface temperature (SST) above 27°C, but also with low-level wind shear. Precipitation shows a similar increasing relationship with both SST and low-level wind shear, except for the highest low-level wind shear. These observations suggest that the threshold for organized deep convection and precipitation in the tropics should consider not only SST, but also vertical wind shear. The longwave cloud radiative feedback, measured as the tropospheric longwave cloud radiative heating per amount of precipitation, is found to generally increase with stronger organized deep convective activity as SST and low-level wind shear increase. Organized deep convective activity, the longwave cloud radiative feedback, and cirrus ice cloud cover per amount of precipitation also appear to be controlled more strongly by SST than by the deviation of SST from its tropical mean. This study hints at the importance of non-thermodynamic factors such as vertical wind shear for impacting tropical convective structure, cloud properties, and associated radiative energy budget of the tropics.

Introduction. Tropical precipitation is largely produced by convection that can be classified into certain types, each of them imposing distinct moistening and heating effects on the atmospheric vertical profile (e.g., Johnson et al. 1999; Elsaesser et al. 2010; Houze et al. 2015; Chen et al. 2021).

Long-lived, horizontally widespread *organized* deep convection dominates the spatiotemporal distribution of the precipitation means and extremes in the current climate, and will regulate how these change with climate warming (Rossow et al. 2013; Tan et al. 2015; Roca and Fiolleau 2020; Semie and Bony 2020). Instead of being a passive factor in how tropical precipitation is statistically realized, organized deep convection drives radiative effects that not only locally help maintain its own development, but also regulate Earth's energy budget through modification of moisture, cloudiness, and large-scale circulation (Houze 1989; Schumacher et al. 2004; Bony et al. 2016, 2020). Differences in simulating organized deep convection and related processes in tropical ascending regions have been suggested to contribute to a spread in future climate projections (Bony et al. 2015; Mauritsen and Stevens 2015; Wolding et al. 2020; Lee et al. 2022). Thus, it is vital to understand what controls the activity of organized deep convection in the tropics.

Sea surface temperature (SST) has been previously shown to strongly regulate tropical deep convection and precipitation. Early pioneering studies showed positive correlations between tropical SST and deep convective activity as measured by outgoing longwave radiative flux, with a "pick-up" of convective activity above SSTs of 26°–27°C observed (Gadgil et al. 1984; Graham and Barnett 1987; Waliser and Graham 1993; Zhang 1993; Lau et al. 1997). Studies utilizing cloud-resolving models have shown SST thresholds for the onset of aggregated convection, a numerical phenomenon possibly relevant to real-world organized deep convection, but this dependence is sensitive to the model and simulation setup (Wing et al. 2017; Wing 2019; Wing et al. 2020). In addition, observations suggest that higher precipitation is collocated with higher SST relative to the tropical mean (SST^*) (Sobel et al. 2002), associated with higher convective instability (Vecchi and Soden 2007) and column saturation fraction (CSF) (Bretherton et al. 2004), both of which imply higher effective buoyancy to support convective systems.

Geophysical Research Letters, vol, 51, issue no. 4, e2023GL106520, doi:10.1029/2023GL106520

Minimal impact of late-season melt events on Greenland ice sheet annual motion.

Ing, R.N., P.W. Nienow, A.J. Sole, A.J. Tedstone, and **K.D. Mankoff**[1,2], 2024

NASA Goddard Institute for Space Studies, New York, NY, USA[1]
Autonomic Integra LLC, New York, NY, USA[2]

Abstract. Extreme melt and rainfall events can induce temporary acceleration of Greenland Ice Sheet motion, leading to increased advection of ice to lower elevations where melt rates are higher. In a warmer climate, these events are likely to become more frequent. In September 2022, seasonally unprecedented air temperatures caused multiple melt events over the Greenland Ice Sheet, generating the highest melt rates of the year. The scale and timing of the largest event overwhelmed the subglacial drainage system, enhancing basal sliding and increasing ice velocities by up to ~240% relative to pre-event velocities. However, ice motion returned rapidly to pre-event levels, and the speed-ups caused a regional increase in annual ice discharge of only ~2% compared to when the effects of the speed-ups were excluded. Therefore, although late melt-season events are forecast to become more frequent and drive significant runoff, their impact on net mass loss via ice discharge is minimal.

Introduction. Across glacier systems worldwide, rapid influxes of surface runoff accessing the ice-bed interface can cause temporary increases in ice motion (Bingham et al., 2008; Gudmundsson et al., 2000). Numerous studies have drawn attention to the potential implications of such “speed-up” events for ice loss from the Greenland Ice Sheet (GrIS), as increased motion causes more ice to be advected to lower, warmer elevations, where surface melt rates are higher (e.g., Doyle et al., 2015; Zwally et al., 2002).

The seasonal cycles of surface melt and ice velocity on land-terminating sectors of the GrIS are coupled through the subglacial drainage system (Davison et al., 2019; van de Wal et al., 2015). Following the onset of the melt season, surface meltwaters begin to access the ice-bed interface (Nienow et al., 2017). Initially, the subglacial drainage system is spatially distributed and inefficient, and becomes overwhelmed by meltwater inputs which causes the basal water pressure to increase (Andrews et al., 2014; Bartholomew et al., 2011). This increase in pressure decreases basal friction leading to an acceleration in ice motion (Bartholomew et al., 2012; Schoof, 2010). As the melt season progresses, the rising supply of meltwater causes the formation of a more efficient channelized subglacial drainage system. The subsequent increased carrying capacity of these channels lowers the basal water pressure and decreases ice motion, with a minimum velocity typically occurring during the late melt-season (mid to late September in west Greenland) (Andrews et al., 2014; Stevens et al., 2016) before slowly accelerating over winter as the efficiency of the subglacial drainage system decreases (Joughin et al., 2008; Sole et al., 2013; Zwally et al., 2002). Although muted due to ocean and fjord processes influencing flow, a similar seasonal cycle in ice velocity can be seen at many marine-terminating glaciers (Moon et al., 2014).

Within the seasonal cycle of ice motion described above, transient speed-up events occur at the margins of the GrIS when there is a large, short-term (<1 day) increase in the meltwater supply to the bed (Bartholomew et al., 2012; Doyle et al., 2015; van de Wal et al., 2008). These rapid influxes of water can result from sudden lake drainages, heavy rainfall, or melt events (e.g., Das et al., 2008; Doyle et al., 2015; Schmid et al., 2023; Shepherd et al., 2009; Tedstone et al., 2013) and overwhelm the capacity of the subglacial drainage system leading to increased basal lubrication (Bartholomaus et al., 2008; Nienow et al., 2005; Sugiyama & Gudmundsson, 2004).

The ice speed-up from melt events can be larger in the late melt-season, when decreasing surface melt and ice creep cause the efficiency of the subglacial drainage system to decrease, making it susceptible to pressurization through minor variations in runoff (Fudge et al., 2009; Nanni et al., 2023).

Geophysical Research Letters, vol. 51, issue no. 6, e2023GL107382, doi:10.1029/2023GL107382

Subseasonal variability of humid heat during the South Asian summer monsoon.

Ivanovich, C.C.[1,2], **R.M. Horton**[1,3], A.H. Sobel, and D. Singh, 2024

NASA Goddard Institute for Space Studies, New York, NY, USA[1]
Earth and Environmental Sciences, Columbia University, New York, NY, USA[2]
Center for Climate Systems Research, Columbia University, New York, NY, USA[3]

Abstract. The South Asian summer monsoon strongly modulates regional temperature and humidity. While extreme dry heat peaks in the pre-monsoon season, recent literature suggests that extreme humid heat can continue to build throughout the monsoon season. Here we explore the influence of monsoon onset and subseasonal precipitation variability on the occurrence of extreme wet bulb temperatures (Tw) across South Asia. We find that extreme Tw events often occur on rainy days during the monsoon season. However, the influence of precipitation on Tw varies with the background climatology of surface specific humidity. In climatologically drier areas, positive Tw anomalies tend to occur when precipitation increases due to either early onset or wet spells during the monsoon. In contrast, in climatologically humid areas, positive Tw anomalies occur during periods of suppressed precipitation, including both delayed onset and dry spells during the monsoon.

Introduction. South Asia is a present-day hotspot for extreme humid heat, with the frequency and intensity of extremes projected to increase in the future. South Asia is one of the only areas to have reached a wet bulb temperature (Tw) beyond the theoretical threshold for human survival (Raymond et al., 2020), posing dire risks to human health and outsized socioeconomic impacts. In recent decades, increases in regional temperature and moisture have boosted the frequency of extreme humid heat events in South Asia (Rogers et al., 2021) and these trends are projected to continue with additional warming (Im et al., 2017; Li et al., 2020; Matthews et al., 2017; Mora et al., 2017; Murari et al., 2015; Saeed et al., 2021; Wang et al., 2021). In this region, humid heat extremes are driven by a variety of mechanisms. A partial list of such mechanisms includes moisture advection (Monteiro & Caballero, 2019), sensible heat flux (Raymond et al., 2021), proximity to warm water bodies (Im et al., 2017), large scale variability (Ivanovich et al., 2022; Speizer et al., 2022), and irrigation (Jha et al., 2022; Krakauer et al., 2020; Mishra et al., 2020), many of which can interact. Better understanding the relationships between monsoon precipitation and humid heat can help determine which types of meteorological drivers are associated with the highest risk for extremes, with potential to improve forecasting and model projections. These results can also help identify the dynamics of simultaneous or sequential rainfall and humid heat, which can cause compound extreme events with complex and understudied impacts on agriculture and human health (Zscheischler et al., 2018).

The South Asian summer monsoons are the main source of humidity and moisture to the region and strongly modulate local dry bulb temperatures (Tdry). Many of the factors driving extreme humid heat in South Asia are influenced by the summer monsoon. While Tdry tends to peak during the pre-monsoon season throughout the region (van Oldenborgh et al., 2018), recent work has suggested that the highest humid heat magnitudes often occur after monsoon onset in parts of South Asia (Raymond et al., 2020; Rogers et al., 2021). Differentiating between dry and humid heat extremes in this region is particularly important given their distinct impacts on plant and human health, respectively, which can both be detrimental to agricultural production (Diaz et al., 2023; Ting et al., 2023). Ivanovich et al. (2022) highlighted that elevated Tw during the June-August season in India is associated with surface level easterly wind anomalies and increased dry bulb temperature and specific humidity, conditions sometimes associated with monsoon breaks. Further, humid heat is rapidly intensifying and increasing in frequency more dramatically than dry heat in this region (Rogers et al., 2021; van Oldenborgh et al., 2018).

Journal of the Atmospheric Sciences, vol. 81, issue no. 5, pp. 819-837, doi:10.1175/JAS-D-23-0072.1

Stickiness: A new variable to characterize the temperature and humidity contributions toward humid heat.

Ivanovich, C.C[1,2], A.H. Sobel, **R.M. Horton**[1,3], and C. Raymond[4], 2024

NASA Goddard Institute for Space Studies, New York, NY, USA[1]
Earth and Environmental Sciences, Columbia University, New York, NY, USA[2]
Lamont-Doherty Earth Observatory, Palisades, NY, USA[3]
NASA Jet Propulsion Laboratory/California Institute of Technology, Pasadena, CA[4]

Abstract. Extreme wet-bulb temperatures (T_w) are often used as indicators of heat stress. However, humid heat extremes are fundamentally compound events, and a given T_w can be generated by various combinations of temperature and humidity. Differentiating between extreme humid heat driven by temperature versus humidity is essential to identifying these extremes' physical drivers and preparing for their distinct impacts. Here we explore the variety of combinations of temperature and humidity contributing to humid heat experienced across the globe. In addition to using traditional metrics, we derive a novel thermodynamic state variable named "stickiness." Analogous to the oceanographic variable "spice" (which quantifies the relative contributions of temperature and salinity to a given water density), stickiness quantifies the relative contributions of temperature and specific humidity to a given T_w. Consistent across metrics, we find that high magnitudes of T_w tend to occur in the presence of anomalously high moisture, with temperature anomalies of secondary importance. This widespread humidity dependence is consistent with the nonlinear relationship between temperature and specific humidity as prescribed by the Clausius–Clapeyron relationship. Nonetheless, there is a range of stickiness observed at moderate-to-high T_w thresholds. Stickiness allows a more objective evaluation of spatial and temporal variability in the temperature versus humidity dependence of humid heat than traditional variables. In regions with high temporal variability in stickiness, predictive skill for humid heat-related impacts may improve by considering fluctuations in atmospheric humidity in addition to dry-bulb temperature.

Introduction. Extreme humid heat events are climate extremes with important societal influence due to their direct link to human and animal heat stress. Physiological research has suggested that humid heat may pose additional risk to human health compared to dry heat due to humidity's influence over humans' thermoregulation efficiency (e.g., Mora et al. 2017; Parsons 2006; Steadman 1979; Fanger 1970). While increased dry-bulb temperatures alone can increase rates of dehydration, over 75% of the heat dissipation by human bodies is associated with evaporative cooling via sweating (Buzan and Huber 2020). The higher the ambient air specific humidity, the more difficult it is for sweat to cool our bodies by evaporation; at extremely high air temperatures, even a moderate amount of evaporative inhibition can cause heat stress. Exposure to this type of heat stress is widespread across the globe, and has been identified as one of the leading causes of death associated with climate extremes (Kovats and Hajat 2008).

Differentiating between extreme humid heat and extreme dry heat is essential to preparing for their individual impacts. At a given temperature, heat stress increases with elevated humidity, posing higher risk to human health and the potential for greater socioeconomic impacts than dry heat. In contrast, the presence of humidity may diminish the effect of extreme heat on crop growth by reducing vapor pressure deficit, for example, in the United States Midwest (Schauberger et al. 2017; Ting et al. 2023), and extreme dry heat has the potential to more strongly prime regions for wildfires (Abatzoglou and Williams 2016; Bowman et al. 2009).

Environmental Research Letters, vol. 19, 114076, doi:10.1088/1748-9326/ad7edc

Temporal connections between extreme precipitation and humid heat.

Johnson, S., **C. Ivanovich**[1,2], **R.M Horton**[1,2], M. Ting, K. Kornhuber, and **C. Lesk**[1], 2024

NASA Goddard Institute for Space Studies, New York, NY, USA[1]
Lamont-Doherty Earth Observatory, Palisades, NY, USA[2]

Abstract. Individually, extreme humid heat and extreme precipitation events can trigger widespread socioeconomic impacts which disproportionately affect vulnerable populations. These impacts might become greater when both events occur in close temporal proximity, for example if emergency responses to heat stress casualties are hindered by flooded roads. Improved understanding of the probabilities and physical mechanisms associated with these events' temporal compounding might uncover causal interrelationships offering avenues for improving early warning systems and projecting changes in a warmer climate. We explore sequential humid heat and rainfall relationships during the local summer season, identifying two classes of temporal relationships. We find that high wet bulb temperature (WBT) anomalies in most mid- to high-latitude and tropical regions are preceded by anomalously low precipitation. In contrast, hot and dry subtropical regions generally experience elevated WBTs during and, to a somewhat lesser extent, before extreme precipitation events. High WBT events are followed by positive precipitation anomalies in many land regions.

Introduction. Heat events are among the most deadly and damaging types of climate extremes (Horton *et al* 2016). Humid heat extremes are a health danger disproportionately affecting the most vulnerable populations, including those with pre-existing health conditions, the elderly, infants, and those without access to protective infrastructure and services such as air conditioning (Romanello *et al* 2022, Diaz *et al* 2023). Heat becomes particularly harmful to human health when combined with high humidity, as high humidity hinders the body's ability to cool itself through sweating (Sherwood and Huber 2010). Extreme precipitation events are likewise a hazard associated with direct loss of life due to flash flooding, but also with damage to infrastructure and agriculture, which is often concentrated in low-lying flood plains alongside vulnerable populations (Caretta *et al* 2022) and urban areas (Hemmati *et al* 2022). However, combinations of humid heat and precipitation are an emerging and often underappreciated hazard in many regions around the world.

Globally, the frequency and intensity of both humid heat events and extreme precipitation have been increasing (Robinson *et al* 2021), and are projected to increase further in the future (IPCC 2021). Raymond *et al* (2020) report a doubling of extreme humid heat events globally over the past 40 years, and populations exposed to humid heat have increased faster than those exposed to high temperatures alone (Rogers *et al* 2021). Coffel *et al* (2017) project more than tenfold increases globally in humid heat by late in the 21st century under RCP 8.5, with even more rapid increases in human exposure. Extreme precipitation trends have likewise been strongly positive across much of the globe (Sun *et al* 2021). As one example, relative to a 1901–1960 base period, in the relatively data-rich contiguous U.S., the frequency of 2-day extreme precipitation events has increased by approximately 40% in the last two decades (Easterling *et al* 2017). The coarse resolution of global climate models and other challenges make it more difficult to project extreme precipitation changes than other variables like temperature. However, diverse methodologies (e.g. Prein *et al* 2017, Lenderink and Attema 2015) strongly support the idea that as a global average the frequency and intensity of extreme precipitation should increase, potentially at rates that far exceed changes in mean precipitation (Zhang *et al* 2017), leading to large increases in population exposed (Chen and Sun 2021).

This concomitant increase in humid heat and extreme precipitation increases the likelihood of both occurring in close temporal proximity (Raymond *et al* 2022). A growing body of research is thus exploring compound extreme events (Zscheischler *et al* 2020) and their impacts (Raymond *et al* 2020).

Communications Earth & Environment, vol. 5, 541, doi:10.1038/s43247-024-01676-1

Increasing contribution of the atmospheric vertical motion to precipitation in a warming climate.

Jun, T., and **D. Rind**[1], 2024

NASA Goddard Institute for Space Studies, New York, NY, USA[1]

Abstract. Global warming already influences precipitation, with more intense precipitation in many locations. Although the 'wet-get-wetter, dry-get-drier' tendency in mean precipitation holds in many locations, the situations for precipitation extremes are more complex, due to changes in dynamic and thermodynamic influences on atmospheric moisture distributions. Here, we build a dynamically interactive atmospheric moisture model for the present (2006–2025) and the future climate (2081–2100), using outputs from coupled ocean-atmosphere general circulation models. We find that the dynamic process of vertical advection of moisture dominates the same-day precipitation, while the smaller impact of the thermodynamic process provides available moisture for several days. As climate warms, we find that the dynamical-induced precipitation more completely exhausts the vertically-integrated moisture and the distribution of the dynamic process's impact on precipitation exhibits a greater spread in the warmer future. The dynamical process is primarily responsible for more extreme heavy precipitation as climate warms, at all latitudes.

Introduction. Societies are vulnerable to precipitation change as precipitation variability has a significant impact on numerous socioeconomic outcomes and human well-being[1,2,3,4,5]. The pattern and magnitude of precipitation are expected to change with global warming as the concentration of atmospheric water vapor is expected to increase[6,7,8]. Although the 'wet-get-wetter, dry-get-drier' (WGWDGD) paradigm[6] applies in many locations, the changes vary by region[9], due to various interacting drivers of precipitation changes[10,11]. Owing to the complexity, and heterogeneity of precipitation change with global warming, building a structural model to represent the underlying physical process of precipitation is necessary to predict the future precipitation change, where contributing factors are parceled out and the mechanism of their interactions is identified.

In previous studies, the atmospheric moisture budget simplifies the analysis of precipitation into the quantification of distinct physical processes[9,12,13,14]. Standard components in the moisture budget include the dynamic and thermodynamic components and horizontal moisture advection. The dynamic process incorporates contributions from the atmospheric circulation where it is embedded[12,15,16,17,18], while the thermodynamic process traces changes in atmospheric water vapor content, which are linked to temperature changes[6,19]. Horizontal moisture advection plays a role as a moisture source for precipitation[20,21].

Studies that associate precipitation change with these individual processes focused on the relative importance of one process over the others[11,12,13,17,22] while neglecting possible interplay among them. However, increased water vapor reduces the magnitude of the required vertical motion to generate the same strength of precipitation, which, with the same magnitude of vertical motion, then leads to stronger precipitation[23,24], suggesting a significant interplay among moisture budget processes in the precipitation process. While the time-averaged moisture budget analysis does not reveal the interactions among the processes and their dynamic evolution, tracing the propagation of a perturbation from a component through the atmospheric moisture system on a daily or sub-daily basis is essential for a complete explanation of the atmospheric moisture dynamics, and the future precipitation changes.

One Earth, vol. 7, issue no. 4, pp. 572-588, doi:10.1016/j.oneear.2024.02.003

Toward a holistic and data-driven framework to evaluate livestock-derived protein systems.

Karl, K.[1,2], R. DeFries, W. Baethgen, M. Furtado, J. Potent, E.M. Leal, **E. Mencos Contreras**[1,2], and **C. Rosenzweig**[1,2], 2024

NASA Goddard Institute for Space Studies, New York, NY, USA[1]
Center for Climate Systems Research, Columbia University, New York, NY, USA[2]

Abstract. The environmental toll of protein production systems, such as greenhouse gas (GHG) emissions and land use associated with the production of livestock-derived foods, poses a substantial challenge for global agricultural sustainability. At the same time, livestock possess significant cultural and economic value for billions, while providing essential macro- and micronutrients. Such tensions fuel a debate on how to optimize livestock production systems, with implications for global nutrition, the environment, and society. Here, we introduce the Protein for Nutrition, Environment, and Society (ProNES) framework to address challenges related to the holistic evaluation of livestock-derived protein systems. ProNES uses publicly available data to comprehensively assess livestock-derived commodities in terms of their nutritional, social, economic, and environmental aspects. The exercise underscores areas where data gaps must be filled for more precise assessments, such as the contributions of livestock production systems to livelihoods across a range of geographic, economic, and sociocultural contexts.

Introduction. Whether the world will be able to produce enough protein to adequately feed a growing population, and whether it can do so without exceeding planetary boundaries, has emerged as a key set of questions for researchers, policymakers, and the private sector alike.[1] In particular, the environmental toll of current protein production and consumption systems has been cited as a reason to advance a global "protein transition" toward more sustainable approaches.[2] Adequately and responsibly meeting global protein demand is a complex and interdisciplinary challenge. It will require a deeper understanding of the biological value of different dietary proteins, as well as a nuanced grasp of the sociocultural and economic importance of protein-rich food commodities.[3,4] This is in addition to the challenge of advancing protein production systems that sit squarely within established global environmental limits and minimize greenhouse gas (GHG) emissions, land use, water use, and biodiversity loss, among other indicators of environmental performance.[5,6,7,8,9]

Given the sheer scale of livestock-derived protein production systems across the globe—such as an estimated 20%–47% of land area dedicated to livestock production, and an annual stock of chickens that reached over 26 billion in 2022—the environmental impacts of livestock-derived protein production systems must be strictly monitored and carefully evaluated.[10,11,12] In addition to their environmental performance, the nutritional contributions of livestock are central to any evaluation of protein systems, because livestock-derived foods are currently a vital source of nutrition for billions, and particularly important for the growth of children in certain regions where diets are often of low quality.[13] At the same time, the overconsumption of red and processed meat can contribute to an assortment of negative health outcomes in many dietary contexts.[14,15] To provide further nuance to the issue, a growing body of research highlights the importance of protein quality in addition to protein quantity to gauge the true nutritional utility of a range of protein-rich food commodities.[16] There are also substantial nutritional differences between processed and unprocessed forms of livestock-derived foods and high levels of variation with respect to the relative consumption levels of processed vs. unprocessed livestock-derived foods across contexts.[17]

Definitions of sustainable agriculture extend well beyond environmental performance and nutritional contributions, however, and often include considerations of the social, economic, and cultural value of the entire agricultural supply chain.[9,18] For example, for many smallholder farming communities, livestock can serve as important forms of transportation, labor, capital storage, risk reduction, and income diversification.

Journal of Geophysical Research Atmospheres, vol. 129, issue no. 16, e2024JD041377, doi:10.1029/2024JD041377

Where dust comes from: Global assessment of dust source attributions with AeroCom models.

Kim, D.[1], M. Chin[1], G. Schuster[2], H. Yu[1], T. Takemura, P. Tuccella, P. Ginoux, X. Liu, Y. Shi, H. Matsui, **K. Tsigaridis[2,3]**, **S.E. Bauer[2,3]**, J.F. Kok, and M. Schulz, 2024

NASA Goddard Space Flight Center, Greenbelt, MD, USA[1]
NASA Langley Research Center, Hampton, VA, USA[2]
NASA Goddard Institute for Space Studies, New York, NY, USA[3]
Center for Climate Systems Research, Columbia University, New York, NY, USA[4]

Abstract. The source of dust in the global atmosphere is an important factor to better understand the role of dust aerosols in the climate system. However, it is a difficult task to attribute the airborne dust over the remote land and ocean regions to their origins since dust from various sources are mixed during long-range transport. Recently, a multi-model experiment, namely the AeroCom-III Dust Source Attribution (DUSA), has been conducted to estimate the relative contribution of dust in various locations from different sources with tagged simulations from seven participating global models. The BASE run and a series of runs with nine tagged regions were made to estimate the contribution of dust emitted in East- and West-Africa, Middle East, Central- and East-Asia, North America, the Southern Hemisphere, and the prominent dust hot spots of the Bodélé and Taklimakan Deserts. The models generally agree in large scale mean dust distributions; however models show large diversity in dust source attribution. The inter-model differences are significant with the global model dust diversity in 30%–50%, but the differences in regional and seasonal scales are even larger. The multi-model analysis estimates that North Africa contributes 60% of global atmospheric dust loading, followed by Middle East and Central Asia sources (24%). Southern hemispheric sources account for 10% of global dust loading, however it contributes more than 70% of dust over the Southern Hemisphere. The study provides quantitative estimates of the impact of dust emitted from different source regions on the globe and various receptor regions including remote land, ocean, and the polar regions synthesized from the seven models.

Introduction. Mineral dust aerosols are small airborne particles, primarily emitted from soils by Aeolian processes including saltation and aerodynamic entrainment (Gillette et al., **1998**; Macpherson et al., **2008**; Marticorena & Bergametti, **1995**; Marticorena et al., **1997**; Shao et al., **2011**). As the most abundant aerosol type by mass in the Earth's atmosphere, mineral dust plays an important role in global climate by interacting with incoming and outgoing radiation, providing liquid and ice cloud nuclei, and affecting atmospheric stability (Colarco et al., **2014**; Creamean et al., **2013**; DeMott et al., **2010**; Evan et al., **2008**; Forster et al., **2007**; Haywood et al., **2005**; Jordan et al., **2020**; Kawai et al., **2023**; Rosenfeld et al., **2014**; Shi et al., **2022**; Shi & Liu, **2019**). Dust has important implications on global biogeochemical cycles through fertilizing terrestrial and ocean ecosystems and modulating carbon uptake (Albani et al., **2014**; Checa-Garcia et al., **2021**; Jickells et al., **2005**; Maher et al., **2010**; Westberry et al., **2023**; Yu et al., **2015**). Also, dust is a major $PM_{2.5}$ aerosol contributor over or near dust source regions across the global (Bauer et al., **2019**; Hand et al., **2017**).

Dust source regions on a global scale have been extensively studied from many previous investigations (e.g., Tegen & Fung, **1995**; Ginoux et al., **2001**, **2012**; Zender et al., **2003**; Shao et al., **2011**; Kok et al., **2021a**, **2021b**, **2023**). The majority of dust mass is emitted from the so-called dust-belt which includes North Africa, the Middle East, and East Asia. Other regions like North America, South America, South Africa, and Australia are also known as important dust source regions contributing dust to the Earth's atmosphere. Once emitted, dust can travel thousands of kilometers across the entire hemisphere, and some of them reach pristine remote areas and the polar regions.

Atmospheric Chemistry and Physics, vol. 24, issue no. 20, pp. 11849-11881, doi:10.5194/acp-24-11849-2024

High ice water content in tropical mesoscale convective systems (a conceptual model).

Korolev, A., Z. Qu, J. Milbrandt, I. Heckman, M. Cholette, M. Wolde, C. Nguyen, G. McFarquhar, P. Lawson, and **A. Fridlind**[1], 2024

NASA Goddard Institute for Space Studies, New York, NY, USA[1]

Abstract. The phenomenon of high ice water content (HIWC) occurs in mesoscale convective systems (MCSs) when a large number of small ice particles with typical sizes of a few hundred micrometers, concentrations of the order of 10^2–10^3 L^{-1}, and IWC exceeding 1 g m^{-3} are present at high altitudes. HIWC regions in MCSs may extend vertically up to 10 km above the melting layer and horizontally up to hundreds of kilometers, filling large volumes of the convective systems. HIWC has great geophysical significance due to its effect on precipitation formation, the hydrological cycle, and the radiative properties of MCSs. It is also recognized as a hazard for commercial aviation operations since it can result in engine power loss and in the malfunctioning of aircraft data probes. This study summarizes observational and numerical simulation efforts leading to the development of a conceptual model for the production of HIWC in tropical MCSs based on the data collected during the HAIC–HIWC campaign. It is hypothesized that secondary ice production (SIP) in the vicinity of the melting layer plays a key role in the formation and sustainability of HIWC. In situ observations suggest that the major SIP mechanism in the vicinity of the melting layer is related to the fragmentation of freezing drops (FFDs). Both in situ data and numerical simulations suggest that the recirculation of drops through the melting layer led to the amplification of SIP. The proposed conceptual model and simulation results motivate further efforts to extend reproducible laboratory measurements.

Introduction. The interest in cloud environments with enhanced ice water content (IWC > 1 g m^{-3}) has emerged in connection with the development of aviation safety envelopes for the operation of commercial aviation. Reports of a growing number of engine power loss events on commercial aircraft flying in the vicinity of convective storm cores has initiated trial field studies of the environmental conditions related to the engine events (Lawson et al., 1998; Strapp et al., 1999). Data obtained provided evidence that engine power loss events result primarily from the ingestion of large concentrations of ice crystals into the engine. The analysis of the Boeing event database showed that the engine power losses typically occur in tropical mesoscale convective systems (MCSs) in the altitude range of 5 to 12 km and the temperature range of −10 to −55 °C (Mason et al., 2006; Mason and Grzych, 2011). The radar reflectivity in the regions of engine events was found to be typically below 30 dBZ (e.g., Mason et al., 2006; Grzych and Mason, 2010; Protat et al., 2016; Wolde et al., 2016). A detailed examination of the information obtained allowed the formulation of a hypothesis that the engine power loss events occur in the presence of high concentrations of small ice crystals constituting high ice water content (HIWC) environments (Lawson et al., 1998; Strapp et al., 2016).

In order to provide a statistically significant data set to assess aviation safety envelopes for engine operations in HIWC environments (FAA Title 14 Code of Federal Regulations Part 33 Appendix D – Mixed-Phase/Glaciated Environmental Envelope and the identical EASA CS-25 Appendix P), the USA's Federal Aviation Administration (FAA) and European Union Aviation Safety Agency (EASA) jointly initiated an international field campaign: European High Altitude Ice Crystals (HAIC) (Dezitter et al., 2013) and North American HIWC (hereafter HAIC–HIWC) (Strapp et al., 2016). The flight operations were conducted out of Darwin, Australia, in 2014 and Cayenne, French Guiana, in 2015. The HAIC–HIWC project was designed to obtain the 99th percentile of total water content (TWC) and characterize ice particle sizes for regulatory purposes. To address the regulatory objectives, cloud environments were sampled along the horizontal traverses at different distances from the convective cores at four temperature levels centered around −10, −30, −40, and −50 °C (± 5 °C) (Strapp et al., 2020).

Field Crops Research, vol. 309, 109306, doi:10.1016/j.fcr.2024.109306

Evaluating differences among crop models in simulating soybean in-season growth.

Kothari, K., R. Battisti, K.J. Boote, S.V. Archontoulis, A. Confalone, J. Constantin, S.V. Cuadra, P. Debaeke, B. Faye, B. Grant, G. Hoogenboom, Q. Jing, M. van der Laan, F.A.M. da Silva, F.R. Marin, A. Nehbandani, C. Nendel, L.C. Purcell, B. Qian, **A.C. Ruane**[1], C. Schoving, E.H.F.M. Silva, W. Smith, A. Soltani, A. Srivastava, N.A. Vieira, and M. Salmerón, 2024

NASA Goddard Institute for Space Studies, New York, NY, USA[1]

Abstract. Crop models are useful tools for simulating agricultural systems that require continued model development and testing to increase their robustness and improve how they describe our current understanding of processes. Coordinated and "blind" evaluation of multiple models using same protocols and experimental datasets provides unique opportunities to further improve models and enhance their reliability. For soybean [*Glycine max* (L.) Merr.], there has been limited coordinated multi-model evaluations for the simulation of in-season plant growth dynamics. We evaluated ten dynamic soybean crop models for their simulation of in-season plant growth using data from five experiments conducted in Argentina, Brazil, France, and USA. We evaluated models after a *Blind* (using only phenology data) and a *Full* calibration (with in-season and end-of-season variables). Calibration reduced model uncertainty by reducing standard bias for the simulation of in-season variables (biomass, leaf, pod, and stem weights, and leaf area index, LAI). However, we found that most models had difficulty in reproducing leaf growth dynamics, with normalized root mean squared error (nRMSE) of 56% for leaf weight and 43% for LAI (across locations and models after *Full* calibration). Models with different levels of complexity and experience were capable of simulating final seed yield at maturity with reasonable accuracy (nRMSE of 8–31% after *Full* calibration). However, the nRMSE for pod weight (of 17–64% after *Full* calibration) was two-fold larger than that of seed yield. Moreover, the models differed in how they simulated timing from sowing to beginning seed growth (47–93 days) and effective seed filling period (18–54 days), owing to model structural differences in defining the reproductive developmental stages. Overall, we identified the following processes that can benefit from further model improvement: leaf expansion and senescence, reproductive phenology, and partitioning to reproductive growth. Simulation of pod wall tissue and individual seed cohorts is another aspect that many models currently lack. Model improvement can benefit from high-temporal resolution experimental datasets that concurrently account for phenology, plant growth, and partitioning. Further, we recommend collecting reproductive phenology in the field consistent with actual dry matter allocation to organs in the models and collecting multiple observations of seed and pod weight to aid model improvement for simulation of seed growth and yield formation.

Introduction. With an annual production of 301 million tons worldwide (FAO, 2020), soybean is the most widely grown legume and a major component of the global food supply. Ensuring high yield stability and the sustainability of soybean production under current and future climate conditions is essential to meet the growing food, feed, and nutrition demand. Process-based crop eco-physiological models are powerful tools to simulate crop growth under climate change and to study potential management and genotype adaptations (Rosenzweig et al., 2014, White et al., 2011). However, models require calibration and evaluation with experimental data prior to their application. While the research focusing on crop model applications has increased in the past decades, the efforts for model evaluation and improvement with detailed field experimental data are lagging (Silva and Giller, 2021). Therefore, new studies that evaluate model simulations with experimental data that include in-season crop growth are paramount to reduce model uncertainty before their application.

Communications Earth & Environment, vol. 5, issue no. 1, 481, doi:10.1038/s43247-024-01638-7

International cooperation was key to stabilize wheat prices after the Russian invasion of Ukraine.

Kuhla, K., **M.J. Puma**[1,2], and C. Otto, 2024

NASA Goddard Institute for Space Studies, New York, NY, USA[1]
Center for Climate Systems Research, Columbia University, New York, NY, USA[2]

Abstract. The Russian invasion of Ukraine in 2022 triggered a global wheat price spike and food insecurities in import-dependent countries. We combine an analysis of the global wheat supply network with an agricultural commodity price model to investigate national impaired supplies and the global annual wheat price hike, respectively, for the trade year 2022. Using a scenario analysis, we show that international cooperation manifested in the Black Sea Grain and Solidarity Lanes initiatives and the removal of export restrictions may have mitigated the 2022 price hike by 13 percentage points. In a worst case scenario – characterized by multi-breadbasket harvest failures, escalating export restrictions, and blocked Ukrainian exports – wheat price increases by 90% compared to the 2000–2020 average. Coping strategies – such as food-secure countries dispersing stocks, reducing wheat as feed, or boosting wheat production – are effective at mitigating the price spike in simplified scenarios. Our findings underscore the imperative of coordinated policy responses to avoid global food supply disruptions.

Introduction. The concentration of production in a few main breadbasket regions and resulting import dependencies of many developing countries renders the global trade network for main food crops like wheat susceptible to system shocks disrupting global supply chains[1,2]. Within the last 20 years, two major world food price crises in 2007/08 and 2010/11 put tens of millions of additional people at risk of food insecurity triggering civil unrest around the globe[3]. Both crises were preceded by simultaneous harvest failures in several main breadbasket regions and aggravated by unilateral export restrictions by many countries, causing disproportionate spikes in food prices[4]. A decade later, the COVID-19 pandemic posed a serious threat to regional[5,6] and global food security[7,8]. In doing so, it disproportionately impacted low- and middle-income populations[9] and societies already grappling with environmental fragility and economic insecurity, such as those in the Sahel region[10]. Further, regional food security was jeopardized in recent years by pests and plagues, including the locust infestation in the Horn of Africa in 2019 and 2020[11], and extreme weather events like the devastating floods and droughts experienced in Nigeria[12]. Compounding extreme weather events in different main production regions can lead to multi-breadbasket failures and thus jeopardize food security also at the global level[1,13]. In the past many countries have responded to global supply failures by unilateral, uncoordinated policy interventions: exporters raised export restrictions and importers winded down restrictions[14]. These interventions and the resulting market uncertainties further amplified agricultural price spikes[15,16]. The intensification of extreme weather events under global warming may exacerbate the risk of multi-breadbasket failures[17], in the absence of adequate adaptation measures[18]. Studies have highlighted that disrupted supply chains[19], financial crisis[20,21], and changes in population and land use[22,23] can put food security at risk in crisis situations.

In early 2022 food price levels were already high due to high fertilizer prices and pandemic-induced supply chain disturbances. The market uncertainties triggered by the Russian invasion of Ukraine then caused monthly prices for agricultural commodities, which Ukraine exports globally such as wheat, corn and sunflower oil, to exceed the peak levels of the two preceding crises[24]. For global food security, the impact on international wheat markets was arguably more critical than other food commodities, because Ukraine and Russia contribute about one-third of the world's wheat exports[25].

Many developing countries, especially in the Middle East, North and Sub-Saharan Africa, and Southeast Asia, heavily rely on wheat imports from either Ukraine or Russia[26]. Moreover, prior to the war, the World Food Program sourced nearly half of its global wheat supplies from Ukraine to support its food assistance[27].

Journal of Geophysical Research Atmospheres, vol. 129, issue no. 11, e2023JD040450, doi:10.1029/2023JD040450

Polar low circulation enhances Greenland's west coast cloud surface warming.

Lac, J., H. Chepfer, **A. Arouf**[1], M.D. Shupe, and M.R. Gallagher, 2024

NASA Goddard Institute for Space Studies, New York, NY, USA[1]

Abstract. Mass loss of the Greenland Ice Sheet (GrIS) plays a major role in the global sea level rise. The west coast of the GrIS has contributed 1,000 Gt of the 4,488 Gt GrIS mass loss between 2002 and 2021, making it a hotspot for GrIS mass loss. Surface melting is driven by changes in the radiative budget at the surface, which are modulated by clouds. Previous works have shown the impact of North Atlantic transport for influencing cloudiness over the GrIS. Here we used space-based lidar cloud profile observations to show that a polar low circulation promotes the presence of low clouds over the GrIS west coast that warm radiatively the GrIS surface during the melt season. Polar low circulation transports moisture and low clouds from the sea to the west of Greenland up over the GrIS west coast through the melt season. The concomitance of the increasing presence of low cloud in fall over the Baffin Sea due to seasonal sea-ice retreat and a maximum occurrence of Polar low circulation in September results in a maximum of low cloud fraction (~14% at 2.5 km above sea level) over the GrIS west coast in September. These low clouds warm radiatively the GrIS west coast surface up to 80 W/m^2 locally. This warming contributes to an average increase of 10 W/m^2 of cloud surface warming in September compared to July on the GrIS west coast. Overall, this study suggests that regional atmospheric processes independent from North Atlantic transport may also influence the GrIS melt.

Introduction. Greenland contains the second largest ice sheet on Earth. In relation to global warming, its melting has accelerated to a loss of 280 Gt/year, corresponding to a contribution of 0.47 mm/year to sea level rise (Van den Broeke et al., 2016). The reliability of Greenland Ice Sheet (GrIS) melt prediction is important for predictions of the future Earth climate, as GrIS disappearance could lead to a global sea-level rise of 7 m (Bamber et al., 2013). Loss of Greenland ice mass occurs in the form of surface melting and ice discharge across the grounding line. Recent Greenland melt acceleration is mainly attributed to surface melting (Enderlin et al., 2014), which has reached a record over the last decades (Nghiem et al., 2012).

Melting of the ice sheet surface is driven by the surface energy budget, which is defined as the difference between the incoming and outgoing energy fluxes at the Greenland surface. This budget takes into account the radiative budget, as well as turbulent energy terms and changes in storage of heat within the ice-sheet. The radiative budget in the visible (shortwave) and thermal infrared (longwave) domains is modulated by the presence of clouds. Part of the longwave radiation emitted by the Greenland surface is absorbed by clouds and re-emitted downward to the surface, causing surface longwave warming relative to clear skies. By blocking the incoming solar shortwave radiation, clouds also produce a shortwave cooling at the surface. Due to the high albedo of the GrIS surface (0.8–0.95 at the Summit station, Miller et al., 2015), the shortwave cooling effect of clouds is weak over Greenland compared to over open water. Thus, in contrast to other regions of the Earth with non icy surfaces, the longwave warming effect of clouds drives the total cloud radiative effect (shortwave cooling plus longwave warming) at the GrIS surface (C. Wang et al., 2019; W. Wang et al., 2019). However, this statement might be contradicted over the narrow coastal band where the GrIS surface albedo can be lower during the melt season (Hofer et al., 2017).

Amongst all cloud types, liquid-bearing clouds are known to play a critical role for surface melt, for instance during extreme melt events such as July 2012 (Bennartz et al., 2013), due to their high surface radiative warming effect produced by their relatively large optical depth compared to ice clouds (Shupe & Intrieri, 2004). They are observed mainly over the southeast and west coasts of the GrIS (Van Tricht et al., 2016). In order to understand the drivers of Greenland's cloud surface warming effect, it is necessary to understand the processes that lead to the presence of these liquid-bearing clouds.

Journal of Advances in Modeling Earth Systems, vol. 16, issue no. 7, e2023MS003918, doi:10.1029/2023MS003918

Reduced order modeling for linearized representations of microphysical process rates.

Lamb, K., **M. van Lier-Walqui**[1,2], S. Santos, and H. Morrison, 2024

NASA Goddard Institute for Space Studies, New York, NY, USA[1]
Center for Climate Systems Research, Columbia University, New York, NY, USA[2]

Abstract. Representing cloud microphysical processes in large scale atmospheric models is challenging because many processes depend on the details of the droplet size distribution (DSD, the spectrum of droplets with different sizes in a cloud). While full or partial statistical moments of droplet size distributions are the typical variables used in bulk models, prognostic moments are limited in their ability to represent microphysical processes across the range of conditions experienced in the atmosphere. Microphysical parameterizations employing prognostic moments are known to suffer from structural uncertainty in their representations of inherently higher dimensional cloud processes, which limit model fidelity and lead to forecasting errors. Here we investigate how data-driven reduced-order modeling can be used to learn predictors for microphysical process rates in bulk microphysics schemes in an unsupervised manner from higher dimensional bin distributions. Using simulations characteristic of marine stratiform clouds, we simultaneously learn lower dimensional representations of droplet size distributions and predict the evolution of the microphysical state of the system. Droplet collision-coalescence, the main process for generating warm rain, is estimated to have an intrinsic dimension of three. This intrinsic dimension provides a lower limit on the number of degrees of freedom needed to accurately represent collision-coalescence in models. We demonstrate how deep learning based reduced-order modeling can be used to discover intrinsic coordinates describing the microphysical state of the system, where process rates such as collision-coalescence are globally linearized. These implicitly learned representations of the DSD retain more information about the DSD than typical moment-based representations.

Introduction. Cloud microphysics, the set of processes that govern the small-scale evolution of cloud particles, remains a major source of uncertainty for numerical weather prediction and in climate models. One major challenge for cloud microphysics is that it is often unclear which predictors should be used to parameterize microphysical processes (Morrison et al., 2020). Clouds are ensembles of a large number of water droplets and ice crystals, and the factors that affect the interaction and growth of cloud particles range from the sub-millimeter scale to the synoptic scale (~1,000 km). Representing cloud microphysical processes requires modeling the evolution of the droplet or particle size distributions (DSD or PSD), since it is too computationally expensive to model the trajectories and evolution of all individual particles in a typical cloud, particularly on the scales required to model atmospheric processes in regional or global models.

Cloud microphysical schemes have typically employed either bulk or bin microphysical models to represent the evolution of the DSD. Bulk microphysics schemes, which are used in large scale weather and climate models, predict only the bulk properties of the DSD (such as cloud mass) within a model grid volume. In bulk schemes, a set of equations (or "parameterizations") describe how these bulk properties evolve due to the effects of the microphysical processes. Most bulk schemes use one, two, or three statistical moments of the DSD. For example, P3 (Predicted Particle Properties scheme) uses M_0 and M_6 in addition to ice mass mixing ratio Q_i (Morrison & Milbrandt, 2015), while the NTU (National Taiwan University) multi-moment bulk microphysics scheme uses M_0, M_2, and M_3 (in addition to Q_i and a M_3-weighted aspect ratio) for ice processes (Tsai & Chen, 2020). For liquid microphysics schemes, the most frequently used moments are M_0, M_3, and M_6, which are equivalent to or roughly proportional to physically observable quantities– the number concentration, mass, and radar reflectivity, respectively (Khain et al., 2015). Paukert et al. (2019) developed a 3-moment scheme using M_0, M_3, and M_6 for warm rain microphysics. In addition, almost all bulk schemes artificially separate precipitating and non-precipitating hydrometeor populations (e.g., by treating cloud droplets and rain droplets as two separate categories).

Communications Earth & Environment, vol. 5, 108, doi:10.1038/s43247-024-01271-4

Labrador Sea's influence on black spruce forests: Insights from tree-ring stable oxygen isotopes.

Larose, J., É. Boucher, A. de Vernal, I. Hermoso de Mendoza, F. Gennaretti, A. Lavergne, L. Andreu-Hayles, and **R.D. Field**[1,2], 2024

NASA Goddard Institute for Space Studies, New York, NY, USA[1]
Department of Applied Physics and Applied Mathematics, Columbia University, New York, NY, USA[2]

Abstract. In eastern Canada, Black spruce (*Picea mariana* Mill. B.S.P.) grows in a wide variety of climates, from maritime-oceanic conditions near the Labrador Sea, to more continental climates, inland. Along this gradient, timing and provenance of heat and moisture that support growth are uncertain, weakening our capacity to predict the response of boreal ecosystems to climate variability. Here, we measured the stable oxygen isotopic composition of black spruce tree-ring cellulose at three sites in eastern Canada and provide evidence of a rapid decrease of Labrador Sea's influence on adjacent ecosystems. Our results report a landwards decrease in the oxygen isotope composition of both tree-ring cellulose ($\delta^{18}O_{TRC}$) and precipitation water ($\delta^{18}O_p$). We also reveal a rapid landwards decoupling between $\delta^{18}O_{TRC}$ variability (1950-2013), maximum temperature and Sea Surface Temperature variations over the Northwest Atlantic. Thus, despite their apparent ecological homogeneity, eastern Canada's black spruce ecosystems rely on heterogeneous sources of heat and moisture.

Introduction. Labrador Sea is a region of deep water formation that drives decadal climate variability in the North Atlantic[1]. Deep waters formed in this sector contribute significantly to the strengthening of the Atlantic Meridional Overturning Circulation (AMOC), with important consequences on climate variability and sea surface temperatures (SSTs)[2]over the whole circum-Atlantic region, and beyond[3,4]. Because of the magnitude and significance of ocean-atmosphere heat and moisture exchanges, one should expect a detectable influence of the Labrador Sea on land ecosystem dynamics. Indeed, in the taiga forest sector of eastern North-America (above 51°N), multiple lines of evidence suggest that temperature-sensitive black spruce (*Picea mariana* (Mill.) B.S.P.) growth variations are teleconnected to ocean–atmosphere interactions in the Northwest Atlantic[5,6,7].

However, the extent of the Labrador Sea's direct influence on adjacent black-spruce-dominated forests remains poorly constrained spatially. Easternmost land masses located close to the Labrador Sea exhibit cold maritime-oceanic conditions[8]. By contrast, westernmost land masses are far more continental[8]. For instance, along this gradient, Nishimura and Laroque[9] observed that black spruce tree growth from stands located close to the Labrador Sea responded to July temperatures, while those located inland (>330 km away from the Labrador Sea) revealed a spatially-coherent response to early (May, June) and late (August) growing season temperatures. The longitudinal East-West shift in black spruce's response was thought to reflect a bio-climatic continentality gradient that increases constraints on black spruce growth, landwards[9]. Across such a continentality gradient, sites located close to the Labrador Sea are expected to get a larger proportion of incoming heat and moisture from a direct oceanic influence. This assumption needs to be better verified especially because westerlies redistribute heat and moisture over much of continental and oceanic regions of Northeastern America. Therefore, any influence from the Northwest Atlantic on inland Canadian climate and ecoystems implies westward transport from the Labrador Sea, in spite of prevailing westerly winds. In order to clarify the extent of this influence, alternative proxies more evocative of a direct oceanic imprint on nearby forest dynamics need to be developed.

Stable oxygen isotopes composition ($\delta^{18}O$) may help determining the spatial extent of the influence of Northwest Atlantic / Labrador Sea air masses on surrounding forest ecosystems. Air masses that originate from oceanic regions contain water vapor enriched in heavy oxygen isotopes (^{18}O). As air masses progress over cold and continental areas, water vapor condenses and precipitates, resulting in heavy isotopes being preferentially removed (ie. rained-out) as part of the thermo-dependent Raleigh distillation process[10].

Geophysical Research Letters, vol. 51, issue no. 10, e2023GL105828, doi:10.1029/2023GL105828

Just how river-like are atmospheric rivers?

LeGrande, A.N.[1,2], J.F. Booth, **C.M. Naud**[1,2], C. Ordaz, and J. Crespo[3], 2024

NASA Goddard Institute for Space Studies, New York, NY, USA[1]
Department of Applied Physics and Applied Mathematics, Columbia University, New York, NY, USA[2]
NASA Jet Propulsion Laboratory, Pasadena, CA, USA[3]

Abstract. Atmospheric Rivers (ARs) are synoptic-scale conduits for poleward transport of heat and water, often associated with extreme rainfall. Using NASA surface heat flux observations and climate model simulations, we assess whether ARs are "rivers", transporting heat and moisture over longer distances, or mostly local convergence. The observations indicate that ARs reduce extratropical surface energy fluxes, even during early development. This damping of surface fluxes during ARs is also simulated in the Goddard Institute for Space Studies ModelE, 2.1 (GISS-E2.1) nudged to (MERRA2) reanalysis winds. Furthermore, water provenance tracers in GISS-E2.1 identify the moisture source for ~7,500 ARs globally during 2018–2022 as farther upstream and equatorward compared to climatology. These results quantitatively show that ARs source relatively less moisture from the surface beneath them and more from a greater distance than during non-AR times.

Introduction. Atmospheric Rivers (ARs) can generate extreme precipitation events, flooding, and contribute ~80% of low to mid latitude and ~30% of high latitude meridional fluxes of water and energy (Woods et al., **2013**; Zhu & Newell, **1998**). Their critical role in the atmosphere makes it important to understand their life cycle. Details of their precipitation are well studied (e.g., Lavers & Villarini, **2013**; Mahoney et al., **2016**; Waliser & Guan, **2017**); however, less has been published regarding energy and moisture sources within ARs (e.g., Bao et al., **2006**).

ARs could result from organized, local convergence associated with an extratropical cyclone (ETC) (e.g., Dacre et al., **2015**), behave as "rivers" representative of synoptic transports of heat and moisture (e.g., Shinoda et al., **2019**; Sodemann & Stohl, **2013**), or, on some occasions, represent a combination of both. Despite this question being examined from multiple observational and modeling perspectives, it remains not fully resolved (Eiras-Barca et al., **2017**; Payne et al., **2020**; Ramos et al., **2016**). For ARs associated with extratropical cyclones (~82% of ARs in the North Pacific; Zhang et al., **2019**), the primary energy source is the atmospheric response to baroclinic instability. However, they also found that only 45% of ETCs are associated with ARs, and this suggests that the moisture component to ARs may depend on unique circulation or surface fluxes. Dacre et al. (**2019**) posit that moisture transported into the AR via a feeder airstream is rained out before traveling too far poleward, based on their ETC-focused moisture budget using reanalysis. If so, then one might expect subsequent moisture is added via surface fluxes. As such, the work herein is focused on the behavior of the ocean surface fluxes under ARs during the events.

One past constraint in determining AR energy sources was that observations of surface winds directly beneath ARs are obscured by precipitation (Bourassa et al., **2019**). This impacted air-sea flux estimates that principally derive from bulk flux equations involving wind speed. The relatively recently (2017) launched NASA Cyclone Global Navigation Satellite System (CYGNSS) GeoPositioning Satellite (GPS) receiver constellation is unique for its ability to measure surface roughness to estimate wind speeds even under heavily precipitating clouds (Ruf et al., **2019**), allowing air-sea fluxes to be estimated with higher fidelity (Crespo et al., **2019**).

Using CYGNSS air-sea fluxes to analyze ETCs, Naud et al. (**2021**) show that the weakest fluxes out of the ocean occur in the storm warm sector where poleward advection of warm air causes surface air temperature to be as warm as the ocean below, limiting energy fluxes out of the ocean. Given that the warm sector of ETCs is often associated with an AR, the Naud et al. (**2021**) result suggests energy fluxed from ocean to atmosphere under AR regions may be small. To test this idea, we examine CYGNSS surface heat fluxes under ARs.

Journal of Geophysical Research: Atmospheres, vol. 129, issue no. 17, e2023JD040179, doi:10.1029/2023JD040179

A GISTEMPv4 observational uncertainty ensemble.

Lenssen, N.[1,2,3], **G.A. Schmidt**[1], **M. Hendrickson**[1,4], P. Jacobs[5], M. Menne, and **R. Ruedy**[1,4], 2024

NASA Goddard Institute for Space Studies, New York, NY, USA[1]
Department of Applied Physics and Applied Mathematics, Columbia University, New York, NY, USA[2]
Climate and Global Dynamics Division, NSF National Center for Atmospheric Research, Boulder, CO, USA[3]
Autonomic Integra LLC, New York, NY, USA[4]
NASA Goddard Space Flight Center, Greenbelt, MD, USA[5]

Abstract. The historical global temperature record is an essential data product for quantifying the variability and change of the Earth system. In recent years, better characterization of observational uncertainty in global and hemispheric trends has become available, but the methodologies are not necessarily applicable to analyses at smaller regional areas, or monthly or seasonal means, where station sparsity and other systematic issues contribute to greater uncertainty. This study presents a gridded uncertainty ensemble of historical surface temperature anomalies from the Goddard Institute for Space Studies (GISS) Surface Temperature (GISTEMP) product. This ensemble characterizes the complex spatial and temporal correlation structure of uncertainty, enabling better uncertainty propagation for climate and applied science in applications of historical temperature products at spatial scales from global to regional and temporal scales from centennial to monthly. This work details the methodology for generating the uncertainty ensemble, presents key statistics of the uncertainty evolution over space and time, and provides best practices for using the uncertainty ensemble in future studies. Summary statistics from the uncertainty ensemble agree well with the previous GISTEMP global uncertainty assessment, providing confidence in both.

Introduction. In recent years, better characterization of uncertainty in historical global and hemispheric temperature trends has become available (Huang et al., **2020**; Lenssen et al., **2019**; Morice et al., **2020**; Rohde & Hausfather, **2020**), but the methodologies are not necessarily applicable to smaller spatiotemporal scales such as regional or monthly averages, where station sparsity and other systematic issues contribute to greater uncertainty. This study describes an ensemble of temperature reconstructions for the Goddard Institute for Space Studies (GISS) Surface Temperature product (GISTEMP) product (Hansen et al., **2010**; Lenssen et al., **2019**) which spans the possible regional and monthly uncertainty while properly accounting for the underlying spatiotemporal correlation structure.

Previous work quantified uncertainty in the GISTEMP estimate of large-scale annual mean series and developed critical components necessary for quantifying the uncertainty in the GISTEMP historical surface temperature record (Lenssen et al., **2019**). Critically, Lenssen et al. (**2019**) formalized the various sources of uncertainty in the GISTEMP procedure and divided total uncertainty into independent, quantifiable components that represented the major sources of uncertainty in the land and ocean analyses. In the Land Surface Air Temperature (LSAT) record, the primary sources of uncertainty are sampling uncertainty and station homogenization uncertainty. Sampling uncertainty is an umbrella term for uncertainties introduced into global and regional means due to incomplete spatial and temporal coverage. Station homogenization uncertainty accounts for possible errors arising from the adjustment of single station records to correct artificial break points due to changes in observing methods or station locations. Using this framework, operational GISTEMP now provides an estimate of global mean uncertainty.

Extending the results of Lenssen et al. (**2019**) to regional and monthly mean temperature is a significant undertaking. There are two primary difficulties: (a) moving from global and large-scale spatial means to small-scale spatial means and (b) quantifying the temporal dependence of the uncertainty to provide accurate estimates of the uncertainty in changes in the mean. The temporal structure of the uncertainty is the most important problem, and is particularly important to capture correctly for accurate uncertainty quantification in global and regional trends.

Ocean Modelling, vol. 188, 102303, doi:10.1016/j.ocemod.2023.102303

The sensitivity of the Equatorial Pacific ODZ to particulate organic matter remineralization in a climate model under pre-industrial conditions.

Lerner, P.[1,2], **A. Romanou**[1,2], D. Nicholson, **M. Kelley**[1], **R. Ruedy**[1,3], and **G. Russell**, 2024

NASA Goddard Institute for Space Studies, New York, NY, USA[1]
Department of Applied Physics and Applied Mathematics, Columbia University, New York, NY, USA[2]
Autonomic Integra LLC, New York, NY, USA[3]

Abstract. Marine oxygen plays a fundamental role in regulating the transfer of organic carbon and nutrients to their dissolved inorganic forms, serving as the terminal electron acceptor for heterotrophic respiration. Oxygen can become limiting to these processes in coastal and open-ocean oxygen deficient zones (ODZs). The maintenance of ODZs depends on the balance between physical processes such as ventilation and biogeochemical processes such as remineralization. These two processes act in opposing directions on ODZs, with ventilation responsible for transporting oxygen from the surface, where it is near saturation with the partial pressure of O_2 in the atmosphere, to deeper oxygen-depleted layers, and remineralization acting to consume oxygen through biogeochemical processes such as microbial degradation throughout the water column. Remineralization is represented in all CMIP6 models, but the actual parameterizations, as well as their magnitude, are widely varying.

In this study, we examine the sensitivity to remineralization of the equatorial Pacific ODZ (O_2 <60μmol/kg) in a model; the NASA GISS Ocean Biogeochemical Model (NOBM-G) embedded in the NASA-GISS coupled atmosphere-ocean model. We find that increasing the remineralization rate shoals the ODZ onset depth (i.e. the regionally averaged upper bound of the ODZ), and decreases ODZ volume and regional-averaged thickness. Changes in biological consumption and vertical convergence of oxygen are identified as the primary contributors to changes in ODZ onset depth. ODZ thickness is mainly influenced by the shoaling of the bottom boundary of the ODZ, which decreases with maximum remineralization rate due to decreasing oxygen consumption and increasing horizontal oxygen convergence in deep waters. On the other hand, vertically-averaged ODZ area has a more complex, non-monotonic relationship with maximum remineralization rate. While these findings suggest an important role for remineralization in determining the shape of the ODZ in our model, the relative importance of remineralization vs. other physical parameterizations remains to be established. While our results reflect the structure of our ocean biogeochemical model, the relationship of remineralization to ODZ characteristics in other models should be examined to better inform model inter-comparisons.

Introduction. Oxygen plays an important role in regulating the amount of CO_2 that can be taken up by the ocean. As the primary electron acceptor in the ocean, oxygen is responsible for over 90% of the loss of particulate organic carbon (POC) in the marine environment (Sarmiento and Gruber, 2006). Changes in oxygen concentration can impact the distribution of carbon and nutrients in the ocean, potentially leading to changes in biological productivity and export of carbon to the deep ocean, which in turn can change the air-sea flux of CO_2 (e.g., Niemeyer et al. (2017)). In most of the ocean, oxygen exists in sufficient quantities such that heterotrophic processes leading to POC remineralization (conversion of organic carbon to dissolved inorganic carbon, DIC) are not dependent on oxygen concentration (Keeling et al., 2010). However, in some regions of the ocean oxygen concentrations reach sufficiently low levels such that aerobic processes are inhibited, decreasing the rate at which organic carbon is converted to DIC. For example, respiratory stress (i.e., hypoxia) in higher trophic level organisms has been shown to occur below oxygen levels of 20–140μmol O_2/kg (Vaquer-Sunyer and Duarte, 2008). Additionally, once oxygen reaches sufficiently low concentrations (at a threshold ranging from 5–20μmol O_2/kg), nitrate replaces oxygen as the primary electron acceptor for the oxidation of organic carbon (Lam and Kuypers, 2011).

Geophysical Research Letters, vol. 51, issue no. 22, e2024GL112006, doi:10.1029/2024GL112006

Investigating the "too bright" issue pertaining to non-PBL clouds over the South Pacific trade-wind region in CMIP6 global climate models.

Li, J.-L.F.[1], K.-M. Xu[2], J.H. Jiang[1], W.-L. Lee, J.-Y. Yu, J.-D. Chern[3], **G.V. Cesana**[4,5], L. Wu[1], and G. Stephens[1], 2024

NASA Jet Propulsion Laboratory, California Institute of Technology, Pasadena, CA, USA[1]
NASA Langley Research Center, Hampton, VA, USA[2]
NASA Goddard Space Flight Center, Greenbelt, MD, USA[3]
NASA Goddard Institute for Space Studies, New York, NY, USA[4]
Center for Climate Systems Research, Columbia University, New York, NY, USA[5]

Abstract. This paper examines the “too bright” issue pertaining to non-planetary boundary layer (PBL) clouds over the South Pacific trade-wind region and its potential link to the falling ice radiative effects (FIREs). We run sensitivity experiments with CESM2-CAM6 (CESM2) global climate model with FIREs on (SON) and off (NOS). The model exhibits more in-cloud liquid water content (CLWC) and droplet above the PBL in NOS, leading to larger shortwave (SW) reflectivity at the top of the atmosphere than in SON over the trade wind regions. CMIP6 models are divided into three subsets: separately calculates the radiative effects of cloud ice and falling ice (SON2), combined (SON1) and without falling ice (NOS). SON2 models exhibit improved CLWC and SW reflectivity similar to CESM2-SON, while NOS and SON1 models are akin to CESM2-NOS owing to weaker surface wind stress and warmer ocean surface, caused by the lack of FIREs over the convective zones.

Introduction. Accurately representing planetary boundary layer (PBL) clouds remains a challenge for fully coupled global climate models (GCMs) (Jian et al., **2021**; Jiang et al., **2012**, **2021**; Li et al., **2008**, **2011**, **2018**, **2023a**; Lin et al., **2014**; Stephens, **2005**, **2008**). These clouds reflect solar radiation, while emitting a similar amount of infrared radiation as the ocean surface. The shortwave (SW) cloud radiative effect (CRE) at the top of the atmosphere (TOA) is mainly determined by cloud fraction (CF), or hydrometeor frequency discussed in Li et al. (**2023b**), cloud liquid water content (CLWC) and in-cloud liquid water content (InLWC) (Bony & Dufresne, **2005**; Mülmenstädt et al., **2021**; Stephens, **2005**, **2008**).

The well-known “too few, too bright” phenomenon is referred to as a specific issue in the portrayal of PBL clouds in the tropics and subtropics in Coupled Model Intercomparison Project Phase 5 (CMIP5: Taylor et al., **2012**) and CMIP6 (Eyring et al., **2016**) models (Bony & Dufresne, **2005**; Boucher et al., **2013**; Klein et al., **2013**; Konsta et al., **2022**; Mueller et al., **2011**; Nam et al., **2012**; Webb et al., **2001**; Zhang et al., **2005**). Conceivably, the “too few, too bright” biases can be a significant contributor to the uncertainties in low-level cloud feedback estimates (Zelinka et al., **2016**). Konsta et al. (**2022**) assessed low-level CF in CMIP6 model simulations that prescribe sea surface temperatures (SST). They found that models tend to depict PBL clouds as overly bright (“too bright”) while underestimating their coverage (“too few”). Nam et al. (**2012**) evaluated outputs of CMIP5 and compared them with various satellite data sets. They demonstrated that models produce excessively bright low-level clouds, even when the low-cloud cover is accurate. They concluded that the impact of these biases on the Earth's radiation budget is mitigated by compensating errors, through underestimating low-cloud cover and overestimating the occurrence of mid- and high-level clouds above low clouds.

The overestimate of non-PBL clouds in the trade-wind region can produce overestimate of solar reflectivity and thus can contribute to the “too bright” issue through overestimate of CLWC. As noted above, Nam et al. (**2012**) used CMIP5 models to first identify this issue. Is it still present in CMIP6 models? What physical mechanism can explain the cause of such an issue?

Communications Earth & Environment, vol. 5, issue no. 1, 295, doi:10.1038/s43247-024-01441-4

Improved constraints on hematite refractive index for estimating climatic effects of dust aerosols.

Li, L., N.M. Mahowald, M. Gonçalves Ageitos, **V. Obiso**[1], **R.L. Miller**[1], C. Pérez García-Pando, C. Di Biagio, P. Formenti, P.G. Brodrick[2], R.N. Clark, R.O. Green[4], R. Kokaly, G. Swayze, and D.R. Thompson[2], 2024

NASA Goddard Institute for Space Studies, New York, NY, USA[1]
NASA Jet Propulsion Laboratory, California Institute of Technology, Pasadena, CA, USA[2]

Abstract. Uncertainty in desert dust composition poses a big challenge to understanding Earth's climate across different epochs. Of particular concern is hematite, an iron-oxide mineral dominating the solar absorption by dust particles, for which current estimates of absorption capacity vary by over two orders of magnitude. Here, we show that laboratory measurements of dust composition, absorption, and scattering provide valuable constraints on the absorption potential of hematite, substantially narrowing its range of plausible values. The success of this constraint is supported by results from an atmospheric transport model compared with station-based measurements. Additionally, we identify substantial bias in simulating hematite abundance in dust aerosols with current soil mineralogy descriptions, underscoring the necessity for improved data sources. Encouragingly, the next-generation imaging spectroscopy remote sensing data hold promise for capturing the spatial variability of hematite. These insights have implications for enhancing dust modeling, thus contributing to

Introduction. Aerosol impacts on climate constitute one of the challenges in estimating current and future climate changes[1]. An important error source arises from absorbing natural aerosols, such as desert dust[1,2,3], because they can both absorb and scatter radiation at short and long wavelengths, giving rise to a complicated relationship with the resulting net (shortwave plus longwave) direct radiative effect (DRE)[2,3]. The absorption capability relative to the scattering by dust aerosols dictates whether they foster or suppress precipitation locally and whether they warm or cool the planet[4,5,6,7]. These climatic impacts are still subject to large uncertainty, primarily due to poorly known attributes of dust aerosols, such as their optical properties[8,9]. To limit computational cost, most global climate models consider dust particles as a globally homogenous mixture of minerals, despite the strong regional variation of mineralogical composition[10,11,12] and, thus, the optical properties of dust aerosols[9,13]. In contrast, recent studies[3,11,14,15,16,17,18,19,20,21] have speciated dust into multiple mineral components, enabling the representation of regional variations of dust composition and resulting complex refractive index (CRI)[14].

Modeling studies[3,16,20] and observations[13,22] have identified two types of iron oxides, specifically hematite and goethite, as key mineral components to estimate dust DRE because of their strong absorption at ultraviolet and visible wavelengths[13,14,19,23], particularly when they are internally mixed with other minerals that are less absorbing[14]. Other light-absorbing oxide types, including manganese-oxides and titanium-oxides[24,25,26], along with iron oxide minerals in addition to hematite and goethite, coexist in dust aerosols. However, measurements consistently indicate that hematite and goethite are the most common types of light-absorbing oxides and predominate in mass over the other types in major dust source regions[11,12,27,28]. Consequently, despite the potential comparability of some other light-absorbing oxide types in terms of the imaginary part of the CRI (referred to as imaginary CRI for brevity), a fundamental parameter linked to the aerosol absorption ability, their overall quantities are typically insufficient to exceed the importance of hematite and goethite for dust absorption within the shortwave spectral range. The imaginary hematite CRI, however, shows over two orders of magnitude difference in the literature (Supplementary Fig. 1)[19], exhibiting strong[29], moderate[30], to weak[31] absorption at visible wavelengths (referred to as STRONG, MODERATE, and WEAK index, respectively). In contrast to this diversity, there is only one set of imaginary goethite CRI[32] available for use, whose accuracy has been questioned[33].

CABI Agriculture and Bioscience, vol. 5, issue no. 1, 109, doi:10.1186/s43170-024-00308-0

Climate change mitigation and adaptation for rice-based farming systems in the Red River Delta, Vietnam.

Li, T., **S.S. McDermid**[1,2], R.O. Valdivia, and P. Sundaram[2], 2024

NASA Goddard Institute for Space Studies, New York, NY, USA[1]
Department of Environmental Studies, New York University, New York, NY, USA[2]

Abstract. Rice is a major contributor to anthropogenic greenhouse gas (GHG) emissions, primarily methane, and at the same time will be negatively impacted by regional climate changes. Identifying rice management interventions to reduce methane emissions while improving productivity is, therefore, critical for climate change mitigation, adaptation, and food security. However, it can be challenging to conduct multivariate assessments of rice interventions in the field owing to the intensiveness of data collection and/or the challenges in testing long-term changes in meteorological and climate conditions. Process-based modeling, evaluated against site-based data, provides an entry point for evaluating the impacts of climate change on rice systems and assessing the impacts, co-benefits, and trade-offs of interventions under historical and future climate conditions.

Introduction. Rice directly feeds ~ 3 billion people and is critical to global food security, farmer livelihoods, and national agricultural economies (Fukagawa and Ziska 2019; Muthayya et al. 2014). Climate change is expected to reduce rice yields globally, by some estimates 10% or more (Peng et al. 2004; Hasegawa et al. 2021), primarily through increases in temperature, reduced and/or highly variable water availability, and via a host of other climate change-mediated changes (e.g. pests and diseases) to agroecosystems (Yuen et al. 2021). While some of these losses may be partly offset by CO_2 fertilization effects (Fukagawa and Ziska 2019; Muthayya et al. 2014; Hasegawa et al. 2018; Jägermeyr et al. 2021; Toreti et al. 2020; Deryng et al. 2016), emerging evidence suggests that higher CO_2 concentrations may also reduce the concentrations of important nutrients, such as zinc and iron, in consumed rice (Zhu et al. 2018). There is thus a need to identify regional, context-specific interventions that can facilitate rice-based farming systems' adaptation to climate change.

At the same time, rice is also a major contributor to climate (and environmental) change, primarily by way of methane emissions that result from the anaerobic conditions created by paddy flood irrigation (Carlson et al. 2016; McDermid et al. 2020), practiced in part to reduce weed pressure. Rice contributes about 10% and 2% of agricultural and total anthropogenic global greenhouse gas (GHG) emissions, respectively, and 8-12% of global methane emissions (Saunois et al. 2020; Crippa et al. 2021; Tubiello et al. 2021). Methane is ~ 21 × more powerful than CO_2 on a 100-year timescale, and it is critical to reduce methane emissions to meet urgent, high-ambition global climate change mitigation targets (IPCC 2018; Masson-Delmotte et al. 2021). Therefore, alongside climate change adaptation, rice farming practices and interventions that also mitigate methane (as well as other GHG) emissions are in increasing demand (Yuan et al. 2021).

Among the range of interventions currently being explored, alternative water management—such as Alternate Wetting and Drying (AWD) in which the rice paddy is irrigated and then allowed to dry to a certain depth before irrigating again (Kosmowski et al. 2023)—has been identified as a means of mitigating methane (CH_4 herein) emissions from rice production (LaHue et al. 2016; Lampayan et al. 2015; Nelson et al. 2015; Carrijo et al. 2017; Setyanto et al. 2018). Furthermore, AWD and similar irrigation practices may help conserve precious freshwater resources in water-scarce regions for future use as warming trends continue (Silalertruksa et al. 2017). Many countries now list water management in rice systems, including AWD, as part of the Nationally Determined Contributions (2020–2022) for either climate change mitigation, adaptation, or both.

Journal of Geophysical Research: Atmospheres, vol. 129, issue no. 7, e2023JD039489, doi:10.1029/2023JD039489

Process modeling of aerosol-cloud interaction in summertime precipitating shallow cumulus over the Western North Atlantic.

Li, X.-Y., H. Wang, M.W. Christensen, J. Chen, S. Tang, S. Kirschler, E. Crosbie[1], L.D. Ziemba[1], D. Painemal[1], A.F. Corral, K.A. McCauley, S. Dmitrovic, A. Sorooshian, M. Fenn[1], J.S. Schlosser[1], S. Stamnes[1], J.W. Hair[1], **B. Cairns[2]**, R. Moore[1], R.A. Ferrare[1], M.A. Shook[1], Y. Choi[1], Diskin, G.S.1, J. DiGangi[1], J.B. Nowak[1], C. Robinson[1], T.J. Shingler[1], K.L. Thornhill[1], and C. Voigt, 2024

NASA Langley Research Center, Hampton, VA, USA[1]
NASA Goddard Institute for Space Studies, New York, NY, USA[2]

Abstract. Process modeling of Aerosol-cloud interaction (ACI) is essential to bridging gaps between observational analysis and climate modeling of aerosol effects in the Earth system and eventually reducing climate projection uncertainties. In this study, we examine ACI in summertime precipitating shallow cumuli observed during the Aerosol Cloud meTeorology Interactions oVer the western ATlantic Experiment (ACTIVATE). Aerosols and precipitating shallow cumuli were extensively observed with in-situ and remote-sensing instruments during two research flight cases on 02 June and 07 June, respectively, during the ACTIVATE summer 2021 deployment phase. We perform observational analysis and large-eddy simulation (LES) of aerosol effect on precipitating cumulus in these two cases. Given the measured aerosol size distributions and meteorological conditions, LES is able to reproduce the observed cloud properties by aircraft such as liquid water content (LWC), cloud droplet number concentration (N_c) and effective radius r_{eff}. However, it produces smaller liquid water path (LWP) and larger N_c compared to the satellite retrievals. Both 02 and 07 June cases are over warm waters of the Gulf Stream and have a cloud top height over 3 km, but the 07 June case is more polluted and has larger LWC. We find that the N_a-induced LWP adjustment is dominated by precipitation feedback for the 2 June precipitating case and there is no clear entrainment feedback in both cases. An increase of cloud fraction due to a decrease of aerosol number concentration is also shown in the simulations for the 02 June case.

Introduction. Aerosol-cloud interaction (ACI) poses the largest uncertainty for accurate climate projection (Seinfeld et al., **2016**). Assuming fixed Liquid Water Path (LWP) and Cloud Fractional Coverage (CFC), increasing the aerosol number concentration N_a leads to a larger cloud droplet number concentration N_c, smaller effective radius r_{eff}, and stronger outgoing shortwave (SW) radiation (Twomey, **1977**). The enhanced SW cloud radiative effect can affect the meteorological state and boundary layer structure of clouds (X.-Y. Li et al., **2023**). Decreased r_{eff} suppresses the precipitation rate by inhibiting the collision-coalescence processes, resulting in a higher LWP and possibly larger CFC (Albrecht, **1989**). This is the conventional wisdom of ACI involving multi-scale, nonlinear processes from aerosol and cloud microphysics to large-scale atmospheric circulations, which are fundamentally poorly understood due to the intractable scale range and strong nonlinearity, and therefore, mathematically poorly represented in Earth System Models (ESMs) (Seinfeld et al., **2016**; Smith et al., **2020**). Besides the strongly nonlinear nature of ACI, it is also in an emergent and non-equilibrium state, which hinders our understanding of processes that determines sinks and sources of aerosol and cloud. One example is the nonlinear interplay among N_a, N_c, and the sink terms of liquid water content (LWC) for summertime shallow cumuli (Seinfeld et al., **2016**). The parameterization of these clouds is responsible for the spread of ESMs in estimating the equilibrium climate sensitivity (ECS) (Zhao et al., **2016**). In addition, even though ACI of shallow cumuli was shown to affect the ECS (Gettelman et al., **2019**), the magnitude is uncertain.

Journal of Ecology., vol. 112, issue no. 11, pp. 2522-2539, doi:10.1111/1365-2745.14416

Effects of water limitation and competition on tree carbon allocation in an Earth system modeling framework.

Lichstein, J.W., T. Zhang, **E. Weng**[1,2], C.E. Farrior, R. Dybzinski, S. Malyshev, E. Shevliakova, R.A. Birdsey, and S.W. Pacala, 2024

NASA Goddard Institute for Space Studies, New York, NY, USA[1]
Center for Climate Systems Research, Columbia University, New York, NY, USA[2]

Abstract.

1. Earth system models (ESMs) have a limited capacity to represent plant functional diversity and shifts in trait distributions. Approaches to improving the representation of this complexity in ESMs include (i) optimality-based approaches that predict trait–environment responses and (ii) explicitly modelling coexistence and community assembly. These approaches are expected to converge only when optimality-based approaches identify competitively dominant strategies, which often differ from strategies that maximize ecosystem functioning or fitness components in monoculture.

2. We used two models, LM3-PPA (a vegetation demographic model designed as an ESM component) and BiomeE (a computationally efficient analog for LM3-PPA), to explore how water limitation affects carbon allocation strategies of canopy trees. We compared competitive allocation strategies and those that maximize biomass or productivity in monoculture. We did not explicitly model coexistence or community assembly. Rather, we used model experiments to identify competitive and maximizing strategies in a two-dimensional trait space under different precipitation and mortality scenarios.

3. At 10 eastern US locations, we simulated historical, wet and dry climate scenarios, novel drought and three different mortality scenarios (low, medium or high sensitivity to water deficit). For each site and scenario, we identified the competitive strategy and three maximizing strategies (maximum biomass, productivity or drought-tolerance).

4. Root: leaf ratios tended to increase and leaf area tended to decrease with increasing water stress (increasing water limitation and its effects on mortality). However, relative to maximizing strategies, competitive strategies shifted towards greater allocation to roots and leaves with increasing water stress.

5. Competitive overinvestments (greater allocation to roots and leaves by competitive strategies compared with maximizing strategies) were robust across different modelling contexts, including vegetation parameter sets (*Acer* vs. *Populus*), models (LM3-PPA vs. BiomeE) and uncalibrated vsersus calibrated BiomeE versions.

6. *Synthesis*: The theoretical prediction that competitive and maximizing allocation strategies differ under water limitation is confirmed for a demographic model designed as an ESM component. Optimality-based trait predictions can simplify representing trait diversity in ESMs but do not always correspond to competitive outcomes. Explicitly modelling coexistence and community assembly in ESMs is challenging but is likely the most general approach to representing trait diversity.

One Earth, vol. 7, issue no. 7, pp. 1187-1201, doi:10.1016/j.oneear.2024.06.013

Critical overview of the implications of a global protein transition in the face of climate change: Key unknowns and research imperatives.

Lumsden, C.L., **J. Jägermeyr**[1,2,3], L. Ziska, and J. Fanzo, 2024

NASA Goddard Institute for Space Studies, New York, NY, USA[1]
Center for Climate Systems Research, Columbia University, New York, NY, USA[2]
Potsdam Institute for Climate Impact Research (PIK), Member of the Leibniz Association, Potsdam, Germany[3]

Abstract. Current dietary protein production and consumption are depleting resources, degrading the environment, and fueling chronic diseases. These human and environmental impacts ignite intense debate on how to shift away from resource-intensive animal-based proteins. While there is significant research across disciplines on shifting supply-demand aspects, knowledge gaps remain in how to transition to optimize nutrition while reducing bidirectional climate change effects. These gaps stymy incentives and policy change to make bold food systems transformations and determine levers to invest in. Here we present a transdisciplinary overview of evidence on proteins' environmental impacts and vulnerability of crop, livestock, and aquatic proteins to climate change. We identify critical unknowns fueling concerns surrounding transitions and propose research directions to increase the likelihood transitions will be environmentally sound and healthy, harnessing genetic crop diversity, managing agricultural landscapes sustainably, and considering cell-based alternatives and pro-equity policies that facilitate healthy choices. Implementing changes requires nuanced, regionally tailored approaches incorporating socio-behavioral, public health, nutrition, and climate science fostering effective debate and solutions promoting sustainability and health.

Introduction. Transitioning food systems and human protein consumption away from carbon- and resource-intensive animal-based proteins to more sustainable, climate-friendlier sources has become a popular topic of analysis and debate. Myriad discussions and publications have been generated—from multiple viewpoints—on shifting protein consumption as a means to promote environmental sustainability and human health.

Such interest has arisen from increasing recognition of the high contribution of food systems to global greenhouse gas (GHG) emissions, particularly those providing animal-based proteins. Food systems currently contribute approximately one-third of total global GHG emissions, with animal-sourced foods a primary driver accounting for two-thirds of food-related GHGs.[1,2,3] Economic and population growth to 2050 without any transition to alternative protein sources is projected to lead to a 21% increase in *per capita* meat consumption and a 63% increase in total consumption and GHG emissions.[4] This impact on GHGs, coupled with the increasing global burden of diet-related non-communicable diseases (NCDs; e.g., obesity, type II diabetes, cardiovascular disease), heightens the urgency to assist populations in adopting dietary patterns and practices that support human and environmental health.

Conversely, there are also substantial unknowns regarding various protein transitions within food systems. Recommendations put forward to improve health and environmental outcomes often fail to address the complexity of protein transitions, the challenges faced by populations to make those changes, and the interdependent nature of their anticipated effects. Proposed solutions are frequently limited in scope regionally and by population impacted, reflect the narrow financial or mission-specific interests of individual groups, and promote overly simplistic resolutions.[5]

Given the dynamic bidirectional relationship between climate change and food systems, and that animal-based protein sources are major contributors to GHG emissions, use excessive resources (land, water), accelerate biodiversity loss, and can lead to diet-related NCDs, there is a merited focus on altering dietary protein sources and consumption to simultaneously improve planetary and human health outcomes.

Atmospheric Measurement Techniques, vol. 17, issue no. 9, pp. 2611-2024, doi:10.5194/amt-17-2611-2024

TROPESS-CrIS CO single-pixel vertical profiles: Intercomparisons with MOPITT and model comparisons for 2020 western US wildfires.

Luo, M.[1], H.M. Worden, **R.D. Field**[2,3], **K. Tsigaridis**[2,4], and **G.S. Elsaesser**[2,3], 2024

NASA Jet Propulsion Laboratory, California Institute of Technology, Pasadena, CA, USA[1]
NASA Goddard Institute for Space Studies, New York, NY, USA[2]
Department of Applied Physics and Applied Mathematics, Columbia University, New York, NY, USA[3]
Center for Climate Systems Research, Columbia University, New York, NY, USA[4]

Abstract. The new TROPESS (TRoposphеric Ozone and its Precursors from Earth System Sounding) profile retrievals of carbon monoxide (CO) from the Cross-track Infrared Sounder (CrIS) are evaluated against Measurement of Pollution in the Troposphere (MOPITT) CO version 9 data. Comparison results that were adjusted to common a priori constraints in the retrieval processes have improved agreement between the two data sets over direct comparisons. TROPESS-CrIS CO profiles are within 5 % of MOPITT but have higher concentrations in the lower troposphere and lower concentrations in the upper troposphere. For the intense western US wildfire events in September 2020, we compare CO fields simulated by the GISS climate model to the two satellite CO observations. We show intermediate steps of the comparison process to illustrate the evaluation of model simulations by deriving the “retrieved” model CO profiles as they would be observed by the satellite. This includes the application of satellite level-2 data along with their corresponding diagnostic operators provided in the TROPESS-CrIS and MOPITT products. The process allows a diagnosis of potential model improvements in modeling fire emissions and pollution transport.

Introduction. As a direct pollutant to Earth's atmosphere, carbon monoxide (CO) is a product of incomplete combustion which has a lifetime of weeks to months. CO has therefore been used as a tracer in atmospheric ozone-related photochemistry and pollution transport studies. High concentrations of CO in source regions can be seen above background concentrations from, for example, biomass burning, traffic, and other fossil fuel combustion in polluted cities and industrial areas (Jacob, 1999). High-CO plumes are seen extending downwind to pollute nearby regions and sometimes circling the globe. For more than 20 years, retrievals of vertical CO profiles or total columns based on satellite measurements of CO absorption bands of 4.7 and 2.3 µm have been made available from several platforms, such as the Measurement of Pollution in the Troposphere (MOPITT) (Drummond et al., 2009), Atmospheric Infrared Sounder (AIRS) (Aumann et al., 2003), Tropospheric Emission Spectrometer (TES) (Beer et al., 2001), Infrared Atmospheric Sounding Interferometer (IASI) (Clerbaux et al., 2009), Cross-track Infrared Sounder (CrIS) (Han et al., 2013), and TROPOspheric Monitoring Instrument (TROPOMI) (Veefkind et al., 2012). In addition, some limited CO data also became available, e.g., from GOSAT (Noël et al., 2022) and GIIRS (Zeng et al., 2023) satellite observations. These satellite CO observations are valuable in tracking and quantifying pollutant emissions, horizontal gradients in pollution patterns, and the pollutant photochemical processes occurring as air moves (Clerbaux et al., 2002). From a long-term and global point of view, the satellite CO observations have been used to track the pollution–time trend in geophysical regions annually and seasonally (Worden et al., 2013; Buchholz et al., 2021). The satellite CO observations have also been used to evaluate parameter variations that drive model simulations of the atmospheric system (Field et al., 2015, 2016; Buchholz et al., 2018).

Journal of Quantitative Spectroscopy and Radiative Transfer, vol. 320, 108972, doi:10.1016/j.jqsrt.2024.108972

Branch dependence of halfwidths: Theoretical analysis of N2-broadened halfwidths of CH3Br in the v6 band.

Ma, Q.[1,2], and C. Boulet, 2024

NASA Goddard Institute for Space Studies, New York, NY, USA[1]
Department of Applied Physics and Applied Mathematics, Columbia University, New York, NY, USA[2]

Abstract. The N_2-broadened halfwidths of CH_3Br in the ν_6 band have been calculated, along with the relaxation matrices W. These calculations employ our modified and refined versions of the Robert-Bonamy formalism. Extensive comparisons between the predicted halfwidths from the models and experimental measurements at T = 296 K are presented. Our latest model very closely matches the measurements. Meanwhile, we considered line mixing effects in the spectral profile of the RQ(j,0) sub-branch. Our method probably yields too large values of the off-diagonal elements of W. Finally, by comparing our calculated halfwidths with the data in HITRAN, we have observed generally good agreement, especially for lines with high values of j. However, the agreement becomes poor for lines with low values of j, deteriorating as j decreases. We identified a factor contributing to this poor agreement: the neglect of branch dependence in the development of HITRAN data. We believe that for lines with low values of j, this oversight undermines the reliability of the halfwidth values of CH_3Br in HITRAN.

Introduction. Methyl bromide (CH_3Br) holds a significant role in atmospheric chemistry. Notably, it is more potent in causing ozone destruction than chlorine (see Ref. [1] for more details). Meanwhile, despite its comparatively shorter atmospheric lifespan among ozone-depleting substances, its capacity to trap heat in the atmosphere significantly contribute to global warming. Accurate spectroscopic parameters of CH_3Br are fundamental in its identification, quantification, atmospheric modeling, climate studies, and understanding its reactivity in the air. This information is crucial in atmospheric applications

Numerous experimental studies have been conducted on this subject, with one particularly important work authored by Jacquemart et al. [2]. In their research, they measured line positions, intensities, self- and N_2-broadened halfwidths in 10-μm spectral region. Moreover, they developed a model based on these measurements, illustrating a rotational dependence on j and k for both self- and N_2-broadened halfwidths. Furthermore, this model found application in the development of HITRAN 2008 for both the 10- and 7 μm spectral regions [3].

Regarding theoretical aspects, the latest calculation of N_2-broadened halfwidths of CH_3Br was conducted by Bousetta et al. [4] utilizing the ATC theory [5]. In their study, they employed the parabolic trajectory model and took into account electrostatic, induction, dispersion interactions. However, it's worth noting that the ATC theory, developed in 1962, is considered somewhat outdated, and in recent times, it has seen decreased utilization among researchers.

Presently, there exist more advanced approaches, including the Robert-Bonamy (RB) model developed in 1979 [6], the Modified Robert-Bonamy (MRB) model developed in 2007 [7], and the Refined Bobert-Bonamy (RRB) model developed in 2013 [8]. Both the MRB and RRB models were formulated by the current authors employing the cumulant expansion instead of the Linked-Cluster theorem utilized by Robert and Bonamy.

A fundamental difference between our approaches and the RB formalism lies in the inclusion or exclusion of the bath average in defining the S_2 operator. In our methodologies, the bath average is conducted in advance during the calculation of S_2 matrix elements. As a result, the S_2 matrix becomes independent of the bath molecule's degrees, significantly reducing its size compared to the RB formalism.

Science of the Total Environment, vol. 949, 174792, doi:10.1016/j.scitotenv.2024.174792

Letter to the Editor regarding Chappell et al., 2023, "Satellites reveal Earth's seasonally shifting dust emission sources".

Mahowald, N., P. Ginoux, G.S. Okin, J. Kok, S. Albani, Y. Balkanski, M. Chin, G. Bergametti, T.F. Eck, C. Pérez García-Pando, A. Gkikas, M. Gonçalves Ageitos, D. Kim, M. Klose, S. LeGrand, L. Li, B. Marticorena, **R.L. Miller**[1], C. Ryder, C. Zender, and Y. Yu, 2024

NASA Goddard Institute for Space Studies, New York, NY, USA[1]

Abstract. Chappell et al. (2023a) recently concluded that North Africa is not the largest source of dust in the world and that the global rate of dust emission is almost two orders of magnitude smaller than estimated by numerous previous studies (e.g., 29 Tg/year versus 1200 to 9000 Tg/year in Huneeus et al., 2011; Ginoux et al., 2012; Klose et al., 2021; Kok et al., 2021a, Kok et al., 2021b; Checa-Garcia et al., 2021; Gliß et al., 2021; Zhao et al., 2022). These conclusions run counter to decades of prior research. Here we first review the data and knowledge we already have about dust, and then discuss the sources of the discrepancies between Chappell et al. (2023a) and previous work.

While Chappell et al. (2023a) concluded that existing dust models greatly overestimate dust emission, particularly in North Africa, their approach fails to consider the available climatological dust data, in contrast to the existing model studies and evaluations. For example, a simple back-of-the-envelope computation indicates that their estimated global annual dust emission rate is 2 orders of magnitude too small and not consistent with the known global atmospheric dust load. A relatively easily observed indicator of the atmospheric dust load is the optical depth over dust regions, which represents the amount of light that is absorbed or reflected by dust aerosols (e.g. Ridley et al., 2016; Balkanski et al., 2007). Combining their estimated ~30 Tg/year global annual emission of dust with diameter less than 10 μm (PM10) with the model-estimated dust lifetime of ~3 days (e.g., Kok et al., 2021a; Gliß et al., 2021), the total amount of dust in the atmosphere would be ~0.25 Tg (3 days*30 Tg/365 days). This corresponds to a global mean dust optical depth ranging from 0.0002 to 0.0005 based on a mid-visible wavelength mass extinction coefficient varying from 0.40 to 0.96 m^2/g (Kok et al., 2021a), respectively. Such values are 2 orders of magnitude lower than observationally constrained values of global mean mid-visible dust optical depth varying from approximately 0.02 to 0.04 (Ridley et al., 2016; Voss and Evan, 2020; Song et al., 2021; Kok et al., 2021a; Gkikas et al., 2022). In order to explain their lower emissions over North Africa, Chappell et al. (2023a) argue that North African dust is not transported away from sources, but recirculated in the regional atmosphere, allowing higher loads to build up. However, relating their low magnitude of emissions of ~30 Tg/year to the observationally constrained global mean dust optical depth would require a dust lifetime on the order of 300 days, which is clearly unphysical. Indeed, such a long lifetime is incompatible with well-documented evidence of the role of meteorological influence on dust transport - for example dust is transported from North African sources across the Atlantic on a timescale of 5–10 days (e.g. Knippertz and Todd, 2012; Weinzierl et al., 2017). Furthermore, well-known documentation of North African wind patterns, trajectory analyses and also the same high-resolution (15 min) SEVIRI satellite analyses used by Chappell et al. (2023a) confirm that dust transport occurs on these time scales (e.g. Ryder et al. (2018), many others.), which disputes the findings of Chappell et al. (2023a).

In addition to the clear underestimation of the global dust emission rate by Chappell et al. (2023a), there is are multiple lines of evidence at that Chappell et al. (2023a) underestimated dust from North Africa the regional scale, as well as the relative contribution of North African dust to the global dust cycle. Chappell et al. (2023a) found that North African dust emission is small (6 Tg/year of PM10 dust) and sparsely distributed across the region.

Earth's Future, vol. 12, issue no. 6, e2023EF004187, doi:10.1029/2023EF004187

Envisioning U.S. climate predictions and projections to meet new challenges.

Mariotti, A., D.C. Bader, **S.E. Bauer**[1], G. Danabasoglu, J.P.P. Dunne, B. Gross, L.R. Leung, S. Pawson[2], W.M Putman[2], V. Ramaswamy, **G.A. Schmidt**[1], and V. Tallapragada, 2024

NASA Goddard Institute for Space Studies, New York, NY, USA[1]
NASA Goddard Space Flight Center, Greenbelt, MD, USA[2]

Abstract. In the face of a changing climate, the understanding, predictions, and projections of natural and human systems are increasingly crucial to prepare and cope with extremes and cascading hazards, determine unexpected feedback and potential tipping points, inform long-term adaptation strategies, and guide mitigation approaches. Increasingly complex socio-economic systems require enhanced predictive information to support advanced practices. Such new predictive challenges drive the need to fully capitalize on ambitious scientific and technological opportunities. These include the unrealized potential for very high-resolution modeling of global-to-local Earth system processes across timescales, reduction of model biases, enhanced integration of human systems and the Earth Systems, better quantification of predictability and uncertainties; expedited science-to-service pathways, and co-production of actionable information with stakeholders. Enabling technological opportunities include exascale computing, advanced data storage, novel observations and powerful data analytics, including artificial intelligence and machine learning. Looking to generate community discussions on how to accelerate progress on U.S. climate predictions and projections, representatives of Federally-funded U.S. modeling groups outline here perspectives on a six-pillar national approach grounded in climate science that builds on the strengths of the U.S. modeling community and agency goals. This calls for an unprecedented level of coordination to capitalize on transformative opportunities, augmenting and complementing current modeling center capabilities and plans to support agency missions. Tangible outcomes include projections with horizontal spatial resolutions finer than 10 km, representing extremes and associated risks in greater detail, reduced model errors, better predictability estimates, and more customized projections to support next generation climate services.

Introduction. Climate change is making extremes like floods, fires, heat waves, and droughts more frequent, more intense, and costlier (Herring et al., 2021; National Academies of Sciences et al., 2016). These hazards often result in multiple, cascading, interconnected, and compounded effects across the natural and human systems. For example, precipitation and wind extremes have direct effects such as flooding and wind damage, as well as indirect effects such as landslides, coastal inundation, and reduced water quality. Similarly, the local dangers of extreme heat, fire, and dust events can be followed by increased air pollution, with the associated human health impacts that can extend over large regions. All these extremes and their associated damage affect society, economies, health, and livelihoods differently depending on environmental specifics under changing conditions. Impacting individual citizens as well as businesses and governments, these extremes can cost lives and tens of billions of dollars in damages each year (NOAA National Centers for Environmental Information (NCEI) U.S, 2022). Disadvantaged and marginalized communities are more vulnerable to the impacts of such extremes (Jay et al., 2023; UN, 2016). It is clear that damages can be reduced by more skillful and earlier forecasts (Vaughan et al., 2016; White et al., 2022). Benefits of improved predictions also include supporting advances in socio-economic activities such as more sophisticated practices for agriculture, water resources, energy management and recreation, among many others. Here we make the case that as we enter the uncharted territory of a changed climate and increasingly complex socio-economic systems, improved predictions and projections (for a definition see Supporting Information S1; SI hereafter) allow better decision making and resilience, and repay the investment several times over.

Open Data Journal Agricultural Research, vol. 10, pp. 14-21, doi:10.18174/odjar.v10i0.18442

Winter wheat experiments to optimize sowing dates and densities in a high-yielding environment in New Zealand: field experiments and AgMIP-Wheat multi-model simulations.

Martre, P., S. Dueri, H. Brown, S. Asseng, F. Ewert, H. Webber, M. George, R. Craigie, **J. Guarin**[1,2,3], D. Pequeno, T. Stella, M. Ahmed, P. Alderman, B. Basso, A. Berger, G. Bracho Mujica, D. Cammarano, Y. Chen, B. Dumont, E. Rezaei, E. Fereres, R. Ferrise, T. Gaiser, Y. Gao, M. Garcia-Vila, S. Gayler, Z. Hochman, G. Hoogenboom, K. Kersebaum, C. Nendel, J. Olesen, G. Padovan, T. Palosuo, E. Priesack, J. Pullens, A. Rodríguez, R. Rötter, M. Ruiz Ramos, M. Semenov, N. Senapati, S. Siebert, A. Srivastava, C. Stöckle, I. Supit, F. Tao, P. Thorburn, E. Wang, T. Weber, L. Xiao, C. Zhao, J. Zhao, Z. Zhao, and Y. Zhu, 2024

NASA Goddard Institute for Space Studies, New York, NY, USA[1]
Center for Climate Systems Research, Earth Institute, Columbia University, New York, NY, USA[2]
Agricultural & Biological Engineering Department, University of Florida, Gainesville, FL, USA[3]

Abstract. This paper describes the data set that was used to test the accuracy of twenty-nine crop models in simulating the effect of changing sowing dates and sowing densities on wheat productivity for a high-yielding environment in New Zealand. The data includes one winter wheat cultivar (Wakanui) grown during six consecutive years, from 2012-2013 to 2017-2018, at two farms located in Leeston and Wakanui in Canterbury, New Zealand. The simulations were carried out in the framework of the Agricultural Model Intercomparison and Improvement Project for wheat (AgMIP-Wheat). Data include local daily weather data, soil profile characteristics and initial conditions, crop measurements at maturity (grain, stem, chaff and leaf dry weight, ear number and grain number, grain unit dry weight), and at stem elongation and anthesis (total above ground dry biomass, leaf number per stem and leaf area index). Several in-season measurements of the normalized difference vegetation index (NDVI) and the fraction of intercepted photosynthetically active radiation (FIPAR) are also available. The crop model simulations include both daily in-season and end-of-season results from twenty-nine wheat models.

Introduction. To meet the growing demand for wheat under increasingly challenging environ-mental conditions, cropping systems must increase productionand one promising avenue is optimizing seeding dates and seeding rates (Bai and Tao 2017, Xin and Tao 2019, Sun et al. 2013, Padovan et al. 2020).Adapting sowing conditions requires an understanding of how crop growth, development and yield are affected by sowing dates and densities, including interactions between canopy development, radiation interceptionand biomass production.The original purpose of the experiments was to investigate if there is a yield advantage from earlier sowing of winter wheat and to determine the optimum plant population for the different sowing dates. Data were collected to quantify the effectsof sowing date and plant population on tiller number, leaf area, dry matter accumulation, lodging, head number and final harvest components. The field trials were conducted by the New Zealand Institute for Plant and Food Research and The Foundation for Arable Research at two farms located in the Canterbury Region of the South Island of New Zealand (Craigie et al., 2015). In this region, winter wheat is usually sown between early April to mid-May, with some farmers sowing in late March in recent years (Craigie et al., 2015). The objective of the trials was to test if sowing earlier (February or early March) and therefore increasing the canopy duration and the intercepted radiation, would increase grain yield.As part of the Agricultural Model Intercomparison and Improvement Project (AgMIP) (Rosenzweig et al. 2013: https://agmip.org/wheat/) twenty-nine process-based wheat crop models were provided with the data from these field experiments, with the goal of evaluating the accuracy of the models in simulating theeffect of varying seeding dates and densities on wheat growth and yield in a high yielding environment.

Nature Plants, vol. 10, pp.1081-1090, doi:10.1038/s41477-024-01739-3

Global nitrogen needs to improve wheat yield under climate change.

Martre, P., S. Dueri, **J.R. Guarin**[1,2,3], F. Ewert, H. Webber, D. Calderini, G. Molero, M. Reynolds, D. Miralles, G. Garcia, H. Brown, M. George, R. Craigie, J.-P. Cohan, J.-C. Deswarte, G. Slafer, F. Giunta, D. Cammarano, R. Ferrise, T. Gaiser, Y. Gao, Z. Hochman, G. Hoogenboom, L.A. Hunt, K.C. Kersebaum, C. Nendel, G. Padovan, **A.C. Ruane**[1], A.K. Srivastava, T. Stella, I. Supit, P. Thorburn, E. Wang, J. Wolf, C. Zhao, Z. Zhao, and S. Asseng, 2024

NASA Goddard Institute for Space Studies, New York, NY, USA[1]
Center for Climate Systems Research, Columbia University, New York, NY, USA[2]
Agricultural and Biological Engineering Department, University of Florida, Gainesville, FL, USA[3]

Abstract. Increasing global food demand will require more food production[1] without further exceeding the planetary boundaries[2] while simultaneously adapting to climate change[3]. We used an ensemble of wheat simulation models with improved sink and source traits from the highest-yielding wheat genotypes[4] to quantify potential yield gains and associated nitrogen requirements. This was explored for current and climate change scenarios across representative sites of major world wheat producing regions. The improved sink and source traits increased yield by 16% with current nitrogen fertilizer applications under both current climate and mid-century climate change scenarios. To achieve the full yield potential—a 52% increase in global average yield under a mid-century high warming climate scenario (RCP8.5), fertilizer use would need to increase fourfold over current use, which would unavoidably lead to higher environmental impacts from wheat production. Our results show the need to improve soil nitrogen availability and nitrogen use efficiency, along with yield potential.

Introduction. Wheat is the most important food crop in the world[5] but even more will be needed to satisfy the increasing demand associated with continuous population and economic growth[6]. However, wheat cropping contributions to biodiversity loss[7], surface and ground water pollution[8], and greenhouse gas emission through fertilizer and pesticide use and mechanization are important[9]. In fact, agriculture, with wheat cropping being a major component, has contributed to the transgression of several of the safe and equitable planetary boundaries in several world regions, mainly due to nitrogen (N) fertilizer use[2]. The recovery efficiency of N fertilizer applied to wheat crops varies greatly (20–90%) between regions and between farms within a region[10]. Globally, wheat crop takes up only 48% of applied N fertilizers in farmers' fields, with most of the remainder being lost to the environment[11]. Not surprisingly, N use efficiency (NUE, the amount of grain yield produced per amount of crop available N) is used as an indicator for monitoring and assessing progress in achieving the United Nations Sustainable Development Goals[12]. While food production needs to continue to increase, it must simultaneously reduce its negative footprint on the environment[13]. Climate change will further challenge both of these[3].

Plant breeding and biotechnology have seen substantial public and private investments to improve crop yield and increase the overall resilience of agriculture to climate change[14]. During the past 7 years, the International Wheat Yield Partnership (IWYP[15]) has contributed to this effort, with the goal to increase wheat yield potential by 50% in 20 years. Previous investments in CIMMYT and other breeding programmes around the world supported a linear increase in grain yield potential since the Green Revolution in the 1960s and 1970s, helping to quadruple global cereal production over the same period[16]. However, in many regions of the world, the translation of genetic yield progress into farmers' fields is increasingly constrained by large yield gaps, that is, the difference between currently achieved yields in farmers' fields and the yield that can be achieved by using the best adapted cultivar with the best current crop and land management practices[17].

Earth System Dynamics, vol. 16, issue no. 1, 317, doi:10.5194/esd-16-317-2025

Towards robust community assessments of the Earth's climate sensitivity.

Marvel, K.D.[1], and M. Webb, 2024

NASA Goddard Institute for Space Studies, New York, NY, USA[1]

Abstract. The eventual planetary warming in response to elevated atmospheric carbon dioxide concentrations is not precisely known. The uncertainty in climate sensitivity (S) primarily results from uncertainties in net physical climate feedback, usually denoted as λ. Multiple lines of evidence can constrain this feedback parameter: proxy-based and model evidence from past equilibrium climates; process-based understanding of the physics underlying changes; and recent observations of temperature change, top-of-the-atmosphere energy imbalance, and ocean heat content. However, despite recent advances in combining these lines of evidence, the estimated range of S remains large. Here, using a Bayesian framework, we discuss three sources of uncertainty – uncertainty in the evidence, structural uncertainty in the model used to interpret this evidence, and differing prior knowledge and/or beliefs – and show how these affect the conclusions we may draw from a single line of evidence. We then propose strategies to combine multiple lines of evidence. We end with three recommendations. First, we suggest that a Bayesian random-effects meta-analysis be used to estimate the evidence and its uncertainty from the published literature. Second, we advocate that the organizers of future assessments clearly specify an interpretive model or a group of candidate models and, in the latter case, use Bayesian model averaging to more heavily weight models that best fit the evidence. Third, we recommend that expert judgment be incorporated via solicitations of priors on model parameters.

Introduction. When radiative forcing (ΔF) is applied to the climate system, it induces a radiative imbalance (ΔN) at the top of the atmosphere and a response (ΔR) of the system itself. To first order, $\Delta R=\lambda\Delta T$, where ΔT is the change in global mean surface temperature. The feedback parameter (λ) thus measures the additional radiative flux density exported to space per unit of temperature change. On sufficiently long timescales, the climate comes into equilibrium ($\Delta N=0$), internal variability is negligible, and we can write a simple energy balance model (denoted M_0) for the climate system. M_0 is expressed as follows:

$$\Delta N = \Delta F + \lambda \Delta T. \quad (1)$$

In the special case where radiative forcing results from a doubling of atmospheric CO_2 relative to its preindustrial concentration of 280 ppm (, the resulting temperature change defines the equilibrium climate sensitivity (S), expressed as

$$S \equiv -\frac{F_{2\times CO_2}}{\lambda}. \quad (2)$$

S is often used as a metric to quantify expected warming in response to radiative forcing but has remained stubbornly uncertain, even as climate models have improved and become more sophisticated. A 2020 community assessment (Sherwood et al., 2020, hereafter referred to as S20) reduced this range using multiple lines of evidence, but the recent Intergovernmental Panel on Climate Change (IPCC) report (Forster, 2021) assessed only “medium confidence” in the upper bound. Is it possible to further narrow the estimated range of S, and can we increase our confidence in this result?

Atmospheric Chemistry and Physics, vol. 24, issue no. 18, pp. 10793-10814, doi:10.5194/acp-24-10793-2024

A thermal-driven graupel generation process to explain dry-season convective vigor over the Amazon.

Matsui, T.[1], D. Hernandez-Deckers, S. Giangrande, T. Biscaro, **A. Fridlind[2]**, and S. Braun[1], 2024

NASA Goddard Space Flight Center, Greenbelt, MD, USA[1]
NASA Goddard Institute for Space Studies, New York, NY, USA[2]

Abstract. Large-eddy simulations (LESs) are conducted for each day of the intensive observation periods (IOPs) of the Green Ocean Amazon (GoAmazon) field campaign to characterize the updrafts and microphysics within deep convective cores while contrasting those properties between Amazon wet and dry seasons. Mean Doppler velocity (V_{dop}) values simulated using LESs are compared with 2-year measurements from a radar wind profiler (RWP) as viewed by statistical composites separated according to wet- and dry-season conditions. In the observed RWP and simulated LES V_{dop} composites, we find more intense low-level updraft velocity, vigorous graupel generation, and intense surface rain during the dry periods compared with the wet periods. To investigate coupled updraft–microphysical processes further, single-day golden cases are selected from the wet and dry periods to conduct detailed cumulus thermal tracking analysis. Tracking analysis reveals that simulated dry-season environments generate more droplet-loaded low-level thermals than wet-season environments. This tendency correlates with seasonal contrasts in buoyancy and vertical moisture advection profiles in large-scale forcing. Employing a normalized time series of mean thermal microphysics, the simulated cumulus thermals appear to be the primary generator of cloud droplets. When subsequent thermals penetrate the ice crystal layer, droplets within the thermals interact with entrained ice crystals, which enhances riming in the thermals. This appears to be a production pathway of graupel/hail particles within simulated deep convective cores. In addition, less-diluted dry-case thermals tend to be elevated higher, and graupel grows further during sedimentation after spilling out from thermals. Therefore, greater concentrations of low-level moist thermals likely result in more graupel/hail production and associated dry-season convective vigor.

Introduction. Deep convection is a fundamental process of turbulence that drives the Earth's general circulation and regulates thermodynamic fields (Emanuel et al., 1994). Deep convection undergoes complex dynamical and microphysical processes throughout its life cycle; these processes appear as towering clouds visible from satellites in different parts of the world (Stephens et al., 2002). As a result, deep convection generates significant amounts of atmospheric latent heat, surface precipitation, and hydrometeors that reflect/absorb solar and infrared radiation, modifying atmospheric circulation and surface energy and mass fluxes (Hartmann, 2016). These complexities in deep convection and feedback processes pose significant challenges with respect to predicting weather and climate using numerical Earth system modeling across different scales (Grabowski and Petch, 2009; Sullivan and Voigt, 2021).

Characteristics of deep convection are unique in different seasons and geographic regimes affected by the local environment. One of the most straightforward yet most robust regime separation concepts is the land–ocean (L–O) contrast (Williams and Stanfill, 2002). Solar radiation increases the surface skin temperature over land more readily than over the ocean due to the smaller heat capacity of soils and vegetation compared with deep water bodies, thus producing stronger surface infrared flux and turbulent heat flux (Matsui and Mocko, 2014). This greater surface energy deepens planetary boundary layers that may trigger deeper convective clouds depending on the atmospheric profiles (Pielke, 2001). Overall, the continental environment tends to promote deeper convection with stronger, wider convective cores (Lucas et al., 1994; Wang et al., 2019), with suppressed warm-rain and enhanced cold-precipitation processes (Williams et al., 2005), often leading to unique drop size distribution characteristics and precipitation partitioning between convective and stratiform process outcomes in different geographic regions (e.g., Tokay and Short, 1996; Giangrande et al., 2012; Dolan et al., 2018).

Atmospheric Measurement Techniques, vol. 17, issue no. 19, pp. 5709-5729, doi:10.5194/amt-17-5709-2024

Pre-launch calibration and validation of the Airborne Hyper-Angular Rainbow Polarimeter (AirHARP) instrument.

McBride, B.A., J.V. Martins, J.D. Cieslak, R. Fernandez-Borda, A. Puthukuddy, X. Xu, N. Sienkiewicz, **B. Cairns**[1], and H.M.J. Barbosa, 2024

NASA Goddard Institute for Space Studies, New York, NY, USA[1]

Abstract. The Airborne Hyper-Angular Rainbow Polarimeter (AirHARP) is a new imaging polarimeter instrument capable of sampling a single Earth target from up to 120 viewing angles, in four spectral channels, and in three linear polarization states across a 114° field of view (FOV). AirHARP is telecentric in the image space and simultaneously images three linear polarization states with no moving parts. These two aspects of the design allow for a simple and efficient quantitative calibration. Using coefficients derived at the center of the lens and the detector flatfields, we can calibrate the entire AirHARP sensor in a variety of laboratory, field, and space environments. We show that this telecentric calibration technique yields a 1σ absolute uncertainty of 0.25 % in degree of linear polarization (DOLP) in the laboratory for all channels and for pixels around the optical axis. To validate across the FOV, we compare our multi-angle reflectance and polarization data with the Research Scanning Polarimeter (RSP) over targets sampled during the NASA Aerosol Characterization from Polarimeter and Lidar (ACEPOL) campaign. We use the error-normalized difference technique to estimate how well the instruments compare relative to their error models. We find that AirHARP and the RSP reasonably agree for reflectance and DOLP within 2 standard deviations of their mutual uncertainty at 550, 670, and 870 nm and over a limited set of ocean and desert scenes. This calibration technique makes the Hyper-Angular Rainbow Polarimeter (HARP) design attractive for new spaceborne climate missions: HARP CubeSat (2020–2022), HARP2 (2024–) on the NASA Plankton, Aerosol, Cloud, ocean Ecosystem (PACE), and beyond.

Introduction. Aerosols and their effect on clouds are one of our largest climate challenges. These particles are difficult to model and measure from satellites. Some aerosols are irregularly shaped, absorbing, and dimly reflecting, and others are spherical and efficient at scattering sunlight. They are transported across the globe from a variety of source regions, perturb the boundary layer, and interact with clouds in different ways, depending on their location in the atmosphere and composition. Aerosols can control how long clouds last, how bright they are, and when they will precipitate (Boucher et al., 2013). This complexity makes it difficult to estimate the impacts of clouds and aerosols on our climate system. However, this uncertainty drives innovation and instrument development. Satellite measurements with a range of spectral, angular, spatial, and polarized capabilities can improve how we measure these properties at global scales (NASA, 2018). Instruments that combine these features, called multi-angle polarimeters (MAPs), may make considerable enhancements to our climate record in this direction (Dubovik et al., 2019). They are highly compatible with current instruments, expand the information content possible in a single measurement, and can be designed to small and cost-effective form factors. Recent studies show that microphysical retrievals done on MAP data are highly attractive for future missions and improving our knowledge of microphysical properties (Mishchenko et al., 2004; Knobelspiesse et al., 2012; Stamnes et al., 2018; Remer et al., 2019). Of these, those that sample with less than or equal to 3 % uncertainty in absolute radiometric calibration and 0.5 % absolute uncertainty in the degree of linear polarization (DOLP) are optimal (NASA 2015, 2021).

Landscape and Urban Planning, vol. 247, 104997, doi:10.1016/j.landurbplan.2023.104997

Post-wildfire neighborhood change: Evidence from the 2018 Camp Fire.

McConnell, K., and **C.V. Braneon**[1,2], 2024

NASA Goddard Institute for Space Studies, New York, NY, USA
Columbia Climate School, CUNY Institute for Demographic Research (CIDR), Carbon Direct, USA[2]

Abstract. As the number of highly destructive wildfires grows, it is increasingly important to understand the long-term changes that occur to fire-affected places. Integrating approaches from social and biophysical science, we document two forms of neighborhood change following the 2018 Camp Fire in the United States, examining the more than 17,000 residential structures within the burn footprint. We found that mobile or motor homes, lower-value residences, and absentee owner residences had a significantly higher probability of being destroyed, providing evidence that housing stock filtering facilitated socially stratified patterns of physical damage. While the relationship between building value and destruction probability could be explained by measures of building density and distance to nearby roads, building type remained an independent predictor of structure loss that we could not fully explain by adding environmental covariates to our models. Using a geospatial machine learning technique, we then identified buildings that had been reconstructed within the burn footprint 20 months after the fire. We found that reconstructed buildings were more likely to have been owner-occupied prior to the fire and had higher average pre-fire property value, suggesting an emerging pattern of cost-burden gentrification. Our findings illustrate the importance of examining the built environment as a driver of socially uneven disaster impacts. Wildfire mitigation strategies are needed for mobile and motor home residents, renters, low-income residents, and dense neighborhoods.

Introduction. The impacts of wildfires on the built environment are growing increasingly acute. In the U.S., the number of housing units exposed to wildfire grew more than twofold in recent decades (Radeloff et al., 2023), and wildfire events in the western U.S. had a 160% higher structure loss rate between 2010 and 2020 compared to the previous decade (Higuera et al., 2023). Concerns over growing wildfire destruction are echoed internationally, with a recent United Nations report emphasizing “the rising threat of extraordinary landscape fires” across many continents (United Nations Environment Programme, 2022). As the number of highly destructive wildfires grows, it is increasingly important to understand the long-term changes that occur to fire-affected places.

Existing research on the dynamics of wildfire and the built environment has documented an extensive set of physical characteristics that influence building destruction outcomes (Alexandre et al., 2016, Gibbons et al., 2012, Syphard et al., 2012, Syphard et al., 2014, Syphard et al., 2017). A small but growing area of research has further described macro-level trends in post-fire building reconstruction (Alexandre et al., 2015, Kramer et al., 2021, Mockrin et al., 2015). We advance this area of study by integrating key concepts from social science research on neighborhood change - shifts in a place’s-built environment, population, or economy over time - to examine socioeconomic differentiation of building destruction and subsequent reconstruction (Zuk et al., 2015).

Our study examines two forms of physical neighborhood change that have not been investigated widely in the context of wildfire: housing stock filtering and cost-burden gentrification. We do so in a case study of the 2018 Camp Fire, which destroyed nearly 19,000 structures in northern California and remains one of the most destructive wildfires in U.S. history. In our study, we test whether socioeconomic-related characteristics of buildings exposed to the fire - building type, building value, and building tenure - were associated with heightened or reduced probability of destruction and subsequent reconstruction. Through this fine-grained examination of the built environment immediately following the Camp Fire and again, 20 months after the event, we illustrate how wildfire can facilitate neighborhood change at different periods of time through a restructuring of the physical landscape.

Geophysical Research Letters, vol. 52, issue no. 2, e2024GL112368, doi:10.1029/2024GL112368

The cloud radiative response to surface warming weakens hydrological sensitivity.

McGraw, Z.[1,2], L.M. Polvani, B. Gasparini, E.K. Van De Koot, and A. Voigt, 2024

NASA Goddard Institute for Space Studies, New York, NY, USA[1]
Department of Applied Physics and Applied Mathematics, Columbia University, New York, NY, USA[2]

Abstract. Precipitation is expected to increase in a warmer global climate, yet how sensitive precipitation is to warming that depends on poorly constrained cloud radiative processes. Clouds respond to surface warming in ways that alter the atmosphere's ability to radiatively cool and hence form precipitation. Here we examine the links between cloud responses to warming, atmospheric radiative fluxes, and hydrological sensitivity in AMIP6 simulations. The clearest impacts come from high clouds, which reduce atmospheric radiative cooling as they rise in altitude in response to surface warming. Using cloud locking, we demonstrate that high cloud radiative changes weaken Earth's hydrological sensitivity to surface warming. The total impact of cloud radiative effects on hydrological sensitivity is halved by interactions between cloud and clear-sky radiative effects yet is sufficiently large to be a major source of uncertainty in hydrological sensitivity.

Introduction. Cloud responses to warming are one of the main uncertainties for projections of future climate (Sherwood et al., 2020; Zelinka et al., 2020). While extensive research has examined how cloud responses alter the extent of global greenhouse gas warming, the question of how these cloud responses affect future precipitation remains largely unexplored. Surface temperature is governed by Earth's top-of-atmosphere (TOA) radiative balance, while precipitation is more directly controlled by radiative fluxes into and out of the atmosphere, from Earth's surface as well as space. In the atmospheric (ATM) energy budget, radiative cooling drives the cycling of latent heat into the atmosphere by condensation, with surface precipitation rates reflecting the net release of latent heat. As clouds are a major term in both the TOA and ATM energy budgets, some of the cloud radiative responses to surface warming that amplify or dampen this warming (i.e., *cloud feedbacks*) will also affect how strongly precipitation responds to surface warming (*hydrological sensitivity* or HS). Here we use recently available methods to establish how cloud radiative processes influence the atmosphere's energetic and hydrological responses.

Over spatial scales of several thousand kilometers or more, any changes in latent heat from precipitation ($L\Delta P$, where L is the latent heat of condensation and P is surface precipitation averaged over months or years) must be balanced by changes in atmospheric radiative cooling ($-\Delta R_{ATM}$) plus changes in surface-to-atmosphere sensible heat flux (ΔSH) (Muller & O'Gorman, 2011; O'Gorman et al., 2012). The atmospheric energy budget is hence a useful framework for understanding precipitation change, despite not directly revealing cause-and-effect relationships on its own. Atmospheric radiative flux changes can be decomposed into a clear-sky component that is calculated by ignoring clouds in calculations of radiative energy fluxes (ΔR_{clear}) and cloud radiative effects (ΔCRE), which are calculated as the difference between the full and clear-sky fluxes. Defining all positive fluxes to add energy into the atmosphere, this relationship can be written as:

$$L\Delta P = -\Delta R_{ATM} - \Delta SH = -\Delta CRE - \Delta R_{clear} - \Delta SH \quad (1)$$

The clear-sky radiative change is the net result of tropospheric temperature and water vapor concentration both increasing as the surface warms. For warming within several degrees of present-day global climate, clear-sky radiative responses overall increase both atmospheric radiative cooling and precipitation (Jeevanjee & Romps, 2018; Liu et al., 2024). Despite this clear-sky basis, much of the intermodel spread in HS has been shown to be associated with cloud radiative responses (Previdi, 2010).

Journal of Climate, vol. 37, issue no. 4, pp. 1449-1464, doi:10.1175/JCLI-D-23-0116.1

Severe global cooling after volcanic super-eruptions? The answer hinges on unknown aerosol size.

McGraw, Z.[1,2], **K. DallaSanta**[1,2], L. Polvani, **K. Tsigaridis**[1,3], **C. Orbe**[1,2], and **S.E. Bauer**[1], 2024

NASA Goddard Institute for Space Studies, New York, NY, USA[1]
Department of Applied Physics and Applied Mathematics, Columbia University, New York, NY, USA[2]
Center for Climate Systems Research, Columbia University, New York, NY, USA[3]

Abstract. Volcanic super-eruptions have been theorized to cause severe global cooling, with the 74 kya Toba eruption purported to have driven humanity to near extinction. However, this eruption left little physical evidence of its severity and models diverge greatly on the magnitude of post-eruption cooling. A key factor controlling the super-eruption climate response is the size of volcanic sulfate aerosol, a quantity that left no physical record and is poorly constrained by models. Here we show that this knowledge gap severely limits confidence in model-based estimates of super-volcanic cooling, and accounts for much of the disagreement among prior studies. By simulating super-eruptions over a range of aerosol sizes, we obtain global mean responses varying from extreme cooling all the way to the previously unexplored scenario of widespread warming. We also use an interactive aerosol model to evaluate the scaling between injected sulfur mass and aerosol size. Combining our model results with the available paleoclimate constraints applicable to large eruptions, we estimate that global volcanic cooling is unlikely to exceed 1.5°C no matter how massive the stratospheric injection. Super-eruptions, we conclude, may be incapable of altering global temperatures substantially more than the largest Common Era eruptions. This lack of exceptional cooling could explain why no single super-eruption event has resulted in firm evidence of widespread catastrophe for humans or ecosystems.

Introduction. Volcanic impacts on climate have been implicated in the Roman Republic's decline and political upheavals in ancient Egypt (McConnell et al. 2020; Manning et al. 2017), among other crises Yet seen from longer time scales, the largest eruptions of recent millennia could be considered modest. Compared to the largest Common Era eruptions, super-eruptions inject into the stratosphere many times more sulfur that forms sunlight-blocking aerosol particles. This has been theorized to cause catastrophic consequences on climate (Rampino and Self 1992; Robock et al. 2009) and human populations (Ambrose 1998; Rampino and Ambrose 2000). However, knowledge of these eruptions and their impacts is limited, as no super-eruption has occurred since the one at Lake Taupo in New Zealand 25 400 years ago (Vandergoes et al. 2013). Here we use models and proxies to constrain super-eruption temperature response as much as is possible with this limited knowledge.

The most studied and debated super-eruption occurred at the site of Lake Toba in Indonesia ~74 000 years ago. This Youngest Toba eruption has been linked to a shift in glacial cycles (Rampino and Self 1992) and the potential near-extinction of humanity, possibly influencing human development (Ambrose 1998). For such extreme impacts, the Toba eruption would need to have caused global cooling many times stronger than the ~0.3°C impact of the much smaller but relatively well-observed 1991 eruption of Mt. Pinatubo (Zanchettin et al. 2022). This might be expected given Toba's injection mass of 70–6600 Tg sulfur dioxide (SO_2) gas into the stratosphere (Black et al. 2021) compared to Pinatubo's 18.4 ± 4.5 Tg SO_2 (Guo et al. 2004). Stratospheric SO_2 undergoes chemical reactions and condenses into liquid aerosol droplets that are primarily composed of sulfuric acid (hereafter referred to as s*ulfate aerosol*, *sulfate particles*, or simply *aerosol*). An extreme injection of stratospheric sulfur is expected to form a dense layer of sulfate that reflects considerable sunlight. However, efforts to identify a strong temperature change contemporaneous with the Toba eruption have proved elusive. Notably, attempts to link fluctuations in ice core temperature proxies to Toba's occurrence have been inconsistent with an attribution to volcanic cooling (Svensson et al. 2013; Crick et al. 2021). Although a millennium-scale cooling was identified in ice core $\delta^{18}O$ records in close temporal proximity to the eruption (Zielinski et al. 1996), this was later found to be incompatible with simulations showing Toba's impacts to end within a few decades of the eruption (Robock et al. 2009).

Geophysical Research Letters, vol. 51, issue no. 13, e2023GL107930, doi:10.1029/2023GL107930

How volcanic aerosols globally inhibit precipitation.

McGraw, Z.[1,2], and L.M. Polvani, 2024

NASA Goddard Institute for Space Studies, New York, NY, USA[1]
Department of Applied Physics and Applied Mathematics, Columbia University, New York, NY, USA[2]

Abstract. Volcanic aerosols reduce global mean precipitation in the years after major eruptions, yet the mechanisms that produce this response have not been rigorously identified. Volcanic aerosols alter the atmosphere's energy balance, with precipitation changes being one pathway by which the atmosphere acts to return toward equilibrium. By examining the atmosphere's energy budget in climate model simulations using radiative kernels, we explain the global precipitation reduction as largely a consequence of Earth's surface cooling in response to volcanic aerosols reflecting incoming sunlight. These aerosols also directly add energy to the atmosphere by absorbing outgoing longwave radiation, which is a major cause of precipitation decline in the first post-eruption year. We additionally identify factors limiting the post-eruption precipitation decline and provide evidence that our results are robust across climate models.

Introduction. Stratospheric aerosols from volcanic eruptions have been linked to widespread disruptions in precipitation observed during the 20th century, most notably a decline in global mean precipitation following the 1991 eruption of Mt. Pinatubo (Adler et al., 2018; Gillett et al., 2004). Global impacts of volcanic eruptions are important to evaluate given potential influences on societies and ecosystems and implications for stratospheric aerosol geoengineering (Proctor et al., 2018; Trenberth & Dai, 2007). While climate models indicate that volcanic aerosols reduce global mean precipitation in the years following eruptions (Iles & Hegerl, 2014; Robock & Liu, 1994), little has been done to understand the underlying mechanisms. This contrasts with efforts to understand regional post-eruption precipitation changes associated with monsoons (Liu et al., 2016; Zhuo et al., 2020) and the intertropical convergence zone (Colose et al., 2016). In this study we identify how precipitation is globally reduced as a consequence of volcanic aerosol presence in the stratosphere.

The atmospheric energy budget is essential for elucidating the mechanisms by which volcanic aerosols alter precipitation, as precipitation reflects the amount of latent heat cycled into the atmosphere through condensation. A perturbation to the climate system initiates a multitude of changes to the atmosphere's energy budget, including radiative, sensible, and latent energy responses. The atmospheric energy budget then tends toward a new equilibrium, with the sum of all energy flux changes close to zero. The precipitation response may be represented as equal to the sum of balancing terms (O'Gorman et al., 2012):

$$L\Delta P \approx \underbrace{-\Delta R_{ATM} - \Delta SH}_{\Delta Q} - \Delta H \qquad (1)$$

Here ΔP is the precipitation anomaly and L is the latent heat of condensation constant. The atmospheric radiative flux anomaly $\Delta R_{ATM} = \Delta R_{TOA} - \Delta R_{SFC}$, is the difference in radiative flux anomalies between the top-of-atmosphere and surface, and ΔSH is surface-to-atmosphere sensible heat flux anomaly. ΔR_{ATM} includes the immediate influence of aerosol-radiation interactions on the net energy flux into the atmosphere (hereafter $\Delta R_{ATM,IRF}$, where IRF is instantaneous radiative forcing, or the atmospheric *aerosol forcing* for short), plus radiative flux responses as the Earth-climate system adjusts to the aerosol presence. ΔH is horizontal transport of dry static energy, which includes circulation responses. ΔH can be neglected at length scales of at least several thousand kilometers (Dagan & Stier, 2020; O'Gorman et al., 2012), and since global mean precipitation is our focus we mostly do so here. The equality in Equation 1 is approximate (≈) because the atmosphere takes time to fully adjust to the stratospheric aerosol layer, which continuously evolves. To simplify our analysis, we define $\Delta Q = -\Delta R_{ATM} - \Delta SH$, the diabatic cooling excluding latent heat (or *diabatic cooling* for short), as in O'Gorman et al. (2012).

Weather and Climate Dynamics, vol. 5, issue no. 1, pp. 251-261, doi:10.5194/wcd-5-251-2024

Replicating the Hadley Cell and subtropical jet disconnect in idealized atmospheric models.

Menzel, M.E.[1,2], D. Waugh, Z. Wu, and T. Reichler, 2024

NASA Goddard Institute for Space Studies, New York, NY, USA[1]
Department of Earth and Planetary Sciences, The Johns Hopkins University, Baltimore, MD, USA[2]

Abstract. Recent work has shown that variability in the subtropical jet's (STJ) latitude, ϕSTJ, is not coupled to that of the Hadley cell (HC) edge, ϕHC, but the robustness of this disconnect has not been examined in detail. Here, we use meteorological reanalysis products, comprehensive climate models, and an idealized atmospheric model to determine the necessary processes for a disconnect between ϕHC and ϕSTJ in the Northern Hemisphere's December–January–February season. We find that a decoupling can occur in a dry general circulation model, indicating that large-scale dynamical processes are sufficient to reproduce the metrics' relationship. It is therefore not reliant on explicit variability in the zonal structure, convection, or radiation. Rather, the disconnect requires a sufficiently realistic climatological basic state. Further, we confirm that the robust disconnect between ϕSTJ and ϕHC across the model hierarchy reveals their differing sensitivities to midlatitude eddy momentum fluxes; ϕHC is consistently coupled to the latitude of maximum eddy momentum flux, but ϕSTJ is not.

Introduction. There is considerable interest in detecting and predicting tropical expansion as a result of increasing greenhouse gases (Seidel et al., 2008; Birner et al., 2014). Early studies examining tropical expansion used various metrics to define the edge of the tropics, including the poleward extent of the Hadley cell (HC) as well as the subtropical jet's (STJ) location. However, studies presented contradicting conclusions based on their choice of metrics (Seidel et al., 2008; Davis and Rosenlof, 2012; Davis and Birner, 2013; Birner et al., 2014). Subsequent comparisons then exposed a disconnect between upper-tropospheric and lower-tropospheric metrics (Solomon et al., 2016; Waugh et al., 2018). Davis and Birner (2017) similarly categorize the upper- and lower-tropospheric metrics as “zonal-circulation” and “meridional-circulation” metrics, respectively. One specific result revealed there is no interannual correlation between the STJ latitude and HC edge in reanalysis products or coupled model output (Waugh et al., 2018; Menzel et al., 2019) and they have distinct responses to increased CO_2 (Davis and Birner, 2017; Menzel et al., 2019).

Historically, large-scale atmospheric circulation in the lower latitudes has been described by axisymmetric theory. In particular, it is dominated by a thermally direct meridional circulation known as the HC (Lorenz, 1967), where the flow is angular momentum conserving and the circulation's poleward extent is determined by energetic constraints (Held and Hou, 1980; Lindzen and Hou, 1988). Additionally, the STJ is attributed to the HC's poleward advection of angular momentum. As the HC's upper branch circulates poleward, the zonal-mean zonal wind must increase to maintain angular momentum conservation and accommodate the flow's decrease in distance to Earth's axis of rotation. This has led to a persistent assumption that the STJ is co-located and co-varies with the edge of the HC.

Although useful to conceptualize zonal-mean flow, axisymmetric theory is limited; the presence of eddies at higher latitudes resulting from non-axisymmetric processes proves a strong influence on HC dynamics (Schneider, 2006). Rather than invoking energetic constraints, the HC's meridional extent is instead determined by baroclinic instabilities (Held, 2000) and can be described by a critical latitude whereby the angular-momentum-conserving flow can no longer remain stable (Walker and Schneider, 2006; Korty and Schneider, 2008). In this vein, HC edge variability is directly related to that of static stability and midlatitude eddies (Davis et al., 2016).

The Planetary Science Journal, vol. 5, 228, doi:10.3847/PSJ/ad769d

Detectability simulations of a NIR surface biosignature on Proxima Centauri b with future space observatories.

Metz, C.O., **N.Y. Kiang**[1], G.L. Villanueva[2], M.N. Parenteau[3], and V. Kofman[2], 2024

NASA Goddard Institute for Space Studies, New York, NY, USA[1]
NASA Goddard Space Flight Center, Greenbelt, MD, USA[2]
NASA Ames Research Center, Moffett Field, CA, USA[3]

Abstract. Telescope missions are currently being designed that will make direct imaging of habitable exoplanets possible in the near future, and studies are needed to quantify the detectability of biosignature features in the planet's reflectance spectrum. We simulated the detectability of a near-infrared-absorbing surface biosignature feature with simulated observations of the nearby exoplanet Proxima Centauri b. We modeled a biosignature spectral feature with a reflectance spectrum based on an anoxygenic photosynthetic bacterial species that has strong absorption at 1 μm, which could make it well suited for life on an M-dwarf-hosted planet. We modeled the distribution of this organism across the planet's surface based on climate states from a 3D general circulation model (GCM) that were Archean- and Proterozoic-like exo-Earth analogs. We included the GCM states' prognostically simulated water clouds and added organic haze into the Archean-like atmospheres. We simulated observations of these Proxima Centauri b scenarios with the LUVOIR-A and B telescope concepts, with LUVOIR-B serving as a proxy to the planned Habitable Worlds Observatory. We calculated the integration times necessary to detect the biosignature and found that it would be detectable on Proxima Centauri b if the organism is moderately abundant (greater than a 1%–4% global surface area coverage), as long as the atmosphere is transmitting in the wavelength range under consideration. Small amounts of methane, clouds, and haze do not greatly impede detectability. We found preliminary evidence that such a biosignature would be detectable on exoplanets within 15 pc, but further investigations are needed to corroborate this.

Introduction. The search for life elsewhere in the Universe is an ancient question but still a relatively young discipline of science. Identifying a sign of life on another planet (known as a "biosignature") is an extremely difficult task for two reasons: (1) the necessary astronomical observations require very high levels of precision, and (2) it is unclear what exactly we are looking for. Life on Earth is only one example of life, and the biochemistry on other planets may be quite different from what we are familiar with. The focus of the present work is item (1), the astronomical technique and technology required for such detections. Much of the work in that field to date has focused on atmospheric biosignatures (e.g., S. D. Domagal-Goldman et al. 2011; J. H. Checlair et al. 2021), primarily because exoplanet atmospheres are more easily detectable than surfaces with the current generation of instruments and techniques (for one, because of refraction when observed in the transit geometry; see A. García Muñoz et al. 2012). Some previous studies have simulated reflectance spectra of exoplanets with potential surface biosignatures (e.g., E. Sanromá et al. 2014; E. W. Schwieterman et al. 2015), but many of them have not simulated noise in the spectra, which makes it difficult to constrain the integration time required to detect these biosignatures.

To observe a spectral biosignature, one needs two things: (1) a recognizable feature in the spectrum that is indicative of the presence of life and (2) a sufficiently high signal-to-noise ratio (SNR) in that wavelength region of the spectrum. A typical requirement for item (2) is that the signal be at least 5 times higher than the standard deviation of the noise. Hereafter, satisfying item (1) will be referred to as "interpretability," and satisfying item (2) will be referred to as "detectability." This work aims to calculate the integration times required to detect surface biosignatures by simulating spectral observations with future space observatories. It is essential to characterize integration times in advance of observations so that one can know whether or not it is possible to detect the desired spectral signatures originating from the target with a given telescope. Telescope time is a rare commodity, and many thousands of hours would likely never be allocated to observing a single target.

Journal of Climate, vol. 37, issue no. 20, pp. 5355-5372, doi:10.1175/JCLI-D-23-0758.1

Southern Hemisphere winter storm tracks respond differently to low and high CO_2 forcings.

Mitevski, I.[2], R. Chemke, **C. Orbe**[1,2], and L.M. Polvani[2], 2024

NASA Goddard Institute for Space Studies, New York, NY, USA[1]
Department of Applied Physics and Applied Mathematics, Columbia University, New York, NY, USA[2]

Abstract. In the Southern Hemisphere, Earth system models project an intensification of winter storm tracks by the end of the twenty-first century. Previous studies using idealized models showed that storm track intensity saturates with increasing temperatures, suggesting that the intensification of the winter storm tracks might not continue further with increasing greenhouse gases. Here, we examine the response of midlatitude winter storm tracks in the Southern Hemisphere to increasing CO_2 from two to eight times preindustrial concentrations in more realistic Earth system models. We find that at high CO_2 levels (beyond $4\times CO_2$), winter storm tracks no longer exhibit an intensification across the extratropics. Instead, they shift poleward, weakening the storm tracks at lower midlatitudes and strengthening at higher midlatitudes. By analyzing the eddy kinetic energy (EKE) budget, the nonlinear storm-track response to an increase in CO_2 levels in the lower midlatitudes is found to stem from a scale-dependent conversion of eddy available potential energy to EKE. Specifically, in the lower midlatitudes, this energy conversion acts to oppositely change the EKE of long and short scales at low CO_2 levels, but at high CO_2 levels, it mostly reduces the EKE of shorter scales, resulting in a poleward shift of the storms. Furthermore, we identify a "tug of war" between the upper and lower temperature changes as the primary driver of the nonlinear-scale-dependent EKE response in the lower midlatitudes. Our results suggest that in the highest emission scenarios beyond the twenty-first century, the storm tracks' response may differ in magnitude and latitudinal distribution from projected changes by 2100.

Introduction. Extratropical storm tracks transport heat, momentum, and moisture, thereby directly influencing Earth's hydrological cycle (Harvey et al. 2014; Schwierz et al. 2010). These storm tracks play a significant role in shaping regional weather and climate by impacting the variability of precipitation, temperature, and winds in extratropical regions (Pfahl and Wernli 2012; Yau and Chang 2020; Chang et al. 2022). Any future changes in storm tracks resulting from increased greenhouse gas (GHG) emissions will have consequential effects on regional climate. Therefore, understanding how storm tracks will change in a warmer world becomes a critically important question to address.

The extratropical storm tracks consist of transient eddies that extract their energy from the mean available potential energy (MAPE) via the process of baroclinic instability (Lorenz 1955; O'Gorman 2010). Since MAPE depends on both the horizontal (meridional) and vertical (static stability) temperature gradients (Lorenz 1955; Peixóto and Oort 1974), changes in the temperature gradients in a warmer climate will directly impact the storm tracks. For example, in a warmer climate, the upper tropical troposphere is projected to warm more than the upper polar troposphere, leading to a stronger upper meridional temperature gradient and increased static stability at lower midlatitudes. Conversely, near the surface, the polar regions are expected to warm more than the tropics, decreasing the lower meridional temperature gradient and static stability at higher midlatitudes (Butler et al. 2010). These opposing effects are expected to differently affect the response of the storms to anthropogenic emissions.

Numerous Earth system model studies have extensively explored the future response of storm tracks to increased GHG concentrations (Yin 2005; Chang et al. 2012; Zappa et al. 2013; Harvey et al. 2014; Lehmann et al. 2014; Harvey et al. 2020; Priestley and Catto 2022). In the Northern Hemisphere, these studies suggest a weakening of summer (JJA) storm tracks, while winter (DJF) storm tracks are expected to strengthen by the end of the twenty-first century only over the North Atlantic/western Europe. In the Southern Hemisphere, summer (DJF) storm tracks are projected to shift poleward, while winter (JJA) storm tracks are anticipated to intensify.

International Food Agribusiness Management Review, vol. 27, issue no. 3, pp. 441-462, doi:10.22434/ifamr1028

The economics of farming expansion in the Brazilian Cerrado under possible effects of climate change.

Monaco, H., C. Ortiz, L. Caetano, C. Müller, and **J. Jägermeyr**[1,2], 2024

NASA Goddard Institute for Space Studies, New York, NY, USA[1]
Center for Climate Systems Research, Columbia University, New York, NY, USA[2]

Abstract. This analysis assesses the financial viability of legally investing in native Cerrado vegetation deforestation for crop production, considering climate change. The study uses data from twelve different crop models based on three different climate models to predict potential future crop yields in cleared land for growing soy and maize. The outcomes show that in many micro-regions, investments in clearing land for crop production would destroy economic value, that is, generate a negative net present value because of low/negative and volatile cashflows driven primarily by future yields as affected by climate. Our analysis was carried out based on present agricultural practices and technology. As climate changes, farmers may adapt their practices, which can lead to more resilient and productive crops, or grow different crops, which could provide better returns on investment in clearing land than the ones resulting from our analysis. Despite various uncertainties, farmers, policy makers and financial institutions should be aware of the climatic and financial risks associated with land clearing in Brazil, mainly in micro-regions in which all scenarios resulted in negative outcomes in the investment analysis.

Introduction. Brazil's Central and Northwestern regions tend to feature flatland and large tables with deep soils, suitable to agriculture with proper fertility adjustments (Silva *et al.*, 2021), on which the native vegetation is known as Cerrado, hence the region's name: the "Cerrados" (Ferraz-Almeida *et al.*, 2021).

The Cerrados in Brazil have an important environmental value. Its deforestation is already bringing several unbalances, among which extreme heat affecting landscape, populations, and crops. A recent study concluded that the value of the various ecosystem services, including water and climate regulation, is estimated at US$5310/ha in present value in 2005's prices, at 10% cost of capital (Flach *et al.*, 2021).

Most of Brazil's agricultural and cattle production expansion have happened on the Cerrado Biome during the past four decades (Rada, 2013). This expansion has accelerated, given the profitability obtained by farmers, and (Daldegan *et al.*, 2019) shows that soy production increased by 9.6 million ha or 128% between 2000 and 2017. Approximately 38% of soy harvested in the 2016–2017 cycle came from land that had once been covered by native vegetation in 1999. The MATOPIBA subregion has been the most affected by this trend.

Although most of the recent expansion has happened on degraded, overgrazed pastureland, there is still a strong activity of converting land under native vegetation into cropland (Daldegan *et al.*, 2019), partly into pastures, given the expansion of agriculture over pastures (Picoli *at al.*, 2020).

Of particular concern are native vegetation plots within crop farms that exceed the minimum conservation (set-aside) requirement by the Brazilian Forest Code that could be legally cleared, of which up to 2.2 million ha are projected to be converted by 2030 (Soterroni *et al.*, 2019).

Commodity production farmers must constantly pursue economies of scale and gains of productivity to remain competitive, as real commodity prices tend to decline over time in high competition markets. This is known as "Cochrane's agricultural treadmill" (Howard, 2009).

Grain and oilseeds demand has been growing following the population growth (Nepstad *et al.*, 2014) and with rising income pulling the demand for animal protein, and demand for feed as consequence (Umberger, 2015). This has sustained farmers' profitability, which has led to expansion in the last agricultural frontiers of the Cerrados.

Natural Hazards and Earth System Sciences, vol. 24, issue no. 2, pp. 445-464, doi:10.5194/nhess-24-445-2024

Improving the fire weather index system for peatlands using peat-specific hydrological input data.

Mortelmans, J., A. Felsberg, G.J.M. De Lannoy, S. Veraverbeke, **R.D. Field**[1,2], N. Andela, and M. Bechtold, 2024

NASA Goddard Institute for Space Studies, New York, NY, USA[1]
Department of Applied Physics and Applied Mathematics, Columbia University, New York, NY, USA[2]

Abstract. The Canadian Fire Weather Index (FWI) system, even though originally developed and calibrated for an upland Jack pine forest, is used globally to estimate fire danger for any fire environment. However, for some environments, such as peatlands, the applicability of the FWI in its current form, is often questioned. In this study, we replaced the original moisture codes of the FWI with hydrological estimates resulting from the assimilation of satellite-based L-band passive microwave observations into a peatland-specific land surface model. In a conservative approach that maintains the integrity of the original FWI structure, the distributions of the hydrological estimates were first matched to those of the corresponding original moisture codes before replacement. The resulting adapted FWI, hereafter called FWI_{peat}, was evaluated using satellite-based information on fire presence over boreal peatlands from 2010 through 2018. Adapting the FWI with model- and satellite-based hydrological information was found to be beneficial in estimating fire danger, especially when replacing the deeper moisture codes of the FWI. For late-season fires, further adaptations of the fine fuel moisture code show even more improvement due to the fact that late-season fires are more hydrologically driven. The proposed FWI_{peat} should enable improved monitoring of fire risk in boreal peatlands.

Introduction. Even though boreal peatlands cover only ∼ 2 %–3 % (4 ×106 km2) of the world's land cover (Xu et al., 2018), it is estimated that they store 600 Gt of carbon (Yu et al., 2010), 25 % of the global soil carbon stock, or twice what is stored in the world's forests (Pan et al., 2011). Under wet conditions, peatlands act as a sink for atmospheric carbon (Gallego-Sala et al., 2018), but due to natural (e.g., drought or lightning-ignited wildfires) and anthropogenic (e.g., drainage for agriculture and forestry) disturbances, this sink can turn into a source (Davies et al., 2013; Granath et al., 2016; Loisel et al., 2021; Turetsky et al., 2002, 2004, 2010; Wieder et al., 2009; Wilkinson et al., 2018). Since peatlands are often considered to be saturated most of the year, they are excluded from many wildfire models (Thompson et al., 2019). On the other hand, the effect of wildfires on peatland carbon stocks has been extensively studied (Gray et al., 2021; Kettridge et al., 2019; Morison et al., 2021; Nelson et al., 2021; Turetsky et al., 2015; Wieder et al., 2009). Furthermore, the link of peat moisture to peat fire probability has received considerable attention (Lukenbach et al., 2015; Thompson et al., 2019; Wilkinson et al., 2018, 2020). With climate change, boreal peatland fires are expected to become more frequent (Turetsky et al., 2015; Wotton et al., 2010) because the boreal region is expected to experience more severe fire weather (hot and dry conditions) by the end of this century (Flannigan et al., 2016; Wang et al., 2014) and the main source of boreal ignitions and burned area, i.e., lightning, is expected to increase (Chen et al., 2021; Flannigan et al., 2013; Krawchuk et al., 2009; Veraverbeke et al., 2017).

Whereas many studies primarily focus on the impact of peat fires (Enayetullah et al., 2022; Gray et al., 2021; Kettridge et al., 2019; Morison et al., 2021; Nelson et al., 2021; Turetsky et al., 2015; Wieder et al., 2009), relatively little attention has been given to improving available approaches of monitoring fire risk originating from drought. The Canadian Forest Fire Weather Index (FWI) system (Van Wagner, 1987) is one of the most well-known systems to rate fire danger based on potential fire spread, fuel consumption, and fire intensity. It relies solely on weather observations such as temperature, relative humidity, precipitation, and wind speed.

Atmospheric Measurement Techniques, vol. 17, issue no. 5, pp. 1577-1597, doi:10.5194/amt-17-1577-2024

Enhancing consistency of microphysical properties of precipitation across the melting layer in the Dual-frequency Precipitation Radar data.

Mroz, K., A. Battaglia, and **A.M. Fridlind**[1], 2024

NASA Goddard Institute for Space Studies, New York, NY, USA[1]

Abstract. Stratiform rain and the overlying ice play crucial roles in Earth's climate system. From a microphysics standpoint, water mass flux primarily depends on two variables: particles' concentration and their mass. The Dual-frequency Precipitation Radar (DPR) on the Global Precipitation Measurement mission core satellite is a spaceborne instrument capable of estimating these two quantities through dual-wavelength measurements. In this study, we evaluate bulk statistics on the ice particle properties derived from dual-wavelength radar data in relation to the properties of rain underneath. Specifically, we focus on DPR observations over stratiform precipitation, characterized by columns exhibiting a prominent bright band, where the melting layer can be easily detected.

Our analysis reveals a large increase in the retrieved mass flux as we transition from the ice to the rain phase in the official DPR product. This observation is in disagreement with our expectation that mass flux should remain relatively stable across the bright band in cold-rain conditions. To address these discrepancies, we propose an alternative retrieval algorithm that ensures a gradual transition of D_m (mean mass-weighted particle melted-equivalent diameter) and the precipitation rate across the melting zone. This approach also helps in estimating bulk ice density above the melting level. These findings demonstrate that DPR observations can not only quantify ice particle content and their size above stratiform rain regions but also estimate bulk density, provided uniform conditions that minimize uncertainties related to partial beam filling.

Introduction. As part of the Global Precipitation Measurement (GPM; Hou et al., 2014) mission, in February 2014, US and Japanese national agencies jointly launched the spaceborne Dual-frequency Precipitation Radar (DPR). The DPR measures at the Ku- (13.6 GHz) and Ka-bands (35.5 GHz), improving on the single-frequency Ku-band (13.8 GHz) radar that was launched in 1997 with the Tropical Rainfall Measuring Mission (TRMM; Kummerow et al., 1998). Not only does GPM have an extended latitude range of 65° S–65° N, compared to TRMM's 36° S–36° N, but it has also improved the system sensitivity. In fact, the Ku-band precipitation radar is now able to detect a minimum radar reflectivity of 15.5 dBZ (Liao and Meneghini, 2022), whereas during the TRMM era, it was 18 dBZ (Heymsfield et al., 2000). Thanks to extended latitudinal coverage, the DPR has shown that the world's largest storms occur primarily over mid- and high-latitude oceans in both hemispheres (Liu and Zipser, 2015) and that the areal coverage of storms overshooting the tropopause over central North America and Argentina rivals that over the tropics (Liu and Liu, 2016).

Here we investigate use of DPR data for the retrieval of the size and the precipitation rate of ice crystals overlying cold rain. Widespread precipitation associated with convection is a primary source of stratiform rain, especially in the tropics. Observational and modeling studies have focused on this topic for decades (e.g., Webster and Stephens, 1980; Chen and Cotton, 1988). However, the climatological significance of fundamentally differing diabatic heating profiles corresponding to regions of convective and stratiform rain was fully realized only about 20 years ago (Houze, 1997). Since then, TRMM measurements have enabled us to assess the frequency and extent of stratiform rain in tropical and subtropical regions. This classification has unveiled the existence of more extensive stratiform rain regions over the ocean, even though the embedded convection is notably more intense over land (Houze et al., 2015; Schumacher and Funk, 2023). Today, identification of the precipitation type as convective, stratiform, or neither is a leading element of DPR retrievals (Awaka et al., 2021).

Earth's Future, vol. 12, issue no. 3, e2023EF003773, doi:10.1029/2023EF003773

Substantial differences in crop yield sensitivities between models call for functionality-based model evaluation.

Müller, C., **J. Jägermeyr**[1,2,3], J.A. Franke, **A.C. Ruane**[1], J. Balkovic, P. Ciais, M. Dury, P. Falloon, C. Folberth, T. Hank, M. Hoffmannn, C. Izaurralde, I. Jacquemin, N. Khabarov, W. Liu, S. Olin, T.A.M. Pugh, X. Wang, K. Williams, F. Zabel, and J.W. Elliott, 2024

NASA Goddard Institute for Space Studies, New York, NY, USA[1]
Center for Climate Systems Research, Columbia University, New York, NY, USA[2]
Potsdam Institute for Climate Impact Research, Member of the Leibniz Association, Potsdam, Germany[3]

Abstract. Crop models are often used to project future crop yield under climate and global change and typically show a broad range of outcomes. To understand differences in modeled responses, we analyzed modeled crop yield response types using impact response surfaces along four drivers of crop yield: carbon dioxide (C), temperature (T), water (W), and nitrogen (N). Crop yield response types help to understand differences in simulated responses per driver and their combinations rather than aggregated changes in yields as the result of simultaneous changes in various drivers. We find that models' sensitivities to the individual drivers are substantially different and often more different across models than across regions. There is some agreement across models with respect to the spatial patterns of response types but strong differences in the distribution of response types across models and their configurations suggests that models need to undergo further scrutiny. We suggest establishing standards in model evaluation based on emergent functionality not only against historical yield observations but also against dedicated experiments across different drivers to analyze emergent functional patterns of crop models.

Introduction. Crop models are often employed to project crop yields under changing conditions such as global warming and associated management change for adaptation (Jägermeyr et al., 2021). Multi-model ensembles are promoted to enhance the robustness of projections (Asseng et al., 2015; Martre et al., 2015), but questions remain on what causes often large differences between projections of individual models (e.g., Jägermeyr et al., 2021; Müller et al., 2021; E. Wang et al., 2022). Global Gridded Crop Models (GGCMs) are especially exposed to this question when applied for assessing climate change impacts (Jägermeyr et al., 2021; Schleussner et al., 2018), adaptation (Franke et al., 2022; Minoli et al., 2019; Zabel et al., 2021), or environmental impacts of agricultural production (W. Liu et al., 2018), because their results are used in downstream analyses, such as in integrated assessment (Ruane et al., 2017) or economic modeling for projecting future land-use change (Stevanović et al., 2016; Wiebe et al., 2015). Even though global gridded crop models are often based on detailed field-scale models or have implemented similar modeling principles in other ecosystem models (Müller et al., 2019) and show similar performance in evaluation against historical, national yield statistics (Franke et al., 2020a, 2020b; Müller et al., 2017), models are subject to substantial uncertainties from both model structure and parametrization (Folberth et al., 2019) as well as from calibration and input data quality (Ruane et al., 2021). This uncertainty shows most prominently in future projections under high-emission climate change scenarios, where models are exposed to driving data far outside the evaluation domain and results show large inter-model differences (Jägermeyr et al., 2021; Müller et al., 2021; Rosenzweig et al., 2014).

Climatic conditions (D. Liu et al., 2020) and soil properties (Qiao et al., 2022) determine yield potentials (Mauser et al., 2009; van Ittersum et al., 2013) and the suitability of different technologies, such as cultivars (Couëdel et al., 2021). Areas with similar climate and soil conditions show similar yield responses to variations in weather conditions, which can be monitored and reported using representative sites (Gommes et al., 2016). D. Liu et al. (2020) have identified the most limiting climate variable(s) across global crop production areas, finding that temperature has generally a higher impact on crop yields than precipitation for maize, rice, soybean, and wheat.

Atmospheric Chemistry & Physics, vol. 24, issue no. 23, pp. 13633-13652, doi:10.5194/acp-24-13633-2024

Can general circulation models (GCMs) represent cloud liquid water path adjustments to aerosol-cloud interactions?

Mülmenstädt, J., **A.S. Ackerman**[1], **A.M. Fridlind**[1], M. Huang, P.-L. Ma, N. Mahfouz, **S.E. Bauer**[1], S.M. Burrows, M.W. Christensen, S. Dipu, A. Gettelman, L.R. Leung, **F. Tornow**[1,2], J. Quaas, A.C. Varble, H. Wang, K. Zhang, and Y. Zheng, 2024

NASA Goddard Institute for Space Studies, New York, NY, USA[1]

Abstract. General circulation models (GCMs), unlike other lines of evidence, indicate that anthropogenic aerosols cause a global-mean increase in cloud liquid water path ($\mathscr{L}$) and thus a negative adjustment to radiative forcing of the climate by aerosol–cloud interactions. In part 1 of this series of papers, we showed that this is true even in models that reproduce the negative correlation observed in present-day internal variability in $\mathscr{L}$ and cloud droplet number concentration (N_d). We studied several possible confounding mechanisms that could explain the noncausal cloud–aerosol correlations in GCMs and that possibly contaminate observational estimates of radiative adjustments. Here, we perform single-column and full-atmosphere GCM experiments to investigate the causal model-physics mechanisms underlying the model radiative adjustment estimate. We find that both aerosol–cloud interaction mechanisms thought to be operating in real clouds – precipitation suppression and entrainment evaporation enhancement – are active in GCMs and behave qualitatively in agreement with physical process understanding. However, the modeled entrainment enhancement has a negligible global-mean effect. This raises the question of whether the GCM estimate is incorrect due to parametric or base-state representation errors or whether the process understanding gleaned from a limited set of canonical cloud cases is insufficiently representative of the diversity of clouds in the real climate. Regardless, even at limited resolution, the GCM physics appears able to parameterize the small-scale microphysics–turbulence interplay responsible for the entrainment enhancement mechanism. We suggest ways to resolve tension between current and future (storm-resolving) global modeling systems and other lines of evidence in synthesis climate projections.

Introduction. Increased aerosol concentration modifies cloud properties by increasing cloud droplet number, which initially makes clouds more reflective. When the aerosol concentration increase is due to an agent external to the climate system such as anthropogenic emissions, this cloud-brightening aerosol–cloud interaction (ACI) exerts a negative radiative forcing (RFaci) on the climate. However, clouds then adjust to the cloud droplet number (N_d) perturbation by changing their liquid water path ($\mathscr{L}$) and cloud coverage; this enhancement or weakening of the instantaneous RFaci is called the radiative adjustment due to $\mathscr{L}$ ($RA_{\mathscr{L}}$) or cloud fraction (RA_f).

General circulation models (GCMs) have long disagreed with other lines of evidence on the sign of $RA_{\mathscr{L}}$, predicting that anthropogenic aerosols increase $\mathscr{L}$ when observational and large-eddy simulation (LES) estimates predict that $\mathscr{L}$ decreases (Bellouin et al., 2020). Recently, Christensen et al. (2023), Varble et al. (2023), and Mülmenstädt et al. (2024b) showed that several Coupled Model Intercomparison sixth-generation GCMs from the Coupled Model Intercomparison Project 6 (CMIP6) generation (Eyring et al., 2016) produce negative correlations between cloud droplet number concentration, N_d, and $\mathscr{L}$ in present-day internal variability. This is welcome news because the inability of GCMs to match observations was interpreted as GCMs' inability to represent enhanced cloud-top entrainment of dry air at high N_d values. Enhanced entrainment is the dominant $RA_{\mathscr{L}}$ mechanism according to assessments based on multiple lines of evidence.

However, even GCMs that produce negative N_d–$\mathscr{L}$ correlations in the present day still predict an $\mathscr{L}$ increase in response to anthropogenic aerosol emissions. In other words, the causal response of the model climate to secular changes in aerosols has the opposite sign to the correlation in present-day internal variability.

Atmospheric Chemistry & Physics, vol. 24, issue no. 12, pp. 7331-7345, doi:10.5194/acp-24-7331-2024

General circulation models simulate negative liquid water path-droplet number correlations, but anthropogenic aerosols still increase simulated liquid water path.

Mülmenstädt, J., E. Gryspeerdt, S. Dipu, J. Quaas, **A.S. Ackerman**[1], **A.M. Fridlind**[1], **F. Tornow**[1,2], **S.E. Bauer**[1], A. Gettelman, Y. Ming, Y. Zheng, P.-L. Ma, H. Wang, K. Zhang, M.W. Christensen, A.C. Varble, L.R. Leung, X. Liu, D. Neubauer, D.G. Partridge, P. Stier, and T. Takemura, 2024

NASA Goddard Institute for Space Studies, New York, NY, USA[1]
Center for Climate Systems Research, Columbia University, New York, NY, USA[2]

Abstract. General circulation models' (GCMs) estimates of the liquid water path adjustment to anthropogenic aerosol emissions differ in sign from other lines of evidence. This reduces confidence in estimates of the effective radiative forcing of the climate by aerosol–cloud interactions (ERFaci). The discrepancy is thought to stem in part from GCMs' inability to represent the turbulence–microphysics interactions in cloud-top entrainment, a mechanism that leads to a reduction in liquid water in response to an anthropogenic increase in aerosols. In the real atmosphere, enhanced cloud-top entrainment is thought to be the dominant adjustment mechanism for liquid water path, weakening the overall ERFaci. We show that the latest generation of GCMs includes models that produce a negative correlation between the present-day cloud droplet number and liquid water path, a key piece of observational evidence supporting liquid water path reduction by anthropogenic aerosols and one that earlier-generation GCMs could not reproduce. However, even in GCMs with this negative correlation, the increase in anthropogenic aerosols from preindustrial to present-day values still leads to an increase in the simulated liquid water path due to the parameterized precipitation suppression mechanism. This adds to the evidence that correlations in the present-day climate are not necessarily causal. We investigate sources of confounding to explain the noncausal correlation between liquid water path and droplet number. These results are a reminder that assessments of climate parameters based on multiple lines of evidence must carefully consider the complementary strengths of different lines when the lines disagree.

Introduction. Aerosol–cloud interactions (ACIs) remain the greatest source of uncertainty in our estimates of anthropogenic perturbations in the Earth's energy budget (Boucher et al., 2014; Forster et al., 2021). In liquid clouds, an anthropogenic aerosol perturbation essentially instantaneously alters the number of cloud droplets (N_d), changing cloud reflectance and thus the shortwave radiation absorbed by the climate system, which exerts a radiative forcing on climate (radiative forcing by aerosol–cloud interactions or RFaci; Twomey, 1977; Boucher et al., 2014). While our knowledge of RFaci is uncertain (Quaas et al., 2020), an even thornier issue is cloud adjustments to the N_d perturbation, where multiple processes acting at different scales from cloud droplets to planetary circulation (Stevens and Feingold, 2009) result in a multiscale dynamics prediction problem that is impervious to any one silver bullet solution (Mülmenstädt and Feingold, 2018). Estimates of ACI adjustments are, therefore, based on multiple, and often conflicting, lines of evidence (Boucher et al., 2014; Bellouin et al., 2020; Forster et al., 2021). Those lines of evidence are, broadly, modeling at the cloud process scale (large eddy simulation or LES), global modeling, and observations at different scales.

In the following, we focus on stratocumulus (Sc) clouds, which play a large role in the energy budget due to their high albedo and frequent occurrence. Our understanding of adjustments in Sc is that two effects compete: an anthropogenic increase in N_d suppresses precipitation (Albrecht, 1989), increasing cloud liquid water path ($\mathscr{L}$); but the N_d increase also promotes increasing turbulent entrainment of subsaturated air at cloud top (Ackerman et al., 2004; Bretherton et al., 2007), decreasing $\mathscr{L}$.

PLOS ONE, vol. 19, issue no. 2, e0298876, doi:10.1371/journal.pone.0298876

Triadic signatures of global refugee and migrant flow networks.

Muneepeerakul, R., J. Johnson, **M.J. Puma**[1,2], and M. Zurek, 2024

NASA Goddard Institute for Space Studies, New York, NY, USA[1]
Center for Climate Systems Research, Columbia University, New York, NY, USA[2]

Abstract. Global refugee and migrant flows form complex networks with serious consequences for both sending and receiving countries as well as those in between. While several basic network properties of these networks have been documented, their finer structural character remains under-studied. One such structure is the triad significance profile (TSP). In this study, the TSPs of global refugee and migrant flow networks are assessed. Results indicate that the migrant flow network's size and TSP remain stable over the years; its TSP shares patterns with social networks such as trade networks. In contrast, the refugee network has been more dynamic and structurally unstable; its TSP shares patterns with networks in the information-processing superfamily, which includes many biological networks. Our findings demonstrate commonality between migrant and social networks as well as between refugee and biological networks, pointing to possible interdisciplinary collaboration—e.g., application of biological network theories to refugee network dynamics—, potentially furthering theoretical development with respect to both network theory and theories on human mobility.

Introduction. Refugee and migrant movements represent the most fundamental [1] and most extreme reactions to natural and human-induced change. When viewed together, these movements form complex networks—with nodes representing countries and edges representing human movements among them—to which network analyses can be applied to gain insights into their structure and dynamics. For example, Davis et al. [2] computed a number of basic network properties of the global migrant flow networks for the period 1960 to 2000 and found increasing transitivity of the network, declining average path length, and a shift towards larger values for degree distributions, noting that these trends "strengthened the 'small-world' behavior." More recently, Abel et al. [3] examined the structure of international migration networks, observing that these networks exhibit stability while having numerous short-term fluctuations over time.

While these efforts above have provided important insights into the basic network properties of the global refugee and migrant flow networks, they are based on low-order properties derived from pairwise relationships. Recent studies on complex networks have indicated that low-order properties alone provide an incomplete picture and highlighted the importance of higher-order network patterns [4–7]. As Lotito et al. [8] put it, "growing empirical evidence is now suggesting that a large number of such interactions are not limited to pairs, but rather occur in larger groups." Therefore, to obtain deeper understanding into human mobility networks, the higher-order structures of these networks need to be examined. One such structure is the "triad significance profile" (TSP) [9], a pattern based on triads or three-node subgraphs.

To be sure, some triadic structure has been studied for human mobility networks, but the focus was on commuting patterns at a city or state level and at a daily timescale (see, e.g., Refs [10, 11]). Here, we focus on more permanent movements (refugees and migrants) at the global scale on an annual timescale or longer. By addressing the subject matter at different spatial and temporal scales, our work complements the existing body of knowledge. Additionally, focusing on the TSP—rather the patterns and dynamics of individual triads—has another unique benefit: complex networks can be grouped based on their TSPs into "superfamilies" [9]. When two networks are part of the same superfamily, a similarity in their structures is implied: a sign of shared underlying dynamics. When this happens for two networks from different fields, it hints at the potential for cross-pollination of the concepts and analytical methods in those fields. This potential has not been explored nor realized for human mobility networks and will be addressed in this paper.

AGU Advances, vol. 5, issue no. 3, e2024AV001287, doi:10.1029/2024AV001287

Discounting water for optimal carbon gain as a basis of stomatal closure.

Nakad, M.[1,2], 2024

NASA Goddard Institute for Space Studies, New York, NY, USA[1]
Center for Climate Systems Research, Columbia University, New York, NY, USA[2]

Abstract. The exchange of carbon dioxide and water vapor between terrestrial ecosystems and the atmosphere is regulated by stomata (small pores in the leaves of plants). Unsurprisingly, environmental factors controlling the opening and closure of stomata has been sought as early as 1800. One approach, popularized in the early 1970s, is a stomatal optimization framework. This framework is based on the hypothesis that plants optimize carbon gain subject to water loss or water availability constraints. This constraint optimization problem was solved in various forms assuming instantaneous adjustments of stomatal aperture to maximize a reward function with no future foresight or legacy effects. Holtzman et al. (2024, **https://doi.org/10.1029/2023av001113**) offers a novel approach that can diagnose the effective timescale over which the reward function maximization must be time-integrated. The developed method thus optimizes an integrated carbon gain function but adjusted by a discount factor subject to water availability in the root zone. The discount factor considers how the plant values carbon gain to save water and its timescale can be inferred from observations because the model is analytically tractable. The results suggest that the most important climate factor that determines this discount timescale is multi-annual mean of the longest dry period during the growing season. The findings highlight how local climate traits influence the spatial variation in ecosystem-level water use strategies. This sets the stage for expanding such a framework to cases where multiple constraints act in concert while operating at distinct time scales.

Introduction. That terrestrial photosynthesis and transpiration are significant contributors to global carbon and water cycles is not in dispute (Gentine et al., **2019**). These key processes are integral to vegetation modeling in land surface schemes, which are typically coupled with climate models to enhance understanding of terrestrial ecosystem response to global change, and vice versa (Sellers et al., **1997**). Plants adjust the opening and closing of their stomata and regulate the exchange of water vapor and carbon dioxide in response to different environmental variables. However, current models face major uncertainty regarding how stomatal conductance responds to changes in the environment, especially soil moisture known to exhibit long memory and persistence (Ghannam et al., **2016**).

Empirical and phenomenological models (e.g., Jarvis, **1976**, and others) have been widely used to predict stomatal conductance. However, there is an understanding deficit in how the parameters of such models vary among species and adapt to a changing environment. In parallel, stomatal optimality theories (e.g., Cowan & GD, **1977**, and others) were developed to describe a universal response of stomatal conductance to environmental factors. These models assume that plants have evolved to optimize a reward function that captures the trade-off between carbon gain and water loss over a yet-to-be-determined time scale. The partial success of these models in predicting many aspects of stomatal responses has captured the attention of the research community. Nevertheless, certain limitations persist for this theory, especially the estimation of the marginal water cost of plant carbon gain parameter.

Stomatal optimization models (e.g., Katul et al., **2010**, and others) maximize a reward function instantaneously rather than over a time interval and differ in their expression of the cost of water use. Typically, this cost is constrained by water availability and accessibility in the rooting zone (Mrad et al., **2019**). However, given the stochastic nature of the environment, plants are expected to optimize their carbon gain over both current and future periods, assuming fluctuating water availability. This can lead to suboptimal behavior when calculating marginal water use efficiency (Feng et al., **2022**). Some studies have introduced optimization schemes over an integrated period, ranging from a typical drydown to the plant's entire lifespan.

International Journal of Climatology, vol. 44, issue no. 8, pp. 2701-2724, doi:10.1002/joc.8476

Recent trends in agriculturally relevant climate in Central America.

Nakamura, J.[3], R. Seager[3], H. Liu[3], F. Cottier, **M.J. Puma**[1,2], D.J. Wrathall, B. Katz, A. de Sherbinin, and S.B. Adamo, 2024

NASA Goddard Institute for Space Studies, New York, NY, USA[1]
Center for Climate Systems Research, Columbia University, New York, NY, USA[2]
Lamont-Doherty Earth Observatory, Palisades, NY, USA[3]

Abstract. This study examines the climatology and trends in climate in Guatemala, Honduras, and El Salvador over the past four decades, against the background of potential impacts on rainfed agriculture, livelihoods, and migration. The results show that there has been a significant warming of surface temperatures, an earlier start to the monsoon, a drier and longer mid-summer drought, and a delay in the second peak of precipitation from September to October. These changes have led to an increase in vapour pressure deficit (VPD) in northern Guatemala and along the Pacific coast in winter. High VPD can stress plants and lead to reduced yields. The study also finds that the thresholds that cause a decline in coffee yield have already been reached in El Salvador, but the average VPD has also risen in Guatemala and Honduras over the past 42 years. Maize yields have also been negatively affected with an inverse relationship with daily maximum temperatures during the summer flowering season. Observed changes and trends in these climate factors are believed to have direct implications for crop yields and livelihoods, potentially driving shifts in migration patterns.

Introduction. Central America, a region that extends from Belize to Panama, is characterized by a tropical monsoonal climate. An extended winter dry season occurs in the period between the retreat and the onset of the monsoon. There are many complexities to the precipitation pattern across Central America due to topography and proximity to water bodies. Spanning the western lowland and inland highland regions, including portions of countries such as Honduras, El Salvador, Guatemala, and Nicaragua, exists a geographic area with a population of around 23 million people (CIESIN, **2018**) commonly referred to as the Central America Dry Corridor (CADC). This contrasts with extensive lowland tropical broadleaf forests in Northern Guatemala, and the Caribbean coast of Honduras and Nicaragua, dominated by smallholder agriculture and large conservation areas, comprising the Meso-American Biological Corridor (MBC). In general, agricultural and livelihood patterns associated with these regions are distinct, with smallholder agriculture dominating in the dry corridor (Pons, **2021**) and large-scale industrialized agriculture and cattle ranching concentrated in areas receiving greater precipitation. Smallholder coffee production is most prevalent where dry and wet areas converge.

Over the preceding decade, the CADC has been afflicted by the most severe droughts witnessed in decades, resulting in disruption for over 1.3 million subsistence agriculturists and labourers, predominantly comprising marginalized Indigenous populations, causing substantial livelihood losses, marked instances of acute food insecurity, and prompting adjustments in their migratory behaviours (Anderson et al., **2023**; Linke et al., **2023**; Pons, **2021**; Stringer et al., **2021**). The primary migrant-sending countries of Central America and the CADC to the US/Mexico border are Guatemala, Honduras, and El Salvador (Angelo, **2021**; Young, **2021**).

Within the prevailing atmospheric circulation characterized by easterly trade winds, the influx of moist air from the Caribbean Sea encounters elevated terrain (Figure **1a**) creating a rain shadow on the western Pacific leeward side in the CADC (Trewartha, **1981**, p. 74). Quesada-Hernández et al. (**2019**) defined the CADC meteorologically using several drought indices and a ratio of potential evaporation to precipitation that changes during normal, dry, and wet years. The brown regions (lower than 14 g/kg) of the monthly climatology of surface specific humidity in Figure **S1** illustrate the more arid regions.

Quarterly Journal of the Royal Meteorological Society, vol. 150, pp.1336-1356, doi:10.1002/qj.4648

A CloudSat-CALIPSO view of cloud and precipitation in the occluded quadrants of extratropical cyclones.

Naud, C.M.[1,2], P. Ghosh, J.E. Martin, **G.S. Elsaesser**[1,2], and D.J. Posselt[3], 2024

NASA Goddard Institute for Space Studies, New York, NY, USA[1]
Center for Climate Systems Research, Columbia University, New York, NY, USA[2]
NASA Jet Propulsion Laboratory, California Institute of Technology, Pasadena, California, USA[3]

Abstract. Using 10 years of satellite-borne radar and lidar observations coupled with a novel method for automated occlusion identification, composite transects of cloud and precipitation across occluded thermal ridges of extratropical cyclones are, for the first time, constructed. These composites confirm that occluded sectors are characterized by the most extensive cloud cover and heaviest precipitation in any of the frontal regions of the cyclone. Hydrometeor frequency in occluded sectors is sensitive to the cyclone's ascent strength but not to the mean precipitable water in the cyclone's environment. This result is in contrast to the strong relationships between hydrometeor frequency and both precipitable water and ascent strength as previously reported in warm frontal regions. In both hemispheres, cloud and precipitation increase with the maximum value of the equivalent potential temperature at 700 hPa within the occluded thermal ridge, until a threshold is reached. For very large values of maximum equivalent potential temperature, hydrometeors become less frequent while precipitation rates increase. It is suggested that this conjunction is a by-product of an increase in the frequency of convection in those instances. While in the Northern Hemisphere occluded sectors exhibit deeper and wider cloud structures than their Southern Hemisphere counterparts, their hydrometeor occurrence frequencies are less. The differences in maximum equivalent potential temperature of the thermal ridges in both hemispheres does not appear to explain the more frequent hydrometeors in the Southern Hemisphere. These relationships offer new perspectives on the interplay between cloud processes and cyclone evolution, as well as new observational constraints for process evaluation of Earth system models.

Introduction. Most of the precipitation in the winter midlatitudes is produced by extratropical cyclones (Hawcroft *et al*., **2012**), whose impacts may also include strong winds, heavy downpours, blizzards, and cold air outbreaks. While these systems are well understood with regard to their formation, development and eventual dissipation, the role of cloud and precipitation processes in their evolution and potential impact is still the subject of active research. While such systems are expected to decrease in number as global warming leads to a gradual decline in the equator-to-pole temperature gradient, attendant increases in atmospheric moisture may enhance their vigor via amplification of the developmental impact of latent heating (e.g., Marciano *et al*., **2015**; Michaelis *et al*., **2017**; Zhang & Colle, **2017**).

Clouds and precipitation typically form along cold and warm frontal boundaries, where frontogenetically induced ascent and moisture convergence drive the water cycle. Such regions of concentrated latent heat release (LHR) have structural, energetic and developmental impacts on the cyclone as revealed by numerous studies (e.g., Binder *et al*., **2016**; Lackmann, **2002**; Sutcliffe & Forsdyke, **1950**; Uccellini, **1990**). Less organized, isolated convective cells have also been implicated in the production of precipitation in extratropical cyclones (e.g., Binder *et al*., **2020**; Crespo & Posselt, **2016**; Oertel *et al*., **2019**; Plummer *et al*., **2015**; Rauber *et al*., **2015**; Rosenow *et al*., **2014**).

Some cyclones entering the post-mature phase of their life cycles undergo the process of occlusion, identified by Bergeron in the context of the Norwegian Cyclone Model and first published in the seminal paper that introduced that model (Bjerknes & Solberg, **1922**). Chief among the structural transformations attending the occlusion process is the development of a thermal ridge connecting the cyclone center to the peak of the warm sector where the cold and warm fronts intersect (Martin, **1999a**, **1999b**; Schultz & Vaughan, **2011**, and references therein).

Earth's Future, vol.12, issue no. 5, e2023EF003987, doi:10.1029/2023EF003987

The changing influence of precipitation on soil moisture drought with warming in the Mediterranean and Western North America.

Nielsen, M.[1,2], **B.I. Cook**[1,3], **K. Marvel**[1,4], M. Ting, and J.E. Smerdon, 2024

NASA Goddard Institute for Space Studies, New York, NY, USA[1]
Department of Earth and Environmental Science, Columbia University, New York, NY, USA[2]
Lamont-Doherty Earth Observatory, Palisades, NY, USA[3]
Project Drawdown, St. Paul, MN, USA[4]

Abstract. Anthropogenic climate change has already affected drought severity and risk across many regions, and climate models project additional increases in drought risk with future warming. Historically, droughts are typically caused by periods of below-normal precipitation and terminated by average or above-normal precipitation. In many regions, however, soil moisture is projected to decrease primarily through warming-driven increases in evaporative demand, potentially affecting the ability of negative precipitation anomalies to cause drought and positive precipitation anomalies to terminate drought. Here, we use climate model simulations from Phase Six of the Coupled Model Intercomparison Project (CMIP6) to investigate how different levels of warming (1, 2, and 3°C) affect the influence of precipitation on soil moisture drought in the Mediterranean and Western North America regions. We demonstrate that the same monthly precipitation deficits (25th percentile relative to a preindustrial baseline) at a global warming level of 2°C increase the probability of both surface and rootzone soil moisture drought by 29% in the Mediterranean and 32% and 6% in Western North America compared to the preindustrial baseline. Furthermore, the probability of a dry (25th percentile relative to a preindustrial baseline) surface soil moisture month given a high (75th percentile relative to a preindustrial baseline) precipitation month is 6 (Mediterranean) and 3 (Western North America) times more likely in a 2°C world compared to the preindustrial baseline. For these regions, warming will likely increase the risk of soil moisture drought during low precipitation periods while simultaneously reducing the efficacy of high precipitation periods to terminate droughts.

Introduction. Anthropogenic climate change has already affected the global hydrological cycle (Durack et al., **2012**; Marvel & Bonfils, **2013**; Marvel et al., **2019**; Zhang et al., **2020**), and many regions are already experiencing longer and more intense agricultural and ecological droughts as a result (Field et al., **2012**; Seneviratne et al., **2021**). Climate models project additional increases in drying and extreme droughts across many regions by 2100 (Cook et al., **2014**, **2020**). While changes in precipitation and its effect on drought are expected to be highly regionally and locally specific, these large-scale increases in drought severity and risk are predominantly caused by the effects of temperature through the direct effects of warming on increasing evaporative demand (Basara et al., **2019**; García-Herrera et al., **2019**; Seager et al., **2015**; Williams et al., **2014**, **2020**) and declining snow and runoff efficiency (Dai et al., **2018**; Marvel et al., **2021**; Vicente-Serrano et al., **2020**; Wanders et al., **2015**).

Coupled with expected temperature changes, climate change will also affect future precipitation characteristics, including total amounts (Dore, **2005**; Held & Soden, **2006**), distribution (Marvel & Bonfils, **2013**), variability (Pendergrass et al., **2017**), event frequency (Papalexiou & Montanari, **2019**), and event intensity (Huang et al., **2020**; Min et al., **2011**). Historically, precipitation is the primary driver of soil moisture drought dynamics (e.g., Seager et al., **2019**). Moisture deficits associated with extended periods of reduced precipitation propagate through the hydrological cycle, reducing water availability in soils, streams, and reservoirs (Mishra & Singh, **2010**). Conversely, large positive precipitation anomalies are the major cause of drought terminations, supplying the moisture needed to overcome existing surface moisture deficits. In many cases, such drought terminations can be abrupt and disruptive when the precipitation causing the termination is connected to extreme phenomena (e.g., atmospheric rivers, tropical cyclones) (Dettinger, **2013**) or is unpredictable on seasonal time scales (Seager, Nakamura, & Ting, **2019**).

Atmospheric Chemistry & Physics, vol. 24, issue no. 9, pp. 5337-5367, doi:10.5194/acp-24-5337-2024

Observationally constrained regional variations of shortwave absorption by iron oxides emphasize the cooling effect of dust.

Obiso, V.[1,2], M. Gonçalves Ageitos, C. Pérez García-Pando, G.L. Schuster[3], **S.E. Bauer**[1], C. Di Biagio, P. Formenti, **J.P. Perlwitz**[1,3], **K. Tsigaridis**[1,5], and **R.L. Miller**[1], 2024

NASA Goddard Institute for Space Studies, New York, NY, USA[1]
Barcelona Supercomputing Center, Barcelona, Spain[2]
Climate, Aerosol, and Pollution Research, LLC, Bronx, NY, USA[3]
NASA Langley Research Center, Hampton, VA, USA[4]
Center for Climate Systems Research, Columbia University, New York, NY, USA[5]

Abstract. The composition of soil dust aerosols derives from the mineral abundances in the parent soils that vary across dust source regions. Nonetheless, Earth system models (ESMs) have traditionally represented mineral dust as a globally homogeneous species. The growing interest in modeling dust mineralogy, facilitated by the recognized sensitivity of the dust climate impacts to composition, has motivated state-of-the-art ESMs to incorporate the mineral speciation of dust along with its effect upon the dust direct radiative effect (DRE). In this work, we enable the NASA Goddard Institute for Space Studies ModelE2.1 to calculate the shortwave (SW) DRE accounting for the regionally varying soil mineralogy. Mineral–radiation interaction at solar wavelengths is calculated according to two alternative coupling schemes: (1) external mixing of three mineral components that are optically distinguished, one of which contains embedded iron oxides; (2) a single internal mixture of all dust minerals with a dynamic fraction of iron oxides that varies regionally and temporally. We link dust absorption to the fractional mass of iron oxides based on recent chamber measurements using natural dust aerosol samples. We show that coupled mineralogy overall enhances the scattering by dust, and thus the global cooling, compared to our control run with globally uniform composition. According to the external mixing scheme, the SW DRE at the top of atmosphere (TOA) changes from −0.25 to, corresponding to a change in the net DRE, including the longwave effect, from −0.08 to. The cooling increase is accentuated when the internal mixing scheme is configured: the SW DRE at the TOA becomes with a net DRE of. The varying composition modifies the regional distribution of single scattering albedo (SSA), whose variations in specific regions can be remarkable (above 0.03) and significantly modify the regional SW DRE. Evaluation against the AErosol RObotic NETwork (AERONET) shows that explicit representation of soil mineralogy and its regional variations reduces the low bias of model dust SSA while improving the range of variability across stations and calendar months. Despite these improvements, the moderate spatiotemporal correlation with AERONET reveals remaining modeling challenges and the need for more accurate measurements of mineral fractions in soils.

Introduction. Dust aerosols are wind-blown soil particles that alter the atmospheric energy and hydrologic cycles by perturbing solar and thermal radiative fluxes (Miller et al., 2014). Estimates of the dust direct radiative effect (DRE) are still largely uncertain, mainly due to poorly constrained dust absorption (Samset et al., 2018). The single scattering albedo (SSA) indicates the fraction of radiative energy extinguished by aerosols through scattering with respect to total extinction, due to both scattering and absorption, and therefore inversely measures the intrinsic aerosol absorptive power. The SSA is a function of the particle size distribution (PSD), complex refractive index (CRI) and shape (Hansen and Travis, 1974; Mishchenko et al., 2002).

Journal of Climate, vol. 37, issue no. 10, pp. 2897-2917, doi:10.1175/JCLI-D-23-0119.1

Coupled stratospheric ozone and Atlantic Meridional Overturning Circulation feedbacks on the Northern Hemisphere midlatitude jet response to 4×CO_2.

Orbe, C.[1,2], **D. Rind**[1], D. Waugh, **J. Jonas**[1,3], X. Zhang, G. Chiodo, **L. Nazarenko**[1,3], and **G.A. Schmidt**[1], 2024

NASA Goddard Institute for Space Studies, New York, NY, USA[1]
Department of Applied Physics and Applied Mathematics, Columbia University, New York, NY, USA[2]
Center for Climate Systems Research, Columbia University, New York, NY, USA[3]

Abstract. Stratospheric ozone, and its response to anthropogenic forcings, provides an important pathway for the coupling between atmospheric composition and climate. In addition to stratospheric ozone's radiative impacts, recent studies have shown that changes in the ozone layer due to 4xCO_2 have a considerable impact on the Northern Hemisphere (NH) tropospheric circulation, inducing an equatorward shift of the North Atlantic jet during boreal winter. Using simulations produced with the NASA Goddard Institute for Space Studies (GISS) high-top climate model (E2.2), we show that this equatorward shift of the Atlantic jet can induce a more rapid weakening of the Atlantic meridional overturning circulation (AMOC). The weaker AMOC, in turn, results in an eastward acceleration and poleward shift of the Atlantic and Pacific jets, respectively, on longer time scales. As such, coupled feedback from both stratospheric ozone and the AMOC result in a two-time-scale response of the NH midlatitude jet to abrupt 4xCO_2 forcing: a "fast" response (5–20 years) during which it shifts equatorward and a "total" response (~100–150 years) during which the jet accelerates and shifts poleward. The latter is driven by a weakening of the AMOC that develops in response to weaker surface zonal winds that result in reduced heat fluxes out of the subpolar gyre and reduced North Atlantic Deep Water formation. Our results suggest that stratospheric ozone changes in the lower stratosphere can have a surprisingly powerful effect on the AMOC, independent of other aspects of climate change.

Introduction. There is large uncertainty in the atmospheric circulation response to increasing greenhouse gases [see Shepherd (2014) and references therein]. Although models generally predict a poleward shift of the midlatitude eddy-driven jet, the magnitude of this shift is highly uncertain (e.g., Vallis et al. 2015; Grise and Polvani 2014) as are its underlying drivers (Shaw 2019). This is especially true in the Northern Hemisphere (NH), where there are opposing thermodynamic influences, i.e., opposite meridional temperature gradient responses at the surface versus the upper troposphere (Shaw et al. 2016). Thus, while enhanced warming in the lower polar troposphere relative to the lower tropical troposphere (i.e., Arctic amplification) contributes to reduced meridional temperature gradients, increases in upper tropospheric tropical warming contribute to enhanced temperature gradients aloft (Butler et al. 2010; Yuval and Kaspi 2020) and it is not clear how these competing processes affect the zonal mean midlatitude jet.

Many processes have been shown to influence the response of meridional temperature gradients to increased CO_2, including polar amplification [see Smith et al. (2019) and references therein] and cloud feedbacks (e.g., Ceppi and Hartmann 2015; Voigt and Shaw 2015). By comparison, composition feedbacks associated with the ozone response to CO_2 have been less well examined although stratospheric ozone changes have been identified as an important pathway coupling composition to climate (Isaksen et al. 2009). In particular, the stratospheric ozone response to 4xCO_2 consists of robust decreases in the tropical lower stratosphere (LS), increases in the tropical upper stratosphere, and increases over high latitudes (Chiodo et al. 2018). In the tropics, the reductions in LS ozone are strongly correlated with the response of stratospheric upwelling [Fig. 6 in Chiodo et al. (2018)], and while the exact details of these changes are model dependent, especially over high latitudes, the general pattern is very consistent among models [e.g., Nowack et al. 2015; Chiodo et al. 2018; Chiodo and Polvani 2019 (hereafter CP2019)].

Journal of Geophysical Research: Atmospheres, vol. 129, issue no. 12, e2023JD040074, doi:10.1029/2023JD040074

Assessing the impact of climate change on atmospheric rivers: A modeling perspective.

Ordaz Osorio, C.[1,2,3], **J.F. Booth**[1,2,3], **A.N. LeGrande**[1,4], and **C.M. Naud**[1,4], 2024

NASA Goddard Institute for Space Studies, New York, NY, USA[1]
Department of Physics, Graduate Center, City University of New York, New York, NY, USA[2]
Department of Earth and Atmospheric Sciences, City College, City University of New York, New York, NY, USA[3]
Center for Climate Systems Research, Columbia University, New York, NY, USA[4]

Abstract. Atmospheric rivers (ARs) play a crucial role in the poleward transport of water vapor, and the AR-associated precipitation is a critical component of global water supplies, making it critical that we understand how ARs may change in the future. To approach this issue, integrations of the NASA Goddard Institute for Space Studies global climate model ModelE version 2.1 (GISSE2.1) are employed. Multiple configurations of the model simulating different climates are analyzed: (a) the last-glacial maximum; (b) present day; (c) the end of the 21st century. The thermodynamic and dynamic components of changes to AR frequency are analyzed using a decomposition method. This method utilizes differences in distinct AR seasonal climatology frequencies derived from various vertically integrated water vapor transport (IVT) thresholds to resolve AR frequency into its components. Global mean state changes in poleward AR frequency for different climates are dominated by precipitable water vapor (PWV) changes. A set of idealized cold and warm climates in which present day sea surface temperatures are uniformly changed are considered for a targeted analysis of the south Pacific Ocean basin. For this analysis, frequency and distribution of AR events in the model runs are analyzed by comparing them to changes in the jet stream as well as the Eulerian storm tracks and low-level baroclinicity. Latitudinal shifts in the ARs in the south Pacific Ocean basin using our integrations are not as tightly coupled to these two storm-related climatological metrics in the midlatitudes but fare better on the poleward side of the storm tracks.

Introduction. Atmospheric rivers (ARs) (Y. Zhu & Newell, **1994**, **1998**) are elongated, filamentary features in the subtropics and midlatitudes that play a crucial role in the global water cycle (Gimeno et al., **2014**). In California, the presence or absence of ARs can determine whether a season is characterized by abundant rainfall or drought conditions (Dettinger et al., **2011**). Likewise, in Chile, a few ARs during JJA account for more than half of the subtropical region's total precipitation (Viale et al., **2018**). The importance of ARs extends beyond regional boundaries, profoundly influencing weather patterns in both California and Chile, where their presence or absence can dictate the onset of either abundant rainfall or drought conditions, respectively. Given the crucial role that ARs play in various regions, including the western coasts of continents (Guan & Waliser, **2015**) as well as the eastern coasts (Kaminski et al., **2023**; Kim et al., **2022**; Ryu et al., **2021**), and in polar regions (Gorodetskaya et al., **2014**; Wille et al., **2022**), it is imperative to understand how ARs will respond to climate change.

The impact of climate change on ARs is reviewed in Payne et al. (**2020**). A couple of main messages from this review include a need to increase our knowledge of ARs globally as well as a better understanding of how ARs relate to large-scale dynamics, particularly for regions outside of the North Pacific and the US West Coast. Ma et al. (**2020**) investigate the poleward shift of ARs in recent decades over the southern hemisphere. Therein, this shift is attributed to anthropogenic forcing and interdecadal SST variability. P. Zhang et al. (**2021**) use a global climate model that treats water vapor primarily as a tracer (Ming & Held, **2018**) to demonstrate that changes to ARs with climate change can be explained primarily by thermodynamics. The authors demonstrate that the main mechanism for ARs is the redistribution of moisture and air mass along constant potential surfaces that is done by extratropical cyclones (ETCs). In the context of the ARTMIP project (Shields et al., **2018**), Shields et al. (**2023**), analyze future AR characteristics. They explore AR characteristics including frequency, intensity, and precipitation. Their findings underscore the significance of AR detection tools and catalogs in shaping projected AR-related precipitation patterns (Shields et al., **2018**, **2023**).

One Earth, vol. 7, issue no. 7, pp. 1250-1265, doi:10.1016/j.oneear.2024.06.012

Human heat stress could offset potential economic benefits of CO2 fertilization in crop production under a high-emissions scenario.

Orlov, A., **J. Jägermeyr**[1,2], C. Müller, A.S. Daloz, F. Zabel, S. Minoli, W. Liu, T.-S. Lin, A.K. Jain, C. Folberth, M. Okada, B. Poschlod, A. Smerald, J.M. Schneider, and J. Sillmann, 2024

NASA Goddard Institute for Space Studies, New York, NY, USA[1]
Center for Climate Systems Research, Columbia University, New York, NY, USA[2]

Abstract. Climate change can significantly affect food production in many ways. Changes in greenhouse gases, temperature, and rainfall directly influence crop productivity, sometimes increasing yield through a mechanism known as the carbon dioxide fertilization effect. However, agricultural production in many countries also relies on physically demanding manual labor, primarily outside, and, as temperatures rise, heat stress on agricultural workers can reduce labor capacity. Consequential climate change impacts on food availability and affordability are a major societal concern, yet the specific and combined impacts on agricultural production remain highly uncertain. An assessment of the future impacts of climate change on the production and prices of four of the world's most consumed crops (maize, wheat, soybean, and rice) reveals that a rise in heat stress will lower agricultural labor capacity and increase labor costs in Africa and Asia. This could offset the potential economic benefits of higher yields due to elevated levels of CO2. Proactive adaptation measures, such as mechanization deployment, are needed to reduce the vulnerability to heat stress.

Under scenarios of high greenhouse gas (GHG) emissions, climate change leads to increasing global temperatures and significant changes in precipitation patterns across regions.[1] Agriculture is especially exposed to climate risks, but, despite recent advances in climate and crop modeling, the climate-induced impacts on agricultural productivity remain highly uncertain.[2,3] The sensitivities of crop models to key drivers of crop yields—such as carbon dioxide, temperature, water, and nitrogen—vary significantly across different crop models.[4] On the one hand, an elevated atmospheric concentration of CO_2 will enhance the productivity of many C_3 crops, including wheat, rice, and soybean, through the CO_2 fertilization effect.[5] At high latitudes, some regions could also experience diminishing temperature limitations (i.e., longer growing seasons) and higher yields due to global warming.[6] On the other hand, crop yields are expected to decline in regions where critical temperature thresholds are already exceeded. This applies especially to C_4 crops (i.e., carbon is fixed initially into a four-carbon compound during photosynthesis, rendering its assimilation more efficient). Maize, a typical C_4 crop adapted to drier climates, assimilates CO_2 more effectively than C_3 crops but benefits little from an increase in atmospheric concentration of CO_2. The most recent crop model simulations based on phase 6 of the Coupled Model Intercomparison Project (CMIP6) indicate a high likelihood of increased yields for soy, rice, and particularly wheat by the middle of the century, whereas maize yields are expected to decline.[3] In addition, the newest scientific evidence shows that climate change will most likely affect crop productivity sooner and more strongly than previously estimated.

Furthermore, apart from direct climate-induced impacts on agriculture (i.e., due to changes in temperature and precipitation), climate change could also indirectly affect agricultural production through climate-induced impacts on capacity and productivity of labor. Agriculture is one of the most labor-intensive sectors, where most physical work is done outdoors and thus is strongly exposed to heat stress.[7] Under high-warming scenarios, heat stress could significantly reduce labor capacity, especially in the tropics.[8,9] More frequent and severe humid heat could increase health risks and reduce the capacity for physical work.[10,11,12] While shifting working hours could potentially reduce the heat-induced loss of labor productivity under current climatic conditions, this adaptation option will become less effective under future high-warming scenarios as both daytime and nighttime temperatures increase.[13]

Annals of the New York Academy of Sciences, vol. 1539, issue no. 1, pp. 49-76, doi:10.1111/nyas.15180

NPCC4: Tail risk, climate drivers of extreme heat, and new methods for extreme event projections.

Ortiz, L., **C. Braneon**[1,2], R. Horton, **D. Bader**[1,3,4], P. Orton, **V. Gornitz**[1,5], B. Rosenzweig, T. McPhearson, L. Smalls-Mantey, H. Sheerazi, F. Montalto, M.R. Golkhandan, C. Evans, A. Degaetano, E. Mallen, L. Carter, K. McConnell, T. Mayo, and M. Buchanan, 2024

NASA Goddard Institute for Space Studies, New York, NY, USA[1]
CUNY Institute for Demographic Research (CIDR), City University of New York, New York City, New York, USA[2]
Center for Climate Systems Research, Columbia University, New York, NY, USA[3]
Lamont-Doherty Earth Observatory, Palisades, NY, USA[4]
Autonomic Integra LLC, New York, NY, USA[5]

Abstract. We summarize historic New York City (NYC) climate change trends and provide the latest scientific analyses on projected future changes based on a range of global greenhouse gas emissions scenarios. Building on previous NPCC assessment reports, we describe new methods used to develop the projections of record for sea level rise, temperature, and precipitation for NYC, across multiple emissions pathways and analyze the issue of the "hot models" associated with the 6th phase of the Coupled Model Intercomparison Project (CMIP6) and their potential impact on NYC's climate projections. We describe the state of the science on temperature variability within NYC and explain both the large-scale and regional dynamics that lead to extreme heat events, as well as the local physical drivers that lead to inequitable distributions of exposure to extreme heat. We identify three areas of tail risk and potential for its mischaracterization, including the physical processes of extreme events and the effects of a changing climate. Finally, we review opportunities for future research, with a focus on the *hot model problem* and the intersection of spatial resolution of projections with gaps in knowledge in the impacts of the climate signal on intraurban heat and heat exposure.

Introduction. While every NPCC assessment report has included a chapter on the state of climate science and projections for NYC, this chapter includes a strengthened emphasis on the equity implications of climate change adaptation.[1, 2] In addition, this chapter addresses emerging issues related to higher-than-expected ECS in several ensemble members from the CMIP6, which simulate higher-than-expected global mean temperatures. Finally, the chapter describes the changing tail and compound risks associated with climate change.

2.1 Chapter Scope and Context. Anthropogenic climate change is fundamentally linked to the rapid increase in GHG emissions propelled by the Industrial Revolution and the European colonial systems that enabled it. "Raw materials from colonies across the British Empire fueled the Industrial Revolution,"[3] land dispossession and forced migration facilitated colonial expansion, and chattel slavery provided unpaid labor to build the British colonies as well as the new American nation.[1, 5-8] In addition, the "political arithmetic" of global trade prompted extreme extraction from the New York metropolitan region's biodiversity into the Atlantic world trading system.[9] Consequently, humanity's climate crisis has its roots in land dispossession, forced migration, as well as human and natural resource extraction orchestrated by European colonial powers.[10, 11] Furthermore, the tremendous variability in vulnerability to climate change (among and within regions) is driven by "patterns of intersecting socio-economic development, unsustainable ocean and land use, inequity, and marginalization" as well as "historical and ongoing patterns of inequity such as colonialism" and structural racism (e.g., Home Owners Loan Corporation redlining in NYC's five boroughs).[12-17]

Vulnerability to climate hazards and stressors (Figure 1)[18] is unequally distributed across NYC as "high levels of social vulnerability are consistently found in areas with lower incomes," aging populations, and higher proportions of Black and Latinx/Hispanic residents.[2]

Atmospheric Measurement Techniques, vol. 17, issue no. 15, pp. 4737-4756, doi:10.5194/amt-17-4737-2024

Global Sensitivity Analysis of simulated polarimetric remote sensing observations over snow.

Ottaviani, M.[1,2], G.H. Myers, and N. Chen, 2024

NASA Goddard Institute for Space Studies, New York, NY, USA[1]
Terra Research Inc, Hoboken, NJ, USA[2]

Abstract. This study presents a detailed theoretical assessment of the information content of passive polarimetric observations over snow scenes, using a global sensitivity analysis (GSA) method. Conventional sensitivity studies focus on varying a single parameter while keeping all other parameters fixed. In contrast, the GSA correctly addresses the covariance of state parameters across their entire parameter space, hence favoring a more correct interpretation of inversion algorithms and the optimal design of their state vectors.

The forward simulations exploit a vector radiative transfer model to obtain the Stokes vector emerging at the top of the atmosphere for different solar zenith angles when the bottom boundary consists of a vertically resolved snowpack of non-spherical grains. The presence of light-absorbing particulates (LAPs), either embedded in the snow or aloft in the atmosphere above in the form of aerosols, is also considered. The results are presented for a set of wavelengths spanning the visible (VIS), near-infrared (NIR), and shortwave infrared (SWIR) region of the spectrum.

The GSA correctly captures the expected, high sensitivity of the reflectance to LAPs in the VIS–NIR and to grain size at different depths in the snowpack in the NIR–SWIR. With adequate viewing geometries, mono-angle measurements of total reflectance in the VIS–SWIR (akin to those of the Moderate Resolution Imaging Spectroradiometer, MODIS) resolve grain size in the top layer of the snowpack sufficiently well. The addition of multi-angle polarimetric observations in the VIS–NIR provides information on grain shape and microscale roughness. The simultaneous sensitivity in the VIS–NIR to both aerosols and snow-embedded impurities can be disentangled by extending the spectral range to the SWIR, which contains information on aerosol optical depth while remaining essentially unaffected when the same particulates are mixed with the snow. Multi-angle polarimetric observations can therefore (i) effectively partition LAPs between the atmosphere and the surface, which represents a notorious challenge for snow remote sensing based on measurements of total reflectance only and (ii) lead to better estimates of grain shape and roughness and, in turn, the asymmetry parameter, which is critical for the determination of albedo. The retrieval uncertainties are minimized when the degree of linear polarization is used in place of the polarized reflectance.

The Sobol indices, which are the main metric for the GSA, were used to select the state parameters in retrievals performed on data simulated for multiple instrument configurations. Improvements in retrieval quality with the addition of measurements of polarization, multi-angle views, and different spectral channels reflect the information content, identified by the Sobol indices, relative to each configuration.

The results encourage the development of new remote sensing algorithms that fully leverage multi-angle and polarimetric capabilities of modern remote sensors. They can also aid flight planning activities, since the optimal exploitation of the information content of multi-angle measurements depends on the viewing geometry. The better characterization of surface and atmospheric parameters in snow-covered regions advances research opportunities for scientists of the cryosphere and ultimately benefits albedo estimates in climate models.

Introduction. The quantification of the surface energy balance of snow-covered regions is of extreme importance for Earth-system model simulations aimed at global climate studies (Hansen and Nazarenko, 2004; Fettweis et al., 2008; van den Broeke et al., 2011; Rae et al., 2012; van Angelen et al., 2012; Tedesco et al., 2013; Alexander et al., 2014; Colgan et al., 2014).

Limnology and Oceanography, vol. 69, no. 12, pp. 2913-2928, doi:10.1002/lno.12719

Dual phosphorus and nitrogen nutrient reduction will be more effective than a phosphorus-only reduction in mitigating diatom and cyanobacterial blooms in Lake Erie, USA-Canada.

Paerl, H.W., J.D. Chaffin, J.H. Cheshire, **H.E. Plaas[1,2],** M.A. Barnard, L.B. Goerlitz, J.S. Braddy, A. Sabo, L.M. Nelson, and L. Yue, 2024

NASA Goddard Institute for Space Studies, New York, NY, USA[1]
Department of Marine, Earth and Atmospheric Sciences, NC State University, Raleigh, NC, USA[2]

Abstract. Lake Erie, USA–Canada plays an important ecological and socioeconomic role but has suffered from chronic eutrophication. In particular, western Lake Erie (WLE) is the site of harmful algal blooms (HABs) which are suspected of being driven by excessive nutrient (phosphorus (P) and nitrogen (N)) inputs. During 2022 and 2023, in situ nutrient dilution and addition bioassays were conducted at a WLE bloom-impacted location to investigate whether a nutrient reduction regime would be effective in limiting phytoplankton growth during the June diatom-dominated spring blooms and August cyanobacteria-dominated summer blooms. The primary objectives of this experiment were to (1) Determine if a proposed 40% P-alone reduction would effectively reduce phytoplankton growth and mitigate blooms and (2) assess whether reductions in both P and N are more effective in controlling phytoplankton biomass than exclusive reductions in either N or P. Samples were analyzed for nutrient concentrations and growth rate responses for specific algal groups, utilizing diagnostic (for major algal groups) photopigments. Results indicated that although both 20% and 40% dilutions led to lower phytoplankton biomass and growth rates, 40% reductions were more effective. Our results support the USA–Canada Great Lakes Water Quality Agreement recommendation of a 40% P reduction, but also indicate that a parallel reduction of N input by 40% would be most effective in controlling bloom magnitudes. Overall, our findings underscore the recommendation that a year-round dual N and P 40% reduction is needed for long-term control of eutrophication and algal blooms, including cyanobacteria and diatoms, in Lake Erie.

Introduction. Rice is the most irrigation-intensive cereal crop, accounting for 30% of global irrigation water use[1]. By 2050, a 50% to 60% increase in global rice production while a 15% increase in irrigation water use are required to feed the growing population[2], which will intensify water competition between agriculture and other sectors, threatening global rice supply[3]. Thus, saving water in rice cultivation is critical to ensure food security of nearly half the world's population with rice as its main staple food.
Alternate wetting and drying (AWD) is a promising and widely recommended water-saving irrigation strategy for paddy rice[4]. With AWD, irrigation water is applied to reflood the field a certain number of days after the subsidence of ponded water. The timing of re-flooding is a key management decision that could be determined by metrics of soil moisture status, such as volumetric or gravimetric water content, soil water potential or field water depth falling below a predetermined threshold[5,6]. Previous studies showed that AWD could reduce irrigation water use by approximately a quarter compared to continuous flooding[7] and might reduce rice yields in some circumstances (such as alkaline soils)[5,7]. Trade-offs between water saving and yield losses remain a fundamental obstacle for large-scale application of AWD.

Science of The Total Environment, vol. 957, 177499, doi:10.1016/j.scitotenv.2024.177499.

Dual nitrogen and phosphorus reductions are needed for long-term mitigation of eutrophication and harmful cyanobacterial blooms in the hydrologically-variable San Francisco Bay Delta, CA.

Paerl, H.W., **H.E. Plaas**, L.M. Nelson, A.S. Korbobo, J.H. Cheshire, L. Yue, and E.P. Preece, 2024

NASA Goddard Institute for Space Studies, New York, NY, USA[1]
Department of Marine, Earth and Atmospheric Sciences, NC State University, Raleigh, NC, USA[2]

Abstract. Cyanobacterial harmful algal blooms (CyanoHABs) are a major concern for water quality, public health and viability of aquatic ecosystems. Increased inputs of nutrients, i.e., nitrogen (N) and phosphorus (P), are known to amplify the occurrence, severity, and duration of CyanoHABs. There is growing concern that CyanoHABs are proliferating along the freshwater to marine continuum, including throughout estuaries. We assessed the influence of nutrient enrichment on the abundance and composition of CyanoHABs and accompanying phytoplankton communities in the San Francisco Bay Delta (SFBD) estuarine ecosystem, a vital resource for California's water supply, fisheries, and recreation. In situ *n*utrient addition bioassays were conducted in June and September 2022, at the end of a record three-year drought period, and May and August 2023, an extremely high rainfall and discharge year. Water was collected from two locations in the SFBD recognized for having CyanoHAB issues, Discovery Bay (DB) and the Stockton Channel (STK). Both sites showed the highest proportion of cyanobacteria in the total phytoplankton community biomass during summer months, and this was particularly noticeable at STK. In June 2022, additions of N and N+P were both shown to increase overall phytoplankton biomass in DB and N+P specifically stimulated cyanobacteria. P alone was not stimulatory. In September 2022, NH_4 promoted the growth of cyanobacteria faster than NO_3, particularly in DB communities. A similar set of responses to N occurred in 2023 in DB, despite major differences in freshwater input between years. In 2022, nutrient additions had no significant stimulatory effects on STK phytoplankton communities, suggesting nutrients were replete throughout the bloom season. However, in 2023 N limitation became more evident in STK, likely due to a dilution effect from the very high freshwater discharge from a record snowpack and reservoir releases, ultimately changing the availability of inorganic N during the CyanoHAB growth period. The combined effect of high flow and nutrient dilution in 2023 was responsible for the reduced CyanoHAB potential. By examining these key differences between seasons in these hydrologically contrasting years, it appears that internal supplies of "legacy P" ensure P availability throughout the summer bloom season regardless of hydrologic variability, while N enrichment plays a key role in stimulating algal production and CyanoHABs under hydrologically variable conditions. Once N was added, P further stimulated biomass production in some cases, indicating potential N+P co-limitation. We conclude that under varying hydrologic conditions, long-term dual N and P input reductions are needed to control eutrophication and CyanoHAB outbreaks throughout the SFBD.

Introduction. Anthropogenic activities have accelerated eutrophication in aquatic systems worldwide due to increased nutrient (nitrogen-N and phosphorus-P) inputs from agricultural, urban and industrial expansion (Conley et al., 2009; Paerl et al., 2016; Wurtsbaugh et al., 2019). Previous research has shown strong links between increased N and P loads and the occurrence and expansion of cyanobacterial harmful algal blooms (CyanoHABs) along the freshwater to marine continuum (Smith and Schindler, 2009; Paerl et al., 2018; Wurtsbaugh et al., 2019).

Natural Hazards, vol. 120, issue no. 4, pp. 3565-3587, doi:10.1007/s11069-023-06288-0

Drought and deluge: the recurrence of hydroclimate extremes during the past 600 years in eastern Australia's Natural Resource Management (NRM) clusters.

Palmer, J.G., D. Verdon-Kidd, K.J. Allen, P. Higgins, **B.I. Cook**[1,2], E.R. Cook[2], C.S.M. Turney, and P.J. Baker, 2024

NASA Goddard Institute for Space Studies, New York, NY, USA[1]
Ocean and Climate Physics, Lamont-Doherty Earth Observatory, Palisades, NY, USA[2]

Abstract. Recent extremes of flood and drought across Australia have raised questions about the recurrence of such rare events and highlighted the importance of understanding multi-decadal climate variability. However, instrumental records over the past century are too short to adequately characterise climate variability on multi-decadal and longer timescales or robustly determine extreme event frequencies and their duration. Palae-oclimate reconstructions can provide much-needed information to help address this problem. Here, we use the 600-year hydroclimate record captured in the eastern Australian and New Zealand Drought Atlas (ANZDA) to analyse drought and pluvial frequency trends for East Australian Natural Resource Management (NRM) clusters. This partitioning of the drought atlas grid points into recognised biophysical areas (i.e. NRM clusters) revealed their differences and similarities in drought intensity and pluvial events over time. We find sustained multi-decadal periods of a wet–dry geographic 'seesaw' between eastern to central and southern NRMs (e.g. 1550–1600 CE and 1700–1750 CE). In contrast, other periods reveal spatially consistent wetting (e.g. 1500–1550 CE) or drying (e.g. 1750–1800 CE). Emerging hot spot analysis further shows that some areas that appear naturally buffered from severe drought during the instrumental period have a greater exposure risk when the longer 600-year record is considered. These findings are particularly relevant to management plans when dealing with the impacts of climate extremes developed at regional scales. Our results demonstrate that integrating and extending instrumental records with palaeo-climate datasets will become increasingly important for developing robust and locally specific extreme event frequency information for managing water resources.

Introduction. Future adaptation planning relies on understanding the environmental impacts of anthropogenic climate change and an appreciation of natural climate variability. While there is a high degree of certainty around the impacts of climate change on temperature, there has been less confidence in the hydroclimatic effects (IPCC 2021). Climate change is thought to have already accelerated the hydrological processes making droughts more severe on a global scale (Mukherjee et al. 2018); however, regional-scale processes, forcings and feedback can modulate the local expression of drought (Cook et al. 2022; Vogel et al. 2019). A further complication is the combination of relatively high variability and short instrumental records that do not adequately capture inherent natural variability and are unlikely to represent the full range of possible wet and dry extremes (Cook et al. 2022)—even without anthropogenically forced climate change. Included within these are a special category of extreme events that are relatively rare, have significant impacts and are of uncertain timing—sometimes described as Black Swans (Taleb 2007)—the lack of a suitable hydroclimate baseline makes it challenging to contextualise recent extremes and plan for the frequency and intensity of climate extremes.

Australia has one of the most variable hydroclimates in the world (Peel et al. 2004) and has experienced three major widespread and protracted droughts in the past 120 years (Verdon-Kidd and Kiem 2009). Over the past two decades alone, parts of Australia have experienced several significant pluvial events (e.g. 2011, 2019 and 2022 CE in Queensland) as well as persistent drought conditions (e.g. 2001–2009 and 2017–2019 CE in Southeast Australia). The estimated economic impact of the 2017–2019 CE drought and subsequent 2019–2020 CE bushfires was A$63 billion (Wittwer and Waschik 2021). A lack of understanding of how unusual such events are presents an obstacle to effective adaptive planning.

Surveys in Geophysics, vol. 45, issue no. 6, pp. 1933-1958, doi:10.1007/s10712-024-09868-2

A multi-satellite perspective on "hot tower" characteristics in the equatorial trough zone.

Pilewskie, J.[1,2], G. Stephens[3], H. Takahashi[3], and T. L'Ecuyer, 2024

NASA Goddard Institute for Space Studies, New York, NY, USA[1]
Center for Climate Systems Research, Columbia University, New York, NY, USA[2]
NASA Jet Propulsion Laboratory, California Institute of Technology, Pasadena, CA, USA[3]

Abstract. In 1979, Herbert Riehl and Joanne Simpson (Malkus) analytically estimated that 1600–2400 undilute convective cores vertically transport energy to the tropopause at any given time within a region where upper-tropospheric energy is only exported from the tropics. The focus of this paper is to update this estimate using modern satellite observations, compare hot tower frequency and intensity characteristics to all deep convective cores that reach the upper troposphere, and document hot tower spatiotemporal variability in relation to precipitation and high cloud properties within the tropical trough zone (between 13 °S and 19 °N). Cloud vertical profiles from CloudSat and CALIPSO measurements supply convective core diameters and proxies for intensity and convective activity, and these proxies are augmented with brightness temperature data from geostationary satellite observations, precipitation information from IMERG, and cloud radiative properties from CERES. Less than 35% of all deep cores are classified as hot towers, and we estimate that 800–1700 hot towers occur at any given time over the course of a day, with the mean maximum core and hot tower frequency occurring at the time of year when peak convective intensity and precipitation occur. Convective objects that contain hot towers frequently contain multiple cores, and the largest systems with five or more distinct cores most frequently occur in regions where organized mesoscale convective systems and the highest climatological mean rain rates are known to occur. Analysis of co-located radar and infrared brightness temperatures reveals that passive observations alone are not sufficient to unambiguously distinguish hot towers using simple brightness temperature thresholds.

Introduction. In 1979, Herbert Riehl and Joanne Simpson (Malkus) analytically estimated that 1600–2400 undilute convective cores vertically transport energy to the tropopause at any given time within a region where upper-tropospheric energy is only exported from the tropics. The focus of this paper is to update this estimate using modern satellite observations, compare hot tower frequency and intensity characteristics to all deep convective cores that reach the upper troposphere, and document hot tower spatiotemporal variability in relation to precipitation and high cloud properties within the tropical trough zone (between 13 °S and 19 °N). Cloud vertical profiles from CloudSat and CALIPSO measurements supply convective core diameters and proxies for intensity and convective activity, and these proxies are augmented with brightness temperature data from geostationary satellite observations, precipitation information from IMERG, and cloud radiative properties from CERES. Less than 35% of all deep cores are classified as hot towers, and we estimate that 800–1700 hot towers occur at any given time over the course of a day, with the mean maximum core and hot tower frequency occurring at the time of year when peak convective intensity and precipitation occur. Convective objects that contain hot towers frequently contain multiple cores, and the largest systems with five or more distinct cores most frequently occur in regions where organized mesoscale convective systems and the highest climatological mean rain rates are known to occur. Analysis of co-located radar and infrared brightness temperatures reveals that passive observations alone are not sufficient to unambiguously distinguish hot towers using simple brightness temperature thresholds.

Australia has one of the most variable hydroclimates in the world (Peel et al. 2004) and has experienced three major widespread and protracted droughts in the past 120 years (Verdon-Kidd and Kiem 2009). Over the past two decades alone, parts of Australia have experienced several significant pluvial events (e.g. 2011, 2019 and 2022 CE in Queensland) as well as persistent drought conditions (e.g. 2001–2009 and 2017–2019 CE in Southeast Australia).

Journal of Environmental Management, vol. 351, 119606, doi:10.1016/j.jenvman.2023.119606

Managing a cyanobacteria harmful algae bloom "hotspot" in the Sacramento — San Joaquin Delta, California.

Preece, E.P., J. Cooke, **H. Plaas**[1,2], A. Sabo[2], L. Nelson[2], and H.W. Paerl[2], 2024

NASA Goddard Institute for Space Studies, New York, NY, USA[1]
Institute of Marine Sciences, University of North Carolina at Chapel Hill, Morehead, City, NC, USA[2]

Abstract. Cyanobacterial harmful algal blooms (CHABs) have become a persistent seasonal problem in the upper San Francisco Estuary, California also known as the Sacramento-San Joaquin Delta (Delta). The Delta is comprised of a complex network of open water bodies, channels, and sloughs. The terminus of the Stockton Channel is an area identified as a CHAB "hotspot." As CHABs increase in severity, there is an urgent need to better understand CHAB drivers to identify and implement mitigation measures that can be used in an estuarine complex like the Delta. We investigated water quality conditions and nutrient dynamics in the Stockton Channel by measuring nutrients in the water column, sediments, and pore waters. *In situ* nutrient addition bioassay experiments were used to assess the effects of nutrient enrichment on total algal/cyanobacterial growth and pigment concentrations. In both June and September, relative to unamended controls, total chlorophyll and cyanobacterial pigment concentrations were unaffected by nutrient additions; hence, the study area showed signs of classical hypereutrophication, with ambient nitrogen and phosphorus present in excess of algal growth requirements. A cyanobacterial bloom, dominated by *Microcystis* spp. was present throughout the study area but was most severe and persistent at the shallowest site at the channel terminus. At this site, *Microcystis* spp. created water quality conditions that allowed for a prolonged bloom from June through September. While targeted nutrient reductions are recommended for long term mitigation, on a shorter timescale, our findings suggest that physical/mechanical controls are the more promising alternative approaches to reduce the severity of CHABs in the terminus of the Stockton Channel.

Introduction. Eutrophication is among the most pressing environmental issues impacting water resources worldwide (Likens, 1972; Smith, 2003; Sepulveda-Jauregui et al., 2018; Beaulieu et al., 2019). In estuaries, the common responses to eutrophication are increased primary productivity, changes in biogeochemical (i.e., nutrient, oxygen) cycling, and reductions in biodiversity (Glibert, 2017). Climate warming is expected to further exacerbate the symptoms of eutrophication, most notably, the increased incidences and severity of cyanobacterial harmful algal blooms (CHABs; Paerl and Huisman, 2008; 2009; Moss, 2011; Lürling et al., 2017).

River dominated coastal systems are particularly at risk of experiencing more severe CHAB events due to the combined effects of nutrient over-enrichment, warming temperatures, and extreme weather events (Paerl, 2023). Indeed, a number of eutrophic estuaries around the world are reporting increased occurrences of CHABs (e.g., Preece et al., 2017; Paerl et al., 2018; Bargu et al., 2019). Cyanobacteria are able to proliferate in the fresh and brackish waters of estuaries, even during extreme climate variability, due to their ability to withstand large changes to water chemistry and physical properties (e.g., stratification and transparency) (Paerl and Huisman, 2008; Lehman et al., 2022).

Large estuarine systems that are prone to CHABs often have "hotspot" regions (i.e., locations where cyanobacteria blooms are most severe and most likely to occur) along the freshwater-marine continuum (Paerl et al., 2018). Mechanisms that create conditions for CHAB hotspots to develop vary by system, but can include; point sources of nutrients, flood management actions that cause freshwater pulses into an estuary, and tropical cyclones and other large storm events (Filippino et al., 2017; Vaičiūtė et al., 2021; Bargu et al., 2023). Size of the system, hydrodynamics, freshwater areas that are hydrologically isolated from high flows, and salinity gradients also influence where hotspots develop (Robson and Hamilton, 2004; Paerl, 2014; Paerl et al., 2018).

Geoscientific Model Development, vol. 17, issue no. 12, pp. 4821-4836, doi:10.5194/gmd-17-4821-2024

Evaluation of CMIP6 model simulations of $PM_{2.5}$ and its components over China.

Ren, F., J. Lin, C. Xu, J.A. Adeniran, J. Wang, R.V. Martin, A. van Donkelaar, M. Hammer, L. Horowitz, S.T. Turnock, N. Oshima, J. Zhang, **S. Bauer**[1], **K. Tsigaridis**[1,2], Ø. Seland, P. Nabat, D. Neubauer, G. Strand, T. van Noije, P. Le Sager, and T. Takemura, 2024

NASA Goddard Institute for Space Studies, New York, NY, USA[1]
Center for Climate Systems Research, Columbia University, New York, NY, USA[2]

Abstract. Earth system models (ESMs) participating in the latest Coupled Model Intercomparison Project Phase 6 (CMIP6) simulate various components of fine particulate matter ($PM_{2.5}$) as major climate forcers. Yet the model performance for $PM_{2.5}$ components remains little evaluated due in part to a lack of observational data. Here, we evaluate near-surface concentrations of $PM_{2.5}$ and its five main components over China as simulated by 14 CMIP6 models, including organic carbon (OC; available in 14 models), black carbon (BC; 14 models), sulfate (14 models), nitrate (4 models), and ammonium (5 models). For this purpose, we collect observational data between 2000 and 2014 from a satellite-based dataset for total $PM_{2.5}$ and from 2469 measurement records in the literature for $PM_{2.5}$ components. Seven models output total $PM_{2.5}$ concentrations, and they all underestimate the observed total $PM_{2.5}$ over eastern China, with GFDL-ESM4 (−1.5 %) and MPI-ESM-1-2-HAM (−1.1 %) exhibiting the smallest biases averaged over the whole country. The other seven models, for which we recalculate total $PM_{2.5}$ from the available component output, underestimate the total $PM_{2.5}$ concentrations partly because of the missing model representations of nitrate and ammonium. Concentrations of the five individual components are underestimated in almost all models, except that sulfate is overestimated in MPI-ESM-1-2-HAM by 12.6 % and in MRI-ESM2-0 by 24.5 %. The underestimation is the largest for OC (by −71.2 % to −37.8 % across the 14 models) and the smallest for BC (−47.9 % to −12.1 %). The multi-model mean (MMM) reproduces the observed spatial pattern for OC ($R = 0.51$), sulfate ($R = 0.57$), nitrate ($R = 0.70$) and ammonium ($R = 0.74$) fairly well, yet the agreement is poorer for BC ($R = 0.39$). The varying performances of ESMs on total $PM_{2.5}$ and its components have important implications for the modeled magnitude and spatial pattern of aerosol radiative forcing.

Introduction. Fine particulate matter ($PM_{2.5}$) influences air quality, human health, and climate change. Exposure to near-surface $PM_{2.5}$ is associated with millions of global premature deaths each year (Zhang et al., 2017; World Health Organization, 2021). $PM_{2.5}$ affects the radiative budget of the climate system directly through scattering and absorption and indirectly via clouds. The effects of atmospheric aerosols on cloud droplet concentrations, cloud distributions, and radiative properties pose large uncertainties in the estimating radiative forcing (Carslaw et al., 2013; Seinfeld et al., 2016). Earth system models (ESMs) are essential tools for studying global climate change. The accuracy of $PM_{2.5}$ simulations in ESMs exhibits a crucial constraint on the reliability of these models in climate change simulation and projection. The Coupled Model Intercomparison Project Phase 6 (CMIP6) provides an opportunity to evaluate $PM_{2.5}$ and its components simulated by the current-generation ESMs which implement interactive aerosol and atmospheric chemistry (Turnock et al., 2020). A total of 21 ESMs participating in CMIP6 provide total $PM_{2.5}$ and/or several component simulations, although the aerosol component species vary across these models. Of these 21 ESMs, 14 models include organic aerosol (OA; converted to organic carbon (OC) in this study by assuming = 1.6), black carbon (BC), sulfate, dust (DST), and sea salt (SSLT). Of these 14 models, 4 also include nitrate, and 5 include ammonium (Table S1).

Journal of Geophysical Research: Biogeosciences, 129, no. 10, e2024JG008143, doi:10.1029/2024JG008143

The impact of drought on terrestrial carbon in the West African Sahel: Implications for natural climate solutions.

Rigatti, E.[2], **S.S. McDermid[1,2]**, **B.I. Cook[1,3]**, and M.G. De Kauwe, 2024

NASA Goddard Institute for Space Studies, New York, NY, USA[1]
Department of Environmental Studies, New York University, New York, NY, USA[2]
Lamont-Doherty Earth Observatory, Palisades, NY, USA[3]

Abstract. Terrestrial ecosystems store more than twice the carbon of the atmosphere and are critical to climate change mitigation efforts. This has led to a proliferation of land-based carbon sequestration efforts, such as re/afforestation associated with the Great Green Wall in the West African Sahel (WAS GGW). However, we currently lack comprehensive assessments of the long-term viability of these ecosystems' carbon storage in the context of increasingly severe climate extremes. The WAS is particularly prone to recurrent and disruptive extremes, exemplified by the persistent and severe late-20th century drought. We assessed the response and recovery of WAS GGW carbon stocks and fluxes to this late-20th century drought, and the subsequent rainfall recovery, by leveraging a suite of terrestrial ecosystem models. While multi-model mean carbon fluxes (e.g., gross primary production, respiration) partly recovered to pre-drought levels, modeled total (above and below ground) ecosystem carbon stock falls to as much as two standard deviations below pre-drought levels and does not recover even ?20 years after the maximum drought anomaly. Furthermore, to the extent that the modeled regional carbon stock recovers, it is nearly entirely driven by atmospheric CO2 trends rather than the precipitation recovery. Uncertainties in regional ecosystem carbon simulation are high, as the models' carbon responses to drought displayed a nearly 10-standard deviation spread. Nevertheless, the multi-model average response highlights the strong and persistent impact of drought on terrestrial carbon storage, and the potential risks of relying on terrestrial ecosystems as a ?natural climate solution? for climate change mitigation.

Introduction. Terrestrial ecosystems store ~2,150 gigatons carbon (GtC) within their soils and vegetation (including live and decomposing biomass), which is more than twice that of the atmosphere (Friedlingstein et al., **2022**). Protecting these carbon stocks is therefore critical to addressing the climate crisis. There is growing interest in buffering and even enhancing terrestrial ecosystems' carbon storage as a “natural climate solution” to meet ambitious climate goals (Griscom et al., **2017**; IPCC, **2018**; Rogelj et al., **2018**; Seddon et al., **2021**; Yin et al., **2023**). Many projects covering a range of ecosystems have been proposed or initiated to these ends (Badgley et al., **2022**; Bastin et al., **2019**; Ellis et al., **2024**; Haya et al., **2023**; Seddon et al., **2021**), including the “Great Green Wall” (GGW) ecosystem restoration effort across the African Sahel (Editorial, **2023**; Goffner et al., **2019**; O’Connor & Ford, **2014**).

However, the viability of these systems for long-term terrestrial carbon storage is uncertain, especially in the context of climate change and increasingly-severe climate extremes (e.g., droughts, heat waves, etc). Extreme events can have significant impacts on the terrestrial carbon cycle and regional stocks (Abram et al., **2021**; Allen et al., **2015**; Brando et al., **2019**; Intergovernmental Panel on Climate Change, **2023**), substantially threatening an ecosystem's capacity as a carbon sink (Van Der Molen et al., **2011**). Even a small shift in the frequency or severity of extreme events can have large implications for carbon cycle dynamics and initiate positive climate-warming feedbacks, compounding the effects of the original disturbance (Frank et al., **2015a**; Reichstein et al., **2013**). Of particular importance is drought, which can affect ecosystems across large spatiotemporal scales. Droughts typically decrease gross primary productivity (GPP) more than respiration (Humphrey et al., **2018**).

Frontiers in Marine Science, vol. 11, 1359149, doi:10.3389/fmars.2024.1359149

Ocean surface radiation measurement best practices.

Riihimaki, L.D., M.F. Cronin, R. Acharya, N. Anderson, J. Augustine, K.A. Balmes, P. Berk, R. Bozzano, A. Bucholtz, K.J. Connell, C. Cox, A.G. Di Sarra, J.B. Edson, C. Fairall, J.T. Farrar, K. Grissom, M.T. Guerra, V. Hormann, K.J. Joseph, C. Lanconelli, F. Melin, D. Meloni, **M. Ottaviani**[1,2], S. Pensieri, K Ramesh, D. Rutan, N. Samarinas, S.R. Smith, S. Swart, A. Tandon, R. Venkatesan, E. Thompson, R.K. Verma, V. Vitale, K.S. Watkins-Brandt, R.A. Weller, C.J. Zappa, and D. Zhang, 2024

NASA Goddard Institute for Space Studies, New York, NY, USA[1]
Terra Research Inc, Hoboken, NJ, USA[2]

Abstract. Ocean surface radiation measurement best practices have been developed as a first step to support the interoperability of radiation measurements across multiple ocean platforms and between land and ocean networks. This document describes the consensus by a working group of radiation measurement experts from land, ocean, and aircraft communities. The scope was limited to broadband shortwave (solar) and longwave (terrestrial infrared) surface irradiance measurements for quantification of the surface radiation budget. Best practices for spectral measurements for biological purposes like photosynthetically active radiation and ocean color are only mentioned briefly to motivate future interactions between the physical surface flux and biological radiation measurement communities. Topics discussed in these best practices include instrument selection, handling of sensors and installation, data quality monitoring, data processing, and calibration. It is recognized that platform and resource limitations may prohibit incorporating all best practices into all measurements and that spatial coverage is also an important motivator for expanding current networks. Thus, one of the key recommendations is to perform interoperability experiments that can help quantify the uncertainty of different practices and lay the groundwork for a multi-tiered global network with a mix of high-accuracy reference stations and lower-cost platforms and practices that can fill in spatial gaps.

Introduction. The radiative balance at the Ocean's surface has a profound impact on the Earth system, affecting the ocean uptake and release of heat, oxygen, carbon dioxide, and aerosols. Solar heating drives ocean and wind circulations. Downwelling solar (shortwave) radiation at the ocean surface is reduced from that at the top of the atmosphere due to reflection and absorption by moisture and particles in the atmosphere, which in turn emit, absorb, and reflect infrared (longwave) radiation. Surface radiation is also a component of the surface energy budget driving ocean heat flux, ocean buoyancy flux, and air-sea exchange processes that impact cloud formation, global circulation, greenhouse gas concentrations, and climate patterns. Sunlight provides energy for photosynthesis supporting marine life.

Accurate measurements of both the solar shortwave (SW) and longwave (LW) radiation at the ocean's surface require not only sensitive high-quality sensors, but also careful installation of the sensor, calibration practices, and treatment of the data. In this paper, we summarize best practices for ocean surface radiation budget measurements developed over the past years by land-based and ocean-based experts, making measurements from a variety of platforms, in a range of environments, and under a range of power, space, and resource constraints. Fundamentally, this set of best practices needs to be applicable to real-world conditions, including those found in remote, harsh regions of the world's oceans. The goal here is to harmonize measurements between ocean and terrestrial-based radiation measurement communities to make a truly global network of Earth surface radiation observations.

Oceanographers began to observe ocean surface radiation to better understand upper ocean dynamics and the processes that govern sea surface temperature and mixed layer depth in the Tropical Ocean Global Atmosphere (TOGA, 1985-1994) program and the World Ocean Circulation Experiment (WOCE, 1990-1998).

Geoscientific Model Development, vol. 17, issue no. 8, pp. 3487-3505, doi:10.5194/gmd-17-3487-2024

Assessing acetone for the GISS ModelE2.1 Earth system model.

Rivera, A., **K. Tsigaridis**[1,2], **G. Faluvegi**[1,2], and D. Shindell, 2024

NASA Goddard Institute for Space Studies, New York, NY, USA[1]
Center for Climate Systems Research, Columbia University, New York, NY, USA[2]

Abstract. Acetone is an abundant volatile organic compound (VOC) in the atmosphere, with important influences on ozone and oxidation capacity. Direct sources include chemical production from other VOCs and anthropogenic emissions, terrestrial vegetation, biomass-burning emissions, and ocean production. Sinks include chemical loss, deposition onto the land surface, and ocean uptake. Acetone also has a lifetime that is long enough to allow transport and reactions with other compounds remote from its sources. The NASA Goddard Institute for Space Studies (GISS) Earth system model ModelE2.1 simulates a variety of Earth system interactions. Previously, acetone had a very simplistic representation in the ModelE chemical scheme. This study assesses a more sophisticated acetone scheme in which acetone is a full 3-dimensional tracer with explicit sources, sinks, and atmospheric transport. We first evaluate the new global acetone budget in the context of past literature. Estimated source and sink fluxes fall within the range of previous models, although total atmospheric burden and lifetime are at the lower end of the published literature. Acetone's new representation in ModelE2.1 also results in more realistic spatial and vertical distributions, which we compare against previous models and field observations. The seasonality of acetone-related processes was also studied in conjunction with field measurements, and these comparisons show promising agreement but also shortcomings at high-emission urban locations, where the model's resolution is too coarse to capture the true behavior. Finally, we conduct a variety of sensitivity studies that explore the influence of key parameters on the acetone budget and its global distribution. An impactful finding is that the production of acetone from precursor hydrocarbon oxidation has strong leverage on the overall chemical source, indicating the importance of accurate molar yields. Overall, our implementation is one that corroborates with previous studies and marks a significant improvement in the development of the acetone tracer in GISS ModelE2.1.

Introduction. Acetone (C_3H_6O) is an abundant oxygenated volatile organic compound (VOC) that has important connections to ozone and the atmosphere's self-cleansing oxidation capacity (Read et al., 2012). Acetone's dynamic presence in Earth's atmosphere can be described through sources, sinks, and mechanisms of transport. Extensive literature has discussed the nature of these sources and sinks, and some are more well constrained than others.

Primary sources of acetone in the atmosphere include anthropogenic sources, terrestrial vegetation, and biomass-burning emissions. Past literature has found the fluxes of these sources to range between 1–2, 30–45, and 2.5–4.5 Tg yr^{-1}, respectively (Beale et al., 2013; Brewer et al., 2017; Elias et al., 2011; Fischer et al., 2012; Folberth et al., 2006; Jacob et al., 2002; Singh et al., 2000; Wang et al., 2020). Chemical production from other VOCs with three or more carbon atoms, each with their own molar yield, is another source of acetone in the atmosphere (Brewer et al., 2017; Fischbeck et al., 2017; Hu et al., 2013; Jacob et al., 2002; Singh et al., 2000; Weimer et al., 2017).

Sinks of acetone include wet and dry deposition as well as chemical loss. Wet deposition occurs within and below clouds due to the solubility of acetone and depends on its Henry's law coefficient (Benkelberg et al., 1995). Dry deposition occurs on the land surface. Chemical loss of acetone forms radicals through photolysis. Past literature has estimated the acetone sinks to be 10 %–30 % dry deposition and 40 %–85 % chemical loss (Arnold et al., 2005; Elias et al., 2011; Fischer et al., 2012; Khan et al., 2015; Singh et al., 1994).

Nature Water, vol. 2, pp. 604-605, doi:10.1038/s44221-024-00266-x

Accelerating Antarctic research amid rapid changes.

Roach, L.A.[1,2], 2024

NASA Goddard Institute for Space Studies, New York, NY, USA[1]
Center for Climate Systems Research, Columbia University, New York, NY, USA[2]

Abstract. We must prioritize diversity, scientific communication and team-based science to keep up with rapid Antarctic ice and climate change.

Introduction. What got me interested in sea ice, during university about ten years ago, was the Antarctic sea ice paradox. When the world was warming, why was Antarctic sea ice expanding? This question has motivated most Antarctic sea ice research for decades. And yet, within only a few years, the trend has reversed. Antarctic sea ice area reached a satellite era record low in 2016, followed by a new record low in 2022, and then another record low in 2023. The pace of change has been dramatic, even during my short research career thus far.

Sea ice plays a crucial role in the global water cycle, acting as a reservoir for relatively fresh water. In the Southern Ocean, the amplitude of the seasonal cycle of sea ice is enormous, with sea ice area expanding sixfold each year, and helping transport freshwater from higher to lower latitudes. Sea ice affects the exposure of Antarctic ice shelves to ocean warming and storms, influencing mass loss from Antarctica's grounded ice, which is one of the most uncertain factors in future sea level rise and paramount for adaptation. Sea ice is essential in climate feedbacks and ecological systems in the Southern Ocean. Given its global importance, that the processes driving Antarctic sea ice expansion are not yet fully-understood, that the record-breaking sea ice lows were not anticipated, and that their drivers remain unclear, one might ask why there hasn't been more research progress.

Several connected factors complicate our understanding of Antarctic sea ice. Antarctic observations are very limited. The Southern Ocean experiences polar night, and visible satellite observations are limited to months with good light, visibility and cloud-free conditions. Being extremely cold, stormy and remote, Antarctica is a challenging destination for field campaigns. Thick sea ice in winter hinders ships and powerful storms hamper crossings. Although coverage is slowly increasing, we still have very limited observations of sea ice thickness and of subsurface ocean water properties in the Southern Ocean, more so than any other ocean on Earth. State-of-the-art climate models struggle with accurate simulation of the Southern Ocean and its sea ice. Biases in this region lead to low confidence in future projections of Antarctic sea ice. Moreover, the processes at play are complicated, and impacted by interactions between the ocean, atmosphere and cryosphere — research domains that can be siloed.

There are inherent climatic and technological limitations that are challenging to address. And, of course, increased research funding is sorely needed (for example, glaciology research funding in the US is minuscule compared to the projected costs of sea level rise mitigation[1]). But we can determine how our polar research community conducts research. From my early-career perspective, here are three key areas where we must improve to rapidly advance understanding in polar science.

First, it is imperative that we make our scientific community more inclusive to all people, and especially newcomers. Ample evidence shows that diverse teams have better performance outcomes. Geoscience remains one of the least diverse scientific fields[2], with many experiencing hostile behaviour[3]. In particular, harassment during remote Antarctic fieldwork is a serious and distressing issue[4]. Preventing misconduct, harassment, and discrimination is the right thing to do by any moral standard and also crucial for improving retention. We all have a duty to uphold standards of conduct every day within our research community and consider how we can make our communities more inclusive. This includes thinking about academic hierarchies and power structures.

Nature Reviews Earth & Environment, vol. 5, issue no. 4, pp. 235-237, doi:10.1038/s43017-024-00542-0

Sea ice in 2023.

Roach, L.A.[1,2], and W.N. Meier, 2024

NASA Goddard Institute for Space Studies, New York, NY, USA[1]
Center for Climate Systems Research, Columbia University, New York, NY, USA[2]

Abstract. Antarctic sea ice extent was the lowest on record in 2023, with an annual mean of 9.81 million km^2, beating the previous minimum of 2022. Arctic sea ice extent was also low, with an annual mean of 10.49 million km^2, but did not break any records.

Key Points.

- Global sea ice extent (Antarctic and Arctic combined) reached a satellite era record daily minimum of 15.86 million km^2 on 31st January 2023.
- Antarctic sea ice extent exhibited record lows in many months of the year, including the lowest monthly summer minimum (1.91 million km^2 in February) and the lowest monthly winter maximum (16.80 million km^2 in September).
- Arctic sea ice anomalies were largest in boreal summer, including a September sea ice extent of 4.37 million km^2, the 5th lowest on record.

Introduction. Sea ice cover in the polar oceans has a key role in climate, ecology and society. It influences global ocean circulation, the radiation budget, global climate sensitivity and ice sheet mass loss[1]; it offers habitats for plankton and wildlife; and it provides a vital lifeline for native communities[2]. Sea ice extent (SIE, the total surface area with at least 15% sea ice concentration) is strongly seasonal. In the Arctic, it typically varies from a maximum of 15 million km^2 in March to a minimum of 6 million km^2 in September, whereas in the Antarctic, it spans from a minimum of 3 million km^2 in February to a maximum of 19 million km^2 in September. Superimposed on these seasonal cycles is longer-term variability (Fig. 1a) driven by anthropogenic greenhouse emissions, ozone depletion and natural internal variability.

To evaluate different configurations of the model or understand model uncertainty, modeling studies involve one-at-a-time sensitivity tests for different injection height approaches (Toll et al., 2015; Wizenberg et al., 2023), aerosol configurations (Forkel et al., 2015; Konovalov et al., 2020; Palacios-Peña et al., 2018), convective transport (Palacios-Peña et al., 2020) or smoke emissions (Carter et al., 2020; Lu & Sokolik, 2013; Pan et al., 2020), but to the best of our knowledge, not simultaneously. Carter et al. (2020), for example, compared model simulations with different biomass burning emissions estimates, but also mention errors in model optics, background aerosols or clouds in satellite retrievals as other possible sources of discrepancy between their model and satellite data. Li et al. (2020) compared particle trajectory-based simulations of a single fire using a 112-member ensemble with different combinations of plume rise scheme, prescribed meteorology, vertical motion and biomass burning estimates. Notably, they found that each of the four emissions estimates produced high-scoring simulations of downwind surface $PM_{2.5}$, highlighting the simultaneous dependence of simulated smoke on the choice of multiple model options.

In the Arctic, sea ice decline has been evident over much of the satellite record: SIE reductions of approximately –3% dec^{-1} in March, approximately –13% dec^{-1} in September and –5% dec^{-1} in the annual mean have been observed, with a record low September (3.57 million km^2) and annual mean (10.42 million km^2) SIE in 2012. Accompanying these SIE declines have been corresponding increases in open water season length and reductions in ice age[3] and thickness.

Earth's Future, vol. 12, issue no. 4, e2023EF003842, doi:10.1029/2023EF003842

Non-linear climate change impacts on crop yields may mislead stakeholders.

Ruane, A.C.[1], **M. Phillips**[1,2,3], **J. Jägermeyr**[1,2], and C. Müller, 2024

NASA Goddard Institute for Space Studies, New York, NY, USA[1]
Center for Climate Systems Research, Columbia University, New York, NY, USA[2]
Autonomic Integra, LLC, Institute for Space Studies, New York, NY, USA[3]

Abstract. We utilize a global warming level (GWL) lens to evaluate global and regional patterns of agricultural impacts as global surface temperature increases, providing a unique perspective on the experience of stakeholders with continued warming in the 21st century. We analyze crop productivity outputs from 11 crop models simulating 5 climate models under 3 emissions scenarios across 4 crops within the AgMIP/ISIMIP Phase 3 ensemble. We categorize regional productivity changes (without adaptation) into 9 characteristic climate change response patterns, identifying consistent increases and decreases as well as non-linear (peak or dip) responses indicative of inflection points reversing trends as GWLs increase. Many maize regions and pockets of wheat, rice and soybean show peak decrease patterns where initial increases may lull stakeholders into complacency or maladaptation before productivity shifts to losses at higher GWLs. Although the GWL perspective has proven useful in connecting diverse climate models and emissions scenarios, we identify multiple pitfalls that recommend proceeding with caution when applying this approach to climate impacts. Chief among these is that carbon dioxide (CO_2) concentrations at any GWL depend on a climate model's transient climate response (TCR). Higher CO_2 concentrations generally benefit crop productivity, so this leads to more pessimistic agricultural projections for so-called “hot” models and can skew multi-model ensemble results as models with high TCR are disproportionately likely to reach higher GWLs. While there are strong connections between many climatic impact-drivers and GWLs, vulnerability and exposure components of food system risk are strongly dependent on development pathways.

Introduction. Future agricultural systems are challenged to balance (a) sustainable increases in productivity and efficiency to ensure food security for growing and developing populations, (b) adaptation to current extremes and future climate change, (c) mitigation of greenhouse gas emissions and other environmental impacts, and (d) incentives for the economic engine that keeps the agricultural sector running (Mbow et al., **2019**; Nabuurs et al., **2023**). Each of these individual challenges is substantial and addressing them simultaneously requires foresight, systems thinking and coordinated planning of proactive solutions (Kerr et al., **2022**; Mbow et al., **2019**; Ruane & Rosenzweig, **2018**; Sillmann et al., **2022**). If farmers and stakeholders throughout the agricultural value chain take a wait-and-see approach they may find themselves without necessary capabilities that could have been possible with early investment in long-term and transformational adaptation solutions (Rickards & Howden, **2012**). Impacts may be particularly severe in places where productivity trends are currently flat or increasing (lowering the concern of stakeholders) but may turn sharply negative in the future leading to a larger gap between adaptation needs and capacity (Ebi et al., **2016**; Kerr et al., **2022**; Sillmann et al., **2022**).

Global mitigation policymaking is largely oriented around benchmark global warming levels (GWLs) such as the 1.5°C and 2.0°C targets that are designated as upper limits in the Paris Agreement (IPCC, **2018**; UNFCCC, **2015**). At a finer scale, adaptation, risk management and the implementation of specific mitigation strategies have a distinct temporal component within dynamic natural and human systems (IPCC, **2022a**), often utilizing information drawn from climate models simulating Shared Socioeconomic Pathways and Representative Concentration Pathways (SSP-RCPs; IPCC, **2022b**; O’Neill et al., **2016**). This set of intertwined perspectives on future climate change motivated special guidance on translating between scenario/time and GWLs in the IPCC (Fischer et al., **2021**).

Journal of Quantitative Spectroscopy and Radiative Transfer, vol. 315, 108849, doi:10.1016/j.jqsrt.2023.108849

Unifying radiative transfer models in computer graphics and remote sensing, Part II: A differentiable, polarimetric forward model and validation.

Salesin, K., K.D. Knobelspiesse[1], **J. Chowdhary**[2,3], P.-W. Zhai, and W. Jarosz, 2024

NASA Goddard Space Flight Center, Greenbelt, MD, USA[1]
NASA Goddard Institute for Space Studies, New York, NY, USA[2]
Department of Applied Physics and Applied Mathematics, Columbia University, New York, NY, USA[3]

Abstract. The constellation of Earth-observing satellites continuously collects measurements of scattered radiance, which must be transformed into geophysical parameters in order to answer fundamental scientific questions about the Earth. Retrieval of these parameters requires highly flexible, accurate, and fast forward and inverse radiative transfer models. Existing forward models used by the remote sensing community are typically accurate and fast, but sacrifice flexibility by assuming the atmosphere or ocean is composed of plane-parallel layers. Monte Carlo forward models can handle more complex scenarios such as 3D spatial heterogeneity but are relatively slower. We propose looking to the computer graphics community for inspiration to improve the statistical efficiency of Monte Carlo forward models and explore new approaches to inverse models for remote sensing. In Part 2 of this work, we demonstrate that Monte Carlo forward models in computer graphics are capable of sufficient accuracy for remote sensing by extending Mitsuba 3, a forward and inverse modeling framework recently developed in the computer graphics community, to simulate simple atmosphere-ocean systems and show that our framework is capable of achieving error on par with codes currently used by the remote sensing community on benchmark results.

Introduction. In Part 1 of this work, we examined the history and current state of the art in radiative transfer models in computer graphics and remote sensing and established our motivation for importing knowledge from computer graphics. In this paper, we take first steps toward putting these concepts into action. Our goal in this work is to develop a framework that can match the accuracy and capabilities of multi-angle, spectral, polarimetric instruments on future satellite missions and can leverage the inherent advantages of Monte-Carlo-based solvers (e.g. three-dimensional geometry and spatial heterogeneity) as well as other special techniques imported from computer graphics (see Part 1). Although in this work we primarily focus on forward modeling, a medium-term goal of our research is to explore differentiable rendering as an engine for inverse modeling. Lastly, a long-term goal of this project is to release this software for use by the remote sensing community, so flexibility and ease of use are also important considerations.

To this end, we extend a forward and inverse modeling framework recently developed in the computer graphics community, Mitsuba 3 [1], to perform simulations of interest to remote sensing. We describe the pre-existing capabilities of Mitsuba 3 and its unique advantages in Section 2 and our extensions to it in Section 3. Lastly, we validate our framework on recent benchmark tests of simple atmosphere-ocean systems that conform to the plane-parallel layers assumption in Section 4 and show that our framework is capable of the accuracy expected for forward models in remote sensing. We plan to apply our framework to three-dimensional spatially varying media in future work.

Journal of Quantitative Spectroscopy and Radiative Transfer, vol. 314, 108847, doi:10.1016/j.jqsrt.2023.108847

Unifying radiative transfer models in computer graphics and remote sensing, Part I: A survey.

Salesin, K., K.D. Knobelspiesse[1], **J. Chowdhary**[2,3], P.-W. Zhai, and W. Jarosz, 2024

NASA Goddard Space Flight Center, Greenbelt, MD, USA[1]
NASA Goddard Institute for Space Studies, New York, NY, USA[2]
Department of Applied Physics and Applied Mathematics, Columbia University, New York, NY, USA[3]

Abstract. The constellation of Earth-observing satellites continuously collects measurements of scattered radiance, which must be transformed into geophysical parameters in order to answer fundamental scientific questions about the Earth. Retrieval of these parameters requires highly flexible, accurate, and fast forward and inverse radiative transfer models. Existing forward models used by the remote sensing community are typically accurate and fast, but sacrifice flexibility by assuming the atmosphere or ocean is composed of plane-parallel layers. Monte Carlo forward models can handle more complex scenarios such as 3D spatial heterogeneity but are relatively slower. We propose looking to the computer graphics community for inspiration to improve the statistical efficiency of Monte Carlo forward models and explore new approaches to inverse models for remote sensing. In Part 1 of this work, we examine the evolution of radiative transfer models in computer graphics and highlight recent advancements that have the potential to push forward models in remote sensing beyond their current periphery of realism.

Introduction. Light collected by sensors observing the Earth's atmosphere and oceans can provide enormous insight into the chemical, physical, and biological processes occurring within. In order to dissect the contributions of such processes to sensor measurements, accurate simulations of how light interacts with real-world phenomena must be developed. To illustrate the immensity of this task, consider that fully accurate simulations of atmosphere–ocean systems must account for scattering and absorption by gases, water droplets, and particulates (aerosols) in the atmosphere; scattering and absorption by gases, liquids, particulates, and organisms in the ocean; scattering at the ocean surface, which may be sprinkled with white caps or sea ice; as well as fluorescence and phosphorescence caused by biological processes. Simulations must also match the capabilities of the sensor to capture angular, spectral, and polarized properties of incoming light. Lastly, these simulations must be computationally efficient — although there is some leeway to sacrifice speed for complexity or vice versa.

In order to be useful to the scientific community, sensor measurements of light must be transformed via simulation into atmospheric or oceanic parameters such as ocean surface roughness; chlorophyll-*a* concentration in the ocean; phase, height, optical thickness, and droplet radius of clouds; and shape, refractive index, optical depth, and vertical distribution of aerosols [1]. The retrieval of all parameters at once for a snapshot of place and time would be ideal, as it would capture their optically interrelated nature. However, this goal is not currently achievable due to both insufficient information per "snapshot" and the limitations of existing retrieval algorithms. More information can be gathered by developing more accurate or more advanced hardware, e.g. sampling more wavelengths in the visible, ultraviolet, and infrared range, sampling multiple viewing angles of the Earth, or detecting the polarization state and angle of incoming light. Many of these enhancements will be added to the instruments on NASA's upcoming Plankton, Aerosol, Cloud, ocean Ecosystem (PACE) mission [2]: the Ocean Color Instrument (OCI) [3], a hyperspectral radiometer, and the Spectro-Polarimeter for Planetary Exploration (SPEXone) [4], [5] and Hyper Angular Rainbow Polarimeter (HARP2) [5], [6], multi-angle polarimeters of different angular and spectral resolutions. In order to harness the unprecedented volume and richness of incoming data to its full potential, more advanced remote sensing algorithms must be developed.

Journal of Atmospheric and Oceanic Technology, vol. 41, issue no. 2, pp. 189-201, doi:10.1175/JTECH-D-23-0001.1

Maximizing the volume of collocated data from two coordinated suborbital platforms.

Schlosser, J.S.[1], R. Bennett, **B. Cairns[2]**, G. Chen[1], B.L. Collister[1], J.W. Hair[1], M. Jones, M.A. Shook[1], A. Sorooshian, K.L. Thornhill[1], L.D. Ziemba[1], and S. Stamnes[1], 2024

NASA Langley Research Center, Hampton, Virginia, USA[1]
NASA Goddard Institute for Space Studies, New York, NY, USA[2]

Abstract. Suborbital (e.g., airborne) campaigns that carry advanced remote sensing and in situ payloads provide detailed observations of atmospheric processes but can be challenging to use when it is necessary to geographically collocate data from multiple platforms that make repeated observations of a given geographic location at different altitudes. This study reports on a data collocation algorithm that maximizes the volume of collocated data from two coordinated suborbital platforms and demonstrates its value using data from the NASA Aerosol Cloud Meteorology Interactions Over the western Atlantic Experiment (ACTIVATE) suborbital mission. A robust data collocation algorithm is critical for the success of the ACTIVATE mission goal to develop new and improved remote sensing algorithms and quantify their performance. We demonstrate the value of these collocated data to quantify the performance of a recently developed vertically resolved lidar + polarimeter–derived aerosol particle number concentration (N_a) product, resulting in a range-normalized mean absolute deviation (NMAD) of 9% compared to in situ measurements. We also show that this collocation algorithm increases the volume of collocated ACTIVATE data by 21% compared to using only nearest-neighbor finding algorithms alone. Additional to the benefits demonstrated within this study, the data files and routines produced by this algorithm have solved both the critical collocation and the collocation application steps for researchers who require collocated data for their own studies. This freely available and open-source collocation algorithm can be applied to future suborbital campaigns that, like ACTIVATE, use multiple platforms to conduct coordinated observations, e.g., a remote sensing aircraft together with in situ data collected from suborbital platforms.

Introduction. Advanced suborbital remote sensing instruments such as multiangle, multispectral polarimeters and multispectral lidar are increasingly used for observations of meteorological, gas, aerosol particle, and cloud properties in the atmosphere. Over the past decade, National Aeronautics and Space Administration (NASA) remote sensing instruments have been deployed in numerous suborbital campaigns that feature multiple aircraft platforms encompassing in situ and remote sensing measurements. This increasing trend of using multiple aircraft is born of the need to both validate remote sensor measurements and retrievals and the need to leverage the strengths of both remote sensing instruments and in situ instruments in studies of the atmosphere.

To leverage data gathered from multiple coordinated aircraft platforms, the data must be collocated. Following the defined convention established by previous works, “collocation” is defined as the act of matching data gathered from separate measurement platforms using predetermined spatial distance and measurement time difference thresholds (Finlon et al. 2022). The exact spatiotemporal threshold that is appropriate for collocating data depends on the type of processes that are of interest. Furthermore, instruments can have either single-pixel swath (i.e., along-track only) or multipixel swath, differing pixel resolutions, and collect data from one-dimensional (1D) point-like in situ data or single-pixel polarimeter data (e.g., x), to 2D image or lidar data (e.g., x, z or x, y), to 3D radar data (e.g., x, y, z), where x is latitude, y is longitude, and z is altitude or depth.

This study aims to add to the traditional methods used for nearest-neighbor finding problems by searching for multiple discrete time segments rather than finding the k nearest neighbors of the entire dataset. This study uses simple brute-force nearest-neighbor finding to serve as the method for nearest-neighbor finding, but there are two possible methods that can be used to optimize the nearest-neighbor finding method process.

Eos, vol. 105, on-line, doi:10.1029/2024EO240514

Lessons learned from running a virtual global workshop.

Schmidt, G.A.[1], J. Arblaster, **K.D. Mankoff**[1,2], A. Pauling, and Q. Li, 2024

NASA Goddard Institute for Space Studies, New York, NY, USA[1]
Autonomic Integra, LLC, Institute for Space Studies, New York, NY, USA[2]

Abstract. The world of academic workshops and conferences is changing. Constrained budgets for meeting organizers and attendees, postpandemic reluctance to travel, concerns about environmental footprints, and the need to be more inclusive are all motivating efforts, including in the sciences, to find workable alternatives to in-person gatherings [Kremser et al., 2024; Fraser and Mancl, 2024]. Meanwhile, widespread access to improved communication technology and the availability of an ever-growing set of online tools are increasingly making remote workshops more viable and effective than in the recent past.

Introduction. Online events are particularly attractive for geographically dispersed groups of participants and—because there is no need to work out location-based logistics—for meeting organizers facing tight constraints on the lead time available for planning. Online events, though they have their own challenges, can also minimize the time commitment for attendees and can enable inclusion of a broader group of perspectives, including in multidisciplinary workshops bringing together experts from different fields.

We are a group of Earth scientists, including modelers and observationalists, interested in quantifying and understanding the impacts of the increasing volumes of meltwater flowing into the ocean from the Greenland and Antarctic ice sheets. This meltwater affects the ocean through sea level and density changes, which can have wider impacts on the climate through ocean temperatures and sea ice changes. Data on these fluxes will be an important input for climate models, such as those used in the Coupled Model Intercomparison Project (CMIP), a vital source of input for international and national climate assessments.

In late 2023, with a looming deadline for submitting input data for the next round of CMIP, we recognized the need for a rapid coordinated global effort to produce datasets characterizing historical freshwater fluxes to support these models. (The deadline was originally in April 2024, although it was subsequently pushed back.) In response, we organized a virtual workshop, held 11–13 February 2024, to gather contributions from a global group of experts. The novel format offered many benefits and was successful, although participant feedback pointed to possible improvements.

Nature, vol. 627, 467, doi:10.1038/d41586-024-00816-z

Climate models can't explain 2023's huge heat anomaly — We could be in uncharted territory.

Schmidt, G.A.[1], 2024

NASA Goddard Institute for Space Studies, New York, NY, USA[1]

Abstract. When I took over as the director of NASA's Goddard Institute for Space Studies, I inherited a project that tracks temperature changes since 1880. Using this trove of data, I've made climate predictions at the start of every year since 2016. It's humbling, and a bit worrying, to admit that no year has confounded climate scientists' predictive capabilities more than 2023 has.

For the past nine months, mean land and sea surface temperatures have overshot previous records each month by up to 0.2 °C — a huge margin at the planetary scale. A general warming trend is expected because of rising greenhouse-gas emissions, but this sudden heat spike greatly exceeds predictions made by statistical climate models that rely on past observations. Many reasons for this discrepancy have been proposed but, as yet no combination of them has been able to reconcile our theories with what has happened.

Introduction. For a start, prevalent global climate conditions one year ago would have suggested that a spell of record-setting warmth was unlikely. Early last year, the tropical Pacific Ocean was coming out of a three-year period of La Niña, a climate phenomenon associated with the relative cooling of the central and eastern Pacific Ocean. Drawing on precedents when similar conditions prevailed at the beginning of a year, several climate scientists, including me, put the odds of 2023 turning out to be a record warm year at just one in five.

El Niño — the inverse of La Niña — causes the eastern tropical Pacific Ocean to warm up. This weather pattern set in only in the second half of the year, and the current spell is milder than similar events in 1997–98 and 2015–16.

However, starting last March, sea surface temperatures in the North Atlantic Ocean began to shoot up. By June, the extent of sea ice around Antarctica was by far the lowest on record. Compared with the average ice cover between 1981 and 2010, a patch of sea ice roughly the size of Alaska was missing. The observed temperature anomaly has not only been much larger than expected, but also started showing up several months before the onset of El Niño.

So, what might have caused this heat spike? Atmospheric greenhouse-gas levels have continued to rise, but the extra load since 2022 can account for further warming of only about 0.02 °C. Other theories put forward by climate scientists include fallout from the January 2022 Hunga Tonga–Hunga Ha'apai volcanic eruption in Tonga, which had both cooling effects from aerosols and warming ones from stratospheric water vapour, and the ramping up of solar activity in the run-up to a predicted solar maximum. But these factors explain, at most, a few hundredths of a degree in warming (Schoeberl, M. R. *et al. Geophys. Res. Lett.* **50**, e2023GL104634; 2023). Even after taking all plausible explanations into account, the divergence between expected and observed annual mean temperatures in 2023 remains about 0.2 °C — roughly the gap between the previous and current annual record.

There is one more factor that could be playing a part. In 2020, new regulations required the shipping industry to use cleaner fuels that reduce sulfur emissions. Sulfur compounds in the atmosphere are reflective and influence several properties of clouds, thereby having an overall cooling effect. Preliminary estimates of the impact of these rules show a negligible effect on global mean temperatures — a change of only a few hundredths of a degree. But reliable assessments of aerosol emissions rely on networks of mostly volunteer-driven efforts, and it could be a year or more before the full data from 2023 are available.

GeoHealth, vol. 8, issue no. 1, e2023GH000970, doi:10.1029/2023GH000970

Premature deaths due to heat exposure: The potential effects of neighborhood-level versus city-level acclimatization within US cities.

Shindell, D., R. Hunter, **G. Faluvegi**[1,2], and L. Parsons, 2024

NASA Goddard Institute for Space Studies, New York, NY, USA[1]
Center for Climate Systems Research, Columbia University, New York, NY, USA[2]

Abstract. For the population of a given US city, the risk of premature death associated with heat exposure increases as temperatures rise, but risks in hotter cities are generally lower than in cooler cities at equivalent temperatures due to factors such as acclimatization. Those living in especially hot neighborhoods within cities might therefore suffer much more than average if such adaptation is only at the city-wide level, whereas they might not experience greatly increased risk if adjustment is at the neighborhood level. To compare these possibilities, we use high spatial resolution temperature data to evaluated heat-related deaths assuming either adjustment at the city-wide or at the neighborhood scale in 10 large US cities. On average, we find that if inhabitants are adjusted to their local conditions, a neighborhood that was 10°C hotter than a cooler one would experience only about 1.0–1.5 excess heat deaths per year per 100,000 persons. By contrast, if inhabitants are acclimatized to city-wide temperatures, the hotter neighborhood would experience about 15 excess deaths per year per 100,000 persons. Using idealized analyses, we demonstrate that current city-wide epidemiological data do not differentiate between these differing adjustments. Given the very large effects of assumptions about neighborhood-level acclimatization found here, as well as the fact that current literature is conflicting on the spatial scale of acclimatization, more neighborhood-level epidemiological data are urgently needed to determine the health impacts of variations in heat exposure within urban areas, better constrain projected changes, and inform mitigation efforts.

Introduction. The existence of large variations in surface air temperatures within cities is well documented (e.g., Hsu et al., **2021**; Huang & Cadenasso, **2016**). Increased heat exposure in specific neighborhoods within urban areas is correlated with a lack of vegetation, larger fractions of areas covered in impermeable surfaces, lower socio-economic status and larger proportion of populations from minority racial groups (e.g., Benz & Burney, **2021**; Hsu et al., **2021**; Huang & Cadenasso, **2016**; Manware et al., **2022**; Parsons et al., **2023**). Exposure to heat extremes is associated with elevated risk of premature death (Ebi et al., **2021**), and therefore the health impact of increased exposures in neighborhoods with strong urban heat islands is widely assumed to be damaging (Stevens et al., **2021**) or modeled as damaging by applying the same superlinear exposure-response function to all populations in a region (Heaviside et al., **2016**).

However, epidemiological research on health outcomes is limited at the neighborhood scale. A few studies have suggested increased death rates within urban heat islands for specific cities, most often for short duration heat waves (Johnson & Wilson, **2009**; Laaidi et al., **2012**) though sometimes for longer periods (Madrigano et al., **2015**). However, others have found relationships that are quite weak in total (e.g., one excess death per million population (Lowe, **2016**)) or found no substantive relationship between urbanization levels (across urban and rural areas) and heat-related death rates (Hattis et al., **2012**). A study focused on local level adjustment found virtually no enhancement of premature heat-related death rates in urban heat island areas over many years in London, suggesting that populations had almost completely acclimatized to neighborhood-level conditions (Milojevic et al., **2016**). Hence the relationship between increased exposures, which are clearly present, and large increases in premature death rates has not been robustly characterized.

Proceedings of National Academy of Sciences of USA, vol. 121, issue no. 5, e2312832120, doi:10.1073/pnas.2312832120

Reductions in premature deaths from heat and particulate matter air pollution in South Asia, China, and the US under decarbonization.

Shindell, D., **G. Faluvegi**[1,2], E. Nagamoto, L. Parsons, and Y. Zhang, 2024

NASA Goddard Institute for Space Studies, New York, NY, USA[1]
Center for Climate Systems Research, Columbia University, New York, NY, USA[2]

Abstract. Following a sustainable development pathway designed to keep warming below 2 °C will benefit human health. We quantify premature deaths attributable to fine particulate matter ($PM_{2.5}$) air pollution and heat exposures for China, South Asia, and the United States using projections from multiple climate models under high- and low-emission scenarios. Projected changes in premature deaths are typically dominated by population aging, primarily reflecting increased longevity leading to greater sensitivity to environmental risks. Changes in $PM_{2.5}$ exposure typically have small impacts on premature deaths under a high-emission scenario but provide substantial benefits under a low-emission scenario. $PM_{2.5}$-attributable deaths increase in South Asia throughout the century under both scenarios but shift to decreases by late century in China, and US values decrease throughout the century. In contrast, heat exposure increases under both scenarios and combines with population aging to drive projected increases in deaths in all countries. Despite population aging, combined $PM_{2.5}$- and heat-related deaths decrease under the low-emission scenario by ~2.4 million per year by midcentury and ~2.9 million by century's end, with ~3% and ~21% of these reductions from heat, respectively. Intermodel variations in exposure projections generally lead to uncertainties of <40% except for US and China heat impacts. Health benefits of low emissions are larger from reduced heat exposure than improved air quality by the late 2090s in the United States. In contrast, in South and East Asia, the $PM_{2.5}$-related benefits are largest throughout the century, and their valuation exceeds the cost of decarbonization, especially in China, over the next 30 y.

Introduction. In the Paris Climate Agreement, the world's nations pledged to keep global warming below 2 °C. Achieving this goal will require a broad transition that emphasizes rapid decarbonization of the global economy along with reductions in emissions of non-CO_2 climate drivers and deforestation (1). Though the avoided climate-related damages are the obvious driver for such a transition, there will be additional benefits that are aligned with Sustainable Development Goals (1). A prominent example is the health benefits of improved air quality since much of the world's CO_2 emissions and air pollution comes from the same activities. These benefits may be particularly salient for several reasons. First, they are large at the global scale, especially those associated with (particulate matter) $PM_{2.5}$ (2). Second, they occur immediately as emissions are reduced, whereas climate-related benefits follow much more slowly (3). Third, many developing countries with historically low CO_2 emissions can rightly claim to have little leverage over the world's climate trajectory yet suffer from high levels of air pollution. These countries might therefore have more incentive to support rapid and deep decarbonization based on the air quality-related benefits than the climate-related benefits.

We therefore study the heat- and $PM_{2.5}$-related health benefits of decarbonization across several countries. Many prior studies have examined the health effects of future heat exposure (4, 5) or air pollution exposure (6–10), but there has been little work to evaluate the effects of both heat and air pollution exposure under the same scenarios. This is primarily due to the limitations of exposure–response functions (ERFs) for heat, which vary substantially by location and have until recently been available only at the city scale or for limited areas, unlike PM exposure for which globally representative functions are widely used (11). Many prior heat-related analyses have therefore studied exposure changes but not the resulting health impacts (12–15).

American Chemical Society EST Air, vol. 1, issue no. 12, pp. 1531-1540, doi:10.1021/acsestair.4c00105

The impact of decarbonization on particulate soiling of solar panels.

Shindell, D., I. Petropoulos, **G. Faluvegi**[1,2], L. Parsons, and M. Bergin, 2024

NASA Goddard Institute for Space Studies, New York, NY, USA[1]
Center for Climate Systems Research, Columbia University, New York, NY, USA[2]

Abstract. Climate researchers have examined many impacts of climate change on energy supply and demand under various scenarios. However, the effect of changing particulate deposition onto solar panel surfaces on solar power production efficiency (i.e., soiling) has not been studied. We therefore characterize probabilistic outcomes across multiple climate models and scenarios. We find large current regional losses (up to 40% without manual cleaning, up to 20% with monthly cleaning and rain removal) in generation that grow slightly under a high-emission scenario, largely due to regional increases in windblown dust. In contrast, under a low-emissions scenario, potential production increases significantly (2–8% interquartile range with only rain removal) due to reduced soiling, especially in regions of Asia and Africa where anthropogenic aerosols are major contributors to soiling. Projected changes vary widely across models in many dusty areas outside of the Sahara and Arabia. Differences can also be large in regions dominated by anthropogenic aerosols, such as Nigeria, eastern China, and northern India, where the full range across modeled potential power production changes extends from −1 to +11% for the end of the century (without manual cleaning), underscoring the need to consider multiple climate models. With large increases in projected solar power deployment, the relatively small potential production increases reported here could nevertheless represent a large dividend in additional energy production. Hence, reductions in air pollution attributable to decarbonization could provide positive feedback under which a greater deployment of solar power (or other renewables) increases the production of solar power, facilitating the transition to renewable energy.

Introduction. Authoritative assessments conducted by the Intergovernmental Panel on Climate Change (IPCC) have concluded that achieving the world's climate goals requires a phase out of unabated fossil fuel combustion by around midcentury. (1,2) Though the primary aim of such a transition is mitigating warming, phasing out fossil fuels would also have enormous effects on air pollution both directly via emissions reductions and indirectly via climate change-induced alterations in factors such as windblown dust. Changes in particulates will have unintended, but potentially important, consequences for solar power generation. Specifically, soiling of solar panels by air pollution and dust will vary, depending upon the emissions from nations around the world. A world with rapid decarbonization would be expected to have markedly less air pollution, leading to reduced losses in solar power generation due to soiling. This may become especially important because providing adequate energy supplies during the fossil fuel phase-out typically relies on massive increases in the deployment of renewables. (1,2) For example, the International Energy Agency (IEA) projects a need for a 20-fold increase in solar power under their net zero by 2050 scenario. (3) We therefore examine how changing particulate deposition under different future scenarios (i.e., high and low emission pathways) will affect solar power production.

We use simulations from the latest climate model intercomparison project (Coupled Model Intercomparison Project's sixth phase or CMIP6) to characterize the distribution of potential futures. We assess differences among CMIP6 models because these models show substantial spread in projected changes in fine particulate matter, (4−7) which as we show can lead to substantially different outcomes in solar power generation. Future projected deposition of particulate matter from CMIP6 models is used as input to a model that estimates how deposited particles affect solar power production, (8) to which we add modest improvements (Methods). To explore a wide range of future possibilities, we examine low- and high-emissions scenarios.

Frontiers in Science, vol. 2, 1349770, doi:10.3389/fsci.2024.1349770

The methane imperative.

Shindell, D., P. Sadavarte, I. Aben, T. de Oliveira Bredariol, G. Dreyfus, L. Höglund-Isaksson, B. Poulter[1], M. Saunois, **G.A. Schmidt[2]**, S. Szopa, K. Rentz, L. Parsons, Z. Qu, **G. Faluvegi[2,3]**, and J.D. Maasakkers, 2024

NASA Goddard Space Flight Center, Greenbelt, MD, USA[1]
NASA Goddard Institute for Space Studies, New York, NY, USA[2]
Center for Climate Systems Research, Columbia University, New York, NY, USA[3]

Abstract. Anthropogenic methane (CH_4) emissions increases from the period 1850–1900 until 2019 are responsible for around 65% as much warming as carbon dioxide (CO_2) has caused to date, and large reductions in methane emissions are required to limit global warming to 1.5°C or 2°C. However, methane emissions have been increasing rapidly since ~2006. This study shows that emissions are expected to continue to increase over the remainder of the 2020s if no greater action is taken and that increases in atmospheric methane are thus far outpacing projected growth rates. This increase has important implications for reaching net zero CO_2 targets: every 50 Mt CH_4 of the sustained large cuts envisioned under low-warming scenarios that are not realized would eliminate about 150 Gt of the remaining CO_2 budget. Targeted methane reductions are therefore a critical component alongside decarbonization to minimize global warming. We describe additional linkages between methane mitigation options and CO_2, especially via land use, as well as their respective climate impacts and associated metrics. We explain why a net zero target specifically for methane is neither necessary nor plausible. Analyses show where reductions are most feasible at the national and sectoral levels given limited resources, for example, to meet the Global Methane Pledge target, but they also reveal large uncertainties. Despite these uncertainties, many mitigation costs are clearly low relative to real-world financial instruments and very low compared with methane damage estimates, but legally binding regulations and methane pricing are needed to meet climate goals.

Introduction. Worldwide efforts to limit climate change are rightly focused on carbon dioxide (CO_2), the primary driver (1). However, since humanity has failed to adequately address climate change for several decades, keeping warming below agreed goals now requires that we address all major climate pollutants. Methane is the second most important greenhouse gas driving climate change. Out of a total observed warming of 1.07°C during the period 2010 to 2019, the Working Group I (WGI) 2021 Intergovernmental Panel on Climate Change (IPCC) Sixth Assessment Report (AR6) attributed 0.5°C to methane emissions (1). However, in many respects, methane mitigation has been neglected relative to CO_2. For example, only ~2% of global climate finance is estimated to go towards methane abatement (2). Similarly, only about 13% of global methane emissions are covered by current policy mechanisms (3). With dramatic climate changes already occurring and methane providing substantial leverage to slow warming in the near future and reduce surface ozone pollution, political will to mitigate methane has recently increased, especially following the Global Methane Assessment (GMA) published by the United Nations Environment Programme (UNEP) and the Climate and Clean Air Coalition (CCAC) in May 2021 (4). The Assessment showed that reducing methane was an extremely cost-effective way to rapidly slow warming and contribute to climate stabilization while also providing large benefits to human health, crop yield, and labor productivity. The GMA also demonstrated that various technical and behavioral options were currently available to achieve such emission cuts. Drawing upon that Assessment and related analysis (5), the United States and European Union launched the Global Methane Pledge (GMP) in November 2021 at the 26th Conference of the Parties to the United Nations Framework Convention on Climate Change (COP26), under which countries set a collective goal of reducing anthropogenic methane emissions by at least 30% (relative to 2020 levels) by 2030. By COP28 in November 2023, participation in the GMP had increased to 155 countries that collectively account for more than half of global anthropogenic methane emissions.

Frontiers in Climate, vol. 6, 1499765, doi:10.3389/fclim.2024.1499765

Climate extremes and risks: links between climate science and decision-making.

Sillmann, J., T.H. Raupach, K.L. Findell, M. Donat, L.M. Alves, L. Alexander, L. Borchert, P.B. de Amorim, C. Buontempo, E.M. Fischer, C.L. Franzke, B. Guan, M. Haasnoot, E. Hawkins, D. Jacob, R. Mahon, D. Maraun, M.A. Morrison, B. Poschlod, **A.C. Ruane**[1], Shampa, T. Stephenson, N. van der Wel, Z. Wang, X. Zhang, and J. Županić, 2024

NASA Goddard Institute for Space Studies, New York, NY, USA[1]

Abstract. The World Climate Research Programme (WCRP) envisions a future where actionable climate information is universally accessible, supporting decision makers in preparing for and responding to climate change. In this perspective, we advocate for enhancing links between climate science and decision-making through a better and more decision-relevant understanding of climate impacts. The proposed framework comprises three pillars: climate science, impact science, and decision-making, focusing on generating seamless climate information from sub-seasonal, seasonal, decadal to century timescales informed by observed climate events and their impacts. The link between climate science and decision-making has strengthened in recent years, partly owing to undeniable impacts arising from disastrous weather extremes. Enhancing decision-relevant understanding involves utilizing lessons from past extreme events and implementing impact-based early warning systems to improve resilience. Integrated risk assessment and management require a comprehensive approach that encompasses good knowledge about possible impacts, hazard identification, monitoring, and communication of risks while acknowledging uncertainties inherent in climate predictions and projections, but not letting the uncertainty lead to decision paralysis. The importance of data accessibility, especially in the Global South, underscores the need for better coordination and resource allocation. Strategic frameworks should aim to enhance impact-related and open-access climate services around the world. Continuous improvements in predictive modeling and observational data are critical, as is ensuring that climate science remains relevant to decision makers locally and globally. Ultimately, fostering stronger collaborations and dedicated investments to process and tailor climate data will enhance societal preparedness, enabling communities to navigate the complexities of a changing climate effectively.

Introduction. Global warming is causing a wide range of weather and climate extremes to become more frequent, intense and widespread (Seneviratne et al., 2021). Every region of the world is experiencing changes in climatic impact-drivers, such as heatwaves, floods, droughts, fire weather, sea level rise, and storm surges (IPCC AR6 2021, 2022). Climate change will continue to cause unprecedented extreme events, such as record-breaking heat waves (Fischer et al., 2021), and will lead to increases in the occurrence of compound events (Raymond et al., 2022). We are thus challenged with “imagining the unimaginable” for better risk preparedness and management.

The World Climate Research Programme (WCRP) envisions a future in which actionable climate information is available for all regions of the world, with climate services providing decision makers with tools enabling them to prepare for, respond to, and build resilience to climate change alongside reducing anthropogenic emissions. Weather and climate information is crucial for climate risk management, as well as for adaptation and mitigation, and needs to be made (or remain) accessible for everyone. The quickly evolving field of climate services is concerned with making climate information accessible and useful to decision makers (Jacob et al., 2024), but there is no one-size-fits-all approach to climate services. Context, user involvement, and collaboration among scientists, practitioners, and users determine the type and usefulness of climate services for adaptation, mitigation, and risk management (Ranasinghe et al., 2021).

Earth System Dynamics, vol. 15, issue no. 6, pp. 1591-1608, doi:10.5194/esd-15-1591-2024

AERA-MIP: Emission pathways, remaining budgets and carbon cycle dynamics compatible with 1.5°C and 2°C global warming stabilization.

Silvy, Y., T.L. Frölicher, J. Terhaar, F. Joos, F.A. Burger, F. Lacroix, M. Allen, R. Bernadello, L. Bopp, V. Brovkin, J.R. Buzan, P. Cadule, M. Dix, J. Dunne, P. Friedlingstein, G. Georgievski, T. Hajima, S. Jenkins, M. Kawamiya, **N.Y. Kiang**[1], V. Lapin, D. Lee, **P. Lerner**[1,2], N. Mengis, E.A. Monteiro, D. Paynter, G.P. Peters, **A. Romanou**[1,2], J. Schwinger, S. Sparrow, E. Stofferahn, J. Tjiputra, E. Tourigny, and T. Ziehn, 2024

NASA Goddard Institute for Space Studies, New York, NY, USA[1]
Applied Physics and Applied Mathematics, Columbia University, New York, NY, USA[2]

Abstract. While international climate policies now focus on limiting global warming to well below 2 °C or pursuing a 1.5 °C level of global warming, the climate modelling community has not provided an experimental design in which all Earth system models (ESMs) converge and stabilize at the same prescribed global warming levels. This gap hampers accurate estimations based on comprehensive ESMs of the carbon emission pathways and budgets needed to meet such agreed warming levels and of the associated climate impacts under temperature stabilization. Here, we apply the Adaptive Emission Reduction Approach (AERA) with ESMs to provide such simulations in which all models converge at 1.5 and 2.0 °C warming levels by adjusting their emissions over time. These emission-driven simulations provide a wide range of emission pathways and resulting atmospheric CO_2 projections for a given warming level, uncovering uncertainty ranges that were previously missing in the traditional Coupled Model Intercomparison Project (CMIP) scenarios with prescribed greenhouse gas concentration pathways. Meeting the 1.5 °C warming level requires a 40 % (full model range: 7 % to 76 %) reduction in multi-model mean CO_2-forcing-equivalent (CO_2-fe) emissions from 2025 to 2030, a 98 % (57 % to 127 %) reduction from 2025 to 2050, and a stabilization at 1.0 (−1.7 to 2.9) PgC yr^{-1} from 2100 onward after the 1.5 °C global warming level is reached. Meeting the 2.0 °C warming level requires a 47 % (8 % to 92 %) reduction in multi-model mean CO_2-fe emissions until 2050 and a stabilization at 1.7 (−1.5 to 2.7) PgC yr^{-1} from 2100 onward. The on-average positive emissions under stabilized global temperatures are the result of a decreasing transient climate response to cumulative CO_2-fe emissions over time under stabilized global warming. This evolution is consistent with a slightly negative zero emissions commitment – initially assumed to be zero – and leads to an increase in the post-2025 CO_2-fe emission budget by a factor of 2.2 (−0.8 to 6.9) by 2150 for the 1.5 °C warming level and a factor of 1.4 (0.9 to 2.4) for the 2.0 °C warming level compared to its first estimate in 2025. The median CO_2-only carbon budget by 2150, relative to 2020, is 800 $GtCO_2$ for the 1.5 °C warming level and 2250 $GtCO_2$ for the 2.0 °C warming level. These median values exceed the median IPCC AR6 estimates by 60 % for the 1.5 °C warming level and 67 % for 2.0 °C. Some of the differences may be explained by the choice of the mitigation scenario for non-CO_2 radiative agents. Our simulations highlight shifts in carbon uptake dynamics under stabilized temperature, such as a cessation of the carbon sinks in the North Atlantic and in tropical forests. On the other hand, the Southern Ocean remains a carbon sink centuries after temperatures stabilize. Overall, this new type of warming-level-based emission-driven simulation offers a more coherent assessment across climate models and opens up a wide range of possibilities for studying both the carbon cycle and climate impacts, such as extreme events, under climate stabilization.

Introduction. Climate goals outlined in international policies, such as the 2015 Paris Agreement (UNFCCC, 2015), primarily focus on global warming levels. The Paris Agreement in particular aims to hold “the increase in the global average temperature to well below 2 °C above pre-industrial levels” and to pursue efforts “to limit the temperature increase to 1.5 °C above pre-industrial levels”. Global warming levels are chosen in international policies as they are often directly correlated to global and regional impacts of climate change (Seneviratne et al., 2016; IPCC, 2018). Hence, each fraction of avoided warming reduces risks for humans and ecosystems (IPCC, 2022).

Atmospheric Measurement Techniques, vol. 17, issue no. 9, pp. 2739-2759, doi:10.5194/amt-17-2739-2024

Retrievals of aerosol optical depth over the western North Atlantic Ocean during ACTIVATE.

Siu, L.W., J.S. Schlosser[1,2], D. Painemal[1], **B. Cairns[3]**, M.A. Fenn[1], R.A. Ferrare[1], J.W. Hair,[1] C.A. Hostetler, L. Li, M.M. Kleb[1], A.J. Scarino[1], T.J. Shingler[1], A. Sorooshian, S.A. Stamnes[1], and X. Zeng, 2024

NASA Langley Research Center, Hampton, Virginia, USA[1]
NASA Postdoctoral Program, NASA Langley Research Center, Hampton, Virginia, USA[2]
NASA Goddard Institute for Space Studies, New York, NY, USA[3]

Abstract. Aerosol optical depth was retrieved from two airborne remote sensing instruments, the Research Scanning Polarimeter (RSP) and Second Generation High Spectral Resolution Lidar (HSRL-2), during the National Aeronautics and Space Administration (NASA) Aerosol Cloud meTeorology Interactions oVer the western ATlantic Experiment (ACTIVATE). The field campaign offers a unique opportunity to evaluate an extensive 3-year dataset under a wide range of meteorological conditions from two instruments on the same platform. However, a long-standing issue in atmospheric field studies is that there is a lack of reference datasets for properly validating field measurements and estimating their uncertainties. Here we address this issue by using the triple collocation method, in which a third collocated satellite dataset from the Moderate Resolution Imaging Spectroradiometer (MODIS) is introduced for comparison. HSRL-2 is found to provide a more accurate retrieval than RSP over the study region. The error standard deviation of HSRL-2 with respect to the ground truth is 0.027. Moreover, this approach enables us to develop a simple, yet efficient, quality control criterion for RSP data. The physical reasons for the differences in two retrievals are determined to be cloud contamination, aerosols near the surface, multiple aerosol layers, absorbing aerosols, non-spherical aerosols, and simplified retrieval assumptions. These results demonstrate the pathway for optimal aerosol retrievals by combining information from both lidars and polarimeters for future airborne and satellite missions.

Introduction. Aerosol particles constitute an important component of the Earth's atmosphere by altering its radiative energy balance. Aerosols impact our climate system directly by scattering and absorbing solar and terrestrial radiation and indirectly by serving as cloud condensation nuclei (CCN) and ice nuclei (IN) (Lohmann and Feichter, 2005; Pöschl, 2005). Changing CCN and IN concentrations can influence the distribution of liquid water, ice, and mixed-phase clouds and the frequency of precipitation. The complex interaction of aerosols with clouds, radiation, and meteorology makes it difficult to probe the feedback and response of our climate system under a perturbation of anthropogenic or natural aerosols (Bellouin et al., 2020; Chen et al., 2014). In the most recent Sixth Assessment Report (AR6) of the Intergovernmental Panel on Climate Change (IPCC), aerosols still represent the largest uncertainty in the global radiative forcing (IPCC, 2023).

To disentangle aerosol–cloud interactions, it is imperative to collect adequate observations for robust statistics across a wide range of cloud regimes. The recent Aerosol Cloud meTeorology Interactions oVer the western ATlantic Experiment (ACTIVATE) epitomizes a coordinated effort to respond to this need (Sorooshian et al., 2023). Being one of the National Aeronautics and Space Administration (NASA) Earth Venture Suborbital-3 (EVS-3) missions, ACTIVATE has three objectives:

- first, to quantify the underlying relationship between the aerosol number concentration, CCN concentration, and cloud drop number concentration;
- second, to develop a better process-level representation of cloud properties and aerosol–cloud interactions in a hierarchy of numerical models;
- finally, to evaluate state-of-the-art remote sensing instruments that are built for retrieving the aerosol and cloud properties (Sorooshian et al., 2019).

Frontiers in Remote Sensing, vol. 5, 1395442, doi:10.3389/frsen.2024.1395442

Summarizing multiple aspects of triple collocation analysis in a single diagram.

Siu, L.W., X. Zeng, A. Sorooshian, **B. Cairns**[1], R.A. Ferrare[2], J.W. Hair[2], C.A. Hostetler[2], D. Painemal[2], and J.S. Schlosser[2], 2024

NASA Goddard Institute for Space Studies, New York, NY, USA[1]
NASA Langley Research Center, Hampton, Virginia, USA[2]

Abstract. With the ongoing expansion of global observation networks, it is expected that we shall routinely analyze records of geophysical variables such as temperature from multiple collocated instruments. Validating datasets in this situation is not a trivial task because every observing system has its own bias and noise. Triple collocation is a general statistical framework to estimate the error characteristics in three or more observational-based datasets. In a triple colocation analysis, several metrics are routinely reported but traditional multiple-panel plots are not the most effective way to display information. A new formula of error variance is derived for connecting the key terms in the triple collocation theory. A diagram based on this formula is devised to facilitate triple collocation analysis of any data from observations, as illustrated using three aerosol optical depth datasets from the recent Aerosol Cloud meTeorology Interactions oVer the western ATlantic Experiment (ACTIVATE). An observational-based skill score is also derived to evaluate the quality of three datasets by taking into account both error variance and correlation coefficient. Several applications are discussed, and sample plotting routines are provided.

Introduction. The development of atmospheric sciences and other branches of Earth system science is inextricably linked to our capability of improving and expanding current atmospheric observing systems (Crutzen and Ramanathan, 2000; Stith et al., 2018; Bluestein et al., 2022). For instance, a dense weather station network provides us with synoptic weather conditions while sounding profiles from radiosondes and dropsondes give us a wealth of information for the vertical structure of the atmosphere over land and ocean (Stith et al., 2018). In addition to *in situ* observations, remotely sensed instruments such as weather radars are able to detect severe weather systems in a timely manner. The advent of satellite meteorology has reshaped our data inventory by making global observations possible (Atlas, 1997). Research aircraft in field campaigns provides a unique platform to collect measurements from both *in situ* and remotely sensed instruments for specific research problems with pressing societal needs (Bluestein et al., 2022).

With more and more new observing systems available, it has become commonplace for more than one instrument observing the same geophysical variable at the same location. Data validation and calibration then become necessary because no observing systems are perfectly built. Stoffelen (1998) recognized this issue and proposed a general statistical framework called triple collocation. For any geophysical variables, triple collocation estimates the error characteristics of three independent datasets without requiring any dataset being the ground truth. Since then, the method has been applied to a wide range of variables such as soil moisture (e.g., Dorigo et al., 2010), sea surface temperature (e.g., O'Carroll et al., 2008), and leaf area index (e.g., Fang et al., 2012), to name a few. The theory of triple collocation has also been clarified, tested, and extended over the years (e.g., Zwieback et al., 2012; Draper et al., 2013; McColl et al., 2014; Su et al., 2014; Yilmaz and Crow, 2014; Gruber et al., 2016; Tsamalis, 2022).

Several performance metrics such as standard error (Stoffelen, 1998) and correlation coefficient (McColl et al., 2014) have been developed for triple collocation analysis. These metrics are usually reported in the form of a map that shows one aspect such as a metric for one dataset (e.g., Dorigo et al., 2010) or a figure that shows another aspect for three datasets (e.g., Tsamalis, 2022). Multiple-panel plots are common in the literature (e.g., McColl et al., 2014; Deng et al., 2023) and some examples are given in Supplementary Material. But this kind of plot is not the most effective way to summarize results. A table that shows multiple aspects may help but different researchers have varying designs and notations (e.g., Su et al., 2014).

The Planetary Science Journal, vol. 5, 175, doi:10.3847/PSJ/ad5830

The CUISINES framework for conducting exoplanet model intercomparison projects, version 1.0.

Sohl, L.E., T.J. Fauchez[3,4], S. Domagal-Goldman, D.A. Christie, R. Deitrick, J. Haqq-Misra, C.E. Harman[5], N. Iro, N.J. Mayne, **K. Tsigaridis[1,2,3]**, G.L. Villanueva[3,4], A.V. Young[3,4], and G. Chaverot, 2024

NASA Goddard Institute for Space Studies, New York, NY, USA[1]
Center for Climate Systems Research, Columbia University, New York, NY, USA[2]
NASA GSFC Sellers Exoplanet Environments Collaboration, USA[3]
NASA Goddard Space Flight Center, Greenbelt, MD, USA[4]
NASA Ames Research Center, Moffet Field, CA, USA[5]

Abstract. As JWST begins to return observations, it is more important than ever that exoplanet climate models can consistently and correctly predict the observability of exoplanets, retrieval of their data, and interpretation of planetary environments from that data. Model intercomparisons play a crucial role in this context, especially now when few data are available to validate model predictions. The CUISINES Working Group of NASA's Nexus for Exoplanet Systems Science supports a systematic approach to evaluating the performance of exoplanet models and provides here a framework for conducting community-organized exoplanet model intercomparison projects (exoMIPs). The CUISINES framework adapts Earth climate community practices specifically for the needs of the exoplanet researchers, encompassing a range of model types, planetary targets, and parameter space studies. It is intended to help researchers to work collectively, equitably, and openly toward common goals. The CUISINES framework rests on five principles: (1) define in advance what research question(s) the exoMIP is intended to address, (2) create an experimental design that maximizes community participation and advertise it widely, (3) plan a project timeline that allows all exoMIP members to participate fully, (4) generate data products from model output for direct comparison to observations, and (5) create a data management plan that is workable in the present and scalable for the future. Within the first years of its existence, CUISINES is already providing logistical support to 10 exoMIPs and will continue to host annual workshops for further community feedback and presentation of new exoMIP ideas.

Introduction. Since the first exoplanet orbiting a main-sequence star was discovered (Mayor & Queloz 1995), the existence of nearly 5600 exoplanets has been confirmed, with over 7500 additional exoplanets awaiting confirmation 13 and the promise of many more discoveries to come from missions such as JWST and the future Habitable Exoplanet Observatory (National Academies of Sciences, Engineering, and Medicine 2023). It is clear even from basic demographics of bulk quantities such as mass and radius that exoplanets are extremely diverse. Not surprisingly, planetary scientists and astrobiologists are eager to explore the "climates" of these worlds—everything from determining the impacts of atmosphere compositions and stellar spectra on global mean temperatures, to the potential for habitable surfaces on rocky planets, to the intricacies of atmospheric (and oceanic) circulation on worlds of all kinds. A full range of atmosphere and related models is available: radiative transfer and retrieval models, 1D radiative–convective equilibrium models (RCEs), energy balance models (EBMs), models of intermediate complexity (MICs), and 3D general circulation models (GCMs). Some of these models were developed specifically for exoplanets. Others have been generalized for broader use from models developed for modern Earth; "recent" (from an astronomical perspective) paleo-Earth, i.e., oxygenated atmospheres of the past several 10^8 yr; and early Earth, marked by habitable conditions and anoxygenic atmospheres (Nisbet & Sleep 2001). With so many exoplanets to simulate, a plethora of models to choose from, and so few data to provide constraints, the planetary science community has been energized to run an ever-increasing number of experiments exploring the possible climates of particular planetary targets or the generalizable effects of stellar spectra and orbital parameters on simplified planetary surfaces such as aqua planets, land planets, and "snowball Earths."

Geophysical Research Letters, vol. 51, issue no. 11, e2024GL108663, doi:10.1029/2024GL108663

Buffering of aerosol-cloud adjustments by coupling between radiative susceptibility and precipitation efficiency.

Song, C., D.T. McCoy, T. Eidhammer, A. Gettelman, I.L. McCoy, D. Watson-Parris, C.J. Wall, **G. Elsaesser**[1,2], and R. Wood, 2024

NASA Goddard Institute for Space Studies, New York, NY, USA[1]
Department of Applied Physics and Applied Mathematics, Columbia University, New York, NY, USA[2]

Abstract. Aerosol-cloud interactions (ACI) in warm clouds are the primary source of uncertainty in effective radiative forcing (ERF) during the historical period and, by extension, inferred climate sensitivity. The ERF due to ACI (ERFaci) is composed of the radiative forcing due to changes in cloud microphysics and cloud adjustments to microphysics. Here, we examine the processes that drive ERFaci using a perturbed parameter ensemble (PPE) hosted in CAM6. Observational constraints on the PPE result in substantial constraints in the response of cloud microphysics and macrophysics to anthropogenic aerosol, but only minimal constraint on ERFaci. Examination of cloud and radiation processes in the PPE reveal buffering of ERFaci by the interaction of precipitation efficiency and radiative susceptibility.

Introduction. Aerosols play an important role in the Earth's energy budget by affecting cloud properties, surface precipitation, and radiation at the top of the atmosphere (Stephens & Ellis, 2008; Twomey, 1991). The change in reflected shortwave radiation from the pre-industrial (PI) to present day (PD) due to anthropogenic perturbations in aerosol is known as aerosol radiative forcing. The radiative forcing from aerosols has larger uncertainty than the radiative forcing from greenhouse gases (GHGs) (Bellouin et al., 2020). The uncertainty in the radiative forcing due to aerosols results in substantial uncertainty in the climate sensitivity to increased greenhouse gases that we can reconcile with the observed temperature record (Andreae et al., 2005; Bellouin et al., 2020; Forster, 2016; Sherwood et al., 2020; Watson-Parris & Smith, 2022; C. Wang, Soden, Yang, & Vecchi, 2021). Longwave radiation is neglected in this study as it has a much smaller effect on aerosol radiative forcing than that from shortwave in warm liquid cloud, but longwave can be important for high altitude, ice-phase cloud (Smith et al., 2020; Zelinka et al., 2014, 2023).

Aerosol-cloud interactions (ACI) in liquid clouds contribute the majority of aerosol forcing (Bellouin et al., 2020). ACI alters the amount of reflected shortwave radiation in liquid cloud in two ways. First, some aerosols serve as cloud condensation nuclei to form cloud droplets. The changes in droplet number concentration (N_d) from changes in CCN concentration alters the cloud reflectivity even without changes in liquid water content (Twomey, 1977). The change in reflected shortwave radiation is termed instantaneous radiative forcing due to ACI (IRFaci). Second, changes in cloud microphysical processes driven by changes in N_d may alter cloud macrophysical properties (cloud extent in space and time, and the amount of condensate in a cloud) (Ackerman et al., 2004). This is termed the cloud adjustment to aerosol. Process understanding and observations suggest that cloud adjustments could lead to increased or decreased cloud amount and optical thickness (Ackerman et al., 2004; Glassmeier et al., 2021; Toll et al., 2019; Wood, 2007). For example, a reduction in cloud droplet size could lead to the suppression of precipitation and consequently would increase cloud lifetime and condensate mass (Albrecht, 1989). Another example of a potential aerosol-cloud adjustment to increasing N_d is enhanced entrainment of dry air at cloud top due to suppressed precipitation and droplet sedimentation, and more rapid evaporation of smaller droplets. These effects enhance PBL drying and can result in reduced cloud lifetime and condensate mass (Ackerman et al., 2004; Bretherton et al., 2007; S. Wang et al., 2003; Wood, 2007).

Atmospheric Chemistry and Physics, vol. 24, issue no. 12, pp. 7421-7446, doi:10.5194/acp-24-7421-2024

Modeling impacts of dust mineralogy on Earth's radiation and climate.

Song, Q., P. Ginoux, M. Gonçalves Ageitos, **R.L. Miller**[1,2], **V. Obiso**[1], and C. Pérez García-Pando, 2024

NASA Goddard Institute for Space Studies, New York, NY, USA[1]
Department of Applied Physics and Applied Mathematics, Columbia University, New York, NY, USA[2]

Abstract. Mineralogical composition drives dust impacts on Earth's climate systems. However, most climate models still use homogeneous dust, without accounting for the temporal and spatial variation in mineralogy. To quantify the radiative impact of resolving dust mineralogy on Earth's climate, we implement and simulate the distribution of dust minerals (i.e., illite, kaolinite, smectite, hematite, calcite, feldspar, quartz, and gypsum) from Claquin et al. (1999) (C1999) and activate their interaction with radiation in the GFDL AM4.0 model. Resolving mineralogy reduces dust absorption compared to the homogeneous dust used in the standard GFDL AM4.0 model that assumes a globally uniform hematite volume content of 2.7 % (HD27). The reduction in dust absorption results in improved agreement with observation-based single-scattering albedo (SSA), radiative fluxes from CERES (the Clouds and the Earth's Radiant Energy System), and land surface temperature from the CRU (Climatic Research Unit) compared to the baseline HD27 model version. It also results in distinct radiative impacts on Earth's climate over North Africa. Over the 19-year (from 2001 to 2019) modeled period during JJA (June–July–August), the reduction in dust absorption in AM4.0 leads to a reduction of over 50 % in net downward radiation across the Sahara and approximately 20 % over the Sahel at the top of the atmosphere (TOA) compared to the baseline HD27 model version. The reduced dust absorption weakens the atmospheric warming effect of dust aerosols and leads to an alteration in land surface temperature, resulting in a decrease of 0.66 K over the Sahara and an increase of 0.7 K over the Sahel. The less warming in the atmosphere suppresses ascent and weakens the monsoon inflow from the Gulf of Guinea. This brings less moisture to the Sahel, which combined with decreased ascent induces a reduction of precipitation. To isolate the effect of reduced absorption compared to resolving spatial and temporal mineralogy, we carry out a simulation where the hematite volume content of homogeneous dust is reduced from 2.7 % to 0.9 % (HD09). The dust absorption (e.g., single-scattering albedo) of HD09 is comparable to that of the mineralogically speciated model on a global mean scale, albeit with a lower spatial variation that arises solely from particle size. Comparison of the two models indicates that the spatial inhomogeneity in dust absorption resulting from resolving mineralogy does not have significant impacts on Earth's radiation and climate, provided there is a similar level of dust absorption on a global mean scale before and after resolving dust mineralogy. However, uncertainties related to emission and distribution of minerals may blur the advantages of resolving minerals to study their impact on radiation, cloud properties, ocean biogeochemistry, air quality, and photochemistry. On the other hand, lumping together clay minerals (i.e., illite, kaolinite, and smectite), but excluding externally mixed hematite and gypsum, appears to provide both computational efficiency and relative accuracy. Nevertheless, for specific research, it may be necessary to fully resolve mineralogy to achieve accuracy.

Introduction. Soil dust aerosols emitted from erodible land surfaces, hereafter referred to as dust, are the most abundant aerosol component in the atmosphere in terms of dry mass. Dust has significant impacts on the Earth's climate systems (atmosphere, ocean, cryosphere) due to its interaction with terrestrial and solar radiation (Sokolik and Toon, 1999), cloud microphysics (Guo et al., 2021), tropospheric chemistry (Bian and Zender, 2003; Paulot et al., 2016), and oceanic and terrestrial biogeochemistry (Mahowald, 2011; Evans et al., 2019; Dunne et al., 2020). In addition, dust particles deposited on snow and ice decrease surface reflectivity and accelerate snowmelt (Skiles et al., 2018; Réveillet et al., 2022).

The Astrophysical Journal, vol. 962, issue no. 1, 83, doi:10.3847/1538-4357/ad1685

Multiple habitable phases on outer exosolar worlds.

Sparrman, V., S. Bladh, and **M.J. Way**[1,2,3], 2024

NASA Goddard Institute for Space Studies, New York, NY, USA[1]
GSFC Sellers Exoplanet Environments Collaboration, NASA Goddard Space Flight Center, MD, USA[2]
Theoretical Astrophysics, Department of Physics and Astronomy, Uppsala University, Uppsala, Sweden[3]

Abstract. As stars evolve to higher luminosities during first ascension of the giant branch, previously frozen terrestrial worlds may thaw and host liquid water on their surfaces. Eventually these outer worlds again become uninhabitable due to receiving too much incident light and their water inventory evaporating. Solar-mass stars experience a sudden decrease in luminosity entering the horizontal branch, which could result in a secondary habitable phase for their outer worlds. The outer worlds' time with habitable surface climates is key in evaluating the possibility of extraterrestrial life arising. The times inside the habitable zone (TIHZ) are calculated for outer worlds orbiting between 5 and 45 au around a Sun-like star. By comparing the TIHZ to time estimates for life to arise on Earth, we evaluate whether such outer worlds are promising candidates in the search for extraterrestrial life. We use two different solar evolution models (PARSEC and Dartmouth) and both optimistic and conservative habitable zone (HZ) definitions. Multiple habitable phases are found for each outer world. Outer worlds with orbits as large as Saturn are found to have a secondary habitable phase which exceeds the first in duration. Generally, the time inside the HZ is found to decrease almost monotonically with orbiting distance. Water loss is calculated after the first habitable phase to determine whether a secondary habitable phase is possible. For all orbiting distances the water loss is insufficient to deplete a water inventory equivalent to that of many moons in the outer solar system.

Introduction. Studies of extraterrestrial habitability aim to help answer the question of whether there is life in the Universe other than what exists here on Earth. As a measure, habitability is fundamentally a judgment and there are therefore many differing definitions. For example, one needs to clarify if one considers habitability for humans, for aqueous life, or for some other type of life which does not require liquid water to function.

Some studies consider habitability of subsurface oceans encased in ice (e.g., Schulze-Makuch & Irwin 2001), nonwater solvents such as a water-ammonia mix (e.g., Fortes 2000), or liquid nitrogen for silicon-based life (e.g., Bains 2004). However, we will focus on the habitability definition of liquid water existing on a surface with an Earth-like atmosphere of N_2–CO_2–H_2O (e.g., Kasting et al. 1993; Kopparapu et al. 2013) or with the addition of methane (e.g., Ramirez & Kaltenegger 2018). Having selected the aqueous habitability definition also limits the habitability candidates to terrestrial bodies, i.e., either (exo)planets or (exo)moons. There are two noteworthy benefits to this consideration of habitability. First, this constrains the habitability modeling problem to climates similar to our own. Second, Ramirez (2018) argues that the identification of Earth-like climates is easier since it is known what atmospheric spectra such a world would produce. This would aid in detecting possibly habitable worlds in future surveys.

The orbiting distance of a terrestrial world is critical in the evaluation of its habitability, as surface liquid water cannot exist on worlds that orbit too close or too far away from their host star. The liquid water habitable zone (HZ) refers to a range of stellar distances wherein an orbiting body is deemed possibly habitable (Huang 1959). The orbital range definition of the HZ can be extended to stellar systems that differ from one another by instead defining the HZ with respect to the incident starlight (instellation) of the orbiting body and the effective temperature of the star (e.g., Kasting et al. 1993; Selsis et al. 2007; Kopparapu et al. 2013). Adding the effective temperature to the definition of the HZ is necessary to account for wavelength-dependent optical properties of the atmosphere in order to compute an effective instellation received at the surface of the orbiting body.

Journal of Advances in Modeling Earth Systems, vol. 16, issue no. 1, e2023MS003748, doi:10.1029/2023MS003748

Evaluation of a stochastic mixing scheme in the deep convective gray zone using a tropical oceanic deep convection case study.

Stanford, M.[1,2,3], A.C. Varble, and H. Morrison, 2024

NASA Goddard Institute for Space Studies, New York, NY, USA[1]
Center for Climate Systems Research, Columbia University, New York, NY, USA[2]
Department of Atmospheric Sciences, University of Utah, Salt Lake City, UT, USA[3]

Abstract. A stochastic horizontal subgrid-scale mixing scheme is evaluated in ensemble simulations of a tropical oceanic deep convection case using a horizontal grid spacing (Δh) of 3 km. The stochastic scheme, which perturbs the horizontal mixing coefficient according to a prescribed spatiotemporal autocorrelation scale, is found to generally increase mesoscale organization and convective intensity relative to a non-stochastic control simulation. Perturbations applied at relatively short autocorrelation scales induce differences relative to the control that are more systematic than those from perturbations applied at relatively long scales that yield more variable outcomes. A simulation with mixing enhanced by a constant factor of 4 significantly increases mesoscale organization and convective intensity, while turning off horizontal subgrid-scale mixing decreases both. Total rainfall is modulated by a combination of mesoscale organization, areal coverage of convection, and convective intensity. The stochastic simulations tend to behave more similarly to the constant enhanced mixing simulation owing to greater impacts from enhanced mixing as compared to reduced mixing. The impacts of stochastic mixing are robust, ascertained by comparing the stochastic mixing ensembles with a non-stochastic mixing ensemble that has grid-scale noise added to the initial thermodynamic field. Compared to radar observations and a higher resolution Δh = 1 km simulation, stochastic mixing seemingly degrades the simulation performance. These results imply that stochastic mixing produces non-negligible impacts on convective system properties and evolution but does not lead to an improved representation of convective cloud characteristics in the case studied here.

Introduction. Simulations of deep moist convection (DMC) are limited by a numerical model's ability to resolve the wide range of process-relevant spatiotemporal scales. An artificial scale separation is inevitably imposed at the grid scale such that subgrid-scale (SGS) processes are parameterized, and the bulk effects of these processes are projected onto the resolved-scale flow. For modern general circulation models (GCMs), climate models, and global numerical weather prediction (NWP) models with horizontal grid spacings (Δ_h) O(10–100) km, DMC is not resolved and must be entirely parameterized. When atmospheric convection was considered in the context of earlier GCM frameworks (e.g., Arakawa & Schubert, 1974), in order to close the set of model equations necessary for predictability, convection parameterizations typically assumed an equilibrium condition (often called the convective quasi-equilibrium assumption, or CQE). Following the approach of Arakawa and Schubert (1974), CQE requires that the time scale of the large-scale forcing be sufficiently slower than the convective adjustment time (i.e., buoyancy dissipation) and that the grid column be large enough to hold a robust cloud ensemble obeying the "law of large numbers"—a requirement of any bulk deterministic parameterization scheme (e.g., Sakradzija et al., 2016).

For ΔhO(1–10) km, these CQE assumptions are violated and the applicability of such convection parameterizations is questionable. However, such kilometer-scale (km-scale) models are still too coarse to resolve individual convective drafts that comprise convective systems (Bryan & Morrison, 2012; Bryan et al., 2003; Lebo & Morrison, 2015). Convection at km scales is thus considered to be only partially resolved, and this range of Δ_h is known as the deep convective "gray zone."

Geoscientific Model Development, vol. 17, issue no. 12, pp. 4791-4819, doi:10.5194/gmd-17-4791-2024

Assessing effects of climate and technology uncertainties in large natural resource allocation problems.

Steinbuks, J., Y. Cai, **J. Jaegermeyr**[1,2,3], and T.W. Hertel, 2024

NASA Goddard Institute for Space Studies, New York, NY, USA[1]
Department of Computer Science, University of Chicago, Chicago, IL, USA[2]
Climate Impacts and Vulnerabilities, Potsdam Institute for Climate Impact Research, Potsdam, Germany[3]

Abstract. The productivity of the world's natural resources is critically dependent on a variety of highly uncertain factors, which obscure individual investors and governments that seek to make long-term, sometimes irreversible, investments in their exploration and utilization. These dynamic considerations are poorly represented in disaggregated resource models, as incorporating uncertainty into large-dimensional problems presents a challenging computational task. In this paper, we apply the SCEQ algorithm (Cai and Judd, 2023) to solve a large-scale dynamic stochastic global land resource use problem with stochastic crop yields due to adverse climate impacts and limits on further technological progress. For the same model parameters and bounded shocks, the range of land conversion is considerably smaller for the dynamic stochastic model than for deterministic scenario analysis.

Introduction. Understanding the future allocation of the world's natural resources is an important research problem for environmental scientists and economists. This involves a thorough understanding of a complex interplay of different factors, including, among others, continuing population increases, shifting diets among the poorest populations in the world, increasing production of renewable energy, including biofuels, and growing demand for ecosystem services, including forest carbon sequestration (Foley et al., 2011). The problem is further confounded by faster-than-expected climate change which is altering the biophysical environment of agriculture and forestry. Moreover, highly uncertain future productivities and valuations of ecosystem services, coupled with medium- to long-term irreversibilities in the extraction of nonrenewable or partially renewable resources, such as long-growth natural forests, give rise to a challenging problem of decision-making under uncertainty.

While there is a large body of research analyzing the problem of natural resource extraction and utilization under uncertainty theoretically or using stylized computational models (see, e.g., Miranda and Fackler, 2004; Tsur and Zemel, 2014, and references therein), quantifying the effects of uncertainty in the natural resource use in a more realistic setting remains a challenging problem. This is because natural resource allocation problems, like environmental policy problems in general, involve highly nonlinear structure and damage functions, important irreversibilities, and long time horizons (Pindyck, 2007). Computationally integrated models of economy and environment are the standard workhorse mechanisms for modeling the long-term allocation of the world's natural resources, including particularly difficult land use problems (see, e.g., Füssel, 2009; Schmitz et al., 2014; Nikas et al., 2019, and references therein). These models have the important advantage of detailed spatial and sectoral (particularly in the energy and agricultural sector) coverage, which allows them to capture a broad range of responses to changes in demand and supply factors affecting the utilization of natural resources. However, given the high computational complexity of these models, they are typically either static or based on myopic expectations, whereby decisions about production, consumption, and resource extraction and conversion are made only on the basis of information in the period of the decision (Babiker et al., 2009). These models, therefore, have limited ability to address important intertemporal questions such as, for example, a dynamic trade-off between conservation, carbon sequestration, and renewable offsets for fossil fuels. Among the few forward-looking dynamic economy and environment models, none explicitly incorporates uncertainty into the determination of the optimal path of natural resource use.[1]

Surveys in Geophysics, vol. 45, issue no. 6, pp.1903-1931, doi:10.1007/s10712-024-09831-1

Tropical deep convection, cloud feedbacks and climate sensitivity.

Stephens, G.L.[1], K.A. Shiro, M.Z. Hakuba[1], H. Takahashi[1], **J.A. Pilewskie[1,2]**, T. Andrews, C.J. Stubenrauch, and L. Wu[1], 2024

NASA Jet Propulsion Laboratory, California Institute of Technology, Pasadena, CA, USA[1]
NASA Goddard Institute for Space Studies, New York, NY, USA[2]
Department of Atmospheric and Oceanic Sciences, University of Wisconsin-Madison, Madison, WI, USA[3]

Abstract. This paper is concerned with how the diabatically-forced overturning circulations of the atmosphere, established by the deep convection within the tropical trough zone (TTZ), first introduced by Riehl and (Malkus) Simpson, in Contr Atmos Phys 52:287–305 (1979), fundamentally shape the distributions of tropical and subtropical cloudiness and the changes to cloudiness as Earth warms. The study first draws on an analysis of a range of observations to understand the connections between the energetics of the TTZ, convection and clouds. These observations reveal a tight coupling of the two main components of the diabatic heating, the cloud component of radiative heating, shaped mostly by high clouds formed by deep convection, and the latent heating associated with the precipitation. Interannual variability of the TTZ reveals a marked variation that connects the depth of the tropical troposphere, the depth of convection, the thickness of high clouds and the TOA radiative imbalance. The study examines connections between this convective zone and cloud changes further afield in the context of CMIP6 model experiments of climate warming. The warming realized in the CMIP6 SSP5-8.5 scenario multi-model experiments, for example, produces an enhanced Hadley circulation with increased heating in the zone of tropical deep convection and increased radiative cooling and subsidence in the subtropical regions. This impacts low cloud changes and in turn the model warming response through low cloud feedbacks. The pattern of warming produced by models, also influenced by convection in the tropical region, has a profound influence on the projected global warming.

Introduction. As the heated air of low latitudes rises and moves poleward, it cools and sinks in the subtropics creating a massive overturning of the atmosphere that stretches from the equator to the poles. This overturing circulation establishes both the main climate zones of Earth and the cloud patterns of these zones. That this rising, heated air at low latitudes is accomplished by the transports of many narrow plumes in deep convection, referred to as hot towers, was one of the most remarkable inferences about the atmosphere made in the mid-20th century by Riehl and Malkus (1958; hereafter R–M). Riehl and Simpson (1979; hereafter R–S) later revisited that study and estimated that about 1600–2400 hot towers must exist at any one time in the deep tropics under an assumption of a fixed size of 5 km.

Figure 1, adapted from Boucher et al. (2013), is a schematic depiction of the major cloud patterns of Earth and, more importantly, a schematic of their connection to the large-scale overturning circulations of the atmosphere. These connections begin with the area of deep convection at lower latitudes in the region referred to as the tropical trough zone (TTZ) by R–M. It is a zone where moisture is transported from higher latitudes at low levels and where heat is moved poleward in the upper levels. The TTZ is fundamental to the way that Earth's heat engine moves heat from low latitudes to higher latitudes and establishes the latitudes where heat transport is toward the winter pole. Deep convection forms in this zone, and its seasonal changes are intimate parts of this transport which relates to the other major cloud types in ways hinted in Fig. 1. This includes high clouds that are directly produced by the convection and the low cloud regimes of the subtropics governed by the overturning circulation convection helps create. The influences of this circulation on clouds and, in turn, the influence of clouds on this circulation are a basic feedback cycle that frames all essential cloud feedbacks that regulate Earth's climate and its response to the forcing of climate change.

Bulletin of the American Meteorological Society, vol. 125, issue no. 4, pp. E760-E777, doi:10.1175/BAMS-D-22-0106.1

Enhancing global food security: Opportunities for the American Meteorological Society.

Stuart, L., M. Hobbins, E. Neibuhr, **A. Ruane**[1], R. Pulwarty, A. Hoell, W. Thiaw, **C. Rosenzweig**[1], F. Muñoz-Arriola, M. Jahn, and M. Farrar, 2024

NASA Goddard Institute for Space Studies, New York, NY, USA[1]

Abstract. Food security is a key pillar of environmental security yet remains one of the world's greatest challenges. Its obverse, food insecurity, negatively impacts health and well-being, drives mass migration, and undermines national security and global sustainable development. Ensuring food security is a delicate balance of myriad concerns within the atmospheric and Earth sciences, agronomy and agriculture engineering, social sciences, economics, monitoring, and policymaking. A Food Security Presidential Session at the American Meteorological Society's (AMS) 2022 Annual Meeting brought together experts across disciplines to tackle issues at the nexus of weather, climate, and food security. The starkest takeaway was the realization that, despite its importance and clear roles for the atmospheric and climate sciences, food security has not been a focus for the AMS community. The aim of this paper is to build on the perspectives shared by this expert panel and to identify overlapping issues and key points of intersection between the food-security community and AMS. We examine 1) the interactions between weather, climate, and the food system and how they influence food security; 2) the time and spatial scales of food security decision support that match weather and climate phenomena; 3) the role of both providers and users of information as well as decision-makers in improving research to operations for food security; and 4) the opportunities for the AMS community to address food security. We conclude that, moving forward, the AMS community is well-positioned to scale up its engagement across the global food system to address existing scientific needs and technology gaps to improve global food security.

Introduction. Food security exists "when all people at all times, have the physical and economic access to sufficient, safe and nutritious food to meet their dietary needs and food preferences for an active and healthy life" (FAO et al. 2021). Shaped by ever-evolving geopolitics, socioeconomic challenges, and environmental pressures, food security lies at the heart of human well-being and prosperity and is key to achieving many of the UN Sustainable Development Goals (SDGs) and those of other global frameworks. Failure to achieve food security can exacerbate vulnerability and inequity, intensify humanitarian crises, and jeopardize international security.

The food system—including the production, distribution, and consumption of food—is highly vulnerable to extreme weather and climate events. The interactions between weather, climate, and the food system have a significant impact on food security by affecting the availability, access, utilization, and stability of food. However, the global food system is also a major driver of climate change, responsible for nearly one-third of global greenhouse gas emissions (GHG) (Crippa et al. 2021). As a result, the food system is not only vulnerable to climate change, but also drives the very shocks that threaten it. Additionally, compounding risks, such as from decreasing biodiversity—which otherwise supports diverse diets, a growing global population, and demographic transitions, and helps to absorb system shocks—are further exposing the food system to climate disruptions and cascading impacts.

Examples of the interactions between weather, climate, and food security can be traced through history. For example, during the 1780s, France suffered a series of failed harvests, a severe drought, an extreme cold snap, and severe storms, all of which resulted in food shortages that raised bread prices to 88% of the average citizen's wages; this led to riots, bloodshed and, ultimately, the French Revolution (Neely 2007). In the late 2000s, drought in Syria exacerbated poverty and social unrest in rural areas, leading to riots and mass displacement (Kelley et al. 2015). More recently, the globally networked nature of risks has become increasingly clear (UNDRR 2021).

Journal of Climate, vol. 37, issue no. 8, pp. 2491-2504, doi:10.1175/JCLI-D-23-0391.1

Systematic differences between the Northern and Southern Hemispheres: Warm frontal ice water path linked to the origin of extratropical cyclones.

Takahashi, H.[1], **C.M. Naud**[2,3], D.J. Posselt[1], and G.A. Duffy, 2024

NASA Jet Propulsion Laboratory, California Institute of Technology, Pasadena, CA, USA[1]
NASA Goddard Institute for Space Studies, New York, NY, USA[2]

Abstract. Extratropical cyclones (ETCs) produce most of the winter precipitation at midlatitudes and are often associated with the most extreme winter weather events. For climate models to accurately predict the occurrence and severity of these extreme events in a changing climate, they need to accurately represent moist processes in general and ice processes in particular. To provide an observational constraint for model evaluation, because cloud cover and precipitation are prevalent in warm-frontal regions, a compositing method is applied to ice retrievals from satellite observations to explore the ice distribution across warm fronts in both hemispheres. Ice water path (IWP) and its variability are compared between Northern Hemisphere (NH) and Southern Hemisphere (SH) warm fronts for different ETC-wide characteristics, as well as for different ETC origination regions. Results reveal that warm-frontal IWP and its variability tend to be higher in the NH than the SH, even when controlling for the ETC strength and environmental precipitable water (PW). IWP differences between NH and SH are found to be primarily related to where the cyclones originate. As the intertropical convergence zone is shifted north, ETCs that originate close to the northern tropics have more PW than those that originate close to the southern tropics. This, in turn, seems to lead to larger IWP in NH frontal clouds than in the SH frontal clouds at a later time. This highlights the importance, for ice amounts generated in warm-frontal regions, of the environmental conditions that an ETC encounters during its genesis phase.

Introduction. Extratropical cyclones (ETCs) and their associated fronts are dominant features of the midlatitudes: their passage is often associated with strong winds, large moisture gradients, and temperature changes. They are the main source of precipitation in the extratropics (Hawcroft et al. 2012; Catto et al. 2012), and play a central role in controlling the meridional transport of energy and moisture from the equator to the poles (e.g., Trenberth and Stepaniak 2003; Shaw et al. 2016). Therefore, they have a significant influence not only on local weather, but also on the global climate. To have confidence in projections of how these systems may change in a future climate, particularly the most extreme events, it is of great importance for climate models to realistically represent cloud and precipitation in these systems. However, the accurate representation of moist processes in general circulation models (GCMs) has been a long-standing challenge. Issues in this representation might explain why the latest generation of GCMs still show biases in their representation of cyclones, and more specifically high-intensity cyclones (Priestley et al. 2020). Possibly related to this, and of importance for projections of high-impact events, there are still discrepancies across model simulations on how atmospheric river precipitation might respond to climate change (Shields et al. 2023).

The bulk of cloud and precipitation in extratropical cyclones occurs in a comma shaped region, the head of which encompasses the center, where sea level pressure is minimum, extending to the east along the warm front and equatorward along the cold front. Precipitation and clouds in the warm-frontal region are formed through the ascent of a poleward flow of relatively warm and moist air, the warm conveyor belt (Browning and Harrold 1969; Carlson 1980; Wernli and Davies 1997; Eckhardt et al. 2004; Madonna et al. 2014; Pfahl et al. 2014). The warm conveyor belt airstream originates in the warm sector boundary layer, in advance of the cold front.

Journal of Geophysical Research: Atmospheres, vol. 129, issue no. 6, e2023JD040489, doi:10.1029/2023JD040489

Constraints on Southern Ocean shortwave cloud feedback from the hydrological cycle.

Tan, C., D.T. McCoy, and **G. Elsaesser**[1,2], 2024

NASA Goddard Institute for Space Studies, New York, NY, USA[1]
Department of Applied Physics and Applied Mathematics, Columbia University, New York, NY, USA[2]

Abstract. Shifts in Southern Ocean (SO, 40–85°S) shortwave cloud feedback (SW_{FB}) toward more positive values are the dominant contributor to higher effective climate sensitivity (ECS) in Coupled Model Intercomparison Project Phase 6 (CMIP6) models. To provide an observational constraint on the SO SW_{FB}, we use a simplified physical model to connect SO SW_{FB} with the response of column-integrated liquid water mass (LWP) to warming and the susceptibility of albedo to LWP in 50 CMIP5 and CMIP6 GCMs. In turn, we predict the responses of SO LWP using a cloud-controlling factor (CCF) model. The combination of the CCF model and radiative susceptibility explains about 50% of the variance in the GCM-simulated SW_{FB} in the SO. Observations of SW radiation fluxes, LWP, and CCFs from reanalysis are used to constrain the SO SW_{FB}. Observations suggest a SO LWP increase in response to warming and albedo susceptibility to LWP that is on the lower end relative to GCMs. The overall constraint on the contribution of SO to global mean SW_{FB} is −0.168 to +0.051 W m^{-2} K^{-1}, relative to −0.277 to +0.270 Wm^{-2} K^{-1}. In summary, observations suggest SO SW_{FB} is less likely to be as extremely positive as predicted by some CMIP6 GCMs, but more likely to range from moderately negative to weakly positive.

Introduction. Quantifying the surface temperature response to a doubling in atmospheric CO_2 concentration, commonly referred to as climate sensitivity, is a fundamental goal of climate science (Boucher et al., 2014; Forster et al., 2023; Houghton et al., 2001). Climate feedback processes such as changes in lapse rate, water vapor, and cloud may dampen or amplify the temperature response to greenhouse gas increase and are critical for estimating climate sensitivity (Bony et al., 2006). Global climate models (GCMs) provide the most direct way to estimate climate sensitivity since they attempt to simulate all relevant processes, including climate feedback (Andrews et al., 2012; Zelinka et al., 2020). Shortwave cloud feedback (SW_{FB}), the shortwave (SW) radiative impact of cloud responses to a surface temperature perturbation, is the largest uncertainty in GCMs' estimate of net climate feedback and by extension, climate sensitivity (Sherwood et al., 2020; Zelinka et al., 2020). The uncertainty in estimating SW_{FB} is strongly driven by difficulties in representing subgrid-scale cloud processes in GCMs (Sherwood et al., 2014; Storelvmo et al., 2015; Webb et al., 2015; Zhao, 2014).

Despite the large intermodel spread in global-mean SW_{FB}, robust regional features have emerged from previous generations of GCMs. For example, positive SW_{FB} in the subtropics has emerged, likely due to decreased cloud coverage with negative SW_{FB} in the middle-to-high latitudes likely attributed to increased cloud optical depth (Ceppi, McCoy, & Hartmann, 2016; Zelinka et al., 2012). Considerable progress has been made on narrowing the possible ranges of tropical and subtropical SW_{FB} using observational constraints (Myers et al., 2021; G. V. Cesana & Del Genio, 2021; G. Cesana et al., 2019; Scott et al., 2020; Klein et al., 2017).

Recent GCMs have suggested a weaker negative Southern Ocean (SO, 40–85°S) SW_{FB}. The ensemble mean SO SW_{FB} of GCMs participating in the sixth phase of the Coupled Model Intercomparison Project (CMIP6) has shifted toward a more positive value relative to CMIP5, leading to the emergence of several GCMs with high effective climate sensitivity (ECS) (ECS ≥4.5 K) (Bodas-Salcedo et al., 2019; Zelinka et al., 2020). Much effort has been made to understand this change within the context of GCM cloud physics (Bjordal et al., 2020; Bodas-Salcedo et al., 2019; Gettelman et al., 2019; Zhang et al., 2019).

Journal of Geophysical Research: Atmospheres, vol. 129, issue no. 8, e2023JD040540, doi:10.1029/2023JD040540

Contributions from cloud morphological changes to the interannual shortwave cloud feedback based on MODIS and ISCCP satellite observations.

Tan, I., M.D. Zelinka, Q. Coopman, B.H. Kahn[1], L. Oreopoulos[2], **G. Tselioudis[3]**, D.T. McCoy, and N. Li, 2024

NASA Jet Propulsion Laboratory, California Institute of Technology, Pasadena, CA, USA[1]
NASA GSFC, Earth Sciences Division, Greenbelt, MD, USA[2]
NASA Goddard Institute for Space Studies, New York, NY, USA[3]

Abstract. The surface temperature-mediated change in cloud properties, referred to as the cloud feedback, continues to dominate the uncertainty in climate projections. A larger number of contemporary global climate models (GCMs) project a higher degree of warming than the previous generation of GCMs. This greater projected warming has been attributed to a less negative cloud feedback in the Southern Ocean. Here, we apply a novel "double decomposition method" that employs the "cloud radiative kernel" and "cloud regime" concepts, to two data sets of satellite observations to decompose the interannual cloud feedback into contributions arising from changes within and shifts between cloud morphologies. Our results show that contributions from the latter to the cloud feedback are large for certain regimes. We then focus on interpreting how both changes within and between cloud morphologies impact the shortwave cloud optical depth feedback over the Southern Ocean in light of additional observations. Results from the former cloud morphological changes reveal the importance of the wind response to warming increases low- and mid-level cloud optical thickness in the same region. Results from the latter cloud morphological changes reveal that a general shift from thick storm-track clouds to thinner oceanic low-level clouds contributes to a positive feedback over the Southern Ocean that is offset by shifts from thinner broken clouds to thicker mid- and low-level clouds. Our novel analysis can be applied to evaluate GCMs and potentially diagnose shortcomings pertaining to their physical parameterizations of particular cloud morphologies.

Introduction. The surface temperature-mediated change in cloud properties, referred to as the cloud feedback, continues to dominate the uncertainty in climate projections. A larger number of contemporary global climate models (GCMs) project a higher degree of warming than the previous generation of GCMs. This greater projected warming has been attributed to a less negative cloud feedback in the Southern Ocean. Here, we apply a novel "double decomposition method" that employs the "cloud radiative kernel" and "cloud regime" concepts, to two data sets of satellite observations to decompose the interannual cloud feedback into contributions arising from changes within and shifts between cloud morphologies. Our results show that contributions from the latter to the cloud feedback are large for certain regimes. We then focus on interpreting how both changes within and between cloud morphologies impact the shortwave cloud optical depth feedback over the Southern Ocean in light of additional observations. Results from the former cloud morphological changes reveal the importance of the wind response to warming increases low- and mid-level cloud optical thickness in the same region. Results from the latter cloud morphological changes reveal that a general shift from thick storm-track clouds to thinner oceanic low-level clouds contributes to a positive feedback over the Southern Ocean that is offset by shifts from thinner broken clouds to thicker mid- and low-level clouds. Our novel analysis can be applied to evaluate GCMs and potentially diagnose shortcomings pertaining to their physical parameterizations of particular cloud morphologies.

The focus of this work is on the shortwave (SW) extratropical cloud optical depth feedback (λ_τ), that is, the contribution of changes in the optical depth (τ) of extratropical clouds to the SW radiation budget in response to rising global 2-m air temperatures holding cloud height and cloud amount fixed.

Remote Sensing of Environment, vol. 303, 113986, doi:10.1016/j.rse.2023.113986

On-orbit calibration and performance of the EMIT imaging spectrometer.

Thompson, D.R.[1], R.O. Green[1], C. Bradley[1], P.G. Brodrick[1], N. Mahowald, E.B. Dor, M. Bennett[1], M. Bernas[1], N. Carmon[1], K.D. Chadwick[1], R.N. Clark, R.W. Coleman[1], E. Cox, E. Diaz[1], M.L. Eastwood[1], R. Eckert[1], B.L. Ehlmann, P. Ginoux, M.G. Ageitos, K. Grant, L. Guanter, D.H. Pearlshtien, M. Helmlinger[1], H. Herzog[1], T. Hoefen, **Y. Huang**[2,3], A. Keebler, O. Kalashnikova[1], D. Keymeulen[1], R. Kokaly, M. Klose, L. Li, S.R. Lundeen[1], J. Meyer, E. Middleton, **R.L. Miller**[2,4], P. Mouroulis[1], B. Oaida[1], **V. Obiso**[2,5], F. Ochoa, W. Olson-Duvall[1], G.S. Okin, T.H. Painter, C. Pérez García-Pando, R. Pollock, V. Realmuto[1], L. Shaw[1], P. Sullivan[1], G. Swayze, E. Thingvold[1], A.K. Thorpe[1], S. Vannan[1], C. Villarreal[1], C. Ung[1], D.W. Wilson[1], and S. Zandbergen[1], 2024

NASA Jet Propulsion Laboratory, California Institute of Technology, Pasadena, CA, USA[1]
NASA Goddard Institute for Space Studies, New York, NY, USA[2]
Karlsruhe Institute of Technology, Karlsruhe, Germany[3]
Center for Climate Systems Research, Columbia University, New York, NY, USA[4]
Barcelona Supercomputing Center, Barcelona, Spain[5]

Abstract. The Earth surface Mineral dust source InvesTigation (EMIT) is a remote visible to shortwave infrared (VSWIR) imaging spectrometer that has been operating onboard the International Space Station since July 2022. This article describes EMIT's on-orbit spectroradiometric calibration and validation. Accurate spectroscopy is vital to achieve consistent mapping results with orbital imaging spectrometers. EMIT takes a unique approach to this challenge, with just six optical elements, no shutter, and no onboard calibration systems. Its simple design focuses on uniformity and stability to enable vicarious spectroradiometric calibration. Our experiments demonstrate that this approach is successful, approaching the fidelity of manual field spectroscopy in some cases, and enabling new and more accurate products across diverse Earth science disciplines. EMIT achieves several notable firsts for an instrument of its class. It demonstrates successful on-orbit adjustments of Focal Plane Array (FPA) alignment with sub-micron precision. It offers spectral uniformity better than 98%. Optical artifacts in the measurement channels are at least three orders of magnitude below the primary solar-reflected surface signals. Its noise performance enables percent-level discrimination in the depths of mineral absorption features. In these aspects, EMIT satisfies the stringent performance needs for the next generation of VSWIR imaging spectrometers to observe the Earth's ecosystems, geology, and water resources.

Introduction. The Visible to Shortwave Infrared (VSWIR) spectral range is sensitive to diverse Earth surface properties, making it useful for a wide range of remote sensing applications. Imaging spectrometers, also known as hyperspectral imagers, acquire rasters of spectra to map geophysical phenomena. They have been used to study terrestrial and aquatic ecosystems, mineral and water resources, greenhouse gas point sources, and more. The first imaging spectrometers were developed over 40 years ago (Goetz and Srivastava, 1985), but they have recently reached a new stage of maturity with orbital instruments conducting global investigations. These missions include the DLR Earth Sensing Imaging Spectrometer, DESIS (Alonso et al., 2019), the PRecursore IperSpettrale della Missione Applicativa, PRISMA (Cogliati et al., 2021), the Hyperspectral Imager Suite, HISUI (Matsunaga et al., 2020), and the Environmental Mapping and Analysis Program, EnMAP (Guanter et al., 2015; Chabrillat et al., 2020). Upcoming missions like the Copernicus Hyperspectral Imaging Mission for the Environment (CHIME; Nieke and Rast, 2018), and the Surface Biology and Geology (SBG) investigation (Cawse-Nicholson et al., 2021) will provide regular coverage of Earth's entire land area and coastal waters. Simultaneously, advances in computing enable more sophisticated algorithms, portending a new era of spectroscopic remote sensing.

Annals of the New York Academy of Sciences, vol. 1539, issue no. 1, vol. 323-334, doi:10.1111/nyas.15150

NPCC4: Climate risk and equity — Advancing knowledge toward a sustainable future — Conclusions.

Towers, J., R. Leichenko, **C. Braneon**[1,2,3], D. Balk, L. Yoon, G. Wagner, J. Ventrella, J.K.W. Tchen, B. Rosenzweig, P. Orton, L. Ortiz, R. Moss, F. Montalto, T. McPhearson, K. McComas, P. Marcotullio, T. Matte, N. Maher, K. Knowlton, **R. Horton**[1,4], S. Foster, D. Bader, and A. Baptista, 2024

NASA Goddard Institute for Space Studies, New York, NY, USA[1]
CUNY Institute for Demographic Research, City University of New York, New York City, New York, USA[2]
Columbia Climate School, Columbia University, New York City, New York, USA[3]
Center for Climate Systems Research, Columbia University, New York, NY, USA[4]

Abstract. This chapter provides an overview of the major themes, findings, and recommendations from NPCC4. It presents summary statements from each chapter of the assessment which identify salient and pressing issues raised and provides recommendations for future research and for enhancement of climate resiliency. The chapter also outlines a set of broader recommendations for future NPCC work and identifies some key topics for the next assessment.

Introduction. The New York City Panel on Climate Change (NPCC) was established to help the city "prepare for and mitigate the expected impact of climate change on New York City's communities, vulnerable populations, public health, natural systems, critical infrastructure, buildings and the economy" (LL42). As an assessment, the NPCC reviews recent advances in biophysical climate science and social science to provide policy-relevant guidance to the city. NPCC4 builds on the prior three NPCC assessments, providing climate projections while deepening areas of prior reports on flooding, health, and equity (see Figure 1). It crafts two new areas of emphasis—on energy and energy insecurity (EI), and tools for future visioning and planning—that further understanding of the impacts of climate risks on the human and ecological systems of New York City (NYC).

Navigating present and future climate risks and related socioeconomic challenges facing the city will require tradeoffs and compromises forged through constructive and scientifically informed public dialogue. To plan and act, community-based organizations, businesses, city government, and other stakeholders will need to continue to integrate scientific and technical information with community values and knowledge. Scientific and technical information are critical to addressing the challenges the city faces and to understanding the technologies and measures that are available to meet them. Scientific and technical information can provide insights and guidance that inform, for example: how to update codes and standards (e.g., Climate Resiliency Design Guidelines) so that new and renovated structures are resilient and efficient; how to identify where, and what kind of flood protection should be prioritized; how to estimate the service loads public infrastructure for stormwater management, sanitation, electric power, and water supply will need to bear; and how to plan public health strategies to manage cascading and compounding extreme events (e.g., co-occurrence of storms, power failures, and heat waves). Community perspectives and local knowledge[1] provide an essential compass to help navigate issues such as growing economic opportunities, improving social welfare, planning transportation systems, and improving access to nature-based solutions (NBS) that contribute to multiple dimensions of well-being. Local knowledge offers complementary information and expertise to biophysical and social science, ensuring that, as the city prepares for the future, it does so in a way that increases civic participation, social cohesion, and community stewardship, all indicators of resiliency. Evidence suggests the integration of different forms of local knowledge (e.g., NOAA's Urban Heat Island mapping program) can improve decision-making associated with climate risk management and community stewardship of, and commitment to, climate resiliency initiatives.[1-3]

Journal of Climate, vol. 37, issue no. 7, pp. 2361-2377, doi:10.1175/JCLI-D-22-0931.1

Predictability of the minimum sea ice extent from winter Fram Strait Ice Area Export: Model versus observations.

Trotechaud, S., B. Tremblay, **J. Williams**[1,2], **J. Romanski**[1,2], **A. Romanou**[1,2], M. Bushuk, W. Merryfield, and R. Msadek, 2024

NASA Goddard Institute for Space Studies, New York, NY, USA[1]
Center for Climate Systems Research, Columbia University, New York, NY, USA[2]

Abstract. Observations show predictive skill of the minimum sea ice extent (Min SIE) from late winter anomalous offshore ice drift along the Eurasian coastline, leading to local ice thickness anomalies at the onset of the melt season—a signal then amplified by the ice–albedo feedback. We assess whether the observed seasonal predictability of September Sea ice extent (Sept SIE) from Fram Strait Ice Area Export (FSIAE; a proxy for Eurasian coastal divergence) is present in global climate model (GCM) large ensembles, namely the CESM2-LE, GISS-E2.1-G, FLOR-LE, CNRM-CM6-1, and CanESM5. All models show distinct periods where winter FSIAE anomalies are negatively correlated with the May Sea ice thickness (May SIT) anomalies along the Eurasian coastline, and the following Sept Arctic SIE, as in observations. Counterintuitively, several models show occasional periods where winter FSIAE anomalies are positively correlated with the following Sept SIE anomalies when the mean ice thickness is large, or late in the simulation when the sea ice is thin, and/or when internal variability increases. More important, periods with weak correlation between winter FSIAE and the following Sept SIE dominate, suggesting that summer melt processes generally dominate over late-winter preconditioning and May SIT anomalies. In general, we find that the coupling between the winter FSIAE and ice thickness anomalies along the Eurasian coastline at the onset of the melt season is a ubiquitous feature of GCMs and that the relationship with the following Sept SIE is dependent on the mean Arctic Sea ice thickness.

Introduction. The Arctic has witnessed major changes in recent decades as a result of anthropogenic greenhouse gas emissions and subsequent polar amplification (Screen and Simmonds 2010; Dai et al. 2019). Since the beginning of the satellite era in the late 1970s, the September sea ice extent (Sept SIE) has declined by −13% per decade (Fetterer et al. 2017 updated daily), the area covered by multiyear ice (MYI) has decreased by more than 50% and the sea ice thickness has declined by 2 m, with a loss of 1.2 m in the 1980s and 1990s alone (Kwok 2018). These changes have major implications for ocean–atmosphere heat and moisture fluxes, solar radiation absorbed at the surface, and liquid freshwater storage in the Arctic, potentially affecting deep convection in the Greenland Sea and, consequently, the global thermohaline circulation (Koenigk et al. 2006; Jahn and Holland 2013). Changes in the sea ice extent can also affect midlatitude weather through atmospheric teleconnections (Screen et al. 2018; Cohen et al. 2020). Also, the changing Arctic sea ice leads to new navigable passages, which affects tourism, economics, and military operations (Stewart et al. 2009; Ebinger and Zambetakis 2009; Sharp 2011), as well as local ice-dependent and obligate species (Vincent et al. 2011).

The then record low Sept SIE of 2007 marked the beginning of a new Arctic, with mainly ice-free conditions in the Chukchi and Beaufort Seas in summer and an increased interest for (sub)seasonal forecasts of sea ice conditions (Stroeve et al. 2014). Initialized GCMs can make skillful predictions when the Sept SIE is near the long-term linear trend, but they have difficulty making skillful predictions for anomalous years that fall outside of the linear trend such as 2012 (Stroeve et al. 2014). With the retreat of the sea ice cover, we see early signs of increased interannual variability, particularly in the Pacific sector of the Arctic (Desmarais and Tremblay 2021), making predictions of the Sept SIE more challenging. The need for skillful forecast of anomalous events such as 2007 motivated the Study of Environmental Arctic Change (SEARCH) Sea Ice Outlook project with the objective of documenting and improving the skill of model forecasts using statistical, numerical and heuristic approaches.

Climate Dynamics, vol. 62, issue no. 9, pp. 9319-9332, doi:10.1007/s00382-024-07396-8



Oceanic cloud trends during the satellite era and their radiative signatures.

Tselioudis, G.[1], W.B. Rossow, F. Bender, L. Oreopoulos[2], and **J. Rémillard**[1,3], 2024

NASA Goddard Institute for Space Studies, New York, NY, USA[1]
NASA Goddard Space Flight Center, Greenbelt, MD, USA[2]
Autonomic Integra, LLC, Institute for Space Studies, New York, NY, USA[3]

Abstract. The present study analyzes zonal mean cloud and radiation trends over the global oceans for the past 35 years from a suite of satellite datasets covering two periods. In the longer period (1984–2018) cloud properties come from the ISCCP-H, CLARA-A3, and PATMOS-x datasets and radiative properties from the ISCCP-FH dataset, while for the shorter period (2000–2018) cloud data from MODIS and CloudSat/CALIPSO and radiative fluxes from CERES-EBAF are added. Zonal mean total cloud cover (TCC) trend plots show an expansion of the subtropical dry zone, a poleward displacement of the midlatitude storm zone and a narrowing of the tropical intertropical convergence zone (ITCZ) region over the 1984–2018 period. This expansion of the 'low cloud cover curtain' and the contraction of the ITCZ rearrange the boundaries and extents of all major climate zones, producing a more poleward and narrower midlatitude storm zone and a wider subtropical zone. Zonal mean oceanic cloud cover trends are examined for three latitude zones, two poleward of 50 ° and one bounded within 50ºS and 50ºN, and show upward or near-zero cloud cover trends in the high latitude zones and consistent downward trends in the low latitude zone. The latter dominate in the global average resulting in TCC decreases that range from 0.72% per decade to 0.17% per decade depending on dataset and period. These contrasting cloud cover changes between the high and low latitude zones produce contrasting low latitude cloud radiative warming and high latitude cloud radiative cooling effects, present in both the ISCCP-FH and CERES-EBAF datasets. The global ocean mean trend of the short-wave cloud radiative effect (SWCRE) depends on the balance between these contrasting trends, which in the CERES dataset materializes as a SW cloud radiative warming trend of 0.12 W/m^2/decade coming from the dominance of the low-latitude positive SWCRE trends while in the ISCCP-FH dataset it manifests as a 0.3 W/m^2/decade SW cloud radiative cooling trend coming from the dominance of the high latitude negative SWCRE trends. The CERES cloud radiative warming trend doubles in magnitude to 0.24 W/m^2/decade when the period is extended from 2016 to 2022, implying a strong cloud radiative heating in the past 6 years coming from the low latitude zone.

Introduction. Clouds modulate both the SW and LW components of the Earth's energy budget and thus play a crucial role in determining the earth's energy imbalance (EEI) which is the primary driver of the ongoing planetary warming (e.g. Loeb et al. 2021; Hansen et al. 2023). Recent studies have shown a near doubling of EEI from 2005 to 2019 in both satellite and in-situ estimates (Loeb et al. 2021). It is therefore crucial to examine and understand cloud property trends in the past decades, in order to better quantify the contribution of cloud property changes to the EEI trends. Cloud properties during the satellite era are derived from operational weather satellite passive radiative retrievals starting in the early 1980s (e.g. ISCCP, CLARA, PATMOS-x), and from research-oriented cloud instrument passive and active retrievals starting in the early 2000s (e.g. MODIS, CloudSat, CALIPSO). This means that a nearly forty-year long record of cloud properties that encompasses several modes of the Earth's shorter term natural variability (ENSO, PDO) is currently available, and it provides a first estimate of longer-term climate trends. While existing cloud products have different sources of uncertainty and different limitations (Stubenrauch et al. 2013, 2024), using them in conjunction can compensate for several of their limitations and provide more reliable estimates of cloud property trends.

Icarus, vol. 413, 116009, doi:10.1016/j.icarus.2024.116009

Composition and speciation of volcanic volatiles on the Moon.

Varnam, M., C.W. Hamilton, **I. Aleinov**[1,2], and J.J. Barnes, 2024

NASA Goddard Institute for Space Studies, New York, NY, USA[1]
Center for Climate Systems Research, Columbia University, New York, NY, USA[2]

Abstract. Lunar volcanic volatiles are crucial for understanding eruption dynamics on the Moon as well as the potential formation, life span, and dissipation of a lunar secondary atmosphere. We review literature concerning volatile content, degassing extent, and speciation during the mare eruption period on the Moon from 4.0 to 1.2 Ga, providing a realistic summary of degassed compositions for the traditional volcanic elements C-O-H-S-F-Cl. The most reliable estimates of lunar volcanic volatiles come from high-titanium (high-Ti) glass beads sampled during the Apollo 17 mission. Analysis of these samples demonstrates that hydrogen is the most abundant element by mole in erupted volcanic gases, so a hydrogen species should be the most abundant molecule in the lunar gas, rather than carbon monoxide. This hydrogen is expected to speciate mostly as H_2, rather than H_2O, at the predicted oxygen fugacity for lunar magma. This difference is important because H_2 more easily escapes from the Moon, whereas H_2O could freeze out on the lunar surface, and potentially persist within permanently shadowed regions near the poles. We also find that sulfur, rather than carbon, is the third most abundant element in lunar volcanic gas, after hydrogen and oxygen.

Introduction. Lunar sample reviews detail the endogenous volatile composition of lunar mare lavas, constraining the volatile abundance and distribution between possible reservoirs in the lunar mantle and crust (e.g., Anand et al., 2014; Basilevsky et al., 2012; McCubbin et al., 2015, McCubbin et al., 2021; Zhang, 2020). These reviews guide investigations into the cause(s) of volatile depletion of the Moon relative to Earth and inform formation and evolution models of the early Earth–Moon system (e.g., Elkins-Tanton and Grove, 2011; Hauri et al., 2017; Lock et al., 2018; McCubbin et al., 2021). These reviews treat degassing during mare eruptions as an error term obscuring the translation of sample measurements to a mantle composition. However, volcanic gas composition (e.g., Kring et al., 2021; Needham and Kring, 2017; Newcombe et al., 2017; Renggli, 2023, Renggli et al., 2023; Rutherford et al., 2017) contributes to active avenues of lunar research, including the possible presence of a transient atmosphere on the Moon during mare volcanism (e.g., Aleinov et al., 2019; Head et al., 2020; Needham and Kring, 2017), the origins of volatiles in permanently shadowed regions (PSRs; e.g., Head et al., 2023; Lucey et al., 2021; Mandt et al., 2022; Prem et al., 2020; The National Academies Press, 2022), and lunar eruption dynamics (e.g., Lo et al., 2021; Wilson and Head, 2017a).

Current models of lunar volcanic gas composition show dramatic differences in not only exsolved species abundance, with H_2O outputs ranging from 0 to 900 μg/g (Needham and Kring, 2017; Rutherford et al., 2017) and CO from 12 to 1280 μg/g (Rutherford et al., 2017), but also relative elemental composition, with H ranging from 1.8 to 81 mol% (Needham and Kring, 2017; Newcombe et al., 2017) and C from 0.3 to 25 mol% (Needham and Kring, 2017; Rutherford et al., 2017). Enthusiastic debate even surrounds the identity of the most abundant gas species, with studies implicating H_2 (Newcombe et al., 2017; Renggli et al., 2023), H_2O (Moitra et al., 2022), CO_2 (Taylor et al., 1991), or CO (e.g., Needham and Kring, 2017; Rutherford et al., 2017; Shearer et al., 2023). Although some variation may reflect regional and lithological differences, we find most variation instead arises from differing methodologies, such as treatment of oxygen fugacity (fO_2) and some studies assuming C saturation in the mantle.

Global and Planetary Change, vol. 239, 104502, doi:10.1016/j.gloplacha.2024.104502

Skill of isotope-enabled climate models for daily surface water vapour in East Asia.

Wang, S., Y. Qian, K. Yoshimura[2], **H. Bong[1,2]**, C. Risi, Z. Wei, H. Pang, W. Xiao, S. Lei, M. Xing, P. Zhao, H. Wu, Y. Shi, D. Wang, and M. Zhang, 2024

NASA Goddard Institute for Space Studies, New York, NY, USA
Atmosphere and Ocean Research Institute, University of Tokyo, Tokyo 169-8555, Japan[2]

Abstract. The isotope-enabled general circulation models (GCM) have been widely applied to simulate the variability of stable isotopes in meteoric water at various time scales. The in-situ observations of water vapour isotopes are an important basis for assessing the performance of isotope-enabled GCMs, although they are still limited. Here we compiled the observations of near-surface water vapour isotopes on a daily scale at 17 stations in East Asia, and assessed the skill and the association between isotope error and meteorological errors on a daily scale. Generally, the spatial pattern and seasonal variability can be well simulated in the isotope-enabled GCMs. The models show better skill for warm and humid backgrounds, which also corresponds to the monsoonal regions with lower latitudes in East Asia. As spatial resolution is finer, the skill of models is better, which can be seen from the two GCMs. According to the correlation coefficient, the improvement of resolution is more obvious in summer than in winter, especially for IsoGSM. In addition, the correlation coefficient in winter is usually larger than that in summer. The daily modelling has good potential to investigate the daily or synoptic climate information in water isotopes. The findings are useful for understanding the applicability of isotope-enabled models in East Asia and the climate factors influencing the skill of isotope-enabled models on a daily basis.

Introduction. Stable hydrogen and oxygen isotopes in meteoric water provide a physical tool to trace the modern and historical water cycle (Bowen et al., 2019; Putman et al., 2021; Dee et al., 2023). Stable isotope fractionation of hydrogen and oxygen results in spatial variations of stable isotope compositions in water vapour and precipitation, responding to temperature and moisture changes during evaporation, transport and condensation (Terzer-Wassmuth et al., 2021; Hu et al., 2022; Wang et al., 2022). Although the mass spectrometer and laser-based methodology have been applied in analysing the stable water isotopes in meteoric water (Putman and Bowen, 2019; Wei et al., 2019; Vystavna et al., 2020, Vystavna et al., 2021), the available in-situ observations of stable isotopes are still sparsely distributed around the world, and the isotope data at better spatial and temporal coverage is needed to examine the environmental signals in stable isotopes.

The isotope-enabled models, especially the general circulation models (GCMs), are an essential supplement to the limited observations and provide spatially evenly distributed simulations of water vapour isotopes (Sturm et al., 2010; Steen-Larsen et al., 2017). Developed for decades, these isotope-enabled models usually perform well in describing large-scale spatial patterns and seasonal variability of meteoric water isotopes (Sturm et al., 2010; Midhun and Ramesh, 2016; Yang et al., 2017). However, simulation accuracy assessments using modern observations are always needed before being applied in modern or past climate studies for a specific location (Zhang et al., 2021; Liu et al., 2023). The knowledge about regimes controlling the skill of models to simulate the water isotopic composition is useful to improve the simulations (Shi et al., 2022).

Compared to the stable isotopes in precipitation, water vapour isotopes usually have advantages in evaluating the isotopic climate models (Galewsky et al., 2016; Wang et al., 2023). The water vapour isotopes provide temporally continuous records of atmospheric processes not only on days with rainfall and snowfall, but also on other days. This is especially useful in arid regions where enough precipitation samples cannot be collected. In addition, the vapour is less affected by below-cloud rain-vapour interactions than the precipitation.

Hydrological Processes, vol. 38, issue no. 9, e15276, doi:10.1002/hyp.15276

Evaluating input data sources for isotope-enabled rainfall-runoff models.

Watson, A., C. Birkel, S. Arciniega-Esparza, J. de Waal, J. Miller, Y. Vystavna, J. van Rooyen, A. Welham, **H. Bong**[1,2], K. Yoshimura, J. Helmschrot, A. Künne, and S. Kralisch, 2024

NASA Goddard Institute for Space Studies, New York, NY, USA[1]
Institute of Industrial Science, The University of Tokyo, Tokyo, Japan[2]

Abstract. Isotope-enabled models provide a means to generate robust hydrological simulations. However, daily isotope-enabled rainfall-runoff models applied to larger spatial scales (>100 km^2) require more input data than conventional non-isotope models in the form of precipitation isotope time series, which are difficult to generate even with point station measurements. Spatially distributed isotope data can be circumvented by isotope-enabled climate models. Here, we evaluate the hydrological simulations of the J2000-isotope enabled hydrological model driven with data from corrected and un-corrected isotope-enabled global and regional climate models (isotope-enabled global spectral model [IsoGSM] and isotope-enabled regional spectral model [IsoRSM], respectively) compared with 1 year of measured reference station and a yearly average precipitation isotope input for a pilot site, the data-scarce sub-humid Eerste River catchment in South Africa. The models driven by all input products performed well for upstream and downstream discharge gauges with Nash Sutcliffe efficiency (NSE) from 0.58 to 0.85 and LogNSE of 0.66 to 0.93. The simulated δ^2H stream isotopes using the reference J2000-iso and J2000-isoRSM were good for the main river with a stream Kling Gupta efficiency (KGE) of between 0.4–0.9 and the top 100 Monte Carlo simulations varying by around 5‰ for δ^2H. For smaller tributaries the model was unable to capture the measured stream isotopes due to biased precipitation isotope inputs. Adjusting the J2000-iso with a bias corrected IsoRSM improved the stream and groundwater isotope simulation and outperformed the model driven by an average yearly precipitation isotope input. Differences in simulated hydrological processes were only evident between the models when evaluating percolation with unrealistic simulations for the standard J2000 model. While the regional climate model is computationally more intensive than its global counterpart, it provided better stream isotope simulations and improvements to simulated percolation. Our results indicate that isotope-enabled climate models can provide useful input data in data scarce regions for hydrological models, where improved water management to address climate change impacts is needed.

Introduction. Stable isotopes, being natural constituents of water, act as sensitive tracers of the hydrological cycle due to their responsiveness to temperature, where the fractionation of heavy to light isotopes is influenced by condensation and evaporation (Dansgaard, 1964; Jasechko et al., 2013). The integration of stable isotopes into hydrological models therefore has the potential to improve the simulation of the hydrological cycle by considering the impact of evaporation and source mixing on moisture feedback between the atmosphere and hydrosphere (Kuppel et al., 2018; Nan et al., 2021b; Stadnyk et al., 2013; Watson, Kralisch, et al., 2024). While isotope-enabled models are beneficial in producing more robust simulations of hydrological processes and water balance estimates (Birkel & Soulsby, 2015; Watson et al., 2023), their more widespread application and use at larger catchment scales beyond 100 km^2 is limited by the availability of spatially-distributed precipitation isotope data (Yang et al., 2023).

The global network of precipitation isotope data (GNIP), managed by the International Atomic Energy Agency, is a global database of stable isotope precipitation data at a monthly resolution (International Atomic Energy Agency, 2008; Vystavna et al., 2020) and some more recent daily datasets. The database is reasonably extensive, covering 100 countries with over 900 monitoring stations across tropical, temperate, arid and polar regions.

Nature Communications, vol. 15, issue no. 4354, doi:10.1038/s41467-024-47872-7

Biodiversity loss reduces global terrestrial carbon storage.

Weiskopf, S., F. Isbell, M.I. Arce-Plata, M. Di Marco, M. Harfoot, J. Johnson, S.B. Lerman, B.W. Miller, T. Morelli, A. Mori, **E. Weng**, and S. Ferrier, 2024

NASA Goddard Institute for Space Studies, New York, NY, USA[1]
Center for Climate Systems Research, Columbia University, New York, NY, USA[2]

Abstract. Natural ecosystems store large amounts of carbon globally, as organisms absorb carbon from the atmosphere to build large, long-lasting, or slow-decaying structures such as tree bark or root systems. An ecosystem's carbon sequestration potential is tightly linked to its biological diversity. Yet when considering future projections, many carbon sequestration models fail to account for the role biodiversity plays in carbon storage. Here, we assess the consequences of plant biodiversity loss for carbon storage under multiple climate and land-use change scenarios. We link a macroecological model projecting changes in vascular plant richness under different scenarios with empirical data on relationships between biodiversity and biomass. We find that biodiversity declines from climate and land use change could lead to a global loss of between *7.44-103.14* PgC (global sustainability scenario) and *10.87-145.95* PgC (fossil-fueled development scenario). This indicates a self-reinforcing feedback loop, where higher levels of climate change lead to greater biodiversity loss, which in turn leads to greater carbon emissions and ultimately more climate change. Conversely, biodiversity conservation and restoration can help achieve climate change mitigation goals.

Introduction. Climate change and biodiversity loss have been increasingly recognized as related crises that are most effectively addressed together[1,2,3,4,5]. Hundreds of experimental studies have consistently found that within a place, more diverse assemblages, and in particular more diverse plant assemblages, have higher standing biomass production and carbon sequestration[6,7,8,9]. There are several possible mechanisms for this phenomenon. Species with different traits and resource requirements may be able to utilize more resources in an ecosystem through reduced competition, increased facilitation, or both, which leads to overall more efficient resource use[10,11,12]. At the same time, more diverse assemblages are more likely to contain the most productive species, which can increase overall functioning[13,14]. Indeed, biodiversity loss can be one of the major drivers of productivity loss within ecosystems, on par with elevated carbon dioxide or effects of drought[15]. Thus, while climate change can affect biodiversity, biodiversity loss can also affect climate change by altering carbon sequestration and storage[4,16]. Despite the contribution that biodiversity itself makes to carbon sequestration, high-level nature-based solution initiatives often focus on increasing the spatial extent of natural ecosystems, particularly forests, and not on their diversity or composition[17].

Similarly, ecosystem service models do not always account for the effects of biodiversity. Models projecting changes in biodiversity, ecosystem functioning, and ecosystem services typically operate independently and do not account for interactions or feedbacks[18,19]. For example, Earth System Models (ESMs) typically model terrestrial ecosystems using a small number of plant functional types and do not include biodiversity-productivity mechanisms[20,21]. Not accounting for biodiversity may lead to inaccurate projections of ecosystem function and ecosystem services. For instance, these estimates assume that remnant habitat patches will provide the same level of function even in the face of significant losses of species diversity[22]. Incorporating biodiversity-ecosystem function relationships could improve model accuracy, especially over long timescales as biodiversity effects become stronger over time[23]. For example, an Australian ecosystem modeling exercise found that including species turnover in marine ecosystem models led to very different outcomes for marine fisheries under different climate change scenarios[24].

Geophysical Research Letters, vol. 51, issue no. 13, e2024GL108512, doi:10.1029/2024GL108512

Meteorology modulates the impact of GCM horizontal resolution on underestimation of midlatitude ocean wind speeds.

Werapitiya, G., D. McCoy, **G. Elsaesser**[1,2], P. Field, and S. Rahimi, 2024

NASA Goddard Institute for Space Studies, New York, NY, USA[1]
Department of Applied Physics and Applied Mathematics, Columbia University, New York, NY, USA[2]

Abstract. We utilize ocean 10-m wind speed (U_{10m}) from the microwave Multi-sensor Advanced Climatology data set to examine the coupling between convective cloud and precipitation processes, synoptic state, and U_{10m} and to evaluate the representation of U_{10m} in global climate models (GCMs). We find that midlatitude U_{10m} is underestimated by GCMs relative to observations. We examine two potential mechanisms to explain this model behavior: cold pool formation in cold air outbreaks (CAOs) associated with downdrafts that enhance U_{10m} and sea surface temperature (SST) gradients affecting U_{10m} through thermally forced surface winds at regional scales. When the effects of the CAO index (*M*) and SST gradients on U_{10m} are accounted for, a relationship between GCM horizontal resolution and U_{10m} appears. The strongest correlation between resolution and U_{10m} is over the western boundary currents characterized by frequent CAOs atop strong SST gradients which drives the strongest surface fluxes on Earth.

Introduction. Near surface wind speed is key to our understanding of the atmospheric state. It is critical to topics ranging from the availability of wind energy over the oceans (Possner & Caldeira, 2017), to how climate is affected through air sea exchanges of heat and gas (Fu et al., 2019), and the transition from shallow to deep convection (Elsaesser & Kummerow, 2013). Surface wind speed also affects dust emissions (Evan, 2018) and is important for setting the cloud feedback (Bodas-Salcedo et al., 2019). Surface winds play an integral role in the Earth's energy and hydrological cycles by setting the atmospheric and oceanic circulation (Alexander & Scott, 1997; Hartmann, 2016). Wind speed magnitude and direction impacts the wind stress that serves as a dominant energy source for the kinetic energy driving the ocean circulation (Ferrari & Wunsch, 2009). The drivers of variability in surface wind speed are complex and include both large scale variability in the atmosphere and processes that are internal to the boundary layer.

The most direct way that surface wind affects the climate system is by setting the flux of energy and momentum between the surface and the atmosphere. This flux can be approximated using the bulk formulas for sensible heat (SH), latent heat (LH) fluxes and momentum fluxes (M):

$$\mathrm{SH} = C_p \rho C_{DH} U_r (\mathrm{T}_s - \mathrm{T}_a)$$

$$\mathrm{LH} = L \rho C_{DE} U_r (q_s - q_a)$$

$$\mathrm{M} = \rho C_{DM} U_r^2$$

where C_p and ρ are the specific heat at constant pressure and density of air; L is the LH of vaporization; C_{DH} and C_{DE} are the heat and moisture flux coefficients, C_{DM} is the momentum exchange coefficient; U_r is the mean wind speed at the standard height; and T and q are the air temperature and specific humidity. Subscripts *s* and *a* indicate values for the surface and the air at the reference level respectively. These formulas are used in global climate models (GCMs) to compute heat and momentum fluxes.

Atmospheric Chemistry and Physics, vol. 24, issue no. 20, pp. 11791-11805, doi:10.5194/acp-24-11791-2024

Aerosol size distribution properties associated with cold-air outbreaks in the Norwegian Arctic.

Williams, A.S., J.L. Dedrick, L.M. Russell, **F. Tornow**[1,2], I. Silber, **A.M. Fridlind**[1], B. Swanson, P.J. DeMott, P. Zieger, and R. Krejci, 2024

NASA Goddard Institute for Space Studies, New York, NY, USA[1]
Center for Climate Systems Research, Columbia University, New York, NY, USA[2]

Abstract. The aerosol particles serving as cloud condensation and ice nuclei contribute to key cloud processes associated with cold-air outbreak (CAO) events but are poorly constrained in climate models due to sparse observations. Here we retrieve aerosol number size distribution modes from measurements at Andenes, Norway, during the Cold-Air Outbreaks in the Marine Boundary Layer Experiment (COMBLE) and at Zeppelin Observatory, approximately 1000 km upwind from Andenes at Svalbard. During CAO events at Andenes, the sea-spray-mode number concentration is correlated with strong over-ocean winds with a mean of 8±4 cm^{-3} that is 71 % higher than during non-CAO conditions. Additionally, during CAO events at Andenes, the mean Hoppel minimum diameter is 6 nm smaller than during non-CAO conditions, though the estimated supersaturation is lower, and the mean number concentration of particles that likely activated in-cloud is 109±61 cm^{-3} with no statistically significant difference from the non-CAO mean of 99±66 cm^{-3}. For CAO trajectories between Zeppelin Observatory and Andenes, the upwind-to-downwind change in number concentration is the largest for the accumulation mode with a mean decrease of 93±95 cm^{-3}, likely attributable primarily to precipitation scavenging. These characteristic properties of aerosol number size distributions during CAO events provide guidance for evaluating CAO aerosol–cloud interaction processes in models.

Introduction. The equatorward transport of polar air masses brings cold air over a relatively warmer open ocean, spurring large turbulent surface fluxes of heat and moisture and creating so-called marine cold-air outbreak (CAO) events. The forming clouds often appear first in the shape of rolls (Brümmer, 1999) before filling in towards a near-overcast deck and then transitioning into a more broken, open-cellular state further downwind (Abel et al., 2017; Lloyd et al., 2018; McCoy et al., 2017; Geerts et al., 2022). Such a cloud regime transition during CAO events is often seen in satellite imagery (e.g., Fig. 1 of Geerts et al., 2022) and has important implications for the regional radiation budget (McCoy et al., 2017). Climate and numerical weather prediction models struggle to accurately capture the clouds associated with CAO events. Such model limitations emerge since important dynamical aspects are unresolved (Field et al., 2017). In addition, there is evidence of strong cloud and aerosol microphysical processes that may modulate the macrophysical structure of clouds. For example, Tornow et al. (2021) found that mid-latitude CAO cloud transitions, which resembled observations, could only be simulated when the number concentration of aerosols serving as cloud condensation nuclei (CCN) was allowed to evolve with time, as aerosol can control the onset of transition-driving precipitation (Abel et al., 2017; Tornow et al., 2021). For polar CAOs of lower temperature, aerosol may additionally provide a reservoir for ice nuclei (e.g., Bigg, 1996). Previous modeling of cold-air outbreaks has typically relied on sparse observational constraints (e.g., Field et al., 2014; Abel et al., 2017; Tornow et al., 2023), illustrating a need for observations of aerosol properties associated with CAO events in order to inform, constrain, and improve model simulations and forecasts.

Aerosol number concentrations in the Arctic are typically very low, with median concentrations consistently less than 400 cm^{-3} (Croft et al., 2016; Pernov et al., 2022; Freud et al., 2017; Tunved et al., 2013). The annual maximum in number concentration at Zeppelin Observatory in Svalbard is during spring due to an increase in accumulation-mode particles (termed Arctic haze), with a maximum in Aitken-mode particles during summer and an annual minimum during fall (Croft et al., 2016; Pernov et al., 2022; Freud et al., 2017; Tunved et al., 2013; Schmale et al., 2022).

Sciences Advances, vol. 10, issue no. 49, eadq3367, doi:10.1126/sciadv.adq3367

Heat disproportionately kills young people: Evidence from wet-bulb temperature in Mexico.

Wilson, A.J., R.D. Bressler, **C. Ivanovich**[1,2,3], C. Tuholske, C. Raymond[4], **R.M. Horton**[1,2,3], A. Sobel, P. Kinney, T. Cavazos, and J.G. Shrader, 2024

NASA Goddard Institute for Space Studies, New York, NY, USA[1]
Department of Earth and Environmental Sciences, Columbia University, New York, NY, USA[2]
Climate School, Columbia University, New York, NY, USA[3]
NASA Jet Propulsion Laboratory, La Cañada Flintridge, CA, USA[4]

Abstract. Recent studies project that temperature-related mortality will be the largest source of damage from climate change, with particular concern for the elderly whom it is believed bear the largest heat-related mortality risk. We study heat and mortality in Mexico, a country that exhibits a unique combination of universal mortality microdata and among the most extreme levels of humid heat. Combining detailed measurements of wet-bulb temperature with age-specific mortality data, we find that younger people who are particularly vulnerable to heat: People under 35 years old account for 75% of recent heat-related deaths and 87% of heat-related lost life years, while those 50 and older account for 96% of cold-related deaths and 80% of cold-related lost life years. We develop high-resolution projections of humid heat and associated mortality and find that under the end-of-century SSP 3?7.0 emissions scenario, temperature-related deaths shift from older to younger people. Deaths among under-35-year-olds increase 32% while decreasing by 33% among other age groups. Analysis of temperature exposure and microdata finds the majority of heat-related deaths are among people under 35 years old.

Introduction. Historically, temperature exposure has caused a large number of premature deaths (*1*–*3*). Heat-related mortality is expected to increase under climate change (*4*–*27*). As the evidence base has grown, multiple studies have found that the elderly are especially vulnerable to heat (*6*, *11*, *14*, *17*, *18*, *28*, *29*). Furthermore, many other studies have expressed particular concern for joint heat and humidity extremes, given the importance of perspiration for human thermoregulation (*30*–*36*).

In this study, we explore the relationship between humid heat and mortality in Mexico, a country that exhibits a unique combination of rich, age-specific, universal mortality microdata and among the most extreme historical humid heat exposures. We find that historically, the majority of heat-related mortality in Mexico has been concentrated among younger people: 75% of heat-related deaths and 87% of heat-related lost life years occur among those under 35 years old. By contrast, the vast majority of cold-related mortality is concentrated among older people: 98% of cold-related deaths and 90% of cold-related lost life years occur among those over 35, with the majority of cold-related deaths occurring among individuals older than 70 years. We then develop projections of humid heat and associated outcomes to assess the future implications of these findings. As in other studies, we find that climate change is expected to increase heat-related mortality while decreasing cold-related mortality. However, we uncover an important source of future climate-driven inequality: The disproportionate impact of heat and cold across age groups reallocates the temperature-related mortality burden from the elderly (who are more affected by cold) to the young (who are more affected by heat). This has important implications for understanding the distributional impacts of climate change and for developing effective policies to adapt to these impacts.

Earth System Science Data, vol. 16, issue no. 11, pp.5405-5428, doi:10.5194/essd-16-5405-2024

PRODEM: An annual series of summer DEMs (2019 through 2022) of the marginal areas of the Greenland Ice Sheet.

Winstrup, M., H. Ranndal, S.H. Larsen, S.B. Simonsen, **K.D. Mankoff**[1,2,3], R.S. Fausto, and L. Sandberg Sørensen, 2024

NASA Goddard Institute for Space Studies, New York, NY, USA[1]
Autonomic Integra, LLC, Institute for Space Studies, New York, NY, USA[2]
Geological Survey of Denmark and Greenland (GEUS), Copenhagen, Denmark[3]

Abstract. Surface topography across the marginal zone of the Greenland Ice Sheet is constantly evolving in response to changing weather, season, climate, and ice dynamics. However, current digital elevation models (DEMs) for the ice sheet are usually based on data from a multi-year period, thus obscuring these changes over time. Here we present four 500 m resolution summer DEMs (PRODEMs) of the Greenland Ice Sheet marginal zone for 2019 through 2022. The PRODEMs cover the marginal zone from the ice edge to 50 km inland, hence capturing all Greenland outlet glaciers. Each PRODEM is based on data fusion of CryoSat-2 radar altimetry and ICESat-2 laser altimetry using regionally varying kriging of elevation anomalies relative to ArcticDEM. The PRODEMs are validated using leave-one-out cross-validation, and PRODEM19 is further validated against an external data set, showcasing their ability to correctly represent surface elevations within the associated spatially varying prediction uncertainties. We observe a general lowering of surface elevations during the 4-year PRODEM period, but the spatial pattern of change is highly complex and with annual changes superimposed. The PRODEMs enable detailed studies of the marginal ice sheet elevation changes. With their high spatio-temporal resolution, the PRODEMs will be of value to a wide range of researchers and users studying ice sheet dynamics and monitoring how the ice sheet responds to changing environmental conditions. PRODEMs from summer 2019 through 2022 are available at https://doi.org/10.22008/FK2/52WWHG (Winstrup, 2024), and we plan to annually update the product henceforth.

Introduction. During the past few decades, the Greenland Ice Sheet has lost mass at an increasing rate (Mankoff et al., 2021; Otosaka et al., 2023; Simonsen et al., 2021; The IMBIE Team, 2020), contributing to global sea level rise (Moon et al., 2018; WCRP Global Sea Level Budget Group, 2018). The largest changes take place near the margin of the ice sheet. Most of the ice sheet margin experiences a large and progressive thinning, but the response is highly heterogeneous, due to the impacts and feedback from temperature, precipitation, and ice flow (Krabill et al., 2004; Sørensen et al., 2018). Coupled ice sheet–climate models suggest that future ice loss from the Greenland Ice Sheet will primarily be driven by changes in surface mass balance, particularly increased ablation at the ice sheet margin due to atmospheric warming (Quiquet and Dumas, 2021).

The ice sheet marginal zone, here defined as a 50 km periphery of the ice sheet, is characterized by a complex interplay of processes. Several feedback loops involve topography and elevation, including, but not limited to, elevation–temperature feedback, local and regional weather, hydrology, and ice dynamics. The elevation–temperature feedback loop means that as the ice sheet thins, the lower surface will be exposed to higher temperatures (van As et al., 2017), leading to increased surface melt and further thinning (Aschwanden et al., 2019; Delhasse et al., 2024). The ice sheet geometry also affects local and regional weather patterns (Ettema et al., 2009). As orographic precipitation is the main driver of Greenland precipitation in coastal areas (Lenaerts et al., 2019), changes in topography may greatly impact precipitation patterns, thereby influencing the surface mass balance. Further, changing surface slopes and ice thicknesses will change both supra- and subglacial hydrological networks, with subsequent impacts on ice flow (Andrews et al., 2018; Maier et al., 2023).

Geophysical Research Letters, vol. 51, issue no. 7, e2023GL107983, doi:10.1029/2023GL107983

Decadal evolution of ice-ocean interactions at a large East Greenland glacier resolved at fjord scale with downscaled ocean models and observations.

Wood, M.[1], A. Khazendar[1], I. Fenty[1], **K.D. Mankoff**[2,3], A.T. Nguyen, K. Schulz, J.K. Willis[1], and H. Zhang[1], 2024

NASA Jet Propulsion Laboratory, California Institute of Technology, Pasadena, CA, USA[1]
NASA Goddard Institute for Space Studies, New York, NY, USA[2]
Autonomic Integra LLC, New York, NY, USA[3]

Abstract. In recent decades, the Greenland ice sheet has been losing mass through glacier retreat and ice flow acceleration. This mass loss is linked with variations in submarine melt, yet existing ocean models are either coarse global simulations focused on decadal-scale variability or fine-scale simulations for process-based investigations. Here, we unite these scales with a framework to downscale from a global state estimate (15 km) into a regional model (3 km) that resolves circulation on the continental shelf. We further downscale into a fjord-scale model (500 m) that resolves circulation inside fjords and quantifies melt. We demonstrate this approach in Scoresby Sund, East Greenland, and find that interannual variations in submarine melt at Daugaard-Jensen glacier induced by ocean temperature variability are consistent with the decadal changes in glacier ice dynamics. This study provides a framework by which coarse-resolution models can be refined to quantify glacier submarine melt for future ice sheet projections.

Introduction. In recent decades, the Greenland ice sheet has been losing mass and is presently contributing approximately 0.5 mm/yr to global sea-level rise (Mankoff et al., 2021). This mass loss is approximately evenly split between enhanced melt on the surface of the ice sheet that runs off to the ocean and increased discharge of ice from Greenland's marine-terminating glaciers. The latter process, termed dynamic mass loss, is instigated by submarine glacier melt which causes glaciers to retreat (Wood et al., 2021) and subsequently accelerate (King et al., 2020), increasing the flux of ice into the ocean (Mankoff et al., 2021). The magnitude of melting depends on the volume and distribution of subglacial discharge at glacier termini, and on the thermal forcing of ocean water (Slater et al., 2015; Xu et al., 2013). Thus, the decadal evolution of submarine melt rates, driven by a combination of variations in regional air and ocean temperatures (Slater & Straneo, 2022) is directly linked to sea-level rise contributions from the ice sheet.

Despite recent advances in our knowledge of the factors contributing to Greenland's ice loss, ice models predicting sea-level rise contributions from the ice sheet systematically underestimate historical ice loss rates, casting doubt on the future projections (Aschwanden et al., 2021; Goelzer et al., 2020). These model-observation differences are largely attributed to uncertainties in the magnitude and variability of submarine melt rates and the subsequent processes that induce dynamic mass loss (Fox-Kemper et al., 2021)—in effect, the oceanic boundary conditions that drive dynamic change in ice sheet models. One of the main sources of this uncertainty arises from a lack of observations and model simulations of ocean properties within Greenland's fjords. From an observational perspective, there are few in situ measurements near Greenland's glaciers, and the majority of those which exist are from recent years after dynamic mass loss had initiated (Mouginot et al., 2019). From an ocean modeling standpoint, most ocean models that resolve fjord circulation and melt are constructed for idealized experiments, are typically forced at their boundary by a single observation, and are run for a period of a few years or less (e.g., Slater et al., 2015; Xu et al., 2013; Zhao et al., 2021). To our knowledge, there are no models, idealized or otherwise, which have been constructed to investigate temperature variability within the fjord network on a decadal scale. As a result, the glaciological modeling community has been left to estimate submarine melt on Greenland's ice from coarse resolution models and sparse ocean observations outside of the fjords.

Nature Astronomy, vol. 8, issue no. 1, pp.101-110, doi:10.1038/s41550-023-02145-z

Inferring chemical disequilibrium biosignatures for proterozoic Earth-like exoplanets.

Young, A.[1], T. Robinson, J. Krissansen-Totton, E.W. Schwieterman, N. Wogan[1], **M. Way**[2,3], **L. Sohl**[2,4], G. Arney[5], C. Reinhard, M. Line, D. Catling, and J. Windsor, 2024

NASA Ames Research Center, Space Science Division, Moffett Field, CA, USA[1]
NASA Goddard Institute for Space Studies, New York, NY, USA[2]
Theoretical Astrophysics Department of Physics and Astronomy, Uppsala University, Uppsala, Sweden[3]
Center for Climate Systems Research, Columbia University, New York, NY, USA[4]
NASA Goddard Space Flight Center, Greenbelt, MD, USA[5]

Abstract. Chemical disequilibrium quantified using the available free energy has previously been proposed as a potential biosignature. However, researchers remotely sensing exoplanet biosignatures have not yet investigated how observational uncertainties impact the ability to infer a life-generated available free energy. We pair an atmospheric retrieval tool to a thermodynamics model to assess the detectability of chemical disequilibrium signatures of Earth-like exoplanets, focusing on the Proterozoic eon when the atmospheric abundances of oxygen–methane disequilibrium pairs may have been relatively high. Retrieval model studies applied across a range of gas abundances revealed that order-of-magnitude constraints on the disequilibrium energy are achieved with simulated reflected-light observations for the high-abundance scenario and high signal-to-noise ratios (50), whereas weak constraints are found for moderate signal-to-noise ratios (20–30) and medium- to low-abundance cases. Furthermore, the disequilibrium-energy constraints are improved by using the modest thermal information encoded in water vapour opacities at optical and near-infrared wavelengths. These results highlight how remotely detecting chemical disequilibrium biosignatures can be a useful and metabolism-agnostic approach to biosignature detection.

Introduction. Exoplanet exploration science is making rapid progress towards the detection and characterization of potentially habitable worlds[1]. Continuing[2,3] and near-future exoplanet strategies[4] will focus on the search for atmospheric gases, including the chemical signatures of life (or biosignatures)[5,6,7]. Recently, the Decadal Survey on Astronomy and Astrophysics 2020 report[4] recommended space-based high-contrast imaging of potentially life-bearing exoplanets as a leading priority for the coming decade. When attempting to infer whether a distant world is inhabited, the chemical disequilibrium is a potential indicator of life and has a long history of study in Solar System planetary environments[8,9,10]. A key example is the coexistence of O_2 and CH_4 in Earth's atmosphere because the strong biological production rates of CH_4 are able to maintain this gas at appreciable levels despite its relatively short chemical lifetime (roughly a decade) in an oxidizing atmosphere.

A primary metric for quantifying chemical disequilibrium involves calculating the difference in chemical energy associated with an observed system and that system's theoretical equilibrium state. Recent work has explored the application of one such metric—the available Gibbs free energy—to Solar System worlds and to Earth's planetary evolution[11,12,13]. Although the available Gibbs free energy is a promising metric for interpreting chemical disequilibrium biosignatures, little is known about how observational uncertainties will impact our ability to constrain the available Gibbs free energy for Earth-like exoplanets, where 'Earth-like' refers to an ocean-bearing, Earth-sized world with surface pressures and temperatures like those on Earth and with an atmosphere dominated by N_2, H_2O and CO_2 with trace amounts of CH_4 and varying levels of O_2.

Exoplanet atmospheric characterization, including the search for biosignature gases, proceeds through retrieval analysis or atmospheric inference (for example, refs. [14,15,16,17,18]). In short, a retrieval framework enables the statistical exploration of atmospheric states that are consistent with a given set of spectral observations, whether these are real or simulated.

Environment Research Climate, vol. 3, issue no. 4, 041005, doi:10.1088/2752-5295/ad929c

Decreased Northern Hemisphere precipitation from consecutive CO_2 doublings is associated with significant AMOC weakening.

Zhang, X., D.W. Waugh, I. Mitevski, **C. Orbe**[1,2], and L.M. Polvani, 2024

NASA Goddard Institute for Space Studies, New York, NY, USA[1]
Department of Applied Physics and Applied Mathematics, Columbia University, New York, NY, USA[2]

Abstract. Previous studies found many climate properties such as northern hemisphere (NH) surface temperature and precipitation respond non-monotonically when CO_2 is increased from 1× to 8×CO_2 relative to pre-industrial levels. Here, we explore the robustness of the non-monotonicity in the NH precipitation response in 11 coupled climate models. Eight models show a decrease in NH precipitation under repeated CO_2 doubling, indicating that the non-monotonic response is a common but not universal result. Although common, the critical CO_2 level where the NH precipitation decrease first occurs differs widely across models, ranging from 2×CO_2 to 8×CO_2. These models also show a prominent weakening in the Atlantic meridional overturning circulation (AMOC) at the same critical CO_2 level, with the AMOC weakening leading the precipitation decrease. The sensitivities of NH precipitation and the AMOC to CO_2 doublings are positively correlated, especially when the AMOC weakens beyond 10 Sv. This suggests that the differences in models' AMOC response can explain their contrasting NH precipitation responses, where models with a large AMOC weakening have decreased NH precipitation. Regionally, this decrease in NH precipitation is the most prominent over the North Atlantic, Europe and the tropical Pacific. Our results suggest that special care must be taken with the use of pattern scaling to inform regional climate decision-making.

Introduction. In a recent study, Mitevski *et al* (2021, hereafter M21) found non-monotonic responses of a range of climate properties to CO_2 forcing in two fully coupled climate models. Specifically, they reported decreased northern hemisphere (NH) surface temperature, expanded Arctic sea ice extent, reduced NH precipitation, contracted subtropical dry zones, and a stronger NH Hadley cell with increasing CO_2 beyond some threshold value, in abrupt forcing simulations spanning 1–8×CO_2. While this surprising behavior was found in both models, the threshold CO_2 concentration beyond which it occurred was different between the two models: it appeared between 2×CO_2 and 3×CO_2 for one model, but between 3×CO_2 and 4×CO_2 for the other model.

The mechanisms behind the non-monotonic response to CO_2 increase have also been explored. M21 found that the non-monotonicity is not present in the slab-ocean versions of the same models, clearly implicating a key role for ocean dynamics. Subsequent studies (Mitevski *et al* 2022, 2023, Orbe *et al* 2023) showed that such ocean dynamics are related to cooling over the North Atlantic (the North Atlantic warming hole, NAWH) and a concurrent weakening of the Atlantic meridional overturning circulation (AMOC). Multiple North Atlantic 'hosing' experiments have demonstrated that a weakened AMOC leads to the NAWH, decreased precipitation over the NH, and a southward shift of the ITCZ in coupled climate models (Zhang and Delworth 2005, Stouffer *et al* 2006, Jackson *et al* 2015, Liu *et al* 2020). The NAWH not only reduces local SSTs and the NH atmospheric moisture content (Jackson *et al* 2015), but also strengthens the meridional SST gradient and changes the cross-equatorial atmospheric heat transport (Moreno-Chamarro *et al* 2019), which explain the NH precipitation decrease.

This non-monotonic response has important implications when extrapolating results from 4×CO_2 simulations to other levels of CO_2 forcing (Chadwick and Good 2013). A particular application is the use of 'pattern scaling' that provides quantitative decision-relevant climate information on a regional scale over a range of scenarios (e.g. Lopez *et al* 2014). Furthermore, given the difference in CO_2 levels at which the non-monotonicity appears, it represents a plausible source of uncertainty in the model spread in response to 4×CO_2 forcing (e.g. Grise and Polvani 2016).

Journal of Geophysical Research: Atmospheres, vol. 129, issue no. 9, e2023JD040437, doi:10.1029/2023JD040437

Precipitation ^{17}O-excess altered during tropical convection: Evidence from monsoon cold surges in Singapore.

Zhang, Y., S. He, B. Wee, **A.N. LeGrande**[1], J. Wang, N. Goodkin, and X. Wang, 2024

NASA Goddard Institute for Space Studies, New York, NY, USA[1]

Abstract. Despite the recent recognition of ^{17}O-excess as a promising new tracer for hydrological processes, our knowledge of the control mechanisms underlying ^{17}O-excess in tropical regions remains limited. To understand how microphysical processes during tropical convection affect precipitation isotope ratios, particularly ^{17}O-excess, in Singapore, we collected precipitation samples at minute intervals from six rain events associated with cold surges during the Northeast Monsoon seasons and analyzed their triple oxygen isotopes. Our results show that precipitation $\delta^{18}O$ decreases in the convective zones and then gradually increases in the stratiform zones, while d-excess exhibits an inverse trend. This correlation between $\delta^{18}O$ and d-excess indicates that rain evaporation plays a crucial role in regulating precipitation isotopes. Moreover, the rain events with a higher upstream rainout amount have lower $\delta^{18}O$ and higher ^{17}O-excess values, suggesting that precipitation $\delta^{18}O$ and ^{17}O-excess likely reflect the integrated upstream convective activity. Microphysical processes associated with upstream convection, such as rain evaporation and vapor recycling, are potential mechanisms that increase ^{17}O-excess values along moisture transport pathways for a rain event, and hence, undermine the effectiveness of ^{17}O-excess as a tracer of moisture source humidity. Contrary to the negative correlation observed in monthly precipitation, there is generally a positive correlation between d-excess and ^{17}O-excess at the event scale. However, this correlation weakens as convective rain intensifies, suggesting that stronger convection can attenuate the positive correlation between d-excess and ^{17}O-excess. Therefore, it is crucial to consider how tropical convection alters ^{17}O-excess when utilizing this tracer to interpret atmospheric dynamics and hydrological processes.

Introduction. Water isotopes ($\delta^{18}O$ and $\delta^{2}H$) along with a secondary parameter d-excess (d-excess = $\delta^{2}H – 8 \times \delta^{18}O$) have been successfully used as natural proxies of hydrological and climatic processes (Craig, 1961; Dansgaard, 1964). Although d-excess was first applied as a proxy of relative humidity (RH) in moisture source regions (Jouzel & Merlivat, 1984), it is also affected by sea surface temperature (SST) in source regions and can be influenced by meteorological parameters at precipitation sites such as RH (Benetti et al., 2014; Johnsen et al., 1989; Kaseke et al., 2018). More recently, a new hydrological tracer, ^{17}O-excess ($^{17}O\text{-excess} = \ln(\delta^{17}O+1) – 0.528 \times \ln(\delta^{18}O+1)$), has been proposed (Barkan & Luz, 2005). Laboratory experiments and theoretical calculations have demonstrated that ^{17}O-excess is primarily controlled by evaporative conditions of moisture source regions and negatively correlated with the RH of these source regions (Angert et al., 2004; Barkan & Luz, 2007). Unlike d-excess, ^{17}O-excess is insensitive to SST, making it potentially a more reliable proxy for the moisture source RH.

Recent advancements in analytical methods (Barkan & Luz, 2005) and instrumentation (Steig et al., 2014) have facilitated the application of ^{17}O-excess in hydrology and, particularly, in paleoclimate studies (e.g., ice cores, sediments and speleothems) to understand historical RH (e.g., Bindeman, 2021; Landais et al., 2008; Sha et al., 2020). However, observations suggest that subsequent processes following source evaporation likely have altered ^{17}O-excess, thereby compromising the ability of precipitation ^{17}O-excess to serve as a proxy of RH from source regions (e.g., He et al., 2021; Landais et al., 2010; Li et al., 2015; Miller, 2018; Pang et al., 2015; Schoenemann & Steig, 2016). In low-latitude regions, contradicting conclusions have been drawn from studies on precipitation ^{17}O-excess. For instance, a study conducted in Okinawa, a subtropical island in Japan, found that precipitation ^{17}O-excess records moisture source humidity conditions (Uechi & Uemura, 2019). In contrast, rain evaporation was observed to significantly alter tropical rainfall in western Africa, leading to a positive correlation between ^{17}O-excess and on-site RH (Landais et al., 2010).

Atmospheric Chemistry & Physics, vol. 24, issue no. 12, pp. 6965-6985, doi:10.5194/acp-24-6965-2024

Influence of atmospheric circulation on the interannual variability of transport from global and regional emissions into the Arctic.

Zheng, C.[2], Y. Wu[2], M. Ting[2], and **C. Orbe**[1,2], 2024

NASA Goddard Institute for Space Studies, New York, NY, USA[1]
Lamont-Doherty Earth Observatory, Palisades, NY, USA[2]

Abstract. Trace gases and aerosols play a crucial role in shaping Arctic climate through their impacts on radiation and chemistry. The concentration of these substances over the Arctic is largely determined by long-range transport originating from midlatitude and tropical source regions. In this study, we explore how atmospheric circulation modulates the interannual variability of long-range transport into the Arctic by utilizing a chemistry–climate model. Idealized tracers, which have fixed lifetimes and spatially varying but temporally fixed surface emissions corresponding to the climatology of anthropogenic emissions of the year 2000, are employed to isolate the role of atmospheric transport from emission and chemistry in modulating interannual variability. Tracers emitted from different source regions are tagged to quantify their relative contributions. Model simulations reveal that tracers from Europe, East Asia, and North America contribute the most to Arctic tracer mass, followed by those from the Tibetan Plateau and South Asia, as well as the Middle East. These regional tracers are predominantly transported into the Arctic middle to upper troposphere, with the exception of tracers from Europe during winter, which are transported into the Arctic lower troposphere. Our analysis shows that the interannual variability of transport into the Arctic for each regional tracer is determined by the atmospheric circulation over the corresponding emission region; i.e., anomalous poleward and eastward winds over the source region promote transport into the Arctic. Considering tracers with global emissions, a southward shift of the midlatitude jet during winter favors increased transport into the Arctic, particularly for tracers emitted over Asia, aligning with previous studies. Comparisons of tracers with different lifetimes indicate that the interannual variability of shorter lifetime tracers is predominantly influenced by regional tracers with shorter transport pathways into the Arctic (e.g., Europe), while the interannual variability of longer lifetime tracers is more contributed by regional tracers with higher emissions (e.g., East Asia).

Introduction. In recent decades, rapid warming has been observed in the Arctic, with a warming rate significantly faster than the global average (e.g., IPCC, 2021). Trace gases and aerosols, primarily transported into the Arctic from emission sources in the midlatitude and the tropics (e.g., Bottenheim et al., 2004; Fisher et al., 2010; Klonecki et al., 2003; Kupiszewski et al., 2013; Law and Stohl, 2007; Rahn and McCaffrey, 1980; Shindell, 2007; Shindell et al., 2008; Stohl, 2006), have substantial impacts on Arctic chemistry as well as Arctic climate via their radiative influences. Shortwave radiative transfer can be modulated by black carbon in the Arctic, as it absorbs sunlight (e.g., Quinn et al., 2006; Warren and Wiscombe, 1980) when deposited onto the Arctic surface or when suspended in the Arctic haze layer, which has been suggested to execute twice as large a climate forcing as carbon dioxide over the Arctic (Hansen and Nazarenko, 2004). Aerosols also modulate longwave radiative transfer, particularly via their indirect effects as they affect the microphysical properties of clouds (Coopman et al., 2018; Garrett and Zhao, 2006; Lubin and Vogelmann, 2006). Additionally, halocarbons originating from midlatitudes influence the production of tropospheric ozone in the Arctic (Atlas et al., 2003; Klonecki et al., 2003), which acts as a greenhouse gas. These influences highlight the importance of comprehending the transport processes responsible for bringing trace gases and aerosols from the midlatitudes and the tropics into the Arctic.

Atmospheric Chemistry & Physics, vol. 24, issue no. 1, pp. 509-532, doi:10.5194/acp-24-509-2024

Exploring the ENSO modulation of the QBO periods with GISS E2.2 models.

Zhou, T.[1,2], **K.J. DallaSanta**[1,3], **C. Orbe**[1,3], **D.H. Rind**[1], **J.A. Jonas**[1,2], **L. Nazarenko**[1,2], **G.A. Schmidt**[1], and **G. Russell**[1], 2024

NASA Goddard Institute for Space Studies, New York, NY, USA[1]
Center for Climate Systems Research, Columbia University, New York, NY, USA[2]
Department of Applied Physics and Applied Mathematics, Columbia University, New York, NY, USA[3]

Abstract. Observational studies have shown that the El Niño–Southern Oscillation (ENSO) exerts an influence on the Quasi-Biennial Oscillation (QBO). The downward propagation of the QBO tends to speed up and slow down during El Niño and La Niña, respectively. Recent results from general circulation models have indicated that the ENSO modulation of the QBO requires a relatively high horizontal resolution, and that it does not show up in the climate models with parameterized but temporally constant gravity wave sources. Here, we demonstrate that the NASA Goddard Institute for Space Studies (GISS) E2.2 models can capture the observed ENSO modulation of the QBO period with a horizontal resolution of 2° latitude by 2.5° longitude but with its gravity wave sources being parameterized interactively. This is because El Niño events lead to more vigorous gravity wave sources generating more absolute momentum fluxes over the equatorial belt, as well as less filtering of these waves into the tropical lower stratosphere through a weakening of the Walker circulation. Various components of the ENSO system, such as the sea surface temperatures, the convective activities, and the Walker circulation, are intimately involved in the generation and propagation of parameterized gravity waves, through which ENSO modulates the QBO period in GISS E2.2 models.

Introduction. The Quasi-Biennial Oscillation (QBO) dominates the interannual variability in the tropical stratosphere (Baldwin et al., 2001), whereas the El Niño–Southern Oscillation (ENSO) is the primary mode of interseasonal–interannual variability over the tropical Pacific Ocean (Wang et al., 2017). It is well known that both the QBO and the ENSO have far-reaching implications for global weather and climate systems (Hamilton et al., 2015; Philander, 1990; Sarachik and Cane, 2010; Domeisen et al., 2019).

The QBO and the ENSO defy linear relationships (Angell, 1986; Xu, 1992; Hu et al., 2012) as highlighted by that fact that while the QBO and ENSO indices are negatively correlated before the 1980s and positively correlated after the 1980s (Garfinkel and Hartmann, 2007; Domeisen et al., 2019; Rao et al., 2020c), they are virtually uncorrelated over the longer periods from 1953 to recent times (Garfinkel and Hartmann, 2007; Geller et al., 2016b, see their Fig. 5 for details). However, Maruyama and Tsuneoka (1988) spotted an intriguing connection between the anomalously short easterly phase of the QBO at 50 hPa in 1987 and the El Niño event that persisted throughout that year. Based on the results from a mechanistic model, Geller et. al. (1997) suggested that the equatorial sea surface temperatures (SSTs) modulate the wave momentum fluxes into the stratosphere and thus the QBO. Remarkably, an observational study conducted by Taguchi (2010) demonstrated that the downward propagation of the QBO tends to speed up during El Niño and slow down during La Niña, whereas the amplitude of the QBO tends to be smaller during El Niño and larger during La Niña, respectively. Using radiosonde data from 10 near-equatorial stations distributed along the Equator, Yuan et al. (2014) found that the ENSO modulation of the QBO period is more robust than that of the QBO amplitude, which is likely due to the fact that the QBO periods are characterized by a high degree of zonal uniformity, whereas the QBO amplitudes exhibit zonal asymmetries of about 10 % (Hamilton et al., 2004, see their Fig. 15).

C. Chapters, Conferences, Workshops, & Other Publications

1. Butler, A.H., D. Shindell, **G. Faluvegi**, A. Bais, E.M. Bednarz, J.S. Daniel, E. Fleming, D. Kinnison, S. Madronich, O. Morgenstern, D. Plummer, R.W. Portmann, S. Tilmes, A.R. Ravishankara, Z. Wang, S. Wei, Q. Zhang, and Y. Zhang, 2024: Chapter 4: Impacts on climate, air quality and the ozone layer. In *Global Nitrous Oxide Assessment*. D.R. Kanter and A.R. Ravishankara, Eds., United Nations Environment Programme and Food and Agriculture Organization, pp. 87-131, doi:10.59117/20.500.11822/46562……228

2. Carroll Steward, K., D. Gosselin, **M. Chandler**, and C.T. Forbes, 2024: Student outcomes of teaching about socioscientific issues in secondary science classrooms: Applications of EzGCM. *J. Sci. Educ. Technol.*, **33**, no. 2, 195-207, doi:10.1007/s10956-023-10068-7…….....229

3. Cesana, G., A.S. Ackerman, T. Vaillant de Guélis, and D.S. Henderson, 2024: Cloud-radiation interactions and cloud-climate feedbacks from an active-sensor satellite perspective. In *Clouds and Their Climatic Impact: Radiation, Circulation, and Precipitation*. S. Sullivan and C. Hoose, Eds., Geophysical Monograph Series, vol. 281, American Geophysical Union, pp. 87-102, doi:10.1002/9781119700357.ch4…….230

4. **Cesana, G.V.**, **A.S. Ackerman**, **A.M. Fridlind**, I. Silber, **A.D. Genio**, M.D. Zelinka, and H. Chepfer, 2024: Better constraining supercooled clouds could reduce projected warming spread. In *Radiation Processes in the Atmosphere and Ocean, 4–8 July 2022, Thessaloniki, Greece*, AIP Conference Proceedings, vol. 2988, AIP Publishing, p. 070009, doi:10.1063/5.0183626……231

5. Järvinen, E., B. van Diedenhoven, N. Magee, S. Neshyba, M. Schnaiter, G. Xu, O. Jourdan, D. Delene, F. Waitz, S. Lolli, and S. Kato, 2024: Ice crystal complexity and link to the cirrus cloud radiative effect. In *Clouds and Their Climatic Impacts*. S.C. Sullivan and C. Hoose, Eds., Geophysical Monograph Series, vol. 271, American Geophysical Union, pp. 47-85, doi:10.1002/9781119700357.ch3……...232

6. Kleese van Dam, K., A. Schlosser, J. Schmutz, B. Bond-Lamberty, K. Fangan, **A.M. Fridlind**, S. Gregurick, D. Niyogi, D. Segre, and P. Weisenhorn, 2024: A Unified Data Infrastructure for Biological and Environmental Research: A Report from the BER Advisory Committee. DOE/SC-0214. U.S. Department of Energy, Office of Science, Biological and Environmental Research Program, doi:10.2172/2331276…….233

7. **Tsigaridis, K.**, **R. Field**, **S.E. Bauer**, M.N. Ross, C. Maloney, **G.A. Schmidt**, and K.H. Rosenlof, 2024: Composition and climate impacts of increasing launches to Low Earth Orbit. In *AIAA SciTech 2024 Forum, 8-12 January 2024, Orlando, FL*, American Institute of Aeronautics and Astronautics, doi:10.2514/6.2024-2168…….....234

8. Werdell, P.J., B. Franz, C. Poulin, J. Allen**, B. Cairns,** S. Caplan, I. Cetinic, S. Craig, M. Gao, O. Hasekamp, A. Ibrahim, K. Knobelspiesse, A. Mannino, J.V. Martins, L. McKinna, G. Meister, F. Patt, C. Proctor, C. Rajapakshe, I. Soto Ramos, J. Rietjens, A. Sayer, and E. Sirk, 2024: Life after launch: A snapshot of the first six months of NASA's Plankton, Aerosol, Cloud, Ocean Ecosystem (PACE) mission. In Sensors, Systems, and Next-Generation Satellites XXVIII: 16-20 September 2024, Edinburgh. S.R. Babu, A. Hélière, and T. Kimura, Eds., Proc. SPIE, vol. 13192, p. 131920E, doi:10.1117/12.3033830…….235

Global Nitrous Oxide Assessment. D.R. Kanter and A.R. Ravishankara, Eds., United Nations Environment Programme and Food and Agriculture Organization, pp. 87-131, doi:10.59117/20.500.11822/46562

Chapter 4: Impacts on climate, air quality and the ozone layer.

Butler, A.H., D. Shindell, **G. Faluvegi**[1,2], A. Bais, E.M. Bednarz, J.S. Daniel, E. Fleming, D. Kinnison, S. Madronich, O. Morgenstern, D. Plummer, R.W. Portmann, S. Tilmes, A.R. Ravishankara, Z. Wang, S. Wei, Q. Zhang, and Y. Zhang, 2024

NASA Goddard Institute for Space Studies, New York, NY, USA[1]
Center for Climate Systems Research, Columbia University, New York, NY, USA[2]

Abstract. The Paris Agreement's temperature goals, which require maintaining net-zero or net-negative emissions of long-lived greenhouse gases, primarily carbon dioxide, cannot be sustainably achieved if nitrous oxide emissions continue to increase. Improved nitrogen management scenarios provide nitrous oxide abatement that is equivalent to reducing carbon dioxide emissions by up to 235 billion tonnes, helping to reach a long-term 1.5°Celsius (or 2.0°Celsius) goal. The air quality improvements resulting from the improved nitrogen management scenarios lead to roughly 4 million avoided premature deaths due to decreased fine particulate matter and ozone exposure over the next decade, and approximately 20 million avoided premature deaths by 2050. The temperature change due to the reduction of cooling aerosols associated with improved agricultural nitrogen management is likely to outweigh the impact of reduced greenhouse gases in the near-term. This would result in modest additional warming for most of the century, stressing the need to accelerate reductions in short-lived climate pollutants and carbon dioxide to counteract this impact. This is similar to the climate impacts of phasing out coal-fired electricity generation, which leads to aerosol-driven short-term warming but carbon dioxide-driven long-term reductions in warming. Reduced emissions of industrial nitrous oxide, however, would provide climate benefits over all timescales as there are minimal co-emissions. If nitrogen oxide and ammonia emissions were already reduced to meet non-climate policy goals, such as air quality improvements, but nitrous oxide emissions not limited, improved agricultural nitrogen management could provide climate benefits over all timescales. Without additional actions, nitrous oxide emissions would lead to around 0.2°Celsius of additional warming by the end of the century. In contrast, improved nitrogen management with technical reductions and associated livestock methane emissions reductions leads to a near-neutral climate impact by the end of the century compared with a high-end emissions scenario in which minimal action is taken. In the same context, improved nitrogen management with technical reductions and societal change as well as associated livestock methane emissions reductions leads to a 0.1°Celsius reduction in warming beginning late in this century.

Nitrous oxide is currently the most significant ozone layer depleting substance being emitted to the atmosphere. This is because anthropogenic nitrous oxide is increasing, and the Montreal Protocol has succeeded in controlling long-lived halogenated ozone-depleting substances (ODS). Without additional controls, future nitrous oxide emissions are expected to grow and to cause additional ozone depletion. The benefits of mitigating nitrous oxide to ozone are much greater by the end of the century than in the near-term. Even though ambitious nitrous oxide abatement strategies only reduce nitrous oxide levels in the atmosphere by a small amount in the next two decades, the benefits accumulate over time. Because nitrous oxide remains in the atmosphere for a long time, the earlier action is taken to reduce nitrous oxide, the sooner those benefits will be realised. Ambitious abatement of nitrous oride emissions would avoid ozone depletion over the next two decades comparable to accelerating the phase down of HCFCs, an action taken by the Parties to the Montreal Protocol in 2007. It could be five times this action when accumulated until 2100. Calculated global ozone depletion avoided by ambitiously abating nitrous oxide emissions, compared to unabated emissions growth, by the end of the 21 st century would amount to about a quarter of the peak historical global ozone depletion caused by substances now controlled under the Montreal Protocol. Ambitious nitrous oxide abatement could avoid cataract cases increasing by 0.2-0.8 per cent and squamous cell carcinoma cases by 2.2-9.8 per cent by 2080-2090, depending on latitude. The lowest levels of ozone this century and beyond are expected to occur if nitrous oxide emissions continue unabated and carbon dioxide and methane are abated consistent with climate goals.

Journal of Science Education and Technology, vol. 33, issue no. 2, pp.195-207, doi:10.1007/s10956-023-10068-7

Student outcomes of teaching about socioscientific issues in secondary science classrooms: Applications of EzGCM.

Carroll Steward, K., D. Gosselin, **M. Chandler**[1,2], and C.T. Forbes, 2024

NASA Goddard Institute for Space Studies, New York, NY, USA[1]
Center for Climate Systems Research, Columbia University, New York, NY, USA[2]

Abstract. Science education literature has highlighted socio-scientific issues (SSI) as an effective pedagogy for teaching science in a social and political context. SSI links science education and real-world problems to engage students in real-world issues, making it ideal for teaching global climate change (GCC). Additionally, technological advances have created a unique opportunity for teaching climate by making previously inaccessible computer-based computational models and data visualizations accessible to the typical K-12 learning environment. Here, we present the findings from the 2020–2021 school year pre-/post-implementation of a 3-week, model-based climate education curriculum module (EzGCM). Results from the three teachers and their students ($n = 240$) within a single high school located in a midwestern state suggest that the technology-enhanced curriculum positively impacted students' knowledge gains, regardless of the teacher who taught the course. We highlight the importance of using interactive tools, such as GCMs, in the classroom to facilitate both conceptual and epistemic learning. The engagement of students with the model and their teachers played a crucial role in enabling students to assess their own misconceptions, shift their belief systems, and develop a deeper understanding of the subject matter.

Introduction. There has been increasing consensus about the impact of anthropogenic changes on Earth's climate over the last few decades in the scientific community. However, this consensus is not fully reflected in current public opinion, suggesting there is much work to be done in fostering climate literacy. The topic of Earth's climate, more specifically global climate change (GCC), has been largely politicized and is "controversial"; it is a complex issue that intersects with larger society in many ways (Jasanoff, 2010; Sadler, 2004, 2009; Zeidler, 2014). This challenge requires an increasing emphasis on promoting climate literacy through formal education, mainly in secondary science classrooms.

Teachers often state a strong sense of responsibility for teaching about Earth's climate but often feel challenged in accomplishing this objective (Carroll Steward et al., 2022). This challenge stems from teachers often feeling underprepared in their science-content knowledge, struggle to find alignments to science standards, and are challenged to integrate climate topics into their instruction (Bhattacharya et al., 2020, 2021b; Carroll Steward et al., 2021). These challenges are compounded by teachers discovering that many of their students struggle to articulate an understanding of Earth's climate, holding many misconceptions regarding this complex system (Bhattacharya et al., 2021b).

Currently, the Next Generation Science Standards (NGSS) identify scientific modeling as a critical performance expectation in secondary science. Climate scientists rely heavily on computer-based computational models and data visualizations (i.e., scientific modeling) from global climate models (GCMs) to explain current climate trends and make projections about the Earth's future climate. The requirements of NGSS and the importance of modeling to climate scientists provide a unique opportunity to teach climate science.

Historically, the computer systems required for these GCMs were inaccessible in typical learning environments due to their complexity and vast data requirements. Fortunately, access to technology has improved so that opportunities to engage students in hands-on climate science have increased. With these advancements, students can engage in the practices of climate science using authentic modeling tools to investigate Earth's climate system and GCC. However, to use these tools effectively, students and teachers require access to well-developed, coherent curriculum resources.

Clouds and Their Climatic Impact: Radiation, Circulation, and Precipitation. S. Sullivan and C. Hoose, Eds., Geophysical Monograph Series, vol. 281, American Geophysical Union, pp. 87-102, doi:10.1002/9781119700357.ch4.

Cloud-radiation interactions and cloud-climate feedbacks from an active-sensor satellite perspective.

Cesana, G.[1,2], **A.S. Ackerman**[1], T. Vaillant de Guélis, and D.S. Henderson, 2024

NASA Goddard Institute for Space Studies, New York, NY, USA[1]
Center for Climate Systems Research, Columbia University, New York, NY, USA[2]

Abstract. Clouds are ubiquitous in the troposphere. Their interactions with radiation may result in either a warming or a cooling of the Earth system and generate diverse climate feedback. The vertical structure of the radiative effects of clouds as well as the response of clouds to global warming (i.e., the cloud feedback) are inadequately constrained within the diversity of current climate models, which limits our ability to project the magnitude of future warming. In this chapter we show how relatively recent active sensor spaceborne observations have narrowed constraints on cloud feedback. The value added beyond what can be retrieved from passive sensors is only just beginning to be exploited.

Introduction: The interactions between cloud particles and radiation modulate the amount of energy that is reflected, emitted, and absorbed by the Earth. Changes in cloud properties (e.g., areal and vertical extent, temperature, emissivity, opacity, and absorptivity profiles) modify their radiative effects, which, in turn, can profoundly affect the radiative balance of the Earth-atmosphere system (Kiehl & Trenberth, 1997; Wielicki et al., 1996) because clouds cover a large part of the troposphere (Cesana & Waliser, 2016; Stubenrauch et al., 2013). For example, liquid clouds are typically more opaque than their frozen counterparts, which corresponds to more reflection of shortwave (SW) radiation and also more absorption and emission of longwave (LW) radiation for a given profile of water content and temperature (e.g., Cesana & Storelvmo, 2017; Rogers & Yau, 1989).

For the past few decades, passive-sensor satellites have been monitoring cloud properties (e.g., Rossow & Schiffer, 1999) and the outgoing and incoming radiative fluxes at the top of the atmosphere (e.g., Wielicki et al., 1996). More recently, active sensors onboard the Cloud-Aerosol Lidar and Infrared Pathfinder Satellite Observations (CALIPSO; Winker et al., 2010) and CloudSat (Stephens et al., 2002) flying in the A-Train Constellation have provided detailed vertical distribution of cloud properties. Combining these new observations with passive-sensor information from other A-Train satellites has made it possible to characterize radiative fluxes at a high vertical resolution for different types of clouds (Hang et al., 2019; L'Ecuyer et al., 2019; Matus & L'Ecuyer, 2017) and has improved previous estimates of surface and top-of-atmosphere (TOA) radiative fluxes (Stephens et al., 2012). The use of such active and passive remote sensing platforms for precipitation is outlined in Chapter 15: Satellite Precipitation Measurements.

To better understand past, present, and future climates, we partly rely on Earth system models (ESMs), which are a simplified version of nature and whose utility and plausibility can be evaluated to some extent through rigorous comparison with pertinent observations. Because of their coarse horizontal mesh of O (100 km), climate models by design do not resolve cloud processes on smaller scales, instead relying on parameterizations that represent the expressions of subgrid processes on the gridbox scale. Often times, such oversimplification results in large cloud biases (e.g., Klein et al., 2013; Zhang et al., 2005). With its more detailed vertical information, CloudSat-CALIPSO observations have exposed biases in climate models (e.g., Cesana & Waliser, 2016; Jiang et al., 2012; Nam et al., 2012) beyond the reach of previous satellite observations. However, it is assumed that simulating the current cloud climatology is a necessary but not sufficient condition to build confidence in the ability of the models to reliably project future climate change.

Radiation Processes in the Atmosphere and Ocean, 4–8 July 2022, Thessaloniki, Greece, AIP Conference Proceedings, vol. 2988, AIP Publishing, p. 070009, doi:10.1063/5.0183626

Better constraining supercooled clouds could reduce projected warming spread.

Cesana, G.V.[1,2], **A.S. Ackerman**[1], **A.M. Fridlind**[1], I. Silber, A.D. Genio, M.D. Zelinka, and H. Chepfer, 2024

NASA Goddard Institute for Space Studies, New York, NY, USA[1]
Center for Climate Systems Research, Columbia University, New York, NY, USA[2]

Abstract. The increase of climate sensitivity to rising greenhouse gas concentrations in the coupled model intercomparison project phase 6 (CMIP6) Earth system models (ESMs) compared to CMIP5 ESMs is primarily attributed to a larger extratropical cloud response to climate change, referred to as cloud feedback. The ratio of supercooled liquid cloud water relative to all cloud water, termed liquid phase ratio (LPR), which has also notably increased in many recent ESMs, is thought to be a primary driver of the extratropical cloud feedback increase. Unlike the preponderance of previous studies that compare native model LPR directly with observations, here we evaluate LPR over three ESM generations against Cloud-Aerosol Lidar and Infrared Pathfinder Satellite Observations (CALIPSO) using an instrument simulator approach, which mimics instrument limitations and uses consistent cloud definitions and resolutions. We find that current coupled model intercomparison project (CMIP) ESMs collectively simulate greater LPR than previous CMIP generations and overestimate LPR compared to observations, contrary to previous findings, likely driven by past inconsistent comparisons of ESM outputs with CALIPSO observations. We further show that greater LPR in ESM present-day climate is unexpectedly correlated with a smaller extratropical cloud feedback, attributable to a decrease of cloud amount exceeding the increase of cloud optical depth. Finally, our results suggest that improving constraints on model LPR using our evaluation framework would likely reduce the spread in CMIP6 climate sensitivities, owing to its effect on extratropical cloud feedback from supercooled clouds.

Introduction: More liquid phase clouds are expected to prevail at the expense of ice clouds in response to climate warming. In general, liquid phase clouds are more reflective than ice clouds for a similar water content and they precipitate less efficiently, which is expected to increase cloud amount and optical depth1 , resulting in more solar radiation reflected back to space, weakening the initial warming through a negative cloud feedback (a relative cooling effect). These changes of cloud amount and optical depth in response to warming are commonly referred to as cloud amount and cloud optical depth feedback, respectively. The contribution of a phase shift to these cloud optical depth and amount feedbacks are maximum in the extratropics (defined as latitudes between 55˚ and 75˚ in both hemispheres), particularly over the Southern Ocean2 , where mixed-phase temperatures (0˚C < T 40-ɔ˚C) are omnipresent in the troposphere. More specifically, the strength of the optical depth feedback seems to depend on the amount of supercooled liquid present at mixed-phase temperatures, where both ice and liquid phases can coexist. Some studies have reported a link between increased liquid water mass relative to all condensed water (LPRmass) in the current climate and reduced negative optical depth feedback in individual ESMs3–5. This possible link is particularly important since the weakening of the Coupled Model Intercomparison Project phase 6 (CMIP6) extratropical negative feedback relative to CMIP5 models has been shown to be the leading cause of larger spread and equilibrium climate sensitivity2 (ECS) in CMIP6 models. Here we evaluate how well CMIP cloud phase is represented against satellite observations and then explore the links between changes in cloud phase and extratropical feedback across CMIP generations.

Clouds and Their Climatic Impacts. S.C. Sullivan and C. Hoose, Eds., Geophysical Monograph Series, vol. 271, American Geophysical Union, pp. 47-85, doi:10.1002/9781119700357.ch3.

Ice crystal complexity and link to the cirrus cloud radiative effect.

Järvinen, E., **B. van Diedenhoven**[1,2], N. Magee, S. Neshyba, M. Schnaiter, G. Xu, O. Jourdan, D. Delene, F. Waitz, S. Lolli, and S. Kato, 2024

NASA Goddard Institute for Space Studies, New York, NY, USA[1]
Center for Climate Systems Research, Columbia University, New York, NY, USA[2]

Abstract. The aim of this chapter is to present emerging information on ice crystal morphology in the nano- and microscale from various sources and explore its impact on ice crystal's single-scattering properties and ultimately on cirrus cloud radiative effect. Increasing amount of observations in the last decade have shown that cirrus ice crystals invariably contain some degree of facet roughness, hollowness, or other morphological complexities that make the crystal shape deviate from that of a pristine hexagonal shape. These morphological complexities are found to be present in a wide variety of environmental conditions. A set of physical and statistical complexity parameters is used to quantify ice crystal complexity depending on the application. Although laboratory studies have shown that complexity parameters tend to increase with increasing crystal growth rate, observations in natural cirrus indicate that complexity parameters only weakly vary at cirrus temperatures below 230 K. Morphological complexities affect the optical properties of ice crystals. Implementing the optical properties of complex ice crystals in climate models has shown that the radiative effect of crystal complexity is a cooling of 1?2 Wm ?2 globally. Due to the prevalence of ice crystal morphological complexities and their influence on cirrus radiative properties, the radiative effect of crystal complexity should be taken into account in future climate models. However, work is still needed to transfer the increasing knowledge of the physical nature of ice crystal complexity into optical particle models and eventually into parameterizations used in models.

Introduction. Cirrus clouds are ubiquitous in Earth's atmosphere. At any given moment, they cover approximately 40–60% of Earth's surface and in the tropics the cirrus cloud coverage can reach up to 70% (e.g., Mace et al., 2009; Matus & L'Ecuyer, 2017; Sassen et al., 2008). Our understanding of cirrus clouds and their role in the climate system has improved greatly in the past decades thanks to new capabilities in modeling, improvements in remote sensing, increased accumulation of in situ data (e.g., with aircraft and balloon-borne measurements), dedicated laboratory and cloud chamber measurements, and development of new instrumentation. While it is generally agreed that cirrus clouds are an important cloud type both from climate and weather perspectives, it is also acknowledged that large gaps exist in our knowledge related to cirrus clouds, leading to substantial uncertainties and possible systematic biases in our predictions of Earth's future climate (Boucher et al., 2013).

Partly, these uncertainties arise from inadequate understanding of microscale physics. Based on data gathered with airborne cloud instruments, it is well known that cirrus ice crystals cover a wide range of crystal sizes from a few micrometers for newly formed crystals to several millimeter sized precipitation particles (e.g., Krämer et al., 2020). It is also known that, unlike spherical liquid droplets, cirrus ice crystals manifest impressively myriad geometries (e.g., Baran, 2009; Lawson et al., 2019). The basic shape of ice crystals often resembles a sixfold radial symmetry that can be attributed to the hexagonal molecular structure of ice. Three facets are most commonly observed: the basal, the prismatic, and the pyramidal. Laboratory studies have shown that the growth rates of these facets are determined by temperature and relative humidity leading to different crystal habits, such as columnar crystals, plate-like crystals, and bullet rosettes (Bailey & Hallett, 2002, 2004, 2009). Variations in atmospheric conditions and interactions with other crystals and supercooled droplets lead to more complex crystal structures. One commonly used scheme to classify ice crystals contains 80 classes for snow and ice (Magono & Lee, 1966).

DOE/SC-0214. U.S. Department of Energy, Office of Science, Biological and Environmental Research Program, doi:10.2172/2331276

A Unified Data Infrastructure for Biological and Environmental Research: A Report from the BER Advisory Committee.

Kleese van Dam, K., A. Schlosser, J. Schmutz, B. Bond-Lamberty, K. Fangan, **A.M. Fridlind**[1], S. Gregurick, D. Niyogi, D. Segre, and P. Weisenhorn, 2024

NASA Goddard Institute for Space Studies, New York, NY, USA[1]

Abstract. The Biological and Environmental Research (BER) program within the U.S. Department of Energy (DOE) Office of Science supports large-scale data generation efforts across its two divisions: Biological Systems Science and Earth and Environmental Systems Sciences. These efforts include user facilities in atmospheric radiation measurements, genomics, metabolomics, proteomics, compute, and imaging. In addition, BER supports the development of plant-based fuels; research in biosystems design, environmental microbiomes, and atmospheric systems; energy flux monitoring; climate-based ecosystem experiments; pathogen biopreparedness; and modeling of climate, urban interfaces, and interactions between people and energy resources. For data access, BER supports community data services at its user facilities, along with specialized data initiatives for Earth and environmental science, climate modeling, genomic and microbial analysis, and multi-sector dynamics modeling.

In October 2022, the BER Advisory Committee (BERAC) received a charge letter from the DOE Office of Science director requesting a review of existing capabilities in data management and infrastructure relevant to BER science. The charge also requested a recommended strategy for next-generation data management and analysis within a unified framework. Further goals included identifying new science opportunities that could be enabled by increased integration of BER's facilities while considering advances in artificial intelligence and machine learning (AI/ML). The charge asked BERAC to examine synergistic investments within DOE and at other agencies and the impact of a more unified data infrastructure on the scientific workforce. To address these goals, the appointed subcommittee established five working groups focusing on (1) environmental science; (2) biological science; (3) diversity, equity, inclusion, and accessibility; (4) BER data services; and (5) unified data infrastructure and artificial intelligence. The subcommittee organized a two-day virtual community workshop that included discussions on new unified data infrastructure-enabled science opportunities, barriers to broader inclusion of minorities, support for early career scientists, and potential unified data infrastructure solutions for BER.

Several science opportunities emerged during subcommittee discussions and workshop breakouts. These crosscutting opportunities apply across much of BER's biological and environmental sciences and represent areas in which the program can significantly impact efforts to understand and manipulate natural and managed resource systems to meet DOE goals. The first opportunity is to leverage decades of collected environmental and biological data to predict biological systems under realistic field conditions at multiple scales. A second opportunity is to develop and test multiscale models that incorporate environment-dependent biological system variables in high resolution. A final opportunity is to make BER data accessible, inclusive, and usable by the broader community. Addressing these challenges will require DOE to encourage shareable, coordinated data collection with standards for field data; develop curated, standardized, and open datasets that can enable multiscale modeling; and make field, environmental, variation, and climate data accessible to support diversity, equity, and inclusion goals.

Introduction. Truly accessible data requires efforts beyond describing a dataset in a publication and making it downloadable. Different expertise is needed to integrate data at different scales, and a challenge for BER is to provide data in a way that enables a nondomain expert to subset these data and perform analyses.

AIAA SciTech 2024 Forum, 8-12 January 2024, Orlando, FL, American Institute of Aeronautics and Astronautics,
doi:10.2514/6.2024-2168

Composition and climate impacts of increasing launches to Low Earth Orbit.

Tsigaridis, K.[1,2], **R. Field**[1,3], **S.E. Bauer**[1,2], M.N. Ross, C. Maloney, **G.A. Schmidt**[1], and K.H. Rosenlof, 2024.

NASA Goddard Institute for Space Studies, New York, NY, USA[1]
Center for Climate Systems Research, Columbia University, New York, NY, USA[2]
Applied Physics and Applied Mathematics, Columbia University, New York, NY, USA[3]

Abstract. We present simulations of an Earth system model in which launch vehicles inject gaseous and particulate combustion products into the stratosphere. We considered two plausible scenarios representative for the year 2050, one with 1000 launches per year and another with 10 times more, all of which assuming heavy lift (80 tons to low Earth orbit; LEO) launches using methane as a proxy for liquefied natural gas (LNG) fuel. An industry-standard plume flowfield model was used to predict emission of gaseous species including carbon monoxide, nitrogen oxides, and water vapor. Black carbon was introduced assuming vacuum emission equal 25% of equivalent kerosene engine. The gas emissions showed marginal or insignificant changes in atmospheric composition, while the black carbon emission was found to be the most influential component. Feedback involve tropopause and stratospheric warming, followed by a moistening of the stratosphere via tropospheric water vapor intrusions, together with a reduction in global albedo. The fact that LNG-fueled rockets could be a concern from aerosol emissions in our simulations, despite burning more efficiently than conventional fuels, underscores the need to better understand actual black carbon emissions from rocket engines in order to accurately predict the global impacts of launch vehicles on future climate.

Introduction. Rocket launches have clear local impacts on atmospheric composition [1], and the number of launches to Low Earth Orbit (LEO) from space agencies and commercial space activities are projected to greatly increase over the next few decades [2]. Better understanding of the broader impacts on air quality, stratospheric ozone, and even climate, under plausible frequency and technological scenarios, including reusable rockets [3], are essential to fully appreciate their potential effects. Depending on the future path of space exploration and utilization, the global rate of orbital launches [4] is projected to accelerate and include an increasing number of heavy lift launch vehicles which would result in much higher rocket engine emissions. Spaceflight is largely unregulated, a situation that could change in the future as the rate of launch emissions increases [5]. Detailed studies of the impacts of emissions from all phases of space flight, from launch to reentry and in all layers of the Earth's atmosphere, are necessary.

The future path of spaceflight technologies and increase in activities are difficult to accurately predict. Nevertheless, current trends and developments can be used to specify plausible future scenarios of launch vehicle emissions from a range of potential technologies (e.g., propellants and payloads) and specific goals (e. g, satellite launches and Mars exploration). Realistic models of rocket engine combustion, afterburning, and launch trajectories provide vertical profiles of emissions, including black carbon particles, nitrogen oxides, water vapor, and other volatiles and relevant byproducts like carbon monoxide. We build upon past work of members of our group [6] performed with the Community Earth System Model (CESM) coupled with the Whole Atmosphere Community Climate Model (WACCM) that includes atmospheric chemistry calculations and aerosol microphysics, and similar work with the Goddard Earth Observing System (GEOS)-Chem model using emissions estimates made for conventional rocket fuel types [7]. Using the National Aeronautics and Space Administration (NASA) Goddard Institute for Space Studies (GISS) Earth system model ModelE, we perform simulations of both the present-day and future (year 2050) climates using realistic emissions for a typical methane fueled heavy lift launch vehicle and plausible, if speculative, number of launches per year. The goal is to both compare the state-of-the-art climate and air quality atmospheric models with high resolution in the vertical and well-resolved stratospheric climate (GISS ModelE and CESM-WACCM), but also to go a step further and understand the future impacts of space launches on climate, as a result of changes induced by the emissions both via gas-phase reactions and aerosol-radiation interactions.

Sensors, Systems, and Next-Generation Satellites XXVIII: 16-20 September 2024, Edinburgh. S.R. Babu, A. Hélière, and T. Kimura, Eds., Proc. SPIE, vol. 13192, p. 131920E, doi:10.1117/12.3033830.

Life after launch: A snapshot of the first six months of NASA's Plankton, Aerosol, Cloud, Ocean Ecosystem (PACE) mission.

Werdell, P.J., B. Franz, C. Poulin, J. Allen, **B. Cairns**[1], S. Caplan, I. Cetinic, S. Craig, M. Gao, O. Hasekamp, A. Ibrahim, K. Knobelspiesse, A. Mannino, J.V. Martins, L. McKinna, G. Meister, F. Patt, C. Proctor, C. Rajapakshe, I. Soto Ramos, J. Rietjens, A. Sayer, and E. Sirk, 2024

NASA Goddard Institute for Space Studies, New York, NY, USA[1]

Abstract. The NASA Plankton, Aerosol, Cloud, ocean Ecosystem (PACE) mission launched from Kennedy Space Center in the early morning of February 8, 2024. Just 63 days later, data from NASA's newest Earth-observing satellite became available to the public. These data will extend and improve upon NASA's 20+ years of global satellite observation of our living oceans, atmospheric aerosols, and cloud and initiate an advanced set of climate-relevant data records. Ultimately, PACE is the first mission to provide daily, global measurements that will enable prediction of the "boom-bust" cycle of fisheries, the appearance of harmful algae, and other factors that affect commercial and recreational industries. PACE also observes clouds and tiny airborne particles known as aerosols that influence air quality and absorb and reflect sunlight, thus warming and cooling the atmosphere. In the months since launch and initial data release, the PACE Project pursued instrument temporal and system vicarious calibrations, executed cross-instrument comparisons, conducted performance assessments, explored synergies with other missions, and released advanced science data products. In parallel, the PACE Validation Science Team left for the field and the Post-launch Airborne eXperiment (PACE-PAX) prepared for its mission. And, most importantly, preliminary science results were realized. Here, we present a snapshot of these activities and their impacts and outcomes, encompassing the first half year of the PACE mission.

Introduction. The Plankton, Aerosol, Cloud, ocean Ecosystem (PACE) mission, launched on 8 February 2024, will extend the continuous high-quality ocean color, atmospheric aerosol, and cloud data records begun by NASA in the late 1990s, building on the heritage of the Coastal Zone Color Scanner (CZCS), Sea-viewing Wide Field-of-view Sensor (SeaWiFS), Moderate Resolution Imaging Spectroradiometer (MODIS), Multi-angle Imaging Spectroradiometer (MISR), and Visible Infrared Imaging Radiometer Suite (VIIRS) [1]. PACE's global hyperspectral imaging radiometer design concept will enable new discoveries in Earth's living ocean, such as the diversity of organisms fueling marine food webs and how aquatic ecosystems respond to environmental change. Its full instrument payload also observes Earth's atmosphere to study clouds, airborne aerosol particles, and the interactions between the two [2, 3]. Looking at the ocean, clouds, and aerosols together improves our knowledge of the roles each plays in our evolving planet. Other applications of PACE science data records – from identifying the frequency, extent, and duration of aquatic harmful algal blooms to improving our understanding of air quality to providing a pathfinder for hyperspectral terrestrial applications – will result in direct economic, recreational, and societal benefits [4, 5]. Ultimately, by extending and expanding NASA's long record of global Earth satellite observations, the PACE mission will monitor our home planet in new and advanced ways in the coming decade. In the first six months since launch (the time of this writing), the PACE Project completed in-orbit commissioning, released radiometric and heritage ocean color science data publicly, pursued instrument on-orbit calibrations, executed cross- instrument comparisons, conducted preliminary performance assessments, released advanced science data products, and reprocessed the full mission time-series. In parallel, a third PACE Science and Applications Team (SAT3) assembled, the PACE Validation Science Team (PVST; https://pace.oceansciences.org/pvstdoi.htm) left for the field and the Post-launch Airborne eXperiment (PACE-PAX, [6]) prepared for deployment.

Author Index

A

Ackerman A.S. 43, 82, 159, 160, 198, 230
Aleinov I. 43, 86, 212
Arouf A. 69, 127

B

Bader D. 77, 142, 170
Barbara J.M. 73
Bauer S.E. 43, 86, 92, 100, 104, 123, 142, 150, 159, 160, 166, 177, 234
Bong H. 76, 213, 214
Braneon C.V. 35, 36, 72, 77, 148, 170, 209

C

Cairns B. 31, 66, 84, 90, 136, 147, 186, 195, 196, 235
Cesana G. 43, 82, 83, 106, 108, 133, 206, 230, 231
Chandler M.A. 229
Chowdhary J. 43, 92, 184, 185
Clifton O.E. 86
Cook B.I. 43, 67, 68, 87, 88, 98, 165, 174, 178
Cowan T.G. 86

D

DallaSanta K.J. 150, 225
Del Genio A.D. 43, 73, 82, 90, 108, 206
DeLessio M. 43, 92
Derras-Chouk A. 77, 93

E

Ehsan M.A. 94
Elsaesser G.S. 43, 95, 100, 116, 139, 164, 198, 206, 216
Erfani S.M.H. 70, 96

F

Faluvegi G.V. 43, 86, 180, 189, 190, 191, 192, 228
Field R.D. 100, 129, 139, 156, 234
Fridlind A.M. 82, 124, 146, 157, 159, 160, 217, 231, 233

G

Gao C.Y. 104
Gornitz V. 77, 114, 170
Guarin J.R. 109, 143, 144

H

Haas H. 111, 112
Hendrickson M. 131
Hickman J.E. 100

I

Ivanovich C.C. 118, 119, 120, 218

J

Jägermeyr J. 75, 102, 105, 109, 113, 135, 138, 155, 158, 169, 183
Jin Z. 83
Jonas J.A. 43, 44, 167, 225

K

Karl K. 101, 122
Kelley M. 43, 86, 132
Kiang N.Y. 43, 107, 153, 194

L

LeGrande A.N. 43, 130, 168, 223
Lerner P. 43, 71, 132
Leitmann-Niimi N.M. 116

M

Ma Q. 140
Mankoff K.D. 117, 187, 219, 220
Marvel K.D. 43, 145, 165
McGraw Z.S. 19, 20, 115, 149, 150, 151
McDermid S.S. 43, 110, 135, 178
Menzel M. 152
Miller R.L. 43, 81, 134, 141, 166, 199, 208

N

Nakad M. 162
Nazarenko L.S. 43, 44, 167, 171, 224, 225
Nielsen M. 165

O

Obiso V. 134, 166, 199, 208
Orbe C. 43, 150, 154, 167, 222, 224, 225
Ottaviani M. 83, 171, 179

P

Perlwitz J.P. 43, 44, 166
Peteet D.M. 74, 114
Phillips M. 105, 183
Pilewskie J. 175, 203
Plaas H.E. 172, 173, 176
Puma M.J. 43, 126, 161

R

Rind D.H. 43, 44, 121, 167, 225
Roach L.A. 181, 182
Robertson A.W. 94
Romanou A. 43, 71, 132, 194, 210
Romanski J. 210
Ruane A.C. 89, 97, 103, 105, 109, 125, 144, 158 184, 193, 204

Author Index

Ruedy	R.A.	43, 44, 131, 132
Russell	G.L.	43, 44, 132, 225
S		
Schmidt	G.A.	2, 13, 14, 15, 16, 22, 24, 33, 34, 43, 44, 71, 85, 131, 142, 167, 187, 188, 192, 225, 234
Sohl	L.E.	43, 197, 221
Stanford	M.W.	201
T		
Tornow	T.	84, 159, 160, 217
Tselioudis	G.	43, 44
Tsigaridis	K.	43, 86, 92, 100, 104, 123, 139, 150, 166, 177, 180, 197, 234
V		
van Lier-Walqui	M.	43, 78, 95, 100, 128
W		
Way	M.J.	43, 80, 91, 200
Weng	E.	43, 137, 215
Westervelt	D.M.	99
Williams	J.	79, 210
Wu	J.	43, 100
Z		
Zhou	T.	75, 106, 225